

**Systematic Manipulation of Siliconoid Clusters:
From Peripheral Functionalization to Heteroatom
Doping**

Dissertation

zur Erlangung des Grades
des Doktors der Naturwissenschaften
der Naturwissenschaftlich-Technischen Fakultät
der Universität des Saarlandes

von

M.Sc. Yannic Heider

Saarbrücken

2020

Tag des Kolloquiums:	25.09.2020
Dekan:	Prof. Dr. Guido Kickelbick
Berichterstatter:	Prof. Dr. David Scheschkewitz Dr. André Schäfer Prof. Dr. Andreas Schnepf
Vorsitz:	Prof. Dr. Christopher Kay
Akademischer Mitarbeiter:	Dr. Volker Huch

Meiner Familie gewidmet

The present dissertation was prepared in the time between January 2017 and May 2020 at the Institute for General and Inorganic Chemistry of the Faculty of Natural Science and Engineering at the Saarland University under the supervision of Prof. Dr. David Scheschkewitz.

Die vorliegende Dissertation wurde in der Zeit zwischen Januar 2017 und Mai 2020 am Institut für Allgemeine und Anorganische Chemie der Naturwissenschaftlich-Technischen Fakultät an der Universität des Saarlandes unter der Aufsicht von Prof. Dr. David Scheschkewitz erstellt.

“Da ist das Ding!”

Oliver Kahn

Abstract

Unsaturated silicon clusters (siliconoids) arise as transient intermediates during the industrial preparation of bulk silicon by chemical vapor deposition of silane precursors. Stable representatives reiterate surface features of silicon materials. The present thesis deals with the systematic manipulation of the ligand periphery and the cluster core of Si_6 siliconoids. The attachment of representative electrophiles at that particular silicon scaffold is now possible at two distinct vertices and their influence on the electronic structure is rationalized. The isolation of boron- and phosphorus-substituted derivatives prompted investigations on the incorporation of the dopant atoms in the cluster core itself. An NHC-stabilized, cyclic Si_2P phosphasilene is shown to dimerize upon Lewis-acid induced abstraction of the donating NHC-ligand. The resulting Si_4P_2 species exhibit cluster structures reminiscent of the corresponding Si_6 siliconoids despite their apparent saturated nature. Access to unsaturated ESi_5 heterosiliconoids ($\text{E} = \text{B}, \text{P}$) was finally gained via a novel dianionic Si_5 cluster, which is obtained by the formal reductive cleavage of a SiTip_2 moiety from the Si_6 siliconoid. The successful incorporation of dopant atoms in siliconoids extends the siliconoid/silicon surfaces analogy to the technological process of silicon doping.

Zusammenfassung

Ungesättigte Siliciumcluster (Silicoide) treten als kurzlebige Zwischenprodukte bei der industriellen Herstellung von Bulk-Silicium durch chemische Gasphasenabscheidung von Silan-Vorstufen auf. Stabile Vertreter weisen Oberflächenmerkmale von Siliciummaterialien auf. Die vorliegende Arbeit befasst sich mit der systematischen Manipulation der Ligandenperipherie und des Clusterkerns von Si_6 -Silicoiden. Die Bindung repräsentativer Elektrophile an diesem bestimmten Siliciumgerüst ist nun an zwei verschiedenen Positionen möglich und ihr Einfluss auf die elektronische Struktur wird rationalisiert. Die Isolierung von Bor- und Phosphor-substituierten Derivaten veranlasste Untersuchungen zum Einbau der Dotierelemente in den Clusterkern selbst. Es wurde gezeigt, dass ein NHC-stabilisiertes, cyclisches Si_2P -Phosphasilen bei Lewis-Säure-induzierter Abstraktion des Donor-NHC-Liganden dimerisiert. Die resultierenden Si_4P_2 -Spezies weisen trotz ihrer augenscheinlich gesättigten Natur Clusterstrukturen auf, die an die entsprechenden Si_6 -Silicoide erinnern. Ungesättigte ESi_5 -Heterosilicoide ($\text{E} = \text{B}, \text{P}$) wurden schließlich über einen neuen dianionischen Si_5 -Cluster zugänglich, der durch die formale reduktive Abspaltung einer SiTip_2 -Einheit vom Si_6 -Silicoid erhalten wird. Der erfolgreiche Einbau von Dotierelementen in Silicoide erweitert die Silicoid/Silicium-Oberflächen Analogie um den technologischen Prozess der Siliciumdotierung.

List of Publications

As part of the present dissertation:

- Yannic Heider*, Nadine E. Poitiers*, Philipp Willmes, Kinga I. Leszczyńska, Volker Huch, David Scheschkewitz. Site-selective functionalization of Si₆R₆ siliconoids. *Chem. Sci.* **2019**, *10*, 4523-4530.
<https://doi.org/10.1039/C8SC05591B>
*These authors contributed equally.
- Yannic Heider, Philipp Willmes, Daniel Mühlhausen, Lukas Klemmer, Michael Zimmer, Volker Huch, David Scheschkewitz. A Three-Membered Cyclic Phosphasilene. *Angew. Chem. Int. Ed.* **2019**, *58*, 1939-1944; *Angew. Chem.* **2019**, *131*, 1956-1964.
English Version: <https://doi.org/10.1002/anie.201811944>
German Version: <http://dx.doi.org/10.1002/ange.201811944>
- Yannic Heider, Philipp Willmes, Volker Huch, Michael Zimmer, David Scheschkewitz. Boron and Phosphorus Containing Heterosiliconoids: Stable p- and n-Doped Unsaturated Silicon Clusters. *J. Am. Chem. Soc.* **2019**, *141*, 19498-19504.
<https://doi.org/10.1021/jacs.9b11181>

Others:

- Philipp Willmes, Kinga Leszczyńska, Yannic Heider, Kai Abersfelder, Michael Zimmer, Volker Huch, David Scheschkewitz. Isolation and Versatile Derivatization of an Unsaturated Anionic Silicon Cluster (Siliconoid). *Angew. Chem. Int. Ed.* **2016**, *55*, 2907-2910; *Angew. Chem.* **2016**, *128*, 2959-2963.
English Version: <https://doi.org/10.1002/anie.201511037>
German Version: <https://doi.org/10.1002/ange.201511037>
- Yannic Heider, David Scheschkewitz. Stable unsaturated silicon clusters (siliconoids). *Dalton Trans.* **2018**, *47*, 7104-7112.
<https://doi.org/10.1039/C8DT01009A>

Acknowledgements/Danksagung

“No one who achieves success does so without acknowledging the help of others. The wise and confident acknowledge this help with gratitude.”

Alfred North Whitehead

In diesem Sinne möchte ich mich an dieser Stelle bei einigen Menschen, die mich durch mein Leben, mein Studium und vor allem meine Promotion begleitet haben, bedanken!

An erster Stelle möchte ich mich ganz herzlich bei **Prof. Dr. Scheschkewitz** dafür bedanken, dass er mir ermöglicht hat nach meiner Masterarbeit auch meine Zeit als Doktorand dem spannenden und interessanten Themengebiet der Silicium-Cluster widmen zu können. Er hat meine Forschung mit seiner kritischen Art, seinen Kommentaren und Vorschlägen auf wissenschaftlicher Ebene stetig vorangetrieben, ohne mir den nötigen Freiraum zu lassen, meine eigenen Ideen und Ziele in das Projekt einbringen und verfolgen zu können. Außerdem möchte ich mich bei Ihm für erlebnisreiche Stunden abseits der Universität auf Tagungen, Konferenzen und vor allem auf den Skipisten der Schweiz bedanken.

Ein ganz besonderes Dankeschön gilt meinen langjährigen Kommilitonen und sehr guten Freunden **Lukas Klemmer**, **Yvonne Kaiser**, **Sascha Grandjean**, **Caroline Hoffmann** und **Thomas Büttner** für die schönen, ereignisreichen und lustigen Jahre, die ich mit ihnen zusammen an und außerhalb der Universität erleben durfte. Sie haben diese Zeit lebenswert gemacht und mir immer das Gefühl gegeben, dass ich mich voll und ganz auf Sie verlassen kann. Besonders **Lukas** und **Yvonne** möchte ich für unsere gemeinsame Zeit im AK Scheschkewitz danken, für ihr aufrichtiges Interesse an meiner Arbeit, ihre Vor- und Ratschläge, angeregte Diskussionen, unsere Dummschwätzereien und diverse feucht-fröhliche Abende.

Ein großes Dankeschön gebührt meinem ehemaligen Betreuer, Mitarbeiter und Freund **Dr. Philipp Willmes** für seine große Unterstützung während meiner Zeit als Student im AK Scheschkewitz. Ich habe sehr viel von ihm gelernt und auch während meiner Zeit als Doktorand noch von unserer guten Zusammenarbeit profitiert. Vielen Dank dafür!

Vielen Dank an alle ehemaligen und aktuellen Mitglieder des Arbeitskreises, der Glasbläserei und der Werkstatt **Dr. Carsten Präsang**, **Dr. Andreas Rammo**, **Dr. Kinga Leszczyńska**, **Dr. David Nieder**, **Dr. Hui Zhao**, **Dr. Cem B. Yildiz**, **Dr. Paresh K. Majhi**, **Dr. Diego M. Andrada**, **Dr. Naim Obeid**, **Dr. Harinath Adimulam**, **Andreas**

Kell, Nadine Poitiers, Marcel Lambert, Marc Hunsicker, Felix Gerlach, Lena Pesch, Andreas Adolf, Britta Schreiber, Eveline Altmeyer und **Sylvia Beetz** für die gute Zusammenarbeit und freundliche Arbeitsatmosphäre.

Vielen Dank an **Daniel Mühlhausen**, der durch seine neugierige Art und seinen Fleiß sehr dazu beigetragen hat, dass mir die Betreuung seiner Bachelorarbeit so viel Spass gemacht hat.

Ein herzliches Dankeschön an **Dr. Volker Huch** für die Durchführung der Kristallstrukturanalysen, an **Dr. Michael Zimmer** für die Unterstützung in Sachen NMR-Spektroskopie und an **Susanne Harling** für die CHN-Analytik.

Ein ganz besonderes Dankeschön möchte ich an die Sekretärin und gute Seele des Arbeitskreises **Bianca Ianuzzi** richten für Ihre offene Art und die bedingungslose Hilfsbereitschaft in bürokratischen Angelegenheiten.

Außerdem möchte ich **Dr. André Schäfer** herzlich dafür danken, dass er sich bereit erklärt hat, das Zweitgutachten dieser Dissertation zu übernehmen.

Ein großes Dankeschön geht an alle meine ehemaligen und aktuellen Teamkollegen und Freunde vom **SV Rockershausen**. Mit ihnen habe ich auf dem Sportplatz und im Clubheim immer den perfekten Ausgleich zu Schule/Studium/Promotion gefunden. Auf dass es noch eine Weile so weitergeht!

Abschließend möchte ich mich noch bei den wichtigsten Menschen in meinem Leben bedanken.

Vielen Dank an alle Ko's, Am's und Anhängsel aus unserem KoHeAm-Clan: **Opa Peter, Oma Uschi, Klaus, Esther, Marc, Sabrina, Jan, Kaarina, Philipp, Lena, Stefan, Beate, Daniel, Nadine, Leo** und **Björn**. Danke, dass wir uns aufeinander verlassen können, dass wir immer zueinander halten und so ein eingeschworener Haufen sind. Bleibt so wie ihr seid! Ihr seid die Besten!

Von ganzem Herzen möchte ich mich bei meiner Freundin **Raphaela De Agazio** für ihre stetige Unterstützung, Aufmerksamkeit und Liebe bedanken. Sie ist mein großer Rückhalt, meine bessere Hälfte und mein Zuhause. Ich liebe dich!

Mein größter Dank gilt meiner Schwester **Michelle Heider** und meinen Eltern **Brigitte** und **Thomas Heider**. Sie haben mich in meinen mittlerweile 28 Jahren immer und in jeglicher Hinsicht bedingungslos unterstützt und zu dem Menschen gemacht, der ich heute bin. Ich liebe euch und bin euch unendlich dankbar!

Content

List of Abbreviations	1
List of Figures	3
List of Schemes	4
List of Tables	7
Preface – Silicon Then and Now	8
1. Introduction	10
1.1. Perspective and Motivation	10
1.2. Saturated Silicon Cages.....	14
1.3. Zintl Ions of Silicon	20
1.3.1. Historical Background.....	20
1.3.2. Solid-State Zintl Phases of Group 14	21
1.3.3. Group 14 Zintl Ions in Solution	21
1.3.4. NMR spectroscopy	24
1.3.5. Functionalization.....	26
1.4. Siliconoids.....	29
1.4.1. Definition	29
1.4.2. Synthesis and Structure	32
1.4.3. Spectroscopic Data and Electronic Properties.....	43
1.4.4. Heterosiliconoids	49
1.4.5. Reactivity	53
1.4.6. Functionalized Siliconoids	57
2. Aims and Scope	59
3. Results and Discussion	61
3.1. Site-selective functionalization of Si_6R_6 siliconoids	61
3.2. A Three-Membered Cyclic Phosphasilene	70

3.3. Boron and Phosphorus Containing Heterosiliconoids: Stable p- and n-Doped Unsaturated Silicon Clusters.....	77
4. Conclusion, Context and Outlook	85
5. References	91
6. Supporting Information	105
6.1. Site-selective functionalization of Si ₆ R ₆ siliconoids (SI).....	105
6.2. A Three-Membered Cyclic Phosphasilene (SI)	153
6.3. Boron and Phosphorus Containing Heterosiliconoids: Stable p- and n-Doped Unsaturated Silicon Clusters (SI)	191
7. Curriculum Vitae	279

List of Abbreviations

222-crypt	4,7,13,16,21,24-Hexaoxa-1,10-diaza-bicyclo[8.8.8]hexacosane
A	Ampere
Å	Angstrom
C	Celsius
cal	Calories
Cp*	Pentamethylcyclopentadienyl (C ₅ Me ₅ ⁻)
CVD	Chemical Vapor Deposition
Dep	Diethylphenyl (2,6-Et ₂ C ₆ H ₃)
DFT	Density Functional Theory
DHA	9,10-Dihydroanthracene
Dip	2,6-Diisopropylphenyl (2,6- <i>i</i> Pr ₂ C ₆ H ₃)
DMAP	4-Dimethylaminopyridine
dmf	<i>N,N</i> -Dimethylformamide
Dmp	Dimethylphenyl (2,6-Me ₂ C ₆ H ₃)
DSC	Differential Scanning Calorimetry
eV	Electronvolt
Et	Ethyl, -C ₂ H ₅
en	Ethylenediamine
Fc	Ferrocene
h	Hour
HOMO	Highest Occupied Molecular Orbital
Hz	Hertz
<i>i</i> Pr	<i>iso</i> -Propyl, -C ₃ H ₇

List of Abbreviations

ⁱ Bu	<i>iso</i> -Butyl, -C ₄ H ₉
IC	Integrated Circuit
K	Kelvin
LUMO	Lowest Occupied Molecular Orbital
M	Molar = mol·L ⁻¹
MAS	Magic Angle Spinning
Me	Methyl, -CH ₃
Mes	Mesityl = 2,4,6-Trimethylphenyl (2,4,6-Me ₃ C ₆ H ₂)
MOSFET	Metal-Oxide-Semiconductor Field-Effect Transistor
ⁿ BuLi	<i>n</i> -Butyllithium
NHC	<i>N</i> -Heterocyclic Carbene
NMR	Nuclear Magnetic Resonance Spectroscopy
Ph	Phenyl
POSS	Polyhedral Oligomeric Silsesquioxane
ppm	Parts Per Million
py	Pyridine
rt	Room Temperature
^t Bu	<i>tert</i> -Butyl, -C ₄ H ₉
T	Tesla
thf	Tetrahydrofuran
TMS	Trimethylsilyl = SiMe ₃
Tip	2,4,6-Triisopropylphenyl (2,4,6- ⁱ Pr ₃ C ₆ H ₂)
UV	Ultraviolet
vis	Visible

List of Figures

- Figure 1:** Moore's Law: The number of transistors on integrated circuit chips (1971-2018) (Source: <https://ourworldindata.org/uploads/2019/05/Transistor-Count-over-time-to-2018.png>; Author: Max Roser, License: Creative Commons Attribution-Share Alike 4.0 International (<https://creativecommons.org/licenses/by-sa/4.0/deed.en>)). 12
- Figure 2:** Schematic representation of the cluster scaffolds of reported saturated polycyclic polysilanes..... 16
- Figure 3:** Structures of silicon-based polyhedral Zintl ions (● = "naked" Si). detected in solid-state ($[\text{Si}_4]^{4-}$ and $[\text{Si}_9]^{4-}$) and solution ($[\text{Si}_4]^{4-}$, $[\text{Si}_5]^{2-}$ and $[\text{Si}_9]^{n-}$ with $n = 2-4$).. 23
- Figure 4:** Reported transition-metal complexes of silicon-based Zintl ions (**21-24**) and the threefold silylated Si_9R_3^- siliconoid **25** (● = Si, ● = "naked" Si; 222-crypt = 4,7,13,16,21,24-hexaoxa-1,10-diaza-bicyclo[8.8.8]hexacosane; R = $\text{SiH}(\text{tBu})_2$).^[203-207] 28
- Figure 5:** Determination of the hemispheroidality parameter Φ in order to distinguish between tetrahedral (left, Φ negative) and hemispheroidal (right, Φ positive) coordination environments (● = "naked" Si, ● = bonded Si atoms, which span the reference plane, ● = residual Si atom of coordination sphere, d = deviation of ● from reference plane, Φ = deviation of ● from reference plane = hemispheroidality parameter). 31
- Figure 6:** Exemplary determination of the hemispheroidality parameter Φ for the "naked" vertex Si5 in the first siliconoid **30**^[247] reported by Scheschkewitz (Si1/Si4 = SiTip₂, Si2/Si3 = SiTip, Si5 = "naked" Si). 34
- Figure 7:** Dominating current vortices in the parent hexasilabenzene isomers **42H** and **43H**. Diatropic vortices are clockwise, paratropic vortices are counterclockwise. The total ring current in **42H** is diatropic and integrates to 9.9 nAT⁻¹. The ²⁹Si NMR chemical shifts are additionally given for **43H**. Partially reproduced from Berger et. al., *Angew. Chem. Int. Ed.* **2010**, 49, 10006-10009^[269] and Abersfelder et. al. *Angew. Chem. Int. Ed.* **2011**, 50, 7936-7939.^[259] 45
- Figure 8:** Molecular orbitals of the parent compound **30H** (a) and schematic representation of the involved atomic orbitals (b). Picture reproduced from Scheschkewitz, *Angew. Chem. Int. Ed.* **2005**, 44, 2954-2956.^[247] 47
- Figure 9:** Comparison of the frontier orbitals of Si₈ siliconoids **34** and **36** and the model compounds **39Dmp** and **43Dip** for pentasila[1.1.1]propellane **39** and its bridged isomer **43**, respectively (● = Si, ● = "naked" Si; R = SiMe₃, R' = tBu, R'' = Dmp = 2,6-Me₂C₆H₃, R''' = Dip = 2,6-iPr₂C₆H₃). Pictures reproduced from Akasaka et. al., *Inorganics* **2018**, 6, 107,^[253] Nied et. al., *J. Am. Chem. Soc.* **2010**, 132, 10264-10265^[257] and Abersfelder et. al. *Angew. Chem. Int. Ed.* **2011**, 50, 7936-7939.^[259] 48

List of Schemes

- Scheme 1:** West's synthesis of the first bicyclo[2.2.2]octasilane **1**, bicyclo[3.3.1]nonasilane **2** and other Si_nMe_m polysilanes ($\bullet = \text{Si}$, $\text{R} = \text{Me}$, $n/m = 6/12$, $10/16$, $10/18$, $11/18$, $13/22$).^[91–93] 14
- Scheme 2:** Syntheses of bicyclo[3.3.1]nonasilane **4**^[94] and bicyclo[2.2.1]heptasilane **5**^[95] exemplary for the synthetic approaches (2): salt elimination reaction (top) and (3) aluminum chloride induced rearrangement (bottom, $\bullet = \text{Si}$, $\text{R} = \text{Me}$, $\text{TMS} = \text{SiMe}_3$). 15
- Scheme 3:** Reduction of tricyclopentasilane **7** to the anionic species **8** and subsequent substitution with TMSCl ($\bullet = \text{Si}$, $\text{SiR}_3 = \text{SiMe}^t\text{Bu}_2$, $\text{TMS} = \text{SiMe}_3$)^[101] 17
- Scheme 4:** Stepwise catenation of bicyclo[1.1.1]pentasilane units to give persilastaffanes **13** and **14** ($\bullet = \text{Si}$, $\text{R} = ^t\text{Bu}$, $\text{TMS} = \text{SiMe}_3$).^[97] 17
- Scheme 5:** Syntheses of the first polyhedral silicon clusters: octasilacubane **15**,^[112] hexasilaprismane **16**^[111] and tetrasilatetrahedron **17**^[109] ($\bullet = \text{Si}$, $\text{R} = \text{SiMe}_2^t\text{Bu}$, $\text{R}' = \text{Dip} = 2,6\text{-}^i\text{Pr}_2\text{C}_6\text{H}_3$, $\text{R}'' = \text{Si}^t\text{Bu}_3$). 18
- Scheme 6:** Generation of tetrasilatetrahedranides **19** and **20** by reductive cleavage of a silyl-substituent from the tetrasilahedranes **17** and **18** ($\bullet = \text{Si}$, **17,19**: $\text{R} = \text{Si}^t\text{Bu}_3$; **18,20**: $\text{R} = \text{SiMe}(\text{CH}(\text{SiMe}_3)_2)_2$).^[110,128] 19
- Scheme 7:** Hypothetical stepwise replacement of the negative charges of the Zintl ion $[\text{Si}_4]^{4-}$ with R^+ substituents to give the anionic and neutral tetrasilahedranes **19,20** and **17,18**, respectively. Conversely, the reductive cleavage of one R -substituent from **17,18** to give anionic **19,20** was successfully demonstrated ($\bullet = \text{Si}$, $\bullet = \text{“naked” Si}$, **17,19**: $\text{R} = \text{Si}^t\text{Bu}_3$; **18,20**: $\text{R} = \text{SiMe}(\text{CH}(\text{SiMe}_3)_2)_2$; remark: R^+ could principally be any electrophile). 26
- Scheme 8:** Synthesis of spiropentasiladiene **26** as side product of cyclotrisilene **27** ($\bullet = \text{Si}$, $\bullet = \text{“naked” Si}$; $\text{R} = ^t\text{BuMe}_2\text{Si}$).^[234] 30
- Scheme 9:** Syntheses of Si_5 siliconoids **30**^[247,249] and **31**^[252] starting from disilenides **28**^[248] and **29** ($\bullet = \text{Si}$, $\bullet = \text{“naked” Si}$; $\text{Cp}^* = \text{pentamethylcyclopentadienyl}$, $\text{A}^- = \text{B}(\text{C}_6\text{F}_5)_4^-$; $^t\text{Bu} = \text{tert-Butyl}$; $\text{TMS} = \text{SiMe}_3$; **30**: $\text{R} = \text{R}' = \text{Tip} = 2,4,6\text{-}^i\text{Pr}_3\text{C}_6\text{H}_2$; **31**: $\text{R-R} = \text{C}((\text{SiMe}_3)_2\text{CH}_2)_2$, $\text{R}' = ^t\text{Bu}$). 33
- Scheme 10:** Thermally induced fragmentation of **31** to give Si_8 siliconoid **32** and silene **33** ($\bullet = \text{Si}$, $\bullet = \text{“naked” Si}$; $\text{R} = \text{SiMe}_3$, $\text{R}' = ^t\text{Bu}$).^[252] 35
- Scheme 11:** Thermal treatment of Si_8 siliconoid **32** results in the rearranged isomers **34** and **35** and the contracted Si_7 siliconoid **36** ($\bullet = \text{Si}$, $\bullet = \text{“naked” Si}$; $\text{R} = \text{SiMe}_3$, $\text{R}' = ^t\text{Bu}$).^[253] 36
- Scheme 12:** Reductive dimerization of pentaiodinated cyclotetrasilane **37** to yield Si_8 siliconoid **38** ($\bullet = \text{Si}$, $\bullet = \text{“naked” Si}$; $\text{R} = \text{Si}(^t\text{Bu})_3$).^[254] 37

- Scheme 13:** Reductive heterocoupling of $\text{Mes}_2\text{SiCl}_2$ and Si_2Cl_6 to yield pentasila[1.1.1]propellane **39** (● = Si, ● = “naked” Si; R = Mes = 2,4,6- $\text{Me}_3\text{C}_6\text{H}_2$).^[257] 37
- Scheme 14:** Reductive dimerization of trichlorinated cyclotrisilane **40** and Cp*-functionalized cyclotrisilene **41** to afford the dismutational isomer of hexasilabenzene **42** and its rearrangement to benzpolarene **43** and Si_{11} siliconoid **44**, respectively (● = Si, ● = “naked” Si; R = Tip = 2,4,6- $\text{iPr}_3\text{C}_6\text{H}_2$).^[51,249,258,259] 38
- Scheme 15:** Synthesis of cyclotetrasilane-fused persilacuneane **45** by reductive tetramerization of tetrachlorinated cyclotetrasilane **46** (● = Si, ● = “naked” Si; R = tBu). 40
- Scheme 16:** Synthesis of cyclopentasilane-fused hexasilabenzvalene **48** by reductive trimerization of tetrachlorinated cyclopentasilane **47** (● = Si, ● = “naked” Si; R = tBu).^[268] 41
- Scheme 17:** Syntheses of mono- and dianionic Si_9 siliconoids **25** and **49** from the Zintl-phase $\text{K}_{12}\text{Si}_{17}$ (● = Si, ● = “naked” Si; 222-crypt = 4,7,13,16,21,24-hexaoxa-1,10-diazabicyclo[8.8.8]hexacosane; R = $\text{SiH}(\text{tBu})_2$).^[207] 42
- Scheme 18:** Synthesis of heteronuclear [1.1.1]propellanes **50a,b** the reduction of a 3:2 mixture of $\text{Mes}_2\text{SiCl}_2$ and ECl_2 with 10 equivalents of lithium naphthalenide solution (● = Si; R = Mes = 2,4,6- $\text{Me}_3\text{C}_6\text{H}_2$; **50a**: E = Ge; **50b**: E = Sn)^[291] 50
- Scheme 19:** Photolysis of the mixed heavy tricyclo[2.1.0.0^{2,5}]pentane precursor **51** to yield the spiro[bispentagerma[1.1.1]propellane **52** (● = Si, $\text{SiR}_3 = \text{SiMe}^t\text{Bu}_2$, $\text{tBu} = \text{tert-Butyl}$).^[293] 51
- Scheme 20:** Syntheses of dismutational (**53a**) and global minimum (**54a,b**) E_2Si_4 heterosiliconoids by treatment of disilene **28** with low-valent dichlorotetraylenes (● = Si, R = Tip = 2,4,6- $\text{iPr}_3\text{C}_6\text{H}_2$, **53**: E = Ge; **54**: E = Sn).^[294] 52
- Scheme 21:** Closed-shell and biradical-type reactivity of the bridgehead bond in pentasila[1.1.1]propellane **39** (● = Si, ● = “naked” Si, R = Mes = 2,4,6- $\text{Me}_3\text{C}_6\text{H}_2$, DHA = 9,10-dihydroanthracene, **55a**: R' = OH, **55b**: R' = OPh, **55c**: R' = SPh, **55d**: R' = SnMe_3).^[257] 54
- Scheme 22:** Reaction of **43** with bromine and iodine to give the corresponding dihalogenated derivatives **57a,b** and its treatment with an excess of iodine to yield the hexaiodinated pentasilane **58** (● = Si, ● = “naked” Si, R = Tip = 2,4,6- $\text{iPr}_3\text{C}_6\text{H}_2$, **57a**: X = Br, **57b**: X = I).^[259] 54
- Scheme 23:** Reaction of **42** with BCl_3 ; estimated yields in crude product are given in brackets (● = Si, ● = “naked” Si, R = Tip = 2,4,6- $\text{iPr}_3\text{C}_6\text{H}_2$).^[51] 55
- Scheme 24:** Reaction of Wiberg’s Si_8 siliconoid **38** with CBr_4 (cleavage of Si_8 framework, preservation of substituents) and I_2 (preservation of Si_8 framework, cleavage of substituents) to give cyclotetrasilane **61** and silyl-substituted bicycloheptasilane **62**, respectively.^[295] 56

- Scheme 25:** Synthesis of anionic siliconoid **63** by the reduction of the dismutational hexasilabenzene isomer **42** or alternatively the direct reduction of the trichlorinated cyclotrisilane precursor **40** (● = Si, ● = “naked” Si, R = Tip = 2,4,6-*i*-Pr₃C₆H₂).^[296] 57
- Scheme 26:** Functionalization of the Si₆ cluster scaffold of **63** with various electrophiles from the Groups 13 to 15^[296] and cluster expansion to the Si₇ siliconoid **65** and the Si₈ siliconoids **67** and **68**^[297] (● = Si, ● = “naked” Si, R = Tip = 2,4,6-*i*-Pr₃C₆H₂, Cp* = 1,2,3,4,5-pentamethylcyclopentadienyl (a) BH₃-SMe₂, (b) ^tBuC(O)Cl, (c) SiCl₄, (d) CIP(NMe₂)₂. **64a**: E = BH₃⁻Li⁺; **64b**: E = C(O)^tBu; **64c**: E = SiCl₃; **64d**: E = P(NMe₂)₂. 58
- Scheme 27:** Synthesis of borate and phosphine substituted Si₆ siliconoids **64a** and **64d** (**64a**: E = BH₃⁻Li⁺, **64d**: E = P(NMe₂)₂, ● = Si, ● = “naked” Si, R = Tip = 2,4,6-*i*-Pr₃C₆H₂). 59
- Scheme 28:** Syntheses of dismutational isomer **42** and global minimum isomer **43** of hexasilabenzene (● = Si, ● = “naked” Si, R = Tip = 2,4,6-*i*-Pr₃C₆H₂). 60
- Scheme 29:** Synthetic routes to *ligato*- and *privo*-functionalized Si₆ benzpolarenes (● = Si, ● = “naked” Si, R = Tip = 2,4,6-*i*-Pr₃C₆H₂). 86
- Scheme 30:** Coordination of the NHC-stabilized three-membered cyclic phosphasilene **70** to iron as a transition-metal center and the Lewis-acid induced NHC-abstraction to yield the saturated Si₄P₂ cluster species **73** and **74** with frameworks reminiscent of the hexasilabenzene isomers **42** and **43** (● = Si, R = Tip = 2,4,6-*i*-Pr₃C₆H₂, NHC = 1,3-diisopropyl-4,5-dimethylimidazol-2-ylidene). 88
- Scheme 31:** Syntheses of monanionic siliconoids *ligato*-**63** and *privo*-**63** and the dianionic Si₅ cluster **75** (● = Si, ● = “naked” Si, R = Tip = 2,4,6-*i*-Pr₃C₆H₂). 89
- Scheme 32:** Syntheses of bis(trimethylsilyl)-substituted Si₅-Cluster **76** and boron- and phosphorus-doped siliconoids **77** and **78** (● = Si, ● = “naked” Si, R = Tip = 2,4,6-*i*-Pr₃C₆H₂ **77**: E = B; **78**: E = P). 90

List of Tables

Table 1: Reported ^{29}Si MAS NMR data for silicon-based binary Zintl phases $A_4\text{Si}_4$, $\text{K}_{12}\text{Si}_{17}$ and ternary Zintl phases $A_7\text{NaSi}_8$, $\text{K}_6\text{Rb}_6\text{Si}_{17}$ (A = alkali metal, δ_{iso} = isotropic chemical shifts). ^[86,159,195–200]	25
Table 2: Reported ^{29}Si NMR data for silicon-based Zintl ions in solution. ^[199–202]	26
Table 3: Comparison of hemispheroidalities Φ and distances between unsubstituted vertices of given siliconoids.	43
Table 4: Comparison of ^{29}Si NMR chemical shifts of given siliconoids.	44

Preface – Silicon Then and Now

Oxygen as indispensable element for life on earth also makes up almost half of the mass of the earth's crust (46.1%).^[1] It might surprise that the second most abundant element turns out to be silicon (rather than the carrier of life itself, carbon) with a mass fraction of around 28.2%,^[1] which only leaves approximately one fourth of the mass for the residual 92 natural elements.

The history of the element silicon goes back to the late 18th century, when Antoine Lavoisier first characterized "*silice*" (silica) as a "salifiable earth", meaning an ore that produces salts upon treatment with acids.^[2,3] Despite presumably having produced the neat metal, he considered it as a compound rather than an element. He concluded that "it is even possible that all substances we call earths may be only metallic oxyds, irreducible by any hitherto known process"^[3] due to their strong affinity to oxygen. In 1808, Sir Humphry Davy proposed the name "silicium", which is derived from the Latin "silex" for flintstone while the ending "-ium" implies a metalloid character.^[4] Conversely, Thomas Thomson argued in 1817 that the "base of silica" shows no metallic character at all but rather resembles the non-metallic elements boron and carbon. Hence, he changed the ending "-ium" to "-on" and coined the present English¹ notation "silicon".^[5] The credit of discovery, however, is usually given to Jöns Jacob Berzelius who was finally able to isolate silicon in its amorphous form and realizing its elemental nature for the first time in 1824.^[6] It took another 30 years until Henri Sainte-Claire Deville reported on the production of silicon in its crystalline state by electrolysis of a mixture of NaCl and AlCl₃, which contained small amounts of SiCl₄.^[7]

Silicon and its compounds show diverse structural, physical and chemical properties and are thus applicable in most areas of today's everyday life: Silicon dioxide and silicates provide the basis for building materials like glass,^[8] ceramics^[9-11] or concrete.^[12,13] Polysiloxanes, polymers with a backbone of alternating silicon and oxygen atoms better known as silicones, are even similarly multifaceted and used, for instance, as lubricants, heat-transfer media, rubbers, paint binders, medicinal implants, seals or insulators.^[14,15] Silicon in its elemental form represents the prototypical semiconductor. Our information technology-centered society would be inconceivable without modern high-performance Si-based devices such as photovoltaic cells, thin-film transistors or microprocessors.^[16-22] In order to meet the resulting high demand,

¹ In contrast, the notation „Silizium/Silicium“ has survived in the German language up to this day.

silicon is industrially produced on a huge scale every year (6.7 million metric tons in 2018 worldwide).^[23] Nowadays, metallurgical grade silicon is almost exclusively produced by the carbothermal or aluminothermal reduction of silicon dioxide. Most high-tech applications require further purification to semiconductor-grade or single crystalline silicon, which is routinely achieved by chemical vapor deposition and the Czochralski or float zone crystal growth processes, respectively.^[17] The indispensability of silicon for the still ongoing “digital revolution”^[24] has prompted the suggestion to refer to the current epoch as the “silicon age”, in reference to the bronze and the iron age of past civilizations.^[25,26]

1. Introduction

1.1. Perspective and Motivation

The word cluster, originating from the old English “clyster”, denotes a bunch or group of something. Synonyms are for example the terms assemblage, collection, array, chunk or batch. The notion of “clusters” is widely used in nearly all sciences: In astronomy, the word cluster is typically used to group families of asteroids, stars or galaxies. The cluster headache is a medicinal term for a neurological disease, while a genetic cluster in biology denotes a group of genes with similar expression. A bunch of computers that are coupled in order to increase the processing power are called a computer cluster. In musicology, a chord comprised of a group of adjacent tones is referred to as a tone cluster.

In chemistry (and physics) arrays of a relatively small number of atoms that are bonded to each other are called clusters and typically regarded as intermediates between molecules and bulk solids on grounds of their size as well as structural and electronic properties. Numerous examples of both transition metal and main group element clusters have been reported. In case of silicon, cage molecules with different composition of the corresponding cluster cores are known: The so-called silsesquioxanes with the general formula $[\text{RSiO}_{1.5}]_x$ are based on silica and exhibit three-dimensional scaffolds of alternating silicon and oxygen atoms, which are substituted by peripheral functionalities R.^[27–31] Since every silicon vertex is connected to three adjacent oxygen atoms the “polyhedral oligomeric silsesquioxanes” (POSS) are regularly referred to as T_x silsesquioxanes with x being the number of silicon atoms in the cluster core. The T_8 silsesquioxane, for instance, exhibits a cubic structure and bears one substituent at every corner of the cube. Spherosilicates are a special case of silsesquioxanes, which feature pending -OR substituents and are thus of the general formula $[\text{ROSiO}_{1.5}]_x$.^[28,31–33] Here, every silicon vertex is bonded to four oxygen atoms, which is why they are designated with the letter Q. The chemistry of heavier silicon chalcogenide cages is much less explored. Still, some examples have been reported including Si_2E_3 bicyclopentanes,^[34,35] double-decker and adamantane-like Si_4E_6 species,^[36,37] Si_4E_3 cages of different shape ($\text{E} = \text{S}, \text{Se}$),^[38,39] polythiadisilabicycles Si_2S_x ($x = 4-6$)^[40] as well as a Si_4Te_6 adamantane.^[39]

Three-dimensional cage molecules with a scaffold that solely consists of silicon atoms can be further subdivided into saturated silicon cages,^[41,42] Zintl ions^[43–50] and siliconoids^[51–53] depending on the inherent connectivity of the atoms, the substitution pattern and their charge. As the name indicates saturated silicon cages feature only saturated, tetracoordinate silicon vertices with at least one stabilizing ligand that is not part of the cluster core itself. In contrast, silicon-based Zintl ions are completely ligand-free or “naked” polyanionic clusters. Finally, the siliconoids as per definition^[51,53] feature at least one unsubstituted silicon vertex with a hemispheroidal coordination environment (all bonds to neighboring cluster atoms pointing into the same half of a sphere) and can be either neutral or negatively charged.

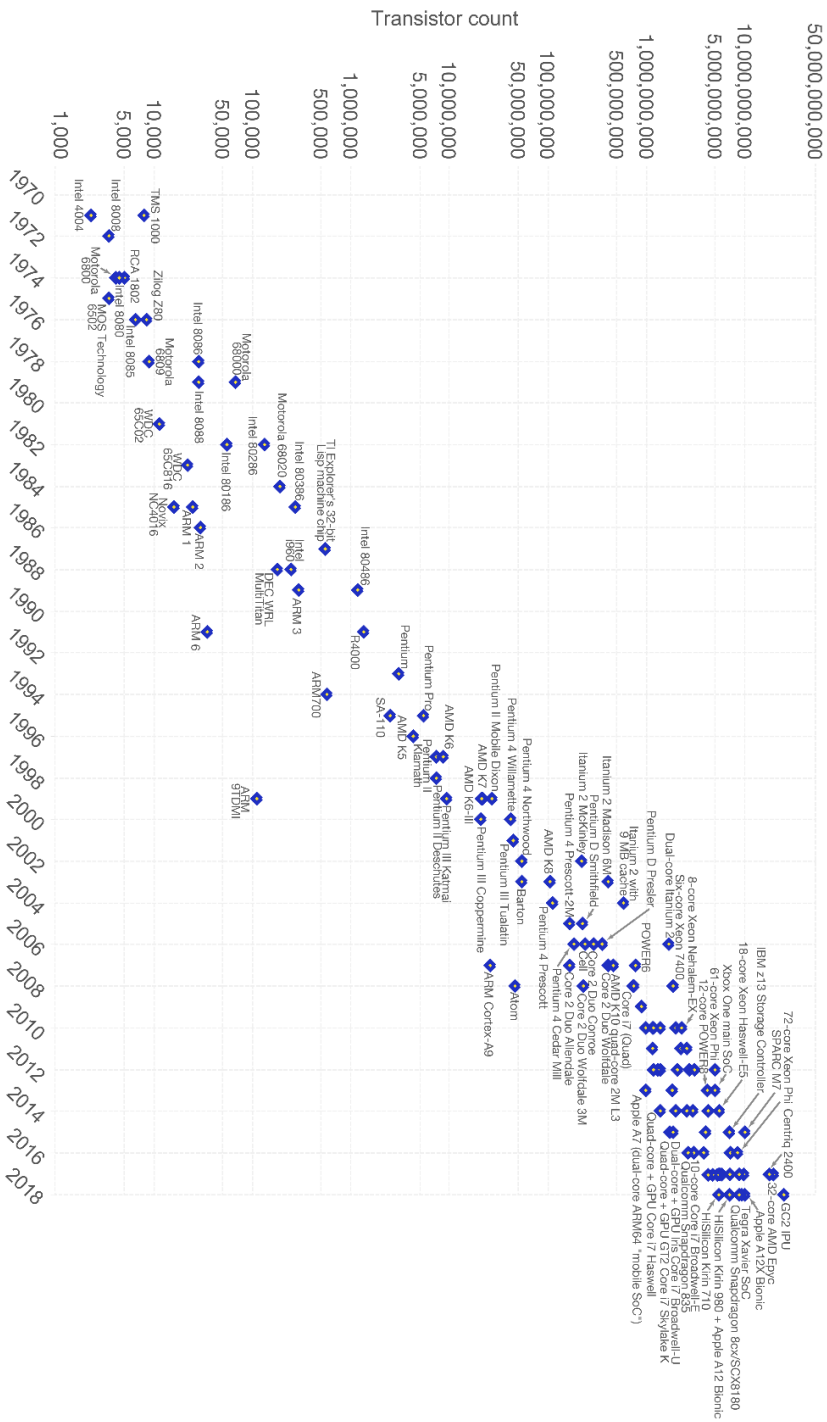
In the following, after a general classification of the scientific relevance of silicon clusters in the context of silicon-based semiconductors, synthetic approaches as well as unique structural and electronic properties of all three sub-categories are reviewed with specific focus on the chemistry of siliconoids.

The inventions of the metal-oxide-semiconductor field-effect transistor (MOSFET) and integrated circuits (IC) in the late 1950's and early 1960's initiated the unprecedented and fascinating rise of silicon as the most important semiconducting material of our time. As early as 1965, Gordon Moore observed the trend that within 6 years after the development of the first transistor, the number of components on a single chip and thus its computing power had roughly doubled every year.^[54] Not seeing any reason why this exponential growth should not continue, at least in the short term, he already predicted that in the future “integrated circuits will lead to such wonders as home computers – or at least terminals connected to a central computer – automatic controls for automobiles, and personal portable communication equipment”^[54] – and how right he was. In 1975, reevaluation of the progress in fabrication of IC's lead to a rule of thumb,^[55] which is nowadays generally known as Moore's law: The number of transistors on a single microprocessor which correlates with the chip's computing power doubles around every two years (Figure 1).^[56–58] As a consequence thereof, the miniaturization of silicon transistors was the main strategy for performance optimization and enhancement of computing power of ICs over the last decades.

1.1. Perspective and Motivation

Moore's Law – The number of transistors on integrated circuit chips (1971-2018)

Moore's law describes the empirical regularity that the number of transistors on integrated circuits doubles approximately every two years. This advancement is important as other aspects of technological progress – such as processing speed or the price of electronic products – are linked to Moore's law.



Data source: Wikipedia (https://en.wikipedia.org/wiki/Transistor_count)
The data visualization is available at [OurWorldInData.org](https://ourworldindata.org). There you find more visualizations and research on this topic.

Licensed under CC-BY-SA by the author Max Roser.

Figure 1: Moore's Law: The number of transistors on integrated circuit chips (1971-2018) (Source: <https://ourworldindata.org/uploads/2019/05/Transistor-Count-over-time-to-2018.png>; Author: Max Roser, License: Creative Commons Attribution-Share Alike 4.0 International (<https://creativecommons.org/licenses/by-sa/4.0/deed.en>)).

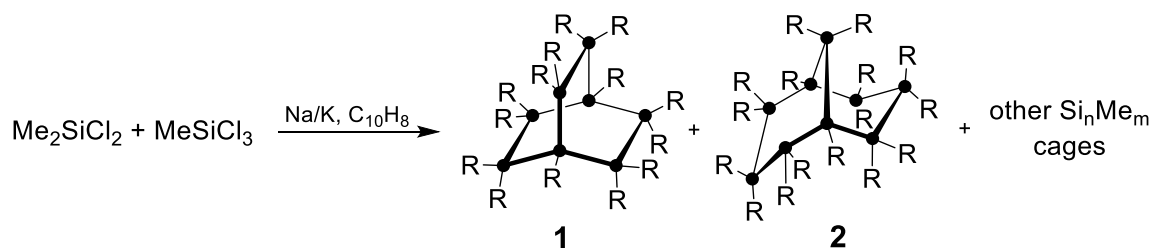
The fabrication of small-sized semiconducting devices is usually achieved by so-called top-down methods like the etching or lithography of bulk silicon. Semiconductor grade amorphous bulk silicon (a-Si) is typically produced by chemical vapor deposition (CVD) of silane precursors (e.g. SiH₄). The optical and electronic properties of the final deposited material are thought to be strongly dependent and thus principally tunable by the incorporation of partially hydrogenated, hence unsaturated silicon clusters of the general formula Si_nH_m ($n > m$, $n = 4$ to ca. 100) that arise as transient intermediates during the gas-phase process.^[59–65] As the experimental evaluation of this premise of an admittedly vague structure-property relationship is far from trivial simply due to the amorphous character of a-Si, numerous computational approaches tried to shed more light on this aspect from a theoretical point of view. Not only surprising structural motifs and stabilities of such unsaturated silicon clusters were computed, but also simulations of deposition dynamics of hydrogenated silicon clusters have been carried out.^[66–75] Remarkably, in particular silicon atoms in surface-near regions of the bulk material show a trend to form cluster-like structures upon a change in their coordination number from four to three or five, respectively.^[76] The chemical reactivity of silicon surfaces is demonstrably determined by unsaturated surface features such as the so-called “buckled dimer” and “dangling bonds” with their free valencies.^[77–79] By definition, these surface atoms must exhibit a hemispheroidal coordination environment. With decreasing size of the components in silicon-based semiconductors the corresponding ratio of surface to volume constantly increases, hence the influence of surface-near incorporated clusters and dangling bonds on the physical and chemical properties becomes progressively more dominant. Therefore, the isolation of stable molecular silicon clusters is of distinctive interest as they serve as analytically accessible model systems for silicon surfaces. In this regard, siliconoids with their “naked”, hemispheroidally coordinated silicon vertices (see Chapter 1.4.1.) mimic the dangling bonds of bulk silicon surfaces and are therefore of particular interest.

Nowadays, the sizes of transistors are typically within the nanoregime, where top-down processes such as etching become more and more technically demanding and expensive. As added complication, transistor sizes are soon expected to hit a limit not only because of excessive heat production on the chips but also due to quantum confinement effects that currently render electronic properties unpredictable and potentially unreliable.^[56–58] A different approach is the targeted bottom-up synthesis of molecular Si-based systems or Si-nanoparticles^[20,80,81] from suitable molecular

precursors resulting in strictly defined structural and (opto-)electronic properties. Although this approach does not remedy the general problem of quantum confinement effects, it might very well help to elucidate structure-property relationships of silicon-based nanomaterials more precisely and thus contribute to a better fundamental understanding of these. A second prospect is the development of more cost-efficient methods for the fabrication of Si-nanodevices. One notable bottom-up approach is the solution-phase preparation of nanoparticles by the reduction of silicon halides with metals.^[82,83] The transient formation of small (poly-)anionic clusters appears to be self-evident during such procedures. The group of Kauzlarich provided firm evidence for this hypothesis and established the direct use of silicon-based Zintl ions (Chapter 1.3.) as a convenient starting material to silicon nanomaterials in a series of papers.^[84–90]

1.2. Saturated Silicon Cages

Saturated polycyclic oligosilanes of the general formula Si_nR_m ($n \leq m$) are usually referred to as silicon cage compounds. Half a century ago in 1970, West reported on the first example of a cage polysilane, namely the bicyclo[2.2.2]octasilane $\text{Si}_8\text{Me}_{14}$ **1**, which was obtained by the reduction of a mixture of Me_2SiCl_2 and MeSiCl_3 with sodium/potassium alloy in the presence of naphthalene (Scheme 1).^[91]

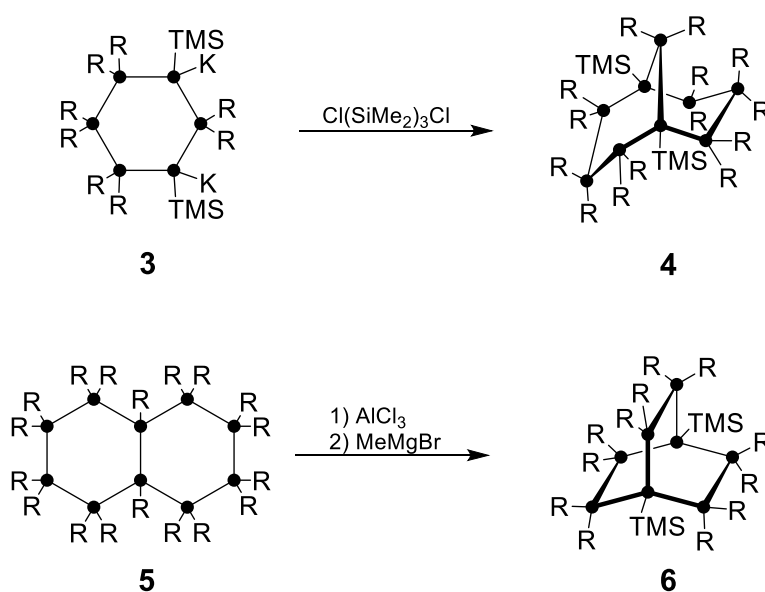


Scheme 1: West's synthesis of the first bicyclo[2.2.2]octasilane **1**, bicyclo[3.3.1]nonasilane **2** and other Si_nMe_m polysilanes ($\bullet = \text{Si}$, $\text{R} = \text{Me}$, $n/m = 6/12, 10/16, 10/18, 11/18, 13/22$).^[91–93]

Only two years later West et al. disclosed an improved synthetic procedure, thus providing access to other polycyclic polysilanes consisting of 6 to 13 silicon atoms.^[92] The molecular structure of the bicyclo[3.3.1]nonasilane $\text{Si}_9\text{Me}_{16}$ **2** was elucidated by an X-Ray diffraction study on single crystals by Stallings in 1976 (Scheme 1).^[93]

1.2. Saturated Silicon Cages

Inspired by West's pioneering work, the groups of Masamune, Ishikawa, Marschner, Iwamoto, Sekiguchi and Scheschkewitz provided further important contributions in the field of saturated silicon cage compounds regarding synthesis and studies on structural and spectroscopic properties. The developed synthetic protocols mainly rely on three different approaches: (1) the Wurtz-type coupling of suitable halogenated precursors with reducing metals as in the case of **1** (Scheme 1); (2) salt elimination reactions between metallated and halogenated (cyclo-)silanes.; (3) aluminum chloride induced rearrangement of (poly)cyclic oligosilanes. Typical examples for the latter two are shown in Scheme 2.



Scheme 2: Syntheses of bicyclo[3.3.1]nonasilane **4**^[94] and bicyclo[2.2.1]heptasilane **5**^[95] exemplary for the synthetic approaches (2): salt elimination reaction (top) and (3) aluminum chloride induced rearrangement (bottom, ● = Si, R = Me, TMS = SiMe₃).

To date, not only examples of alkyl-, aryl-, silyl- and even halide-substituted polysilanes with bicyclic (**A-E**),^[91–100] tricyclic (**F-K**)^[51,101–106] and tetracyclic (**L**)^[102,107,108] cluster scaffolds are known, but also representatives of silicon-based polyhedra such as tetrahedra (**M**),^[109,110] prismanes (**N**),^[51,111] cubanes (**O**)^[112–115] and a twenty-atomic silafullerane (**P**)^[116] (Chart 1).

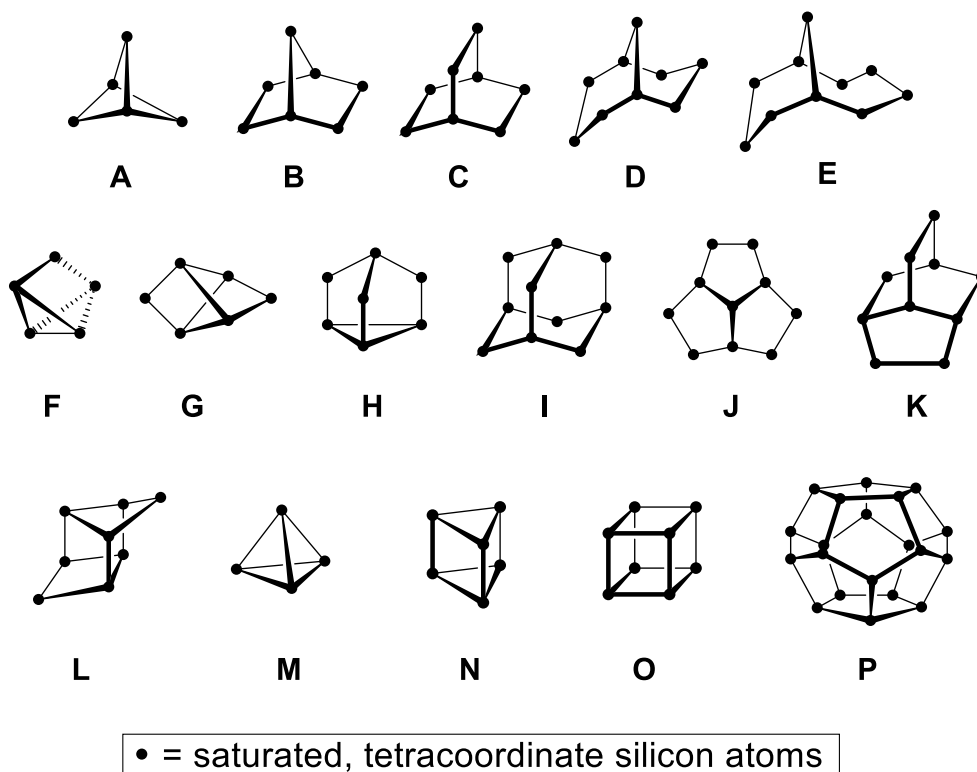
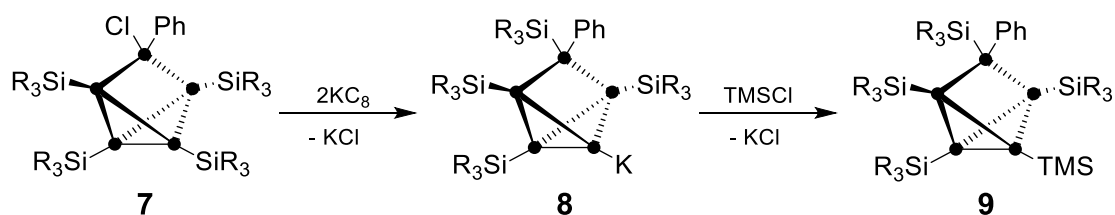


Figure 2: Schematic representation of the cluster scaffolds of reported saturated polycyclic polysilanes.

While these compounds are very interesting from a fundamental point of view alone, permethylated polysilanes have been applied as thermal precursors for the fabrication of silicon carbide fibers.^[117,118] The electronic structure of oligo- and polysilanes is usually determined by σ -conjugation between Si-Si single bonds, which has been extensively discussed in the literature, especially in the case of the corresponding linear and ladder congeners.^[41,100,117–121] The resulting optical and photochemical properties (the σ - σ^* transitions of oligo- and polysilanes result in UV/vis-absorptions at $\lambda = 250\text{--}400\text{ nm}$) suggest possible applications in microlithography, electroluminescent diodes or as photoinitiators.^[118,119,122,123] In the case of cage oligosilanes, studies on their utilization in materials science has not yet been reported although initial efforts regarding their functionalization might pave the way to more applicable extended systems or the embedding of the corresponding clusters in materials: The chloro-functionalized pentasilatricyclo[2.1.0.0^{2,5}]pentane **7**, for instance, can be reduced to the corresponding anionic cage **8**.^[101] A subsequent proof-of-principle substitution reaction with Me_3SiCl demonstrated the potential of **8** to act as nucleophilic transfer reagent of the tricyclic silicon scaffold (Scheme 3).^[101]

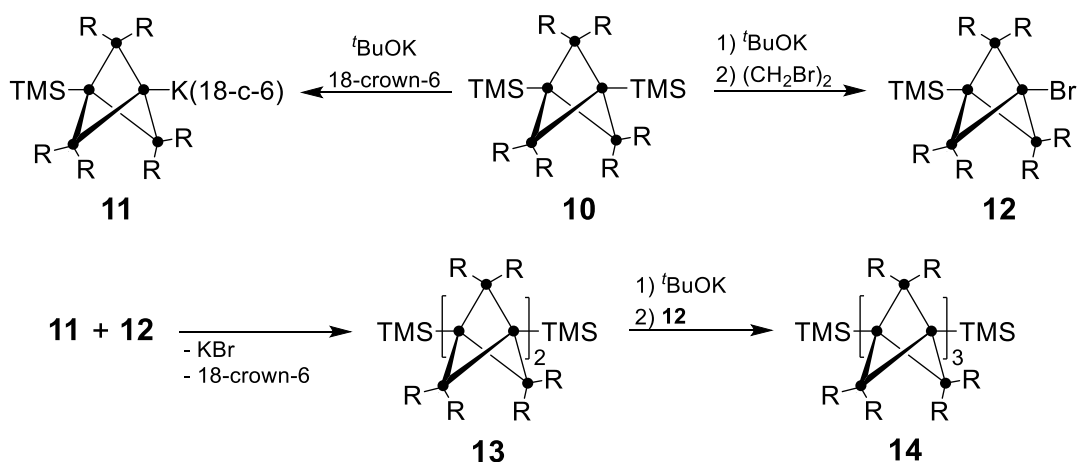
1.2. Saturated Silicon Cages



Scheme 3: Reduction of tricyclopentasilane **7** to the anionic species **8** and subsequent substitution with TMSCl ($\bullet = \text{Si}$, $\text{SiR}_3 = \text{SiMe}^t\text{Bu}_2$, $\text{TMS} = \text{SiMe}_3$)^[101]

In addition to **7**, other cages of the types **G** and **J** were directly obtained as the halide-functionalized derivatives. In addition, post-functionalization of type **C** octasilanes provides a reliable access to a variety of bridgehead-functionalized derivatives.^[98–100,124] Interestingly, a phenyl-substituted bicyclo[2.2.2]octasilane exhibits intramolecular charge-transfer fluorescence, which hints at the potential of silicon clusters to possibly compete with their linear congeners in terms of photochemical properties.^[125]

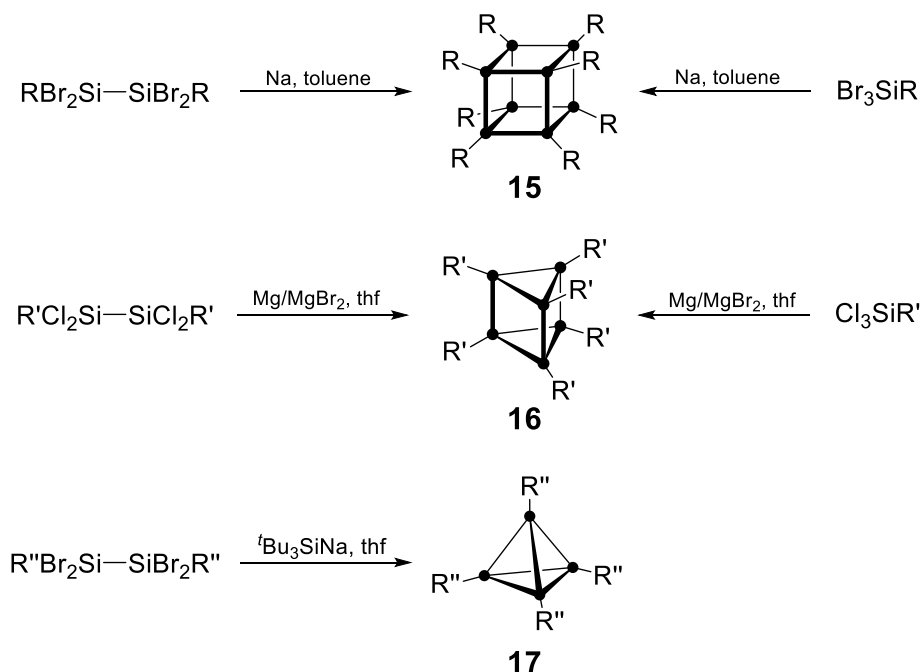
As a first example of an extended chain of silicon clusters, the group of Iwamoto reported the successful stepwise synthesis of persilastaffanes with one, two and three catenated bicyclo[1.1.1]pentasilane units, respectively (Scheme 4).



Scheme 4: Stepwise catenation of bicyclo[1.1.1]pentasilane units to give persilastaffanes **13** and **14** ($\bullet = \text{Si}$, $\text{R} = ^t\text{Bu}$, $\text{TMS} = \text{SiMe}_3$).^[97]

Particularly appealing from an aesthetic point of view are silicon cage compounds with polyhedral structure. In 1988, H. Matsumoto described the reduction of either 2,2,3,3-tetrabromotetrasilane or 1,1,1-tribromodisilane with sodium in toluene to give

the very first octasilacubane cage compound **15**.^[112] Only five years later, the Sakurai/Sekiguchi and Wiberg groups obtained the even smaller hexasilaprismane **16**^[111] and tetrasilatetrahedrane **17**,^[109] respectively (Scheme 5). Notably, the precursors employed for the preparation of **15-17** bear a close resemblance to one another, yet their reduction results in three different polyhedral cluster structures. Apparently, the shape and size of the reduction products strongly depend on the choice of stabilizing ligands, leaving groups, reducing agents and the solvent, which also holds true for the generation of saturated cage compounds of types **A-J** (Figure 2). In fact, this observation is a manifestation of the general rule that larger substituents enforce larger exohedral and therefore smaller endohedral bonding angles.



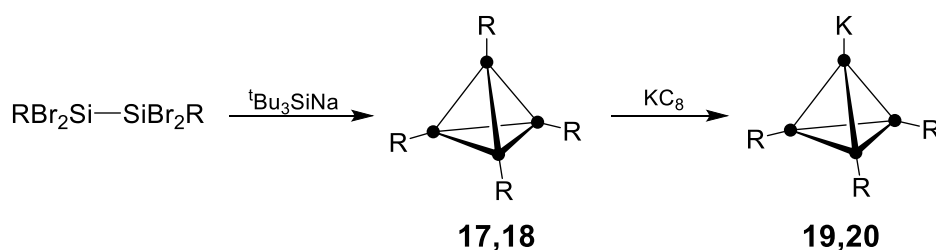
Scheme 5: Syntheses of the first polyhedral silicon clusters: octasilacubane **15**,^[112] hexasilaprismane **16**^[111] and tetrasilatetrahedron **17**^[109] (● = Si, R = SiMe₂^tBu, R' = Dip = 2,6-ⁱPr₂C₆H₃, R'' = Si^tBu₃).

Later, the group of Lerner developed a convenient one-pot-synthesis for the generation of Wiberg's tetrasilatetrahedrane **17**^[126] and a second example of a Si₆R₆ hexasilaprismane was reported by the Scheschkewitz group.^[51] Further representatives of Si₈R₈ octasilacubanes with varying ligands have been isolated and characterized by the groups of H. Matsumoto,^[113] Sekiguchi^[114] and N. Matsumoto.^[115] The group of Unno demonstrated that octasilacubanes can be halogenated upon ring-opening to give functionalized tetracyclic cages of type **J** (Figure 2).^[107,108] Subsequent

1.2. Saturated Silicon Cages

reduction results in the recovery of the intact octasilacubane system.^[124] Similar reactivity was reported for the tetrasilahedrane **17**, which can be oxidatively opened with iodine to the corresponding unsaturated cyclotetrasilene.^[127]

To date, only two examples of functionalized silicon clusters with uncompromised polyhedral scaffold were reported by the groups of Sekiguchi and Klapötke: The reductive cleavage of a silyl-substituent from tetrasilatetrahedranes **17** and **18** gives access to the corresponding anionic species **19** and **20** (Scheme 6).^[110,128] Reactivity studies of **19** and **20**, however, cast doubts on their capability of the nucleophilic transfer of the unperturbed tetrahedral Si₄ cluster core, which is apparently rather prone to σ -bond cleavage.^[128,129]



Scheme 6: Generation of tetrasilatetrahedranides **19** and **20** by reductive cleavage of a silyl-substituent from the tetrasilahedranes **17** and **18** (● = Si, **17,19**: R = Si^tBu₃; **18,20**: R = SiMe(CH(SiMe₃)₂).^[110,128]

1.3. Zintl Ions of Silicon

1.3.1. Historical Background

Ligand-free, polyanionic clusters of p-block elements are known as Zintl ions. Their chemistry finds its beginning around 130 years ago in 1891, when Joannis reported on the generation of deep green solutions on mixing of the pure elements sodium and lead in liquid ammonia.^[130] Shortly thereafter, in the early 20th century, especially the work of Kraus, Smyth and Peck contributed to the assumption that solutions of alkali metals and main-group elements contain highly reduced species of the more electronegative p-block element.^[131–134] It was Eduard Zintl who finally shed more light on this hypothesis in 1931. In comprehensive studies, Zintl and co-workers reacted solutions of sodium in liquid ammonia with soluble salts of a huge variety of main group elements.^[135] They observed that elements of the Groups 1 to 3 regularly form insoluble intermetallic phases or alloys. In contrast, the electronegativity difference between the alkali metal and the main group element of the Groups 4 to 7 exceeds a certain value so that they rather form soluble “salt-like” compounds with discrete anions. With the help of potentiometric titrations, they determined the composition of these salts. The deep green solution formed from sodium and lead in liquid ammonia (first described by Joannis around 40 years earlier) was found to mainly contain Na_4Pb_9 .^[135] Further corroboration was obtained from the dissolution of preformed solid alloys of sodium and lead in liquid ammonia, which results in the same solutions of Na_4Pb_9 .^[136] According to Zintl, the idealized complete electron transfer from the electropositive alkali metal to the electronegative p-block element must result in the formation of polyanionic species containing more than one atom. At this point, however, Zintl believed that the corresponding lead polyanion were a complex of a central Pb^{4-} anion coordinated by eight additional neutral lead atoms. In the meantime, several reports on structure elucidations of nine-atomic polyanionic clusters of the tetrel elements have been published demonstrating the polyhedral nature of the species (see following chapters). In an obituary notice on Eduard Zintl in 1941, Fritz Laves proposed to refer to the above-mentioned border between the Groups 1-3 and the Groups 4-7 in the periodic table as the “Zintl border” in honor of Zintl's pioneering work. In analogy, the salt-like phases of alkali metals with elements right from the “Zintl border” are called “Zintl phases”.^[137] Several review articles have already highlighted the manifold aspects of Zintl ion chemistry in past decades.^[43–50] The following

chapters will mainly focus on the chemistry of silicon-based Zintl ions with some references to their heavier congeners of Group 14.

1.3.2. Solid-State Zintl Phases of Group 14

Solid Zintl phases of the tetrel elements can be easily synthesized by simple melting of the elements in the appropriate molar ratio. For a long time, only the composition of the resulting salt-like solids was known. In 1953, Shoemaker was finally able to identify the structure of the alleged polyanionic species in the alloy NaPb as an $[\text{Pb}_4]^{4-}$ tetrahedron with the help of an X-ray diffraction study.^[138] Somewhat surprisingly, the detection of the larger nine-atomic $[\text{E}_9]^{4-}$ cluster (E = Group 14 element) in solid-state took another 44 years until Sevov accomplished the structure determination of the Zintl phase Cs_4Ge_9 in 1997.^[139] Up to date, the $[\text{E}_4]^{4-}$ and $[\text{E}_9]^{4-}$ are the most frequently occurring Zintl clusters and typically present in solid binary phases of the general formula A_4E_4 ^[140–146] and A_4E_9 ,^[139,147–151] respectively, while both can also be found coexistent in $\text{A}_{12}\text{E}_{17}$ ^[152–155] phases in a 2:1 ratio (A = alkali metal, E = Group 14 element). Besides that, ternary Zintl phases $\text{A}_7\text{A}'\text{E}_8$ ^[156–159] and $\text{K}_6\text{Rb}_6\text{Si}_{17}$ ^[160] with two different alkali metals incorporated are known. Notably, in the case of silicon the nine-atomic Zintl ions $[\text{Si}_9]^{4-}$ are only found in $\text{A}_{12}\text{Si}_{17}$ phases, while phases of the type A_4Si_9 remain elusive.

Despite the omnipresence of the $[\text{E}_4]^{4-}$ and $[\text{E}_9]^{4-}$ cluster species in solid Zintl phases of the tetrel elements, there are also few reports on phases containing polyanions of different charge and shape: In case of tin, the eight-atomic $[\text{Sn}_8]^{6-}$ cluster with a square-antiprismatic shape was reported by Sevov.^[161] Butterfly-shaped $[\text{E}_4]^{6-}$ anions are present in Ba_3E_4 phases (E = Si, Ge).^[162,163] Furthermore, Zintl phases containing “Y-shaped” $[\text{Si}_4]^{12-}$ stars,^[164,165] five-membered $[\text{E}_5]^{6-}$ rings (E = Si-Pb)^[164–169] or even six-membered $[\text{E}_6]^{10-}$ rings (E = Si, Ge)^[170,171] are known.

1.3.3. Group 14 Zintl Ions in Solution

While solid Zintl phases are insoluble in common organic solvents due to their strong polarity due to effective charge separation, they can be dissolved in liquid ammonia at

low temperatures. Phases of the types A_4E_9 and $A_{12}E_{17}$ show better solubility than the corresponding A_4E_4 phases owing to their lower charge per atom. In the early 1970's, Kummer and Diehl employed ethylenediamine (en) as alternative solvent and were able to isolate and structurally characterize the compound $Na_4Sn_9 \cdot 7en$, which for the first time provided proof for the retention of the discrete polyanions of Zintl phases upon dissolution.^[172–174] Higher quality crystalline material from solutions containing $[E_9]^{4-}$ Zintl ions was later obtained by changing the solvent^[175] and especially by employing cation sequestering agents such as cryptands^[176,177] or crown-ethers.^[178] It took almost another 40 years until Korber demonstrated that also the smaller $[E_4]^{4-}$ species ($E = Sn, Pb$) can be preserved in solution.^[179] In case of the heavier atoms tin and lead, solutions of their Zintl ions can be prepared directly by dissolving the pure elements in liquid ammonia at low temperatures. The corresponding germanium and silicon analogues are only available by the dissolution of the appropriate Zintl phases synthesized at high temperature that contain the precast cluster polyanions.

For a long time, the silicon-based Zintl anions $[Si_4]^{4-}$ and $[Si_9]^{4-}$ remained elusive in solution. As A_4Si_4 phases are virtually insoluble in liquid ammonia or comparable solvents and A_4Si_9 phases do not exist, attempts to isolate the silicides from solution relied on the extraction of $A_{12}Si_{17}$ phases containing both $[Si_4]^{4-}$ and $[Si_9]^{4-}$ in a 2:1 ratio with liquid ammonia. First evidence for the presence of $[Si_4]^{4-}$ and $[Si_9]^{4-}$ in these solutions was provided by the isolation of corresponding transition-metal complexes (see Chapter 1.3.5.) and NMR-spectroscopical data (see Chapter 1.3.4.). The highly reduced tetrahedral $[Si_4]^{4-}$ cluster exhibits a large ratio of charge per atom of -1 , and is thus very prone to oxidation reactions, which is generally considered the main reason for the difficulties in the isolation of this species. In the larger $[Si_9]^{4-}$ Zintl ion, every cluster vertex bears an average charge of only -0.44 . $[Si_9]^{4-}$ should therefore be viable in solution. In comparison to its heavier congeners $[E_9]^{4-}$ ($E = Ge, Sn, Pb$), however, the four negative charges are distributed over a smaller volume due to the smaller atomic radius of the silicon atoms suggesting higher reactivity and thus lower stability in solution. Indeed, while reports on the first solvate crystal structures of $[E_9]^{4-}$ date back to the 1970s ($E = Ge$ ^[180], Sn ^[172]) and 1990s ($E = Pb$ ^[181]), respectively, the isolation and structural characterization of the corresponding tetraanionic nonasilicide remained elusive until Korber's reports on the ammoniates $Rb_4Si_9 \cdot (NH_3)_x$ ($x = 4.75$ and $x = 5$) in 2009 and 2010.^[160,182] Very recently, the groups of Fässler and Korber also structurally characterized $K_8[Si_9][Si_4] \cdot (NH_3)_{14.6}$ and $Rb_{1.2}K_{2.8}Si_4 \cdot (NH_3)_7$ providing further

direct evidence that also the smaller, highly charged $[\text{Si}_4]^{4-}$ cluster is retained in solution.^[183,184]

Prior to these pioneering works, the dissolution of $\text{A}_{12}\text{Si}_{17}$ phases resulted in the loss of one electron and thus the isolation of the oxidized $[\text{Si}_9]^{3-}$ cluster anion.^[185] With mild oxidants such as Ph_3GeCl , Me_3SnCl or $t\text{BuCl}$ the targeted generation of the corresponding dianionic species $[\text{Si}_9]^{2-}$ is possible.^[186] Furthermore, two examples of the isolation of a $[\text{Si}_5]^{2-}$ species were reported, the formation mechanism of which remains obscure.^[182,185] The structures of all known silicon-based polyhedral Zintl ions are depicted in Figure 3.

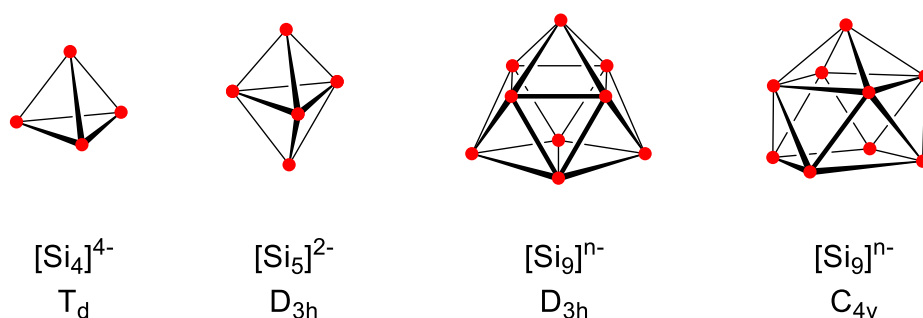


Figure 3: Structures of silicon-based polyhedral Zintl ions (\bullet = “naked” Si) detected in solid-state ($[\text{Si}_4]^{4-}$ and $[\text{Si}_9]^{4-}$) and solution ($[\text{Si}_4]^{4-}$, $[\text{Si}_5]^{2-}$ and $[\text{Si}_9]^{n-}$ with $n = 2-4$).

According to the so-called Zintl-Klemm concept,^[46,48,50,187-189] the valence electrons of the electropositive alkali metal in Zintl phases are completely transferred to the more electronegative p-block element. In line with the (8-N) rule, the subtraction of the average concentration of valence electrons from 8 gives the average number of bonds per main-group atom. This allows for an electron-precise description of the resulting structure, which often resembles known allotropes of the corresponding isoelectronic element. As an example, in the case of $[\text{Si}_4]^{4-}$ every silicon atom formally exhibits five valence electrons and thus forms three bonds to adjacent silicon atoms. The tetrahedral structure of the tetraanionic Si_4 cluster is indeed reminiscent of the well-known P_4 tetrahedron. Alternatively, the cluster shapes of silicon-based Zintl ions can be rationalized by the Wade-Mingos Rules, which have been developed to describe bonding situations in borane and carborane cluster species by Kenneth Wade and expanded towards other main group and transition metal species by Mike Mingos.^[190-193] In this approach, every silicon atom provides two electrons for cluster bonding and thus for both the $[\text{Si}_4]^{4-}$ and the $[\text{Si}_5]^{2-}$ species 12 skeletal electrons are available. While

$[\text{Si}_5]^{2-}$ forms a *closo* ($2n+2$) trigonal-bipyramidal framework, the *nido* ($2n+4$) cluster of $[\text{Si}_4]^{4-}$ is derived by removal of one apical vertex, which results in a (pseudo-) tetrahedral appearance (Figure 3). Depending on the charge, the nine-atomic Zintl ions of silicon adopt either a *closo* tricapped trigonal antiprism with D_{3h} symmetry ($[\text{Si}_9]^{2-}$, $2n+2 = 20$ electrons, Figure 3) or a *nido* monocapped square antiprism with C_{4v} symmetry ($[\text{Si}_9]^{4-}$, $2n+4 = 22$ electrons, Figure 3). Accordingly, the trianionic $[\text{Si}_9]^{3-}$ Zintl cluster possesses 21 skeletal electrons and its structure should be somewhere in between the former two, which was experimentally confirmed by Sevov et al. in 2004.^[185]

Unsurprisingly, the structurally characterized silicon-based Zintl clusters known to date regularly show slight to pronounced distortions from the perfect D_{3h} and C_{4v} symmetries, which can be regarded as a manifestation of the low energy barrier between the two conformations.^[46,48]

1.3.4. NMR spectroscopy

In the context of the synthesis of silicon nanoparticles from the Zintl phase Na_4Si_4 , the group of Kauzlarich reported the corresponding ^{29}Si MAS NMR signal of the $[\text{Si}_4]^{4-}$ tetrahedron in solid-state for the first time in 2001.^[86] The high-field shift of the two resonances detected for the two independent crystallographic sites at $\delta = -365.5$ ppm and $\delta = -361.2$ ppm was explained by the donation of electrons from the electropositive sodium atoms to the electronegative silicon atoms, which is in line with the Zintl-Klemm concept described in the previous chapter. This explanation was adopted in several other reports on MAS NMR studies on solid-state Zintl phases and is nowadays widely accepted. The rationalization of the similarly high-field shifted ^{31}P NMR resonance of the isoelectronic P_4 tetrahedron by magnetically induced cluster currents,^[194] however, casts doubt on the regularly cited explanation in the case of $[\text{Si}_4]^{4-}$ and surely demands future in-depth theoretical investigations in this regard. All reported ^{29}Si MAS NMR chemical shifts for silicon-based Zintl phases are summarized in Table 1.^[86,159,195–200] The decreasing shielding of the silicides with increasing atomic number of the counter cation was tentatively attributed to the less efficient transfer of electrons from the alkali metal to silicon despite the increasing electronegativity difference.

1.3. Zintl Ions of Silicon

Table 1: Reported ^{29}Si MAS NMR data for silicon-based binary Zintl phases A_4Si_4 , $\text{K}_{12}\text{Si}_{17}$ and ternary Zintl phases A_7NaSi_8 , $\text{K}_6\text{Rb}_6\text{Si}_{17}$ (A = alkali metal, δ_{iso} = isotropic chemical shifts).^[86,159,195–200]

Zintl phase	A	$\delta_{\text{iso}}^{29}\text{Si}$ [ppm]
A_4Si_4	Na	-365.5 / -361.2
	Na	-364 (broad)
	Na	-365.5 / -361.2
	K	-346.2 / -322.6
	Rb	-304.3 / -292.0
	Cs	-188.8
$\text{A}_{12}\text{Si}_{17}$	K	$[\text{Si}_4]^{4-}$: -326 / -317 / -316
		$[\text{Si}_9]^{4-}$: -344 / -331 / -322 / -320
A_7NaSi_8	K	-369.7 / -357.2
	Rb	-344.0 / -324.3
	Cs	-279.4 / -234.6
$\text{A}_6\text{A}'_6\text{Si}_{17}$	K/Rb	-311 (broad)

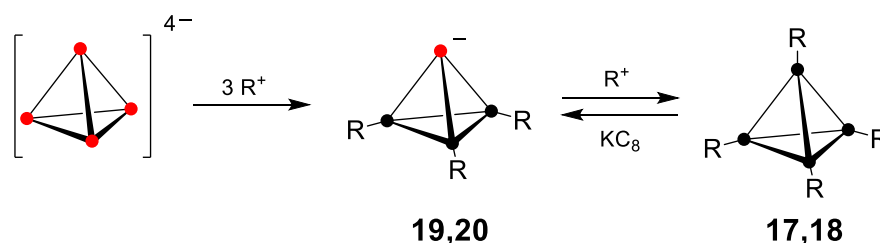
In 2013, the groups of Korber and Gschwind characterized the bare silicide $[\text{Si}_4]^{4-}$ in solution.^[200] The ^{29}Si NMR resonance at $\delta = -323.0$ ppm was detected using a ^{29}Si isotopically enriched sample of the Zintl phase $\text{K}_6\text{Rb}_6\text{Si}_{17}$. The moderate upfield shift of 12 ppm compared to the corresponding ^{29}Si MAS NMR spectrum of the solid starting material was rationalized by dissociation of the ions and thus enhanced charge separation in solution. This assumption was corroborated by comparison with the situation in case of the analogous tetrastannide $[\text{Sn}_4]^{4-}$, which gives rise to an upfield shifted signal ($\Delta\delta = -98$ ppm) in the ^{119}Sn NMR spectrum in the presence of [2.2.2]cryptand as cation sequestering agent in a similar manner.^[200] In the last two years, the groups of Korber, Gschwind and Fässler extended the list of soluble Zintl ions detected by ^{29}Si NMR spectroscopy with $[\text{Si}_5]^{2-}$ and $[\text{Si}_9]^{2-}$ as well as the protonated species $[\mu\text{-HSi}_4]^{3-}$, $[\text{HSi}_9]^{3-}$ and $[\text{H}_2\text{Si}_9]^{2-}$ ^[199,201,202] (Table 2). Almost without exception, all species show the typical high-field shifted resonances close to those observed for the corresponding solid Zintl phases (Table 1 and Table 2). Only the apical vertices in the dianionic Si_5 species give rise to an extremely low-field shifted resonance at $\delta = +348.7$ ppm.^[202] Unfortunately, this unusual offset of the ^{29}Si NMR signals of two adjacent vertices in the same cluster core was not explained in more detail. While in the nine-atomic species, protonation takes place at a distinct vertex, the smaller four-atomic congener was found to be protonated at one edge of the tetrahedral scaffold under formation of a 3c-2e SiHSi bond.^[202]

Table 2: Reported ^{29}Si NMR data for silicon-based Zintl ions in solution.^[199–202]

Dissolved Zintl phase	Detected Zintl ion	Solvent	$\delta^{29}\text{Si}$ [ppm]
$\text{K}_6\text{Rb}_6\text{Si}_{17}$	$[\text{Si}_4]^{4-}$	NH_3	-323.0
$\text{K}_6\text{Rb}_6\text{Si}_{17}$	$[\mu\text{-HSi}_4]^{3-}$	NH_3	-404.5 / -327.8
$\text{K}_6\text{Rb}_6\text{Si}_{17}$	$[\text{Si}_5]^{2-}$	NH_3	-347.8 / +348.7
$\text{K}_{12}\text{Si}_{17}$	$[\text{Si}_9]^{2-}$	py- d_5 / thf- d_8 (1:1)	-309.4
$\text{K}_6\text{Rb}_6\text{Si}_{17}$	$[\text{HSi}_9]^{3-}$	NH_3	-358.5 / -158.5
$\text{K}_{12}\text{Si}_{17}$	$[\text{H}_2\text{Si}_9]^{2-}$	py- d_5 / thf- d_8 (1:1)	-346.1

1.3.5. Functionalization

In principal, the multiple negative charges of Zintl anions could be expected to exhibit a certain nucleophilicity and thus be suitable starting materials to access partially substituted derivatives with reduced charge by treatment with appropriate electrophiles. The formal stepwise addition of n R^+ substituents to the smallest silicon-based Zintl cluster $[\text{Si}_4]^{4-}$ would result in the corresponding ligand-stabilized anionic cage compounds $\text{Si}_4\text{R}_n^{(4-n)-}$ ($n = 1-3$) or even the neutral tetrahedrane ($n = 4$). This hypothetical reaction would thus establish a link between the Zintl anion $[\text{Si}_4]^{4-}$ and Wiberg's iconic tetrasilatetrahedrane **17**^[109] as well as the corresponding monoanionic Si_4R_3^- species **19**^[128] (Scheme 7) and thus conceptually connect the fields of Zintl ion chemistry (Chapter 1.3.) and saturated silicon cage compounds (Chapter 1.2.).



Scheme 7: Hypothetical stepwise replacement of the negative charges of the Zintl ion $[\text{Si}_4]^{4-}$ with R^+ substituents to give the anionic and neutral tetrasilatetrahedranes **19,20** and **17,18**, respectively. Conversely, the reductive cleavage of one R -substituent from **17,18** to give anionic **19,20** was successfully demonstrated ($\bullet = \text{Si}$, $\color{red}\bullet =$ "naked" Si , **17,19**: $\text{R} = \text{Si}^t\text{Bu}_3$; **18,20**: $\text{R} = \text{SiMe}(\text{CH}(\text{SiMe}_3)_2)_2$; remark: R^+ could principally be any electrophile).

This intriguing concept has not been realized experimentally in the case of silicon-based Zintl anions until recently. The associated difficulties are generally attributed to the high negative charge of Zintl anions leading to the insolubility in common organic solvents and an exceptionally high reduction potential. A first step in the opposite direction has been taken by the groups of Sekiguchi and Klapötke, who were able to reductively cleave one R-substituent from neutral tetrasilatetrahedranes **17** and **18** to give the corresponding monoanionic clusters **19** and **20**.^[110,128] Even though the strongly reduced charge in **19** and **20** as compared to the tetraanionic bare silicide $[\text{Si}_4]^{4-}$ should alleviate the mentioned difficulties, even in these cases a successful electrophilic substitution upon retainment of the unperturbed silicon tetrahedron is still eagerly awaited. The only example of a rational chemical transformation of the smallest silicon-based Zintl ion $[\text{Si}_4]^{4-}$ is the reaction of a solution of $\text{K}_6\text{Rb}_6\text{Si}_{17}$ in liquid ammonia with mesityl copper, which results in the formation of the corresponding complex $[(\text{MesCu})_2\text{Si}_4]^{4-}$ **21**^[203] (Figure 4). The central Si_4 tetrahedron in **21** is capped by two η^3 -coordinated CuMes fragments and thus retains its tetraanionic charge. The isolation of **21** provided initial evidence for the persistence of the highly charged $[\text{Si}_4]^{4-}$ in solution prior to the first reports on crystal structures of solvates of $[\text{Si}_4]^{4-}$ by Korber^[184] and Fässler^[183].

The lower charge per atom and the apparently somewhat higher stability in solution (see Chapter 1.3.3.) of the bigger $[\text{Si}_9]^{4-}$ species suggest an improved control of its reaction behavior. Indeed, more examples of transition-metal complexes have been reported in comparison to $[\text{Si}_4]^{4-}$. Treatment of solutions of $\text{K}_{12}\text{Si}_{17}$ with ZnPh_2 and $\text{NHC}^{\text{Dip}}\text{CuCl}$ resulted in the formation of the corresponding η^4 -coordinated transition-metal complexes $[\text{Si}_9\text{Zn-Ph}]^{3-}$ **22**^[204] and $[\text{Si}_9\text{Cu-NHC}^{\text{Dip}}]^{3-}$ **23**,^[205] respectively (Figure 4). A comparable reaction of $\text{K}_6\text{Rb}_6\text{Si}_{17}$ with $[\text{Ni}(\text{CO})_2(\text{PPh}_3)_2]$ in liquid ammonia yields the binuclear complex $[\text{Si}_9\text{Ni}(\text{CO})_2]_2^{8-}$ **24**.^[206] Here, the nickel centers bridge two $[\text{Si}_9]^{4-}$ moieties over a central Si_4Ni_2 six-membered ring (Figure 4). Recently, the group of Fässler finally reported on the first example of a successful threefold silylation of the $[\text{Si}_9]^{4-}$ motif to give the anionic $[\text{Si}_9(\text{SiH}(\text{tBu})_2)_3]^-$ cluster **25**^[207] (Figure 4, see also Chapter 1.4.2.), which might pave the way for more extensive investigations regarding the functionalization of silicon-based Zintl ions in the future.

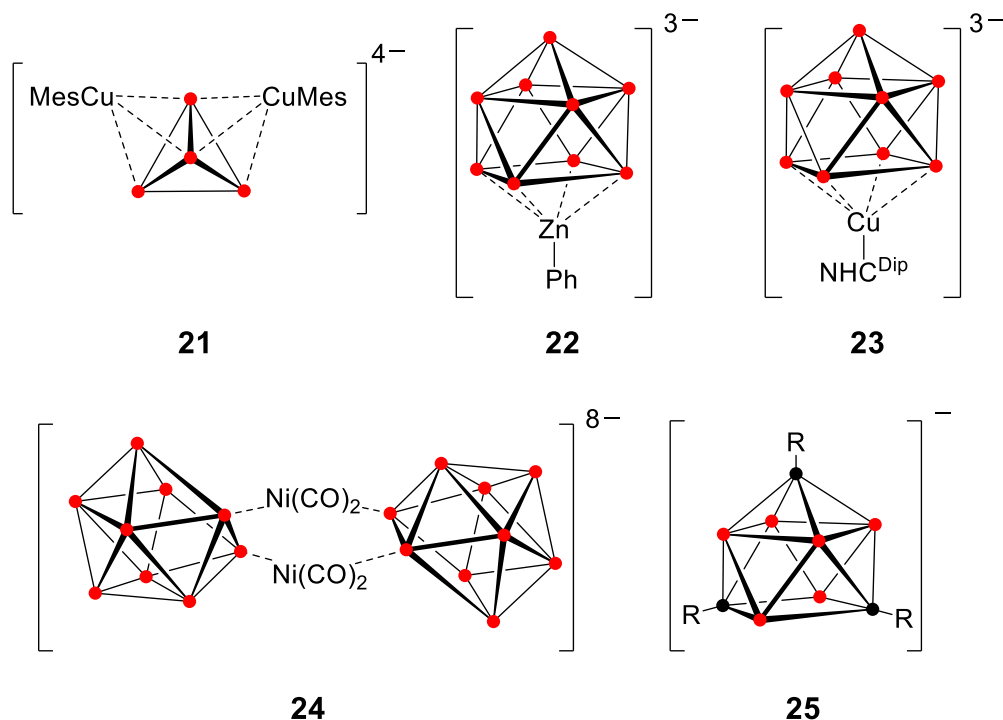


Figure 4: Reported transition-metal complexes of silicon-based Zintl ions (**21-24**) and the threefold silylated Si₉R₃⁻ siliconoid **25** (● = Si, ● = “naked” Si; 222-crypt = 4,7,13,16,21,24-hexaoxa-1,10-diaza-bicyclo[8.8.8]hexacosane; R = SiH(^tBu)₂).^[203–207]

The reactivity of heavier Group 14 Zintl anions (in particular those of germanium) is much more widely explored and has been subject to various review articles.^[45–49] Besides the herein described oxidative coupling reactions, the generation of transition-metal complexes and the synthesis of endohedrally filled Zintl clusters, especially the targeted silylation,^[208–212] arylation/alkenylation^[213–216] and catenation^[217–226] of germanium-based Zintl ions have moved into focus in recent years.

1.4. Siliconoids

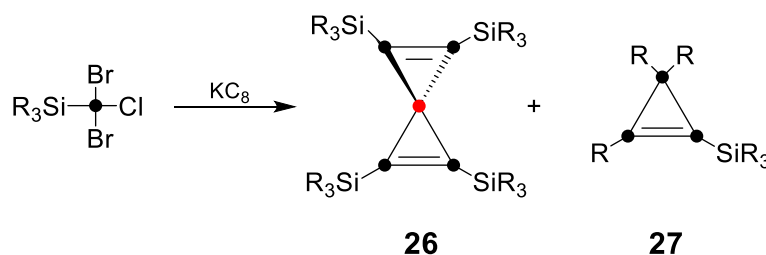
1.4.1. Definition

Around the turn of the millennium the Schnöckel group pioneered a synthetic route to stable, molecular Group 13 clusters by treatment of metastable solutions of monohalides MX (M = Al, Ga; X = halide) with nucleophilic scavenging reagents.^[227–230] Remarkably, examples with up to 84 metal atoms in the cluster core and diameters of up to two nanometers have been reported.^[231] In this regard, Schnöckel introduced the term “metalloid”^[227–229] to describe these kind of clusters, which feature more metal-metal than metal-ligand bonds and as well as exposed cluster atoms that are completely free of peripheral bonds.^[229] As a consequence of these “naked” vertices with a formal oxidation state of zero, the average oxidation state of the cluster atoms is between 0 (as in the element) and +I (as in the low-valent precursors). Therefore, and due to the occasional resemblance of the scaffolds to excerpts of the neat metal's solid-state structure, they are regularly considered as molecular model systems for the elemental bulk.

Initiated by various reports on the isolation of related cluster compounds of tin and germanium, Schnepf expanded Schnöckel's concept of “metalloid clusters” to Group 14 elements in 2007.^[232] Accordingly, in a Group 14 metalloid cluster of the general formula E_nR_m ($n > m$) “naked” and substituted tetrel atoms coexist. The average oxidation state is set between 0 and +I per definition despite the fact that the standard low-valent oxidation state in Group 14 is +II (rather than +I as in Group 13). This definition is backed by the fact that even Group 14 halides of the oxidation state +I become dominant in the gas phase at the high temperatures applied during the synthetic procedure. Nonetheless, the more recent isolation of $Ge_{14}Br_8(PEt_3)_4$ as one of the metastable germanium precursors derived from such a high temperature process provided strong hints at the intermediacy of germanium(II) bromide.^[233] In order to emphasize their proposed intermediacy during the CVD fabrication of a-Si (see Chapter 1.1.), our group coined the notation “siliconoid” for unsaturated, molecular silicon clusters with at least one “naked” cluster vertex irrespective of the average oxidation state.^[51] By employing the presence of such a hemispheroidally coordinated vertex as a sole criterion to decide whether a silicon cluster can be regarded as a siliconoid, we avoid ambiguities in case of systems containing electron-precise

moieties with silicon in the oxidation state +IV, potentially raising the average oxidation state above a certain threshold.

With the empirical formula of $\text{Si}_5(\text{Si}^t\text{BuMe}_2)_3)_4$ and the resulting average oxidation state of the silicon atoms within the bicyclic scaffold, Kira's spiropentasiladiene **26**^[234] (Scheme 8), for instance, does fulfill the criteria of a metalloid cluster according to Schnöckel and Schnepf, but should not be referred to as a siliconoid according to our own definition due to its electron-precise nature and the resulting absence of a hemispheroidally coordinated silicon vertex.



Scheme 8: Synthesis of spiropentasiladiene **26** as side product of cyclotrisilene **27** (● = Si, ● = “naked” Si; R = $^t\text{BuMe}_2\text{Si}$).^[234]

Due to the increasing importance of surface features at the nanoscale and below, the resemblance of “naked”, hemispheroidally coordinated vertices in siliconoids to the so-called dangling bonds of silicon surfaces, is an integral aspect of their use as molecular model systems in order to allow for a better understanding of the chemical reactivity of such surfaces at various scales by making use of the vast analytic toolbox of molecular chemistry. In many cases, hemispheroidal coordination of a vertex in a silicon cluster is obvious and can be readily distinguished from regular tetrahedral coordination environments by visual inspection. For borderline cases, we recently proposed a quantitative geometrical approach, which allows for the facile identification of hemispheroidal coordination environments and provides an index for the degree of hemispheroidality, the hemispheroidality parameter Φ .

As per definition, (pseudo-)tricoordinate vertices must always be hemispheroidally coordinated with the trigonal planar case being the only exception. For tetracoordinate vertices, the procedure is slightly less straightforward (Figure 5). In a first step, a reference plane is defined by those three directly bonded cluster vertices for which the sum of angles about the atom in question is closest to 360° (step 1). The deviation d of the fourth atom of the coordination sphere from this plane is measured and arbitrarily

set to a negative value (step 2). As a consequence, the deviation Φ of the scrutinized atom from the plane is negative if it resides on the same side as the reference atom used in step 2 and positive if it is located on the other side. This value Φ is the called the hemispheroidality parameter. Positive Φ values indicate a hemispheroidal coordination environment, negative Φ values a (distorted) tetrahedral coordination environment and $\Phi = 0$ the exceptional planar tetracoordinate case (step 3).

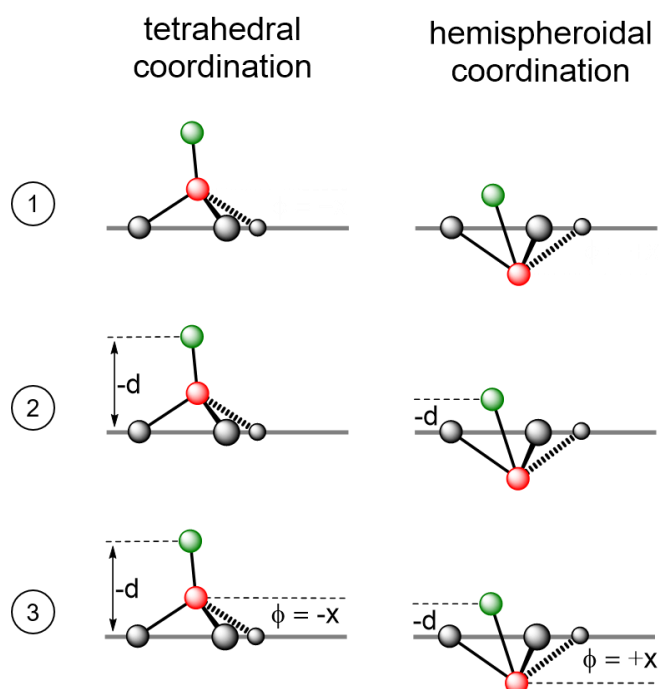
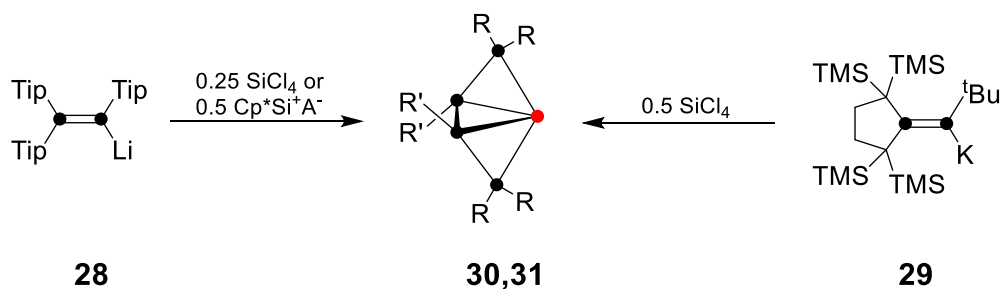


Figure 5: Determination of the hemispheroidality parameter Φ in order to distinguish between tetrahedral (left, Φ negative) and hemispheroidal (right, Φ positive) coordination environments (\bullet = “naked” Si, \circ = bonded Si atoms, which span the reference plane, \bullet = residual Si atom of coordination sphere, d = deviation of \bullet from reference plane, Φ = deviation of \bullet from reference plane = hemispheroidality parameter).

1.4.2. Synthesis and Structure

As already mentioned in the previous chapter, the syntheses of metalloids clusters of the Group 13 elements mainly rely on protocols involving metastable solutions of low-valent monohalides of the appropriate metal.^[227–231] Comparable approaches allowed for the generation of numerous metalloids in the case of germanium,^[232,235–237] tin^[232,237,238] and lead.^[232] In the case of silicon however, potential (meta-)stable low-valent (pseudo-)halide precursors were not accessible before 2006, when Roesky reported on the successful isolation of the first monomeric amidinate-stabilized chlorosilylene.^[239] Even though further representatives became available in the meantime,^[240–246] synthetic protocols for the generation of siliconoids based on Si(II)(pseudo-)halide precursors are still unknown. Instead, three alternative synthetic strategies were established and have been proven convenient in recent years: (1) the usage of disilenide precursors, which are heavier analogues of vinyl anions, (2) the reductive coupling of two or more suitable halogenated precursors, which is highly reminiscent of the most popular approach towards saturated silicon cages (see Chapter 1.2.) and (3) the partial substitution of silicon-based Zintl anions.

Method (1) lead to the first stable siliconoid with a hemispheroidally coordinated vertex, which could be successfully synthesized and isolated by Scheschkewitz in 2005.^[247] The treatment of a fourfold excess of lithium disilenide **28** with SiCl₄ affords the Si₅ siliconoid **30** in 37% yield (Scheme 9). The systematic formation of the by-product of the oxidation of **28**, the peraryl-substituted tetrasilabutadiene, suggests that **28** simultaneously acts as both nucleophile and reducing agent in this reaction. Notably, the disilenide **28** itself is accessible by reductive coupling of Tip₂SiCl₂,^[248] which corresponds to method (2) for the synthesis of siliconoids. In a collaborative effort of the groups of Jutzi and Scheschkewitz, **30** was also detected as one of the products of the reaction of **28** with half an equivalent of the SiCp* cation (Scheme 9).^[249] Notably, the hydrogen-substituted parent species **30H** (R = R' = H) is only a transition state on the potential energy surface of Si₅H₆.^[247] This computational result had initially cast doubts on the constitution of **30**,^[250] which, however, were rebutted by the identification of **30Dip** (R = R' = 2,6-diisopropylphenyl) as a local minimum.^[249] In addition, Iwamoto and co-workers later demonstrated that the five-atomic cluster core of **30** can also be stabilized by a different set of ligands. Accordingly, potassium disilenide **29**^[251] reacts with SiCl₄ to give the closely related Si₅ siliconoid **31** with two *tert*-Butyl and two 1,4-butylene substituents in 63% yield (Scheme 9).^[252]



Scheme 9: Syntheses of Si₅ siliconoids **30**^[247,249] and **31**^[252] starting from disilenes **28**^[248] and **29** (● = Si, ● = “naked” Si; Cp* = pentamethylcyclopentadienyl, A⁻ = B(C₆F₅)₄⁻; ^tBu = *tert*-Butyl; TMS = SiMe₃; **30**: R = R' = Tip = 2,4,6-Pr₃C₆H₂; **31**: R-R = C((SiMe₃)₂CH₂)₂, R' = ^tBu).

Both **30** and **31** feature an unsubstituted vertex that is hemispheroidally coordinated with relatively small Φ values of 0.1915 Å (**30**) and 0.1826 Å (**31**). The general procedure for the determination of Φ as outlined in Chapter 1.4.1., will be demonstrated in an exemplary manner on the solid-state structure of the first siliconoid **30** with a five-atomic scaffold (Figure 6). The vertices Si2/Si3 and Si1/Si4 are each substituted by one and two Tip-ligands, respectively. Only Si5 is completely free of bonds other than those to the adjacent vertices Si1 to Si4 and its coordination environment is thus to be determined as follows: as the largest sum of angles around Si5 is the one involving Si1, Si3 and Si4 (323.76°), the reference plane is defined by these three atoms (step 1). The distance d of the fourth atom of the coordination sphere of Si5 from the reference plane is arbitrarily set to a negative value (Si2, $d = -1.4434$ Å, step 2). As the “naked” silicon vertex Si5 is located on the other side of the reference plane it shows a positive deviation and thus a positive hemispheroidality parameter Φ (Si5, $\Phi = 0.1915$ Å, step 3). Si5 therefore exhibits a hemispheroidal coordination environment (Figure 6).

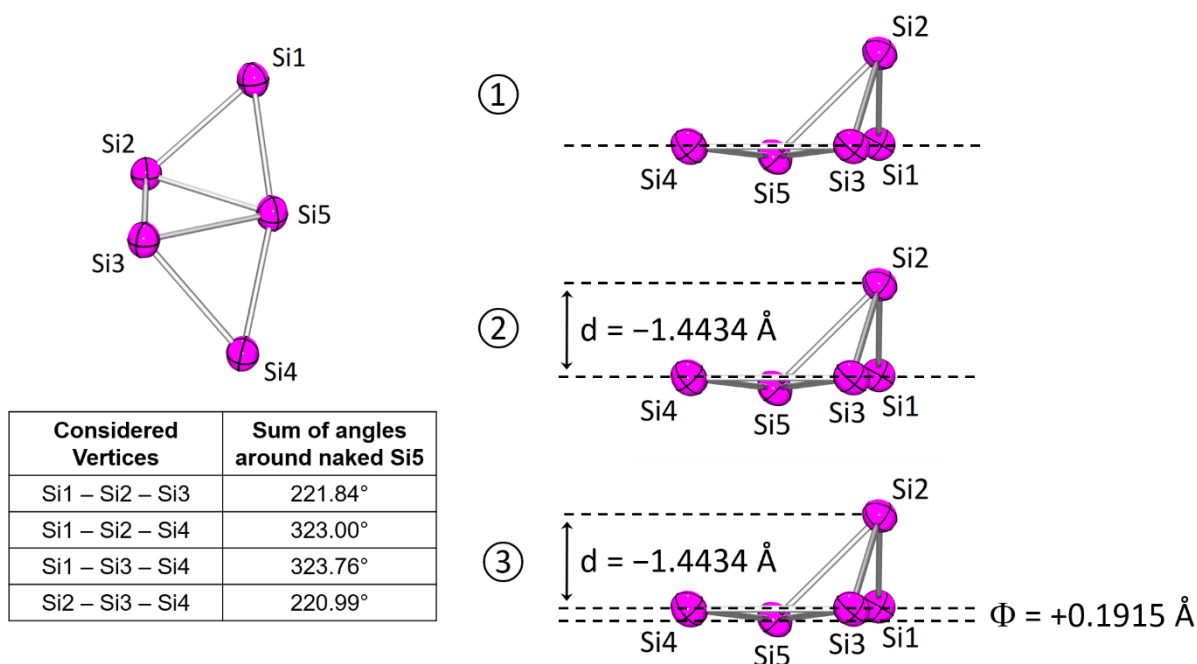
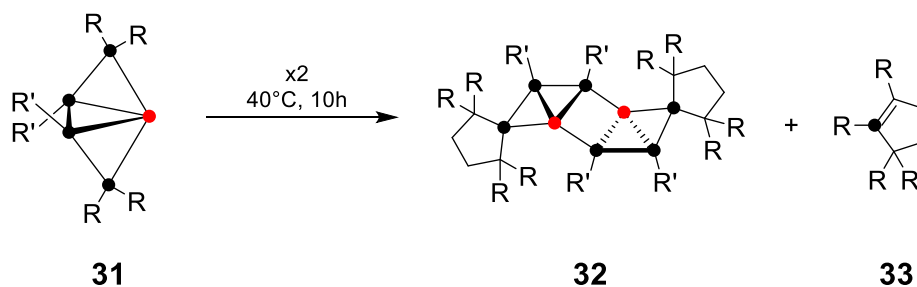


Figure 6: Exemplary determination of the hemispheroidality parameter Φ for the “naked” vertex Si5 in the first siliconoid **30**^[247] reported by Scheschkewitz (Si1/Si4 = SiTip₂, Si2/Si3 = SiTip, Si5 = “naked” Si).

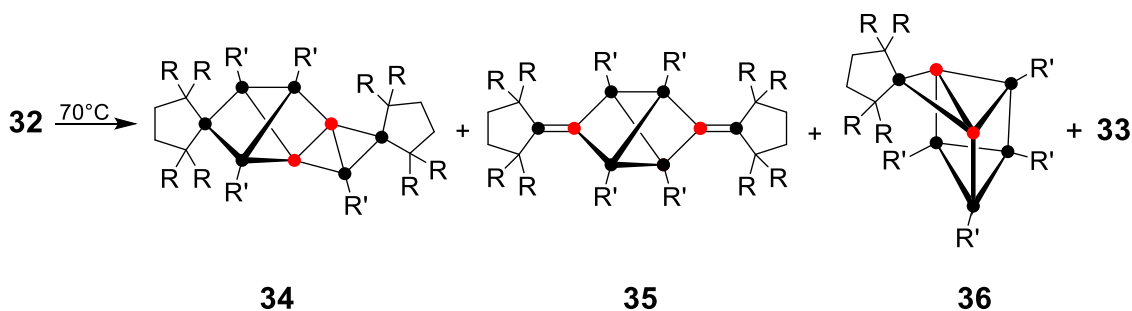
The silicon scaffolds of **30** and **31** appear to be highly distorted due to transannular interactions. Structural features are exemplary reproduced for **30**: In fact, the mono substituted vertices of the central three-membered rings also show slight hemispheroidities ($\Phi = +0.1243 \text{ \AA}$ and $+0.1307 \text{ \AA}$), despite the presence of a stabilizing ligand. While the bond length between the formally sp^2 -hybridized SiR vertices (2.306 \AA) is expectedly somewhat shorter than a Si-Si single bond, the two transannular distances to the “naked” silicon vertex are somewhat longer (2.343 and 2.337 \AA) and fall within the usual range of a single bond. The two planes defined by R-SiR-SiR₂ are almost perpendicular to one another with a torsion angle of 88.7° .

Thermal treatment of Iwamoto’s Si₅ siliconoid **31** at 40°C for 10 hours results in the extrusion of a dialkylsilylene, which readily isomerizes to the thermodynamically favored silene **33**. Dimerization of the apparently unstable Si₄ intermediate affords the Si₈ siliconoid **32** with two “naked” Si vertices in 61% yield (Scheme 10).^[252]



Scheme 10: Thermally induced fragmentation of **31** to give Si_8 siliconoid **32** and silene **33** (● = Si, ● = “naked” Si; R = SiMe_3 , R' = $t\text{Bu}$).^[252]

The ladderane-like siliconoid **32** seems to be a rather electron-precise species. The “naked” silicon atoms clearly do not interact with one another as indicated by the long distance of 3.149 Å between the two.^[252] Despite the symmetrical substitution pattern in **32**, only one of the two “naked” silicon vertices exhibits a hemispheroidal coordination sphere ($\Phi = +0.0124$), while the other is strongly distorted tetrahedral ($\Phi = -0.0311$). Notably, both only marginally deviate from the tetragonal-planar case. In 2018, the group of Iwamoto reported the thermal rearrangement of **32** into its Si_8R_8 isomers **34** and **35** alongside the formation of siliconoid **36** with a contracted Si_7R_6 cluster core (Scheme 11).^[253] $^1\text{H-NMR}$ monitoring suggested that **34** is initially formed, which after a longer period at higher temperatures is either rearranged to **35** or undergoes fragmentation to **36** and the corresponding silylene, which under these conditions rapidly isomerizes to silene **33** as previously observed during the generation of the starting material **32**. Consequently, the yields strongly depend on the reaction time: After 3h at 70°C **34**, **35** and **36** are observed in 26%, 3% and 28% yields, respectively. Heating for another 19 hours leads to the complete consumption of **34**, while **35** and **36** are formed in 6% and 59% yields. All three species were isolated by fractionate recrystallization and subjected to X-ray diffraction analysis.

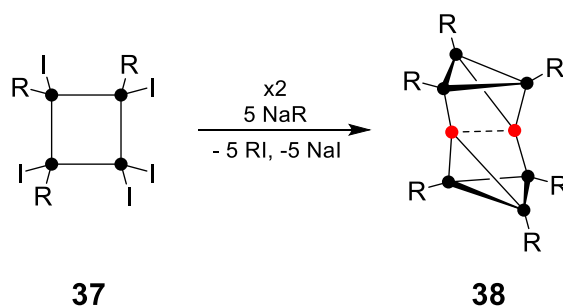


Scheme 11: Thermal treatment of Si_8 siliconoid **32** results in the rearranged isomers **34** and **35** and the contracted Si_7 siliconoid **36** (● = Si, ● = “naked” Si; R = SiMe_3 , R' = tBu).^[253]

The Si_8 siliconoid **34** exhibits two unsubstituted vertices, which are both part of a bicyclo[1.1.0]tetrasilane and a tricyclo[2.2.0.0^{2,5}]hexasilane moiety. They adopt the typical hemispheroidal coordination with Φ values of +0.6530 Å and +0.5293 Å, respectively and show an interatomic distance of 2.5477 Å, which is longer than the typical Si-Si single bond but much shorter than in the precursor **32** (3.149 Å), indicating the presence of a weak bonding interaction. The second Si_8R_8 isomer **35** is constituted of a central tricyclo[2.2.0.0^{2,5}]hexasilane moiety that is flanked by two almost perpendicular double bonds ($\tau = 87,3^\circ$). As the substituent-free atoms of the cluster scaffold of **35** are part of electron-precise double bonds and exhibit perfectly trigonal-planar coordination environments, **35** must not be called a siliconoid. In contrast, the Si_7R_6 cluster **36** with a contracted cluster core features two tetracoordinate, unsubstituted silicon vertices with large Φ values of +0.998 Å and +1.0191 Å, undoubtedly proving its status as siliconoid. The distance between the two is 2.6829 Å and thus intermediate between the corresponding distances in **32** (3.149 Å) and **34** (2.5477 Å). The scaffold as a whole can either be seen as a hexasila[2.1.1]propellane with two of the propeller blades connected to each other or an edge-bridged hexasilaprismane.

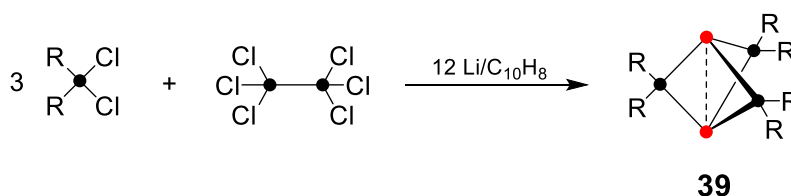
On grounds of the observed high thermal stability of the ligand-stabilized, polyhedral tetrasilatetrahedrane **17**,^[109] Wiberg postulated in 2005 that the catenation of two tetrahedrane moieties by a salt metathesis reaction between corresponding metallated and halogenated derivatives, comparable to the synthesis of Iwamoto's persilastaffanes **13** and **14**,^[97] should be within reach. While an electron-precise Si-Si single bond could be anticipated for such a bis(tetrasilatetrahedrane), related results suggest its likely instability: The full reductive dehalogenation of pentaiodinated cyclotetrasilane **37** (in turn obtained by complete iodination of tetrahedrane **17**) with

supersilyl-sodium ($\text{Na}(\text{Si}^t\text{Bu}_3)$) results in the Si_8R_6 siliconoid **38** as dimerization product with a central dumbbell of two “naked” silicon vertices that is side-on sandwiched between two almost coplanar ligand-stabilized three-membered rings (Scheme 12).^[254] The Si-Si bond between the unsubstituted vertices, albeit short (2.29 Å), still results in a hemispheroidal coordination environment with Φ values of +0.0984 Å and +0.1233 Å.



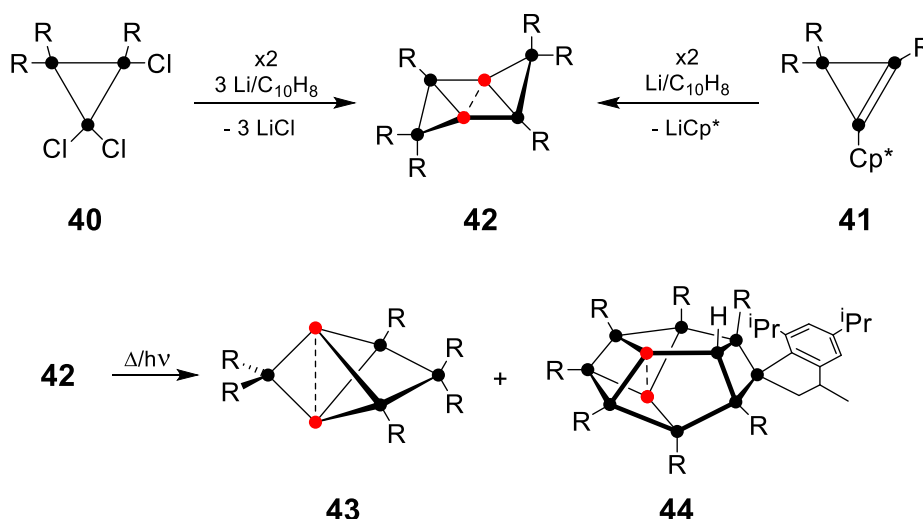
Scheme 12: Reductive dimerization of penta-iodinated cyclotetrasilane **37** to yield Si_8 siliconoid **38** (● = Si, ● = “naked” Si; R = Si^tBu_3).^[254]

In the closing remarks of his 1991 review article about strained-ring and double-bond systems of Group 14 elements, Masamune pointed out that the synthesis of a pentasila[1.1.1]propellane, a disilyne and a tetrasilahedrane were the main challenges in silicon chemistry at the time.^[255] While the latter was not long in coming with Wiberg’s tetrasilahedrane **17** of 1993,^[109] the first structural characterization of a disilyne only dates back to 2004.^[256] Almost 20 years after Masamune’s statement, Breher et al. finally obtained the first pentasila[1.1.1]propellane **39** by reduction of a mixture of $\text{Mes}_2\text{SiCl}_2$ and Si_2Cl_6 (ratio 3:1) with lithium/naphthalene, albeit in very low yields (10% spectroscopically, 1% crystalline; Scheme 13).^[257]



Scheme 13: Reductive heterocoupling of $\text{Mes}_2\text{SiCl}_2$ and Si_2Cl_6 to yield pentasila[1.1.1]propellane **39** (● = Si, ● = “naked” Si; R = Mes = 2,4,6- $\text{Me}_3\text{C}_6\text{H}_2$).^[257]

The two “naked” bridgehead atoms show distinct hemispheroidal coordination environments with Φ values of +1.3227 Å and +1.3134 Å and are bonded to three SiR₂ bridges arranged in a perfectly eclipsed manner. The nature of the bonding between bridgehead atoms at a distance of 2.636 Å has been the topic of numerous theoretical and experimental investigations and will be addressed in more detail in Chapter 1.4.3. The first isomer of the today still hypothetical hexasilabenzene was isolated by Sakurai and Sekiguchi as the hexasilaprismane **16** (see Chapter 1.2.).^[51,111] While **16** can be considered as an electron-precise species, the product of reductive dimerization of the trichlorinated cyclotrisilane **40** is strongly delocalized. The tricyclic Si₆R₆ isomer **42** with a chair-like conformation was obtained in 52% yield by Scheschkewitz et al. (Scheme 14) and exhibits an unusual type of aromaticity due its dismutational substitution pattern.^[258] Alternatively, **42** can be accessed by the reduction of a pentamethylcyclopentadienyl-substituted cyclotrisilene precursor **41**.^[249] The thermal or photolytically induced rearrangement of **42** results in the formation of the bridged-propellane type siliconoid **43** (58% yield). As side product, the Si₁₁ siliconoid **44** with two unsubstituted silicon vertices could be identified and isolated in very low yields of 2.6% (Scheme 14).^[51] Thus far, **44** represents the siliconoid with the highest number of silicon atoms in the cluster scaffold, that could be fully characterized, even though the mechanism of its formation remains obscure.

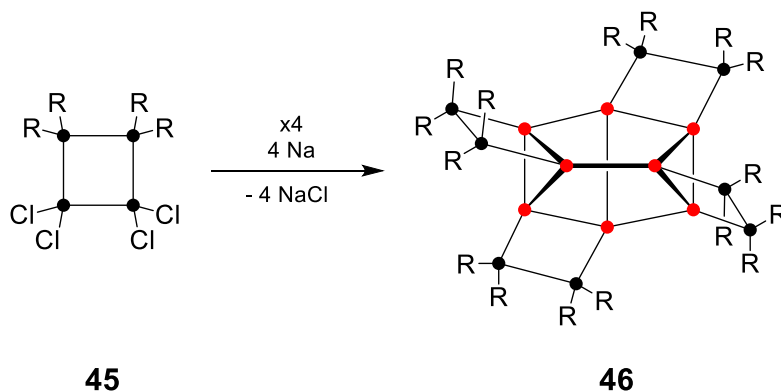


Scheme 14: Reductive dimerization of trichlorinated cyclotrisilane **40** and Cp*-functionalized cyclotrisilene **41** to afford the dismutational isomer of hexasilabenzene **42** and its rearrangement to benzpolarene **43** and Si₁₁ siliconoid **44**, respectively (● = Si, ● = “naked” Si; R = Tip = 2,4,6-^tPr₃C₆H₂).^[51,249,258,259]

In a hypothetical hexasilabenzene, every silicon atom should bear one substituent and therefore exhibit the oxidation state +I. The less uniform substitution pattern in siliconoid **42** with two SiR₂(+II), two SiR(+I) and two “naked” Si(0) atoms can be formally derived by a twofold dismutation. Consequently, the cluster scaffold features a central rhomboidal, unsaturated Si₄ plane consisting of the two “naked” and the two monosubstituted vertices, which is bridged by two opposing saturated SiTip₂ moieties in a chair-like manner. In order to give credit to the dismutated arrangement of substituents and the circumstance that **42** nevertheless shows a cyclic delocalization of electrons around the central four-membered ring, the term “dismutational isomer of hexasilabenzene” was coined (see also Chapter 1.4.3.). In contrast, the skeleton of the thermal isomerization product **43** is rather reminiscent of the pentasila[1.1.1]propellane **39**,^[257] but with an additional SiTip₂ silylene unit bridging two wings of the propellane motif. This “bridged propellane” scaffold was calculated to be the global minimum on the Si₆R₆ potential energy surface and is therefore validly regarded the thermodynamical analogue of benzene in the case of silicon.^[259,260] Considering the fact that graphene is constituted of condensed benzene units, it might come as no surprise that the global minimum structure of **43** was subsequently suggested to be a preferred repeating motif in silicon nanosheets,^[261] which obviously makes it particularly attractive regarding the desired access to the elusive^[262–265] heavier graphene congener, silicene. The distances between the “naked” bridgehead vertices in **42** (2.7287 Å) and **43** (2.7076 Å) are unusually elongated, which indicates the absence of a direct bonding interaction between the two. This assumption is strongly supported by their electron densities that were determined by Stalke making use of X-ray diffraction at high 2θ angles.^[266] The resulting (pseudo-)tricoordinate coordination spheres allow for strong hemispheroidalization around the unsubstituted vertices as shown by their Φ values of +1.1151 Å (**42**) and +1.3535 Å (**43**). The considerably shorter bond length in **44** (2.4976 Å; Φ = +0.5361 Å and +0.3109 Å) was tentatively attributed to the staggered arrangement of the central propellane-like unit allowing for a stronger bonding interaction.^[51]

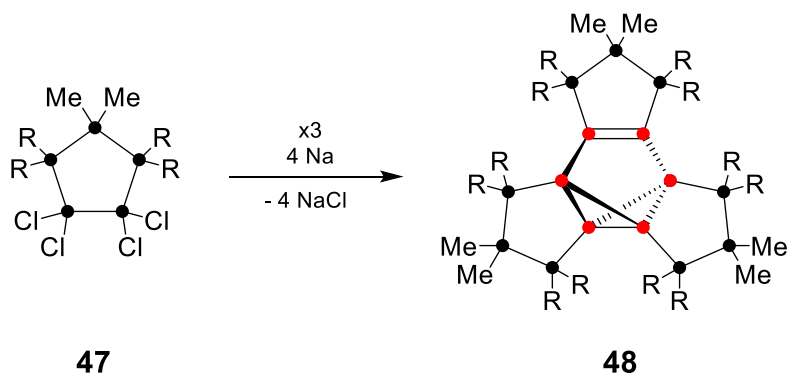
In 2013, Kyushin and co-workers reported the reductive tetramerization of the tetrachlorinated cyclotetrasilane **45** with sodium metal to give the C₂-symmetric octasilacuneane **46** in 15% yield (Scheme 15).^[267] Apparently, **46** represents a borderline case of a siliconoid as it does not feature an obviously “naked” silicon atom at first inspection. However, if the annulated disilane moieties are considered as part

of the cluster core, all eight vertices of the central cuneane motif are potential candidates for hemispheroidal coordination. While four of these exhibit more or less electron-precise distorted tetrahedral coordination environments ($\Phi = -0.1990 \text{ \AA}$ and $\Phi = -0.2426 \text{ \AA}$), the other four are indeed hemispheroidally coordinated, albeit by very small margins ($\Phi = +0.0368 \text{ \AA}$ and $\Phi = +0.0555 \text{ \AA}$). It is therefore legitimate to refer to **46** as a siliconoid according to our definition.



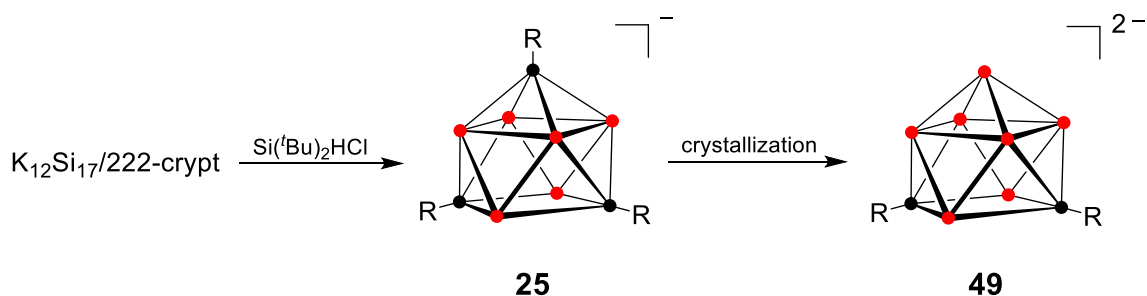
Scheme 15: Synthesis of cyclotetrasilane-fused persilacuneane **45** by reductive tetramerization of tetrachlorinated cyclotetrasilane **46** (● = Si, ● = “naked” Si; R = ‘Bu).

A similar borderline case appears to be the cyclopentasilane-fused hexasilabenzvalene **48**, which was isolated by the same group (Scheme 16).^[268] Once more, the six silicon atoms of the central benzvalene moiety can be regarded as unsubstituted vertices of the core if the annulated, stabilizing Si_3 bridges are taken as part of the siliconoid scaffold. Obviously, the tricoordinate silicon atoms of the localized double bond, that show large *trans*-bent angles ($\theta = 36.5^\circ$ and 42.5°), must be hemispheroidally coordinated per definition and thus cannot be decisive for the classification of **48** as a siliconoid. Since all other “naked” silicon atoms in question are tetrahedrally coordinated with Φ values ranging from -0.0756 \AA to -0.1677 \AA , **48** should not be referred to as a siliconoid.



Scheme 16: Synthesis of cyclopentasilane-fused hexasilabenzvalene **48** by reductive trimerization of tetrachlorinated cyclopentasilane **47** (● = Si, ● = "naked" Si; R = ^tBu).^[268]

The siliconoids discussed so far were prepared by the aforementioned synthetic methods (1) and (2), namely the usage of disilenides as starting materials or the full reductive dehalogenation of suitable precursors. Very recently, the group of Fässler succeeded for the first time in employing silicon-based Zintl anions as precursors to anionic siliconoids (see also Chapter 1.3.5.). Treatment of the activated Zintl phase $K_{12}Si_{17}/222$ -crypt in thf solution with six equivalents of $Si(^tBu)_2HCl$ allows for the isolation and characterization of the trisubstituted, monoanionic Si_9 siliconoid **25**.^[207] An X-ray diffraction study on single crystals revealed the loss of one silyl-substituent during the crystallization process (possibly by disproportionation), which resulted in the formation of the corresponding disubstituted, dianionic species **49** (Scheme 17).^[207] All seven exposed cluster atoms show distinct hemispheroidalization ($\Phi = +1.2680 \text{ \AA}$ to $+1.5848 \text{ \AA}$). The Si-Si bonds lengths within the dianionic siliconoid framework (2.405 \AA to 2.7818 \AA) are somewhat shorter than in the bare, tetraanionic Si_9^{4-} Zintl cluster (2.423 \AA to 2.881 \AA),^[160,183] presumably due to the much lower Coulomb repulsion of the two remaining negative charges.



Scheme 17: Syntheses of mono- and dianionic Si_9 siliconoids **25** and **49** from the Zintl-phase $K_{12}Si_{17}$ (● = Si, ● = “naked” Si; 222-crypt = 4,7,13,16,21,24-hexaoxa-1,10-diaza-bicyclo[8.8.8]hexacosane; R = $SiH(tBu)_2$).^[207]

The hemispheroidalities Φ of the “naked” vertices of the discussed siliconoids and the hexasilabenzvalene species **48** are summarized in Table 3. In case of clusters with more than one exposed vertex, the distances between the unsubstituted vertices are also indicated.

The “naked” bridgehead vertices in siliconoids with a central propellane motif (**36**, **39**, **43**) and those in the dismutational isomer of hexasilabenzene **42** can be regarded as (pseudo-)tricoordinate due to their long interatomic distance. As a result, they regularly exhibit strongly hemispheroidal coordination environments with Φ values, typically being greater than 1 Å, which is only exceeded by the dianionic, disubstituted Zintl-type siliconoid **49** with its greatest Φ value even surpassing 1.5 Å. Iwamoto’ and Kyushin’s Si_8 clusters **32**, **46** and **48** are to be considered as borderline cases as their “naked” vertices show only marginal deviation from the tetracoordinate planar case ($\Phi = 0$). However, since all unsubstituted vertices in **46** are distorted tetrahedrally coordinate as can be seen from negative Φ values, the status as siliconoid is not justified according to the hemispheroidality parameters. “Naked” cluster atoms with negative Φ values are also present in **32** and **48**, yet they fulfill the criterion for siliconoids as they feature at least one slightly hemispheroidalized cluster atoms with a positive Φ value.

1.4. Siliconoids

Table 3: Comparison of hemispheroidalities Φ and distances between unsubstituted vertices of given siliconoids.

Siliconoid	Number of "naked" vertices	Si _u -Si _u [Å]	ϕ values [Å]	Hemispheroidal coordination?
30	1	—	+ 0.1915	✓
31	1	—	+ 0.1826	✓
32	2	3.149	+ 0.0124/−0.0311	✓
34	2	2.5477	+ 0.6530/+0.5293	✓
36	2	2.6829	+ 0.998/+1.0191	✓
38	2	2.29	+ 0.0984/+0.1233	✓
39	2	2.636	+ 1.3227/+1.3134	✓
42	2	2.7287	+ 1.1151	✓
43	2	2.7076	+ 1.3535	✓
44	2	2.4976	+ 0.5361/+0.3109	✓
46	8	2.3320 – 2.4100	+ 0.0555/+ 0.0368/ − 0.1990/− 0.2426	✓
48	6	2.3188 – 2.3683	− 0.0756/ −0.0959/ −0.1594/ −0.1677	✗
49	7	2.4292 – 2.7818	+1.5566/+1.2882/ +1.2850/+1.2680/ +1.2804/+1.5848/ +1.5807	✓

1.4.3. Spectroscopic Data and Electronic Properties

Siliconoids not only exhibit structural peculiarities but also unusual electronic properties, which in most cases are not to be individually considered but rather depend on each other. As a prime example, the hemispheroidally coordinated, "naked" vertices in siliconoids typically give rise to distinctively high-field shifted ^{29}Si NMR signals, which is highly reminiscent of the NMR spectroscopic properties of silicon-based Zintl ions (see Chapter 1.3.4.). In contrast to $[\text{Si}_4]^{4-}$ and $[\text{Si}_9]^{4-}$ Zintl clusters, but in a similar manner as $[\text{Si}_5]^{2-}$, silicon vertices of one and the same siliconoid scaffold can also show ^{29}Si NMR resonances at very low field. The resulting wide distributions of ^{29}Si NMR chemical shifts (see Table 4) with differences between the two signals observed

at highest and lowest field of up to 448.8 ppm in the case of **43** reflect the characteristic electronic anisotropy of siliconoids and thus one of their main distinctive attributes.

Table 4: Comparison of ^{29}Si NMR chemical shifts of given siliconoids.

Siliconoid	Most low-field signal δ (^{29}Si) [ppm]	Most high-field signal δ (^{29}Si) [ppm]	Range ($\Delta\delta_{\text{min}}-\delta_{\text{max}}$) [ppm]
30	7.4	-124.8	132.2
31	60.0	-69.5	129.5
32	24.6	-26.8	51.4
34	64.7	-191.9	256.6
36	123.3	-159.5	282.8
38	—	—	—
39	25.5	-273.2	298.7
42	124.6	-89.3	213.9
43	174.6	-274.2	448.8
44	26.2	-78.7	104.9
46	35.4	-71.8	107.2
48	187.3	-84.6	271.9
25	-175.2	-358.8	183.6

While most reports on siliconoids lack explanations for the observed NMR spectroscopic peculiarities, they were rationalized in the case of the hexasilabenzene isomers **42** and **43** on the basis of theoretically calculated magnetically induced cluster currents in the corresponding parent species **42H** and **43H**.^[259,269] In both cases, the “naked” bridgehead atoms are surrounded by a diatropic current vortex, which exerts a strong magnetic shielding effect resulting in the observed high-field shifted resonances in the ^{29}Si NMR spectra (Figure 7, Table 4). In contrast, the monosubstituted vertices in **42** and the disubstituted vertex in **43**, which are directly adjacent to the “naked” atoms, are surrounded by a paratropic current loop leading to a pronounced magnetic deshielding of their ^{29}Si NMR signals (Figure 7, Table 4). This is particularly noteworthy as these vertices are tetracoordinate and would therefore be considered as electron-precise in a first approximation. Usually, tetracoordinate silicon atoms rarely display chemical shifts at lower field than about 90 ppm even in the case

of base-stabilized silylium cations.^[270–273] The topologies of the frontier molecular orbitals in **43** and related species were discussed as complementary explanation for the observed low-field shifted resonances of the untethered propeller blades in the context of stable heterosiliconoids featuring germanium and tin atoms in the bridgehead positions, respectively (see Chapter 1.4.4.).

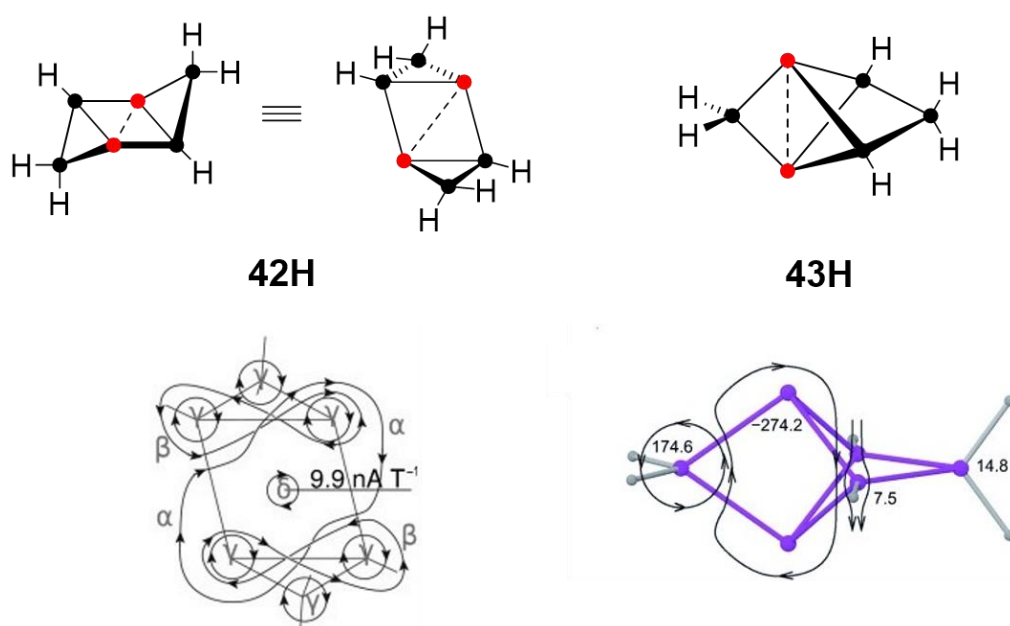


Figure 7: Dominating current vortices in the parent hexasilabenzene isomers **42H** and **43H**. Diatropic vortices are clockwise, paratropic vortices are counterclockwise. The total ring current in **42H** is diatropic and integrates to 9.9 nA T^{-1} . The ^{29}Si NMR chemical shifts are additionally given for **43H**. Partially reproduced with permission from Berger et. al., *Angew. Chem. Int. Ed.* **2010**, *49*, 10006-10009^[269] and Abersfelder et. al. *Angew. Chem. Int. Ed.* **2011**, *50*, 7936-7939.^[259]

The overall induced molecular current in both hexasilabenzene isomers is diamagnetic with around 10 nA T^{-1} and thus almost identical to what was found for the prototypical 6π -Hückel-aromatic benzene. However, planar Hückel-aromatic compounds must feature a central paramagnetic vortex, despite the overall diamagnetic ring current. Conversely, siliconoids **42** and **43** feature a central diatropic current loop, which is rather akin to the situation in compounds featuring spherical aromaticity such as P_4 .^[194] Nevertheless, **42** shows delocalization of six electrons, albeit restricted to the central, planar four-membered ring according to theoretical investigations.^[258] Whereas in benzene 6π -electrons contribute to the aromatic system, the cyclic delocalization in **42** involves two π -, two σ - and two nonbonding electrons.^[258] As already outlined in Chapter 1.4.2., the term “disputational aromaticity” was established for this

phenomenon based on the dismutated substitution pattern of the silicon scaffold in comparison to the highly symmetrical benzene. This novel type of aromaticity apparently results in a surprising stability as **42** can be exposed to air in its solid state for hours without any sign of decomposition. The global minimum framework of siliconoid **43** on the other hand decomposes within minutes when exposed to air, but shows extraordinary thermal stability allowing for its transfer into the gas-phase with only minor traces of decomposition.

The structure and in particular the nature of the central bridgehead bond in [1.1.1]propellane and its heavier congeners were and still are thoroughly discussed in the literature. As early as 1972, theoretical investigations by Stohrer/Hoffmann^[274] and Newton/Schulmann^[275] on the carbon-derivative revealed the bonding situation between the bridgehead atoms to be far from trivial as seemingly contradictory results did not allow the unambiguous determination of the nature of their interaction as bonding or nonbonding: On the one hand, the calculated bond lengths and the symmetric appearance of the HOMO suggested the existence of a central bond in a closed-shell singlet ground state rather than a diradical. On the other hand, the total overlap population between the bridgehead vertices was found to be negative, which rather indicated a nonbonding interaction. More recent results by Shaik and co-workers suggested a so-called “charge-shift” bridgehead bond.^[276,277] In the meantime, numerous other reports on both theoretical and experimental investigations with the intention to clarify the nature of the bridgehead bond were published and reviewed.^[278–280] This still ongoing discussion is not only restrained to the carbon-based [1.1.1]propellane but also focuses on the corresponding heavier homologues.^[279,281–284] The first successful synthesis of a pentasil[1.1.1]propellane **39** allowed the experimental evaluation of predicted properties for the first time. Here, the bridgehead bond was found to be 2.636 Å, which is unusually elongated (ca 13%) in comparison to a regular Si-Si single bond suggesting a rather weak bonding interaction. Considering the calculated reaction energy for the addition of dihydrogen to the bridgehead bond, the Si-Si bond strength was estimated to be around 174 kJ/mol and thus considerably weaker than in normal disilanes (ca. 306-322 kJ/mol).^[257] The longest wavelength absorption observed at $\lambda = 396$ nm was assigned to the electronic transition from the cluster-bonding HOMO to the LUMO on grounds of TD-DFT calculations. The fact, that **39** shows both closed-shell and biradicaloid reactivity (see Chapter 1.4.5.) underlines the abnormal, ambiguous nature of the central Si-Si bridge.

Theoretical investigations on the electronic structure of the highly distorted scaffold of the first ever reported Si₅ siliconoid **30** revealed it to be a transition state in the case of the corresponding parent compound. In this case, the bis-homoaromatic isomer, where both SiR₂ bridges are on the same side of the central three-membered ring represents the minimum structure being 14.8 kcal/mol lower in energy.^[247] Apparently, the kinetically stabilizing effect of the sterically demanding Tip groups in **30** is sufficiently great to force the scaffold into a local energy minimum. The extreme distortion of the silicon skeleton results in an almost orthogonal set of two p-orbitals at the formally sp²-hybridized silicon atoms (Figure 8). The energetic separation of HOMO and HOMO-1 (0.14 eV) is only marginal, while the HOMO-2 is around 1.1 eV lower in energy.^[247] Hence formally, the Heilbronner criterion for Möbius aromaticity (4n mobile electrons) is fulfilled.^[285] Indeed, the topology of the HOMO-1 is reminiscent of a Möbius array (Figure 8) just as in the so called Möbius benzene, which was calculated by Johnson in 1996.^[286]

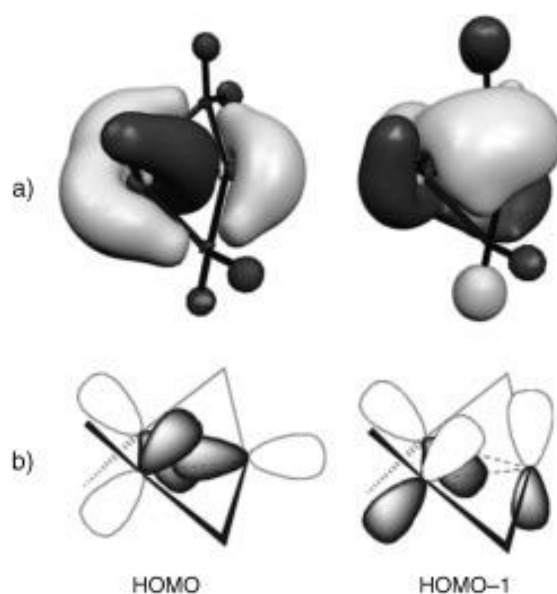


Figure 8: Molecular orbitals of the parent compound **30H** (a) and schematic representation of the involved atomic orbitals (b) Picture reproduced with permission from D. Scheschkewitz, *Angew. Chem. Int. Ed.* **2005**, *44*, 2954-2956.^[247]

Surprisingly, an EI-MS experiment of **30** revealed a peak at $m/z = 1415.9$, which corresponds to a Si₇Tip₆ species. Apparently, the expansion of the cluster with two additional silicon atoms must take place upon heating prior to evaporation into the gas phase as a similar behavior could not be observed using milder ionization techniques. This assumption finds further corroboration in an exothermic process at 144°C

detected by DSC.^[247] In stark contrast, siliconoid **31** does not show tendency for cluster expansion but rather releases a silylene unit upon heating in benzene (see Chapter 1.4.2.). The resulting intermediate heavy bicyclic bridgehead alkene dimerizes to siliconoid **32** but can also be trapped with DMAP (= 4-dimethylaminopyridine). Unfortunately, no further information on the electronic structure of the dimerized Si₈ species **32** were given by the authors in this case.^[252] According to DFT calculations on the thermal rearrangement product **34**, the HOMO and LUMO are mainly represented by the σ and σ^* orbitals of the bridgehead bond between the “naked” silicon vertices, respectively (Figure 9). The corresponding orbitals of the cluster contraction product **36** rather contribute to the HOMO-1 and the LUMO, while the HOMO involves cluster bonding σ -orbitals,^[253] comparable to what was found for the model compounds pentasila[1.1.1]propellane **39Dmp** (Dmp = 2,6-Me₂C₆H₃)^[257] and its closely related bridged isomer **43Dip** (Dip = 2,6-iPr₂C₆H₃)^[259] (Figure 9).

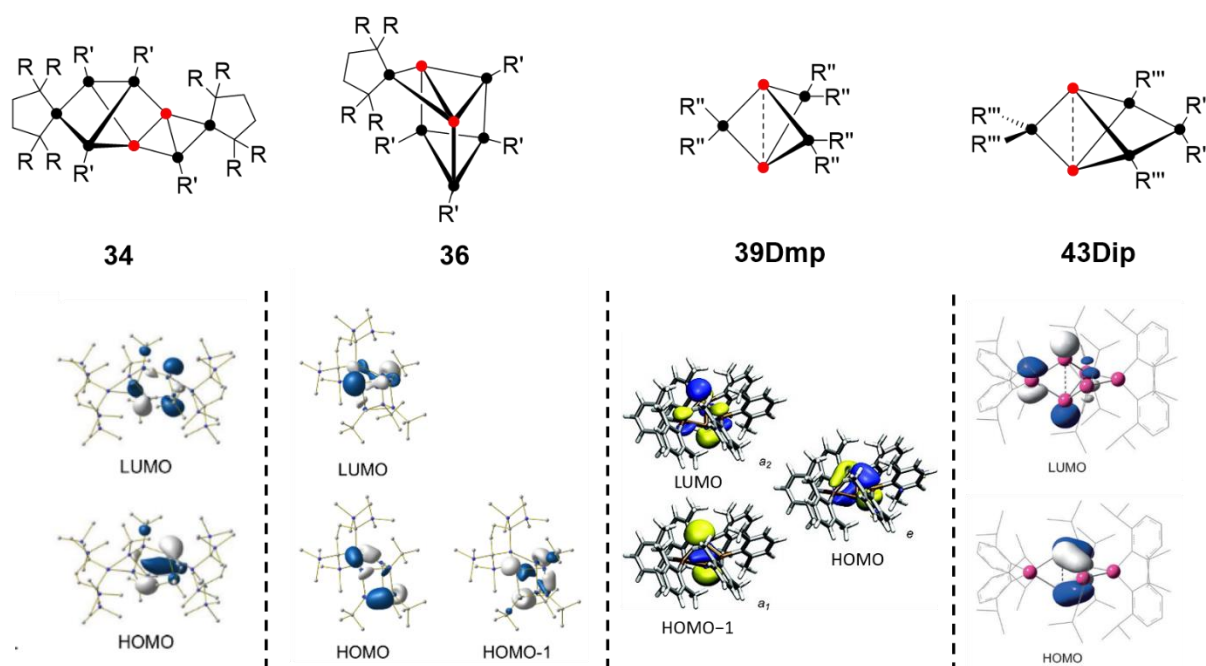


Figure 9: Comparison of the frontier orbitals of Si₈ siliconoids **34** and **36** and the model compounds **39Dmp** and **43Dip** for pentasila[1.1.1]propellane **39** and its bridged isomer **43**, respectively (● = Si, ● = “naked” Si; R = SiMe₃, R' = ^tBu, R'' = Dmp = 2,6-Me₂C₆H₃, R''' = Dip = 2,6-iPr₂C₆H₃). Pictures reproduced with permission from Akasaka et. al., *Inorganics* **2018**, 6, 107,^[253] Nied et. al., *J. Am. Chem. Soc.* **2010**, 132, 10264-10265^[257] and Abersfelder et. al. *Angew. Chem. Int. Ed.* **2011**, 50, 7936-7939.^[259]

The large skeleton of siliconoid **46** with overall 16 silicon atoms and a central cuneane motif of eight vertices shows well-developed σ -conjugation. The UV/vis spectrum lacks

distinctive absorption bands, but tails to ca. $\lambda = 570$ nm with small shoulders at $\lambda = 345$ nm and $\lambda = 380$ nm, which was attributed to close energies of frontier orbitals and thus severe overlap of intrinsically discrete absorption bands.^[267] The observed tailing is a characteristic feature of saturated polyhedral silicon cages and was also reported for hexasilaprismanes^[51,111] and octasilacubanes.^[112,113] On grounds of these findings, octasilacuneane **46** was labelled an “intermediate model between small organosilicon molecules and silicon semiconductors” in terms of electronic properties by the authors.^[267]

The extremely high-field shifted ²⁹Si NMR signal ($\delta = -358.8$ ppm) of the unsubstituted vertices in the monoanionic siliconoid **25** is comparable to what was observed for the very recently reported protonated Zintl species $[\text{HSi}_9]^{3-}$ ($\delta = -358.5$ ppm)^[202] and $[\text{H}_2\text{Si}_9]^{2-}$ ($\delta = -346.1$ ppm),^[199] which might be expected as both are derived from the bare, tetraanionic $[\text{Si}_9]^{4-}$ Zintl cluster. Apparently, substitution of the scaffold with a proton in or silyl groups causes a considerable deshielding of the vertices in question ($[\text{HSi}_9]^{3-}$: $\delta = -158.5$ ppm and **25**: $\delta = -175.2$ ppm), even though the resonance still appears deep in the high-field region. An intrinsic atomic orbital charge analysis revealed that the negative charge in **25** is perfectly delocalized over the six unsubstituted silicon atoms, while the two negative charges in **49** are unsymmetrically distributed.

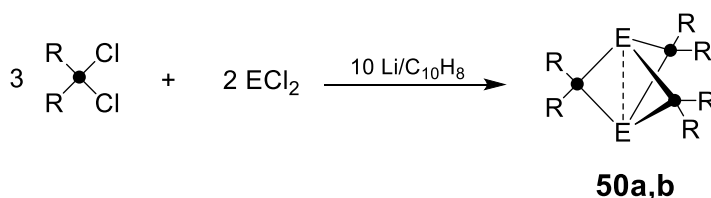
1.4.4. Heterosiliconoids

Unsaturated homonuclear clusters of germanium and tin were reported well before the first silicon derivatives became available. A complete account on these derivatives, is beyond the scope of this silicon-centered overview. The reader is referred to excellent and comprehensive reviews in this regard.^[46,47,232,235–238] In order to provide suitable context for this sub-chapter on heterosiliconoids, i.e. siliconoids with partial replacement of the core atoms by atoms other than silicon, the developments in case of heavier propellanes and related species shall be briefly summarized by way of example.

The report on the first pentastanna-propellane by Sita and Bickerstaff dates back to 1989.^[287] A second example could be generated by the group of Drost in 2002.^[288] One year before the isolation of the iconic pentasila[1.1.1]propellane **39**, the group of Breher

isolated the corresponding germanium species in 2009.^[289] As concerns bridged propellanes, Wesemann isolated a hexastannabenzene Sn_6R_6 with a scaffold identical to the – in this case preceding – global minimum hexasilabenzene isomer **42**.^[290] With synthetic protocols for homonuclear siliconoids as well as their heavier congeners established, the question naturally arose whether heteronuclear derivatives would be accessible as well. Indeed, a few examples are known to date and discussed in the following.

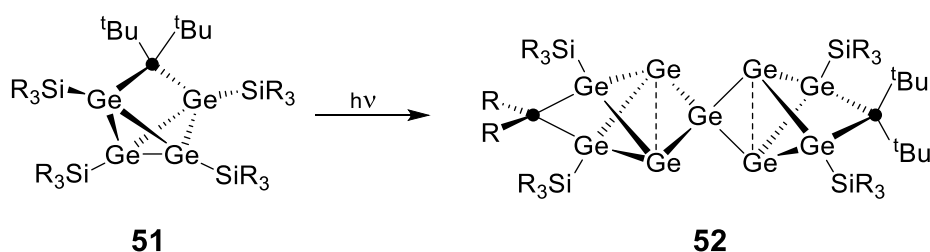
Breher's heteronuclear [1.1.1]propellanes **50a,b** of the general formula $\text{E}_2\text{Si}_3\text{Mes}_6$ were synthesized by the reductive heterocoupling of $\text{Mes}_2\text{SiCl}_2$ and the corresponding low-valent dichlorides of germanium and tin in a 3:2 ratio with 10 equivalents of lithium/naphthalene (Scheme 18).^[291] The crystalline yields are with 4% (**50a**) and 12% (**50b**) rather low, yet still higher than for the homonuclear silicon analogue **39** (1%). Notably, no other [1.1.1]propellane species with an alternative occupancy of the cluster positions with E and Si atoms were observed in the reaction mixtures leading to the conclusion that the low-valent tetrylene(II)chlorides ECl_2 were the sole source of the atoms in the bridgehead positions. The pronounced thermal stability of **50a,b** without rearrangement of atoms or ligand scrambling was taken as another indication for the preference of heavier atoms to be located at a “naked” or unsubstituted position of the scaffold.



Scheme 18: Synthesis of heteronuclear [1.1.1]propellanes **50a,b** the reduction of a 3:2 mixture of $\text{Mes}_2\text{SiCl}_2$ and ECl_2 with 10 equivalents of lithium naphthalenide solution (● = Si; R = Mes = 2,4,6- $\text{Me}_3\text{C}_6\text{H}_2$; **50a**: E = Ge; **50b**: E = Sn).^[291]

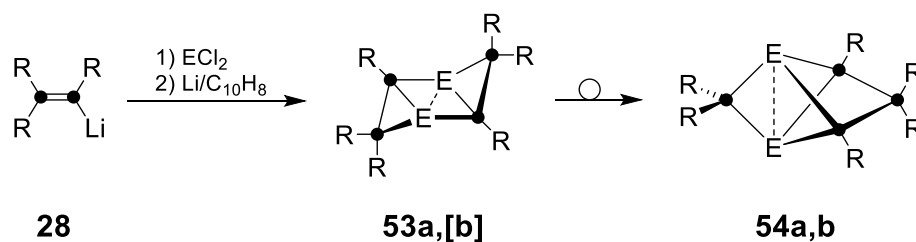
The distances between the bridgehead vertices are 0.1 Å (**50a**) and 0.27 Å/0.342 Å (**50b**) shorter than in the corresponding homonuclear congeners Ge_5Mes_6 ^[289] and Sn_5R_6 (R = Dep = 2,6- $\text{Et}_2\text{C}_6\text{H}_3$ ^[287] or R = 2,6-(OⁱPr)₂ C_6H_3 ^[288]) presumably due to the smaller size of the bridging SiMes_2 propeller blades in the case of **50a,b**. The thus indicated stronger bond interaction between the bridgehead atoms was confirmed by cyclic voltammetry, UV/vis spectroscopy and DFT calculations, which additionally

revealed a correlation with the singlet and triplet A_2 transitions.^[291] This corroborates the principal feasibility of manipulating the inherent structural and electronic properties of heavy Group 14 cluster species by the selective labelling with heteroatoms, which was initially demonstrated by Power in the context of his $\text{Ge}_2\text{Sn}_3[1.1.1]$ propellane.^[292] In 2013, Sekiguchi and co-workers reported the formation of the spirobis(pentagerma[1.1.1]propellane) species **52** in 18% yield by photolysis of the saturated tricyclic precursor **51** (Scheme 19). On grounds of DFT calculations and the typically long interatomic distance (2.8292 Å) between the bridgehead germanium vertices, which is comparable to the value found in Breher's pentagermapropellane (2.869 Å), they classified **52** as a singlet tetraradicaloid.



Scheme 19: Photolysis of the mixed heavy tricyclo[2.1.0.0^{2,5}]pentane precursor **51** to yield the spiro[bispentagerma[1.1.1]propellane **52** (● = Si, $\text{SiR}_3 = \text{SiMe}^t\text{Bu}_2$, $^t\text{Bu} = \text{tert-Butyl}$).^[293]

Treatment of disilenide **28** with an equimolar amount of $\text{GeCl}_2 \cdot \text{dioxane}$ and subsequent reduction of the postulated intermediate, disilyl-substituted chlorogermylene, with lithium/naphthalene solution affords the digermatetrasilane-analogue **53a** of the dismutational isomer of hexasilabenzene **42** in 42% yield (Scheme 20). In solution, **53a** slowly isomerizes to its alleged global minimum isomer **54a** at room temperature. This process can be accelerated by moderate heating to 65°C and is then complete after 12 hours. Under identical reaction conditions the utilization of SnCl_2 instead of GeCl_2 directly yields **54b** with a bridged propellane scaffold in 22% yield (Scheme 20). The fact that the probable intermediate, dismutational Sn_2Si_4 isomer [**53b**], could not even be detected spectroscopically at -80°C suggests a very low thermal stability.



Scheme 20: Syntheses of dismutational (**53a**) and global minimum (**54a,b**) E_2Si_4 heterosiliconoids by treatment of disilenide **28** with low-valent dichlorotetrylenes ($\bullet = Si$, $R = Tip = 2,4,6\text{-}i\text{-}Pr_3C_6H_2$, **53**: $E = Ge$; **54**: $E = Sn$).^[294]

Heteroatomic siliconoids feature electronic anisotropies similar to their all-silicon archetypes^[258,259,269] as indicated by multinuclear NMR spectroscopy. The bridgehead tin vertices in **50b** and **54b** give rise to high-field shifted resonances in the ^{119}Sn spectra (**50b**: $\delta = -1348$ ppm,^[291] **54b**: $\delta = -1260$ ppm^[294]) just as the corresponding “naked” silicon vertices in the closely related **39**^[257] and **43**^[259] (see Table 4). Furthermore, the $SiTip_2$ bridge directly adjacent to the bridgehead atoms in all $E_2Si_4Tip_6$ species ($E = Si, Ge, Sn$) is strongly deshielded. However, somewhat surprisingly the deshielding effect enhances with increasing atomic number of the bridgehead atoms (Si_6Tip_6 **43**: $\delta^{29}Si = 174.6$ ppm; $Ge_2Si_4Tip_6$ **54a**: $\delta^{29}Si = 236.0$ ppm; $Sn_2Si_4Tip_6$ **54b**: $\delta^{29}Si = 284.5$ ppm). In the case of the all-silicon global minimum isomer of hexasilabenzene **43**, these large distributions of NMR chemical shifts were explained by the two nonbonding electrons at the bridgehead positions being involved in three-dimensional magnetically induced cluster currents (see Chapter 1.4.3.).^[259,269] However, theoretical calculations on the homologous series of parent compounds $E_2Si_4H_6$ ($E = Si, Ge, Sn, Pb$) revealed that the induced current strengths and topologies are almost identical in every case and therefore cannot explain the increasing deshielding going down the group. Additionally, relativistic effects were found to be negligible in this regard.^[294] During more in-depth investigations the HOMOs and LUMOs were found to be primarily located at the bridgehead vertices and the directly adjacent untethered $SiTip_2$ propeller blade with orthogonal symmetries, which is a geometrical prerequisite for the HOMO-LUMO excitation to contribute to the paramagnetic term of the chemical shielding tensor. With increasing atomic number of the bridgehead vertices, the HOMO-LUMO gap is narrowed. The paramagnetic term is progressively increasing, thus shifting the corresponding ^{29}Si NMR signal of the untethered propeller blade downfield.^[294] The overall downfield shift may thus be attributed to a synergy of magnetically induced

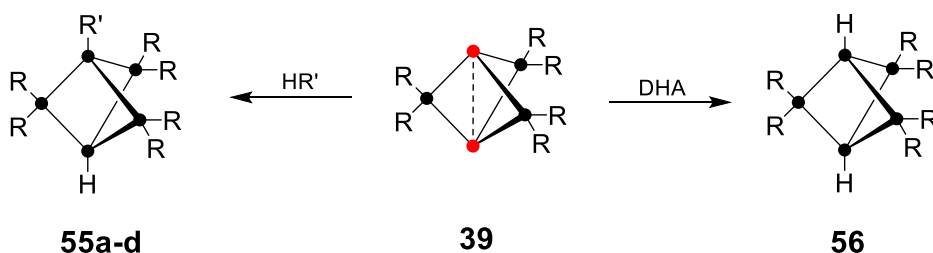
cluster currents (see Chapter 1.4.3.) and contributions of the HOMO-LUMO excitation to the paramagnetic term of the chemical shielding tensor. Heterosiliconoids **54a,b** are further examples that validate the hypothesis of the tunability of electronic properties of siliconoids by the implementation of heteroatoms.

All heteronuclear clusters discussed in this chapter do not feature a “naked”, hemispheroidally coordinated silicon atom as the “naked” vertices are occupied by the heavier germanium or tin atoms. Since they can be formally derived from their all-silicon counterparts, the designation as “heterosiliconoids” seems nonetheless to be justified.

1.4.5. Reactivity

The chemistry of siliconoids is obviously still in its infancy as the report on the first example (**31**) dates back only to 2005. Accordingly, the initial focus rested on the exploration of synthetic pathways and the comprehensive characterization of these compounds regarding both structural (Chapter 1.4.2.) and electronic features (Chapters 1.4.3. and 1.4.4.). As a consequence, relatively few examples of their reactivity have been reported to date. While in many cases thermally or photolytically induced rearrangement reactions, including cluster contraction or expansion, were observed (see previous chapters), there are also few examples of siliconoids being employed as actual reactants.

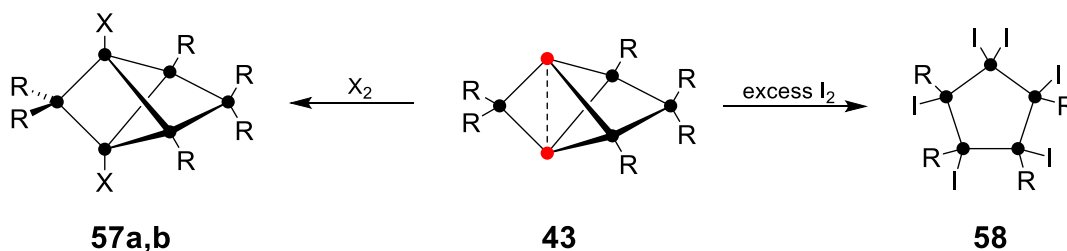
Preliminary reactivity studies on Breher's pentasila[1.1.1]propellane **39** were performed on NMR-tube scales in order to gain further insight into the nature of the central bridgehead bond. On the one hand, **39** shows closed-shell reactivity as HR' reagents (R' = OH, OPh, SPh) are readily added across the bridgehead bond to give the corresponding bicyclo[1.1.1]pentasilanes **55a-c** (Scheme 21). On the other hand, similar additions of the typical radical-type reagents Me₃SnH and H₂-sources such as 9,10-dihydroanthracene (DHA) indicate that **39** can also react as biradicaloid (Scheme 21).^[257] These findings provide experimental support for the theoretically manifested electronic ambiguity of the central bridgehead bonds in [1.1.1]propellanes.



Scheme 21: Closed-shell and biradical-type reactivity of the bridgehead bond in pentasila[1.1.1]propellane **39** (● = Si, ● = “naked” Si, R = Mes = 2,4,6-Me₃C₆H₂, DHA = 9,10-dihydroanthracene, **55a**: R' = OH, **55b**: R' = OPh, **55c**: R' = SPh, **55d**: R' = SnMe₃).^[257]

In contrast, heterosiliconoids **50a,b** with germanium and tin atoms in the bridgehead positions, respectively, are stable against H₂O, PhOH and DHA. However, both show radical-type reactivity as their treatment with FcS-SFc (Fc = ferrocene) results in the corresponding addition of the disulfide across the bridge upon homolytic S-S bond cleavage. While the Sn₂Si₃ species **50b** is inert towards Me₃SnH, the germanium analogue **50a** gives the corresponding addition product in quantitative yield.^[291] Once more, these findings underline the impact of heteroatom doping on electronic properties and thus reactivity of siliconoids.

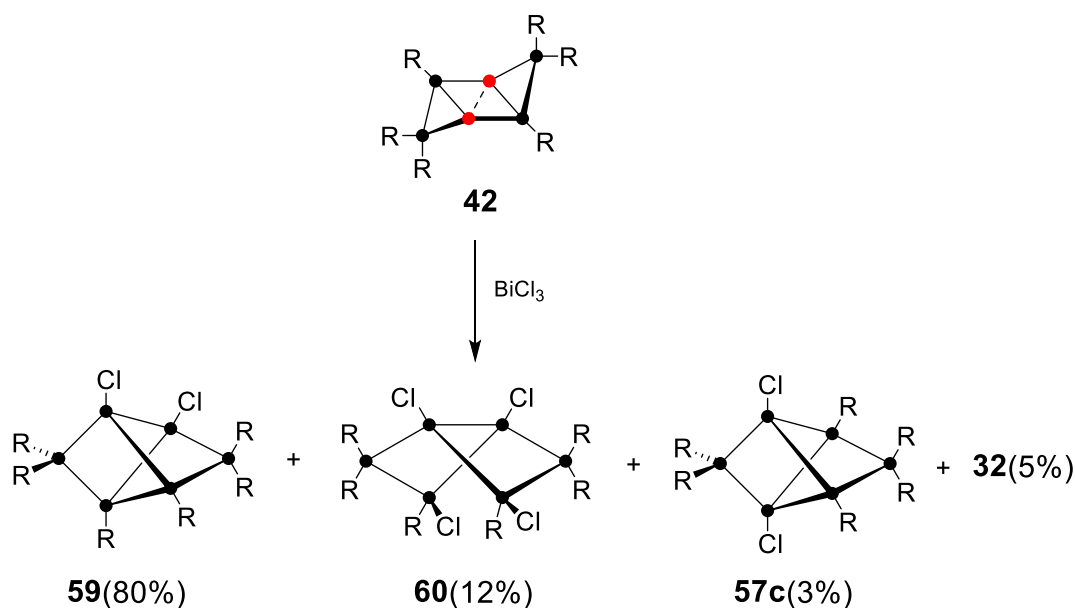
Addition of neat bromine and iodine to the bridgehead bond of the global minimum bridged propellane isomer of hexasilabenzene **43** affords the corresponding dihalogenated derivatives **57a** (X = Br) and **57b** (X = I) in 27% and 64% yield, respectively (Scheme 22). Treatment of **43** with an excess of iodine in refluxing toluene results in the formation of the highly functionalized, hexaiodinated pentasilane **58** by the expulsion of one silicon vertex (Scheme 22).



Scheme 22: Reaction of **43** with bromine and iodine to give the corresponding dihalogenated derivatives **57a,b** and its treatment with an excess of iodine to yield the hexaiodinated pentasilane **58** (● = Si, ● = “naked” Si, R = Tip = 2,4,6-*i*-Pr₃C₆H₂, **57a**: X = Br, **57b**: X = I).^[259]

The somewhat counterintuitive shortening of the bridgehead bond upon the addition of Br₂ (**57a**: 2.6547 Å) and I₂ (**57b**: 2.6810 Å) as compared to the siliconoid precursor **43** (2.7076 Å) was – following Bent's rule – attributed to an increased s-character of the cluster bonds causing an overall contraction of the silicon framework. The vertices of the now saturated cluster unsurprisingly show a much narrower distribution of ²⁹Si NMR chemical shifts ranging from δ = -77.4 ppm to δ = 21.2 ppm in the typical region for small saturated silicon rings, indicating the loss of the siliconoid-typical electronic anisotropy upon substitution of the former “naked” silicon vertices.

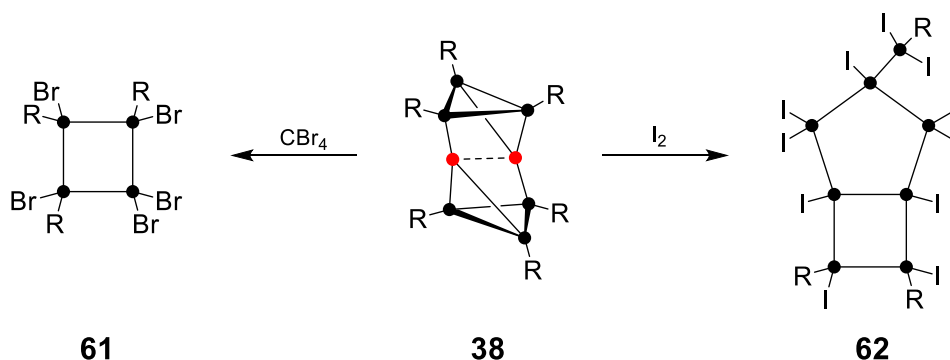
In contrast to the findings for **43**, the reaction of the dismutational isomer of hexasilabenzene **42** with bromine or iodine gives complex reaction mixtures, which could not be analyzed in further detail. Even with BiCl₃ as comparably mild chlorination agent, no uniform conversion to a single product was observed. In this case, however, the individual compounds could be isolated by extraction of the reaction mixture with hexane and subsequent fractional crystallization (Scheme 23).



Scheme 23: Reaction of **42** with BiCl₃; estimated yields in crude product are given in brackets (● = Si, ● = “naked” Si, R = Tip = 2,4,6-*i*-Pr₃C₆H₂).^[51]

The main product **59** displays a cluster scaffold reminiscent of the global minimum skeleton of **43**. In contrast to the observed 1,3-substitution during the reaction of **43** with bromine and iodine, the chlorine atoms end up adjacent to one another in 1,2 position. The corresponding 1,3-derivative **57c** is only formed as a side product in very low yield (3%). Further side products are the thermal rearrangement product of

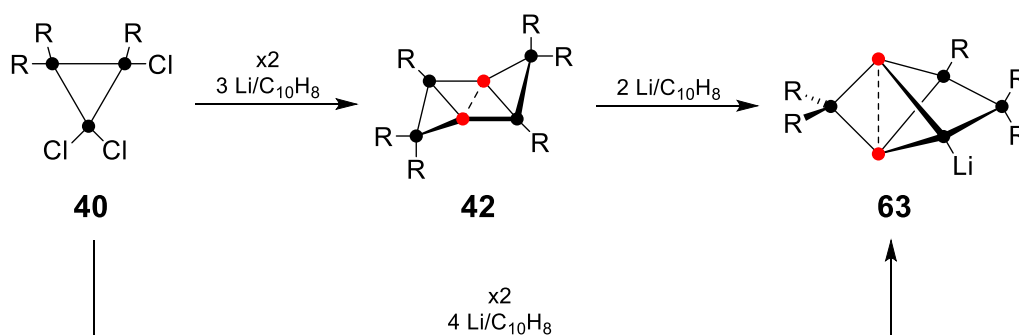
42, the global minimum isomer of hexasilabenzene **43** (5% yield) and the tetrachlorinated bicyclohexasilane **60** (12% yield). Since **60** could not be generated by treatment of a pure sample of **59** with BiCl_3 , σ -bond chlorination during the formation of **59** must take place prior to the chlorine addition to the “naked” bridgehead vertices. These initial studies demonstrate that the reactivity of the dismutational isomer of hexasilabenzene **42** is far from trivial and suggest more in-depth future investigations. The distance between the unsubstituted silicon vertices in Wiberg’s Si_8 siliconoid **38** (2.29 Å) is distinctively shorter than in other examples (see Table 3) indicating a stronger bond interaction. It could therefore be expected to be less prone towards addition reactions to the central Si_2 dumbbell. Indeed, treatment of **38** with mild halogenation reagents (CCl_4 , SnCl_4 , CBr_4 , I_2) does not result in the simple addition of X_2 ($\text{X} = \text{Cl}, \text{Br}, \text{I}$) to the bridgehead bond but rather results in multiple σ -bond oxidations.^[295] The reactions with CCl_4 and CBr_4 proceed via the cleavage of the silicon scaffold but with preservation of the number of substituents to give a trichlorocyclotrisilane and a pentachlorohousane species in the case of CCl_4 and the pentabrominated cyclotetrasilane **61** in the case CBr_4 (Scheme 24). In contrast, treatment of **38** with SnCl_4 and I_2 results in the halogenative cleavage of substituents, while the eight-atomic silicon framework is preserved, yet with different connectivity and shape. Thus, a hexachlorinated tetracyclooctasilane, and the silyl-substituted bicycloheptasilane **62** were obtained (Scheme 24).



Scheme 24: Reaction of Wiberg’s Si_8 siliconoid **38** with CBr_4 (cleavage of Si_8 framework, preservation of substituents) and I_2 (preservation of Si_8 framework, cleavage of substituents) to give cyclotetrasilane **61** and silyl-substituted bicycloheptasilane **62**, respectively.^[295]

1.4.6. Functionalized Siliconoids

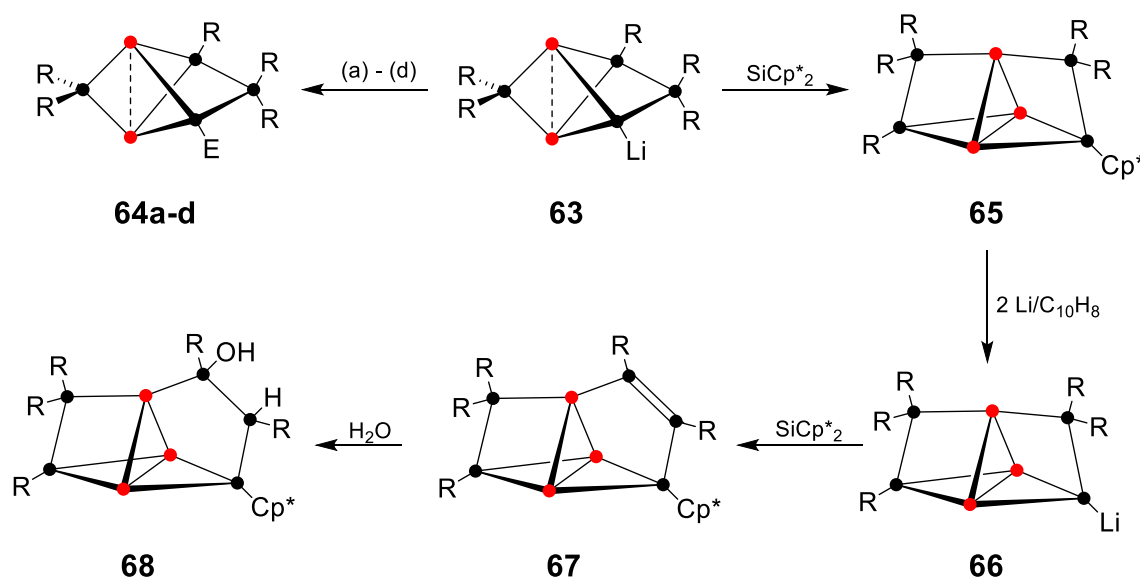
In order to apply molecular siliconoids as precursors for extended, possibly conjugated systems, the availability of functionalized derivatives is an inevitable prerequisite. As already discussed in the previous chapter, initial experimental investigations regarding the reactivity of siliconoids mainly involved addition reactions of suitable reagents across the bridgehead bonds between the “naked”, hemispheroidally coordinated vertices. As a consequence, the siliconoids are generally transformed into saturated, yet functionalized silicon clusters or rings that lack both typical structural and electronic features of siliconoids in all cases. In 2016, our group reported the reductive cleavage of a Tip-substituent from the dismutational hexasilabenzene isomer **42** to result in the anionic siliconoid **63** with a bridged propellane cluster scaffold identical to the global minimum hexasilabenzene isomer **43** in 62% yield (Scheme 25).^[296] With the two “naked”, hemispheroidally coordinated vertices, which are remarkably not compromised by the reduction, and the newly generated negatively charged silicon center, **63** constitutes the – at the time – missing link between neutral siliconoids (Chapter 1.4.2.) and bare, polyanionic Zintl clusters (Chapter 1.3.). Notably, the use of an additional equivalent of reducing agent during the synthesis of **42** directly yields the anionic siliconoid **63** in 51% yield, thus conveniently avoiding the isolation of **42**.



Scheme 25: Synthesis of anionic siliconoid **63** by the reduction of the dismutational hexasilabenzene isomer **42** or alternatively the direct reduction of the trichlorinated cyclotrisilane precursor **40** (● = Si, ● = “naked” Si, R = Tip = 2,4,6-*i*-Pr₃C₆H₂).^[296]

The distance between the unsubstituted vertices in **63** (2.5506 Å) is remarkably shorter in comparison to its neutral all-Tip substituted congener **43** (2.7076 Å). The retention of the hallmark electronic anisotropy in **63** is reflected in the ²⁹Si NMR data: While the signals for the “naked” silicon atoms expectedly appear at high field (δ = -237.3 ppm

and $\delta = -238.2$ ppm), the adjacent deshielded SiTip₂ moiety gives rise to a resonance at $\delta = 159.6$ ppm. In reactions with various electrophiles from the Groups 13 to 15, anionic siliconoid **63** was proven to be an excellent synthon for the transfer of the intact Si₆ siliconoid framework to give the first representatives of functionalized siliconoids **64a-d** (Scheme 26). In addition, treatment of **63** with decamethylsilicocene SiCp*₂ yields the Si₇ siliconoid **65** with three unsubstituted silicon vertices (Scheme 26), thus achieving the atomically precise expansion of the siliconoid cluster.^[297]



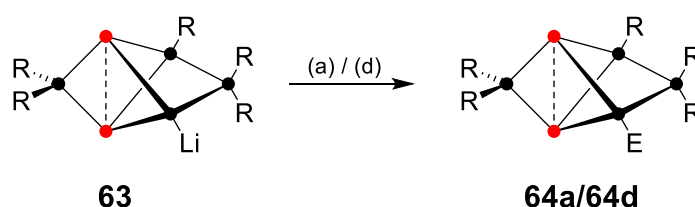
Scheme 26: Functionalization of the Si₆ cluster scaffold of **63** with various electrophiles from the Groups 13 to 15^[296] and cluster expansion to the Si₇ siliconoid **65** and the Si₈ siliconoids **67** and **68**^[297] (● = Si, ● = “naked” Si, R = Tip = 2,4,6-*i*-Pr₃C₆H₂, Cp* = 1,2,3,4,5-pentamethylcyclopentadienyl (a) BH₃·SMe₂, (b) ^tBuC(O)Cl, (c) SiCl₄, (d) ClP(NMe₂)₂. **64a**: E = BH₃⁻Li⁺; **64b**: E = C(O)tBu; **64c**: E = SiCl₃; **64d**: E = P(NMe₂)₂).

Reductive cleavage of the Cp*⁻-ligand in **65** and subsequent treatment of the corresponding anionic Si₇ species **66** with SiCp*₂ even lead to the Si₈ species **67**, which, however, could only be crystallized as the corresponding product of hydrolysis of the exohedral Si=Si bond **68**.

2. Aims and Scope

The report on the first isolation of an anionic siliconoid (**64**) provided two important pieces of information regarding the chemistry of siliconoids: (1) The reductive aryl-group cleavage from neutral siliconoids is a powerful synthetic tool for the generation of anionic derivatives without compromising the “naked”, unsubstituted vertices and (2) the intact silicon scaffold can be subsequently transferred to a variety of electrophiles from the Groups 13 to 15 in simple salt metathesis reactions. Based on preliminary results,^[298–300] a major objective of this work was the extension of the scope of the reductive cleavage of substituents to include other neutral siliconoid starting materials as well as the application of additional electrophilic main-group reagents to the anionic derivatives. The available data suggested that the electronic structure of the siliconoid cluster cores might be manipulated by peripheral functionalization. Therefore, the thorough investigation, comparison and possibly rationalization of the electronic influence of different peripherally attached functionalities were further central objectives of this thesis.

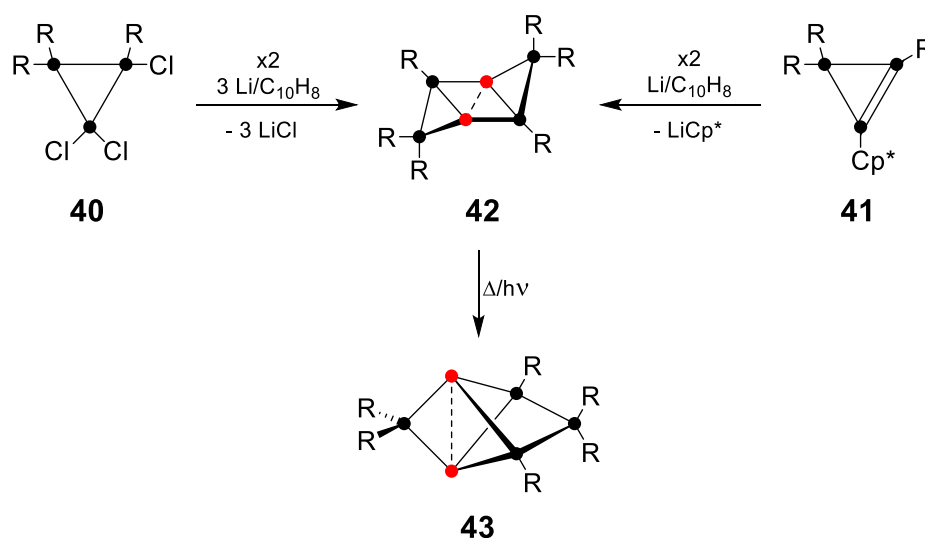
As already outlined in the introduction, siliconoids can be regarded as molecular model systems for silicon surfaces as their hemispheroidally coordinated vertices are highly reminiscent of the so called “dangling bonds” (Chapter 1.1.). The successful attachment of a Group 13 and a Group 15 atom to a siliconoid cluster core in the borate and phosphine substituted Si_6 siliconoids **64a** and **64d** is especially intriguing, as this represents a first step towards the extension of the given analogy to the industrially important technological process of silicon doping (Scheme 27).



Scheme 27: Synthesis of borate and phosphine substituted Si_6 siliconoids **64a** and **64d** (**64a**: $\text{E} = \text{BH}_3^- \text{Li}^+$, **64d**: $\text{E} = \text{P}(\text{NMe}_2)_2$, ● = Si, ● = “naked” Si, R = Tip = 2,4,6- $\text{Pr}_3\text{C}_6\text{H}_2$).

2. Aims and Scope

The logical next step would be the incorporation of dopant atoms into the cluster core itself, which was therefore another main objective of this work. The dismutational isomer **42** and the global minimum isomer **43** of the hypothetical hexasilabenzene are readily available as neutral Si_6 siliconoids by reduction of either the trichlorinated cyclotrisilane **40** or the Cp^* -functionalized low-valent cyclotrisilene **41** (Scheme 28).



Scheme 28: Syntheses of dismutational isomer **42** and global minimum isomer **43** of hexasilabenzene (\bullet = Si, \bullet = "naked" Si, R = Tip = 2,4,6- $\text{Pr}_3\text{C}_6\text{H}_2$).

By analogy, one possibly expedient synthetic strategy towards a molecularly doped siliconoid is the synthesis and subsequent reductive dimerization of precursors that already contain the desired heteroatom. Particularly encouraging in this regard is the successful isolation of mixed Group 14 heterosiliconoids by a similar approach (Scheme 20, Chapter 1.4.4.). Preliminary results in our group provided first evidence that reactions of lithium disilene **28** with low-valent phosphorus species in the formal oxidation state +I yield small Si_2P rings, which could be appropriate precursor molecules.

3. Results and Discussion

3.1. Site-selective functionalization of Si₆R₆ siliconoids

Yannic Heider*, Nadine E. Poitiers*, Philipp Willmes, Kinga I. Leszczyńska, Volker Huch, David Scheschkewitz, *Chem. Sci.* **2019**, *10*, 4523-4530.

<https://doi.org/10.1039/C8SC05591B>

These authors contributed equally.

The above cited article was published by the Royal Society of Chemistry (RSC) as an “Open Access” article and is licensed under a “Creative Commons Attribution-NonCommercial 3.0 Unported (CC BY-NC 3.0)” License (<https://creativecommons.org/licenses/by-nc/3.0/>).

The results described within this article are additionally concluded and put into context in Chapter 4.

Contributions of the Authors:

Yannic Heider: Lead: Synthesis, and characterization of privo-functionalized Si₆ siliconoids (R = CPh, COtBu, P(NMe₂)₂, SiCl₃, BH₃⁻); Equal (N.P.): Conceptualization, Visualization, Investigation, Methodology, Data Curation, Formal Analysis, Writing – Review and Editing of the Supporting Information; Equal (P.W.): Synthesis and characterization of privo-anionic Si₆ siliconoid; Supporting: Writing – Review and Editing of the manuscript.

Nadine E. Poitiers: Lead: Writing – Review and Editing of the manuscript, Synthesis and characterization of ligato-functionalized Si₆ siliconoids (R = TMS, CPh); Equal (Y.H.): Conceptualization, Visualization, Investigation, Methodology, Data Curation, Formal Analysis, Writing – Review and Editing of the Supporting Information

Philipp Willmes: Equal (Y.H.): Synthesis and characterization of privo-anionic Si₆ siliconoid; Lead: Synthesis and characterization of privo-TMS substituted Si₆ siliconoid; Supporting: Investigation, Methodology.

Kinga I. Leszczyńska: Supporting: Supervision.

Volker Huch: Lead: X-ray analysis.

David Scheschkewitz: Lead: Project administration, Supervision, Acquisition of funding and resources; Supporting: Writing – Review and Editing.

Cite this: *Chem. Sci.*, 2019, 10, 4523

All publication charges for this article have been paid for by the Royal Society of Chemistry

Received 14th December 2018
Accepted 7th March 2019

DOI: 10.1039/c8sc05591b

rsc.li/chemical-science

Introduction

Partially substituted neutral silicon clusters (siliconoids)^{1–4} are fleeting intermediates during the production of silicon from molecular precursors and can typically only be detected in the gas phase.^{5–9} The synthesis of stable derivatives has attracted considerable interest as the unsubstituted vertices of siliconoids are reminiscent of the free valences at bulk and nano surfaces of silicon, the so-called “dangling bonds”.^{10–13} Since the report on the first stable siliconoid Si₅R₆ with one “naked” vertex in a hemispheroidal coordination environment by one of us,¹⁴ numerous examples have been prepared by the groups of Wiberg,¹⁵ Breher,¹⁶ Kyushin,^{17,18} Iwamoto,¹⁹ Fässler²⁰ and ourselves.^{14,21–23} The Si₆R₆ isomers **1** (ref. 22) and **2** (ref. 23) are lower energy isomers of the hypothetical hexasilabenzene and as such prime examples of the often drastic differences between carbon and silicon (Scheme 1). While of the known C₆H₆ isomers, benzene is by far the lowest in energy, the tricyclic **2** corresponds to the global minimum isomer of Si₆H₆ and can therefore be considered as the silicon analogue of benzene on grounds of thermodynamic stability.^{23,24}

The functionalization of such clusters is a prerequisite for the further development of their chemistry and ultimately the

Krupp-Chair of General and Inorganic Chemistry, Saarland University, 66123 Saarbrücken, Germany. E-mail: scheschkewitz@mx.uni-saarland.de

† Electronic supplementary information (ESI) available: CCDC 1877380 (**5a**), 1877381 (**5b**), 1877378 (**4Li**), 1877379 (**6a**), 1877382 (**6c**), 1877383 (**6f**). For ESI and crystallographic data in CIF or other electronic format see DOI: 10.1039/c8sc05591b

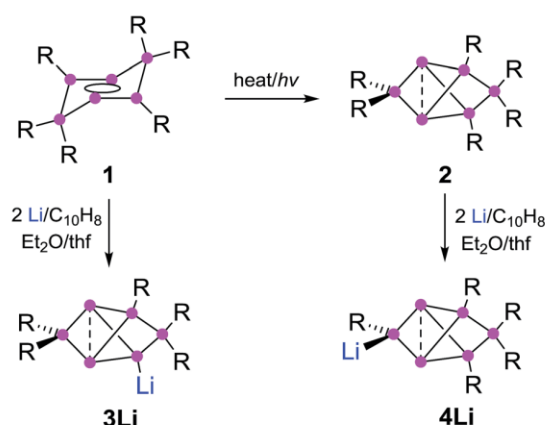
‡ These authors contributed equally.

Site-selective functionalization of Si₆R₆ siliconoids†

Yannic Heider,‡ Nadine E. Poitiers,[§] Philipp Willmes, Kinga I. Leszczyńska, Volker Huch and David Scheschkewitz^{§*}

The recent progress in the synthesis of partially substituted neutral silicon clusters (siliconoids) revealed unique structures and electronic anisotropies that are reminiscent of bulk and nano surfaces of silicon. Here, we report the selective 2-lithiation of the global minimum Si₆R₆ siliconoid at a different vertex than in the previously reported isomeric 4-lithiated derivative (R = 2,4,6-triisopropylphenyl). In order to enable an intuitive distinction of the vertices of the global minimum Si₆R₆ scaffold (which can be considered the silicon analogue of benzene in terms of thermodynamic stability), we introduce a novel nomenclature in analogy to the *ortho*–*meta*–*para* nomenclature of disubstituted benzenes. By treatment of the 2-lithiated Si₆ cluster with Me₃SiCl, SiCl₄, H₃B·SMe₂, (Me₂N)₂PCl as well as with carboxylic acid chlorides RCOCl (R = ^tBu, Ph) various 2-functionalized Si₆ clusters were obtained and characterized in solution and – in most cases – the solid state. The structural and spectroscopic effect of the position of the newly introduced functional group is discussed by comparison to the corresponding 4-functionalized derivatives.

application of their fascinating electronic properties in extended materials. Compared to the related Zintl anions of the heavier group 14 elements,^{25–31} which are (poly)anionic, completely unsubstituted deltahedral clusters, siliconoids are partially substituted yet exhibit a similarly wide dispersion of ²⁹Si NMR shifts.^{14,16–18,22,24} Very recently, the protonation of silicon Zintl anions to partially H-substituted anionic siliconoids was reported independently by the groups of Fässler and Gschwind/Korber.^{30,31} We had previously described the reductive functionalization of the dismutational Si₆R₆ isomer **1** to the



Scheme 1 Synthesis of **3Li** (ref. 32) and **4Li** (this work) from dismutational hexasilabenzene isomer **1** and from the global minimum isomer **2** (Tip = 2,4,6-triisopropylphenyl).



anionic siliconoid **3Li** as well as its reactivity with several representative electrophiles of groups 13 to 15.^{32,33}

Herein, we show that reduction of the global minimum isomer **2** under similar conditions selectively affords the regiomeric anionic Si₆ siliconoid **4Li** instead of **3Li** by cleavage of an aryl substituent in the 2-position of the bridged propellane scaffold (Scheme 1). In order to account for the rapidly increasing number of species with the thermodynamically favored bridged-propellane scaffold and unequivocally distinguish between the different vertices, we propose a novel terminology for this structural motif, inspired by the well-established *ortho*–*meta*–*para* nomenclature for disubstituted benzenes.^{34–37} The functionalization of **3Li** and **4Li** with selected electrophiles is shown to result in several sets of regiomeric derivatives allowing for the systematic comparison of the structural and spectroscopic consequences of the functional group's position.

Results and discussion

Nomenclature of Si₆ siliconoids

Structures with [1.1.1]propellane motif have intrigued experimentalists and theorists alike ever since the early 1970s,^{38,39} because of their non-classical structure containing bridgehead atoms in an umbrella-type hemispheroidal coordination environment. The bonding situation between the bridgehead atoms of [1.1.1]propellanes can be described by biradical or ionic contributions to the electronic ground state^{40–43} and was discussed by Shaik *et al.* as a “charge-shift-bond”.^{44,45} The Si₆ siliconoids **2** and **3Li** show a closely related structure having two propeller blades bridged by one SiTip₂ moiety. Strongly deshielded ²⁹Si NMR signals had been explained by a cluster-like delocalization of the two electrons in question.²³ Electron density determinations of the Si₆ siliconoid **2** confirmed the absence of direct bonding between the bridgehead silicon vertices.⁴⁶ For nomenclature purposes,^{47,48} the Si₆ scaffold is nonetheless formally considered as tetracyclic system with a direct connection between the hemispheroidally coordinated vertices that are depicted in the schemes as a dashed line.

The high thermodynamic stability of Si₆ siliconoid **2** as the alleged global minimum of the Si₆H₆ potential energy surface^{23,24} suggests a considerable prevalence of this structural motif. This received first corroboration by the successful synthesis of mixed group 14 systems⁴⁹ and a Sn₆ derivative recently.⁵⁰ Saturated variations of the six-atom scaffold occur in numerous other species throughout main group chemistry.^{51–54} In the past, the tetracyclic core structure has been variously referred to as “edge-capped trigonal bipyramid”⁵⁵ “doubly edge-bridged tetrahedron”⁵⁶ or “bridged propellane”.²³ As these terminologies do not seem to do justice to the ubiquity of the structural motif, we propose a novel term that echoes the relationship to the iconic benzene molecule and – at the same time – takes into account the extraordinary polarization of **2** and related species.^{39,57–64} We thus suggest the term “benzpolarene” – in analogy to benzvalene – for the tetracyclic arrangement of vertices in the cluster core of **2** and **3Li**. In addition, we feel that the availability of the first Si₆ siliconoid regiomers described

herein requires a descriptive nomenclature not unlike the well-established *ortho*, *meta* and *para* prefixes used for disubstituted benzenes. The prefixes thus proposed in the following reflect the characteristic bonding situation of each vertex (Chart 1).

The latin words for “naked” (lat. nudus), “bonded” (lat. ligatus), “remote” (lat. remotus) and “deprived” (lat. privus) served as inspirations. The *nudo* prefix is assigned to the unsubstituted (“naked”) bridgehead silicon atoms in 1,3-position, the *ligato* prefix to the mono-substituted vertices (4,6-position) bonded to one substituent each, the *remoto* prefix to the remote bridge in 5-position and the *privo* prefix to the characteristically deshielded (“deprived” of electrons) atom in 2-position.

Functionalization in *ligato* position

In addition to the previously reported persilabenzpolarenes,^{32,33} we investigated two further reactions of siliconoid **3Li** with electrophiles. The novel *ligato* functionalized siliconoids **5a,b** were thus obtained by treatment of **3Li** in benzene at room temperature with Me₃SiCl and benzoyl chloride, respectively (Scheme 2). The reactions proceed quantitatively according to ²⁹Si NMR spectroscopy. The siliconoids **5a,b** were isolated as single crystals and fully characterized by X-ray analysis, NMR spectroscopy, UV/Vis (Table 1) and by IR spectroscopy in case of the CO containing species.

The ²⁹Si NMR spectra of **5a,b** show the typical distribution of chemical shifts for *ligato* functionalized persilabenzpolarenes as recently reported by our group for **5c–f**.^{32,33} The two unsubstituted bridgehead silicon atoms give rise to two ²⁹Si signals in a range of –257 to –280 ppm (Table 1). The C_{2v} symmetry of the benzpolarene scaffold of **2** is lowered to C_s in the substituted cases. As we had shown by VT NMR studies for some of the *ligato*-functionalized species,³² hindered rotation further reduces the symmetry so that the two seemingly identical *nudo* atoms become diastereotopic. The resonances of the SiTip₂ groups in *privo* position are strongly deshielded with signals at 169.9 (**5a**) and 174.7 ppm (**5b**). The surprisingly downfield shifted signals (for tetracoordinate silicon atoms) had been rationalized by invoking magnetically induced cluster currents or – in a complementary manner – by the strong LUMO contribution at this atom.^{49,65,66} The ²⁹Si NMR chemical shifts of the remaining cluster vertices are located in the typical range for saturated silicon atoms and vary only slightly with the introduced functionality. The longest wavelength absorption bands in the UV/Vis are observed at λ_{max} = 459 nm (**5a**) and 477 nm (**5b**). The characteristic CO stretching mode in the IR of **5b** at ν = 1605 cm^{–1} compares well with that of **5c**.^{32,33} Single crystals

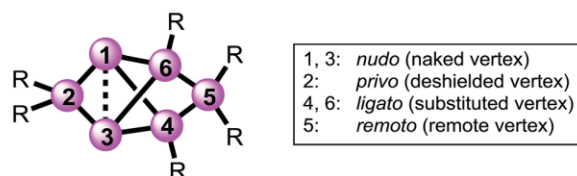
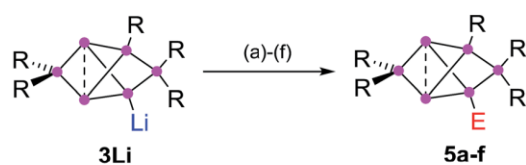


Chart 1 Proposed prefixes for unique assignment of vertices in bridged propellane-type (“benzpolarene”) siliconoids.





Scheme 2 Synthesis of *ligato*-functionalized siliconoids **5a–f**. Reagents: (a) Me_3SiCl , (b) PhCOCl , (c) ${}^t\text{BuCOCl}$, (d) $\text{CIP}(\text{NMe}_2)_2$, (e) SiCl_4 , (f) $\text{BH}_3 \cdot \text{SMe}_2$. **5a**: E = Me_3Si , **5b**: E = COPh and the previously reported³² **5c**: E = CO^tBu , **5d**: E = $\text{P}(\text{NMe}_2)_2$, **5e**: E = SiCl_3 , **5f**: E = BH_3^- .

were obtained in 45% (**5a**) and 66% (**5b**) yield and the structures confirmed by X-ray diffraction studies (Fig. 1).⁶⁷ The distances between the unsubstituted bridgehead silicon atoms Si1 and Si3 are slightly shorter than in the global minimum isomer,²³ in line with the observations for the previously reported *ligato* functionalized persilabenzpolarenes **3Li** and **5c–f**.^{32,33} The distance between the *ligato* positions Si4 and Si6 of **5a–f** increases with decreasing distance between the *nudo* positions Si1 and Si3, presumably in order to minimize strain (Table 1). Apparently, the variation of the *ligato* functionality of the benzpolarene structures **5a–f** directly influences the bonding between the unsubstituted silicon atoms Si1 and Si3.

Synthesis of *privo* lithiated siliconoid **4Li**

The reduction of the dismutational isomer of hexasilabenzene **1** had yielded the lithiated siliconoid with a benzpolarene scaffold **3Li** and thus a functionalized derivative of the Si_6H_6 global minimum isomer **2**.^{32,33} In order to probe the possible intermediacy of **2**, its reduction with lithium/naphthalene was investigated (Scheme 3).

Treatment of **2** with 2.2 equivalents of $\text{Li}/\text{C}_{10}\text{H}_8$ in Et_2O and thf indeed results in the complete and uniform conversion into

a novel anionic Si_6 species as confirmed by ${}^{29}\text{Si}$ NMR spectroscopy. The six resonances show a similar chemical shift distribution as in **3Li**, but with distinctly different values suggesting the functionalization had taken place in another position of the benzpolarene scaffold (Table 1). The reduction product **4Li** was fully characterized by X-ray diffraction on single crystals, NMR spectroscopy and UV/Vis spectroscopy.

A strongly deshielded ${}^{29}\text{Si}$ NMR signal at 267.9 ppm is significantly broadened (presumably due to coupling to the quadrupolar ${}^7\text{Li}$ -nucleus) and only shows a cross-peak to the aromatic H atoms of a single Tip ligand in the 2D ${}^1\text{H}/{}^{29}\text{Si}$ correlation spectrum. These observations led us to conclude that the anionic functionality of **4Li** is located at the tetra-coordinate silicon atom in the *privo* position Si2. The ${}^{29}\text{Si}$ chemical shift of 267.9 ppm is particularly remarkable as saturated silyl anions typically show resonances at much higher field often deep in the negative ppm region.⁶⁹ According to our previous calculations,⁶⁶ the magnetically induced cluster currents circumvent the *privo* position and thus cause its pronounced deshielding even in case of the peraryl-substituted benzpolarene **2**. On the basis of a complementary explanation referring to the topology of the LUMO,⁴⁹ this phenomenon is probably due to the pronounced silylene character of the *privo* atom. The presence of a directly attached electron-releasing substituent could lead to an increased localization of the vacant p orbital in the *privo* position and thus to the observed even more pronounced deshielding. The signals for the *remoto* SiTip_2 and the two *ligato* SiTip units appear at $\delta = 15.3$ and $100.2/-43.8$ ppm, respectively. The reason for the large difference between the chemical shifts is unclear although the electronic environments of the *ligato* atoms are certainly dominated by their relative position to the anionic functionality and the lithium counter cation in *privo* position. The unsubstituted bridgehead silicon atoms in the *nudo* positions are apparently

Table 1 Comparison of NMR spectroscopic and structure data of *ligato* functionalized siliconoids **5a–f** and *privo* functionalized siliconoids **6a–f**

Position of E	Comp.	Functional group (E)	Si1, Si3 [ppm]	Si2 [ppm]	Si4 [ppm]	λ_{max} [nm]	$\Delta\text{Si1–Si3}$ [Å]	$\Delta\text{Si4–Si6}$ [Å]	$\sigma_m^{a,67}$	Hemispheroidality ^b ϕ [Å]
—	2	Tip ²³	–274.2	174.6	–7.5	473	2.7076(8)	2.9037	0.08	1.3535
<i>ligato</i>	3Li	Li ³²	–230.9, –232.6	152.2	–66.8	364	2.5506(9)	3.2243	—	1.2805
<i>privo</i>	4Li	Li	–222.2, –231.4	267.9	–43.8	468	2.5562(10)	2.9171(11)	—	1.3078
<i>ligato</i>	5a	TMS	–257.8, –266.6	169.9	–3.7	459	2.6176(5)	2.9643(8)	–0.04	1.3283
<i>ligato</i>	5b	COPh	–263.0, –279.0	174.7	–26.5	477	2.6598(9)	2.8854(8)	0.34	1.3333
<i>ligato</i>	5c	CO^tBu ³²	–264.7, –271.1	171.8	–27.4	475	2.6430(6)	2.9095	0.27	1.3458
<i>ligato</i>	5d	$\text{P}(\text{NMe}_2)_2$ (ref. 32)	–256.0, –261.4	168.7	–33.8	475	2.6231(5)	2.9508	0.18	1.3498
<i>ligato</i>	5e	SiCl_3 (ref. 32)	–252.3, –264.2	175.4	12.9	460	2.635(1)	2.8920	0.48	1.3409
<i>ligato</i>	5f	BH_3 (ref. 32)	–257.3, –265.0	161.2	–4.8	475	2.620(1)	2.9988	–0.48	1.3153
<i>privo</i>	6a	TMS	–242.0, –253.3	193.6	–15.9	469	2.6118(6)	2.9482(6)	–0.04	1.3308
<i>privo</i>	6b	COPh	–268.5, –271.1	166.2	–16.2	—	—	—	0.34	—
<i>privo</i>	6c	CO^tBu	–263.1, –265.8	173.1	–14.5	473	2.6350(5)	2.9641(7)	0.27	1.3439
<i>privo</i>	6d	$\text{P}(\text{NMe}_2)_2$	–246.0, –256.1	186.5	–16.9	—	—	—	0.18	—
<i>privo</i>	6e	SiCl_3	–251.6, –258.9	161.7	–6.4	—	—	—	0.48	—
<i>privo</i>	6f	BH_3^-	–243.3, –255.6	237.3	–28.8	454	2.6024(8)	2.9431(7)	–0.48	1.3155

^a For substituents BH_3^- and Tip no Hammett parameters are available. The Hammett parameters of similar compounds were used for the correlation plots in Fig. 4: $\text{B}(\text{OH})_3^-$ for BH_3^- and $(\text{C}_6\text{H}_5)_4\text{C}(\text{HMe}_2)$ for the Tip substituent (see ref. 68). ^b The hemispheroidality ϕ is the distance of a naked cluster vertex from the plane spanned by its three substituents. Its value is taken as a measure for the degree of hemispheroidality of the vertex. For a detailed explanation see ref. 4.



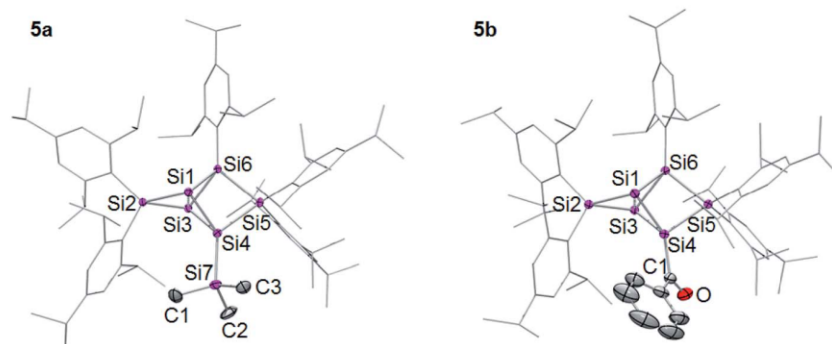
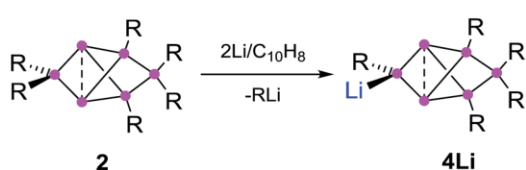


Fig. 1 Structures of **5a,b** in the solid state (thermal ellipsoids at 50% probability). Hydrogen atoms and co-crystallized pentane omitted. a: E = SiMe₃, b: E = COPh.



Scheme 3 Synthesis of *privo*-lithiohexasilabenzpolarene **4Li** by reduction with 2 equivalents of Li/C₁₀H₈.

not compromised by the reduction and give rise to two signals at the usual high field at $\delta = -222.2$ and -231.4 ppm, comparable to the corresponding signals of the *ligato* lithiated **3Li**. The constitution of the reduction product of benzpolarene **2** was finally proven as the *privo* functionalized **4Li** by X-ray diffraction on single crystals (Fig. 2).⁶⁷

The distance between the bridgehead silicon atoms (Si1–Si3 2.5562(10) Å) is similar to that in **3Li**, but shorter than in the fully Tip-substituted siliconoid **2** and the *ligato* functionalized siliconoids **5a–b**. This shortening is tentatively attributed to delocalization of the lone-pair of the anionic silicon vertex into cluster bonding orbitals. The formation of the two regioisomeric derivatives is predominantly a consequence of the

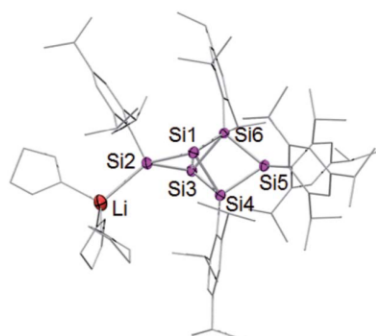


Fig. 2 Structure of **4Li** in the solid state (thermal ellipsoids at 50% probability). Hydrogen atoms and co-crystallized solvent molecules omitted.

different topologies of the LUMOs of both the dismutational Si₆R₆ isomer **1** and the benzpolarene isomer **2**. The initial reduction plausibly occurs at the unsubstituted vertices of the starting materials (A, D), which provide dominant contributions to the respective LUMOs.^{22,23} Other important LUMO contributions are located precisely at the silicon vertices to which the preferentially eliminated aryl groups are bonded. The subsequent isomerizations are likely driven by the very low energy of the benzpolarene scaffold (Scheme 4). The lithiated regioisomer **3Li** is formed due to a *syn* TipLi elimination (B) followed by a cyclobutene–bicyclobutane rearrangement (C). In case of the reduction of the benzpolarene isomer **2**, we suggest an orbital- and strain-controlled TipLi elimination followed by a 1,2-migration of the lithium counteraction (F) to yield **4Li**.

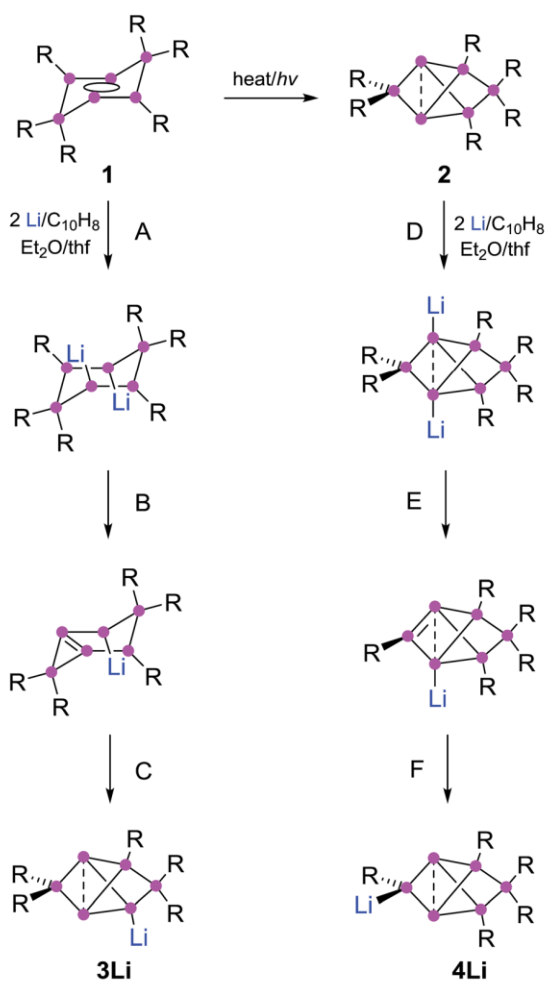
Functionalization in *privo* position

In order to evaluate the suitability of *privo* lithiated siliconoid **4Li** as nucleophilic transfer reagent for the intact unsaturated Si₆ scaffold, we treated it with several electrophiles (Me₃SiCl, PhCOCl, ^tBuCOCl, CIP(NMe₂)₂, SiCl₄, BH₃·SMe₂). Indeed, the corresponding *privo* substituted siliconoids **6a–f** are obtained by straightforward combination of the reagents in toluene at room temperature (Scheme 5).

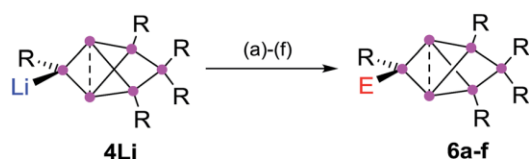
According to ²⁹Si NMR spectra, the reactions lead to full conversion of **4Li** to the *privo* functionalized siliconoids **6a–f**. Crystallization of **6a,c,f** from concentrated hexane solutions affords single crystals in moderate to good yields (**6a**: 66%; **6c**: 27%; **6f**: 78%), which were fully characterized by multinuclear NMR spectroscopy, UV/Vis spectroscopy and X-ray diffraction (Fig. 3).⁶⁷ In case of **6b,d,e**, the reactions were only performed on the NMR scale and characterized by multinuclear NMR spectroscopy. The ²⁹Si NMR data of the *privo* substituted species display a similarly wide dispersion in chemical shifts as the corresponding *ligato* isomers. The ²⁹Si NMR spectra of **6a–f** thus show two signals in the high-field region for the *nudo* positions and a strongly deshielded signal for the *privo* silicon atom, which carries one Tip substituent and the functional group E in this case.

The UV/Vis spectra of the isolated products **6a,c,f** and **4Li** show the position of the longest wavelength absorption





Scheme 4 Mechanistic explanation of the regioselective formation of 3Li and 4Li.



Scheme 5 Synthesis of *privo*-functionalized siliconoids 6a–d. Reagents: (a) Me_3SiCl , (b) PhCOCl , (c) ${}^t\text{BuCOCl}$, (d) $\text{CIP}(\text{NMe}_2)_2$, (e) SiCl_4 , (f) $\text{BH}_3 \cdot \text{SMe}_2$. 6a: E = Me_3Si , 6b: E = COPh , 6c: E = CO^tBu , 6d: E = $\text{P}(\text{NMe}_2)_2$, 6e: E = SiCl_3 , 6f: E = BH_3^- .

maximum to strongly depend on the substituents of the Si_6 scaffold (λ_{max} : 6a 469 nm; 6c 473 nm; 6f 454 nm; 4Li 468 nm). As in case of the *ligato* functionalized species, it can presumably be assigned to the vertical HOMO–LUMO singlet excitation.

The distances between the bridgehead silicon atoms Si_1 – Si_3 in the crystal structure of 6a,c,f (6a 2.6118(6), 6c 2.6350(5), 6f 2.6024(6) Å) are longer than in the *ligato* lithiated siliconoid 3Li^{32,33} and *privo* lithiated siliconoid 4Li, but slightly shorter than

in the *ligato* functionalized siliconoids 5a,c,f. This is in line with a more effective σ donation in the *privo* position. While for siliconoids 5a–f, a reciprocal interdependency between the distances of Si_1 – Si_3 and Si_4 – Si_6 is observed, no such relationship is present in case of the *privo* functionalized siliconoids 6a–f.

The ${}^{29}\text{Si}$ NMR resonances of the *privo* silicon atom are strongly influenced by the nature of the pending functionality. The signal is shifted to higher field with increasing electron-withdrawing power of the substituent: $\text{Li} > \text{BH}_3 > \text{TMS} > \text{P}(\text{NMe}_2)_2 > \text{Tip} > \text{CO}^t\text{Bu} > \text{COPh} > \text{SiCl}_3$. This sequence correlates nicely with the Hammett parameter σ_m ,^{70–73} which is based on the relative reaction kinetics of a second substitution in the *meta* position of benzene relative to the functionality in question.

Correlation with Hammett parameters σ

Fig. 4 shows the two correlations between the ${}^{29}\text{Si}$ NMR chemical shift at the *privo* position of compounds 2, 5a–f and 6a–f and the Hammett parameter σ_m drawn separately for the two synthetically accessible positions of the functional group. The correlations with the σ_p Hammett parameter are similar, but slightly less satisfactory (see ESI†).

The plot for the *ligato* functionalized compounds 5a–f (Fig. 3, top) shows a linear relationship ($R^2 = 0.912$). The response of the ${}^{29}\text{Si}$ chemical shift, however, is moderate as indicated in its range (160 to 180 ppm) and the resulting slope ($m = 14.346$ ppm). Electron-withdrawing substituents in *ligato* position result in a stronger deshielding of the *privo* atom in the ${}^{29}\text{Si}$ NMR (5b,c,d,e) while electron-donating groups exert the opposite effect (5a,f). The σ_m value for the Tip substituent (red triangle in Fig. 4) had to be approximated by that of C_6H_5 -4-CHMe₂ (ref. 68) and was therefore disregarded for the linear fit. Surprisingly, there is no apparent correlation of the Hammett parameters with the ${}^{29}\text{Si}$ chemical shifts of the *nudo* silicon atoms Si_1 and Si_3 (Table 1).

In case of the *privo* functionalized benzpolarenes (6a–f), the correlation of the Hammett parameters σ_m is even better with a very good linear dependency ($R^2 = 0.978$). This is due to a markedly stronger response than in case of *ligato* functionalization with a slope of $m = -79.76$ ppm and a consequently larger chemical shift range (160 to 240 ppm). The stronger influence of the functional group is readily explained by its direct attachment to the silicon atom in question (Si_2) vs. an additional distance of two Si–Si bonds in case of *ligato* functionalization. Remarkably, the slope of the linear fit is negative proving a reciprocal relationship between the electron-withdrawing strength of the substituent and its deshielding effect in the *privo* position. We had shown previously that the formal substitution of the *nudo* silicon atoms by germanium or tin results in a pronounced deshielding of the *privo* positions as well, which we tentatively rationalized by the strong influence of the LUMO shape on the paramagnetic contribution to the chemical shift.⁴⁹

In contrast to our findings, in the case of mono-substituted carbon-based benzenes, the correlation of the Hammett parameter σ_p with the chemical shift of the *para*-carbon atom is known,⁷⁴ i.e. the ring atom opposite to the one carrying the functional group.



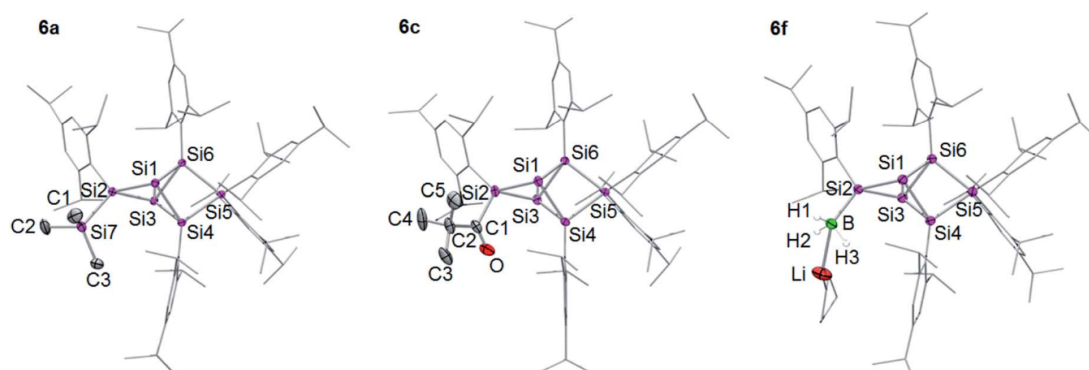


Fig. 3 Structures of **6a**, **6c** and **6f** in the solid state (thermal ellipsoids at 50% probability). Hydrogen atoms and co-crystallized solvent molecules omitted. a: E = TMS, c: E = CO^tBu, f: E = BH₃⁻.

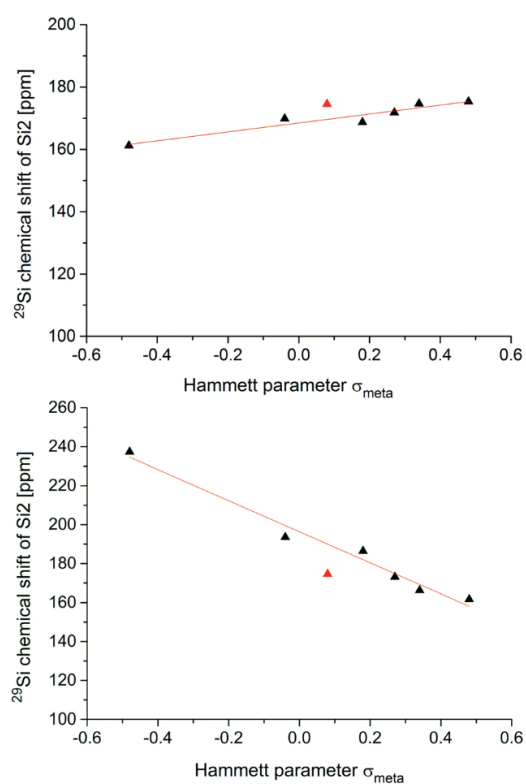


Fig. 4 Plots of the Hammett parameters σ_m vs. ^{29}Si chemical shifts of the *privo* silicon vertices of *ligato* (**5a–f**; top) and *privo* functionalized hexasilabenzpolarenes (**6a–f**; bottom). The data pair marked with red triangles corresponds to the unfunctionalized hexaaryl derivative **2**.

Conclusion

Si₆ siliconoids **1** and **2** can be selectively reduced to yield derivatives of the global minimum isomer of the Si₆H₆ potential energy surface with an anionic functionality at distinct vertices. In order to distinguish between the different positions of the

tricyclic Si₆ scaffold, we propose a nomenclature that refers to the characteristic environment of the four conceivable symmetry-independent positions: *nudo*, *privo*, *ligato* and *remoto*. The anisotropic electronic structure of the global minimum Si₆H₆ scaffold is accounted for by the introduction of “benzpolarene” as unique name for this ever more frequently occurring structural motif. The *privo* lithiated hexasilabenzpolarene is accessible by reductive cleavage of one of the Tip groups of the perarylated derivative, while the *ligato* lithiated isomer had been obtained from the dismutational isomer previously. The *privo* derivative is shown to be an equally suitable nucleophilic reagent for the transfer of the uncompromised benzpolarene framework. The electronic influence of the functional groups in two distinct positions is rationalized on the basis of linear correlations with the Hammett parameter σ_m . With the possibility of functionalization in different positions of the Si₆ scaffold the construction of larger systems comprising Si₆ siliconoid motifs has become a viable option, which is currently being investigated in our laboratory.

Conflicts of interest

There are no conflicts to declare.

Acknowledgements

Funding by the Deutsche Forschungsgemeinschaft (DFG SCHE906/4-1 and 4-2) and COST Action CM1302 (Smart Inorganic Polymers) is gratefully acknowledged.

Notes and references

- 1 F. Breher, *Coord. Chem. Rev.*, 2007, **251**, 1007.
- 2 T. Iwamoto and S. Ishida, *Chem. Lett.*, 2014, **43**, 164.
- 3 S. Kyushin in *Organosilicon Compounds: Theory and Experiment (Synthesis)*, ed. V. Y. Lee, Academic Press, 2017, vol. 1, ch. 3.
- 4 Y. Heider and D. Scheschkewitz, *Dalton Trans.*, 2018, **47**, 7104.
- 5 T. M. I. Davidson, *J. Organomet. Chem.*, 1970, **24**, 97.



- 6 G. A. Rechtsteiner, O. Hampe and M. F. Jarrold, *J. Phys. Chem. B*, 2001, **105**, 4188.
- 7 H. Murakami and T. Kanayama, *Appl. Phys. Lett.*, 1995, **67**, 2341.
- 8 W. M. M. Kessels, M. C. M. Van De Sanden and D. C. Schram, *Appl. Phys. Lett.*, 1998, **72**, 2397.
- 9 M. Watanabe, H. Murakami, T. Miyazaki and T. Kanayama, *Appl. Phys. Lett.*, 1997, **71**, 1207.
- 10 Y. Ge and J. D. Head, *Int. J. Quantum Chem.*, 2003, **95**, 617.
- 11 G. Hadjisavvas, G. Kopidakis and P. Kelires, *Phys. Rev. B*, 2001, **64**, 125413.
- 12 M. F. Jarrold, *Science*, 1991, **252**, 1085.
- 13 H. Neergaard Waltenburg and J. T. Yates Jr, *Chem. Rev.*, 1995, **95**, 1589.
- 14 D. Scheschkewitz, *Angew. Chem., Int. Ed.*, 2005, **44**, 2954.
- 15 G. Fischer, V. Huch, P. Payer, S. K. Vasisht, M. Veith and N. Wiberg, *Angew. Chem., Int. Ed.*, 2005, **44**, 7884.
- 16 D. Nied, R. Köppe, W. Klopper, H. Schnöckel and F. J. Breher, *Am. Chem. Soc.*, 2010, **132**, 10264.
- 17 A. Tsurusaki, C. Iizuka, K. Otsuka and S. Kyushin, *J. Am. Chem. Soc.*, 2013, **135**, 16340.
- 18 S. Ishida, K. Otsuka, Y. Toma and S. Kyushin, *Angew. Chem., Int. Ed.*, 2013, **52**, 2507.
- 19 T. Iwamoto, N. Akasaka and S. Ishida, *Nat. Commun.*, 2014, **5**, 5353.
- 20 L. J. Schiegerl, A. J. Karttunen, W. Klein and T. F. Fässler, *Chem. Eur. J.*, 2018, **24**, 19171.
- 21 K. Abersfelder, S. Russell, H. S. Rzepa, A. J. P. White, P. R. Haycock and D. Scheschkewitz, *J. Am. Chem. Soc.*, 2012, **134**, 16008.
- 22 K. Abersfelder, A. J. P. White, H. S. Rzepa and D. Scheschkewitz, *Science*, 2010, **327**, 564.
- 23 K. Abersfelder, A. J. P. White, R. J. F. Berger, H. S. Rzepa and D. Scheschkewitz, *Angew. Chem., Int. Ed.*, 2011, **50**, 7936.
- 24 M. Moteki, S. Maeda and K. Ohno, *Organometallics*, 2009, **28**, 2218.
- 25 E. Zintl and A. Z. Harder, *Z. Phys. Chem. Abt. A*, 1931, **154**, 47.
- 26 F. T. Fässler, *Struct. Bond.*, 2011, **140**, 91.
- 27 S. Scharfe, F. Kraus, S. Stegmaier, S. Schier and T. F. Fässler, *Angew. Chem., Int. Ed.*, 2011, **50**, 3630.
- 28 J. M. Goicoechea and S. C. Sevov, *J. Am. Chem. Soc.*, 2004, **126**, 6860.
- 29 M. Waibel and T. F. Fässler, *Inorg. Chem.*, 2013, **52**, 5861.
- 30 T. Henneberger, W. Klein and T. F. Fässler, *Z. Anorg. Allg. Chem.*, 2018, **644**, 1018.
- 31 C. Lorenz, F. Hastreiter, K. Hioe, N. Lokesh, S. Gärtner, N. Korber and R. M. Gschwind, *Angew. Chem., Int. Ed.*, 2018, **57**, 12956.
- 32 P. Willmes, K. Leszczyńska, Y. Heider, K. Abersfelder, M. Zimmer, V. Huch and D. Scheschkewitz, *Angew. Chem., Int. Ed.*, 2016, **55**, 2907.
- 33 K. I. Leszczyńska, V. Huch, C. Präsang, J. Schwabedissen, R. J. F. Berger and D. Scheschkewitz, *Angew. Chem., Int. Ed.*, 2019, DOI: 10.1002/anie.201811331.
- 34 K. Lonsdale, *Nature*, 1928, **122**, 810.
- 35 E. D. Glending, R. Faust, A. Streitwieser, K. Peter, C. Vollhardt and F. Weinhold, *J. Am. Chem. Soc.*, 1993, **115**(23), 10952.
- 36 E. G. Cox, *Rev. Mod. Phys.*, 1958, **30**(1), 159–162.
- 37 T. C. Dinadayalane, U. D. Prikakumar and G. N. J. Sastry, *J. Phys. Chem. A*, 2004, **108**, 11433.
- 38 M. D. Newton and J. M. Schulman, *J. Am. Chem. Soc.*, 1972, **93**, 773.
- 39 A. M. Dilmac, E. Spuling, A. de Meijere and S. Bräse, *Angew. Chem., Int. Ed.*, 2017, **56**, 5684.
- 40 F. Breher, *Coord. Chem. Rev.*, 2007, **251**, 1007.
- 41 P. P. Power, *Chem. Rev.*, 2003, **103**, 789.
- 42 H. Grützmacher and F. Breher, *Angew. Chem., Int. Ed.*, 2002, **41**, 4006.
- 43 D. Nied and F. Breher, *Chem. Soc. Rev.*, 2011, **40**, 3455.
- 44 S. Shaik, P. Maitre, G. Sini and C. P. Hiberty, *J. Am. Chem. Soc.*, 1992, **114**, 7861.
- 45 W. Wu, J. Gu, J. Song, S. Shaik and P. C. Hiberty, *Angew. Chem., Int. Ed.*, 2009, **48**, 1407.
- 46 D. Kratzert, D. Leusser, J. J. Holstein, B. Dittrich, K. Abersfelder and D. S. D. Stalke, *Angew. Chem., Int. Ed.*, 2013, **52**, 4478.
- 47 IUPAC Nomenclature of Organic Chemistry 1957, *J. Am. Chem. Soc.*, 1960, **82**, 5545.
- 48 International Union of Pure and Applied Chemistry, *Nomenclature of Organic Chemistry, sections A, B, C, D, E, F, H*, Pergamon Press, 1979 edn, 1979.
- 49 A. Jana, V. Huch, M. Repisky, R. J. F. Berger and D. Scheschkewitz, *Angew. Chem., Int. Ed.*, 2014, **53**, 3514.
- 50 C. P. Sindlinger and L. Wesemann, *Chem. Sci.*, 2014, **5**, 2739.
- 51 M. Veith, *Angew. Chem., Int. Ed.*, 1987, **26**, 1.
- 52 Y. Xiong, S. Yao, M. Brym and M. Driess, *Angew. Chem.*, 2017, **119**, 4595.
- 53 Y. Peng, H. Fan, H. Zhu, H. W. Roesky, J. Magull and C. E. Hughes, *Angew. Chem., Int. Ed.*, 2004, **43**, 3443.
- 54 T. Iwamoto, K. Uchiyama, K. Chizuko and M. Kira, *Chem. Lett.*, 2007, **36**, 368.
- 55 K. Raghavachari and V. Logovinsky, *Phys. Rev. Lett.*, 1985, **55**, 2853.
- 56 D. Nieder, C. B. Yildiz, A. Jana, M. Zimmer, V. Huch and D. Scheschkewitz, *Chem. Commun.*, 2016, **52**, 2799.
- 57 L. R. Sita and R. D. Bickerstaff, *J. Am. Chem. Soc.*, 1989, **111**, 6454.
- 58 D. Nied, W. Klopper and F. Breher, *Angew. Chem.*, 2009, **121**, 1439.
- 59 L. R. Sita and I. Kinoshita, *J. Am. Chem. Soc.*, 1990, **112**, 8839.
- 60 L. R. Sita and I. Kinoshita, *J. Am. Chem. Soc.*, 1991, **113**, 5070.
- 61 L. R. Sita and I. Kinoshita, *J. Am. Chem. Soc.*, 1992, **114**, 7024.
- 62 A. F. Richards, M. Brynda and P. P. Power, *Organometallics*, 2004, **23**, 4009.
- 63 A. F. Richards, M. Brynda, M. M. Olmstead and P. P. Power, *Organometallics*, 2004, **23**, 2841.
- 64 C. Drost, M. Hildebrand and P. Lönnecke, *Main Group Met. Chem.*, 2002, **25**, 93.
- 65 J. Juselius, D. Sundholm and J. Gauss, *Chem. Phys.*, 2004, **121**, 3952.



- 66 R. J. F. Berger, H. S. Rzepa and D. Scheschkewitz, *Angew. Chem., Int. Ed.*, 2010, **49**, 10006.
- 67 Details of crystal structure analyses are available in the ESI. CCDC 1877380 (**5a**), 1877381 (**5b**), 1877378 (**4Li**), 1877379 (**6a**), 1877382 (**6c**) and 1877383 (**6f**) contain the supplementary crystallographic data for this paper.†
- 68 C. Hansch, A. Leo and R. W. Taft, *Chem. Rev.*, 1991, **91**, 165.
- 69 H. W. Lerner, *Coord. Chem. Rev.*, 2005, **249**, 781.
- 70 L. P. Hammett, *Trans. Faraday Soc.*, 1938, **34**, 156.
- 71 L. P. Hammett, *Physical Organic Chemistry*, McGraw Hill, 1940, p. 184.
- 72 H. H. Jaffe, *Chem. Rev.*, 1953, **53**, 191.
- 73 L. P. Hammett, *Physical Organic Chemistry*, 2nd edn, McGraw-Hill, New York, 1970.
- 74 H. Spiesecke and W. G. Schneider, *J. Chem. Phys.*, 1961, **35**, 731.



3.2. A Three-Membered Cyclic Phosphasilene

Reproduced with permission from Yannic Heider, Philipp Willmes, Daniel Mühlhausen, Lukas Klemmer, Michael Zimmer, Volker Huch, David Scheschkewitz, *Angew. Chem. Int. Ed.* **2019**, *58*, 1939-1944; *Angew. Chem.* **2019**, *131*, 1956-1964. Copyright © (2019) Wiley-VCH Verlag GmbH & Co. KGaA.

English Version: <https://doi.org/10.1002/anie.201811944>

German Version: <http://dx.doi.org/10.1002/ange.201811944>

The results described within this communication are additionally concluded and put into context in Chapter 4.

Contributions of the Authors:

Yannic Heider: Lead: Conceptualization, Visualization, Writing – Review and Editing, Investigation, Methodology, Data Curation, Formal Analysis, Synthesis, and characterization of Si₄P₂ species; Equal (P.W.): Characterization of Si₂P species; Supporting: Theoretical Studies; Supporting: CP/MAS NMR and VT-NMR.

Philipp Willmes: Lead: Synthesis of Si₂P species and Si₂PFe species; Equal (Y.H.): Characterization of Si₂P species, Investigation, Formal Analysis.

Daniel Mühlhausen: Supporting: Investigation, Methodology, Formal Analysis of Si₄P₂ species (Bachelor-Thesis).

Lukas Klemmer: Lead: Theoretical studies.

Michael Zimmer: Lead: CP/MAS NMR and VT-NMR.

Volker Huch: Lead: X-ray analysis.

David Scheschkewitz: Lead: Project administration, Supervision, Acquisition of funding and resources; Supporting: Writing – Review and Editing.

Coordination Chemistry

International Edition: DOI: 10.1002/anie.201811944

German Edition: DOI: 10.1002/ange.201811944

A Three-Membered Cyclic Phoshasilene

Yannic Heider, Philipp Willmes, Daniel Mühlhausen, Lukas Klemmer, Michael Zimmer, Volker Huch, and David Scheschkewitz*

Dedicated to Professor Dietmar Stalke on the occasion of his 60th birthday

Abstract: Small unsaturated phosphacycles are versatile reagents owing to their strain and the added functionality of the double bond and the phosphorus lone pair. Herein we report the synthesis and isolation of the smallest possible cyclic phoshasilene as a stable adduct with an N-heterocyclic carbene (NHC). First reactivity studies show a) that the PSi_2 ring is a competent ligand to the $\text{Fe}(\text{CO})_4$ fragment via the phosphorus lone pair and b) that the abstraction of the NHC by BPh_3 results in the rapid head-to-head or head-to-tail dimerization of the PSi_2 unit. The relatively facile NHC cleavage indicates that the $\text{P}=\text{Si}$ double bond is available for further manipulation.

Heavier congeners of alkenes have been continuously attracting considerable attention since the report on the first distannene by Lappert in 1973.^[1] During the following decade, the use of sterically demanding substituents for the kinetic stabilization of homo- or heteronuclear heavier double bonds allowed the isolation of stable examples for almost the entire p block.^[2] Regarding the pivotal role of phosphorus as an n-type dopant in the silicon semiconductor industry, the combination of these two elements on a molecular level has been of special interest: First reports on the spectroscopic (Bickelhaupt, 1984^[3]) and structural characterization (Niecke, 1993^[4]) of stable acyclic phoshasilenes with a $\text{Si}=\text{P}$ double bond paved the way to further breakthroughs concerning synthesis and reactivity.^[5] Recently, stable silylene–base adducts were employed as precursors, typically giving donor-stabilized and thus ylidic $\text{Si}=\text{P}$ bonds with a tetracoordinate silicon atom.^[5c] Our group reported the 1,3-migration of the amino group of intermediate *P*-aminophosphino disilenes as a convenient synthetic procedure.^[6]

In contrast, only a few cyclic compounds with one or more $\text{Si}=\text{P}$ double bonds are known. Examples include the heavy cyclobutadienes **I**^[7] and **II**,^[7,8] the heavy cyclobutene anion congener **III**^[9] as well as heavier hetero-analogues of the cyclopentadiene cation **IV**^[10] and benzene **V**^[11] (Figure 1). Three-membered cyclic phoshasilenes are notably absent

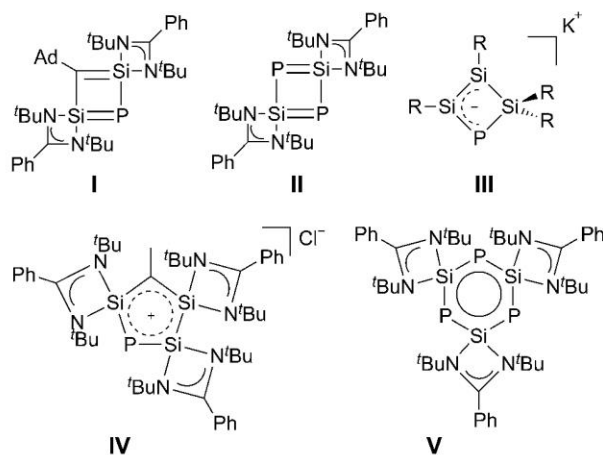


Figure 1. Reported examples of heterocycles with formal $\text{Si}=\text{P}$ double bonds. Ad = adamantyl, Tip = 2,4,6-triisopropylphenyl.^[7–11]

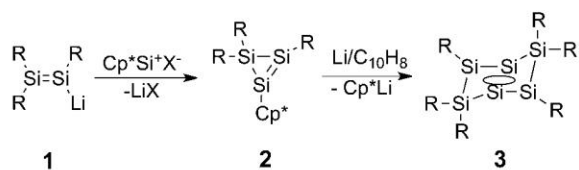
from the literature; even reports on saturated three-membered rings of silicon and phosphorus (Si_2P ^[12] and SiP_2 ^[13]) as well as phoshasilirenes with an endocyclic $\text{P}=\text{C}$ double bond^[14] are scarce. This is even more surprising in light of the well-established chemistry of the corresponding phosphorus–carbon analogues,^[15] which has proven particularly useful for the generation of transient phosphinidenes, that is, mono-coordinate phosphorus(I) species.^[16] We now report on the synthesis and characterization of an unsaturated PSi_2 ring as a complex with an N-heterocyclic carbene (NHC). First reactivity studies regarding the ligand properties and cleavage of the NHC surprisingly reveal a behavior closely resembling that of related species with only Group 14 elements in the scaffold.^[17]

A few years ago, in a cooperation with the Jutzi group, we demonstrated the capability of the Cp^*Si^+ cation^[18] to act as a stoichiometric source of silicon in the reaction with lithium disilene **1**.^[19] Reductive cleavage of the Cp^* ligand from the resulting Cp^* -functionalized cyclotrisilene **2**^[20] resulted in dimerization to the dismutational isomer of hexasilabenzene **3** (Scheme 1).^[20]

Inspired by these findings, we now considered the use of a phosphorus(I) cation as electrophile. In a series of papers, Macdonald and co-workers had established the facile synthesis of cationic phosphorus(I) synthons.^[21] Whereas the reaction of disilene **1** with a 1,2-bis(diphenylphosphino)ethane (dpe)-coordinated P^+ cation^[21a] did not yield tangible results, treatment of **1**^[19] with an equimolar amount of the

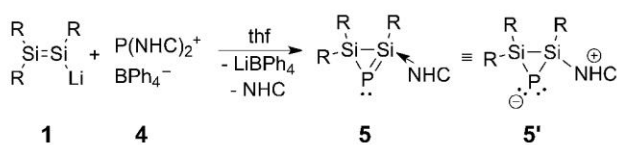
[*] M. Sc. Y. Heider, Dr. P. Willmes, B. Sc. D. Mühlhausen, M. Sc. L. Klemmer, Dr. M. Zimmer, Dr. V. Huch, Prof. Dr. D. Scheschkewitz
Krupp-Lehrstuhl für Allgemeine und Anorganische Chemie
Universität des Saarlandes
Campus, C4.1, 66123 Saarbrücken (Germany)
E-mail: scheschkewitz@mx.uni-saarland.de

Supporting information and the ORCID identification number(s) for the author(s) of this article can be found under:
<https://doi.org/10.1002/anie.201811944>.



Scheme 1. Reported synthesis of Cp*-functionalized cyclotrisilene **2** and its reductive dimerization to the dismutational isomer of hexasilabenzene **3**. R = Tip, Cp* = pentamethylcyclopentadienyl, [A⁻] = [B(C₆F₅)₄]⁻, C₁₀H₈ = naphthalene.^[20]

NHC-stabilized P^I cation **4**^[21b] in thf indeed leads to a uniform conversion into the donor-stabilized cyclic phosphasilene **5** (Scheme 2).



Scheme 2. Synthesis of cyclic phosphasilene **5** (this work) by treatment of disilene **1**^[19] with NHC-stabilized P^I cation **4**^[21b]. R = Tip, NHC = 1,3-diisopropyl-4,5-dimethylimidazol-2-ylidene.

Yellow single crystals of **5** were obtained in good yields (84%) from pentane. An X-ray diffraction study revealed the coordination of the N-heterocyclic carbene moiety to the otherwise monosubstituted silicon center of the disilaphosphirene motif (Figure 2).^[22] The distance between the silicon and the carbenic carbon atom (Si1–C1 1.957(2) Å) is in the typical range for acyclic NHC-stabilized phosphasilenes (1.928–1.9707 Å)^[23] as well as NHC complexes of related low-valent silicon species (1.9221–1.985 Å).^[24] The Si1–Si2 bond length of 2.3082(6) Å is at the short end of values reported for Si–Si single bonds. Both Si–P bonds (P–Si1 2.170(1) Å; P–Si2 2.196(1) Å) are significantly shorter than the average Si–P single bond (2.25 Å),^[25] and of similar length as those in heterocycles **I–V** (2.1515–2.2012 Å).^[7–11] The nearly identical Si–P bond lengths suggest a dominating ylidic contribution to the electronic structure as in **5'** (Scheme 2). On the other hand, back-donation from the anionic phosphorus center into σ* orbitals at the silicon centers has been

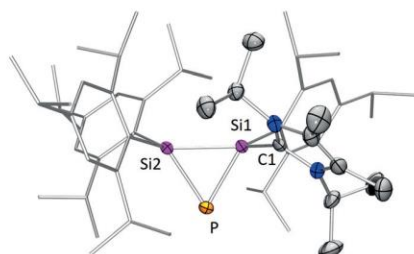


Figure 2. Molecular structure of **5** in the solid state (thermal ellipsoids at 50%, H atoms omitted). Selected bond lengths [Å] and angles [°]: Si1–C1 1.950(4), Si1–Si2 2.294(1), Si1–P 2.170(1), Si2–P 2.196(1); Si1–P–Si2 63.38(4).

suggested to shorten the endocyclic bonds even in saturated three-membered rings of heavier main-group elements.^[12c,26] The slightly shorter Si1–P bond could thus be attributed to partial double bond character.

DFT calculations on **5** at the M06-ZX(D3)/def2-TZVPP level of theory support this interpretation. The HOMO consists almost exclusively of the p_z orbital at the phosphorus center. Its strictly non-bonding nature lends further support to a predominantly ylidic structure (Figure 3; see **5'** in Scheme 2). The second lone pair at phosphorus is represented by the HOMO–1 and shows significant back-donation to both silicon centers, which is in line with the observed shortening of the Si–P bonds. As frequently observed for NHC complexes of low-coordinate main-group species, the LUMO is primarily located at the NCN moiety of the carbene ligand (Figure 3).

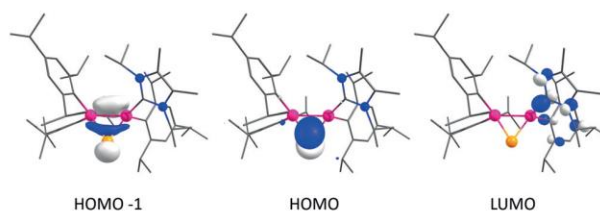
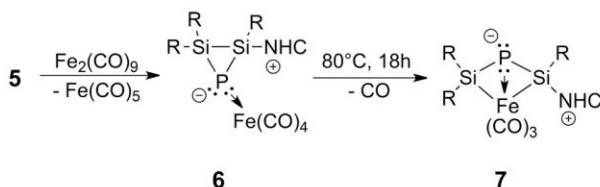


Figure 3. Selected Kohn–Sham orbitals of **5** (isovalue 0.07465).

In analogy to reported NHC complexes of germanium-(II),^[27] a solution of crystallized **5** displays two signals in the ³¹P NMR spectrum at δ = –252.0 and –267.9 ppm (ratio 1:0.88) as well as four doublets in the ²⁹Si NMR spectrum between δ = –68.7 and –73.6 ppm. The two sets of signals were tentatively attributed to the hindered rotation of the Tip groups and/or the NHC. Indeed, the ratio of the two signals changes with increasing temperature. VT-NMR analysis revealed a significant broadening upon heating although coalescence could not be reached within the accessible temperature window (243–353 K; see the Supporting Information). The presence of only one conformer in the solid state, however, was confirmed by multinuclear CP/MAS NMR spectroscopy (³¹P CP/MAS NMR: δ = –249.2 ppm; ²⁹Si CP/MAS NMR: δ = –70.6 and –75.4 ppm). Surprisingly, both ³¹P NMR resonances split into slightly broadened (pseudo)triplets (*J*_{P,H} = 8.5 and 12.8 Hz) in the ¹H-coupled spectra. Four ¹H NMR signals at δ = 8.62, 6.70, 6.43, and 6.26 ppm (assigned to the *ortho*-¹Pr-CH atoms of Tip groups and the NHC) also show abnormal coupling patterns. A ¹H{³¹P} NMR spectrum as well as a ³¹P/¹H correlation experiment unambiguously identified the hydrogen atoms coupling to the phosphorus nucleus (see the Supporting Information): In the minor conformer, the phosphorus center couples to one ¹Pr-CH of the NHC ligand and one of the Tip substituents in *trans* position relative to the NHC. In the major conformer, two ¹Pr-CH hydrogen atoms of the two remaining Tip groups couple to the phosphorus atom. In the solid-state structure, relatively short distances between phosphorus and the H atoms in question (2.5416 Å and 2.5339 Å) confirm this assignment to the major conformer.

The high-field ^{31}P resonance is comparable to those of saturated Si_2P cycles ($\delta = -241.4$ to -325 ppm),^[12] and in line with ylidic formulation **5**. The heterocycles **I**, **IV**, and **V** with formal $\text{Si}=\text{P}$ bonds show similar high-field ^{31}P NMR resonances while the ^{29}Si NMR signals appear at slightly lower field ($\delta^{31}\text{P} = -272.1$ to -241.9 ppm; $\delta^{29}\text{Si} = -5.1$ to 70.6 ppm).^[7,10,11] The small $^{31}\text{P}/^{13}\text{C}$ coupling constants of the ^{13}C NMR signals of the carbenic carbon atoms strongly support exclusive coordination of the NHC to the silicon centers in both conformers ($^2J_{\text{C-P}} = 8.5$ and 4.9 Hz). The $^1J_{\text{P-Si}}$ coupling constants ($^1J_{\text{P-Si}} = 91.1$ to 107.2 Hz) are comparable to those of heterocycles **I–V** ($^1J_{\text{P-Si}} = 75.45$ to 138.2 Hz).^[7–11] In both conformers, the $^1J_{\text{P-Si}}$ coupling constant for the formal $\text{Si}=\text{P}$ double bond is significantly larger ($\Delta^1J_{\text{P-Si}} = 16.1$ Hz and 7.1 Hz) than the one for the $\text{Si}-\text{P}$ single bond. The UV/vis absorption spectrum of **5** shows a broad shoulder at $\lambda_{\text{max}} = 370$ to 420 nm, which is due to an excitation at $\lambda_{\text{calc}} = 379$ nm on grounds of TD-DFT calculations at the M06-2X(D3)/def2-TZVPP//BP86(D3)/def2-SVP level of theory. The main contributing transitions are HOMO \rightarrow LUMO (49%) and HOMO \rightarrow LUMO+1 (38%). A second, more intense absorption band at $\lambda_{\text{max}} = 336$ nm ($\epsilon = 8700\text{M}^{-1}\text{cm}^{-1}$) corresponds to an excitation at $\lambda_{\text{calc}} = 322$ nm, and is mainly composed of the transitions HOMO $-1\rightarrow$ LUMO, HOMO $-1\rightarrow$ LUMO+1, and HOMO \rightarrow LUMO+2 (see the Supporting Information).

The considerable electron density at the phosphorus center of **5** should allow for coordination to metal centers. Indeed, reaction of **5** with an equimolar amount of diiron nonacarbonyl in toluene leads to complete conversion into the anticipated tetracarbonyliron complex **6** after 12 hours (Scheme 3). The observed NMR chemical shifts for **6** are very



Scheme 3. Synthesis of $\text{Fe}(\text{CO})_4$ complex **6** and transformation into FePSi_2 bicyclo[1.1.0]butane derivative **7**. R = Tip, NHC = 1,3-diisopropyl-4,5-dimethylimidazol-2-ylidene.

similar to those of **5**: In the ^{31}P NMR spectrum, once again two resonances for two (presumably rotational) isomers are observed at $\delta = -244.8$ and -266.3 ppm in the typical region for Si_2P three-membered rings,^[12a,b] although in a distinctly different ratio (10:1 vs. approximately 1:1 for **5**). Owing to the low natural abundance of ^{29}Si , only the major isomer could be detected in the ^{29}Si NMR spectrum as two doublets at $\delta = -59.5$ ($^1J_{\text{P-Si}} = 75.6$ Hz) and -62.6 ppm ($^1J_{\text{P-Si}} = 60.1$ Hz). Notably, the $^1J_{\text{P-Si}}$ coupling constants are significantly smaller in comparison to those of **5**, indicating a lower s-character of the endocyclic bonds, in line with an increased s-character of the phosphorus lone pair coordinating to the iron center. Unsurprisingly, the carbonyl ligands give rise to only one low-field doublet in the ^{13}C NMR spectrum at $\delta = 221.9$ ppm, as it is well established that Berry pseudo-rotation allows for

a facile exchange of the CO ligands in metal carbonyls, which is very fast on the NMR timescale.^[28] The magnitude of the $J_{\text{C-P}}$ coupling constant (11.3 Hz) is in accordance with a 2J coupling and thus supports the presence of a direct Fe–P interaction.^[12c,29,30]

In contrast to the single CO signal in the ^{13}C NMR spectrum, five IR stretching bands of carbonyl moieties are resolved at $\nu = 2020, 1944, 1930, 1906,$ and 1890cm^{-1} as IR spectroscopy is several orders of magnitude faster. The shift to smaller wavenumbers in comparison with those of the corresponding N-heterocyclic carbene complexes indicates a somewhat stronger σ -donor ability of **5** (e.g., $\text{NHC}^{\text{Dip}}\text{Fe}(\text{CO})_4$: $\nu = 2035, 1947, 1928, 1919\text{cm}^{-1}$; $\text{NHC}^{\text{Dip}} = \text{C}\{\text{N}(\text{Ar})\text{CH}\}_2$, Ar = 2,6-diisopropylphenyl).^[31]

An X-ray diffraction study (Figure 4)^[22] on orange single crystals of **6**, obtained from a concentrated toluene solution in excellent yields (91%), revealed a P–Fe distance of $2.2874(4)$ Å. This distance is longer than that of typical

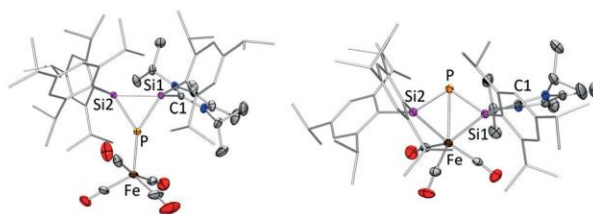
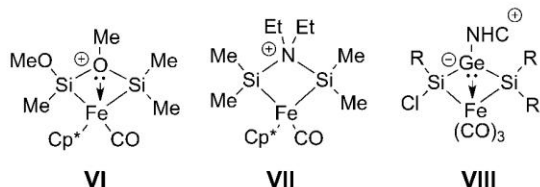


Figure 4. Molecular structures of **6** (left) and **7** (right) in the solid state (thermal ellipsoids at 50%, H atoms omitted). Selected bond lengths [Å] and angles [°]: **6**: Si1–C1 1.954(1), Si1–Si2 2.3755(5), Si1–P 2.1635(5), Si2–P 2.1838(5), P–Fe 2.2874(4); Si1–P–Si2 66.243(16); **7**: Si1–C1 1.990(3), Si1–P 2.173(1), Si2–P 2.214(1), P–Fe 2.4981(8), Si1–Fe 2.3342(9), Si2–Fe 2.3958(9).

P–Fe bonds (2.08 – 2.245 Å),^[29,32] presumably due to high steric congestion. A similar elongation has been reported for a tetracarbonyl iron complex of a phosphatrisilabicyclo[1.1.0]butane derivative (2.3181 Å) bearing sterically demanding substituents.^[12c] The iron center is trigonal-bipyramidally coordinated by the phosphorus atom and four CO ligands. While the donor–acceptor bond between silicon and the NHC (Si1–C1 $1.9542(13)$ Å) is almost the same as in **5** ($1.950(4)$ Å), the Si1–Si2 bond length has significantly increased ($2.3755(5)$ Å), and is now in the typical region for Si–Si single bonds. In contrast, both the Si1–P ($2.1635(5)$ Å) and the Si2–P bonds ($2.1838(5)$ Å) are slightly shortened compared to those in **5**, suggesting a more anionic character of the phosphorus center, which implies a larger electron back-donation ability. The UV/vis spectrum of **6** shows a broad absorption band at $\lambda_{\text{max}} = 340$ to 460 nm.

Upon heating to 80°C in toluene for 18 hours, **6** is converted into the heteronuclear FePSi_2 bicyclo[1.1.0]butane analogue **7** with concomitant release of one equivalent of CO (Scheme 3). In comparison to **6**, both silicon nuclei are considerably deshielded, giving rise to signals at $\delta = 30.8$ ppm ($^1J_{\text{Si-P}} = 110.9$ Hz) and $\delta = 26.5$ ppm ($^1J_{\text{Si-P}} = 138.6$ Hz), which is consistent with coordination to the electropositive iron center. Comparable alkoxysilyl- and aminosilyl-bridged sily-

lene iron complexes **VI** and **VII** as well as the analogous compound **VIII** with an isolobal NHC-stabilized germylene unit instead of the phosphorus center in **7** have been reported by the group of Ogino^[33] and ourselves^[17b] (Scheme 4).



Scheme 4. Reported transition-metal complexes **VI–VIII** for comparison. R = Tip, NHC = 1,3-diisopropyl-4,5-dimethylimidazol-2-ylidene.^[17b,33]

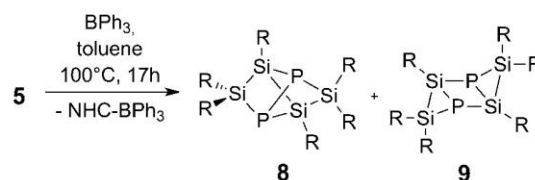
Whereas in these cases, low-field shifts in the ²⁹Si NMR spectra from $\delta = 89.6$ to $\delta = 127.4$ ppm indicated pronounced π -complex character according to the Dewar–Chatt–Duncanson model,^[34] the ²⁹Si NMR chemical shifts of **7** suggest considerable back-donation from the iron center. This assertion is supported by the ³¹P NMR resonance at very high field at $\delta = -378.6$ ppm indicating considerable accumulation of charge density at the phosphorus center. The IR stretching bands of the CO ligands at $\nu = 1969$, 1904, and 1878 cm^{-1} , however, are located at even lower frequencies than in the related compound **VIII** ($\nu = 1982$, 1920, 1916 cm^{-1}), supporting the presence of strong back-donation from the iron center to the carbonyl ligands as well. Therefore, the σ -donator strength of the SiPSi pincer ligand system in **7** must be exceptionally strong.

The molecular structure of **7** was confirmed by an X-ray diffraction study on red single crystals that had been grown in moderate yields (48 %) from a concentrated toluene solution (Figure 4).^[22] The Fe–P bond of 2.4981(8) Å is unusually long, indicating a rather weak interaction between the phosphorus and the metal center. This is in accordance with the detection of a singlet resonance in the ¹³C NMR spectrum at $\delta = 219.9$ ppm for the carbonyl carbon nuclei, with the ³¹P coupling being apparently too small for detection. Consequently, the iron center can be considered as five-coordinate in a distorted trigonal-bipyramidal arrangement. Notably, the Si1–P (2.173(1) Å) and the Si1–Fe (2.3342(9) Å) bonds involving the NHC-coordinated silicon atom are slightly shorter than those of the SiTip₂ unit (Si2–P 2.214(1) Å), Si2–Fe 2.3958(9) Å), presumably owing to lower steric congestion of the NHC ligand. Disregarding the metal center, the sum of bond angles ($R_2\text{SiP } 340.2^\circ$; $R(\text{NHC})\text{SiP } 339.5^\circ$) of both silicon atoms suggests slightly less pyramidal coordination than in **VIII** ($R_2\text{SiGe } 334.5^\circ$; $R(\text{Cl})\text{SiGe } 332.9^\circ$).^[17b] We tentatively attribute this counterintuitive observation to the geometric effect of the smaller phosphorus atom compared to germanium, which gives rise to more acute inner angles at the silicon centers. In contrast to **6**, bicyclobutane analogue **7** with two chiral centers (P and Si1) shows only one set of signals in the NMR spectra. We assume that the weak interaction between iron and phosphorus as indicated by the long distance (P–Fe 2.4981(8) Å) facilitates planarization of the four-membered

Si₂PFe ring and thus inversion of the bicyclic moiety in solution. The UV/vis spectrum of **7** shows a very broad absorption band at $\lambda_{\text{max}} = 350\text{--}475$ nm, which is comparable to that of **6** ($\lambda_{\text{max}} = 340$ to 460 nm).

With proof of principle for the good ligand properties of **6** established, we pondered whether a stronger Lewis acid would also coordinate to the exposed phosphorus center or rather abstract the stabilizing NHC. Spontaneous^[35] as well as Lewis-acid-induced^[23a] abstractions of the carbene from NHC-stabilized acyclic phosphasilenes have already been demonstrated to result in either the corresponding donor-free double bond moiety^[23a] or its dimerization to yield a Si₂P₂ four-membered ring.^[35] Heating of **5** with BPh₃ to 100 °C in toluene indeed leads to the formation of the NHC–borane complex^[23a] as detected by ¹H and ¹¹B NMR spectroscopy. After 17 hours, conversion into a product mixture with several ³¹P NMR signals between $\delta = +92$ to -381 ppm is typically complete. Light-yellow and pale-yellow single crystals were obtained by fractional crystallization from a hexane solution, which allowed for the identification of two products by X-ray analysis: the dimerization products, Si₄P₂ isomers **8** (ca. 58 %) and **9** (ca. 14 %; Scheme 5 and Figure 5).^[22] This strongly resembles the reactivity of Iwamoto's base-stabilized Si₄ bridgehead disilene towards BPh₃.^[17f]

While **8** features a cluster motif reminiscent of the global minimum isomer of hexasilabenzene^[36] and a Si₂P₄ cage compound derived from white phosphorus,^[37] **9** adopts a chair-like conformation comparable to the so-called disubstituted isomer of hexasilabenzene.^[38] Apparently, a head-



Scheme 5. Dimerization of **5** upon Lewis-acid-induced NHC abstraction to afford Si₄P₂ isomers **8** and **9**. R = Tip, NHC = 1,3-diisopropyl-4,5-dimethylimidazol-2-ylidene.

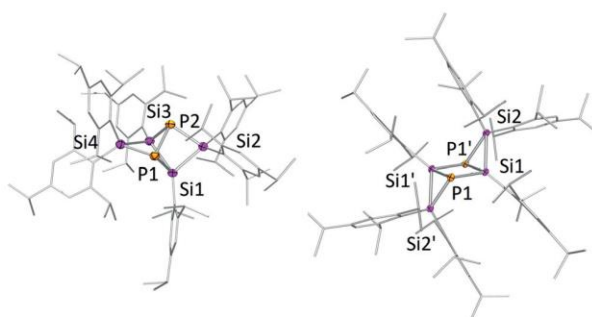


Figure 5. Molecular structure of **8** (left) and **9** (right) in the solid state (thermal ellipsoids at 50%, H atoms omitted). Selected bond lengths [Å] and angles [°]: **8**: P1–P2 2.243(1), P1–Si1 2.281(1), P1–Si4 2.3000(1), Si1–Si3 2.462(1), Si1–Si2 2.354(1); P1–Si4–Si3 76.12 (6), P2–P1–Si1 79.48(6), Si1–Si2–P2 76.83 (6); **9**: P1–Si1 2.2372(4), P1–Si2' 2.3002(4), P1–Si1' 2.3210(4), Si1–Si2 2.3008(4); Si1–Si2–P1' 60.59(1), P1–Si1–P1' 97.56(1), Si1–P1–Si1' 82.44(1).

to-tail [2+2] cycloaddition reaction of two three-membered phosphasilene moieties leads to formation of the cluster motif in **9**. The formation mechanism of **8** on the other hand is less apparent. A plausible possibility is the initial formation of a head-to-head dimer, which then rearranges to **8** under release of steric strain.

The C_2 -symmetric and thus chiral scaffold of **8** renders the two phosphorus centers diastereotopic, giving rise to two broad doublets in the ^{31}P NMR spectrum in C_6D_6 solution at $\delta = -120.6$ and -134.4 ppm with equal intensities and $^1J_{\text{P,P}}$ coupling constants of 163 Hz and a distinct roofing effect. In a VT-NMR study, both doublets significantly broadened with rising temperature. At $T = 320$ K, the P–P coupling disappeared in the increased half-width of the signals (about 380 Hz). The CP/MAS ^{31}P NMR spectrum also shows two broad resonances at $\delta = -122.2$ and -136.9 ppm, with the resolution being insufficient for the detection of the P–P coupling. Similarly, the ^{29}Si spectrum in C_6D_6 solution and the CP/MAS ^{29}Si NMR spectrum of **8** both show two very broad signals at $\delta = 32.1$, -1.4 ppm and $\delta = 32.2$, -3.7 ppm, respectively.

An X-ray diffraction study on single crystals of **8** revealed the molecular structure as the aforementioned tetracyclic scaffold (Figure 5).^[22] The P–P bond is with 2.243(1) Å a typical single bond (2.22 Å)^[25] and shorter than those of a Si_2P_4 compound with a similar tetracyclic scaffold (2.280 to 2.296 Å).^[37] In contrast, both the Si–P (2.281(1)–2.300(1) Å) and the Si–Si bonds (2.354(1)–2.462(1) Å) are slightly longer than the corresponding typical single bonds (2.25 and 2.34 Å, respectively)^[25] and those of the related Si_2P_4 cluster (Si–P: 2.275 to 2.295 Å; Si–Si: 2.28 to 2.296 Å).^[37] Both phosphorus vertices show strong pyramidalization (Σ of angles: P1 262.6°; P2 260.9°). Compound **9** features a centrosymmetric diamond-shaped Si_2P_2 moiety with two short (2.2372(4) Å) and two long Si–P bonds (2.3210(4) Å). The internal angles amount to 97.56(1)° and 82.44(1)° at the silicon and phosphorus centers, respectively. The long edges are bridged by opposing SiTip₂ moieties, resulting in the chair-like appearance. The Si–Si bonds are 2.3004(1) Å long, and thus shorter than a typical single bond (2.34 Å).^[25] The phosphorus atoms in **9** exhibit an even greater pyramidalization (Σ of angles 245.2°) than in **8** (Σ of angles: P1 262.6°; P2 260.9°).

Owing to its inversion symmetry, only one singlet ^{31}P NMR resonance for the two phosphorus nuclei was detected at $\delta = -182.9$ ppm, which is shifted by about 50 ppm upfield compared to **8**. This is in line with only two upfield-shifted signals in the ^{29}Si NMR spectrum at $\delta = -83.6$ and -91.4 ppm, which are both split into doublets of doublets due to coupling with the chemically equivalent, but magnetically inequivalent P atoms ($J = 21.7$ – 107.1 Hz). The reported thermally induced rearrangement of dismutational hexasilabenzene isomer **3**^[38] to its global-minimum isomer^[36] prompted us to also investigate if **8** can be thermally isomerized to **9** or vice versa. While no tangible results in this regard have been obtained to date, both **8** and **9** decomposed/rearranged to the same, yet unidentified product upon melting at temperatures $T > 220$ °C.

In conclusion, we have reported on the isolation and full characterization of the smallest possible cyclic phosphasilene

as an NHC adduct. First aspects of its reactivity were disclosed, namely the coordination to transition-metal centers and the abstraction of the NHC by a Lewis acid. Further studies with a view towards the P=Si moiety as well as ring opening of the strained PSi_2 cycle are currently underway in our laboratory.

Acknowledgements

Funding by the Deutsche Forschungsgemeinschaft (DFG SCHE906/4-1 and 4-2) and COST Action CM1302 (Smart Inorganic Polymers) is gratefully acknowledged.

Conflict of interest

The authors declare no conflict of interest.

Keywords: coordination chemistry · heavier multiple bonds · phosphorus · silicon · small rings

How to cite: *Angew. Chem. Int. Ed.* **2019**, *58*, 1944–1944
Angew. Chem. **2019**, *131*, 1958–1964

- [1] P. J. Davidson, M. F. Lappert, *J. Chem. Soc. Chem. Commun.* **1973**, 317.
- [2] a) P. P. Power, *J. Chem. Soc. Dalton Trans.* **1998**, 2939–2951; b) R. C. Fischer, P. P. Power, *Chem. Rev.* **2010**, *110*, 3877–3923; c) V. Y. Lee, A. Sekiguchi, J. Escudí, H. Ranaivonjatovo, *Chem. Lett.* **2010**, *39*, 312–318.
- [3] C. N. Smit, F. M. Lock, F. Bickelhaupt, *Tetrahedron Lett.* **1984**, *25*, 3011–3014.
- [4] H. R. G. Bender, E. Niecke, M. Nieger, *J. Am. Chem. Soc.* **1993**, *115*, 3314–3315.
- [5] a) M. Driess, R. Janoschek, *J. Mol. Struct.* **1994**, *313*, 129–139; b) M. Driess, *Adv. Organomet. Chem.* **1996**, *39*, 193–230; c) V. Nesterov, N. C. Breit, S. Inoue, *Chem. Eur. J.* **2017**, *23*, 12014–12039.
- [6] P. Willmes, M. J. Cowley, M. Hartmann, M. Zimmer, V. Huch, D. Scheschke, *Angew. Chem. Int. Ed.* **2014**, *53*, 2216–2220; *Angew. Chem.* **2014**, *126*, 2248–2252.
- [7] S. S. Sen, S. Khan, H. W. Roesky, D. Kratzert, K. Meindl, J. Henn, D. Stalke, J. P. Demers, A. Lange, *Angew. Chem. Int. Ed.* **2011**, *50*, 2322–2325; *Angew. Chem.* **2011**, *123*, 2370–2373.
- [8] S. Inoue, W. Wang, C. Präsang, M. Asay, E. Irran, M. Driess, *J. Am. Chem. Soc.* **2011**, *133*, 2868–2871.
- [9] T. P. Robinson, M. J. Cowley, D. Scheschke, J. M. Goicoechea, *Angew. Chem. Int. Ed.* **2015**, *54*, 683–686; *Angew. Chem.* **2015**, *127*, 693–696.
- [10] S. S. Sen, J. Hey, M. Eckhardt, R. Herbst-Irmer, E. Maedl, R. A. Mata, H. W. Roesky, M. Scheer, D. Stalke, *Angew. Chem. Int. Ed.* **2011**, *50*, 12510–12513; *Angew. Chem.* **2011**, *123*, 12718–12721.
- [11] A. E. Seitz, M. Eckhardt, A. Erlebach, E. V. Peresypkina, M. Sierka, M. Scheer, *J. Am. Chem. Soc.* **2016**, *138*, 10433–10436.
- [12] a) M. Driess, H. Pritzko, *Z. Anorg. Allg. Chem.* **1996**, *622*, 858–862; b) M. Driess, S. Rell, H. Pritzko, R. Janoschek, *Angew. Chem. Int. Ed. Engl.* **1997**, *36*, 1326–1329; *Angew. Chem.* **1997**, *109*, 1384–1387; c) P. Willmes, L. Junk, V. Huch, C. B. Yildiz, D. Scheschke, *Angew. Chem. Int. Ed.* **2016**, *55*, 10913–10917; *Angew. Chem.* **2016**, *128*, 11074–11078.
- [13] a) M. Baudler, H. Jongbloed, *Z. Anorg. Allg. Chem.* **1979**, *458*, 9–21; b) K. F. Tebbe, *Z. Anorg. Allg. Chem.* **1980**, *468*, 202–212;

- c) M. Weidenbruch, M. Herrndorf, A. Schäfer, *J. Organomet. Chem.* **1985**, 295, 7–14; d) M. Driess, H. Pritzkow, S. Rell, R. Janoschek, *Inorg. Chem.* **1997**, 36, 5212–5217.
- [14] a) A. Schäfer, M. Weidenbruch, W. Saak, S. Pohl, *Angew. Chem. Int. Ed. Engl.* **1987**, 26, 776–777; *Angew. Chem.* **1987**, 99, 806–807; b) R. Okazaki, *Pure Appl. Chem.* **1996**, 68, 895–900.
- [15] a) F. Mathey, M. Regitz in *Compr. Heterocycl. Chem. II* (Eds.: A. R. Katritzky, C. W. Rees, E. F. V. Scriven), Elsevier, Amsterdam, **1996**, pp. 277–304; b) F. Mathey, M. Regitz in *Phosphorus-Carbon Heterocycl. Chem.* (Ed.: F. Mathey), Elsevier, Amsterdam, **2001**, pp. 17–55.
- [16] a) L. L. Liu, J. Zhou, L. L. Cao, R. Andrews, R. L. Falconer, C. A. Russell, D. W. Stephan, *J. Am. Chem. Soc.* **2018**, 140, 147–150; b) S. G. A. Van Assema, F. J. J. De Kanter, M. Schakel, K. Lammertsma, *Organometallics* **2006**, 25, 5286–5291; c) R. Streubel, H. Wilkens, A. Ostrowski, C. Neumann, F. Ruthe, P. G. Jones, *Angew. Chem. Int. Ed. Engl.* **1997**, 36, 1492–1494; *Angew. Chem.* **1997**, 109, 1549–1550; d) H. Wilkens, F. Ruthe, P. G. Jones, R. Streubel, *Chem. Commun.* **1998**, 1529–1530; e) F. Mercier, B. Deschamps, F. Mathey, *J. Am. Chem. Soc.* **1989**, 111, 9098–9100.
- [17] a) K. E. Litz, J. E. Bender IV, J. W. Kampf, M. M. Banaszak Holl, *Angew. Chem. Int. Ed. Engl.* **1997**, 36, 496–498; *Angew. Chem.* **1997**, 109, 516–518; b) A. Jana, M. Majumdar, V. Huch, M. Zimmer, D. Scheschkewitz, *Dalton Trans.* **2014**, 43, 5175–5181; c) K. Inomata, T. Watanabe, H. Tobita, *J. Am. Chem. Soc.* **2014**, 136, 14341–14344; d) A. Jana, V. Huch, H. S. Rzepa, D. Scheschkewitz, *Angew. Chem. Int. Ed.* **2015**, 54, 289–292; *Angew. Chem.* **2015**, 127, 291–295; e) D. Nieder, C. B. Yildiz, A. Jana, M. Zimmer, V. Huch, D. Scheschkewitz, *Chem. Commun.* **2016**, 52, 2799–2802; f) T. Iwamoto, N. Akasaka, S. Ishida, *Nat. Commun.* **2014**, 5, 5353.
- [18] P. Jutzi, A. Mix, B. Rummel, W. W. Schoeller, B. Neumann, H.-G. Stammer, *Science* **2004**, 305, 849–851.
- [19] D. Scheschkewitz, *Angew. Chem. Int. Ed.* **2004**, 43, 2965–2967; *Angew. Chem.* **2004**, 116, 3025–3028.
- [20] K. Leszczyńska, K. Abersfelder, M. Majumdar, B. Neumann, H.-G. Stammer, H. S. Rzepa, P. Jutzi, D. Scheschkewitz, *Chem. Commun.* **2012**, 48, 7820–7822.
- [21] a) B. D. Ellis, M. Carlesimo, C. L. B. Macdonald, *Chem. Commun.* **2003**, 1946–1947; b) B. D. Ellis, C. A. Dyker, A. Decken, C. L. B. Macdonald, *Chem. Commun.* **2005**, 1965; c) E. L. Norton, K. L. S. Szekely, J. W. Dube, P. G. Bomben, C. L. B. Macdonald, *Inorg. Chem.* **2008**, 47, 1196–1203.
- [22] CCDC 1873591 (5), 1873592 (6), 1873593 (7), 1873594 (8), and 1873595 (9) contain the supplementary crystallographic data for this paper. These data can be obtained free of charge from The Cambridge Crystallographic Data Centre.
- [23] a) H. Cui, J. Zhang, C. Cui, *Organometallics* **2013**, 32, 1–4; b) D. Dhara, D. Mandal, A. Maiti, C. B. Yildiz, P. Kalita, N. Chrysochos, C. Schulzke, V. Chandrasekhar, A. Jana, *Dalton Trans.* **2016**, 45, 19290–19298; c) A. W. Kyri, P. K. Majhi, T. Sasamori, T. Agou, V. Nesterov, J. D. Guo, S. Nagase, N. Tokitoh, R. Streubel, *Molecules* **2016**, 21, 1309; d) S. Roy, P. Stollberg, R. Herbst-Irmer, D. Stalke, D. M. Andrada, G. Frenking, H. W. Roesky, *J. Am. Chem. Soc.* **2015**, 137, 150–153.
- [24] a) R. S. Ghadwal, H. W. Roesky, S. Merkel, J. Henn, D. Stalke, *Angew. Chem. Int. Ed.* **2009**, 48, 5683–5686; *Angew. Chem.* **2009**, 121, 5793–5796; b) Y. Wang, Y. Xie, P. Wei, R. B. King, H. F. Schaefer III, P. V. R. Schleyer, G. H. Robinson, *Science* **2008**, 321, 1069–1072; c) M. J. Cowley, V. Huch, H. S. Rzepa, D. Scheschkewitz, *Nat. Chem.* **2013**, 5, 876–879; d) A. Jana, I. Omlor, V. Huch, H. S. Rzepa, D. Scheschkewitz, *Angew. Chem. Int. Ed.* **2014**, 53, 9953–9956; *Angew. Chem.* **2014**, 126, 10112–10116; e) T. Yamaguchi, A. Sekiguchi, M. Driess, *J. Am. Chem. Soc.* **2010**, 132, 14061–14063.
- [25] P. Rademacher, *Größe und Gestalt von Molekülen*, Verlag Chemie, Weinheim, **1987**.
- [26] K. Abersfelder, D. Scheschkewitz, *J. Am. Chem. Soc.* **2008**, 130, 4114–4121.
- [27] P. A. Rupar, M. C. Jennings, K. M. Baines, *Organometallics* **2008**, 27, 5043–5051.
- [28] a) S. T. Wilson, N. J. Coville, J. R. Shapely, J. A. Osborn, *J. Am. Chem. Soc.* **1974**, 96, 4038–4040; b) F.-W. Grevels, J. Jacke, W. E. Klotzbücher, C. Krüger, K. Seevogel, Y.-H. Tsay, *Angew. Chem. Int. Ed. Engl.* **1987**, 26, 885–887; *Angew. Chem.* **1987**, 99, 960–961; c) F.-W. Grevels, J. Jacke, K. Seevogel, *J. Mol. Struct.* **1988**, 174, 107–112.
- [29] J.-J. Brunet, R. Chauvin, O. Diallo, B. Donnadiou, J. Jaffart, D. Neibecker, *J. Organomet. Chem.* **1999**, 584, 390–395.
- [30] A. H. Cowley, R. A. Kemp, J. C. Wilburn, *Inorg. Chem.* **1981**, 20, 4289–4293.
- [31] S. Warratz, L. Postigo, B. Royo, *Organometallics* **2013**, 32, 893–897.
- [32] a) H. Y. Liu, K. Eriks, A. Prock, W. P. Giering, *Organometallics* **1990**, 9, 1758–1766; b) A. H. Cowley, R. E. Davis, K. Remadna, *Inorg. Chem.* **1981**, 20, 2146–2152; c) P. E. Riley, R. E. Davis, *Inorg. Chem.* **1980**, 19, 159–165.
- [33] a) K. Ueno, H. Tobita, M. Shimoi, H. Ogino, *J. Am. Chem. Soc.* **1988**, 110, 4092–4093; b) H. Tobita, K. Ueno, M. Shimoi, H. Ogino, *J. Am. Chem. Soc.* **1990**, 112, 3415–3420; c) K. Ueno, S. Ito, K. Endo, H. Tobita, S. Inomata, H. Ogino, *Organometallics* **1994**, 13, 3309–3314.
- [34] a) M. J. S. Dewar, *Bull. Soc. Chim. Fr.* **1951**, 18, C71–C79; b) J. Chatt, L. A. Duncanson, *J. Chem. Soc.* **1953**, 2939–2947.
- [35] K. Hansen, T. Szilvási, B. Blom, M. Driess, *Angew. Chem. Int. Ed.* **2015**, 54, 15060–15063; *Angew. Chem.* **2015**, 127, 15274–15277.
- [36] K. Abersfelder, A. J. P. White, R. J. F. Berger, H. S. Rzepa, D. Scheschkewitz, *Angew. Chem. Int. Ed.* **2011**, 50, 7936–7939; *Angew. Chem.* **2011**, 123, 8082–8086.
- [37] Y. Xiong, S. Yao, M. Driess, *Angew. Chem. Int. Ed.* **2007**, 46, 4511–4513; *Angew. Chem.* **2007**, 119, 4595–4597.
- [38] K. Abersfelder, A. J. P. White, H. S. Rzepa, D. Scheschkewitz, *Science* **2010**, 327, 564–566.

Manuscript received: October 17, 2018

Revised manuscript received: November 29, 2018

Accepted manuscript online: December 13, 2018

Version of record online: January 18, 2019

3.3. Boron and Phosphorus Containing Heterosiliconoids: Stable p- and n-Doped Unsaturated Silicon Clusters

Reprinted with permission from Yannic Heider, Philipp Willmes, Volker Huch, Michael Zimmer, David Scheschkewitz, *J. Am. Chem. Soc.* **2019**, *141*, 19498-19504. Copyright © (2019) American Chemical Society.

<https://doi.org/10.1021/jacs.9b11181>

The results described within this article are additionally concluded and put into context in Chapter 4.

Contributions of the Authors:

Yannic Heider: Lead: Conceptualization, Visualization, Writing – Review and Editing, Investigation, Methodology, Data Curation, Formal Analysis, Theoretical studies; Supporting: CP/MAS NMR and VT-NMR.

Philipp Willmes: Supporting: Preliminary results.

Volker Huch: Lead: X-ray analysis.


Michael Zimmer: Lead: CP/MAS NMR and VT-NMR.

David Scheschkewitz: Lead: Project administration, Supervision, Acquisition of funding and resources; Supporting: Writing – Review and Editing.

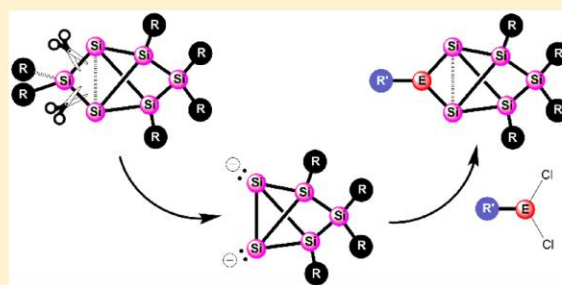
Boron and Phosphorus Containing Heterosiliconoids: Stable p- and n-Doped Unsaturated Silicon Clusters

Yannic Heider,¹ Philipp Willmes, Volker Huch, Michael Zimmer, and David Scheschkewitz*¹

Krupp-Chair for General and Inorganic Chemistry, Saarland University, 66123 Saarbrücken, Germany

 Supporting Information

ABSTRACT: Unsaturated silicon clusters (siliconoids) are short-lived intermediates during the transition from molecules to the elemental bulk; stable representatives reiterate surface features of silicon materials. The incorporation of suitable heteroatoms into the cluster scaffold of stable siliconoids extends this analogy to the technological process of silicon doping. Here, we report boron- and phosphorus-containing heterosiliconoids with BSi_5 and PSi_5 core based on the global minimum Si_6R_6 platform (dubbed benzpolarene for its relationship to benzene). The reductive cleavage of an SiR_2 moiety ($\text{R} = 2,4,6\text{-iPr}_3\text{C}_6\text{H}_2$) from Si_6R_6 selectively yields a dianionic $\text{Si}_5\text{R}_4^{2-}$ cluster as its lithium salt. Treatment with Me_3SiCl affords the corresponding trimethylsilyl-substituted $(\text{Me}_3\text{Si})_2\text{Si}_5\text{R}_4$. Reaction of $\text{Si}_5\text{R}_4^{2-}$ with $\text{iPr}_2\text{NECl}_2$ ($\text{E} = \text{B}, \text{P}$) yields the unprecedented p- and n-doped heterosiliconoids $\text{iPr}_2\text{NESi}_5\text{R}_4$. Their peculiar electronic features are compared to those of the hexasilabenzpolarene starting material on grounds of NMR spectroscopy, X-ray diffraction, and DFT calculations.



INTRODUCTION

Modern society is built on microelectronic devices and therefore vitally depends on semiconducting materials of the highest purity such as the most widely employed silicon. The purification of elemental silicon on a multiton scale, mainly by chemical vapor deposition of molecular silane precursors, is doubtlessly a key development of modern society. The chemical processes during deposition of bulk silicon and particularly of thin films are still a central research focus^{1–4} as they provide the basis for the tuning of the material's electronic properties through deliberate manipulation of composition and structure.^{5,6} The partially substituted silicon clusters (siliconoids)^{7–12} occurring as intermediates during the deposition are thought to persist in the (initially amorphous) silicon to some extent, which results in a much wider bandgap than in the annealed crystalline state.^{13–21} Stable representatives are accessible by the use of bulky substituents that confer kinetic inertness to the otherwise highly reactive species. Siliconoids echo characteristic structural and electronic features of bulk and nanoscale silicon surfaces, particularly with their unsubstituted, hemispheroidally coordinated vertices.^{10,11}

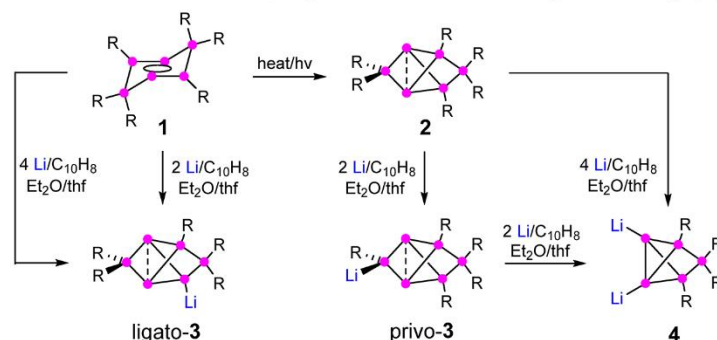
Changes in composition of silicon materials, that is the incorporation of dopants such as boron or phosphorus, are typically achieved by admixture of diborane(6) (B_2H_6) or phosphane (PH_3) at a late stage of silicon purification for band gap engineering in the crystalline state.^{22–27} The superconductivity of cubic silicon at high boron concentrations and temperatures near 0 K constitutes an extreme manifestation of the effect of heteroatoms on electronic properties of silicon.²⁸ While a few stable examples of heterosiliconoids containing

heavier Group 14 elements, namely, germanium and tin, are known,^{29–31} related species with Group 13 and/or 15 elements have so far only been observed in the gas phase or were calculated theoretically.^{32–35} We recently reported the functionalization of the dismutational isomer (1)⁷ and the global minimum isomer (2)⁸ of the still hypothetical hexasilabenzene by reductive cleavage of one of the aryl substituents (Scheme 1). As distinct functionalized derivatives of 2 were obtained regiospecifically in both cases,^{36,37} the peculiar stability of this type of Si_6 scaffold became once more obvious. We therefore coined the term “benzpolarene” as a simple nomenclature in reference to its relationship to benzene. Inspired by the *ortho-meta-para* nomenclature of disubstituted benzenes, we also introduced the prefixes *privo*, *nudo*, *ligato*, and *remoto* for the unambiguous reference to the four distinct positions in the benzpolarene scaffold.³⁷ With the presence of a negatively charged silicon vertex and an otherwise uncompromised siliconoid framework with two unsubstituted vertices, *ligato-3* and *privo-3* helped close the conceptual gap between neutral siliconoids and the ligand-free multiply charged Zintl anions of silicon,^{38–41} which have garnered attention as potential high-capacitance electrode material for lithium ion batteries.^{42–44} While silicon-based Zintl anions have only recently been used as starting material for siliconoids with partial substitution by hydrogen, silyl or stannyl groups,^{40,41,45–47} *ligato-3* and *privo-3* are excellent reagents for the nucleophilic transfer of the unperturbed

Received: October 17, 2019

Published: November 15, 2019

Scheme 1. Syntheses of Monoanionic Siliconoids *ligato-3*³⁶ and *privo-3*³⁷ and the Novel Dianionic Si₅ Cluster 4 (This Work) from the Two Hexasilabenzene Isomers 1⁷ and 2⁸ (Magenta Circles = Si; R = Tip = 2,4,6-*i*-Pr₃C₆H₂)



cluster framework toward various electrophiles from Groups 13 to 15.^{36,37} In particular, the successful grafting of boron- and phosphorus-containing moieties to the periphery of the cluster encouraged us to investigate the incorporation of these two elements into the cluster scaffold itself and thus obtain true heterosiliconoids containing the two elements typically employed for p- and n-doping of elemental silicon.

Based on the pronounced electron deficit of the hexasilabenzpolarene scaffold in the *privo* position as manifested in the appearance of the LUMO,⁸ we anticipated that an excess of reducing agent might cleave this vertex to yield a vicinal dianionic Si₅ cluster.

RESULTS AND DISCUSSION

While *ligato-3* turned out to be inert toward an excess of lithium/naphthalene, treatment of *privo-3* with 2 equiv of Li/C₁₀H₈ indeed affords the lithium salt of dianionic **4** in an NMR-spectroscopically quantitative manner (Scheme 1). Notably, **4** is also accessible in a one-pot reaction by directly treating the benzpolarene **2** with four equivalents of Li/C₁₀H₈. Formally, the *privo*-SiTip₂ moiety of **2** is cleaved during the reduction and the two former unsubstituted *nudo*-vertices end up being lithiated instead. Owing to the high symmetry of the silicon scaffold, the ²⁹Si NMR spectrum of **4** in C₆D₆ shows only three broad resonances at $\delta = 55.7$, -90.1 , and -298.3 ppm in a 1:2:2 ratio. The broadening of the signals is tentatively attributed to solution equilibria involving aggregates of different sizes as well as varying amounts of coordinating solvent molecules and/or partial dissociation into solvent separated ions pairs. Indeed, the ⁷Li NMR spectrum of a solution of **4** in toluene-*d*₈ shows up to six distinct resonances at low temperature (see Supplementary Figures 5–7). Dilithiated **4** is isolated as a dark ochre microcrystalline powder by precipitation from hexane in good yields (69%). A preliminary X-ray diffraction study on single crystals grown from a hexane/toluene mixture unambiguously confirmed the constitution of **4** as the corresponding dimer [4]₂·(THF)₃ in the solid state despite the rather low quality of the data set (see Supplementary Table 1 and Figure 28). The four lithium cations form a central diamond shape and thus connect the two dianionic Si₅ moieties. Notably, only three of the four central lithium atoms are coordinated by one donating THF molecule, while the fourth remains exposed. This is also reflected in the ⁷Li CP/MAS NMR spectrum with three signals at $\delta = 5.80$, 2.28, and -0.57 ppm (ratio 1:2:1, see Supplementary Figure 8). Meanwhile, the ²⁹Si CP/MAS

NMR spectrum confirms the *pseudo*-symmetry of the Si₅ moieties with only three resonances at $\delta = 42.4$, -100.5 , and -290.6 ppm (1:2:2, see Supplementary Figure 4). In order to obtain higher quality X-ray data, we prepared a highly diluted solution of **4** in hexane out of which small amounts of single crystals of [4]₂·(THF)₂ could be isolated after several weeks. In this case, the inversion-symmetric structural model could be refined with only minor disorder problems due to cocrystallized hexane molecules (Figure 1). The following discussion will therefore exclusively refer to [4]₂·(THF)₂.

As in [4]₂·(THF)₃, the four central lithium cations in [4]₂·(THF)₂ are arranged in a planar diamond-shape at the center of the dimer. Only Li2 and Li2' are coordinated by a donating thf-ligand in this case, while the coordination spheres of Li1 and Li1' are saturated through coordination by the *ligato*-

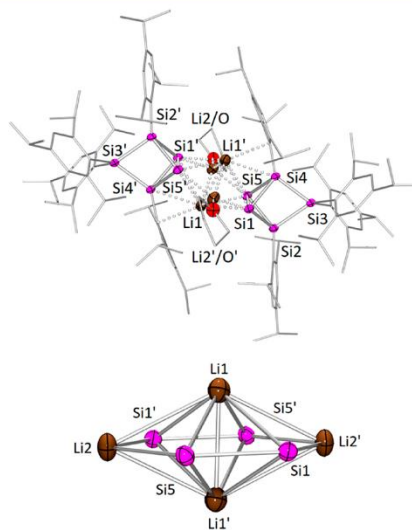
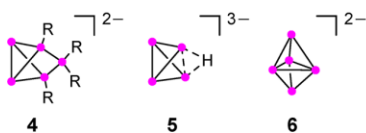


Figure 1. Molecular structure in the solid state of the dimer of dianionic Si₅ cluster [4]₂·(THF)₂ (top) and close-up of the central hexagonal bipyramidal arrangement of the four anionic silicon vertices with their lithium counter cations (bottom). Thermal ellipsoids are displayed at 50% probability. Hydrogen atoms, carbon ellipsoids, and cocrystallized solvent molecules are omitted for clarity. Selected bond lengths [Å]: Si1–Si5 2.5524(6), Si1–Si2 2.3822(6), Si1–Si4 2.3229(6), Si1–Li1 2.858(3), Si2–Li1 2.785(3), and Li1–Li1' 2.793(7).

bonded Tip substituents, which becomes apparent in pronounced bending of this aryl groups toward the Li atom in question. This phenomenon is regularly observed in aryl-substituted lithiosilanes and was rationalized by the group of Strohmann.⁴⁸ The corresponding torsion angles Si–C_i–C_o–C_m in [4]₂·(THF)₂ (169.14° and 166.63°) are even larger than those in phenyl substituted lithiosilanes (170.5–179.4°)⁴⁸ despite the sterically more demanding Tip-substituent. This is also reflected in the much shorter Si4–Li1' distance (2.785 Å) compared to the corresponding one between Si2 and Li1 (4.007 Å). Disregarding the counter cations, the silicon cluster core of 4 consists of a Si₄Tip₂²⁻ tetrahedron, which is edge-bridged by an additional SiTip₂ moiety. It is hence closely related to the edge-on protonated smallest deltahedral Zintl ion [μ-HSi₄]³⁻ 5, recently detected in solution by Korber et al. (Chart 1).⁴⁵ The distance between the anionic vertices (Si1–

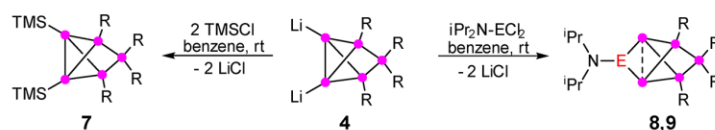
Chart 1. Comparison of the Stable Dianionic Silicon Cluster 4, the Elusive Edge-on Protonated Zintl Anion 5,⁴⁴ and the Dianionic Bare Pentasilicide 6^{45,49} (Magenta Circles = Si; R = Tip = 2,4,6-*i*-Pr₃C₆H₂)



Si5 2.5524(6) Å) in [4]₂·(THF)₂ is similar to the equatorial Si–Si bond lengths in dianionic pentasilicide [Si₅]²⁻ 6 (2.535 Å).⁴⁹ Incidentally, this also holds true for the distance between the *nudo*-Si centers in monoanionic siliconoids *ligato*-3 (2.5506 Å)³⁶ and *privo*-3 (2.5562 Å).³⁷ All other bond lengths show values close to standard single bonds and are thus comparable to those observed for homoatomic benzpolarene-type siliconoids.^{7–11,36,37}

The remarkable upfield shifted ²⁹Si NMR resonance of the anionic silicon vertices in 4 (δ = –298.3 ppm) is reminiscent of those of 5 (δ²⁹Si = –404.5 and –327.8 ppm)⁴⁵ and the equatorial vertices in 6 (δ²⁹Si = –347.8 ppm)⁴⁵ and other silicon based Zintl-anions in general.^{50–52} Despite the recently reported protonation as well as one case in which it was employed as ligand,^{45,53} the functionalization of Si₄⁴⁻ via nucleophilic substitution is unknown due to the multiple negative charges and the ensuing exceptionally high reduction potential and inherent insolubility in conventional solvents.³⁹ In contrast, the dianionic Si₅ cluster compound 4, which mimics both structural and electronic features of bare silicides, readily dissolves in common organic solvents such as benzene, toluene, and THF and is stable in solution under argon up to several weeks at room temperature depending on the solvent. As a proof-of-principle reaction, the addition of 2 equiv of Me₃SiCl to a solution of 4 in benzene promptly affords the anticipated bis(trimethylsilyl)-substituted neutral Si₅ cluster 7

Scheme 2. Syntheses of Bis(trimethylsilyl)-Substituted Si₅-Cluster 7 and Boron- and Phosphorus-Doped Siliconoids 8 and 9 (Magenta Circles = Si; E = B, P; R = Tip = 2,4,6-*i*-Pr₃C₆H₂)



19500

DOI: 10.1021/jacs.9b11181
J. Am. Chem. Soc. 2019, 141, 19498–19504

in quantitative spectroscopic yield (Scheme 2). The ²⁹Si NMR spectrum of 7 shows four resonances at δ = 34.7, 1.7, –81.3, and –231.3 ppm (ratio 1:2:2:2). The molecular structure in the solid state as determined by X-ray diffraction on single crystals is shown in Figure 2 and revealed a distinctly shorter

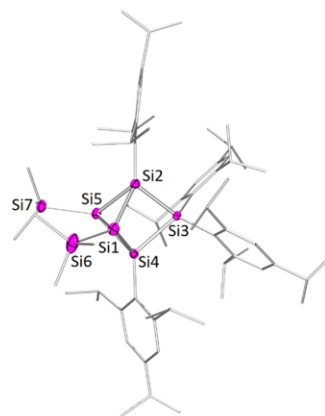


Figure 2. Molecular structure in the solid state of the bis-(trimethylsilyl)-substituted Si₅-cluster 7. Thermal ellipsoids are displayed at 50% probability. Hydrogen atoms, carbon ellipsoids, and cocrystallized solvent molecules are omitted for clarity. Selected bond lengths [Å]: Si1–Si5 2.469(1), Si1–Si2 2.302(1), Si1–Si4 2.338(1), Si1–Si6 2.332(1), and Si2–Si3 2.376(1).

Si1–Si5 bond distance (2.469(1) Å) compared to that in the dianionic precursor [4]₂·(THF)₂ (2.5524(6) Å), albeit still longer than the typical Si–Si single bond. The much longer bond in [4]₂·(THF)₂ can therefore be attributed to Coulomb repulsion of the directly neighbored negative charges. Despite the formally electron-precise and saturated nature of 7, however, the trimethylsilyl-substituted bridgehead silicon vertices Si1 and Si5 exhibit hemispheroidal coordination environments with hemisphericity parameters of φ = 0.2541 Å and φ = 0.3121 Å.^{10,11,37} This surprising observation is tentatively attributed to the steric strain in the bicyclobutane moiety, which enforces the observed lengthening of the bridgehead Si–Si bond even in the absence of Coulomb repulsion and thus shifts electron density into the nonbonding perimeter of the cluster scaffold.

Encouraged by this finding, we considered dichlorides of boron and phosphorus as electrophiles toward 4 with the intention of restoring the six-atomic benzpolarene-scaffold of 2 with the *privo*-Si vertex being formally substituted by a heteroatom. Indeed, the addition of dichloro-*N,N*-diisopropylaminoborane or -phosphane, respectively, to a solution of the dianionic Si₅-cluster 4 in benzene at room temperature readily yields the anticipated heteroatomic siliconoids 8 and 9 (Scheme 2). Although saturated six-vertex cages of silicon

and phosphorus^{54,55} as well as phosphine-functionalized Zintlions of germanium⁵⁶ are known, there is no precedence for the incorporation of either Group 13 or 15 vertices into the scaffold of unsaturated silicon clusters such as siliconoids or Zintl anions. Both **8** and **9** were fully characterized by multinuclear NMR spectroscopy and X-ray diffraction (Figures 3 and 4). The pronounced electronic anisotropy and the

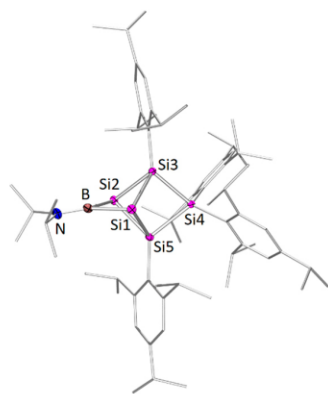


Figure 3. Molecular structure in the solid state of heteronuclear siliconoid **8**. Thermal ellipsoids are displayed at 50% probability. Hydrogen atoms, carbon ellipsoids, and cocrystallized solvent molecules are omitted for clarity. Selected bond lengths [Å]: Si1–B 2.031 (1), Si1–Si2 2.5911(4), Si1–Si3 2.3270(4), Si3–Si4 2.3816(4), and B–N 1.374(2).

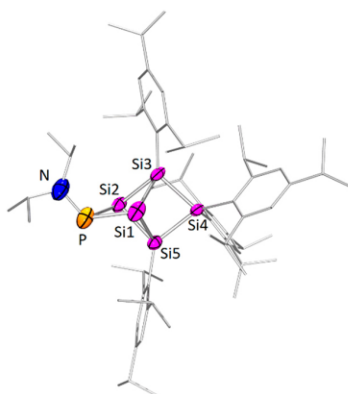


Figure 4. Molecular structure in the solid state of heteronuclear siliconoid **9**. Thermal ellipsoids are displayed at 50% probability. Hydrogen atoms, carbon ellipsoids, and cocrystallized solvent molecules are omitted for clarity. Selected bond lengths [Å]: Si1–P 2.314(2), Si1–Si2 2.613(1), Si1–Si3 2.391(2), Si3–Si4 2.38(1), and P–N 1.651(3).

resulting unusual wide dispersion of ²⁹Si NMR chemical shifts of homonuclear siliconoids are some of their hallmarks.^{10,11} Besides the frequently observed upfield shifted resonances for unsubstituted silicon vertices, all Si₆ siliconoids with a benzpolarene scaffold^{7–11} show a distinct deshielding of the tetracoordinate *privo*-position in the ²⁹Si NMR spectra slightly depending on the electronic nature of pending functionalities.³⁷ On grounds of calculations, this had been attributed to a paratropic cluster current vortex surrounding the silicon center in this particular position.^{8,57} A complementary

explanation referred to the LUMO topology indicating pronounced silylene character at the *privo* vertex.³¹ This deshielding effect can be regarded as a spectroscopic fingerprint of the uncompromised benzpolarene cluster scaffold.

The boron atom in the *privo*-position in **8** also gives rise to a low-field shifted resonance at $\delta = 83.3$ ppm in the ¹¹B NMR spectrum and three signals at $\delta = 39.0, -43.3,$ and -288.6 ppm (ratio 1:2:2) in the ²⁹Si NMR spectrum including the anticipated upfield resonance for the unsubstituted silicon vertices. Although silyl-substituted amino boranes systematically show ¹¹B NMR shifts at up to $\delta = 72.1$ ppm,⁵⁸ most neutral aminoboranes typically give rise to ¹¹B NMR resonances between $\delta = 6.5$ ppm and $\delta = 47.6$ ppm.⁵⁹ In fact, the detected ¹¹B signal of **8** is close to the range of terminal and bridging aminoborylene complexes of transition metals ($\delta = 86.6$ – 119.1 ppm).⁶⁰ The unusual deshielding at the boron vertex of **8** may thus be attributed to a certain borylene character. A similar picture emerges for the phosphorus-doped siliconoid **9**, which gives rise to a ³¹P NMR resonance at $\delta = 386.7$ ppm. The strongly low-field shifted resonance in comparison to common tricoordinate aminophosphanes ($\delta = 42.9$ – 177.7 ppm)⁶¹ is even approaching the range of chemical shifts observed for amino-substituted diphosphenes ($\delta = 448.8$ – 577.6 ppm)⁶² but still far away from the maximal deshieldings observed in transition metal phosphinidene complexes.⁶³ Due to the presence of the symmetry breaking lone pair at the phosphorus atom of **9**, each silicon vertex gives rise to an individual ²⁹Si NMR signal ($\delta = 153.7, 8.2, -76.7, -225.8,$ and -240.0 ppm). The two high-field resonances are characteristic for the *nudo* positions of benzpolarenes; the assignment is confirmed by the absence of a cross-peak to a Tip group in the ²⁹Si NMR spectrum. The signal of the *ligato* silicon vertex *trans* to the phosphorus lone pair at 153.7 ppm is strongly deshielded compared to other neutral benzpolarene-type siliconoids.^{7–11,36,37} The isoelectronic anionic benzpolarene *privo*-3 alone displays a similar low-field shifted resonance for one *ligato*-vertex (100.2 ppm). As *privo*-3 and **9** share the presence of a lone pair at the *privo*-position of the benzpolarene scaffold, we speculate that the nonbonding electron density at this position desymmetrizes the magnetically induced cluster currents typical for benzpolarenes.⁵⁷ This phenomenon is also reflected in different Si–P coupling constants for the *nudo*-silicon vertices ($J_{P-Si} = 105.4$ and 124.4 Hz). Furthermore, while one *ligato*-silicon vertex gives rise to a doublet resonance in the ²⁹Si NMR spectrum with a coupling constant of $^2J_{P-Si} = 41.0$ Hz, the other one shows no coupling at all.

For further confirmation of the structures of **8** and **9**, we calculated their ²⁹Si, ³¹P, and ¹¹B NMR chemical shifts at the OLYP/def2-TZVPP//BP86/def2-SVP and the OLYP/pcS-2//BP86/def2-SVP levels of theory.⁶⁴ The good agreement of both the optimized structure and the calculated chemical shifts with the experimental data leaves no doubt about the integrity of the cluster scaffolds of **8** and **9** in solution (see Supplementary Tables 15 and 16).

An X-ray analysis on single crystals of **8** and **9** unambiguously confirmed their constitutions (Figures 3 and 4). Severe disorder of the organic substituents in **9**, however, led to a less than satisfactory refinement of the model (see the Supporting Information for details). The following discussion of structural parameters is therefore limited to the boron-containing heterosiliconoid **8** (Figure 3): The Si–B bond

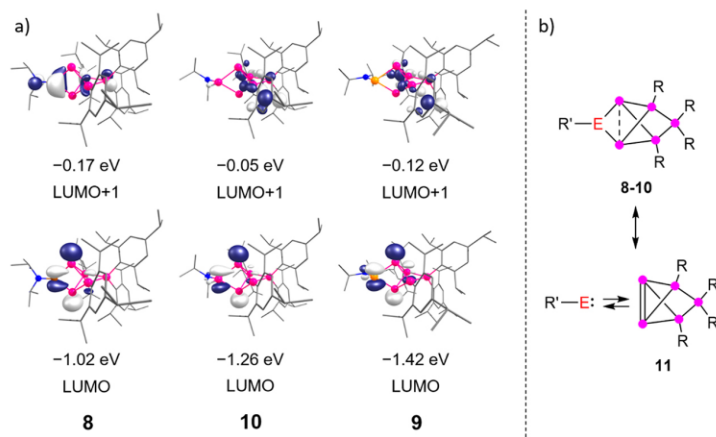


Figure 5. (a) Comparison of the LUMOs and LUMO+1s of the doped siliconoids **8** and **9** and the model system **10** (isocontour value: 0.051840). (b) Representation of **8–10** as complexes of the hypothetical neutral Si₅Tip₄ moiety **11** with the free borylene, silylene, and phosphinidene, respectively (magenta circles = Si; R = Tip = 2,4,6-Pr₃C₆H₂; R' = NⁱPr₂; E = B, SiH, P).

lengths (Si1–B 2.031(1) and Si2–B 2.038(1) Å) in **8** are marginally longer than the exohedral Si–B bonds of both *ligato*- and *privo*-borate substituted hexasilabenzpolarenes (2.009³⁶ and 2.023 Å³⁷), which is very likely due to the higher steric demand of the NⁱPr₂ substituent. However, they are still shorter than those in a cyclic amino-substituted boracyclopentasilane (2.109 and 2.112 Å)⁵⁸ which is tentatively attributed to the more pronounced back-donation ability of the tetramethylpiperidinyl ligand employed in the latter case. The distance between the *nudo*-vertices (2.5911(4) Å) is slightly larger than that in the monoanionic siliconoids *ligato*-**3** (2.5506 Å)³⁶ and *privo*-**3** (2.5562 Å)³⁷ and the dianionic Si₅ precursor [4]₂·(THF)₂ (2.5524(6) Å) but shorter than those in all neutral homoatomic hexasilabenzpolarenes (2.6024–2.7076 Å).³⁷ The shortening can be attributed to the smaller atomic radius of boron compared to silicon. All other endohedral bonds in **8** are comparable to those observed for homoatomic benzpolarene-type siliconoids.^{7–11,36,37} To gain further insight into the electronic structures of **8** and **9**, we calculated their frontier orbitals at the M06-2X/def2-SVPP//BP86/def2-SVP level of theory. The homoatomic model system **10** in which the *privo* silicon atom carries one hydrogen and one NⁱPr₂ group was also calculated to allow for comparison in the absence of substituent effects. As in the case of **2**,⁸ the HOMO of all three species corresponds to cluster bonding electrons rather than the predominantly nonbonding orbitals at the unsubstituted bridgehead atoms (see Supplementary Table 13). The LUMOs are depicted in Figure 5a and consist mainly of three parallel p-orbitals, one of which is centered at the *privo* and the collinear other two at the *nudo*-positions. While the topology of the LUMO is barely affected by the nature of the *privo*-vertex, its energy is by 0.4 eV lower for **9** than for **8**.

Compared to the Si₆ model system **10**, a boron atom at the *privo*-position raises the LUMO energy ($\Delta E = 0.24$ eV), while a phosphorus atom causes the opposite effect ($\Delta E = 0.16$ eV). Whereas a similar juxtaposition of the corresponding all-Tip substituted compounds reveals an analogous situation for **2** and **9**_{Tip}, the LUMOs of **2** and **8**_{Tip} are almost equal in energy (see Supplementary Table 14). Unsurprisingly, the back-bonding of the NⁱPr₂ group exerts the strongest influence on

the electronic structure of the cluster core when attached to the electron-deficient boron center as in **8**. The topology of the LUMOs of **2**, **8**, and **9** at the *privo*-positions strongly resembles the LUMOs of the corresponding free silylene, borylene, and phosphinidenes, respectively. The homo and hetero persilabenzpolarene structures may therefore be regarded as complexes of the latter with a hypothetical neutral Si₅Tip₄ moiety **11** with a strongly *cis*-bent Si=Si double bond (Figure 5b). In the case of **8**, this point of view is additionally supported by the LUMO+1 with a dominant contribution of a second p orbital at the boron center, which is perpendicular to the one contributing to the LUMO just like in free borylene. The LUMO+1s of **10** and **9** on the other hand are mainly distributed over the *ligato*-bonded Tip-ligands.

In conclusion, the dianionic R₄Si₅ cluster **4** is accessible by reductive cleavage of one vertex of the neutral Si₆ benzpolarene **2**. The doubly lithiated scaffold of **4** is reminiscent of tetrahedral Zintl anions of silicon in terms of structural and electronic properties. In contrast to Zintl anions, however, the high solubility and stability in common organic solvents at ambient temperatures allows for the facile derivatization of **4** with electrophiles, for instance, the straightforward reaction with 2 equiv of Me₃SiCl. In addition, **4** turned out to be a valuable synthon for the generation of unprecedented molecular heterosiliconoids **8** and **9** with boron and phosphorus directly incorporated into the cluster scaffold. Full characterization of **8** and **9** including theoretical investigations confirmed the integrity of the electronic benzpolarene signature despite the substitution of the *privo*-silicon vertex by the heteroatoms.

■ ASSOCIATED CONTENT

Supporting Information

The Supporting Information is available free of charge at <https://pubs.acs.org/doi/10.1021/jacs.9b11181>.

- Crystallographic data of [4]₂·(THF)₃ (CIF)
- Crystallographic data of **7** (CIF)
- Crystallographic data of **9** (CIF)
- Crystallographic data of **8** (CIF)
- Crystallographic data of [4]₂·(THF)₂ (CIF)

Experimental procedures; NMR, CP-MAS NMR, and UV-vis spectra; X-ray crystallographic data; computational details (PDF)

AUTHOR INFORMATION

Corresponding Author

*scheschkewitz@mx.uni-saarland.de

ORCID

Yannic Heider: 0000-0001-5822-7601

David Scheschkewitz: 0000-0001-5600-8034

Notes

The authors declare no competing financial interest.

ACKNOWLEDGMENTS

Funding by the Deutsche Forschungsgemeinschaft (DFG SCHE 906/4-1 and 4-2) is gratefully acknowledged.

REFERENCES

- Filtvedt, W. O.; Holt, A.; Ramachandran, P. A.; Melaaen, M. C. Chemical vapor deposition of silicon from silane: review of growth mechanisms and modeling/scaleup of fluidized bed reactor. *Sol. Energy Mater. Sol. Cells* **2012**, *107*, 188–200.
- Ramanujam, J.; Verma, A. Photovoltaic properties of a-Si:H films grown by plasma enhanced chemical vapor deposition: a review. *Mater. Express* **2012**, *2*, 177–196.
- Tonokura, K.; Koshi, M. Reaction kinetics in silicon chemical vapor deposition. *Curr. Opin. Solid State Mater. Sci.* **2002**, *6*, 479–485.
- Hadjisavvas, G.; Kopidakis, G.; Kelires, P. C. Structural models of amorphous silicon surfaces. *Phys. Rev. B: Condens. Matter Mater. Phys.* **2001**, *64*, 125413.
- Venema, L. Silicon electronics and beyond. *Nature* **2011**, *479*, 309.
- Teo, B. K.; Sun, X. H. Silicon-based low-dimensional nanomaterials and nanodevices. *Chem. Rev.* **2007**, *107*, 1454–1532.
- Abersfelder, K.; White, A. J. P.; Rzepa, H. S.; Scheschkewitz, D. A tricyclic aromatic isomer of hexasilabenzene. *Science* **2010**, *327*, 564–566.
- Abersfelder, K.; White, A. J. P.; Berger, R. J. F.; Rzepa, H. S.; Scheschkewitz, D. A stable derivative of the global minimum on the Si₆H₆ potential energy surface. *Angew. Chem., Int. Ed.* **2011**, *50*, 7936–7939.
- Abersfelder, K.; Russell, A.; Rzepa, H. S.; White, A. J. P.; Haycock, P. R.; Scheschkewitz, D. Contraction and expansion of the silicon scaffold of stable Si₆R₆ isomers. *J. Am. Chem. Soc.* **2012**, *134*, 16008–16016.
- Iwamoto, T.; Ishida, S. Silicon compounds with inverted geometry around silicon atoms. *Chem. Lett.* **2014**, *43*, 164–170.
- Heider, Y.; Scheschkewitz, D. Stable unsaturated silicon clusters (siliconoids). *Dalton Trans.* **2018**, *47*, 7104–7112.
- Akasaka, N.; Ishida, S.; Iwamoto, T. Transformative Si₈R₈ siliconoids. *Inorganics* **2018**, *6*, 107.
- Raghavachari, K.; Logovinsky, V. Structure and bonding in small silicon clusters. *Phys. Rev. Lett.* **1985**, *55*, 2853–2856.
- Jarrold, M. F. Nanosurface chemistry on size-selected silicon clusters. *Science* **1991**, *252*, 1085–1092.
- Watanabe, M. O.; Murakami, H.; Miyazaki, T.; Kanayama, T. Three types of stable structures of hydrogenated silicon clusters. *Appl. Phys. Lett.* **1997**, *71*, 1207–1209.
- Meleshko, V.; Morokov, Y.; Schweigert, V. Structure of small hydrogenated silicon clusters: global search of low-energy states. *Chem. Phys. Lett.* **1999**, *300*, 118–124.
- Rechtsteiner, G. A.; Hampe, O.; Jarrold, M. F. Synthesis and temperature-dependence of hydrogen-terminated silicon clusters. *J. Phys. Chem. B* **2001**, *105*, 4188–4194.
- Yu, D. K.; Zhang, Q.; Lee, S. T. Structural properties of hydrogenated silicon nanocrystals and nanoclusters. *J. Appl. Phys.* **2002**, *92*, 7453–7458.
- Ning, N.; Rinaldi, S. M.; Vach, H. An atomic-scale study of hydrogenated silicon cluster deposition on a crystalline silicon surface. *Thin Solid Films* **2009**, *517*, 6234–6238.
- Shcherbina, Y. S.; Torchynska, T. V. Optical and structural investigation of Si nanoclusters in amorphous hydrogenated silicon. *Thin Solid Films* **2010**, *518*, S204–S207.
- Haertelt, M.; Lyon, J. T.; Claes, P.; de Haeck, J.; Lievens, P.; Fielicke, A. Gas-phase structures of neutral silicon clusters. *J. Chem. Phys.* **2012**, *136*, 064301.
- Spear, W. E.; Le Comber, P. G. Substitutional doping of amorphous silicon. *Solid State Commun.* **1975**, *17*, 1193–1196.
- Spear, W. E.; Le Comber, P. G. Electronic properties of substitutionally doped amorphous Si and Ge. *Philos. Mag.* **1976**, *33*, 935–949.
- Aspnes, D. E.; Studna, A. A.; Kinsbron, E. Dielectric properties of heavily doped crystalline and amorphous silicon from 1.5 to 6.0 eV. *Phys. Rev. B: Condens. Matter Mater. Phys.* **1984**, *29*, 768–779.
- Stutzmann, M.; Biegelsen, D. K.; Street, R. A. Detailed investigation of doping in hydrogenated amorphous silicon and germanium. *Phys. Rev. B: Condens. Matter Mater. Phys.* **1987**, *35*, 5666–5701.
- Lengyel, I.; Jensen, K. F. A chemical mechanism for in situ boron doping during silicon chemical vapor deposition. *Thin Solid Films* **2000**, *365*, 231–241.
- Murota, J.; Sakuraba, M.; Tillack, B. Atomically controlled processing for doping in future Si-based devices. *ECS Trans.* **2011**, *37*, 181–188.
- Bustarret, E.; Marcenat, C.; Achatz, P.; Kačmarčík, J.; Lévy, F.; Huxley, A.; Ortéga, E.; Bourgeois, E.; Blase, X.; Débarre, D.; Boulmer, J. Superconductivity in doped cubic silicon. *Nature* **2006**, *444*, 465–468.
- Nied, D.; Oña-Burgos, P.; Klopfer, W.; Breher, F. Tuning the gap: electronic properties and radical-type reactivities of heteronuclear [1.1.1]propellanes of heavier group 14 elements. *Organometallics* **2011**, *30*, 1419–1428.
- Ito, Y.; Lee, V. Y.; Gornitzka, H.; Goedecke, C.; Frenking, G.; Sekiguchi, A. Spirobis(pentagerma[1.1.1]propellane: a stable tetraradicaloid. *J. Am. Chem. Soc.* **2013**, *135*, 6770–6773.
- Jana, A.; Huch, V.; Repisky, M.; Berger, R. J. F.; Scheschkewitz, D. Dismutational and global-minimum isomers of heavier 1,4-dimetallatetrasilabenzenes of group 14. *Angew. Chem., Int. Ed.* **2014**, *53*, 3514–3518.
- Truong, N. X.; Haertelt, M.; Jaeger, B. K. A.; Gewinner, S.; Schöllkopf, W.; Fielicke, A.; Dopfer, O. Characterization of neutral boron-silicon clusters using infrared spectroscopy: the case of Si₆B. *Int. J. Mass Spectrom.* **2016**, *395*, 1–6.
- Lu, S.-J.; Xu, X.-L.; Cao, G.-J.; Xu, H.-G.; Zheng, W.-J. Structural evolution and bonding properties of BSi_n^{-/0} (n = 4–12) clusters: size-selected anion photoelectron spectroscopy and theoretical calculations. *J. Chem. Phys.* **2018**, *149*, 174314.
- Chang, Y.; Li, G.; Gao, A.; Chen, H.; Li, Q. The geometric, energetic, and electronic properties of charged phosphorus-doped silicon clusters, PSi_n^{+/PSi_n⁻} (n = 1–8). *Theor. Chem. Acc.* **2011**, *130*, 1009–1022.
- Nigam, S.; Majumder, C.; Kulshreshtha, S. K. Structural and electronic properties of Si_n, Si_n⁻ and PSi_{n-1} clusters (2 ≤ n ≤ 13): theoretical investigation based on ab initio molecular orbital theory. *J. Chem. Phys.* **2006**, *125*, 074303.
- Willmes, P.; Leszczyńska, K.; Heider, Y.; Abersfelder, K.; Zimmer, M.; Huch, V.; Scheschkewitz, D. Isolation and versatile derivatization of an unsaturated anionic silicon cluster (siliconoid). *Angew. Chem., Int. Ed.* **2016**, *55*, 2907–2910.
- Heider, Y.; Poitiers, N. E.; Willmes, P.; Leszczyńska, K. I.; Huch, V.; Scheschkewitz, D. Site-selective functionalization of Si₆R₆ siliconoids. *Chem. Sci.* **2019**, *10*, 4523–4530.

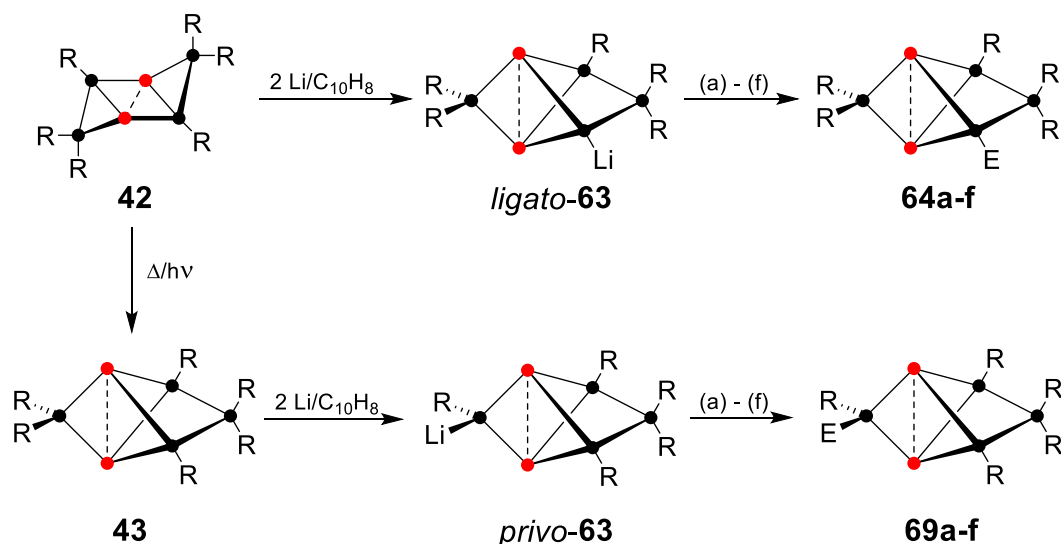
- (38) Scharfe, S.; Kraus, F.; Stegmaier, S.; Schier, A.; Fässler, T. F. Zintl ions, cage compounds, and intermetallic clusters of group 14 and group 15 elements. *Angew. Chem., Int. Ed.* **2011**, *50*, 3630–3670.
- (39) Fässler, T. F. Relationships between soluble zintl anions, ligand-stabilized cage compounds, and intermetallic clusters of tetrel (Si-Pb) and pentel (P-Bi) elements. In *Zintl Ions. Structure and Bonding*; Fässler, T. F., Ed.; Springer, Berlin, Heidelberg, 2011; Vol. 140.
- (40) Schiegerl, L. J.; Karttunen, A. J.; Klein, W.; Fässler, T. F. Anionic siliconoids from zintl phases: $R_3Si_9^{2-}$ with six and $R_2Si_9^{2-}$ with seven unsubstituted exposed silicon cluster atoms ($R=Si(tBu)_2H$). *Chem. - Eur. J.* **2018**, *24*, 19171–19174.
- (41) Schiegerl, L. J.; Karttunen, A. J.; Klein, W.; Fässler, T. F. Silicon clusters with six and seven unsubstituted vertices via a two-step reaction from elemental silicon. *Chem. Sci.* **2019**, *10*, 9130–9139.
- (42) Kulova, T. L.; Skundin, A. M.; Pleskov, Y. V.; Terukov, E. I.; Kon'kov, O. I. Lithium insertion into amorphous silicon thin-film electrodes. *J. Electroanal. Chem.* **2007**, *600*, 217–225.
- (43) Key, B.; Bhattacharyya, R.; Morcrette, M.; Seznéc, V.; Tarascon, J.-M.; Grey, C. P. Real-time investigations of structural changes in silicon electrodes for lithium-ion batteries. *J. Am. Chem. Soc.* **2009**, *131*, 9239–9249.
- (44) Michan, A. L.; Divitini, G.; Pell, A. J.; Leskes, M.; Ducati, C.; Grey, C. P. Solid electrolyte interphase growth and capacity loss in silicon electrodes. *J. Am. Chem. Soc.* **2016**, *138*, 7918–7931.
- (45) Hastreiter, F.; Lorenz, C.; Hioe, J.; Gärtner, S.; Lokesh, N.; Korber, N.; Gschwind, R. M. Elusive zintl ions $[\mu-HSi_4]^{3-}$ and $[Si_5]^{2-}$ in liquid ammonia: protonation states, sites, and bonding situation evaluated by NMR and theory. *Angew. Chem., Int. Ed.* **2019**, *58*, 3133–3137.
- (46) Schiegerl, L. J.; Karttunen, A. J.; Tillmann, J.; Geier, S.; Raudaschl-Sieber, G.; Waibel, M.; Fässler, T. F. Charged Si_9 clusters in neat solids and the detection of $[H_2Si_9]^{2-}$ in solution: a combined NMR, Raman, mass spectrometric, and quantum chemical investigation. *Angew. Chem., Int. Ed.* **2018**, *57*, 12950–12955.
- (47) Lorenz, C.; Hastreiter, F.; Hioe, J.; Lokesh, N.; Gärtner, S.; Korber, N.; Gschwind, R. M. The structure of $[HSi_9]^{3-}$ in the solid state and its unexpected highly dynamic behavior in solution. *Angew. Chem., Int. Ed.* **2018**, *57*, 12956–12960.
- (48) Strohmman, C.; Däschlein, C. Bent phenyl groups in lithiosilanes – crystal structures and interpretation of this unanticipated feature. *Chem. Commun.* **2008**, 2791–2793.
- (49) Goicoechea, J. M.; Sevov, S. C. Naked deltahedral silicon clusters in solution: synthesis and characterization of Si_9^{3-} and Si_5^{2-} . *J. Am. Chem. Soc.* **2004**, *126*, 6860–6861.
- (50) Goebel, T.; Ormeci, A.; Pecher, O.; Haarmann, F. The silicides M_xSi_4 with $M = Na, K, Rb, Cs$, and Ba_2Si_4 – NMR spectroscopy and quantum mechanical calculations. *Z. Anorg. Allg. Chem.* **2012**, *638*, 1437–1445.
- (51) Neumeier, M.; Fendt, F.; Gärtner, S.; Koch, C.; Gärtner, T.; Korber, N.; Gschwind, R. M. Detection of the elusive highly charged zintl ions Si_4^{4-} and Sn_4^{4-} in liquid ammonia by NMR spectroscopy. *Angew. Chem., Int. Ed.* **2013**, *52*, 4483–4486.
- (52) Scherf, L. M.; Pecher, O.; Griffith, K. J.; Haarmann, F.; Grey, C. P.; Fässler, T. F. Zintl phases $K_{4-x}Na_xSi_4$ ($1 \leq x \leq 2.2$) and K_2NaSi_8 : synthesis, crystal structures, and solid-state NMR spectroscopic investigations. *Eur. J. Inorg. Chem.* **2016**, *2016*, 4674–4682.
- (53) Waibel, M.; Kraus, F.; Scharfe, S.; Wahl, B.; Fässler, T. F. $[(MesCu)_2(\eta^3-Si_4)]^{4-}$: a mesitylcopper-stabilized tetrasilicide tetraanion. *Angew. Chem.* **2010**, *122*, 6761–6765.
- (54) Xiong, Y.; Yao, S.; Brym, M.; Driess, M. Consecutive insertion of a silylene into the P_4 tetrahedron: facile access to strained SiP_4 and Si_3P_2 cage compounds. *Angew. Chem., Int. Ed.* **2007**, *46*, 4511–4513.
- (55) Heider, Y.; Willmes, P.; Mühlhausen, D.; Klemmer, L.; Zimmer, M.; Huch, V.; Scheschke, D. A three-membered cyclic Phosphasilene. *Angew. Chem., Int. Ed.* **2019**, *58*, 1939–1944.
- (56) Geitner, F. S.; Klein, W.; Fässler, T. F. Synthesis and reactivity of multiple phosphine- functionalized nonagermanide clusters. *Angew. Chem.* **2018**, *130*, 14717–14721.
- (57) Berger, R. J. F.; Rzepa, H. S.; Scheschke, D. Ring currents in the dismutational aromatic isomer Si_6R_6 . *Angew. Chem., Int. Ed.* **2010**, *49*, 10006–10009.
- (58) Markov, J.; Fischer, R.; Wagner, H.; Noormofidi, N.; Baumgartner, J.; Marschner, C. Open, cyclic, and bicyclic compounds of double silylated phosphorus and boron. *Dalton Trans.* **2004**, 2166–2169.
- (59) Odom, J. D.; Moore, T. F.; Goetze, R.; Nöth, H.; Wrackmeyer, B. Nuclear magnetic resonance studies of boron compounds XVI carbon-13 studies of organoboranes: phenylboranes and boron-substituted aromatic heterocycles. *J. Organomet. Chem.* **1979**, *173*, 15–32.
- (60) Braunschweig, H.; Dewhurst, R. D.; Gessner, V. H. Transition metal borylene complexes. *Chem. Soc. Rev.* **2013**, *42*, 3197–3208.
- (61) Wrackmeyer, B.; Köhler, C.; Milius, W.; Grevy, J. M.; García-Hernández, Z.; Contreras, R. Aminophosphanes with bulky amino groups: molecular structure, coupling constants $^1J(^{31}P, ^{15}N)$ and $^2J(^{31}P, ^{29}Si)$, and isotope-induced chemical shifts $^1\Delta^{14/15}N(^{31}P)$. *Heteroat. Chem.* **2002**, *13*, 667–676.
- (62) Schrödel, H.-P.; Schmidpeter, A. The ^{31}P -chemical shift of diphosphenes. *Phosphorus, Sulfur Silicon Relat. Elem.* **1997**, *129*, 69–76.
- (63) Cowley, A. H. Terminal phosphinidene and heavier congeneric complexes. The quest is over. *Acc. Chem. Res.* **1997**, *30*, 445–451.
- (64) Leszczyńska, K. I.; Huch, V.; Präsang, C.; Schwabedissen, J.; Berger, R. J. F.; Scheschke, D. Atomically precise expansion of unsaturated silicon clusters. *Angew. Chem., Int. Ed.* **2019**, *58*, 5124–5128.

4. Conclusion, Context and Outlook

The reductive cleavage of an aryl group from the dismutational isomer of hexasilabenzene **42** cleanly affords the anionic siliconoid *ligato-63*^[296] with a tricyclic scaffold corresponding to that of the global minimum isomer **43**, which in turn results in the anionic Si₆ siliconoid *privo-63* with the negative charge being located at a different vertex of the otherwise identical cluster scaffold, when reduced under identical conditions.

In the first part of this PhD thesis, the experimental procedure for the synthesis of *privo-63* was optimized so that it can now be routinely isolated in multigram scale as microcrystalline powder in good yields of up to 60%. Just as in the case of the reported anionic siliconoid *ligato-63*, the corresponding *privo*-lithiated derivative was proven to be capable of the nucleophilic transfer of the unperturbed Si₆ framework towards a series of electrophiles from the Groups 13 to 15 (Scheme 29).

During the course of these investigations, the term “benzpolarene” was coined for the six-atomic silicon scaffold of **43** and its derivatives in order to emphasize the thermodynamic analogy to benzene (global minimum structure on the Si₆R₆ potential energy surface) and the inherent pronounced polarization. Furthermore, with two anionic siliconoids and their derivatives in hand that feature the identical benzpolarene framework but are functionalized at two different vertices, we felt the need for a nominal distinction. Thus, we introduced a nomenclature in the style of the well-known *ortho*, *meta*, *para* prefixes generally used in the context of disubstituted benzenes in order to distinguish between the *privo*-, two *nudo*-, two *ligato*- and a *remoto*-position in the Si₆ benzpolarene scaffold.



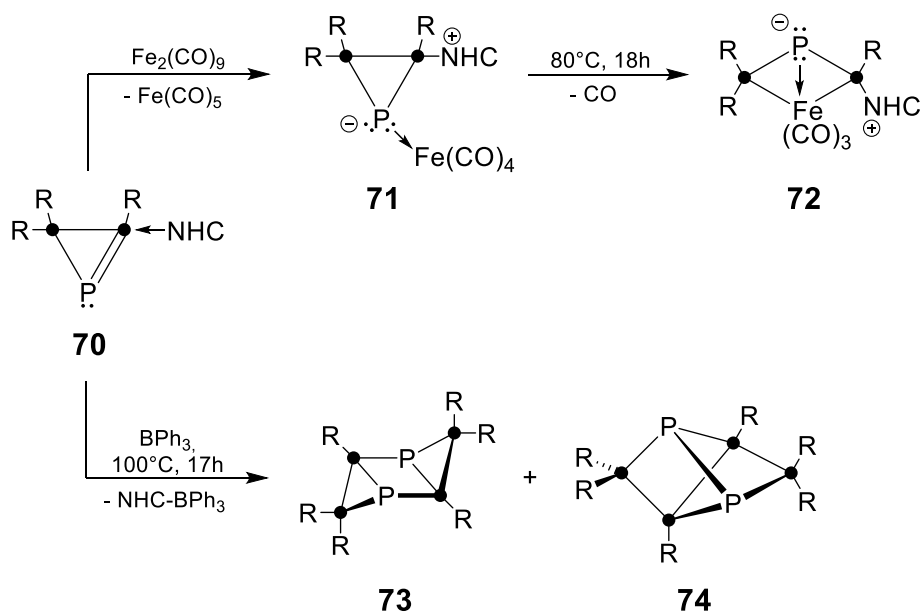
	Reagent	E
(a)	BH ₃ ·SMe ₂	BH ₃ ⁺ Li ⁻
(b)	^t BuC(O)Cl	C(O) ^t Bu
(c)	SiCl ₄	SiCl ₃
(d)	(NMe ₂) ₂ PCl	P(NMe ₂) ₂
(e)	PhC(O)Cl	C(O)Ph
(f)	Me ₃ SiCl	SiMe ₃

Scheme 29: Synthetic routes to *ligato*- and *privo*-functionalized Si₆ benzpolarenes (● = Si, ● = “naked” Si, R = Tip = 2,4,6-ⁱPr₃C₆H₂).

The evaluation and comparison of the spectroscopic data of the functionalized siliconoids *privo-63*, *ligato-63*, **64a-f** and **69a-f** revealed the peripherally attached functionalities to have a strong influence on the inherent electronic structure of the siliconoid cluster core. This is primarily reflected in a substituent-dependent shift of the low-field ²⁹Si NMR resonance of the *privo*-vertex, which is expectedly more pronounced in the case of the *privo*-functionalized derivatives with the substituent directly attached to the silicon atom in question. The observed effect was quantitatively rationalized making use of the Hammett parameters σ_m , which represent a measure for the electronegativity or -positivity of a given pending moiety. Notably, the same substituent has an opposite effect, when attached in the *privo*- or *ligato*-position, respectively: While electronegative substituents in *ligato*-position cause a deshielding of the *privo*-Si vertex, a corresponding shielding effect can be observed upon direct attachment in *privo*-position. While the chemistry of the iconic benzene is probably one of the most comprehensively investigated research areas in organic chemistry, the

complete opposite was true for its thermodynamic counterpart in the case of silicon (**43**) until very recently. With the present work, we certainly do not only contribute to a better fundamental understanding in this regard but also provide synthetic tools, which might set a launch for a faster and more comprehensive development of this emerging research area.

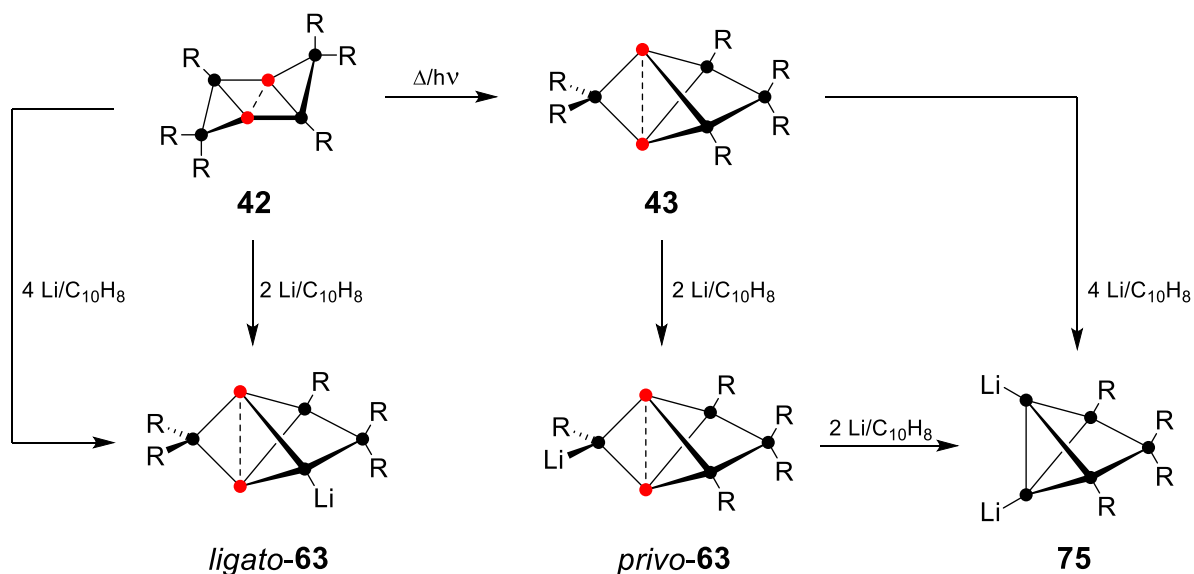
As already highlighted in the “Aims and Scope” section (Chapter 2), the successful attachment of boron and phosphorus as the prototypical dopant atoms in silicon industry to the benzpolarene Si₆ cluster core in **64a/d** and **69a/d** can be regarded a first step towards doping at a molecular level. In order to achieve the major second goal of this work, namely the incorporation of one or more dopant atoms in the cluster core itself, the initial focus rested on the identification of suitable precursors, which already contain the desired heteroatom. Very recently, the NHC-stabilized cyclic phosphasilene **70** could be isolated in our group for the first time and was already proven to be capable of acting as a donor to transition metals in the iron complex **71**. A subsequent thermally induced rearrangement afforded the Si₂PFe species **72** with a central bicyclobutane motif (Scheme 30). As **70** bears a certain resemblance to the three-membered Si₃ rings **40** and **41**, which serve as precursors to Si₆ siliconoids, it was considered as possible precursor to a Si₄P₂ cluster species. In a first step, the complete characterization of **70** was performed including X-ray diffraction studies on recrystallized samples, additional analytical methods like CP/MAS-NMR spectroscopy, 2D NMR spectroscopy and theoretical calculations. The unsaturated three-membered Si₂P ring was shown to exist as two rotational isomers in solution, of which only one is present in the solid state. The formal Si=P double bond exhibits a strong ylidic character due to the donation of the NHC-ligand to the unsaturated silicon center. In a next step, the Lewis-acid induced cleavage of the NHC-ligand was proven to indeed lead to the desired dimerization to the two Si₄P₂ cluster species **71** and **72** (Scheme 30). Both cluster frameworks are highly reminiscent of the dismutational isomer of hexasilabenzene **42** and hexasilabenzpolarene **43**, respectively. Owing to the additional valence electron of phosphorus in comparison to silicon, however, the Si₄P₂ clusters are completely saturated and lack the typical electronic features of the related, unsaturated Si₆ siliconoids as displayed by NMR and UV/vis spectroscopic data.



Scheme 30: Coordination of the NHC-stabilized three-membered cyclic phosphasilene **70** to iron as a transition-metal center and the Lewis-acid induced NHC-abstraction to yield the saturated Si_4P_2 cluster species **73** and **74** with frameworks reminiscent of the hexasilabenzene isomers **42** and **43** ($\bullet = \text{Si}$, $\text{R} = \text{Tip} = 2,4,6\text{-}i\text{Pr}_3\text{C}_6\text{H}_2$, $\text{NHC} = 1,3\text{-diisopropyl-4,5-dimethylimidazol-2-ylidene}$).

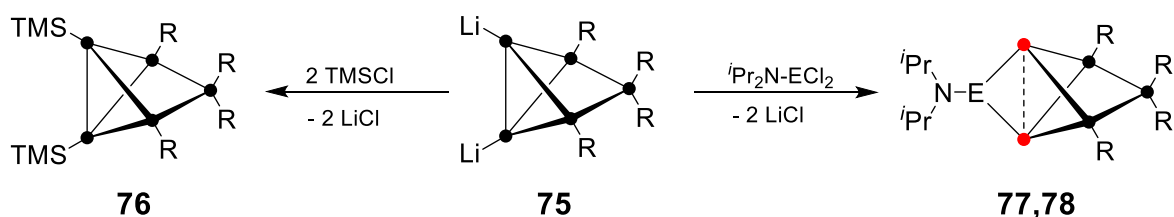
A two-electron oxidation to the corresponding dicationic species would result in an isoelectronic species; a corresponding investigation was prevented by the poor selectivity of the NHC-abstraction and associated low yields of **71** and **72**. A possible future approach could be the one-electron oxidation of the cyclic phosphasilene precursor **68**, which is available in multigram scale. The subsequent dimerization of the intermediate radical species upon liberation of the NHC-ligand might directly lead to a desired dicationic, unsaturated and thus molecularly doped siliconoid cluster. An alternative synthetic pathway for the incorporation of dopant atoms in the cluster core of siliconoids itself became finally available with the isolation of the dianionic Si_5 cluster species **75**.

Owing to the pronounced electron deficit in the *privo*-position of the hexasilabenzpolarene scaffold, the treatment of the anionic siliconoid *privo*-**63** with two equivalents of lithium/naphthalene solution resulted in the formation of the dianionic Si_5 cluster **75** upon cleavage of this exact vertex (Scheme 31). Notably, **75** is also accessible by direct reduction of the corresponding neutral precursor **43** with four equivalents of reductant, while the closely related, anionic *ligato*-**63** isomer proved to be inert under comparable reaction conditions (Scheme 31).



Scheme 31: Syntheses of monanionic siliconoids *ligato-63* and *privo-63* and the dianionic Si₅ cluster **75** (● = Si, ● = “naked” Si, R = Tip = 2,4,6-*i*-Pr₃C₆H₂).

An X-ray diffraction study on single crystals and CP/MAS NMR studies revealed the existence of **75** as its dimer in the solid-state with a central Si₄Li₂ hexagon. Corresponding VT-NMR studies suggest an equilibrium of different aggregates in solution. The dianionic Si₅ cluster species **75** is highly reminiscent of the smallest silicon-based Zintl ion [Si₄]⁴⁻ in terms of structural as well as electronic features. However, in contrast to Zintl ions, **75** can be readily dissolved in common organic solvents, which is a big advantage regarding the possible functionalization or even the construction of extended supramolecular systems based on siliconoids. Indeed, the facile twofold derivatization of **75** with Me₃SiCl in benzene to give the neutral bis(trimethylsilyl)-substituted Si₅ cluster **76** provided proof for the capability of the anionic charges in **75** to act as nucleophilic functionalities (Scheme 32). In a next step, the treatment of **75** with dichlorides of boron and phosphorus allowed for the isolation of the unprecedented heterosiliconoids **77** and **78** (Scheme 32). With the corresponding dopant atoms being directly incorporated in the cluster core and still featuring “naked” silicon vertices, they represent the first examples of molecularly doped, unsaturated siliconoid clusters and can therefore be regarded model systems for p-type or n-type doped silicon surfaces.



Scheme 32: Syntheses of bis(trimethylsilyl)-substituted Si_5 -Cluster **76** and boron- and phosphorus-doped siliconoids **77** and **78** (● = Si, ● = “naked” Si, R = Tip = 2,4,6- $i\text{Pr}_3\text{C}_6\text{H}_2$ **77**: E = B; **78**: E = P).

Full characterization of **77** and **78**, including X-ray diffraction studies on single crystals, multinuclear NMR spectroscopy, CP/MAS NMR spectroscopy, UV/vis spectroscopy and theoretical investigations confirmed both the structural and electronic analogy of the six-atomic scaffolds to the corresponding hexasila-species **43** irrespective of the nature of the atom in *privo*-position of the benzpolarene scaffold: The boron and the phosphorus atom in **77** and **78**, respectively, are similarly deshielded as the *privo*-Si vertex in **43** and give rise to resonances in the low-field regions of the ^{11}B NMR and ^{31}P NMR spectra, while the signals for the “naked” silicon vertices appear at the typical high-field in the ^{29}Si NMR spectra. The appearance of the calculated frontier orbitals at the *privo* vertex is very similar in all cases and resemble those of free borylene, silylene and phosphinidene. The corresponding orbital energies suggest that the HOMO-LUMO gap of the benzpolarene framework might be tunable by targeted manipulation of not only the *privo*-atom itself but also the pending functionalities. A future priority will be the use of the novel Si_5 dianionic cluster **75** as starting material to larger silicon-based systems. With two available nucleophilic functionalities, the linkage or catenation of two or more Si_5 moieties as well as their attachment to or embedding in nanomaterials should be within reach.

5. References

- [1] *CRC Handbook of Chemistry and Physics*, 97th edition, CRC Press, Boca Raton, Florida, **2016-2017**.
- [2] A.-L. de Lavoisier, *Traité Élémentaire de Chimie: Présenté Dans Un Ordre Nouveau et d'après Les Découvertes Modernes*, Cuchet, Paris, **1789**.
- [3] A.-L. de Lavoisier, *Elements of Chemistry: In a New Systematic Order Containing All the Modern Discoveries*, William Creech, Edinburgh, **1799**.
- [4] D. Humphry in *Philos. Trans. R. Soc. London*, London, **1808**, pp. 333–370.
- [5] T. Thomson, *A System of Chemistry in Four Volumes*, Baldwin, Cradock And Joy, London, **1817**.
- [6] J. J. Berzelius, *Ann. Phys.* **1824**, 77, 169–230.
- [7] H. S.-C. Deville, in *C. R. Hebd. Seances Acad. Sci.*, Paris, **1854**, pp. 321–326.
- [8] B. H. W. S. De Jong, R. G. C. Beerkens, P. A. van Nijnatten, E. Le Bourhis in *Ullmann's Encycl. Ind. Chem.* **2011**.
- [9] L. R. Pinckney in *Ullmann's Encycl. Ind. Chem.* **2013**.
- [10] W. Roger Cannon, E. Gugel, G. Leimer, G. Woetting, R. B. Heimann in *Ullmann's Encycl. Ind. Chem.* **2011**.
- [11] C. Barry Carter, M. Grant Norton, *Ceramic Materials: Science and Engineering*, Springer, New York, **2013**.
- [12] J. Kropp in *Ullmann's Encycl. Ind. Chem.* **2012**, 723–744.
- [13] P. C. Hewlett, *Lea's Chemistry of Cement and Concrete Fourth Edition*, Elsevier, **2003**.
- [14] H.-H. Moretto, M. Schulze, G. Wagner in *Ullmann's Encycl. Ind. Chem.* **2012**, 32, 675–712.
- [15] M. Andriot, J. DeGroot, R. Meeks, E. Gerlach, M. Jungk, A. Wolf, D. Corning, S. Cray, T. Easton, A. Mounthey, et al. *Inorg. Polym.* **2009**.
- [16] M. Mizutori, R. Yamada in *Ullmann's Encycl. Ind. Chem.* **2012**, 32, 357–394.
- [17] W. Zulehner, B. Neuer, G. Rau in *Ullmann's Encycl. Ind. Chem.* **2012**, 32, 573–601.
- [18] L. Venema, *Nature* **2011**, 479, 309.
- [19] B. K. Teo, X. H. Sun, *Chem. Rev.* **2007**, 107, 1454–1532.
- [20] W. Lu, C. M. Lieber, *Nat. Mater.* **2007**, 6, 841–850.
- [21] J. K. Rath, B. Stannowski, P. A. T. T. Van Veenendaal, M. K. Van Veen, R. E. I.

- Schropp, *Thin Solid Films* **2001**, 395, 320–329.
- [22] M. L. Snedaker, Y. Zhang, C. S. Birkel, H. Wang, T. Day, Y. Shi, X. Ji, S. Kraemer, C. E. Mills, A. Moosazadeh, et al., *Chem. Mater.* **2013**, 25, 4867–4873.
- [23] *Mineral Commodity Summaries 2019*, U.S. Geological Survey, Reston, Virginia, **2019**.
- [24] I. Bojanova, *IT Professional* **2014**, 16, 8–12.
- [25] J. Dabrowski, H.-J. Müssig, *Physics Today* **2001**, 54, 76–77.
- [26] *Fundamental Aspects of Silicon Oxidation* (Eds.: Y. J. Chabal), Springer, Berlin Heidelberg, **2001**.
- [27] J. D. Lichtenhan, *Comments Inorg. Chem.* **1995**, 17, 115–130.
- [28] R. H. Baney, M. Itoh, A. Sakakibara, T. Suzuki, *Chem. Rev.* **1995**, 95, 1409–1430.
- [29] K. Tanaka, Y. Chujo, *J. Mater. Chem.* **2012**, 22, 1733–1746.
- [30] Y. Kawakami, *React. Funct. Polym.* **2007**, 67, 1137–1147.
- [31] P. G. Harrison, *J. Organomet. Chem.* **1997**, 542, 141–183.
- [32] Ł. John, *Mater. Sci. Eng., C* **2018**, 88, 172–181.
- [33] P. A. Agaskar, *Colloids Surf.* **1992**, 63, 131–138.
- [34] H. Yoshida, Y. Takahara, T. Erata, W. Ando, *J. Am. Chem. Soc.* **1992**, 114, 1098–1100.
- [35] N. Choi, K. Asano, W. Ando, *Organometallics* **1995**, 14, 3146–3148.
- [36] M. Unno, Y. Kawai, H. Shioyama, H. Matsumoto, *Organometallics* **1997**, 16, 4428–4434.
- [37] M. Unno, D. Ishii, H. Matsumoto, *Bull. Chem. Soc. Jpn.* **1999**, 72, 2469–2473.
- [38] J. Keuter, K. Schwedtmann, A. Hepp, K. Bergander, O. Janka, C. Doerenkamp, H. Eckert, C. Mück-Lichtenfeld, F. Lips, *Angew. Chem. Int. Ed.* **2017**, 56, 13866–13871.
- [39] K. Schwedtmann, A. Hepp, K. Schwedtmann, J. J. Weigand, F. Lips, *Eur. J. Inorg. Chem.* **2019**, 2, 4719–4726.
- [40] N. Choi, K. Asano, N. Sato, W. Ando, *J. Organomet. Chem.* **1996**, 516, 155–165.
- [41] A. Sekiguchi, H. Sakurai, *Adv. Organomet. Chem.* **1995**, 37, 1–38.
- [42] S. Kyushin in *Organosilicon Compounds*, (Ed. V. Y. Lee), Academic Press, **2017**, pp. 69–144.
- [43] J. D. Corbett, *Chem. Rev.* **1985**, 85, 383–397.

- [44] J. D. Corbett in *Struct. Bonding*, Vol.87 (Ed. D. M. P. Mingos), Springer, Berlin, Heidelberg, **1997**, pp. 157–193.
- [45] S. Scharfe, T. F. Fässler, *Philos. Trans. R. Soc., A* **2010**, 368, 1265–1284.
- [46] S. Scharfe, F. Kraus, S. Stegmaier, A. Schier, T. F. Fässler, *Angew. Chem. Int. Ed.* **2011**, 50, 3630–3670.
- [47] T. F. Fässler in *Struct. Bonding*, Vol. 140, (Ed. T. F. Fässler), Springer, Berlin, Heidelberg, **2011**, pp. 91–131.
- [48] S. Gärtner, N. Korber in *Comprehensive Inorganic Chemistry II (Second Edition)*, (Eds. J. Reedjik, K. Poeppelmeier), Elsevier, **2013**, pp. 251–267.
- [49] R. J. Wilson, B. Weinert, S. Dehnen, *Dalton Trans.* **2018**, 47, 14861–14869.
- [50] T. F. Fässler, *Coord. Chem. Rev.* **2001**, 215, 347–377.
- [51] K. Abersfelder, A. Russell, H. S. Rzepa, A. J. P. White, P. R. Haycock, D. Scheschkewitz, *J. Am. Chem. Soc.* **2012**, 134, 16008–16016.
- [52] T. Iwamoto, S. Ishida, *Chem. Lett.* **2014**, 43, 164–170.
- [53] Y. Heider, D. Scheschkewitz, *Dalton Trans.* **2018**, 47, 7104–7112.
- [54] G. E. Moore, *Electronics* **1965**, 38, 114ff. (Reprinted: DOI: 10.1109/nssc.2006.4785860).
- [55] G. E. Moore at *International Electron Devices Meeting*, Washington D.C., **1975**, pp. 35–40.
- [56] S. E. Thompson, S. Parthasarathy, *Mater. Today* **2006**, 9, 20–25.
- [57] C. A. Mack, *IEEE Trans. Semicond. Manuf.* **2011**, 24, 202–207.
- [58] M. M. Waldrop, *Nature*, **2016**, 530, 144–147.
- [59] Y. S. Shcherbyna, T. V. Torchynska, *Thin Solid Films* **2010**, 518, 204–207.
- [60] K. T. T. Miyazaki, T. Uda, I. Stich, *Chem. Phys. Lett.* **1996**, 261, 346–352.
- [61] W. M. M. Kessels, M. C. M. Van De Sanden, D. C. Schram, *Appl. Phys. Lett.* **1998**, 72, 2397–2399.
- [62] H. Murakami, T. Kanayama, *Appl. Phys. Lett.* **1995**, 67, 2341–2343.
- [63] T. V. Torchynska, *Superlattices Microstruct.* **2009**, 45, 267–270.
- [64] G. Belomoin, J. Therrien, A. Smith, S. Rao, R. Twesten, S. Chaieb, M. H. Nayfeh, L. Wagner, L. Mitas, *Appl. Phys. Lett.* **2002**, 80, 841–843.
- [65] D. K. Yu, R. Q. Zhang, S. T. Lee, *J. Appl. Phys.* **2002**, 92, 7453–7458.
- [66] M. O. Watanabe, H. Murakami, T. Miyazaki, T. Kanayama, *Appl. Phys. Lett.* **1997**, 71, 1207.
- [67] Y. Ge, J. D. Head, *Int. J. Quantum Chem.* **2003**, 95, 617–626.

- [68] I.-S. Hwang, M.-S. Ho, T. Tsong, *Phys. Rev. Lett.* **1999**, *83*, 120–123.
- [69] V. Meleshko, Y. Morokov, V. Schweigert, *Chem. Phys. Lett.* **1999**, *300*, 118–124.
- [70] N. Ning, H. Vach, *J. Phys. Chem. A*, **2010**, *114*, 3297–3305.
- [71] N. Ning, S. M. Rinaldi, H. Vach, *Thin Solid Films* **2009**, *517*, 6234–6238.
- [72] M. F. Jarrold, *Science*, **1991**, *252*, 1085–1092.
- [73] K. Raghavachari, V. Logovinsky, *Phys. Rev. Lett.* **1985**, *55*, 2853–2856.
- [74] J. T. Lyon, P. Gruene, A. Fielicke, G. Meijer, E. Janssens, P. Claes, P. Lievens, *J. Am. Chem. Soc.* **2009**, *131*, 1115–1121.
- [75] W. S. Verwoerd, *Surf. Sci.* **1980**, *99*, 581–597.
- [76] G. Hadjisavvas, G. Kopidakis, P. C. Kelires, *Phys. Rev. B*, **2001**, *64*, 125413.
- [77] H. N. Waltenburg, J. T. Yates, *Chem. Rev.* **1995**, *95*, 1589–1673.
- [78] J. M. Buriak, *Chem. Rev.* **2002**, *102*, 1271.
- [79] J. Yoshinobu, *Prog. Surf. Sci.* **2004**, *77*, 37–70.
- [80] H. Mizuta, S. Oda in *European Nano Systems Workshop*, Paris, **2005**.
- [81] A. Fasoli, W. I. Milne, *Mater. Sci. Semicond. Process.* **2012**, *15*, 601–614.
- [82] J. R. Heath, *Science*, **1992**, *258*, 1131–1133.
- [83] R. K. Baldwin, K. A. Pettigrew, E. Ratai, M. P. Augustine, S. M. Kauzlarich, *Chem. Commun.* **2002**, *17*, 1822–1823.
- [84] C. S. Yang, R. A. Bley, S. M. Kauzlarich, H. W. H. Lee, G. R. Delgado, *J. Am. Chem. Soc.* **1999**, *121*, 5191–5195.
- [85] R. A. Bley, S. M. Kauzlarich, *J. Am. Chem. Soc.* **1996**, *118*, 12461–12462.
- [86] D. Mayeri, B. L. Phillips, M. P. Augustine, S. M. Kauzlarich, *Chem. Mater.* **2001**, *13*, 765–770.
- [87] B. M. Nolan, T. Henneberger, M. Waibel, T. F. Fässler, S. M. Kauzlarich, *Inorg. Chem.* **2015**, *54*, 396–401.
- [88] K. A. Pettigrew, Q. Liu, P. P. Power, S. M. Kauzlarich, *Chem. Mater.* **2003**, *15*, 4005–4011.
- [89] T. M. Atkins, M. C. Cassidy, M. Lee, S. Ganguly, C. M. Marcus, S. M. Kauzlarich, *ACS Nano* **2013**, *7*, 1609–1617.
- [90] D. Neiner, H. W. Chiu, S. M. Kauzlarich, *J. Am. Chem. Soc.* **2006**, *128*, 11016–11017.
- [91] A. Indriksons, R. West, *J. Am. Chem. Soc.* **1970**, *92*, 6704–6705.
- [92] R. West, A. Indriksons, *J. Am. Chem. Soc.* **1972**, *94*, 6110–6115.

- [93] W. Stallings, J. Donohue, *Inorg. Chem.* **1976**, *15*, 524–529.
- [94] M. Zirngast, J. Baumgartner, C. Marschner, *Organometallics* **2008**, *27*, 6472–6478.
- [95] M. Ishikawa, M. Watanabe, J. Iyoda, H. Ikeda, M. Kumada, *Organometallics* **1982**, *1*, 317–322.
- [96] Y. Kabe, T. Kawase, J. Okada, O. Yamashita, M. Goto, S. Masamune, *Angew. Chem. Int. Ed. Engl.* **1990**, *29*, 794–796.
- [97] T. Iwamoto, D. Tsushima, E. Kwon, S. Ishida, H. Isobe, *Angew. Chem. Int. Ed.* **2012**, *51*, 2340–2344.
- [98] R. Fischer, T. Konopa, S. Ullly, J. Baumgartner, C. Marschner, *J. Organomet. Chem.* **2003**, *685*, 79–92.
- [99] W. Setaka, N. Hamada, M. Kira, *Chem. Lett.* **2004**, *33*, 626–627.
- [100] A. Wallner, M. Hölbling, J. Baumgartner, C. Marschner, *Silicon Chem.* **2007**, *3*, 175–185.
- [101] V. Y. Lee, T. Yokoyama, K. Takanashi, A. Sekiguchi, *Chem. Eur. J.* **2009**, *15*, 8401–8404.
- [102] Y. Kabe, M. Kuroda, Y. Honda, O. Yamashita, T. Kawase, S. Masamune, *Angew. Chem. Int. Ed. Engl.* **1988**, *27*, 1725–1727.
- [103] T. Iwamoto, K. Uchiyama, C. Kabuto, M. Kira, *Chem. Lett.* **2007**, *36*, 368–369.
- [104] R. Fischer, J. Baumgartner, G. Kickelbick, K. Hassler, C. Marschner, *Chem. Eur. J.* **2004**, *10*, 1021–1030.
- [105] J. Fischer, J. Baumgartner, C. Marschner, *Science*, **2005**, *310*, 825.
- [106] A. Tsurusaki, Y. Koyama, S. Kyushin, *J. Am. Chem. Soc.* **2017**, *139*, 3982–3985.
- [107] M. Unno, K. Higuchi, M. Ida, H. Shioyama, S. Kyushin, H. Matsumoto, M. Goto, *Organometallics* **1994**, *13*, 4633–4640.
- [108] M. Unno, H. Masuda, H. Matsumoto, *Silicon Chem.* **2002**, *1*, 377–381.
- [109] N. Wiberg, C. M. M. Finger, K. Polborn, *Angew. Chem. Int. Ed. Engl.* **1993**, *32*, 1054–1056.
- [110] M. Ichinohe, M. Toyoshima, R. Kinjo, A. Sekiguchi, *J. Am. Chem. Soc.* **2003**, *125*, 13328–13329.
- [111] A. Sekiguchi, T. Yatabe, C. Kabuto, H. Sakurai, *J. Am. Chem. Soc.* **1993**, *115*, 5853–5854.
- [112] H. Matsumoto, K. Higuchi, Y. Hoshino, *J. Chem. Soc., Chem. Commun.* **1988**, *3*, 1083–1084.

- [113] H. Matsumoto, K. Higuchi, S. Kyushin, M. Goto, *Angew. Chem. Int. Ed. Engl.* **1992**, *31*, 1354–1356.
- [114] A. Sekiguchi, T. Yatabe, H. Kamatani, C. Kabuto, H. Sakurai, *J. Am. Chem. Soc.* **1992**, *114*, 6260–6262.
- [115] K. Furukawa, M. Fujino, N. Matsumoto, *Appl. Phys. Lett.* **1992**, *60*, 2744–2745.
- [116] J. Tillmann, J. H. Wender, U. Bahr, M. Bolte, H. W. Lerner, M. C. Holthausen, M. Wagner, *Angew. Chem. Int. Ed.* **2015**, *54*, 5429–5433.
- [117] R. West, *J. Organomet. Chem.* **1986**, *300*, 327–346.
- [118] R. D. Miller, J. Michl, *Chem. Rev.* **1989**, *89*, 1359–1410.
- [119] H. A. Fogarty, D. L. Casher, R. Imhof, T. Schepers, D. W. Rooklin, J. Michl, *Pure Appl. Chem.* **2003**, *75*, 999–1020.
- [120] S. Kyushin, H. Matsumoto, *Adv. Organomet. Chem.* **2003**, *49*, 133–166.
- [121] M. Kosa, M. Karni, Y. Apeloig, *Organometallics* **2007**, *26*, 2806–2814.
- [122] A. Fujii, K. Yoshimoto, M. Yoshida, Y. Ohmori, K. Yoshino, *Jpn. J. Appl. Phys.* **1995**, *34*, 1365–1367.
- [123] S. Hayase, *Prog. Polym. Sci.* **2003**, *28*, 359–381.
- [124] M. Unno, H. Shioyama, M. Ida, H. Matsumoto, *Organometallics* **1995**, *14*, 4004–4009.
- [125] W. Setaka, N. Hamada, C. Kabuto, M. Kira, *Chem. Commun.* **2005**, *906*, 4666–4668.
- [126] F. Meyer-Wegner, S. Scholz, I. Sanger, F. Schodel, M. Bolte, M. Wagner, H.-W. Lerner, *Organometallics* **2009**, *28*, 6835–6837.
- [127] N. Wiberg, H. Auer, H. Noth, J. Knizek, K. Polborn, *Angew. Chem. Int. Ed.* **1998**, *37*, 2869–2872.
- [128] T. M. Klapotke, S. K. Vasisht, G. Fischer, P. Mayer, *J. Organomet. Chem.* **2010**, *695*, 667–672.
- [129] T. M. Klapotke, S. K. Vasisht, P. Mayer, *Eur. J. Inorg. Chem.* **2010**, 3256–3260.
- [130] A. Joannis in *C. R. Hebd. Seances Acad. Sci.*, Paris, **1891**, *113*, 795–798.
- [131] C. A. Kraus, *J. Am. Chem. Soc.* **1907**, *29*, 1557–1571.
- [132] C. A. Kraus, *J. Am. Chem. Soc.* **1922**, *44*, 1216–1239.
- [133] F. H. Smyth, *J. Am. Chem. Soc.* **1917**, *39*, 1299–1312.
- [134] E. B. Peck, *J. Am. Chem. Soc.* **1918**, *40*, 335–347.
- [135] E. Zintl, J. Goubeau, W. Dullenkopf, *Zeitschrift fur Phys. Chemie A* **1931**, *154*, 1–46.

- [136] E. Zintl, A. Harder, *Z. Phys. Chem. A* **1931**, 154, 47–91.
- [137] F. Laves, *Naturwissenschaften* **1941**, 29, 244–255.
- [138] R. E. Marsh, D. P. Shoemaker, *Acta Crystallogr.* **1953**, 6, 197–205.
- [139] V. Queneau, S. C. Sevov, *Angew. Chem. Int. Ed. Engl.* **1997**, 36, 1754–1756.
- [140] J. Witte, H. G. Von Schnering, *Z. Anorg. Allg. Chem.* **1964**, 327, 260–273.
- [141] Y. Grin, M. Baitinger, R. Kniep, H. G. Von Schnering, *Z. Kristallogr. - New Cryst. Struct.* **1999**, 214, 453–454.
- [142] M. Baitinger, Y. Grin, R. Kniep, H. G. Von Schnering, *Z. Kristallogr. - New Cryst. Struct.* **1999**, 214, 457–458.
- [143] M. Baitinger, K. Peters, M. Somer, W. Carrillo-Cabrera, Y. Grin, R. Kniep, H. G. Von Schnering, *Z. Kristallogr. - New Cryst. Struct.* **1999**, 214, 455–456.
- [144] H. G. Von Schnering, J. Llanos, J. H. Chang, K. Peters, E. M. Peters, R. Nesper, *Z. Kristallogr. - New Cryst. Struct.* **2005**, 220, 324–326.
- [145] H. G. Von Schnering, M. Schwarz, J. H. Chang, K. Peters, E. M. Peters, R. Nesper, *Z. Kristallogr. - New Cryst. Struct.* **2005**, 220, 525–527.
- [146] T. Goebel, Y. Prots, F. Haarmann, *Z. Kristallogr. - New Cryst. Struct.* **2008**, 223, 187–188.
- [147] E. Todorov, S. C. Sevov, *Inorg. Chem.* **1998**, 37, 3889–3891.
- [148] V. Queneau, S. C. Sevov, *Inorg. Chem.* **1998**, 37, 1358–1360.
- [149] S. Bobev, S. C. Sevov, *Polyhedron* **2002**, 21, 641–649.
- [150] C. Hoch, M. Wendorff, C. Röhr, *Acta Crystallogr., Sect. C: Cryst. Struct. Commun.* **2002**, 58, 45–46.
- [151] S. Ponou, T. F. Fässler, *Z. Anorg. Allg. Chem.* **2007**, 633, 393–397.
- [152] H. G. Von Schnering, M. Baitinger, U. Bolle, W. Carrillo-Cabrera, J. Curda, Y. Grin, F. Heinemann, J. Llanos, K. Peters, A. Schmeding, et al., *Z. Anorg. Allg. Chem.* **1997**, 623, 1037–1039.
- [153] V. Quéneau, E. Todorov, S. C. Sevov, *J. Am. Chem. Soc.* **1998**, 120, 3263–3264.
- [154] W. Carrillo-Cabrera, R. Cardoso Gil, M. Somer, Ö. Persil, H. G. Von Schnering, *Z. Anorg. Allg. Chem.* **2003**, 629, 601–608.
- [155] C. Hoch, M. Wendorff, C. Röhr, *J. Alloys Compd.* **2003**, 361, 206–221.
- [156] J. Llanos, R. Nesper, H. G. von Schnering, *Angew. Chem. Int. Ed. Engl.* **1983**, 22, 7000.
- [157] H. G. von Schnering, M. Schwarz, R. Nesper, *Angew. Chem. Int. Ed. Engl.* **1986**,

- 25, 566–567.
- [158] T. Goebel, F. Haarmann, *Z. Anorg. Allg. Chem.* **2008**, 634, 2040–2040.
- [159] O. Pecher, M. Esters, A. Görne, B. Mausolf, A. Ormeci, F. Haarmann, *Z. Anorg. Allg. Chem.* **2014**, 640, 2169–2176.
- [160] S. Joseph, C. Suchentrunk, F. Kraus, N. Korber, *Eur. J. Inorg. Chem.* **2009**, 4641–4647.
- [161] S. Bobev, S. C. Sevov, *Angew. Chem. Int. Ed.* **2000**, 39, 4108–4110.
- [162] F. Zürcher, R. Nesper, *Angew. Chem. Int. Ed.* **1998**, 37, 3314–3318.
- [163] U. Aydemir, A. Ormeci, H. Borrmann, B. Böhme, F. Zürcher, B. Uslu, T. Goebel, W. Schnelle, P. Simon, W. Carrillo-Cabrera, et al., *Z. Anorg. Allg. Chem.* **2008**, 634, 1651–1661.
- [164] R. Nesper, H. G. von Schnering, J. Curda, *Chem. Ber.* **1986**, 119, 3576–3590.
- [165] T. K.-J. Köster, E. Salager, A. J. Morris, B. Key, V. Seznec, M. Morcrette, C. J. Pickard, C. P. Grey, *Angew. Chem. Int. Ed.* **2011**, 50, 12591–12594.
- [166] U. Frank, W. Müller, *Z. Naturforsch.* **1975**, 30b, 313–315.
- [167] R. Nesper, J. Curda, H. G. Von Schnering, *J. Solid State Chem.* **1986**, 62, 199–206.
- [168] P. Na, N. Basn, N. Eusn, N. Dame, *Inorg. Chem.* **2004**, 43, 6490–6494.
- [169] I. Todorov, S. C. Sevov, *Inorg. Chem.* **2005**, 44, 5361–5369.
- [170] H. G. Von Schnering, U. Bolle, J. Curda, K. Peters, W. Carrillo-Cabrera, M. Somer, M. Schultheiss, U. Wedig, *Angew. Chem. Int. Ed. Engl.* **1996**, 35, 984–986.
- [171] U. Bolle, W. Carrillo-Cabrera, K. Peters, H. G. von Schnering, *Z. Kristallogr. - New Cryst. Struct.* **1998**, 213, 689.
- [172] D. Kummer, L. Diehl, *Angew. Chem. Int. Ed. Engl.* **1970**, 9, 895.
- [173] L. Diehl, K. Khodadadeh, D. Kummer, J. Strähle, *Chem. Ber.* **1976**, 109, 3404–3418.
- [174] L. Diehl, K. Khodadadeh, D. Kummer, J. Strähle, *Z. Naturforsch.* **1976**, 31b, 522–524.
- [175] A. Nienhaus, S. D. Hoffmann, T. F. Fässler, *Z. Anorg. Allg. Chem.* **2006**, 632, 1752–1758.
- [176] J. D. Corbett, D. G. Adolphson, D. J. Merryman, P. A. Edwards, F. J. Armatis, *J. Am. Chem. Soc.* **1975**, 97, 6267–6268.
- [177] J. D. Corbett, P. A. Edwards, *J. Chem. Soc. Chem. Commun.* **1975**, 984–985.

- [178] T. F. Fässler, R. Hoffmann, *Angew. Chem. Int. Ed.* **1999**, *38*, 543–546.
- [179] K. Wiesler, K. Brandl, A. Fleischmann, N. Korber, *Z. Anorg. Allg. Chem.* **2009**, *635*, 508–512.
- [180] C. H. E. Belin, J. D. Corbett, A. Cisar, *J. Am. Chem. Soc.* **1977**, *99*, 7163–7169.
- [181] J. Campbell, D. A. Dixon, H. P. A. Mercier, G. J. Schrobilgen, *Inorg. Chem.* **1995**, *34*, 5798–5809.
- [182] S. Joseph, C. Suchentrunk, N. Korber, *Z. Naturforsch.* **2010**, *65b*, 1059–1065.
- [183] C. B. Benda, T. Henneberger, W. Klein, T. F. Fässler, *Z. Anorg. Allg. Chem.* **2017**, *643*, 146–148.
- [184] C. Lorenz, S. Gärtner, N. Korber, *Z. Anorg. Allg. Chem.* **2017**, *643*, 141–145.
- [185] J. M. Goicoechea, S. C. Sevov, *J. Am. Chem. Soc.* **2004**, *126*, 6860–6861.
- [186] J. M. Goicoechea, S. C. Sevov, *Inorg. Chem.* **2005**, *44*, 2654–2658.
- [187] E. Zintl, *Angew. Chem.* **1939**, *52*, 1–48.
- [188] W. Klemm, *Proc. Chem. Soc.* **1958**, 329–341.
- [189] R. Nesper, *Z. Anorg. Allg. Chem.* **2014**, *640*, 2639–2648.
- [190] K. Wade, *Inorg. Nucl. Chem. Lett.* **1972**, *8*, 559–562.
- [191] K. Wade, *Adv. Inorg. Chem. Radiochem.* **1976**, *18*, 1–66.
- [192] D. M. P. Mingos, *Nature Phys. Sci.* **1972**, *236*, 99–102.
- [193] R. E. Williams, *Chem. Rev.* **1992**, *92*, 177–207.
- [194] B. M. Cossairt, C. C. Cummins, A. R. Head, D. L. Lichtenberger, R. J. F. Berger, F., S. A. Hayes, N. W. Mitzel, G. Wu, *J. Am. Chem. Soc.* **2010**, *132*, 8459–8465.
- [195] J. He, D. D. Klug, K. Uehara, K. F. Preston, C. I. Ratcliffe, J. S. Tse, *J. Phys. Chem. B.* **2001**, *105*, 3475–3485.
- [196] T. Goebel, Y. Prots, A. Ormeci, O. Pecher, F. Haarmann, *Z. Anorg. Allg. Chem.* **2011**, *637*, 1982–1991.
- [197] T. Goebel, A. Ormeci, O. Pecher, F. Haarmann, *Z. Anorg. Allg. Chem.* **2012**, *638*, 1437–1445.
- [198] L. M. Scherf, O. Pecher, K. J. Griffith, F. Haarmann, C. P. Grey, T. F. Fässler, *Eur. J. Inorg. Chem.* **2016**, *2016*, 4674–4682.
- [199] L. J. Schiegerl, A. J. Karttunen, J. Tillmann, S. Geier, G. Raudaschl-Sieber, M. Waibel, T. F. Fässler, *Angew. Chem. Int. Ed.* **2018**, *57*, 12950–12955.
- [200] M. Neumeier, F. Fendt, S. Gärtner, C. Koch, T. Gärtner, N. Korber, R. M. Gschwind, *Angew. Chem. Int. Ed.* **2013**, *52*, 4483–4486.
- [201] C. Lorenz, F. Hastreiter, J. Hioe, N. Lokesh, S. Gärtner, N. Korber, R. M.

- Gschwind, *Angew. Chem. Int. Ed.* **2018**, *57*, 12956–12960.
- [202] F. Hastreiter, C. Lorenz, J. Hioe, S. Gärtner, N. Lokesh, N. Korber, R. M. Gschwind, *Angew. Chem. Int. Ed.* **2019**, *58*, 3133–3137.
- [203] M. Waibel, F. Kraus, S. Scharfe, B. Wahl, T. F. Fässler, *Angew. Chem. Int. Ed.* **2010**, *49*, 6611–6615.
- [204] J. M. Goicoechea, S. C. Sevov, *Organometallics* **2006**, *25*, 4530–4536.
- [205] F. S. Geitner, T. F. Fässler, *Chem. Commun.* **2017**, *53*, 12974–12977.
- [206] S. Joseph, M. Hamberger, F. Mutzbauer, O. Härtl, M. Meier, N. Korber, *Angew. Chem. Int. Ed.* **2009**, *48*, 8770–8772.
- [207] L. J. Schiegerl, A. J. Karttunen, W. Klein, T. F. Fässler, *Chem. Eur. J.* **2018**, *24*, 19171–19174.
- [208] O. Kysliak, C. Schrenk, A. Schnepf, *Inorg. Chem.* **2015**, *54*, 7083–7088.
- [209] K. Mayer, L. J. Schiegerl, T. Kratky, S. Günther, T. F. Fässler, *Chem. Commun.* **2017**, *53*, 11798–11801.
- [210] F. Li, S. C. Sevov, *Inorg. Chem.* **2012**, *51*, 2706–2708.
- [211] O. Kysliak, T. Kunz, A. Schnepf, *Eur. J. Inorg. Chem.* **2017**, 805–810.
- [212] O. Kysliak, A. Schnepf, *Dalton Trans.* **2016**, *45*, 2404–2408.
- [213] M. W. Hull, S. C. Sevov, *Inorg. Chem.* **2007**, *46*, 10953–10955.
- [214] M. W. Hull, S. C. Sevov, *Angew. Chem. Int. Ed.* **2007**, *46*, 6695–6698.
- [215] C. B. Benda, J. Q. Wang, B. Wahl, T. F. Fässler, *Eur. J. Inorg. Chem.* **2011**, 4262–4269.
- [216] M. W. Hull, S. C. Sevov, *J. Am. Chem. Soc.* **2009**, *131*, 9026–9037.
- [217] C. Schenk, A. Schnepf, *Angew. Chem. Int. Ed.* **2007**, *46*, 5314–5316.
- [218] C. Schenk, F. Henke, G. Santiso-Quiñones, I. Krossing, A. Schnepf, *Dalton Trans.* **2008**, 4436–4441.
- [219] F. Henke, C. Schenk, A. Schnepf, *Dalton Trans.* **2009**, 9141–9145.
- [220] O. Kysliak, C. Schrenk, A. Schnepf, *Inorg. Chem.* **2017**, *56*, 9693–9697.
- [221] A. Nienhaus, R. Hauptmann, T. F. Fässler, *Angew. Chem. Int. Ed.* **2002**, *41*, 3213–3215.
- [222] M. M. Bentlohner, W. Klein, Z. H. Fard, L. A. Jantke, T. F. Fässler, *Angew. Chem. Int. Ed.* **2015**, *54*, 3748–3753.
- [223] S. Frischhut, M. M. Bentlohner, W. Klein, T. F. Fässler, *Inorg. Chem.* **2017**, *56*, 10691–10698.
- [224] A. Ugrinov, S. C. Sevov, *J. Am. Chem. Soc.* **2002**, *124*, 10990–10991.

- [225] A. Ugrinov, S. C. Sevov, *Inorg. Chem.* **2003**, *42*, 5789–5791.
- [226] M. S. Denning, J. M. Goicoechea, *Dalton Trans.* **2008**, 5882–5885.
- [227] A. Purath, R. Köppe, H. Schnöckel, *Angew. Chem. Int. Ed.* **1999**, *38*, 2926–2928.
- [228] A. Schnepf, G. Stösser, H. Schnöckel, *J. Am. Chem. Soc.* **2000**, *122*, 9178–9181.
- [229] A. Schnepf, H. Schnöckel, *Angew. Chem. Int. Ed.* **2002**, *41*, 3532–3552.
- [230] H. Schnöckel, *Dalton Trans.* **2005**, 3131–3136.
- [231] A. Schnepf, H. Schnöckel, *Angew. Chem. Int. Ed.* **2001**, *40*, 711–715.
- [232] A. Schnepf, *Chem. Soc. Rev.* **2007**, *36*, 745–758.
- [233] T. Kunz, C. Schrenk, A. Schnepf, *Angew. Chem. Int. Ed.* **2018**, *57*, 4088–4092.
- [234] T. Iwamoto, M. Tamura, C. Kabuto, M. Kira, *Science*, **2000**, *290*, 504–507.
- [235] A. Schnepf, *Eur. J. Inorg. Chem.* **2008**, 1007–1018.
- [236] A. Schnepf, *New J. Chem.* **2010**, *34*, 2079–2092.
- [237] C. Schenk, F. Henke, A. Schnepf, *Phosphorus, Sulfur Silicon Relat. Elem.* **2011**, *186*, 1370–1374.
- [238] A. Schnepf, *Phosphorus, Sulfur Silicon Relat. Elem.* **2016**, *191*, 662–664.
- [239] C. W. So, H. W. Roesky, J. Magull, R. B. Oswald, *Angew. Chem. Int. Ed.* **2006**, *45*, 3948–3950.
- [240] Y. Wang, Y. Xie, P. Wei, R. B. King, H. F. Schaefer III, P. V. R. Schleyer, G. H. Robinson, *Science*, **2008**, *321*, 1069–1072.
- [241] R. S. Ghadwal, H. W. Roesky, S. Merkel, J. Henn, D. Stalke, *Angew. Chem. Int. Ed.* **2009**, *48*, 5683–5686.
- [242] S. S. Sen, H. W. Roesky, D. Stern, J. Henn, D. Stalke, *J. Am. Chem. Soc.* **2010**, *132*, 1123–1126.
- [243] A. C. Filippou, O. Chernov, G. Schnakenburg, *Angew. Chem. Int. Ed.* **2009**, *48*, 5687–5690.
- [244] H. Cui, C. Cui, *Dalton Trans.* **2011**, *40*, 11937–11940.
- [245] F. Uhlemann, R. Köppe, A. Schnepf, *Z. Anorg. Allg. Chem.* **2014**, *640*, 1658–1664.
- [246] J. Teichmann, M. Wagner, *Chem. Commun.* **2018**, *54*, 1397–1412.
- [247] D. Scheschkewitz, *Angew. Chem. Int. Ed.* **2005**, *44*, 2954–2956.
- [248] D. Scheschkewitz, *Angew. Chem. Int. Ed.* **2004**, *43*, 2965–2967.
- [249] K. Leszczyńska, K. Abersfelder, M. Majumdar, B. Neumann, H.-G. Stammer, H. S. Rzepa, P. Jutzi, D. Scheschkewitz, *Chem. Commun.* **2012**, *48*, 7820–7822.

- [250] K. Takeuchi, D. Uemura, S. Inagaki, *J. Phys. Chem. A* **2005**, *109*, 8632–8636.
- [251] T. Iwamoto, M. Kobayashi, K. Uchiyama, S. Sasaki, S. Nagendran, H. Isobe, M. Kira, *J. Am. Chem. Soc.* **2009**, *131*, 3156–3157.
- [252] T. Iwamoto, N. Akasaka, S. Ishida, *Nat. Commun.* **2014**, *5*, 5353.
- [253] N. Akasaka, S. Ishida, T. Iwamoto, *Inorganics* **2018**, *6*, 107.
- [254] G. Fischer, V. Huch, P. Mayer, S. K. Vasisht, M. Veith, N. Wiberg, *Angew. Chem. Int. Ed.* **2005**, *44*, 7884–7887.
- [255] T. Tsumaraya, S. A. Batcheller, S. Masamune, *Angew. Chem. Int. Ed. Engl.* **1991**, *30*, 902–930.
- [256] A. Sekiguchi, R. Kinjo, M. Ichinohe, *Science*, **2004**, *305*, 1755–1758.
- [257] D. Nied, R. Köppe, W. Klopfer, H. Schnöckel, F. Breher, *J. Am. Chem. Soc.* **2010**, *132*, 10264–10265.
- [258] K. Abersfelder, A. J. P. White, H. S. Rzepa, D. Scheschkewitz, *Science*, **2010**, *327*, 564–566.
- [259] K. Abersfelder, A. J. P. White, R. J. F. Berger, H. S. Rzepa, D. Scheschkewitz, *Angew. Chem. Int. Ed. Engl.* **2011**, *50*, 7936–7939.
- [260] M. Moteki, S. Maeda, K. Ohno, *Organometallics* **2009**, *28*, 2218–2224.
- [261] S. Marutheeswaran, P. D. Pancharatna, M. M. Balakrishnarajan, *Phys. Chem. Chem. Phys.* **2014**, *16*, 11186–11190.
- [262] T. P. Kaloni, G. Schreckenbach, M. S. Freund, U. Schwingenschlögl, *Phys. Status Solidi RRL*. **2016**, *10*, 133–142.
- [263] J. Zhao, H. Liu, Z. Yu, R. Quhe, S. Zhou, Y. Wang, C. C. Liu, H. Zhong, N. Han, J. Lu, et al., *Prog. Mater. Sci.* **2016**, *83*, 24–151.
- [264] S. Balendhran, S. Walia, H. Nili, S. Sriram, M. Bhaskaran, *Small* **2015**, *11*, 640–652.
- [265] H. Oughaddou, H. Enriquez, M. R. Tchalala, H. Yildirim, A. J. Mayne, A. Bendounan, G. Dujardin, M. Ait Ali, A. Kara, *Prog. Surf. Sci.* **2015**, *90*, 46–83.
- [266] D. Kratzert, D. Leusser, J. J. Holstein, B. Dittrich, K. Abersfelder, D. Scheschkewitz, D. Stalke, *Angew. Chem. Int. Ed.* **2013**, *52*, 4478–4482.
- [267] S. Ishida, K. Otsuka, Y. Toma, S. Kyushin, *Angew. Chem. Int. Ed.* **2013**, *52*, 2507–2510.
- [268] A. Tsurusaki, C. Iizuka, K. Otsuka, S. Kyushin, *J. Am. Chem. Soc.* **2013**, *135*, 16340–16343.
- [269] R. J. F. Berger, H. S. Rzepa, D. Scheschkewitz, *Angew. Chem. Int. Ed.* **2010**,

- 49, 10006–10009.
- [270] J. B. Lambert, S. Zhang, S. M. Ciro, *Organometallics* **1994**, *13*, 2430–2443.
- [271] J. B. Lambert, L. Kania, S. Zhang, *Chem. Rev.* **1995**, *95*, 1191–1201.
- [272] V. H. G. Rohde, P. Pommerening, H. F. T. Klare, M. Oestreich, *Organometallics* **2014**, *33*, 3618–3628.
- [273] A. Simonneau, T. Biberger, M. Oestreich, *Organometallics* **2015**, *34*, 3927–3929.
- [274] W.-D. Stohrer, R. Hoffmann, *J. Am. Chem. Soc.* **1972**, *94*, 779–786.
- [275] M. D. Newton, J. M. Schulman, *J. Am. Chem. Soc.* **1972**, *94*, 773–778.
- [276] S. Shaik, P. Maitre, G. Sini, P. C. Hiberty, *J. Am. Chem. Soc.* **1992**, *114*, 7861–7866.
- [277] W. Wu, J. Gu, J. Song, S. Shaik, P. C. Hiberty, *Angew. Chem.* **2009**, *121*, 1435–1438.
- [278] K. B. Wiberg, F. H. Walker, *J. Am. Chem. Soc.* **1982**, *104*, 5239–5240.
- [279] A. M. Dilmaç, E. Spuling, A. de Meijere, S. Bräse, *Angew. Chem. Int. Ed.* **2017**, *56*, 5684–5718.
- [280] M. S. Gordon, K. A. Nguyen, M. T. Carroll, *Polyhedron* **1991**, *10*, 1247–1264.
- [281] P. von R. Schleyer, R. Janoschek, *Angew. Chem. Int. Ed. Engl.* **1987**, *26*, 1267–1268.
- [282] W. W. Schoeller, T. Dabisch, T. Busch, *Inorg. Chem.* **1987**, *26*, 4383–4389.
- [283] F. Breher, *Coord. Chem. Rev.* **2007**, *251*, 1007–1043.
- [284] D. Nied, F. Breher, *Chem. Soc. Rev.* **2011**, *40*, 3455–3466.
- [285] E. Heilbronner, *Tetrahedron Lett.* **1964**, *29*, 1923–1928.
- [286] R. P. Johnson, K. J. Daoust, *J. Am. Chem. Soc.* **1996**, *118*, 7381–7385.
- [287] L. R. Sita, R. D. Bickerstaff, *J. Am. Chem. Soc.* **1989**, *111*, 6454–6456.
- [288] C. Drost, M. Hildebrand, P. Lönnecke, *Main Group Met. Chem.* **2002**, *25*, 93–98.
- [289] D. Nied, W. Klopfer, F. Breher, *Angew. Chem. Int. Ed.* **2009**, *48*, 1411–1416.
- [290] C. P. Sindlinger, L. Wesemann, *Chem. Sci.* **2014**, *5*, 2739–2746.
- [291] D. Nied, P. Oña-Burgos, W. Klopfer, F. Breher, *Organometallics* **2011**, *30*, 1419–1428.
- [292] A. F. Richards, M. Brynda, P. P. Power, *Organometallics* **2004**, *23*, 4009–4011.
- [293] Y. Ito, V. Y. Lee, H. Gornitzka, C. Goedecke, G. Frenking, A. Sekiguchi, *J. Am. Chem. Soc.* **2013**, *135*, 6770–6773.
- [294] A. Jana, V. Huch, M. Repisky, R. J. F. Berger, D. Scheschkewitz, *Angew. Chem.*

- Int. Ed. Engl.* **2014**, *53*, 3514–8.
- [295] N. Wiberg, S. K. Vasisht, G. Fischer, P. Mayer, V. Huch, M. Veith, *Z. Anorg. Allg. Chem.* **2007**, *633*, 2425–2430.
- [296] P. Willmes, K. Leszczyńska, Y. Heider, K. Abersfelder, M. Zimmer, V. Huch, D. Scheschkewitz, *Angew. Chem. Int. Ed.* **2016**, *55*, 2907–2910.
- [297] K. I. Leszczyńska, V. Huch, C. Präsang, J. Schwabedissen, R. J. F. Berger, D. Scheschkewitz, *Angew. Chem. Int. Ed.* **2019**, *58*, 5124–5128.
- [298] K. Abersfelder, PhD thesis, Imperial College London (UK), **2012**.
- [299] P. Willmes, PhD thesis, Saarland University (Germany), **2016**.
- [300] Y. Heider, Master-thesis, Saarland University (Germany), **2016**.

6. Supporting Information

6.1. Site-selective functionalization of Si_6R_6 siliconoids (SI)

Supporting Information:

Site-Selective Functionalization of Si₆R₆ SiliconoidsYannic Heider,[‡] Nadine E. Poitiers,[‡] Philipp Willmes, Kinga Leszczyńska, Volker Huch,
and David Scheschkewitz*

Krupp-Chair of General and Inorganic Chemistry, Saarland University, D-66123 Saarbrücken, Germany

Contents

<u>General Methods</u>	<u>S2</u>
<u>1. Preparation, data and spectra (NMR, UV-vis, IR) of:</u>	<u>S3</u>
<i>ligato</i> -TMS-substituted siliconoid 5a	S3
<i>ligato</i> -Benzoyl-substituted siliconoid 5b	S7
<i>privo</i> -Lithiated Anionic siliconoid 4Li	S11
<i>privo</i> -TMS-substituted siliconoid 6a	S16
<i>privo</i> -Benzoyl-substituted siliconoid 6b	S20
<i>privo</i> -Pivaloyl-substituted siliconoid 6c	S22
<i>privo</i> -Bis(dimethylamino)phosphinyl-substituted siliconoid 6d	S28
<i>privo</i> -Trichlorosilyl-substituted siliconoid 6e	S31
<i>privo</i> -Borate-substituted siliconoid 6f	S34
<u>2. Details on X-ray Diffraction Studies</u>	<u>S40</u>
<u>3. Plots of the Hammett parameter σ_m/σ_p vs ²⁹Si chemical shift of Si2</u>	<u>S46</u>

General

All manipulations were carried out under a protective atmosphere of argon, by using a glovebox or standard Schlenk techniques. Ethereal solvents were dried by heating to reflux over Na/benzophenone and distilled and stored under an atmosphere of argon. Hydrocarbons were dried over sodium or potassium. NMR spectra were recorded on a Bruker Avance III 300 NMR spectrometer (^1H = 300.13 MHz, ^{13}C = 75.46 MHz, ^{29}Si = 59.6 MHz, ^7Li = 116.64 MHz, ^{11}B = 96.3 MHz) and/or a Bruker Avance IV 400 NMR spectrometer (^1H = 400.13 MHz, ^{13}C = 100.6 MHz, ^{29}Si = 59.6 MHz) UV/Vis spectra were recorded on a Perkin-Elmer Lambda 35 spectrometer in quartz cells with a path length of 0.1 cm. Infrared spectra were measured with a Bruker Vertex 79 in a platinum ATR diamond cell. Elemental analyses were performed on an elemental analyzer Leco CHN-900 and/or an elemental vario Micro Cube. They are mostly low in carbon, which is tentatively attributed to incomplete combustion due to the formation of silicon carbide. Compounds **1**, **2** and **3** were prepared according to our published procedures.^{21, 22, 31, 32}

General procedure for the synthesis of *privo* and *ligato* functionalized siliconoids **5a-b** and **6a-f**.

The respective compounds are prepared by treating 1 equivalent of the anionic siliconoid **3Li** or **4Li** with 1 equivalent of Me_3SiCl (**5a**, **6a**), benzoylchloride (**5b**, **6b**), pivaloyl chloride (**6c**), $(\text{Me}_2\text{N})_2\text{PCl}$ (**6d**), SiCl_4 (**6e**), or $\text{H}_3\text{B}\cdot\text{SMe}_2$ (**6f**) in benzene or toluene at room temperature. After stirring for the indicated period of time, all volatiles are removed in vacuo and the crude product is filtered from hexane and crystallized from hexane or pentane.

Preparation of ligato-Trimethylsilyl-2,2,5,5,6-pentakis(2',4',6'-triisopropylphenyl)tetracyclo**[2.2.0.0^{1,3}.0^{3,6}]hexasilane (5a)**

Quantities: **3Li**, 325 mg (0.21 mmol); Me₃SiCl 25.24 mg (0.23 mmol); benzene (5 mL); stirring 4 h; crystallization from pentane. Yield: 120 mg (45 %) red crystals. **¹H-NMR** (300.13 MHz, tol-d₈, 223 K): δ = 7.61, 7.28 (C₁₀H₈), 7.21 (m, overlapping with C₁₀H₈, 3 H, Ar-H), 7.09 – 6.81 (m, overlapping with benzene-d₆, 12 H, Tip-CH), 5.32 (sept, ³J_{HH} = 6.44, 1H, Tip-*i*Pr-CHMe₂), 5.07 (sept, ³J_{HH} = 6.44, 1 H, Tip-*i*Pr-CHMe₂), 4.44 (sept, ³J_{HH} = 6.44, 2 H, Tip-*i*Pr-CHMe₂), 3.96 (sept, ³J_{HH} = 6.44, 2 H, Tip-*i*Pr-CH₃), 3.55 (sept, ³J_{HH} = 6.44, 1H, Tip-*i*Pr-CHMe₂), 3.28 (m, overlapping, together 3H, Tip-*i*Pr-CHMe₂), 2.73 (m, overlapping, together 6H, Tip-*i*Pr-CHMe₂), 2.22 (br, 2H, Tip-*i*Pr-CH₃), 1.98 (br, 2H, Tip-*i*Pr-CH₃), 1.76 (br, 3H, Tip-*i*Pr-CH₃), 1.53 - 1.07 (br, together 96H, Tip-*i*Pr-CH₃), 0.22 (s, 9H, Si-CH₃). **¹³C-NMR** (75.46 MHz, tol-d₈, 223 K): δ = 156.47, 155.65, 154.41, 154.15, 153.82, 153.15, 152.95, 151.94, 151.59, 150.59, 150.42, 150.14, 148.99, 148.89, 139.32, 139.07 (Ar-C), 133.88, 128.15, 126.06 (C₁₀H₈), 123.61, 123.45, 123.21, 123.04, 122.47, 122.08, 121.91, 121.24, 121.05 (Ar-CH), 38.37, 36.22, 36.09, 35.90, 35.14, 34.84, 34.46, 34.25, 32.05, 29.31 (Tip-*i*Pr-CH), 29.1884, 28.49, 27.26, 26.23, 25.35, 24.96, 24.58, 24.24, 24.05, 23.85, 23.42, 22.80 (Tip-*i*Pr-CH₃), 22.56 (Tip-*i*Pr-CH₂), 14.12 (Tip-*i*Pr-CH₃), 2.94 (Si-CH₃). **²⁹Si-NMR** (59.62 MHz, tol-d₈, 223 K): δ = 169.9 (s, *privo*-SiTip₂), 25.8 (s, *remoto*-SiTip₂), 11.3 (s, *ligato*-SiTip), -3.7 (s, *ligato*-Si-SiMe₃), -42.5 (s, SiMe₃), -257.8 (s, *nudo*-Si), -266.6 (s, *nudo*-Si). **Elemental analysis** calculated for C₈₁H₁₃₀Si₇: C, 74.81; H, 10.08. Found: C, 74.1; H, 9.95.

6. Supporting Information

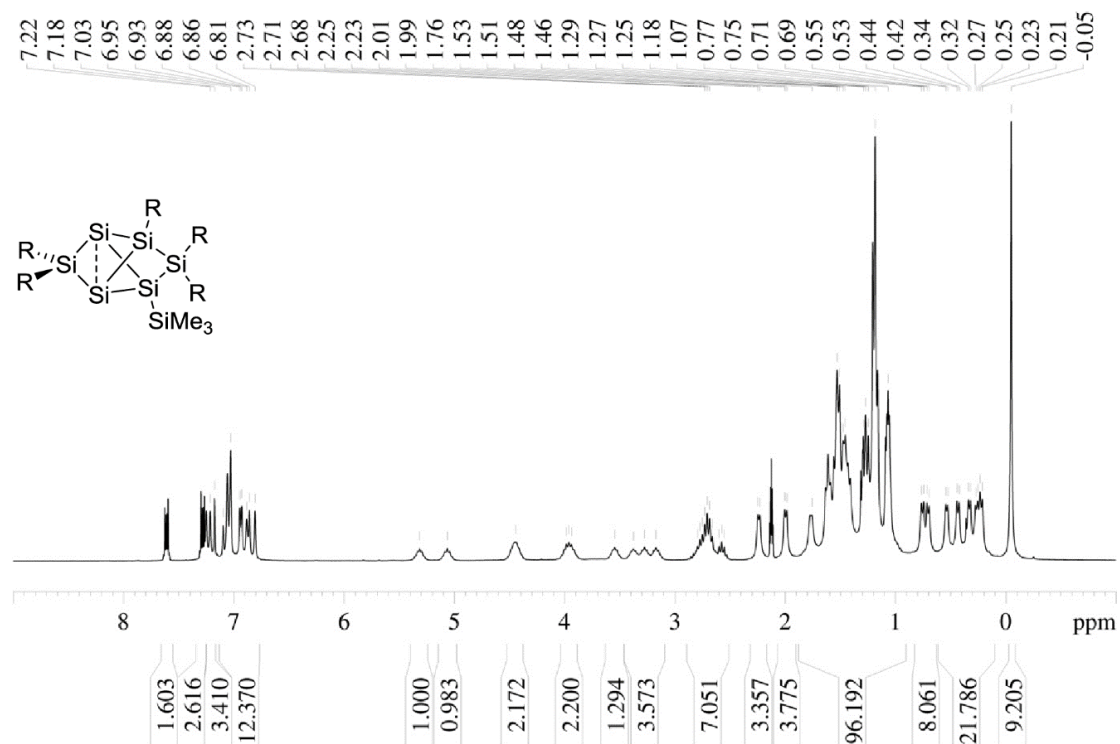


Figure S1: ^1H NMR of **5a** in C_6D_6 (300 MHz).

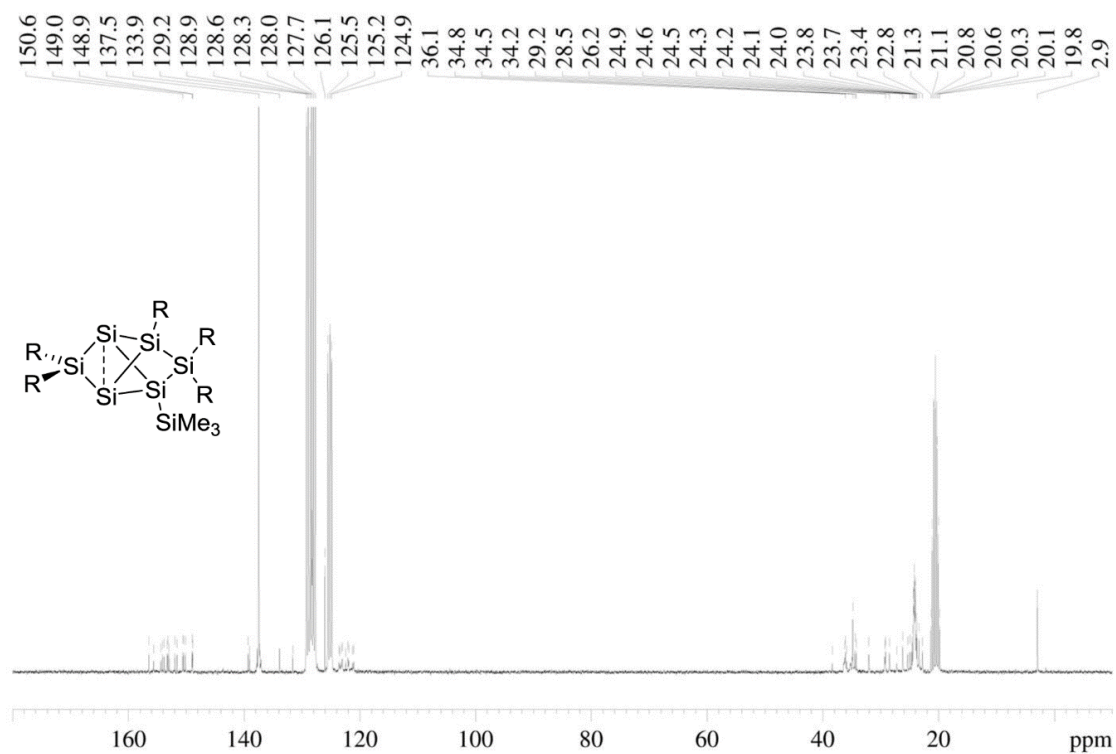


Figure S2: ^{13}C NMR of **5a** in C_6D_6 (75.5 MHz).

6. Supporting Information

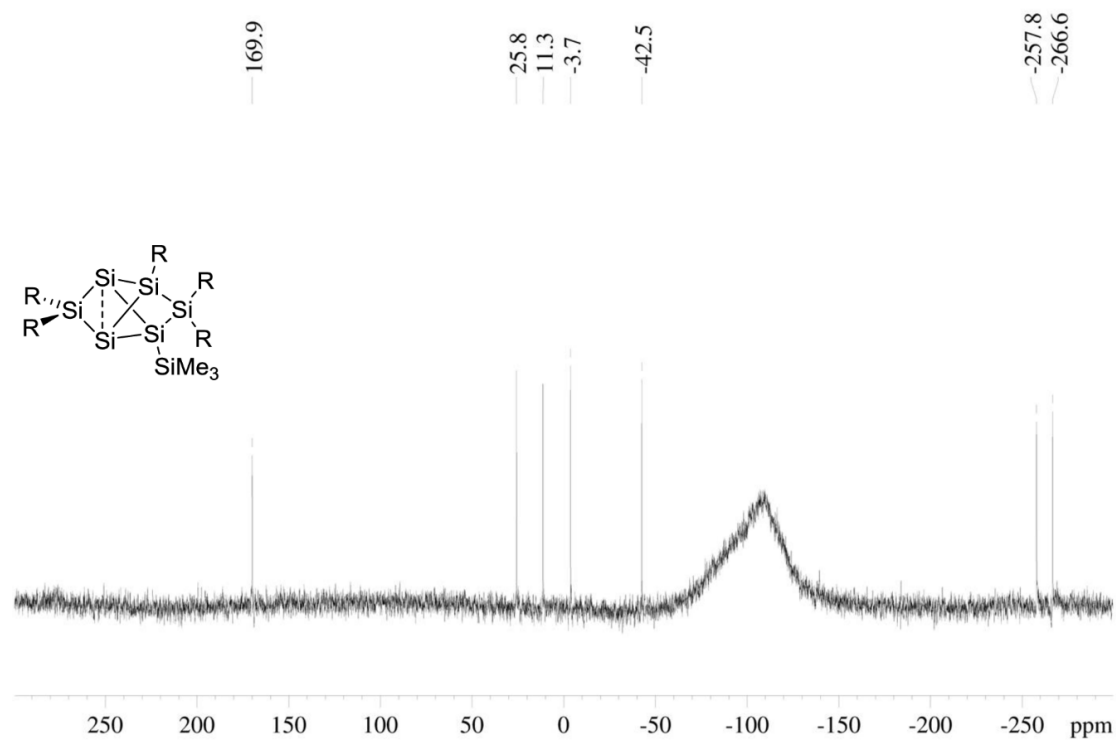


Figure S3: ²⁹Si NMR of **5a** in C₆D₆ (59.6 MHz).

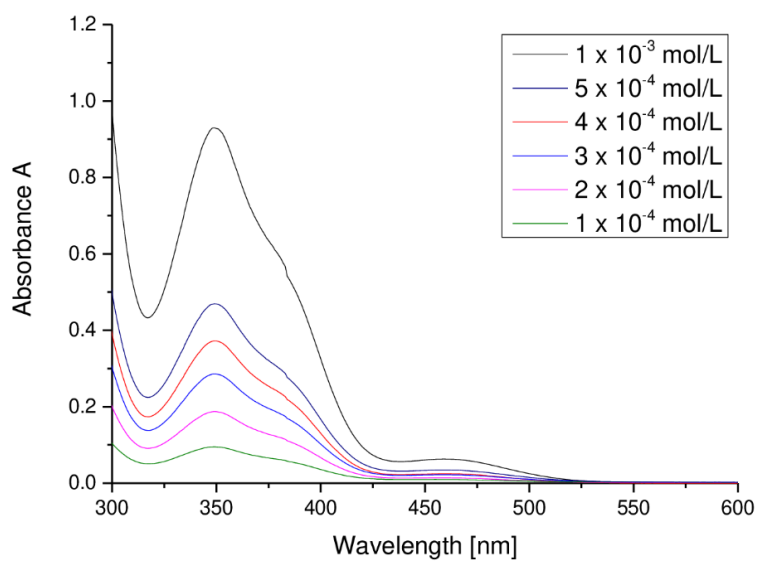


Figure S4: UV-Vis spectrum of **5a** in hexane at different concentrations.

6. Supporting Information

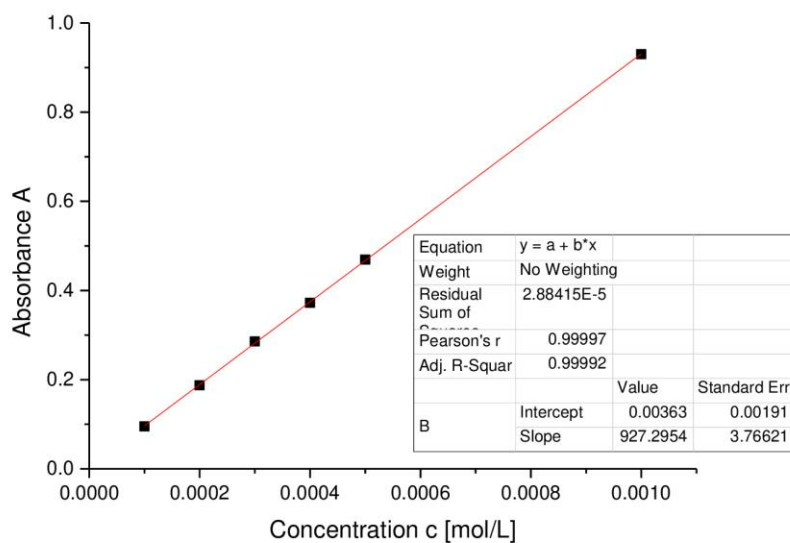


Figure S5: Determination of ϵ ($9273 \text{ M}^{-1} \text{ cm}^{-1}$) by linear regression of absorptions ($\lambda = 349 \text{ nm}$) of **5a** against concentration.

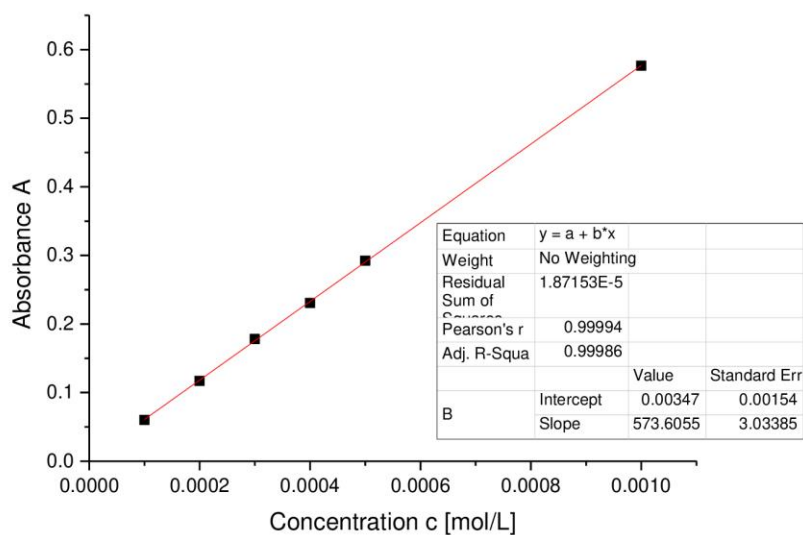


Figure S6: Determination of ϵ ($5736 \text{ M}^{-1} \text{ cm}^{-1}$) by linear regression of absorptions ($\lambda = 382 \text{ nm}$) of **5a** against concentration.

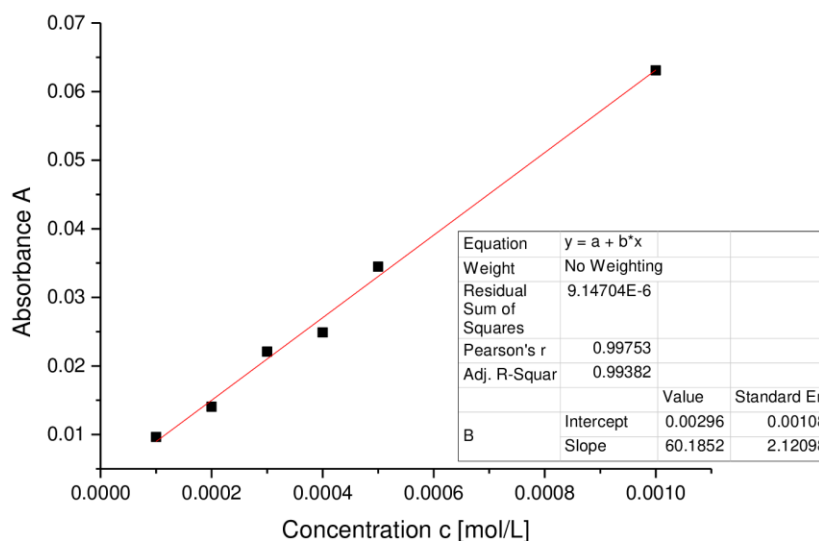


Figure S7: Determination of ϵ ($602 \text{ M}^{-1} \text{ cm}^{-1}$) by linear regression of absorptions ($\lambda = 459 \text{ nm}$) of **5a** against concentration.

Preparation of ligato-Benzoyl-2,2,5,5,6-pentakis(2',4',6'-triisopropyl-phenyl)tetracyclo

[2.2.0.0^{1,3}.0^{3,6}] hexasilane (5b)

Quantities: **3Li**, 500 mg (0.32 mmol); benzoylchloride 49.24 mg (0.35 mmol); benzene; stirring 4 h; crystallization from pentane. Yield: 270 mg (66 %) red crystals.

¹H-NMR (300.13 MHz, benzene-*d*₆, 300 K): $\delta = 7.87$ (m, 1H, Ar-H) 7.62, 7.24 (*C*₁₀H₈), 7.07 - 6.79 (br, overlapping with benzene-*d*₆, 8H Tip-CH), 6.73 (s, 1H, Tip-CH), 5.05 - 4.82 (m, 2H, Tip-^{*i*}Pr-CHMe₂), 4.38 - 4.13 (m, 2H, Tip-^{*i*}Pr-CHMe₂), 4.03 - 3.48 (m, 4H, Tip-^{*i*}Pr-CHMe₂), 3.22 - 2.89 (m, 2H, Tip-^{*i*}Pr-CHMe₂), 2.82 - 2.48 (m, 5H, Tip-^{*i*}Pr-CHMe₂) 2.33 (sept, ³J_{HH} = 6.8 Hz, 1H, Tip-^{*i*}Pr-CHMe₂), 2.1, 2.07 (br, 3H, Tip-^{*i*}Pr-CH₃), 1.87 - 0.12 (m, overlapping with hexane, 112H, Tip-^{*i*}Pr-CH₃). **¹³C-NMR** (75.46 MHz, benzene-*d*₆, 300 K): $\delta = 155.99, 154.64, 152.59, 151.01, 150.59, 150.23, 149.53, 143.49, 136.75, 136.38, 136.09$ (Ar-C), 133.90 (*C*₁₀H₈), 132.42, 128.89 (Ar-CH), 128.19 (*C*₁₀H₈), 127.87, 127.55 (Ar-C), 125.88 (*C*₁₀H₈), 123.55, 123.09, 122.51, 122.24, 122.04, 121.32, 120.99 (br, Ar-CH), 37.61, 36.79, 36.39, 35.99, 35.52, 34.34, 34.59, 34.49, 34.27, 34.17, 33.86 (Tip-^{*i*}Pr-CH), 28.21, 28.11, 27.34, 27.19, 27.09, 25.54, 24.92, 24.74, 24.28, 24.28, 24.05, 23.86, 23.76, 23.53, 23.24 (Tip-^{*i*}Pr-CH₃), 22.54 (Tip-^{*i*}Pr-CH₂), 22.43, 14.11 (Tip-^{*i*}Pr-CH₃). **²⁹Si-NMR** (59.62 MHz, benzene-*d*₆, 300 K): $\delta = 174.7$ (s, *privo*-SiTip₂), 17.1 (s, *ligato*-SiTip), 8.7 (s, *remoto*-SiTip₂), -26.5 (s, *ligato*-Si-C=O), -263.0 (s, *nudo*-Si), -279.0 (s, *nudo*-Si).

Elemental analysis calculated for C₈₂H₁₂₀OSi₆: C, 76.33; H, 8.91. Found: C, 74.96; H, 9.60.

6. Supporting Information

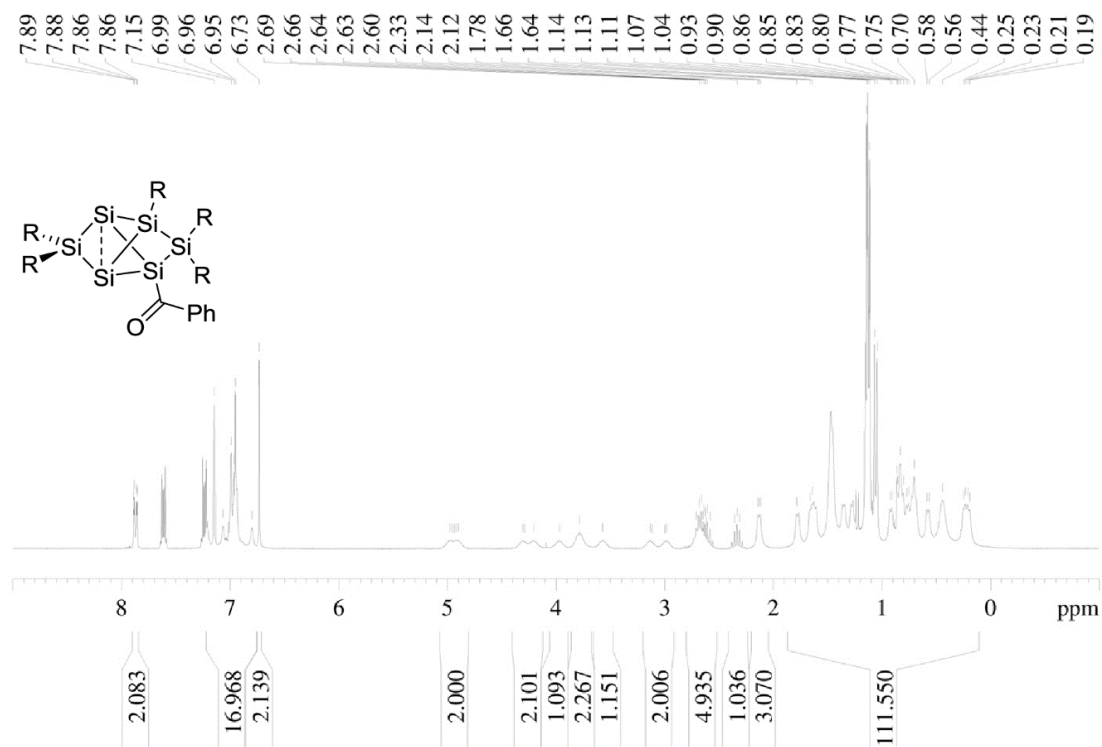


Figure S8: ^1H NMR of **5b** in C_6D_6 (300 MHz).

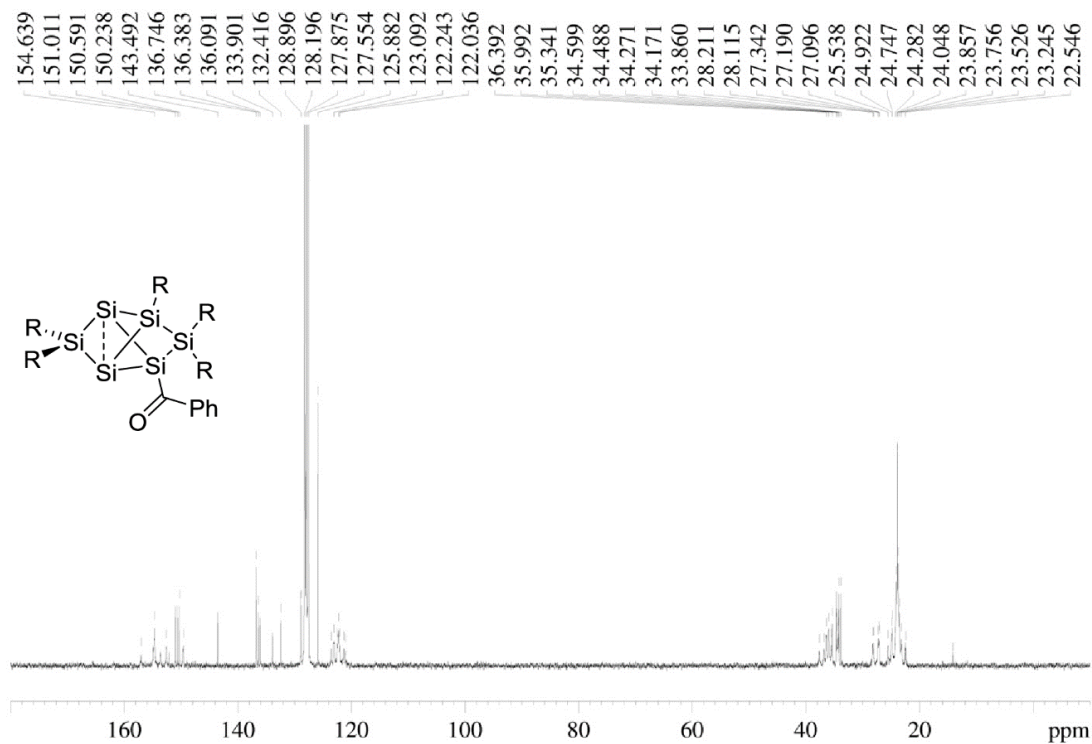


Figure S9: ^{13}C NMR of **5b** in C_6D_6 (75.5 MHz).

6. Supporting Information

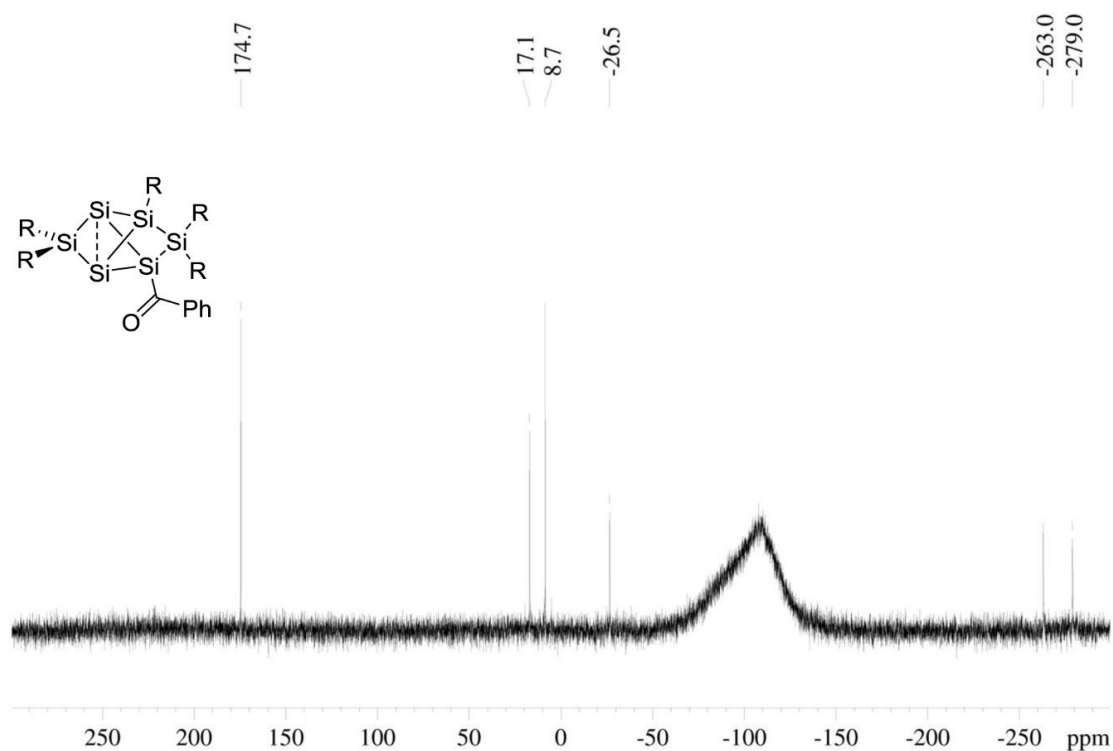


Figure S10: ^{29}Si NMR of **5b** in C_6D_6 (59.6 MHz).

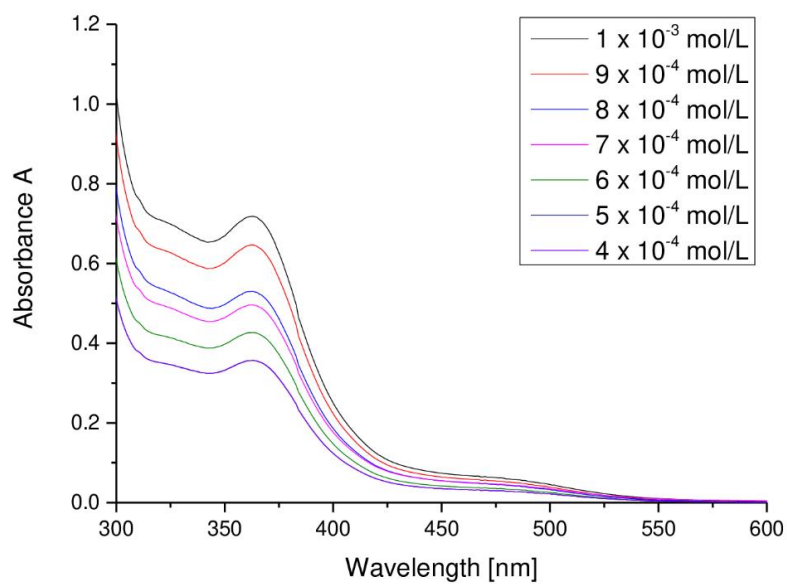


Figure S11: UV-Vis spectrum of **5b** in hexane at different concentrations.

6. Supporting Information

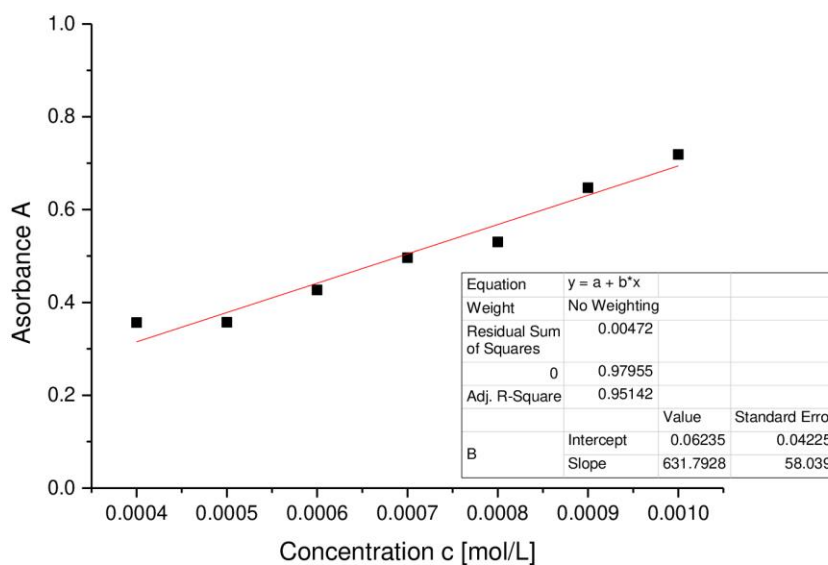


Figure S12: Determination of ϵ ($6318 \text{ M}^{-1} \text{ cm}^{-1}$) by linear regression of absorptions ($\lambda = 363 \text{ nm}$) of **5b** against concentration.

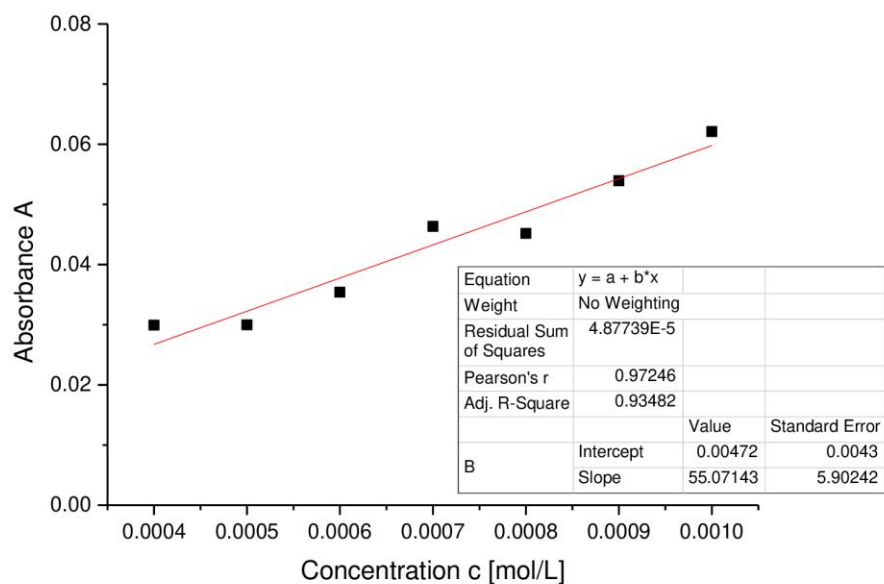


Figure S13: Determination of ϵ ($551 \text{ M}^{-1} \text{ cm}^{-1}$) by linear regression of absorptions ($\lambda = 477 \text{ nm}$) of **5b** against concentration.

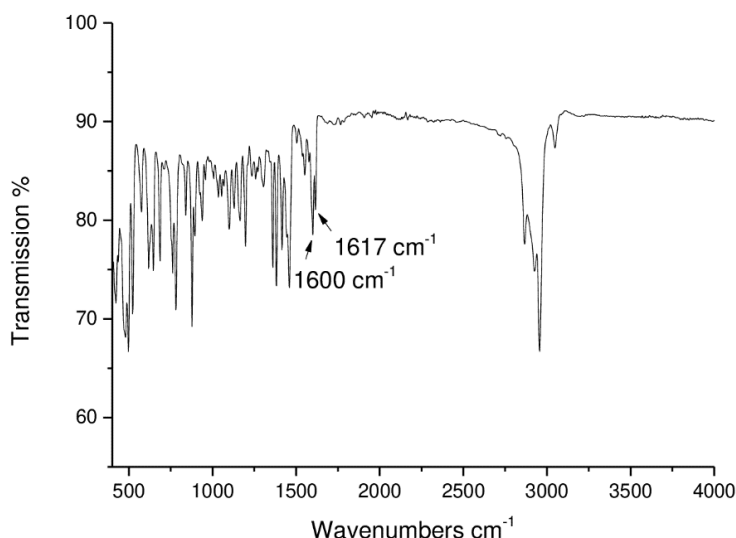


Figure S14: Infrared spectrum of **5b** (powder).

Preparation of *privo*-Lithiated anionic siliconoid **4Li**

***privo*-Lithio-2,4,5,6-pentakis(2',4',6'-triisopropylphenyl) tetracyclo [2.2.0.0^{1,3}.0^{3,6}]hexasilane (**4Li**)**

A solution of 2.39 g of siliconoid **3** (1.72 mmol) in 6 mL of Et₂O is cooled to -78°C. Lithium/naphthalene solution in thf (7.6 mL, 0.5 M, 3.78 mmol) is added dropwise and the resulting reaction mixture allowed warming to room temperature overnight with vigorous stirring. All volatiles are removed in vacuum and the resulting residue is washed three times with hexane. The final product **4Li** remains as pale-orange microcrystals. (1.42 g; 60% yield). ¹H NMR (300.13 MHz, benzene-d₆, 300K): δ = 7.28 (d, 1H, Tip-H), 7.27 (d, 1H, Tip-H), 7.05 (d, 1H, Tip-H), 7.00 (s, 2H, Tip-H), 6.94 (d, 1H, Tip-H), 6.93 (s, 1H, Tip-H), 6.84, 6.83 (each d, each 1H, Tip-H), 5.45 (sept, 1H, ⁱPr-CH), 5.15 – 5.00 (m, 2H, ⁱPr-CH), 4.57 (sept, 1H, ⁱPr-CH), 4.45 (sept, 1H, ⁱPr-CH), 4.18 (sept, 2H, ⁱPr-CH), 3.64 (sept, 1H, ⁱPr-CH), 3.44 – 3.30 (m, 2H, ⁱPr-CH), 3.04 (t, 8H, thf), 2.83 – 2.65 (m, 5H, ⁱPr-CH), 2.17, 2.14 (each d, together 6H, ⁱPr-CH₃), 1.74 (t, 6H, ⁱPr-CH₃), 1.67, 1.62, 1.57 (each d, each 3H, ⁱPr-CH₃), 1.50 (d, 9H, ⁱPr-CH₃), 1.45 (d, 3H, ⁱPr-CH₃), 1.25 – 1.11 (m, 38H, ⁱPr-CH₃ and thf), 0.95 (d, 6H, ⁱPr-CH₃), 0.75 (t, 6H, ⁱPr-CH₃), 0.69 – 0.62 (m, 9H, ⁱPr-CH₃), 0.37, 0.34 (each d, together 6H, ⁱPr-CH₃). ⁷Li NMR (116.6 MHz, benzene-d₆, 300K): δ = 0.29 (s). ¹³C NMR (75.5 MHz, benzene-d₆, 300K): δ = 158.3, 156.4, 156.1, 156.0, 153.8, 153.5, 152.5, 152.5, 151.0, 149.3, 148.8, 148.4, 148.3, 147.5, 146.3, 140.9, 139.8, 131.7, 131.5 (Ar-C), 123.0, 122.6, 122.4, 122.2, 121.4, 121.3, 120.9, 120.1, 119.8 (Ar-CH), 68.5 (thf), 36.8, 36.7, 36.5, 36.3, 36.1, 36.0, 35.1, 34.9, 34.8, 34.7, 34.6, 30.2, 28.1, 27.8, 27.5, 27.1, 26.7, 25.6 (Tip-ⁱPr-CH and Tip-ⁱPr-CH₃), 25.2 (thf), 25.2, 24.9, 24.9, 24.8, 24.7, 24.6, 24.5, 24.3, 24.2, 23.6, 22.6, 22.0 (Tip-

6. Supporting Information

ⁱPr-CH and Tip-ⁱPr-CH₃). ²⁹Si NMR (59.6 MHz, benzene-d₆, 300K): δ = 267.9 (br, *privo*-SiTiLi), 100.2 (s, *ligato*-Si), 15.3 (s, *remoto*-Si), -43.8 (s, *ligato*-Si), -222.2 (s, *nudo*-Si), -231.4 (s, *nudo*-Si). **Elemental analysis** calculated for C₈₃H₁₃₁LiO₂Si₆: C, 74.60; H, 9.88. Found: C, 72.68; H, 9.51.

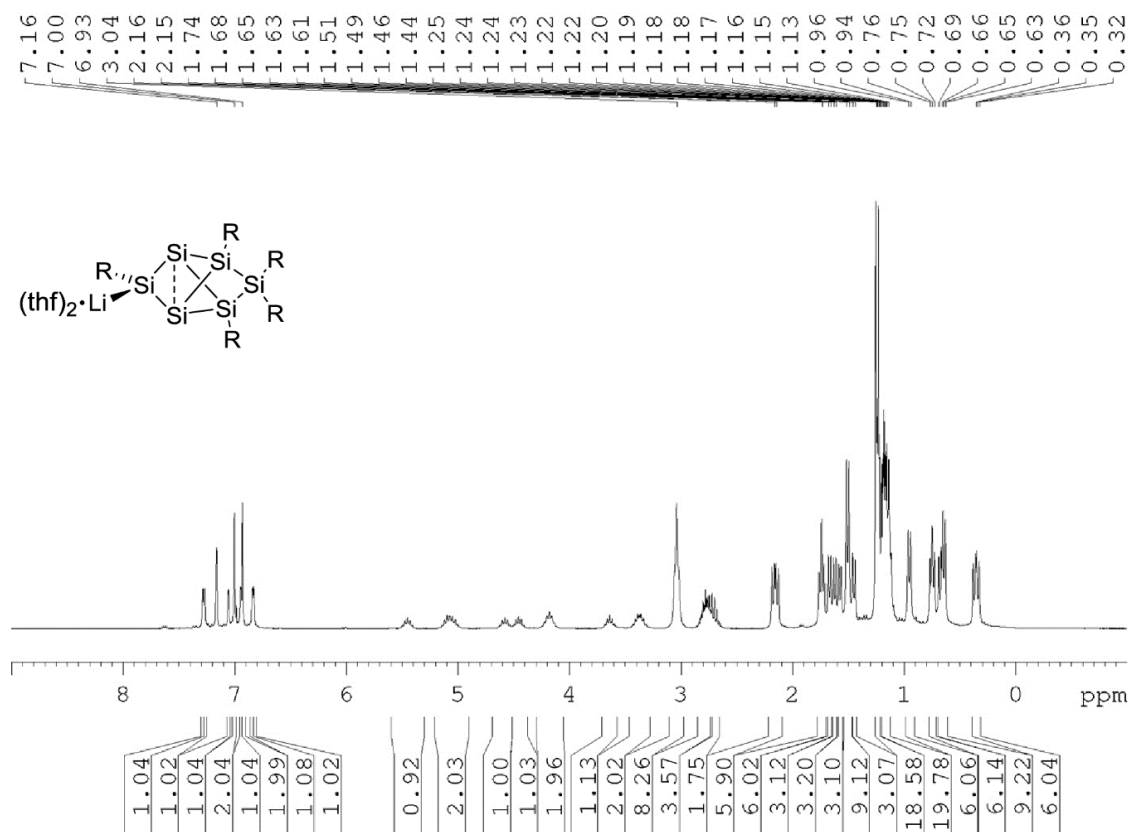


Figure S15: ¹H NMR of **4Li** in C₆D₆ (300 MHz).

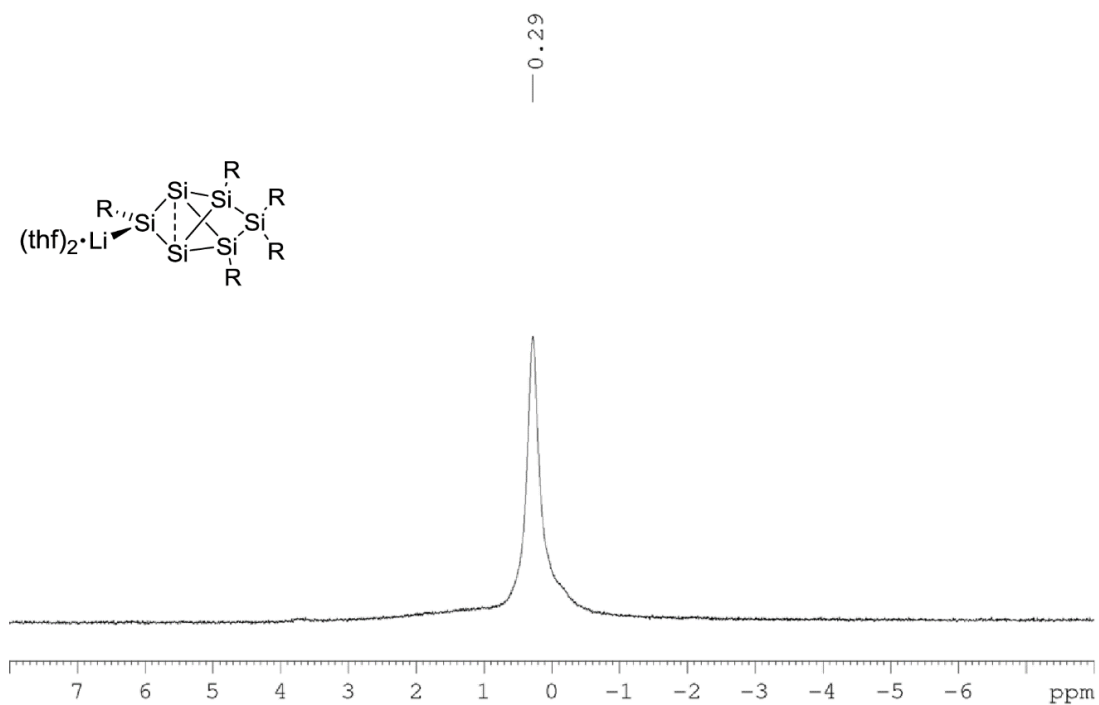


Figure S16: ^7Li NMR of **4Li** in C_6D_6 (116.6 MHz).

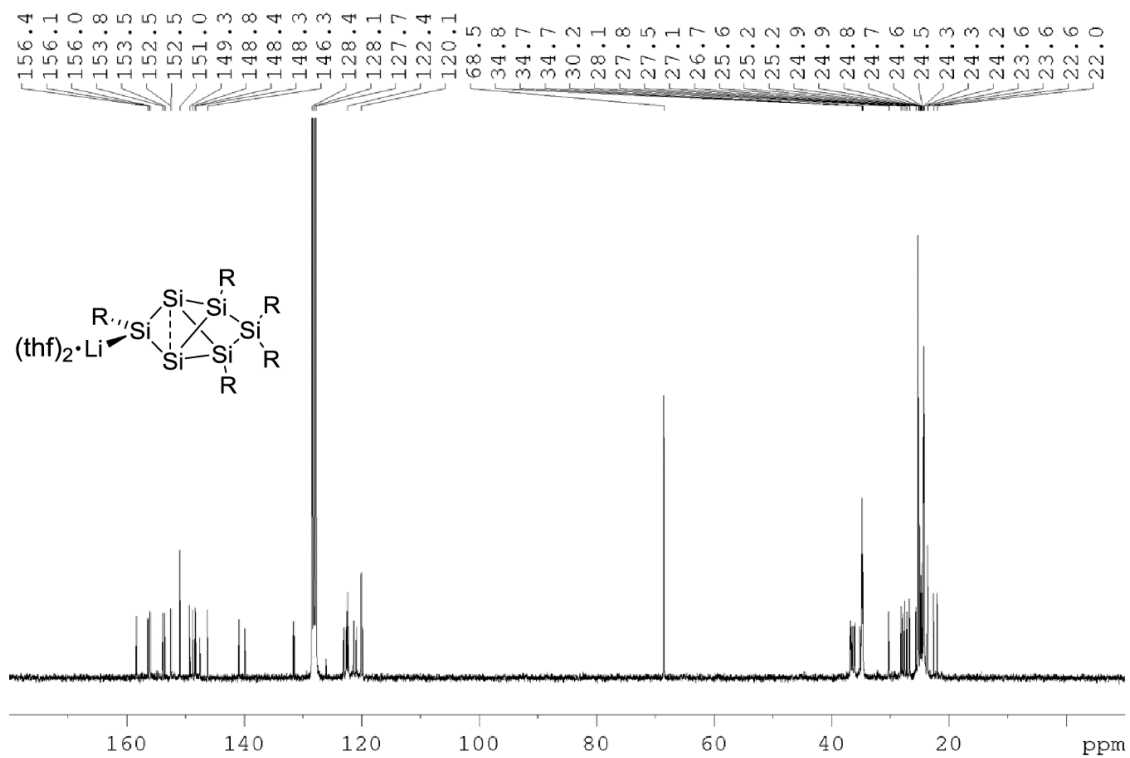


Figure S17: ^{13}C NMR of **4Li** in C_6D_6 (75.5 MHz).

6. Supporting Information

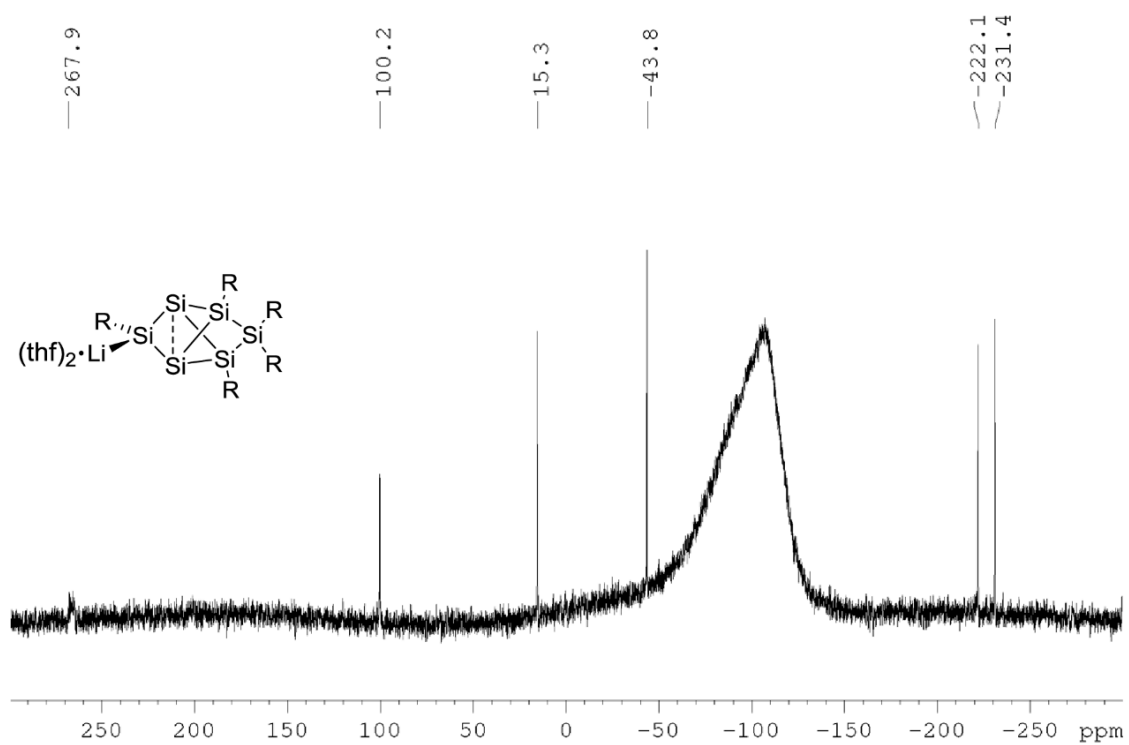


Figure S18: ^{29}Si NMR of **4Li** in C_6D_6 (59.6 MHz).

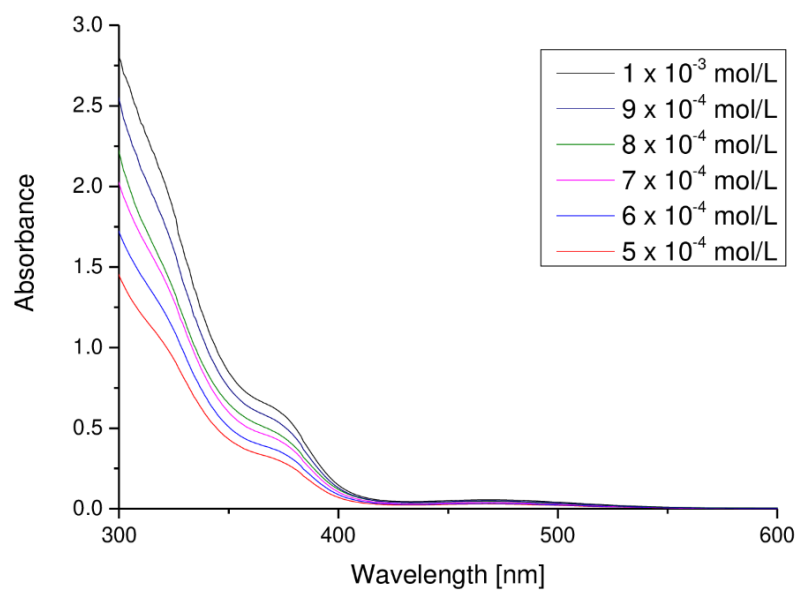


Figure S19: UV-Vis spectrum of **4Li** in hexane at different concentrations.

6. Supporting Information

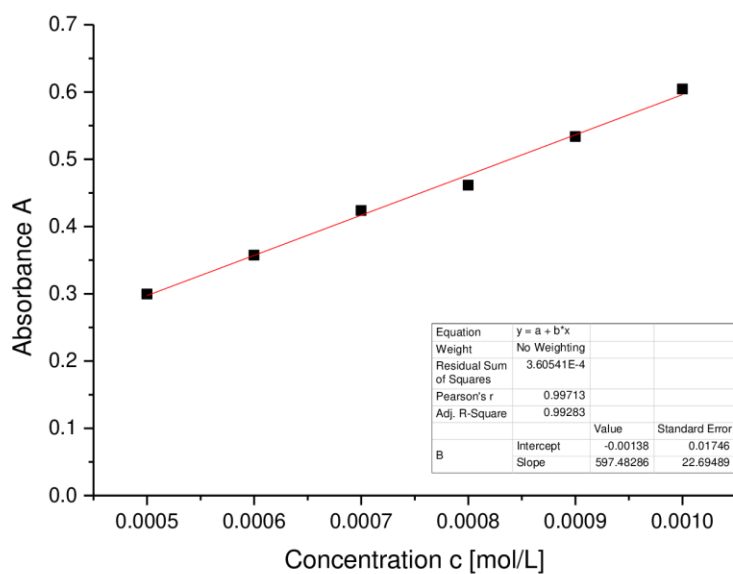


Figure S20: Determination of ϵ ($5974 \text{ M}^{-1} \text{ cm}^{-1}$) by linear regression of absorptions ($\lambda = 373 \text{ nm}$) of **4Li** against concentration.

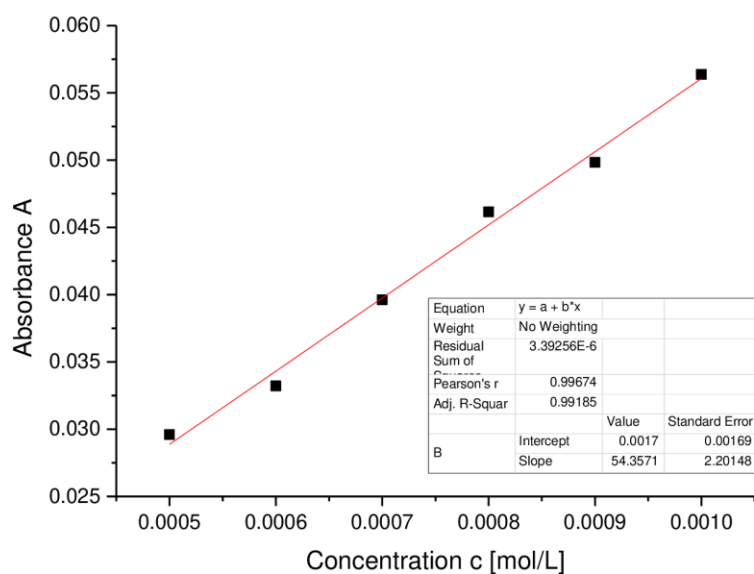


Figure S21: Determination of ϵ ($543 \text{ M}^{-1} \text{ cm}^{-1}$) by linear regression of absorptions ($\lambda = 468 \text{ nm}$) of **4Li** against concentration.

Preparation of *privo*-Trimethylsilyl-2,4,5,6-pentakis(2',4',6'-triisopropylphenyl)tetracyclo**[2.2.0.0^{1,3}.0^{3,6}]hexasilane (6a)**

Quantities: **4Li**, 104 mg (0.078 mmol); Me₃SiCl 11 μ L (9.39 mg, 0.086 mmol); toluene (2 mL); stirring 2.5 h; crystallization from hexane. Yield: 65 mg (66 %) orange crystals.

¹H NMR (300.13 MHz, benzene-d₆, 300K): δ = 7.27 (d, 2H, Tip-H), 7.07, 7.01, 6.97, 6.91, 6.83 (each d, each 1H, Tip-H), 6.80 (d, 2H, Tip-H), 6.75 (d, 1H, Tip-H), 4.93 (m, 2H, ⁱPr-CH), 4.37 (sept, 1H, ⁱPr-CH), 4.06 (sept, 2H, ⁱPr-CH), 3.74, 3.63 (each m, each 1H, ⁱPr-CH), 3.57 (t, 10H, thf), 3.37 (m, 2H, ⁱPr-CH), 2.71 (m, 6H, ⁱPr-CH), 2.14 (d, 3H, ⁱPr-CH₃), 2.05 (d, 3H, ⁱPr-CH₃), 1.82 (d, 3H, ⁱPr-CH₃), 1.67 (m, 7H, ⁱPr-CH₃), 1.57 (m, 14H, ⁱPr-CH₃), 1.43 (br, 10H, thf), 1.24, 1.21, 1.20, 1.18, 1.17, 1.16, 1.15, 1.13, 1.11, 1.08 (each d, overall 36H, ⁱPr-CH₃), 0.79 (d, 3H, ⁱPr-CH₃), 0.67 (t, 6H, ⁱPr-CH₃), 0.51 (m, 6H, ⁱPr-CH₃), 0.40, 0.38 (each d, overall 6H, ⁱPr-CH₃), 0.29 (d, 3H, ⁱPr-CH₃), -0.15 (s, 9H, Si(CH₃)₃). ¹³C NMR (75.5 MHz, benzene-d₆, 300K): δ = 157.1, 156.9, 156.6, 156.1, 153.7, 153.2, 152.6, 152.0, 150.7, 150.2, 149.9, 149.4, 149.2, 138.7, 138.3, 134.8, 129.1, 126.9, 123.7 (Ar-C), 123.1, 122.8, 122.6, 122.4, 122.2, 122.1, 121.7, 121.6, 121.3, 121.0 (Ar-CH), 37.7, 37.6, 37.3, 36.9, 36.7, 36.4, 35.1, 35.0, 34.8, 34.7, 34.6, 34.5, 27.8, 27.6, 27.4, 27.1, 27.0, 26.5, 26.4, 26.2, 25.7, 25.4, 25.3, 25.1, 25.0, 24.9, 24.6, 24.4, 24.3, 24.1, 24.0, 23.9, 22.6 (Tip-ⁱPr-CH and Tip-ⁱPr-CH₃), 1.5 (Si(CH₃)₃). ²⁹Si NMR (59.6 MHz, benzene-d₆, 300K): δ = 193.6 (s, *privo*-Si(Tip)SiMe₃), 29.2 (s, *remoto*-SiTip₂), 22.4 (s, *ligato*-SiTip), -11.2 (s, SiMe₃), -15.9 (s, *ligato*-SiTip), -242.0 (s, *nudo*-Si), -253.3 (s, *nudo*-Si). **Elemental analysis** calculated for C₇₈H₁₂₄Si₇: C, 74.45; H, 9.93. Found: C, 71.65; H, 9.83.

6. Supporting Information

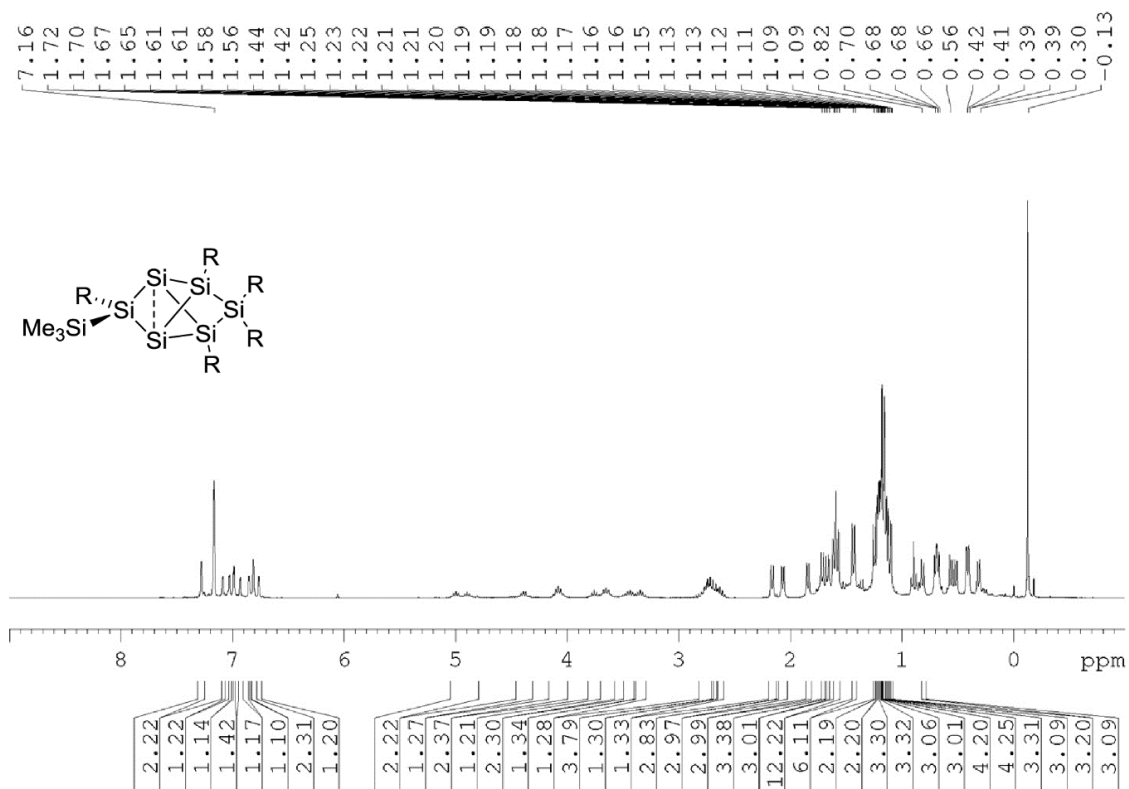


Figure S22: ^1H NMR of **6a** in C_6D_6 (300 MHz).

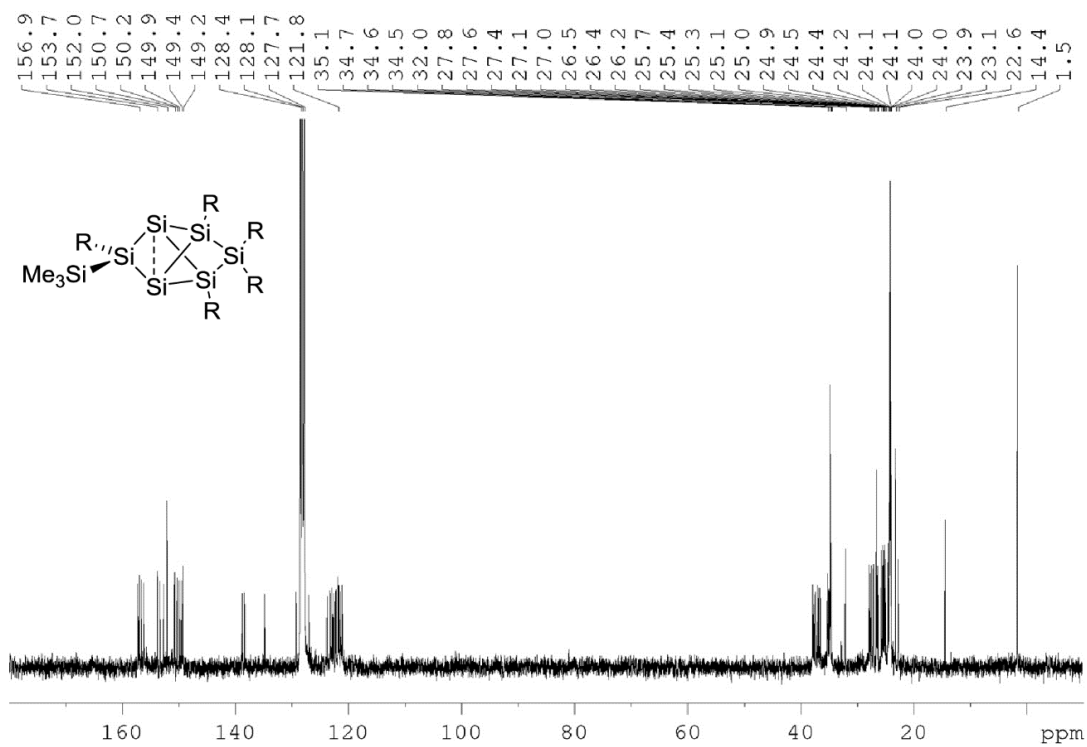


Figure S23: ^{13}C NMR of **6a** in C_6D_6 (75.5 MHz).

6. Supporting Information

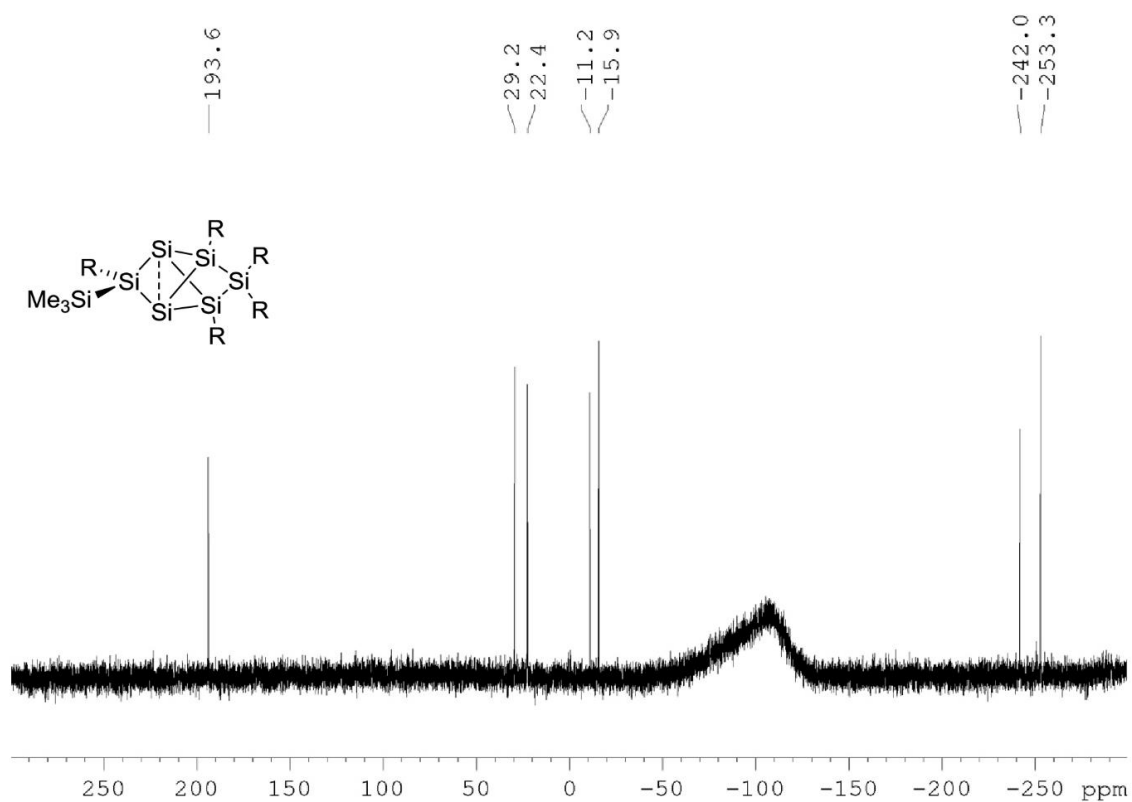


Figure S24: ^{29}Si NMR of **6a** in C_6D_6 (59.6 MHz).

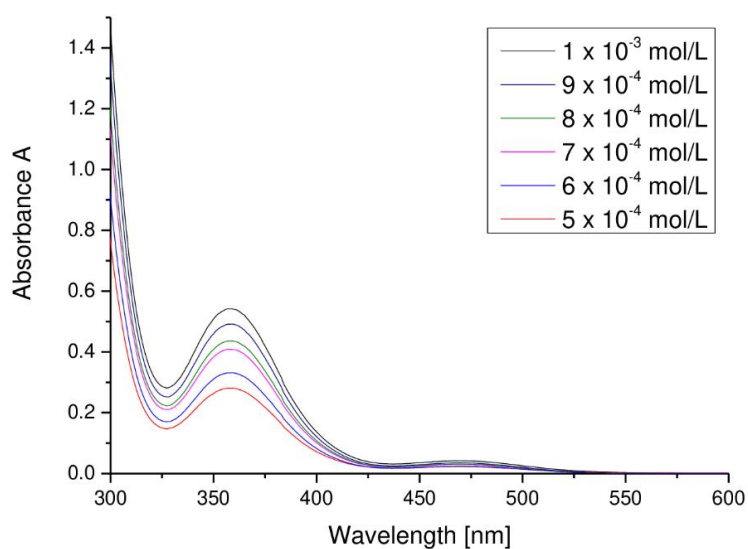


Figure S25: UV-Vis spectrum of **6a** in hexane at different concentrations.

6. Supporting Information

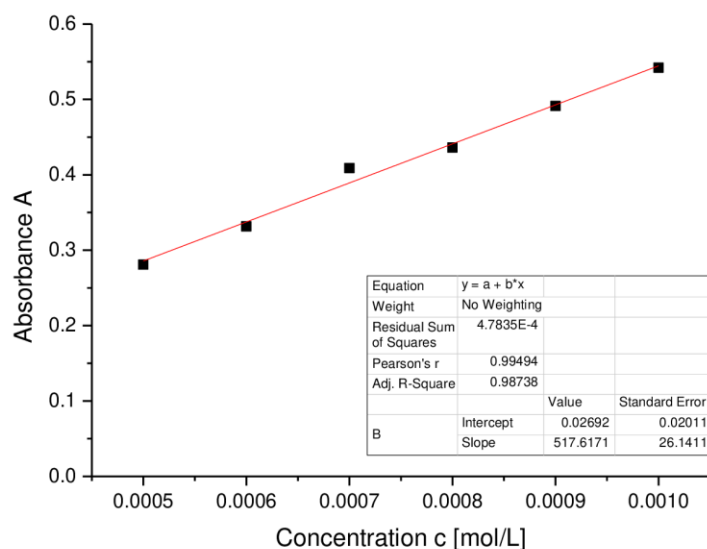


Figure S26: Determination of ϵ ($5176 \text{ M}^{-1} \text{ cm}^{-1}$) by linear regression of absorptions ($\lambda = 357 \text{ nm}$) of **6a** against concentration.

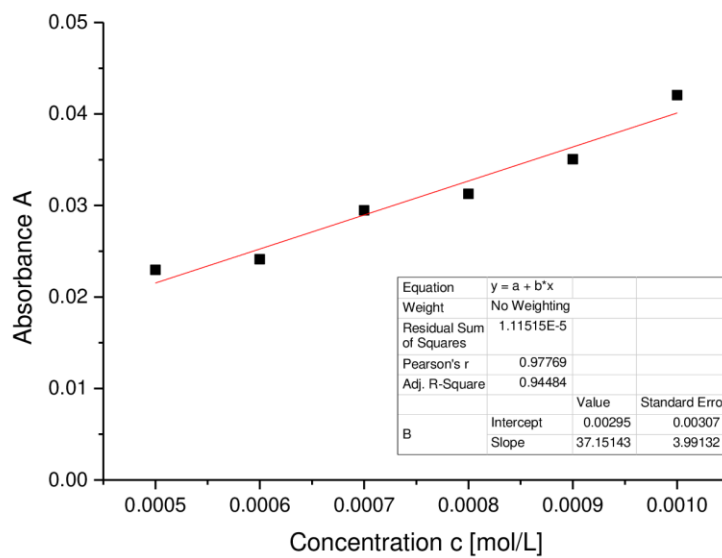


Figure S27: Determination of ϵ ($371 \text{ M}^{-1} \text{ cm}^{-1}$) by linear regression of absorptions ($\lambda = 469 \text{ nm}$) of **6a** against concentration.

Preparation of privo-Benzoyl-2,4,5,5,6-pentakis(2',4',6'-tri-iso-propylphenyl)tetracyclo***[2.2.0.0^{1,3}.0^{3,6}] hexasilane (6b)***

Quantities: **4Li**, 89.5 mg (0.06 mmol); benzoyl chloride 7.5 μ L (9.1 mg, 0.065 mmol); toluene; stirring 0.5 h; The crude product was thoroughly dried in vacuo and characterized by multinuclear NMR spectroscopy.

¹H NMR (300.13 MHz, benzene-d₆, 300K): δ = 7.72 (s), 7.70 (d), 7.26 (d), 7.24 (br), 7.07 (d), 6.96 (d), 6.89 (d), 6.87 (s), 6.81 (t), 6.77 (m), 6.74 (s), 5.06 – 5.02 (m), 4.90 – 4.85 (m), 4.30 – 4.20 (m), 4.15 – 4.02 (m), 3.70 – 3.63 (m), 3.30 – 3.19 (m), 2.86 – 2.55 (m), 2.14 (d), 2.04 (d), 1.87 (d), 1.63 – 1.33 (m), 1.25 – 1.06 (m), 0.80 (d), 0.74 (d), 0.70 – 0.62 (m), 0.47 (d), 0.39 (d), 0.31 (d). **¹³C NMR** (75.5 MHz, benzene-d₆, 300 K): δ = 226.9 (CO), 156.8, 156.5, 156.1, 156.1, 154.3, 153.7, 153.4, 153.3, 152.2, 152.0, 151.4, 150.8, 150.6, 149.6, 149.5, 149.1, 140.5, 138.5, 138.4, 133.5, 132.4, 128.9, 126.5, 126.1, 123.5, 123.2, 122.9, 122.4, 122.2, 121.9, 121.5, 121.3, 121.2 (Ar-C and Ar-CH), 37.4, 37.1, 36.6, 35.2, 34.8, 34.6, 34.5 (Tip-*i*Pr-CH and Tip-*i*Pr-CH₃), 32.0 (hexane), 27.6, 27.4, 27.1, 26.7, 26.5, 26.1, 25.9, 25.7, 25.6, 25.4, 25.3, 24.9, 24.7, 24.5, 24.1, 24.1, 24.0, 23.9, 23.5, 23.1, 22.9, 22.7, 22.6 (Tip-*i*Pr-CH and Tip-*i*Pr-CH₃), 14.4 (hexane). **²⁹Si NMR** (59.6 MHz, benzene-d₆, 300 K): δ = 166.2 (s, *privo*-Si(Tip)COPh), 30.9 (s, *remoto*-SiTip₂), -3.6 (s, *ligato*-SiTip), -16.2 (s, *ligato*-SiTip) -269.5 (s, *nudo*-Si) -271.1 (s, *nudo*-Si).

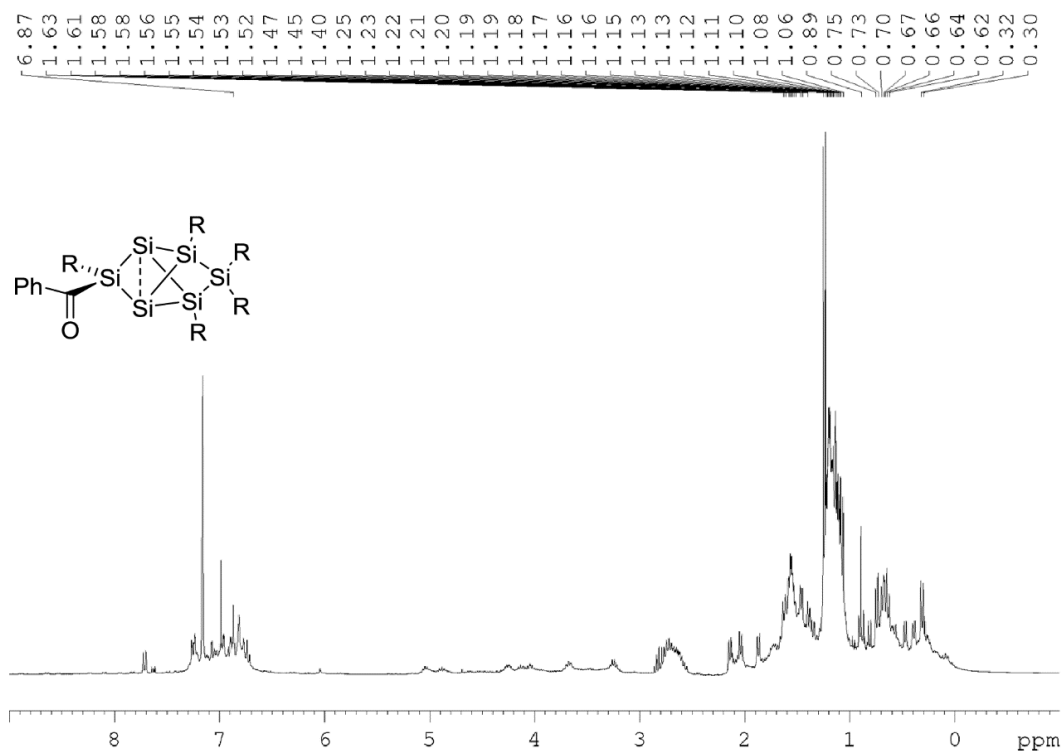


Figure S28: ¹H NMR of **6b** in C₆D₆ (300 MHz).

6. Supporting Information

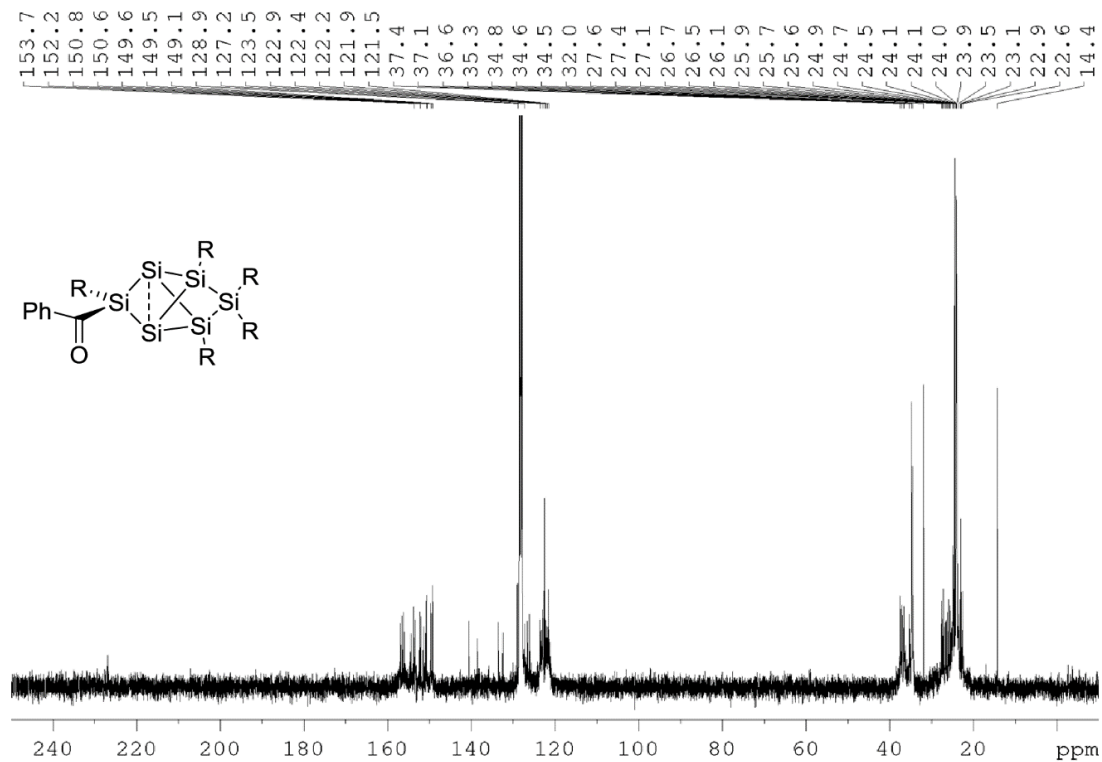


Figure S29: ^{13}C NMR of **6b** in C_6D_6 (75.5 MHz).

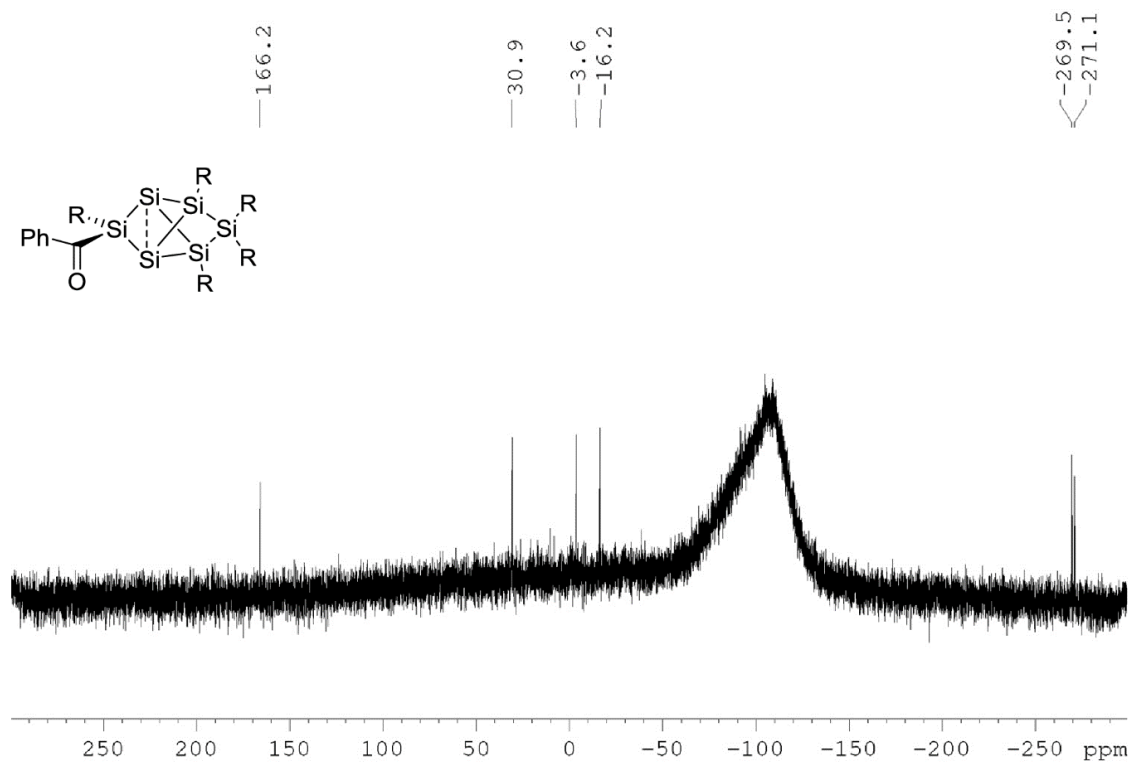


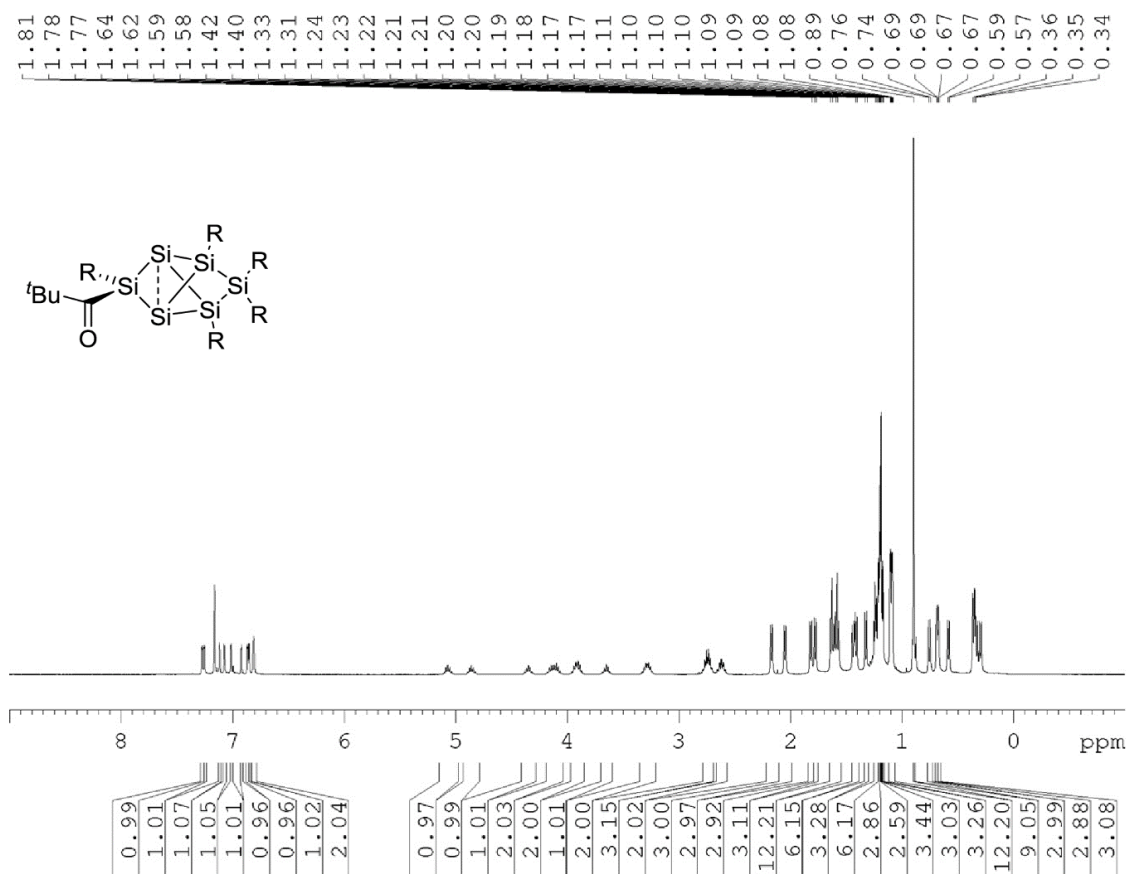
Figure S30: ^{29}Si NMR of **6b** in C_6D_6 (59.6 MHz).

Preparation of privo-Pivaloyl-2,4,5,5,6-pentakis(2',4',6'-triisopropylphenyl)tetracyclo[2.2.0.0^{1,3}.0^{3,6}]hexasilane (6c)

Quantities: **4Li**, 150.7 mg (0.11 mmol); pivaloyl chloride 13.9 μ L (13.6 mg, 0.11 mmol); toluene (2.5 mL); stirring 0.5 h; crystallization from hexane. Yield: 39 mg (27 %) orange crystals.

¹H NMR (400.13 MHz, benzene-*d*₆, 300K): δ = 7.27, 7.25, 7.12, 7.07, 7.01, 6.92, 6.86, 6.85 (each d, each 1H, Tip-H), 6.80 (t, 2H, Tip-H), 5.07, 4.86, 4.35 (each sept, each 1H, ⁱPr-CH), 4.18 – 4.06 (m, 2H, ⁱPr-CH), 3.96 – 3.87 (m, 2H, ⁱPr-CH), 3.65 (s, 1H, ⁱPr CH), 3.32 – 3.23 (m, 2H, ⁱPr-CH), 2.78 – 2.70 (m, 3H, ⁱPr-CH), 2.65 – 2.58 (m, 2H, ⁱPr-CH), 2.17, 2.05, 1.81, 1.78 (each d, each 3H, ⁱPr-CH₃), 1.64 – 1.56 (m, 12H, ⁱPr-CH₃), 1.44, 1.41, 1.32 (each d, each 3H, ⁱPr-CH₃), 1.25 – 1.17 (m, 21H, ⁱPr-CH₃), 1.11 – 1.08 (m, 12H, ⁱPr-CH₃), 0.89 (s, 9H, ^tBu-CH₃), 0.75, 0.69, 0.67, 0.58 (each d, each 3H, ⁱPr-CH₃), 0.36 – 0.28 (m, 12H, ⁱPr-CH₃). **¹³C NMR** (100.6 MHz, benzene-*d*₆, 300K): δ = 238.7 (CO), 157.1, 156.9, 155.9, 155.4, 154.2, 153.8, 153.5, 153.2, 152.1, 151.8, 151.6, 150.6, 150.5, 149.5, 149.3, 138.5, 138.4, 133.6, 128.2, 127.9 (Ar-C), 126.6, 123.6, 123.0, 122.9, 122.7, 122.4, 122.2, 122.0, 121.5, 120.6 (Ar-CH), 49.4 (CMe₃), 37.7, 37.5, 37.3, 37.2, 37.0, 36.7, 36.5, 35.3, 35.0, 35.0, 34.7, 34.6, 34.6, 32.0, 29.0, 27.4, 26.8 (Tip-ⁱPr-CH and Tip-ⁱPr-CH₃), 26.8 (^tBu-CH₃), 26.2, 26.1, 25.7, 25.7, 25.5, 25.4, 25.2, 25.1, 25.0, 24.9, 24.8, 24.5, 24.1, 24.1, 24.1, 24.0, 23.9, 23.6, 23.1, 22.4, 14.4 (Tip-ⁱPr-CH and Tip-ⁱPr-CH₃). **²⁹Si NMR** (59.6 MHz, benzene-*d*₆, 300 K): δ = 173.1 (s, *privo*-Si(Tip)CO^tBu) 30.9 (s, *remoto*-SiTip₂), -1.7 (s, *ligato*-SiTip), -14.5 (s, *ligato*-SiTip) -263.1 (s, *nudo*-Si) -265.8 (s, *nudo*-Si). Elemental analysis calculated for C₈₀H₁₂₄OSi₆: C, 75.64, H; 9.84. Found: C, 74.29; H, 10.05.

6. Supporting Information



6. Supporting Information

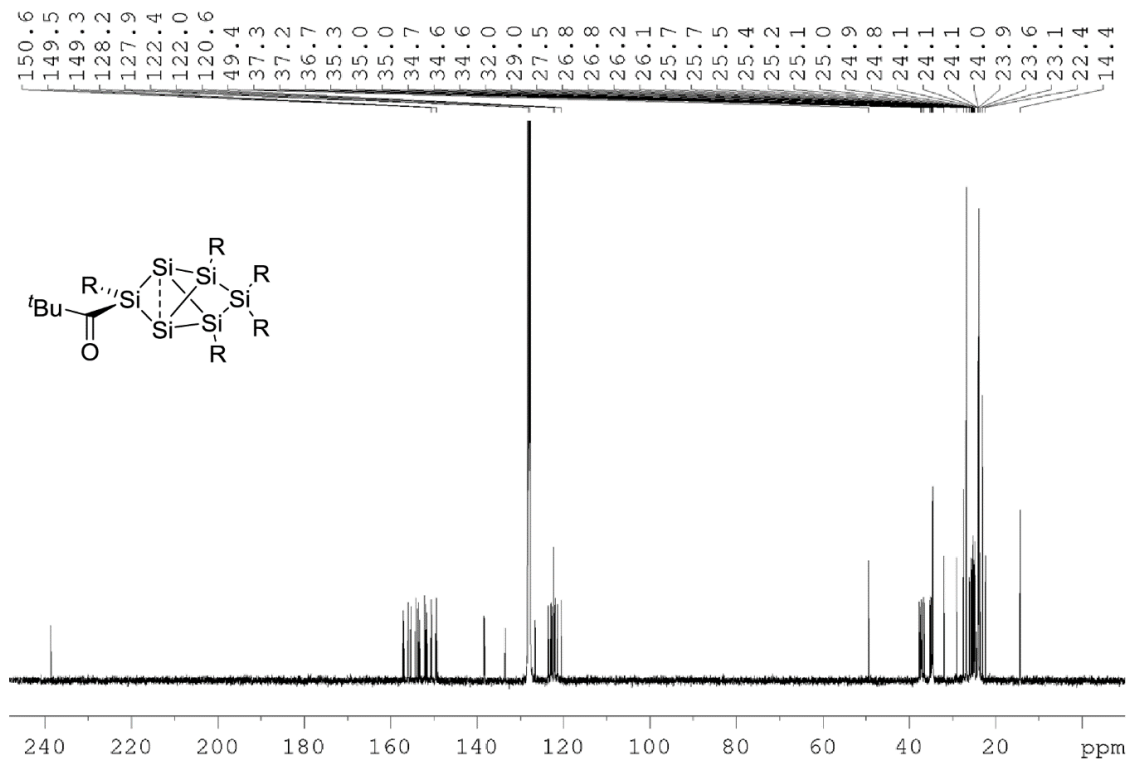


Figure S32: ^{13}C NMR of **6c** in C_6D_6 (100.6 MHz).

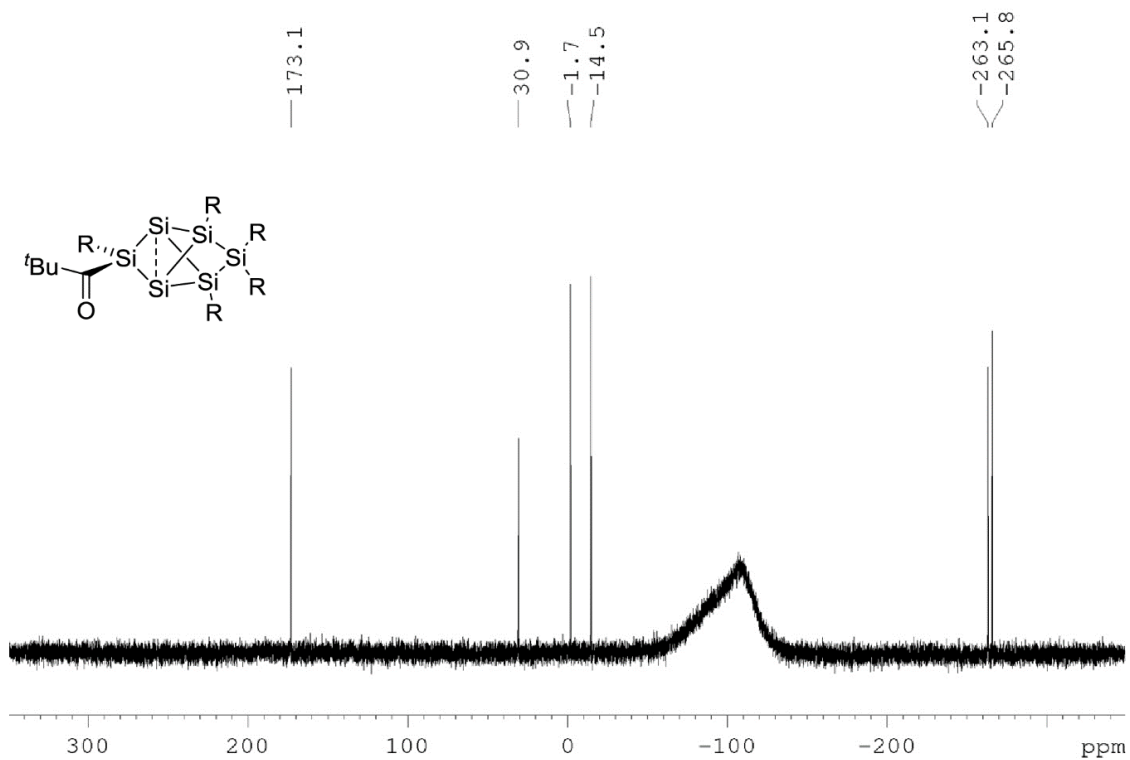


Figure S33: ^{29}Si NMR of **6c** in C_6D_6 (59.6 MHz).

6. Supporting Information

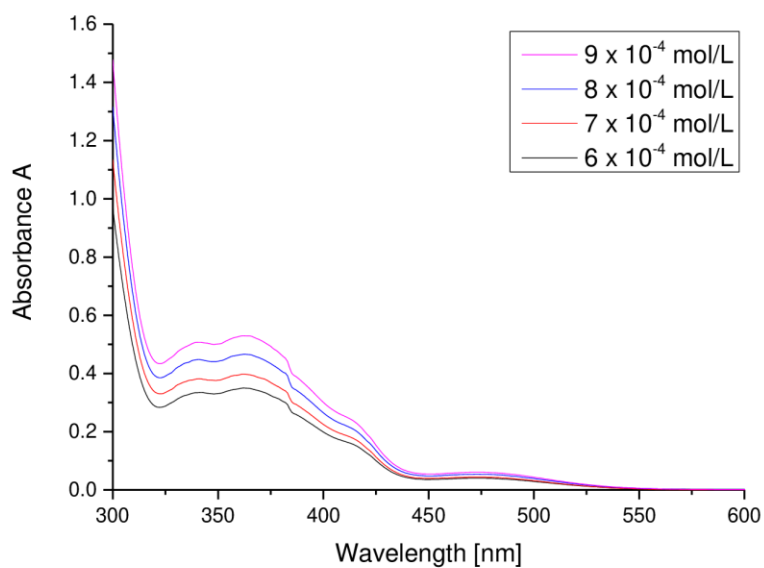


Figure S34: UV-Vis spectrum of **6c** in hexane at different concentrations.

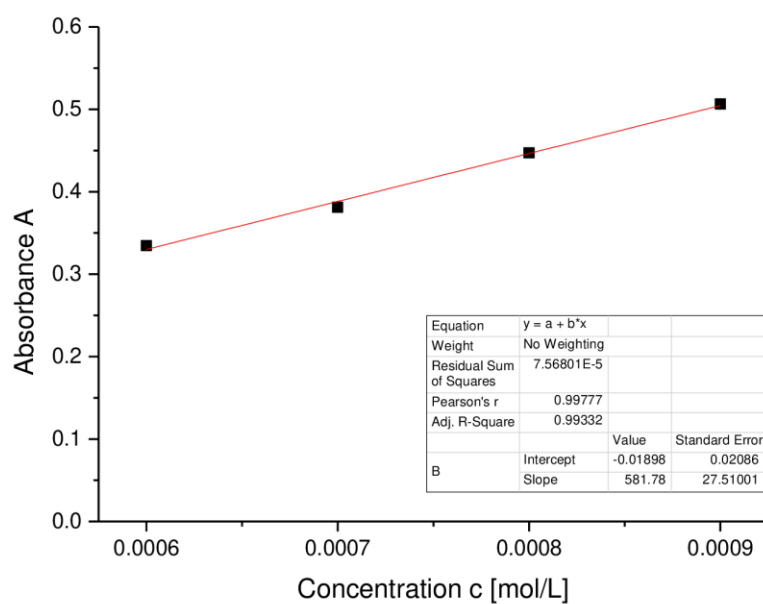


Figure S35: Determination of ϵ ($5817 \text{ M}^{-1} \text{ cm}^{-1}$) by linear regression of absorptions ($\lambda = 342 \text{ nm}$) of **6c** against concentration.

6. Supporting Information

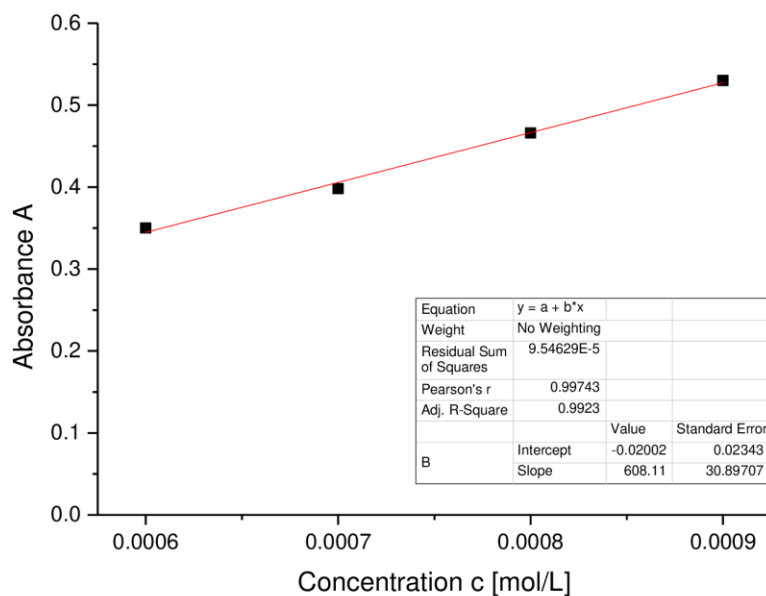


Figure S36: Determination of ϵ ($6081 \text{ M}^{-1} \text{ cm}^{-1}$) by linear regression of absorptions ($\lambda = 362 \text{ nm}$) of **6c** against concentration.

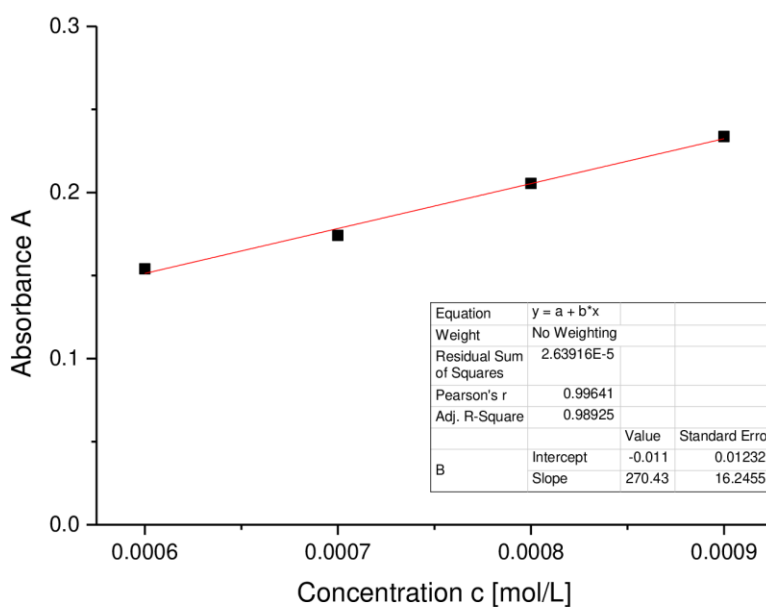


Figure S37: Determination of ϵ ($2704 \text{ M}^{-1} \text{ cm}^{-1}$) by linear regression of absorptions ($\lambda = 415 \text{ nm}$) of **6c** against concentration.

6. Supporting Information

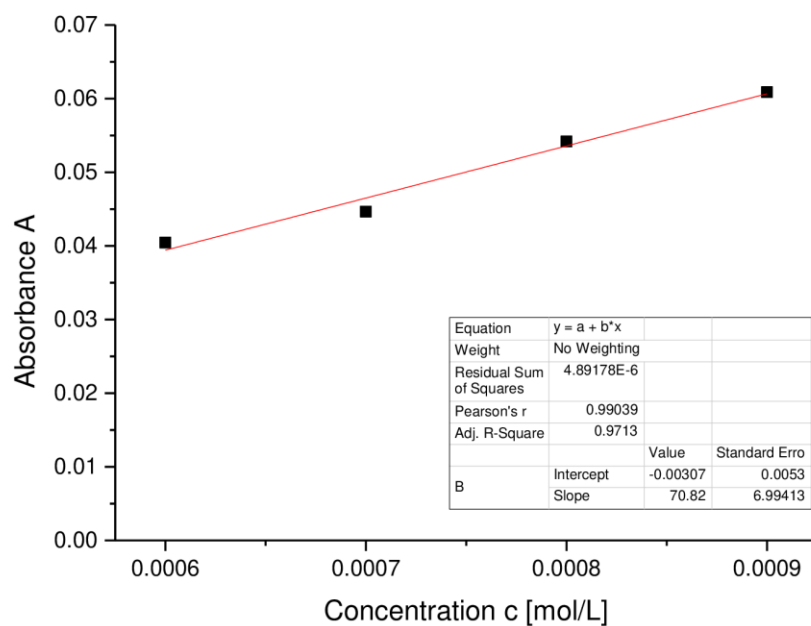


Figure S38: Determination of ϵ ($708 \text{ M}^{-1} \text{ cm}^{-1}$) by linear regression of absorptions ($\lambda = 473 \text{ nm}$) of **6c** against concentrations.

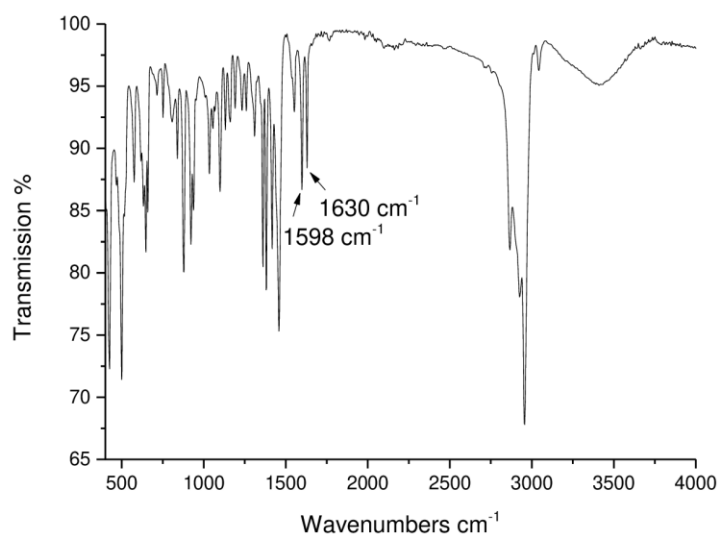


Figure S39: Infrared spectrum of **6c** (powder).

Preparation of *privo*-Bis(dimethylamino)phosphanyl-2,4,5,5,6-pentakis(2',4',6'tri-iso-propyl-phenyl)-tetracyclo[2.2.0.0^{1,3}.0^{3,6}] hexasilane (6d)

Quantities: **4Li**, 102.8 mg (0.077 mmol); (Me₂N)₂PCl 11.2 μL (11.9 mg, 0.077 mmol); benzene-d₆ (0.6 mL); NMR scale. The crude product was thoroughly dried in vacuum and characterized by multinuclear NMR spectroscopy.

¹H NMR (300.13 MHz, benzene-d₆, 300K): δ = 7.28 (d, 2H, Tip-H), 7.09 (s, 1H, Tip-H), 6.99 (s, 1H, Tip-H), 6.91 (s, 1H, Tip-H), 6.87 (s, 1H, Tip-H), 6.81 (s, 2H, Tip-H), 6.79 (s, 1H, Tip-H), 5.06 (sept, 1H, ⁱPr-CH), 4.88 (sept, 1H, ⁱPr-CH), 4.41 (sept, 1H, ⁱPr-CH), 4.19 – 4.08 (m, 2H, ⁱPr-CH), 4.01 – 3.95 (m, 2H, ⁱPr-CH), 3.65 (sept, 1H, ⁱPr-CH), 3.47 (sept, 1H, ⁱPr-CH), 3.35 (sept, 1H, ⁱPr-CH), 2.78 – 2.65 (m, 5H, ⁱPr-CH), 2.58 (d, ³J_{PH} = 9.89 Hz, 6H, N(CH₃)₂), 2.30 (d, ³J_{PH} = 9.19 Hz, 6H, N(CH₃)₂), 2.19 (d, 3H, ⁱPr-CH₃), 2.06 (d, 3H, ⁱPr-CH₃), 1.86 (d, 3H, ⁱPr-CH₃), 1.79 (d, 3H, ⁱPr-CH₃), 1.70 (d, 3H, ⁱPr-CH₃), 1.65 – 1.57 (m, 12H, ⁱPr-CH₃), 1.44 (t, 6H, ⁱPr-CH₃), 1.22 – 1.14 (m, 27H, ⁱPr-CH₃), 1.11 – 1.07 (m, 6H, ⁱPr-CH₃), 0.84 (d, 3H, ⁱPr-CH₃), 0.72 (d, 3H, ⁱPr-CH₃), 0.68 (d, 3H, ⁱPr-CH₃), 0.55 (d, 3H, ⁱPr-CH₃), 0.45 – 0.39 (m, 9H, ⁱPr-CH₃), 0.31 (d, 3H, ⁱPr-CH₃). **¹³C NMR** (75.5 MHz, benzene-d₆, 300 K): δ = 157.4, 157.1, 156.9, 156.5, 156.3, 156.0, 155.9, 154.5, 153.7, 153.6, 153.3, 152.0, 151.8, 151.2, 151.0, 150.7, 150.3, 149.9, 149.3, 149.1 (Ar-C), 123.7, 123.1, 122.8, 122.5, 122.2, 122.1, 121.9, 121.7, 121.6, 121.4 (Ar-CH), 47.2 (d, ²J_{CP} = 9.54 Hz, N(CH₃)₂), 46.0 (d, ²J_{C-P} = 14.79 Hz, N(CH₃)₂), 40.7, 39.5, 38.4, 37.6, 37.4, 37.2, 37.1, 36.9, 36.4, 35.2, 34.8, 34.7, 34.6, 34.5, 28.4, 27.8, 27.4, 26.9, 26.6, 26.4, 26.3, 25.6, 25.4, 25.3, 25.2, 25.1, 25.0, 24.9, 24.8, 24.5, 24.5, 24.1, 24.1, 24.0, 24.0, 22.4 (Tip-ⁱPr-CH and Tip-ⁱPr-CH₃). **²⁹Si NMR** (59.6 MHz, benzene-d₆, 300 K): δ = 186.5 (d, ¹J_{SiP} = 97.44 Hz, *privo*-Si(Tip)P(NMe₂)₂), 28.0 (d, ¹J_{SiP} = 7.52 Hz, *remoto*-SiTip₂), 13.7 (d, ¹J_{SiP} = 20.87 Hz, *ligato*-SiTip), -16.9 (s, *ligato*-SiTip), -246.0 (d, ¹J_{SiP} = 33.40 Hz, *nudo*-Si), -256.1 (d, ¹J_{SiP} = 8.28 Hz, *nudo*-Si). **³¹P NMR** (121.5 MHz, benzene-d₆, 300 K): δ = 121.3 (s, ¹J_{SiP} = 97.44 Hz).

6. Supporting Information

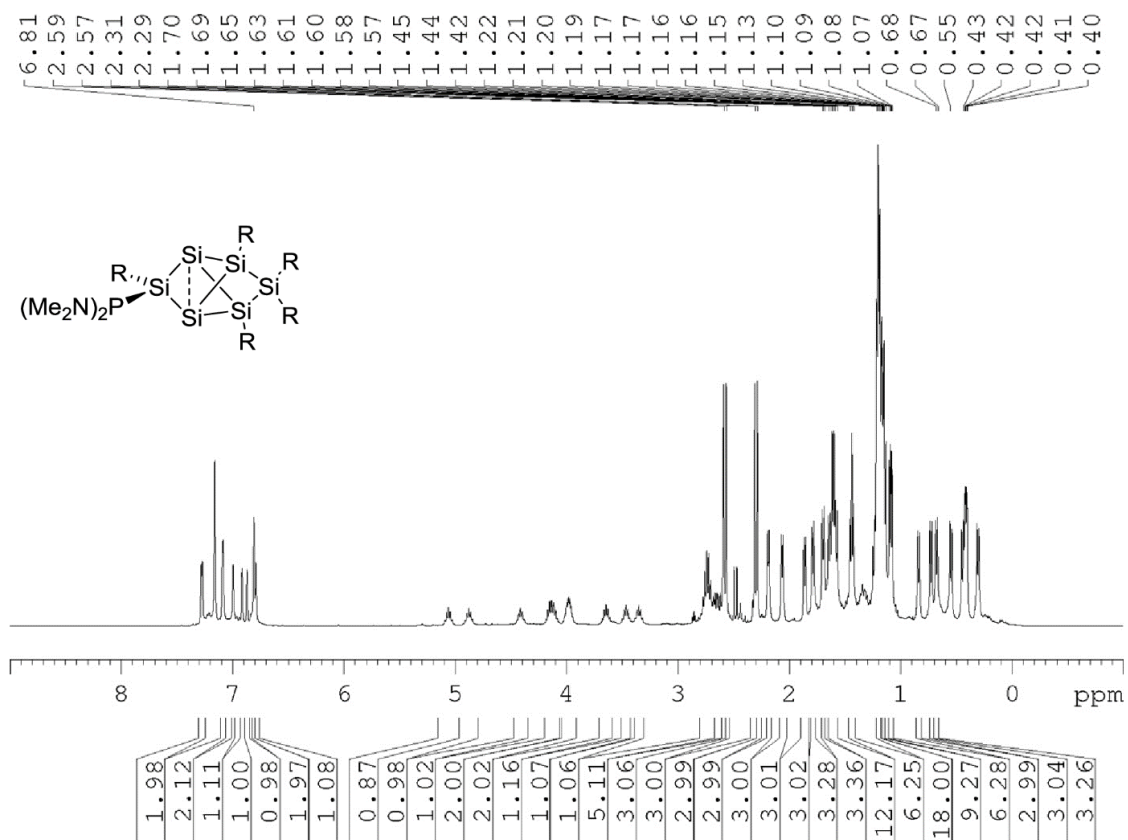


Figure S40: ^1H NMR of **6d** in C_6D_6 (400 MHz).

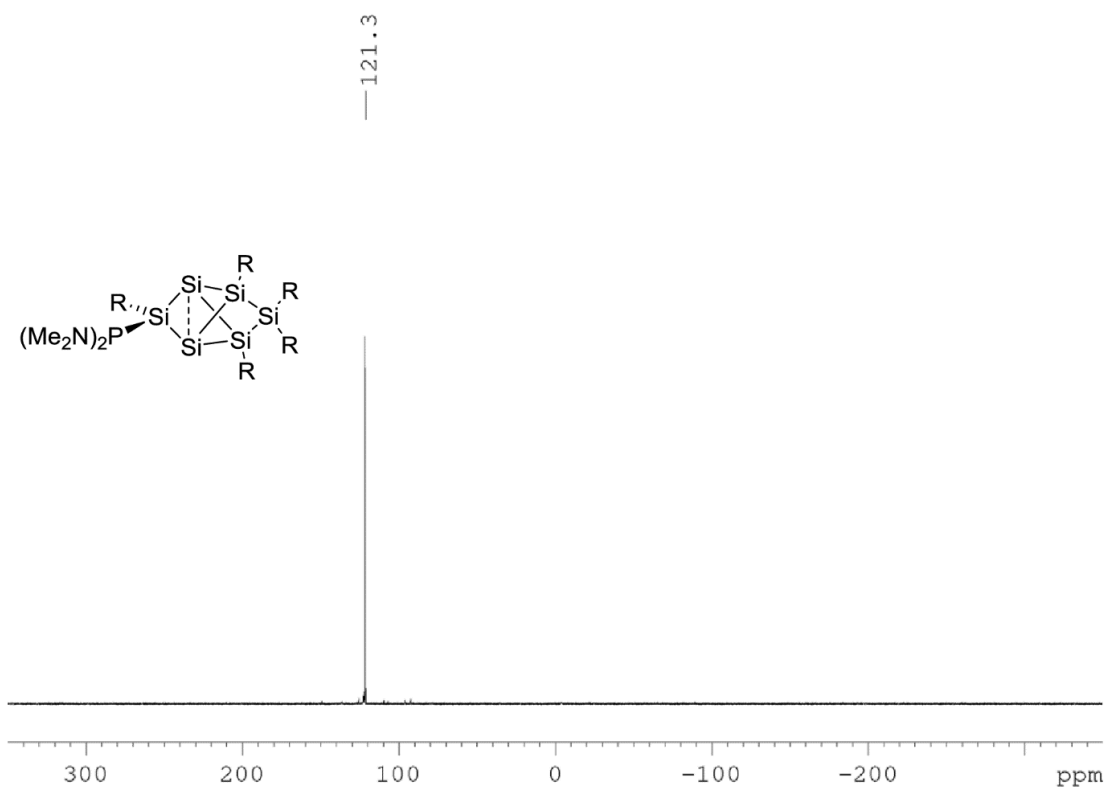


Figure S41: ^{31}P NMR of **6d** in C_6D_6 (121.5 MHz).

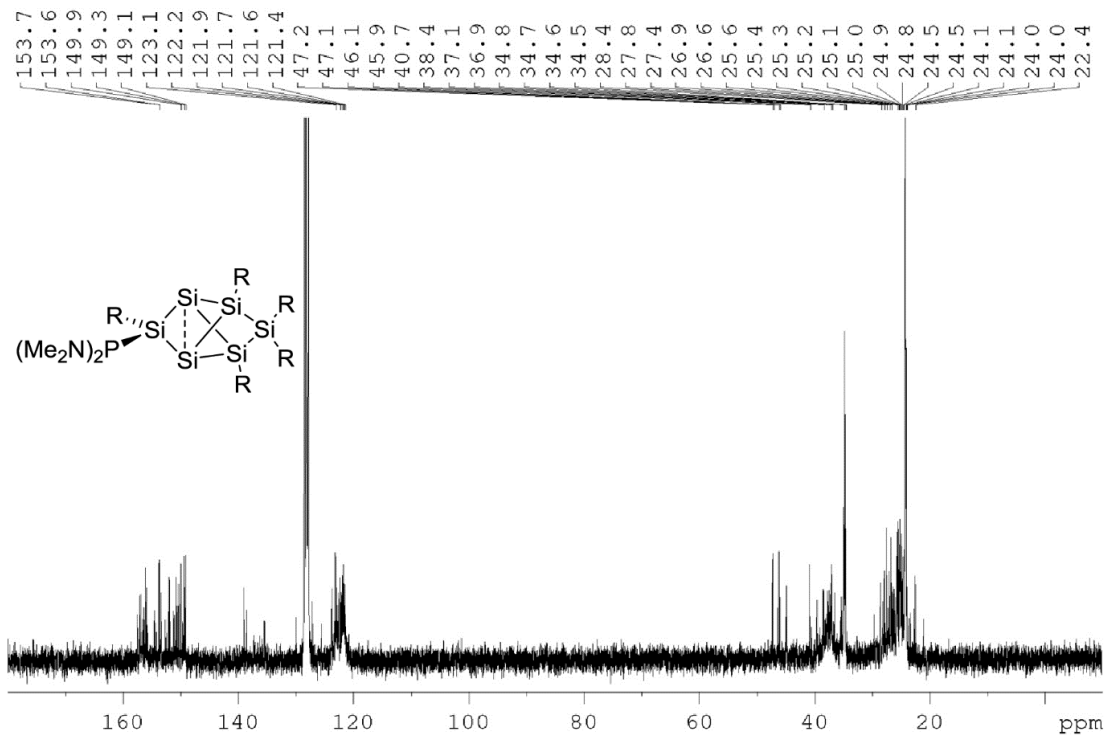


Figure S42: ^{13}C NMR of **6d** in C_6D_6 (75.5 MHz).

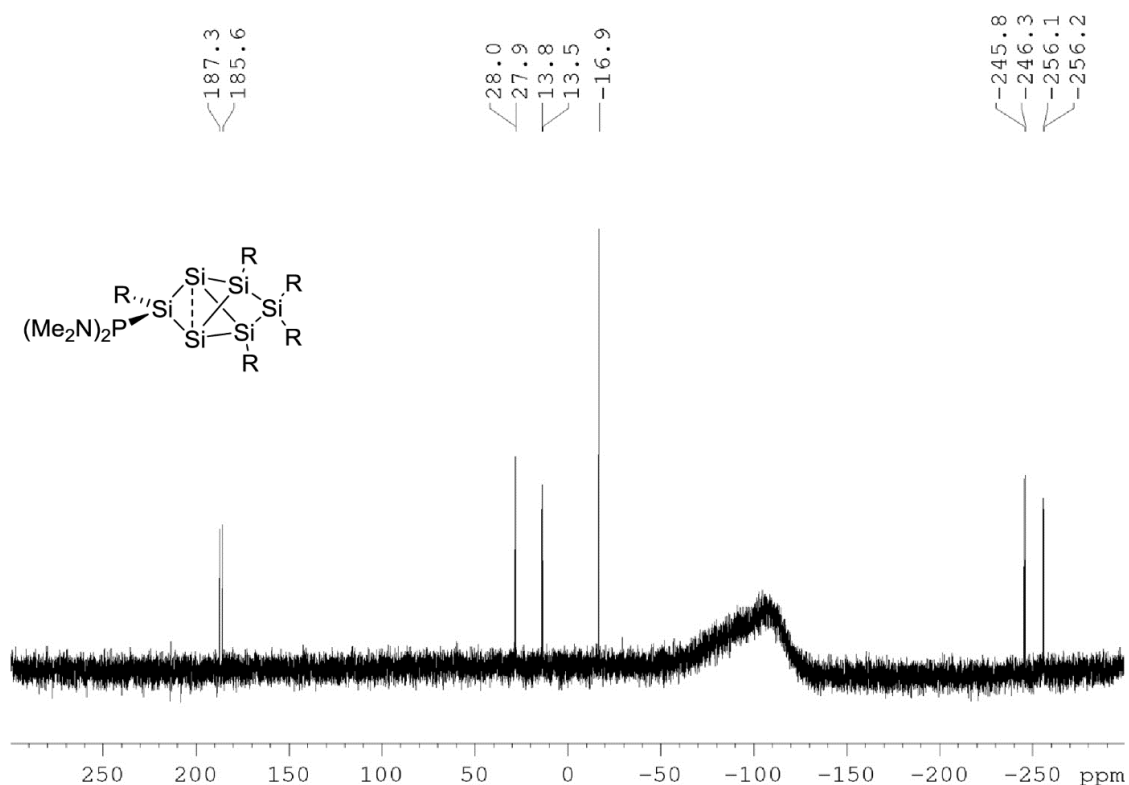


Figure S43: ^{29}Si NMR of **6d** in C_6D_6 (59.6 MHz).

***privo*-Trichlorosilyl-2,4,5,5,6-pentakis(2',4',6'-tri-iso-propyl-phenyl)tetracyclo[2.2.0.0^{1,3}.0^{3,6}]hexasilane (**6e**)**

Quantities: **4Li**, 81.8 mg (0.061 mmol); SiCl_4 7.7 μL (11.4 mg, 0.067 mmol); benzene- d_6 (0.6 mL); NMR scale. The crude product was thoroughly dried in vacuo and characterized by multinuclear NMR spectroscopy.

^1H NMR (300.13 MHz, benzene- d_6 , 300K): δ = 7.25 (s, 2H, Tip-H), 7.10 (d, 1H, Tip-H), 7.04 (d, 1H, Tip-H), 6.97 (d, 1H, Tip-H), 6.90 (d, 1H, Tip-H), 6.82 (d, 1H, Tip-H), 6.78 (s, 2H, Tip-H), 6.74 (d, 1H, Tip-H), 4.89 (sept, 1H, ^iPr -CH), 4.74 (sept, 1H, ^iPr -CH), 4.28 (sept, 1H, ^iPr -CH), 4.01 – 3.79 (m, 3H, ^iPr -CH), 3.72 – 3.52 (m, 2H, ^iPr -CH), 3.39 – 3.20 (m, 2H, ^iPr -CH), 2.78 – 2.52 (m, 5H, ^iPr -CH), 2.13 (d, 3H, ^iPr -CH₃), 2.03 (d, 3H, ^iPr -CH₃), 1.81 (d, 6H, ^iPr -CH₃), 1.62 (d, 3H, ^iPr -CH₃), 1.60 – 1.50 (m, 15H, ^iPr -CH₃), 1.39 (d, 3H, ^iPr -CH₃), 1.24 (d, 3H, ^iPr -CH₃), 1.21 – 1.05 (m, 30H, ^iPr -CH₃), 0.77 (d, 3H, ^iPr -CH₃), 0.65 (d, 6H, ^iPr -CH₃), 0.53 (d, 3H, ^iPr -CH₃), 0.46 (d, 3H, ^iPr -CH₃), 0.38 – 0.35 (m, 6H, ^iPr -CH₃), 0.28 (d, 3H, ^iPr -CH₃). ^{13}C NMR (75.5 MHz, benzene- d_6 , 300 K): δ = 157.0, 156.7, 156.6, 156.2, 154.4, 154.1, 153.8, 153.6, 152.0, 151.8, 151.3, 150.8, 149.9, 149.7, 137.8, 137.5, 130.1, 127.6, 125.3(Ar-C), 123.9, 123.3, 122.9, 122.8, 122.4, 122.3, 122.2, 122.1, 121.5 (Ar-CH), 38.3, 37.8, 37.6, 37.5, 37.1, 36.5, 36.5, 35.4, 35.1, 34.7, 34.7, 34.6, 34.6, 34.5, 27.8, 27.4, 27.3, 27.1, 27.0, 26.7, 26.5, 26.1, 25.6, 25.2, 25.1, 25.0, 24.6, 24.1,

6. Supporting Information

24.0, 23.9, 23.8, 23.7, 22.9, 22.5 (Tip-ⁱPr-CH and Tip-ⁱPr-CH₃). ²⁹Si NMR (59.6 MHz, benzene-d₆, 300 K):
 δ = 161.7 (privo-Si(Tip)SiCl₃), 35.2 (s, *remoto*-SiTip₂), 12.0 (s, *ligato*-SiTip), 7.4 (SiCl₃), -6.4 (s, *ligato*-SiTip), -251.6 (s, *nudo*-Si), -258.9 (s, *nudo*-Si).

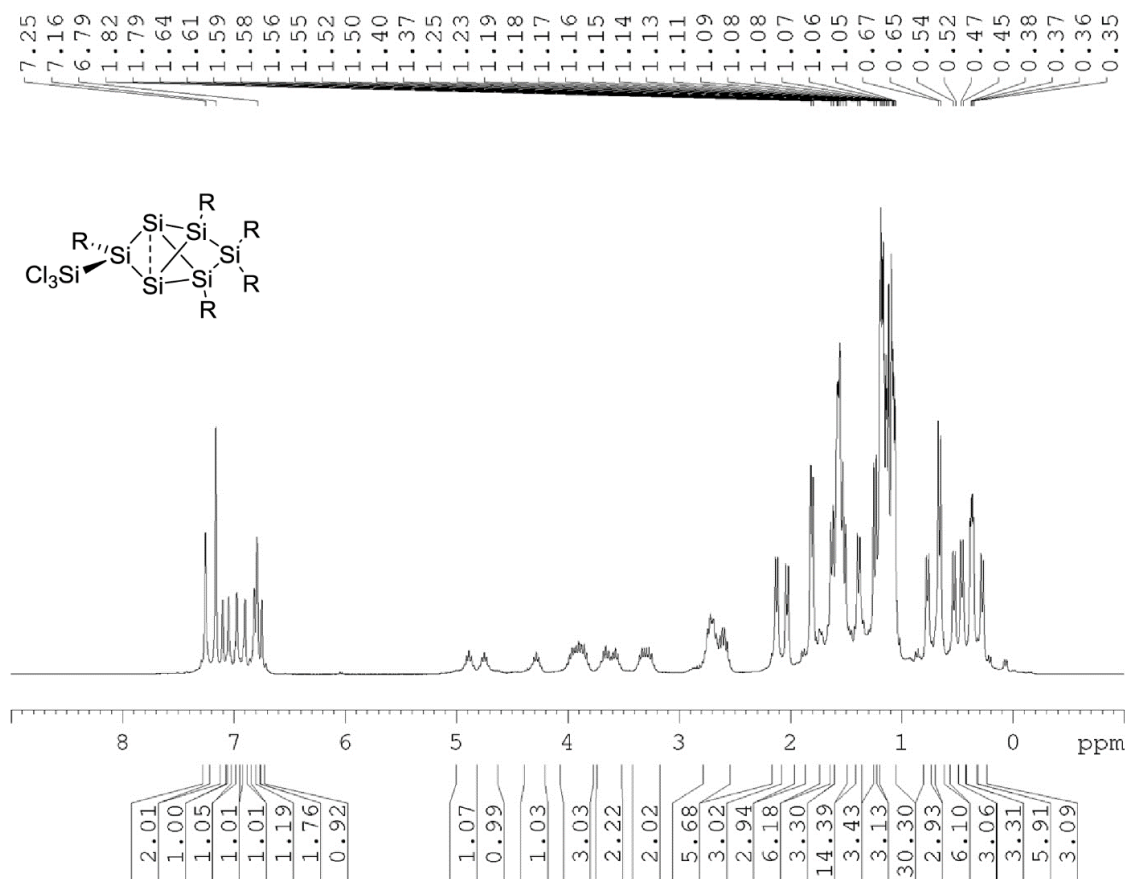


Figure S44: ¹H NMR of **6e** in C₆D₆ (300 MHz).

6. Supporting Information

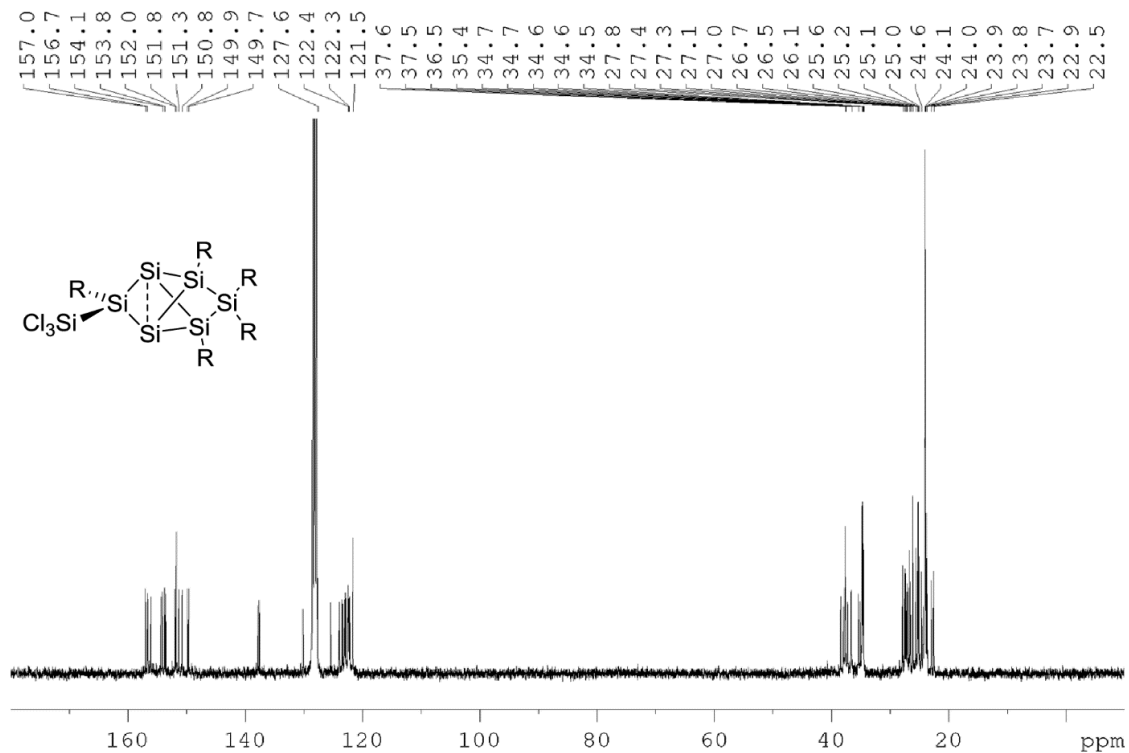


Figure S45: ^{13}C NMR of **6e** in C_6D_6 (75.5 MHz).

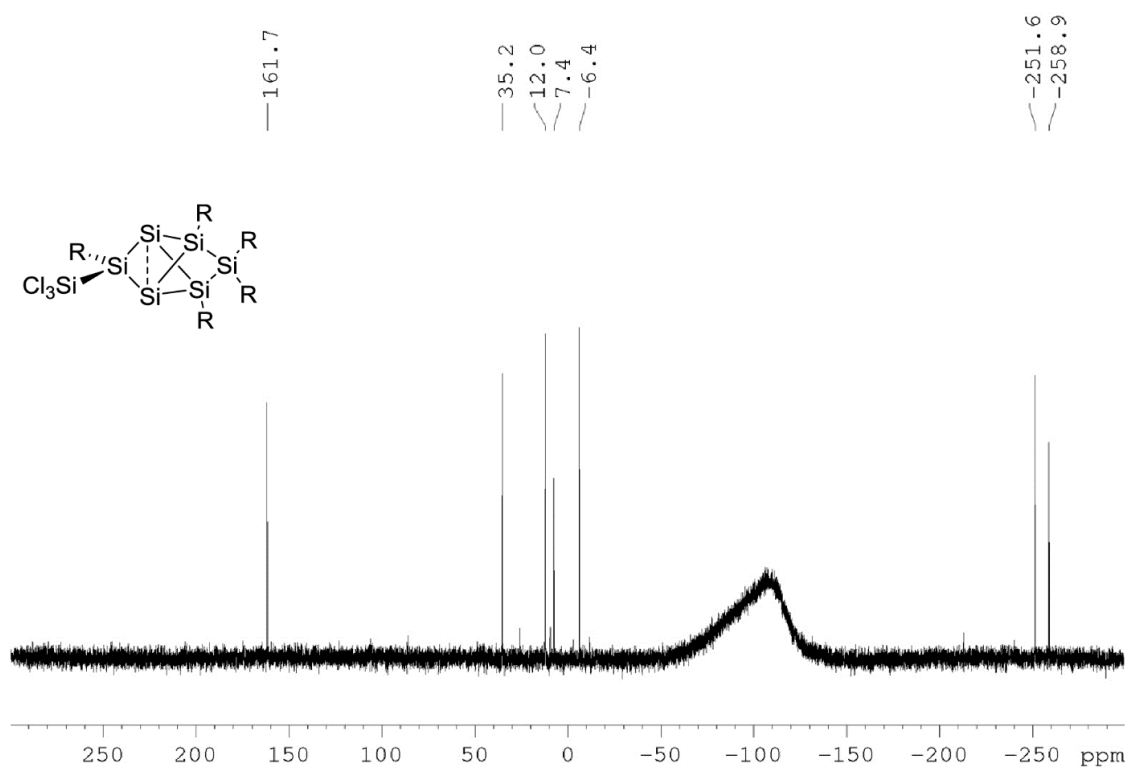


Figure S46: ^{29}Si NMR of **6e** in C_6D_6 (59.6 MHz).

Preparation of *privo*-Lithium-2,4,5,5,6-pentakis(2',4',6'-triisopropylphenyl)tetracyclo[2.2.0.0.0^{1,3}.0^{3,6}]hexasilan-2-ylborate (6f)

Quantities: **4Li**, 53.4 mg (0.04 mmol); H₃B·SMe₂ 4.2 μL (3.4 mg, 0.04 mmol); toluene (1 mL); stirring 1 h; crystallization from hexane. Yield: 40 mg (78 %) yellow crystals.

¹H NMR (300.13 MHz, benzene-d₆, 300K): δ = 7.27, 7.24, 7.09, 6.97, 6.94 (each d, each 1H, Tip-H), 6.89 (s, 2H, Tip-H), 6.81, 6.80, 6.68 (each d, each 1 H, Tip-H), 5.16, 5.05, 4.77 (each sept, each 1H, ⁱPr-CH), 4.30 (m, 3H, ⁱPr-CH), 3.79, 3.69 (each sept, each 1H, ⁱPr-CH), 3.33 (m, 2H, ⁱPr-CH), 3.07 (br, 7H, thf), 2.72 (m, 5H, ⁱPr-CH), 2.14, 2.10, 1.78, 1.71 (each d, each 3H, ⁱPr-CH₃), 1.61 (m, 12H, ⁱPr-CH₃), 1.47, 1.42, 1.37 (each d, each 3H, ⁱPr-CH₃), 1.20 (m, 30H, ⁱPr-CH₃), 1.19 (m, thf), 0.63 (m, 18H, ⁱPr-CH₃), 0.35 (m, 9H, ⁱPr-CH₃). ⁷Li NMR (116.6 MHz, benzene-d₆, 300K): δ = -0.58 (s). ¹¹B NMR (96.3 MHz, benzene-d₆, 300K): δ = -36.4 (q, ¹J_{BH} = 82.3 Hz, BH₃). ¹³C NMR (75.5 MHz, benzene-d₆, 300K): δ = 156.8, 156.5, 156.4, 155.9, 153.5, 153.3, 152.0, 151.9, 149.3, 149.0, 148.8, 148.6, 148.4, 148.1, 142.7, 139.9, 139.4, 130.6, 128.8 (Ar-C), 123.1, 122.7, 122.4, 122.2, 121.6, 121.0, 120.8, 120.3, 119.6 (Ar-CH), 36.9, 36.7, 36.6, 36.1, 35.9, 35.2, 34.7, 34.6, 34.5, 34.4, 33.8, 28.5, 27.5, 27.5, 27.3, 27.0, 26.4, 26.3, 25.7, 25.5, 25.2, 25.1, 25.0, 24.9, 24.8, 24.7, 24.6, 24.4, 24.3, 24.1, 24.0, 24.0, 23.9, 23.9, 23.8, 23.6, 22.5, 22.0 (Tip-ⁱPr-CH and Tip-ⁱPr-CH₃). ²⁹Si NMR (59.6 MHz, benzene-d₆, 300K): δ = 237.3 (br, *privo*-Si(Tip)BH₃), 21.7 (s, *ligato*-SiTip), 21.1 (s, *remoto*-SiTip₂), -28.8 (s, *ligato*-SiTip), -243.3 (s, *nudo*-Si), -255.6 (s, *nudo*-Si). **Elemental analysis** calculated for C₇₉H₁₂₆BLiOSi₆: C, 74.24; H, 9.94. Found: C, 70.10; H, 9.50.

6. Supporting Information

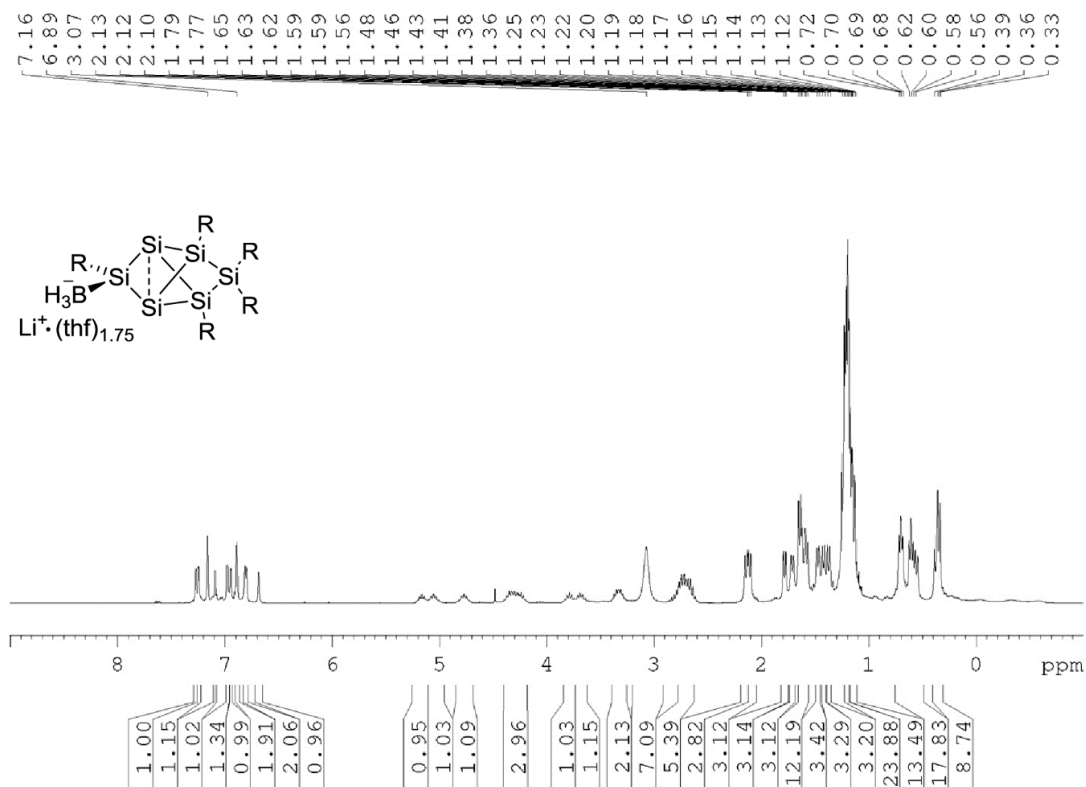


Figure S47: ¹H NMR of **6f** in C₆D₆ (300 MHz).

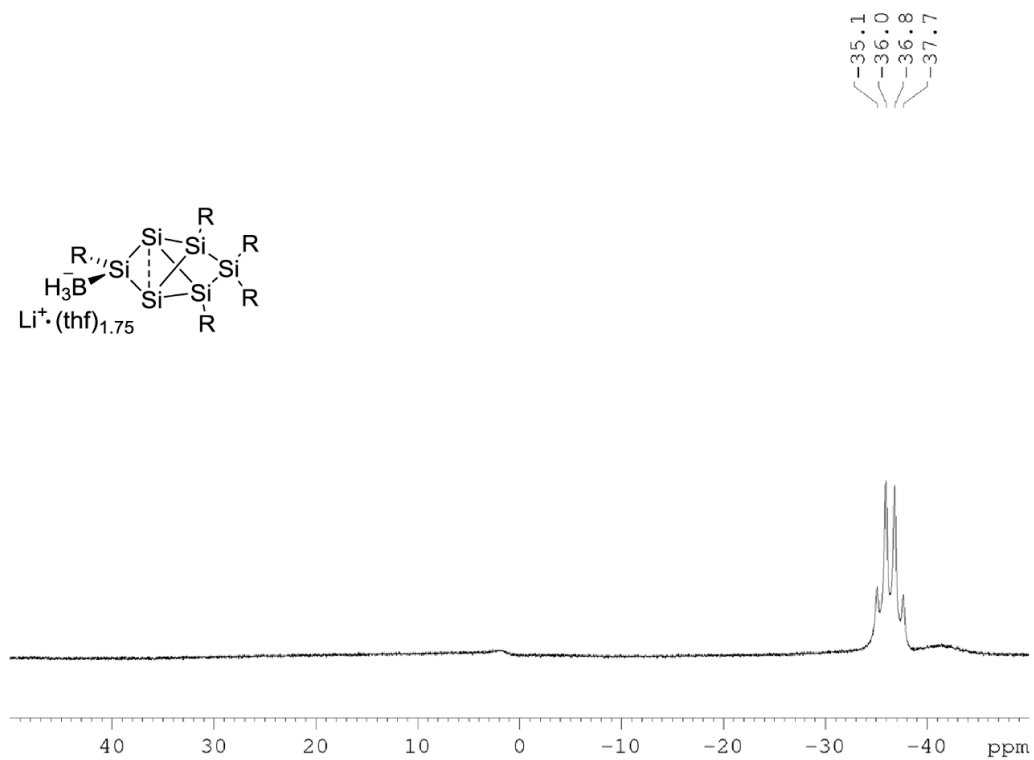


Figure S48: ¹¹B NMR of **6f** in C₆D₆ (96.3 MHz).

6. Supporting Information

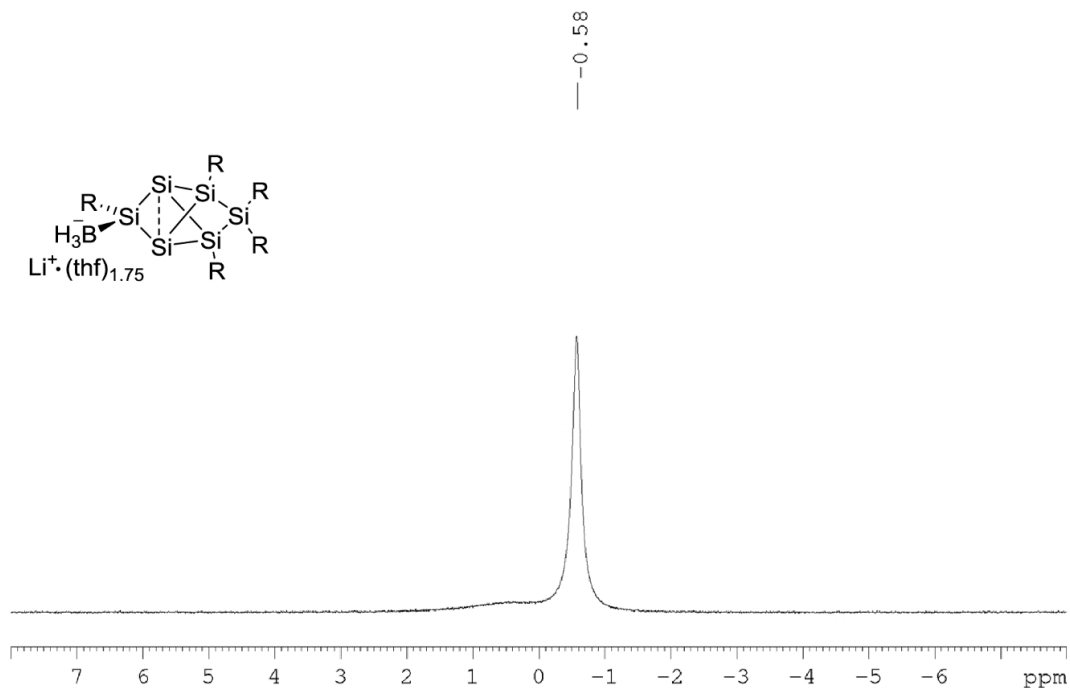


Figure S49: ⁷Li NMR of **6f** in C₆D₆ (116.6 MHz).

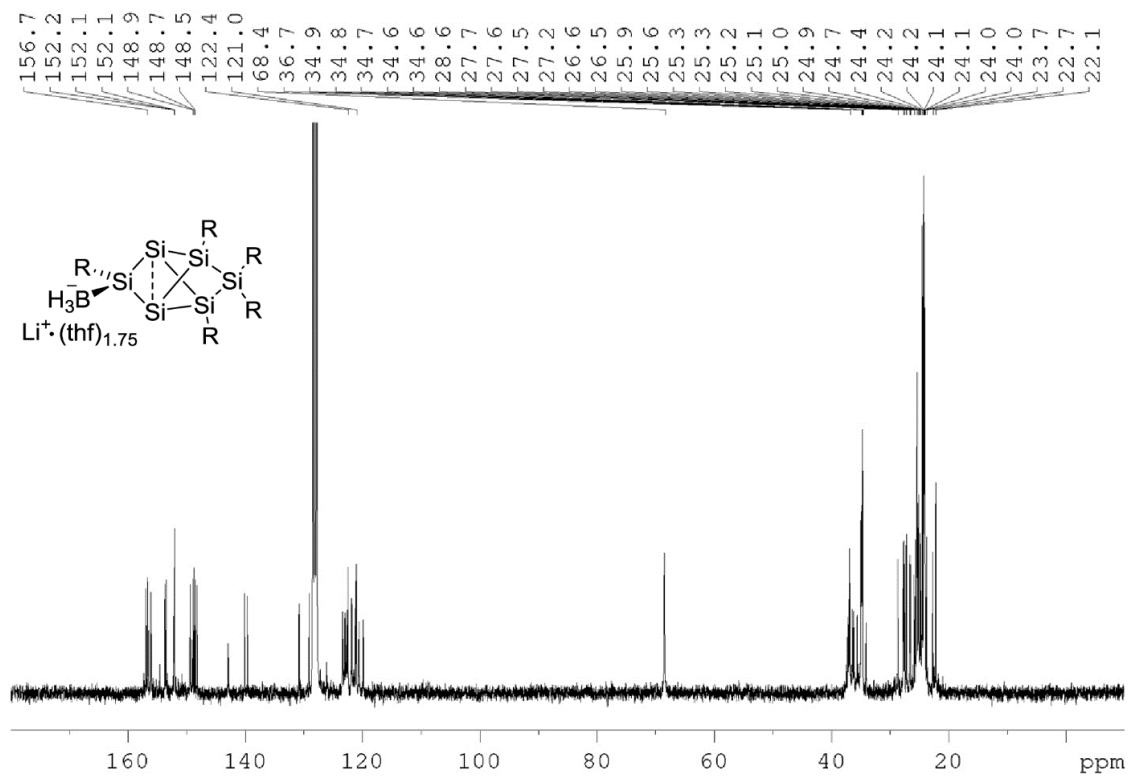


Figure S50: ¹³C NMR of **6f** in C₆D₆ (75.5 MHz).

6. Supporting Information

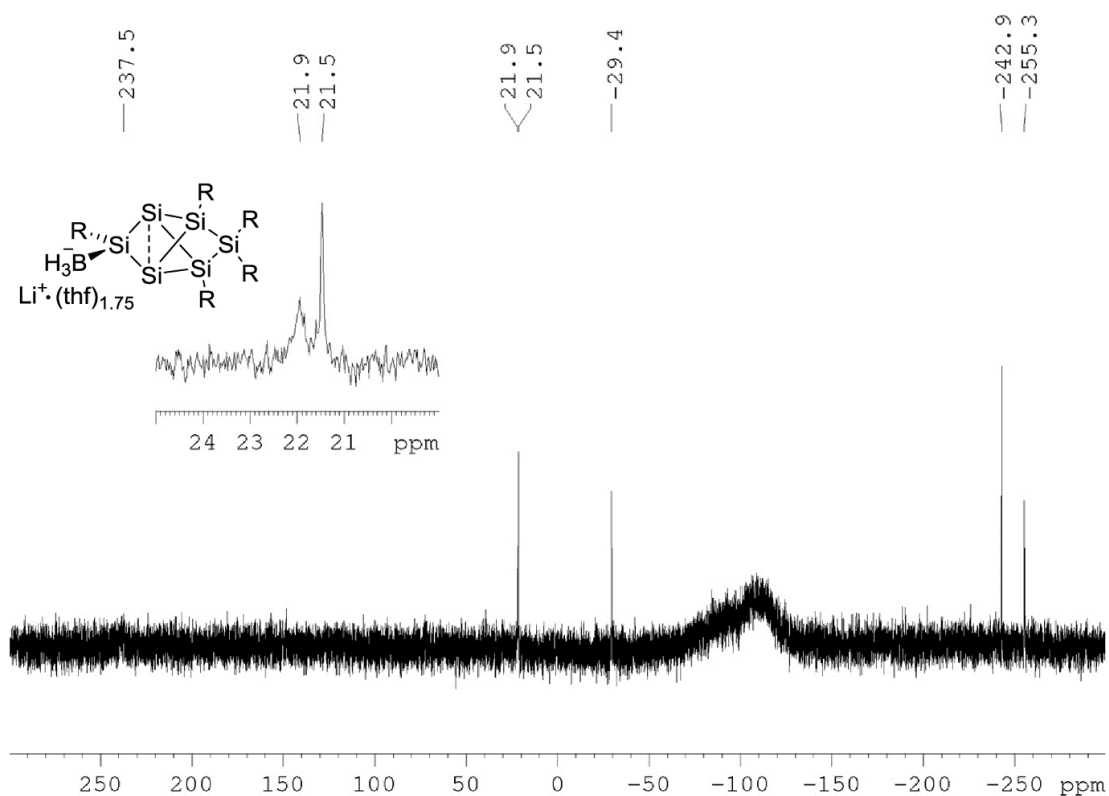


Figure S51: ²⁹Si NMR of **6f** in C₆D₆ (59.6 MHz; lb = 1)

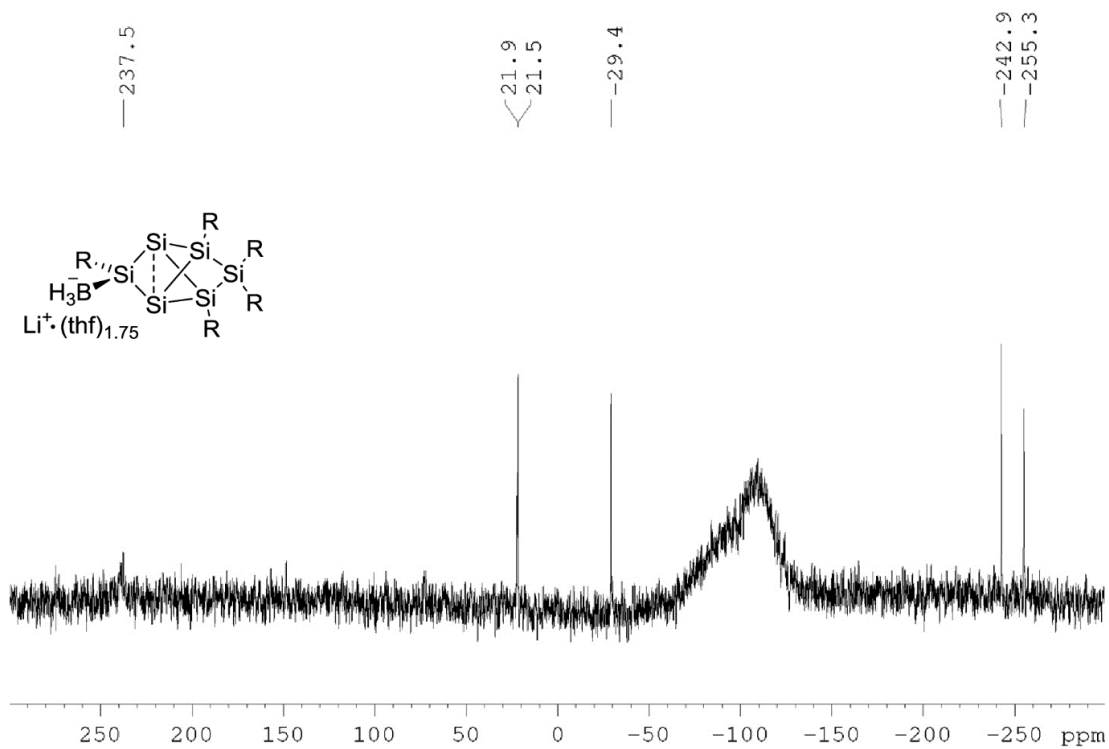


Figure S52: ²⁹Si NMR of **6f** in C₆D₆ (59.6 MHz; lb = 6)

S37

6. Supporting Information

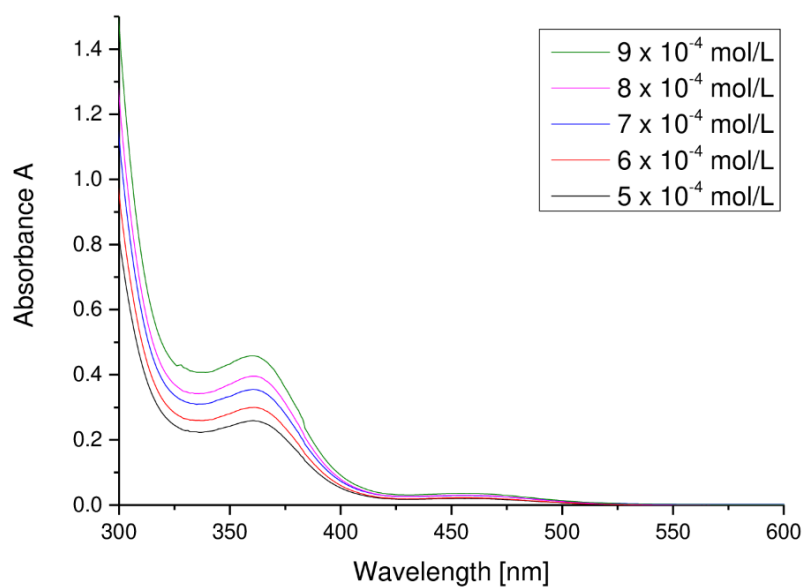


Figure S53: UV-Vis spectrum of **6f** in hexane at different concentrations.

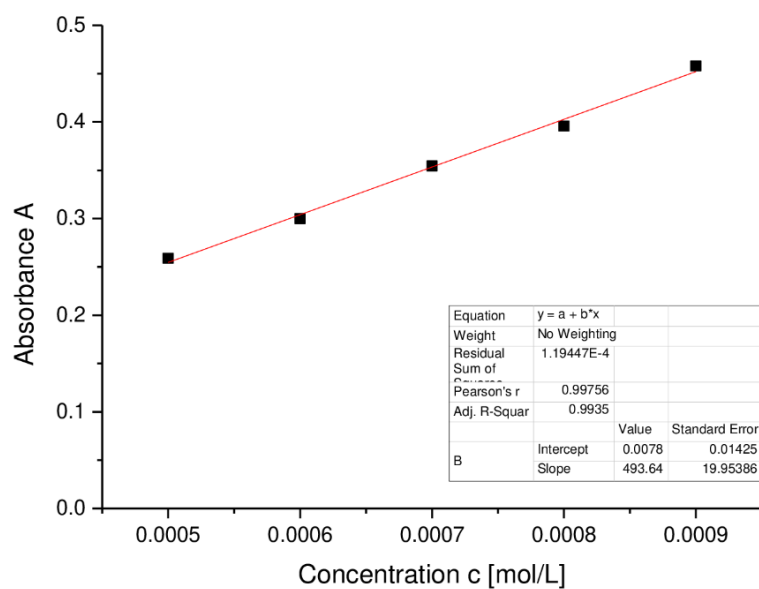


Figure S54: Determination of ϵ ($4936 \text{ M}^{-1} \text{ cm}^{-1}$) by linear regression of absorptions ($\lambda = 361 \text{ nm}$) of **6f** against concentration.

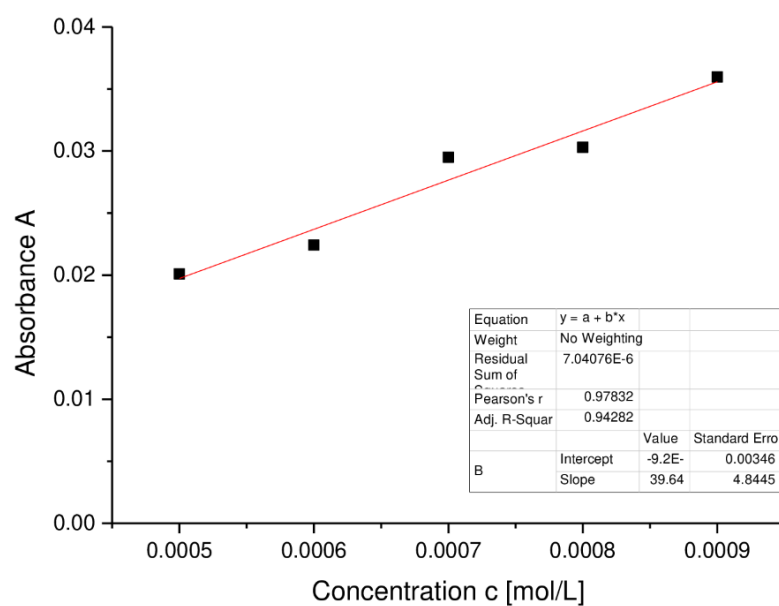


Figure S55: Determination of $\epsilon(396 \text{ M}^{-1} \text{ cm}^{-1})$ by linear regression of absorptions ($\lambda = 454 \text{ nm}$) of **6f** against concentration.

Details on X-ray Diffraction Studies**Table S1.** Crystal data and structure refinement for *ligato*-TMS-substituted siliconoid **5a** (CCDC-1877380).

Identification code	sh3711	
Empirical formula	C ₇₈ H ₁₂₄ Si ₇ , 0.5(C ₅ H ₁₂)	
Formula weight	1294.47	
Temperature	132(2) K	
Wavelength	0.71073 Å	
Crystal system	Monoclinic	
Space group	C2/c	
Unit cell dimensions	a = 38.1514(15) Å	α = 90°.
	b = 12.7134(5) Å	β = 94.456(3)°.
	c = 33.8416(11) Å	γ = 90°.
Volume	16364.7(11) Å ³	
Z	8	
Density (calculated)	1.051 Mg/m ³	
Absorption coefficient	0.155 mm ⁻¹	
F(000)	5688	
Crystal size	0.546 x 0.393 x 0.223 mm ³	
Theta range for data collection	1.071 to 29.218°.	
Index ranges	-52 ≤ h ≤ 52, -17 ≤ k ≤ 17, -46 ≤ l ≤ 46	
Reflections collected	160059	
Independent reflections	22155 [R(int) = 0.0358]	
Completeness to theta = 25.242°	100.0 %	
Absorption correction	Semi-empirical from equivalents	
Max. and min. transmission	0.7458 and 0.7025	
Refinement method	Full-matrix least-squares on F ²	
Data / restraints / parameters	22155 / 83 / 836	
Goodness-of-fit on F ²	1.031	
Final R indices [I > 2σ(I)]	R1 = 0.0431, wR2 = 0.1036	
R indices (all data)	R1 = 0.0584, wR2 = 0.1118	
Extinction coefficient	n/a	
Largest diff. peak and hole	0.779 and -0.649 e.Å ⁻³	

6. Supporting Information

Table S2. Crystal data and structure refinement for *ligato*-benzoyl-substituted siliconoid **5b** (CCDC-1877381).

Identification code	sh3716	
Empirical formula	C ₈₂ H ₁₂₀ O Si ₆	
Formula weight	1290.31	
Temperature	132(2) K	
Wavelength	0.71073 Å	
Crystal system	Monoclinic	
Space group	P2 ₁ /c	
Unit cell dimensions	a = 18.8229(6) Å	α = 90°.
	b = 28.6659(10) Å	β = 107.786(2)°.
	c = 30.7990(12) Å	γ = 90°.
Volume	15824.1(10) Å ³	
Z	8	
Density (calculated)	1.083 Mg/m ³	
Absorption coefficient	0.147 mm ⁻¹	
F(000)	5632	
Crystal size	0.672 x 0.453 x 0.385 mm ³	
Theta range for data collection	0.993 to 27.929°.	
Index ranges	-22 ≤ h ≤ 24, -37 ≤ k ≤ 35, -40 ≤ l ≤ 40	
Reflections collected	152878	
Independent reflections	37861 [R(int) = 0.0485]	
Completeness to theta = 25.242°	99.9 %	
Absorption correction	Semi-empirical from equivalents	
Max. and min. transmission	0.7456 and 0.6696	
Refinement method	Full-matrix least-squares on F ²	
Data / restraints / parameters	37861 / 192 / 1743	
Goodness-of-fit on F ²	1.081	
Final R indices [I > 2σ(I)]	R1 = 0.0648, wR2 = 0.1395	
R indices (all data)	R1 = 0.1038, wR2 = 0.1598	
Extinction coefficient	n/a	
Largest diff. peak and hole	0.801 and -0.476 e.Å ⁻³	

6. Supporting Information

Table S3. Crystal data and structure refinement for *privo*-lithiated anionic siliconoid **4Li** (CCDC-1877378).

Identification code	sh3618	
Empirical formula	C ₈₇ H ₁₃₉ Li O ₃ Si ₆	
Formula weight	1408.45	
Temperature	175(2) K	
Wavelength	0.71073 Å	
Crystal system	Triclinic	
Space group	P-1	
Unit cell dimensions	a = 14.2918(16) Å	$\alpha = 109.652(5)^\circ$.
	b = 16.4145(18) Å	$\beta = 104.243(4)^\circ$.
	c = 21.516(3) Å	$\gamma = 99.970(4)^\circ$.
Volume	4422.6(9) Å ³	
Z	2	
Density (calculated)	1.058 Mg/m ³	
Absorption coefficient	0.138 mm ⁻¹	
F(000)	1544	
Crystal size	0.696 x 0.647 x 0.466 mm ³	
Theta range for data collection	1.362 to 27.284°.	
Index ranges	-18<=h<=18, -21<=k<=20, -27<=l<=27	
Reflections collected	69055	
Independent reflections	19545 [R(int) = 0.0443]	
Completeness to theta = 25.242°	100.0 %	
Absorption correction	Semi-empirical from equivalents	
Max. and min. transmission	0.7455 and 0.6196	
Refinement method	Full-matrix least-squares on F ²	
Data / restraints / parameters	19545 / 411 / 1006	
Goodness-of-fit on F ²	1.064	
Final R indices [$I > 2\sigma(I)$]	R1 = 0.0628, wR2 = 0.1581	
R indices (all data)	R1 = 0.0952, wR2 = 0.1885	
Extinction coefficient	n/a	
Largest diff. peak and hole	0.975 and -0.428 e.Å ⁻³	

6. Supporting Information

Table S4. Crystal data and structure refinement for *privo*-TMS-substituted siliconoid **6a** (CCDC-1877379).

Identification code	sh3668	
Empirical formula	C ₇₈ H ₁₂₄ Si ₇ , C ₆ H ₁₄	
Formula weight	1344.57	
Temperature	152(2) K	
Wavelength	0.71073 Å	
Crystal system	Monoclinic	
Space group	P2 ₁ /c	
Unit cell dimensions	a = 21.0070(7) Å	α = 90°.
	b = 20.4182(7) Å	β = 95.4324(13)°.
	c = 19.9183(7) Å	γ = 90°.
Volume	8505.1(5) Å ³	
Z	4	
Density (calculated)	1.050 Mg/m ³	
Absorption coefficient	0.152 mm ⁻¹	
F(000)	2960	
Crystal size	0.480 x 0.380 x 0.166 mm ³	
Theta range for data collection	0.974 to 28.755°.	
Index ranges	-27 ≤ h ≤ 28, -27 ≤ k ≤ 25, -24 ≤ l ≤ 26	
Reflections collected	68739	
Independent reflections	22100 [R(int) = 0.0376]	
Completeness to theta = 25.242°	100.0 %	
Absorption correction	Semi-empirical from equivalents	
Max. and min. transmission	0.7458 and 0.6844	
Refinement method	Full-matrix least-squares on F ²	
Data / restraints / parameters	22100 / 26 / 1278	
Goodness-of-fit on F ²	1.032	
Final R indices [I > 2σ(I)]	R1 = 0.0473, wR2 = 0.1158	
R indices (all data)	R1 = 0.0737, wR2 = 0.1319	
Extinction coefficient	n/a	
Largest diff. peak and hole	0.783 and -0.504 e.Å ⁻³	

6. Supporting Information

Table S5. Crystal data and structure refinement for *privo*-pivaloyl-substituted siliconoid **6c** (CCDC-1877382).

Identification code	sh3824	
Empirical formula	C ₈₀ H ₁₂₄ O Si ₆ , 0.5(C ₆ H ₁₄)	
Formula weight	1313.41	
Temperature	152(2) K	
Wavelength	0.71073 Å	
Crystal system	Triclinic	
Space group	P-1	
Unit cell dimensions	a = 13.3961(3) Å	α = 67.9010(10)°.
	b = 18.2592(5) Å	β = 70.1540(10)°.
	c = 19.4141(4) Å	γ = 76.3090(10)°.
Volume	4106.08(17) Å ³	
Z	2	
Density (calculated)	1.062 Mg/m ³	
Absorption coefficient	0.143 mm ⁻¹	
F(000)	1442	
Crystal size	0.374 x 0.306 x 0.220 mm ³	
Theta range for data collection	1.179 to 33.864°.	
Index ranges	-20 ≤ h ≤ 20, -28 ≤ k ≤ 28, -30 ≤ l ≤ 30	
Reflections collected	127205	
Independent reflections	33036 [R(int) = 0.0356]	
Completeness to theta = 25.242°	100.0 %	
Absorption correction	Semi-empirical from equivalents	
Max. and min. transmission	0.7467 and 0.7205	
Refinement method	Full-matrix least-squares on F ²	
Data / restraints / parameters	33036 / 77 / 872	
Goodness-of-fit on F ²	1.032	
Final R indices [I > 2σ(I)]	R1 = 0.0544, wR2 = 0.1381	
R indices (all data)	R1 = 0.0908, wR2 = 0.1578	
Extinction coefficient	n/a	
Largest diff. peak and hole	1.580 and -0.722 e.Å ⁻³	

6. Supporting Information

Table S6. Crystal data and structure refinement for *privo*-borate-substituted siliconoid **6f** (CCDC-1877383).

Identification code	sh3732	
Empirical formula	C ₁₅₈ H ₂₅₂ B ₂ Li ₂ O ₂ Si ₁₂ , 2(C ₆ H ₆)	
Formula weight	2712.38	
Temperature	192(2) K	
Wavelength	0.71073 Å	
Crystal system	Monoclinic	
Space group	P2 ₁ /c	
Unit cell dimensions	a = 17.8496(8) Å	α = 90°.
	b = 24.9370(10) Å	β = 99.856(2)°.
	c = 20.3519(9) Å	γ = 90°.
Volume	8925.2(7) Å ³	
Z	2	
Density (calculated)	1.009 Mg/m ³	
Absorption coefficient	0.133 mm ⁻¹	
F(000)	2968	
Crystal size	0.778 x 0.754 x 0.306 mm ³	
Theta range for data collection	1.158 to 29.617°.	
Index ranges	-24 ≤ h ≤ 24, -34 ≤ k ≤ 22, -28 ≤ l ≤ 28	
Reflections collected	96855	
Independent reflections	25096 [R(int) = 0.0341]	
Completeness to theta = 25.242°	100.0 %	
Absorption correction	Semi-empirical from equivalents	
Max. and min. transmission	0.7459 and 0.6970	
Refinement method	Full-matrix least-squares on F ²	
Data / restraints / parameters	25096 / 192 / 950	
Goodness-of-fit on F ²	1.403	
Final R indices [I > 2σ(I)]	R1 = 0.0643, wR2 = 0.1752	
R indices (all data)	R1 = 0.0991, wR2 = 0.1926	
Extinction coefficient	n/a	
Largest diff. peak and hole	1.192 and -0.383 e.Å ⁻³	

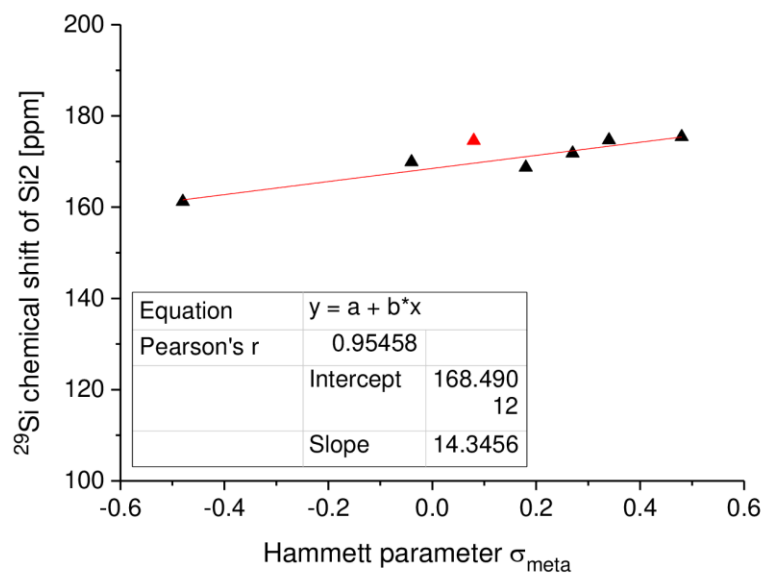
Plot of the Hammett parameter σ_m/σ_p vs ^{29}Si chemical shift of Si2

Figure S56: Plot of the Hammett parameter σ_m vs ^{29}Si chemical shift of Si2 for substituents in *ligato* position of **5a-f** and **2**.

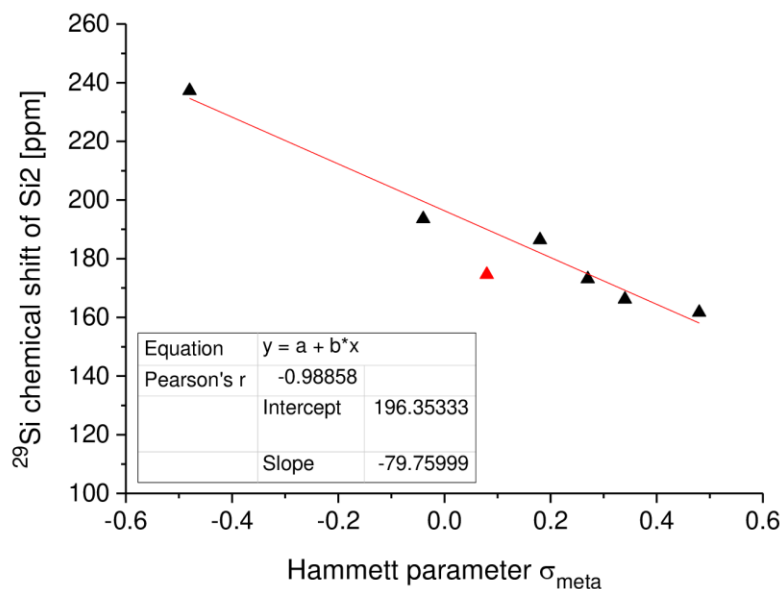


Figure S57: Plot of the Hammett parameter σ_m vs ^{29}Si chemical shift of Si2 for substituents in *privo* position of **6a-f** and **2**.

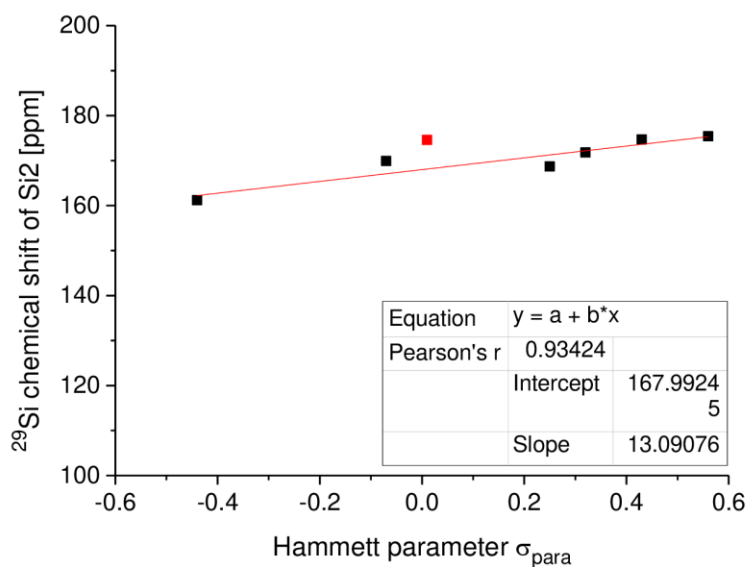


Figure S58: Plot of the Hammett parameter σ_p vs ^{29}Si chemical shift of Si2 for substituents in *ligato* position of **5a-f** and **2**.

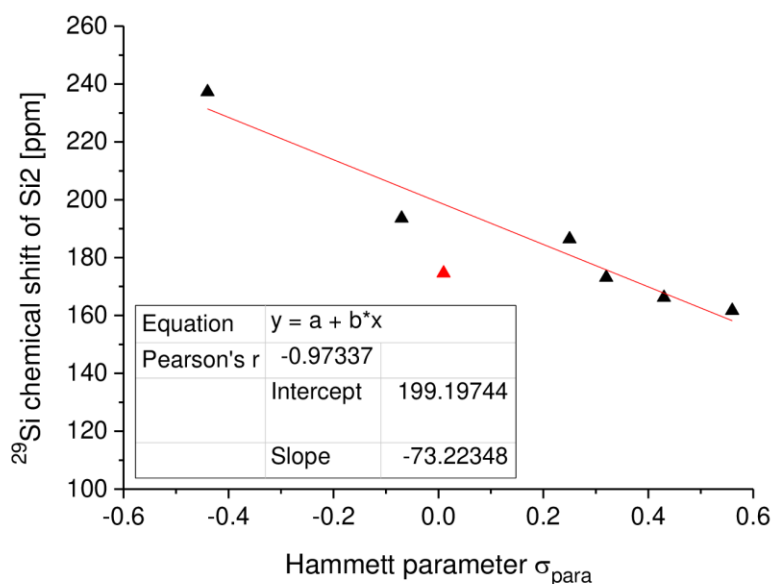


Figure S59: Plot of the Hammett parameter σ_p vs ^{29}Si chemical shift of Si2 for substituents in *privo* position of **6a-f** and **2**.

6.2. A Three-Membered Cyclic Phosphasilene (SI)



Supporting Information

A Three-Membered Cyclic Phosphasilene

*Yannic Heider, Philipp Willmes, Daniel Mühlhausen, Lukas Klemmer, Michael Zimmer, Volker Huch, and David Scheschkewitz**

anie_201811944_sm_miscellaneous_information.pdf

Author Contributions

Y.H. Conceptualization: Supporting; Formal analysis: Lead; Investigation: Supporting; Methodology: Equal; Supervision: Supporting; Visualization: Lead; Writing – original draft: Lead; Writing – review & editing: Supporting

P.W. Formal analysis: Equal; Investigation: Supporting; Supervision: Supporting

D.M. Formal analysis: Supporting; Methodology: Supporting

M.Z. Data curation: Lead; NMR studies: Lead

V.H. Data curation: Lead; Formal analysis: Lead; x-ray studies: Lead

D.S. Conceptualization: Lead; Funding acquisition: Lead; Project administration: Lead; Resources: Lead; Supervision: Lead; Writing – review & editing: Lead.

Table of Contents**1. Experimental Procedures** **2**

General and data and plots of spectra of:

NHC-stabilized 2,2,3-tris(2,4,6-triisopropylphenyl)-2H-1,2,3-phosphadisilirene **5**

2-(1,3-diisopropyl-4,5-dimethyl-1H-imidazol-3-ium-2-yl)-2,3,3-tris(2,4,6-triisopropylphenyl)-1,2,3-phosphadisiliran-1-ide tetracarbonyl iron **6**

1,3-diisopropyl-4,5-dimethyl-2-(1,3,3-tris(2,4,6-triisopropylphenyl)disilaphosph-2-en-1-ylidene)-2,3-dihydro-1H-imidazole tricarbonyl iron **7**

3,3,4,5,6,6-hexakis(2,4,6-triisopropylphenyl)-1,2-diphospha-3,4,5,6-tetrasilatricyclo[2.2.0.0²,5]hexane **8**
and 2,3,3,5,6,6-hexakis(2,4,6-triisopropylphenyl)-1,4-diphospha-2,3,5,6-tetrasilatricyclo[3.1.0.0²,4]hexane **9**

2. Details on X-ray Diffraction Studies **23****3. Details on theoretical calculations** **33****4. References** **35****5. Authors Contributions** **35**

1. Experimental Procedures**General**

All manipulations were carried out under a protective atmosphere of argon, using Schlenk techniques or in a glove box. Solvents were purified by a PureSolvMD5 solvent purification system by Innovative Technology. UV/Vis spectra were acquired using a PerkinElmer Lambda 35 spectrometer using quartz cells with a path length of 0.1 cm. Infrared spectra were recorded on a Shimadzu IRAffinity-1S spectrometer. NMR spectra were recorded on a Bruker Avance III HD 400 MHz spectrometer. Solid-state NMR spectra were recorded on a Bruker AV400WB spectrometer. C₆D₆ was dried over potassium, then distilled under argon. Tetrahydrofuran-d₈ was dried over Na/K alloy, then distilled under argon. Elemental analyses were carried out with an elemental vario Micro Cube. Disilene **1**^[1] and P(I) cation **4**^[2] were prepared according to literature procedures.

NHC-stabilized 2,2,3-tris(2,4,6-triisopropylphenyl)-2H-1,2,3-phosphadisilirene 5

A solution of 2.03 g (2.38 mmol) of disilene **1**^[1] in 50 mL of thf is cooled to -78°C and rapidly added to a -78°C cold solution of 1.69g of P(I) cation **4**^[2] in 70 mL of thf. The orange-reddish reaction mixture is stirred and allowed to warm to room temperature within 4.5 hours. After stirring for another 30 minutes at room temperature the reaction mixture is filtered and the filtrate reduced to dryness in vacuo. The solid residue is digested with hexane and filtered again. After the solvent is evaporated under reduced pressure one equivalent of free 1,3-diisopropyl-4,5-dimethylimidazol-2-ylidene that is formed in the course of the reaction is sublimed out in high vacuum (1×10^{-5} mbar, 3h). The residue is dissolved in pentane and standing overnight yields 1.76 g (84%) of NHC-stabilized phosphasilene **5** as yellow crystals. (m.p. 200-205°C, dec.)

¹H NMR (400.13 MHz, C₆D₆, 300K): δ = 8.62 (sept, 1H, NHC-ⁱPr-CH), 7.16 (br, 3H, Tip-H), 7.12 (s, 2H, Tip-H), 7.09 (d, 1H, Tip-H), 7.06 (d, 1H, Tip-H), 7.05 (d, 1H, Tip-H), 7.03 (d, 1H, Tip-H), 7.02 (d, 1H, Tip-H), 6.99 (t, 2H, Tip-H), 6.74 – 6.65 (m, 1H, Tip-ⁱPr-CH), 6.47 – 6.38 (m, 1H, Tip-ⁱPr-CH), 6.31 – 6.19 (m, 2H, Tip-ⁱPr-CH overlapping with NHC-ⁱPr-CH), 5.37 (sept, 1H, NHC-ⁱPr-CH), 5.15 (sept, 1H, NHC-ⁱPr-CH), 4.93, 4.62, 4.47, 4.17 (each sept, each 1H, Tip-ⁱPr-CH), 4.03 – 3.93 (m, 2H, Tip-ⁱPr-CH), 3.91 – 3.81 (m, 3H, Tip-ⁱPr-CH), 2.86 – 2.70 (m, 6H, Tip-ⁱPr-CH), 1.83 (d, 3H, Tip-ⁱPr-CH₃), 1.74 (t, 6H, Tip-ⁱPr-CH₃), 1.62 – 1.45 (m, 34H, Tip-ⁱPr-CH₃ and NC(CH₃)=C(CH₃)N), 1.39 (s, 3H, NC(CH₃)=C(CH₃)N), 1.37 (d, 3H, NHC-ⁱPr-CH₃), 1.36, 1.34 (each d, each 3H, Tip-ⁱPr-CH₃), 1.29 (d, 6H, x), 1.28 – 1.23 (m, 32H, Tip-ⁱPr-CH₃ and NHC-ⁱPr-CH₃), 1.21, 1.19 (each d, each 3H, x), 1.17 (br s, 3H, Tip-ⁱPr-CH₃), 1.15 (br s, 3H, x), 0.99 (d, 3H, NHC-ⁱPr-CH₃), 0.93 (d, 6H, Tip-ⁱPr-CH₃ and NHC-ⁱPr-CH₃), 0.87 (d, 3H, x), 0.64 – 0.52 (m, 21H, Tip-ⁱPr-CH₃ and NHC-ⁱPr-CH₃), 0.45, 0.31 (each d, each 3H, NHC-ⁱPr-CH₃). Due to the ratio of isomers in solution (1 : 0.88) integrations of the major isomer were larger by this very factor and rounded down to full numeric values for simplify matters.

¹³C NMR (100.6 MHz, C₆D₆, 300K): δ = 162.4 (d, ²J_{C-P} = 8.5 Hz, NCN), 159.3 (d, ³J_{C-P} = 2.1 Hz, Tip-C), 158.3 (d, ³J_{C-P} = 2.1 Hz, Tip-C), 157.7 (d, ³J_{C-P} = 1.4 Hz, Tip-C), 157.1 (d, ²J_{C-P} = 4.9 Hz, NCN), 156.3, 155.9, 156.7, 155.4, 155.2, 154.3, 152.9, 151.6, 149.9, 149.2, 149.0, 149.0, 148.8, 147.7, 147.6, 144.9 (each s, Tip-C) 144.8 (d, ³J_{C-P} = 6.4 Hz, Tip-C), 143.1 (d, ³J_{C-P} = 6.4 Hz, Tip-C), 138.9 (d, ³J_{C-P} = 7.7 Hz, Tip-C), 137.6 (d, ³J_{C-P} = 4.5 Hz, Tip-C), 135.9 (d, ³J_{C-P} = 3.9 Hz Tip-C), 133.0 (d, ³J_{C-P} = 6.0 Hz, Tip-C), 128.7 (Tip-C), 127.9, 126.4, 125.7, 125.0, 124.5, 124.1, 124.0, 122.3, 122.0, 121.9, 121.6, 121.5, 121.5, 120.6, 120.6, 120.2 (Tip-CH and NC(CH₃)=C(CH₃)N), 53.2, 53.0, 52.8 (NHC-ⁱPr-CH) 48.3 (d, J_{C-P} = 23.3 Hz, NHC-ⁱPr-CH), 36.5, 35.8, 35.8, 35.6, 35.4, 35.4, 35.3, 34.7, 34.7, 34.6, 34.5, 34.5, 29.5, 28.1, 27.4, 27.3, 26.5, 26.1, 26.1, 26.0, 25.9, 25.8, 25.8, 25.8, 25.7, 25.6, 25.5, 25.4, 25.4, 25.2, 25.0, 24.9, 24.8, 24.7, 24.5, 24.4, 24.3, 24.3, 24.2, 24.2, 24.1, 24.0, 23.7, 21.4, 21.3, 21.1, 21.0, 20.7, 20.7, 20.3, 20.1, 20.0 (Tip-ⁱPr-CH, Tip-ⁱPr-CH₃ and NHC-ⁱPr-CH₃), 10.4, 10.1, 10.1, 9.9 (NC(CH₃)=C(CH₃)N).

³¹P{¹H} NMR (162.0 MHz, C₆D₆, 300K): δ = -252.0, -267.9 (ratio 1 : 0.88).

³¹P NMR (162.0 MHz, C₆D₆, 300K): δ = -252.0 (^{TS}J_{P-H} = 8.5 Hz), -267.9 (^{TS}J_{P-H} = 12.8 Hz).

³¹P CP/MAS NMR (162.0 MHz, 13kHz): δ = -249.2.

²⁹Si NMR (79.5 MHz, C₆D₆, 300K): δ = -68.7 (¹J_{P-Si} = 91.1 Hz), -68.9 (¹J_{P-Si} = 107.2 Hz), -69.8 (¹J_{P-Si} = 104.3 Hz), -73.6 (¹J_{P-Si} = 97.2 Hz).

²⁹Si CP/MAS NMR (79.5 MHz, 13kHz): δ = -70.6 (¹J_{P-Si} = 87.1 Hz), -75.4 (¹J_{P-Si} = 87.1 Hz).

UV/Vis (hexane): $\lambda_{\text{max}}(\epsilon)$ = 336 nm (8700 M⁻¹cm⁻¹).

Elemental analysis: calculated for C₅₆H₈₉N₂PSi₂: C, 76.65%; H, 10.22%; N, 3.19%. Found: C, 76.27; H, 10.03; N, 2.50.

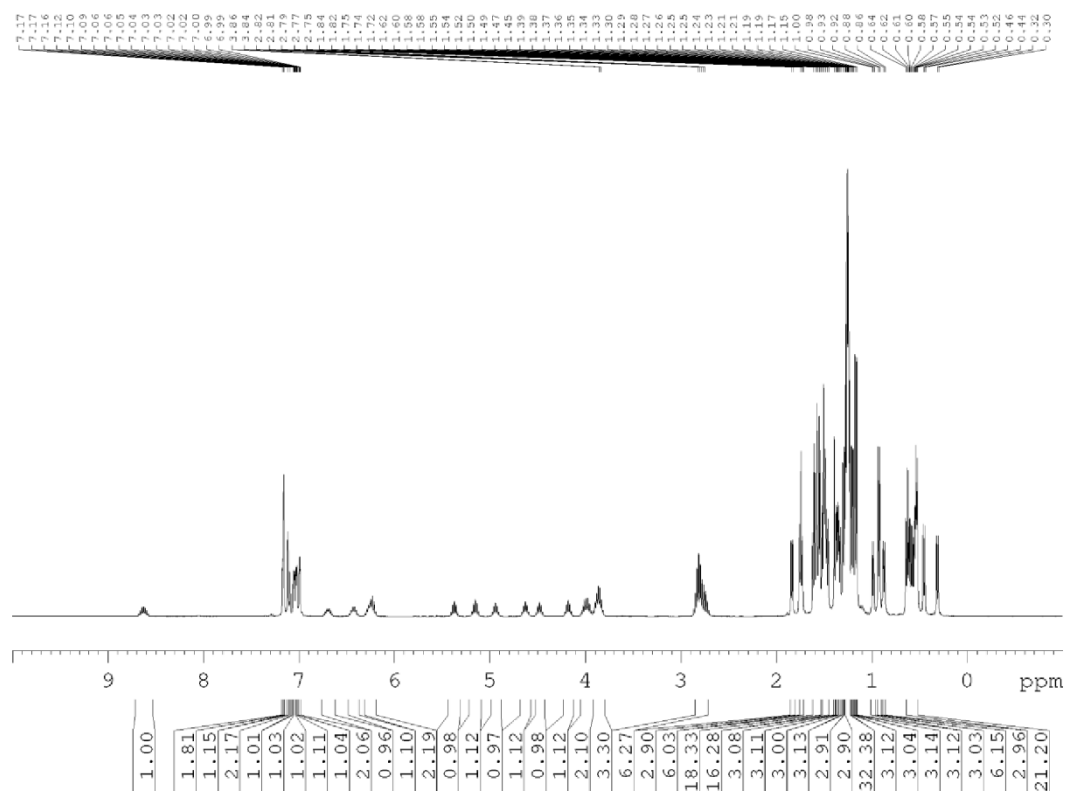


Figure S1: ^1H NMR spectrum of **5** in C_6D_6 at 300 K.

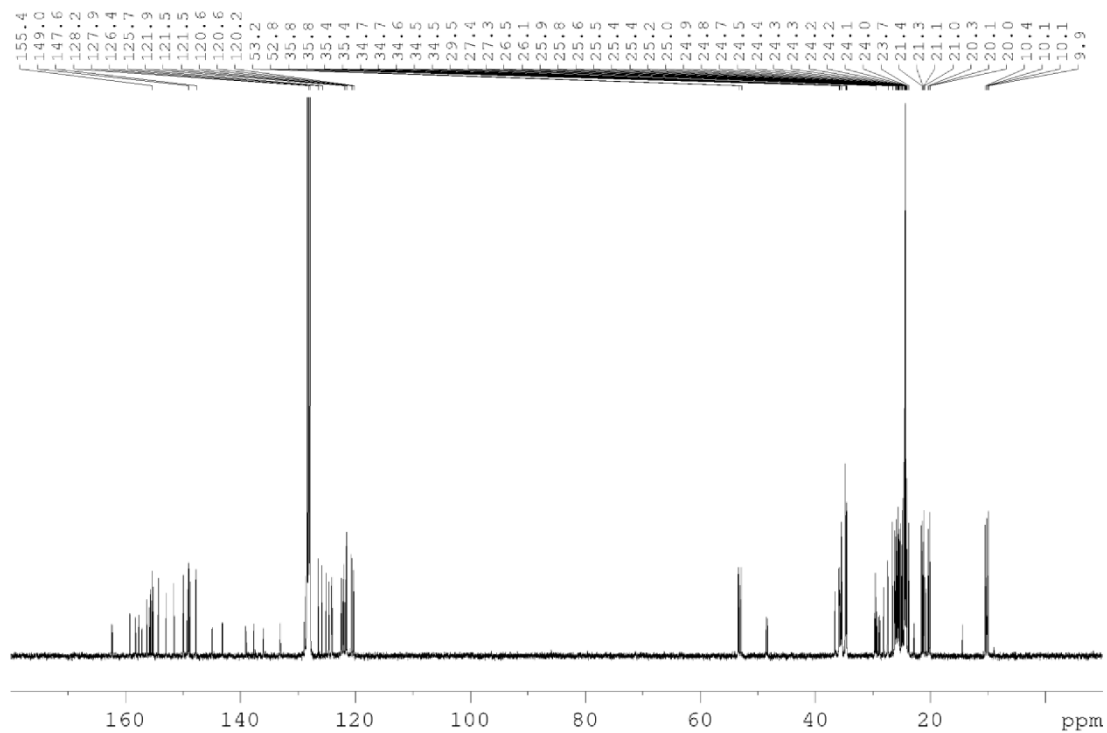


Figure S2: ^{13}C NMR spectrum of **5** in C_6D_6 at 300 K.

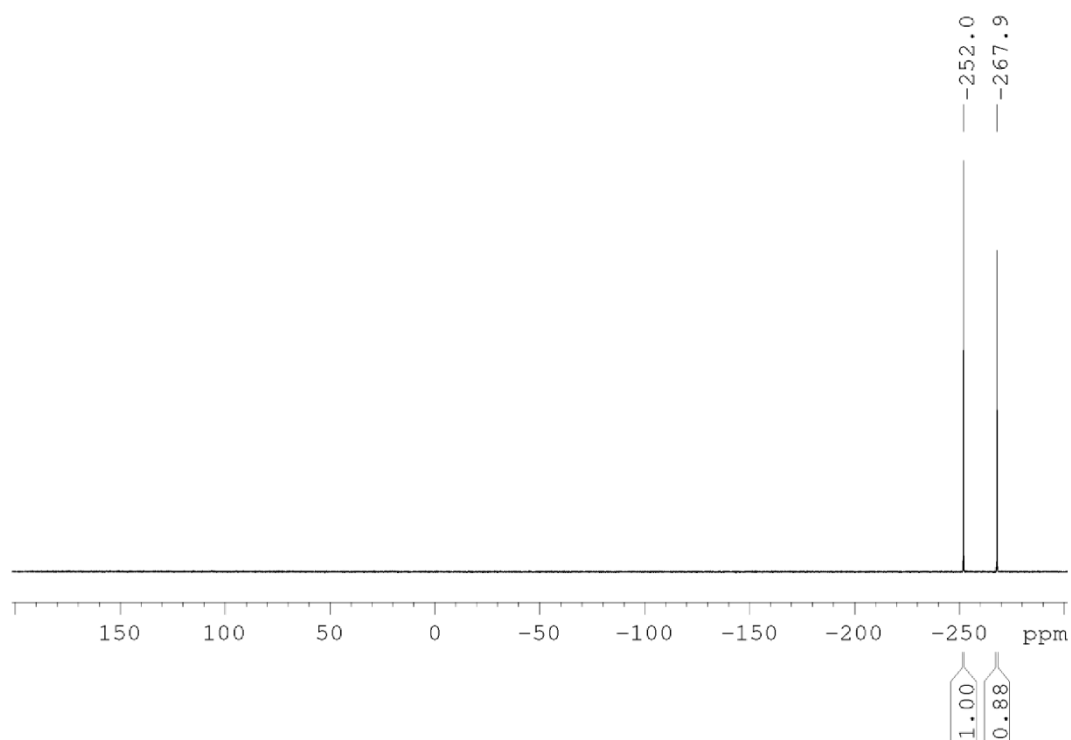


Figure S3: $^{31}\text{P}\{^1\text{H}\}$ NMR spectrum of **5** in C_6D_6 at 300 K.

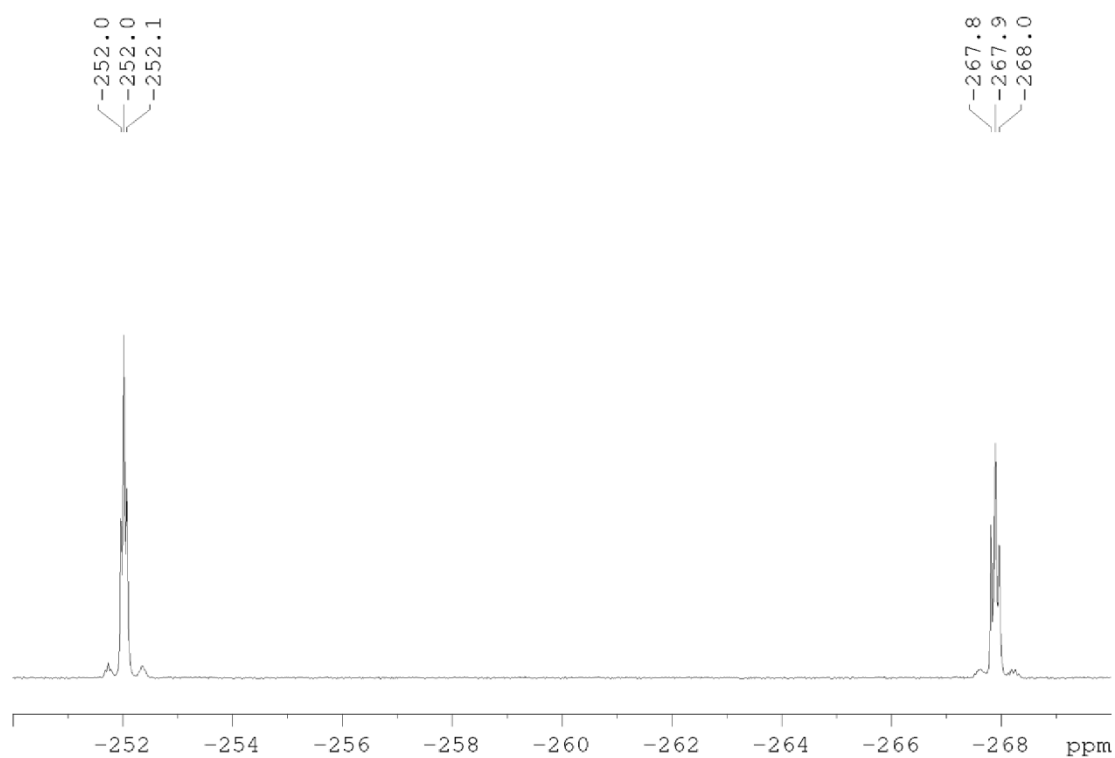


Figure S4: ^{31}P NMR resonances of **5** in C_6D_6 at 300 K without ^1H decoupling.

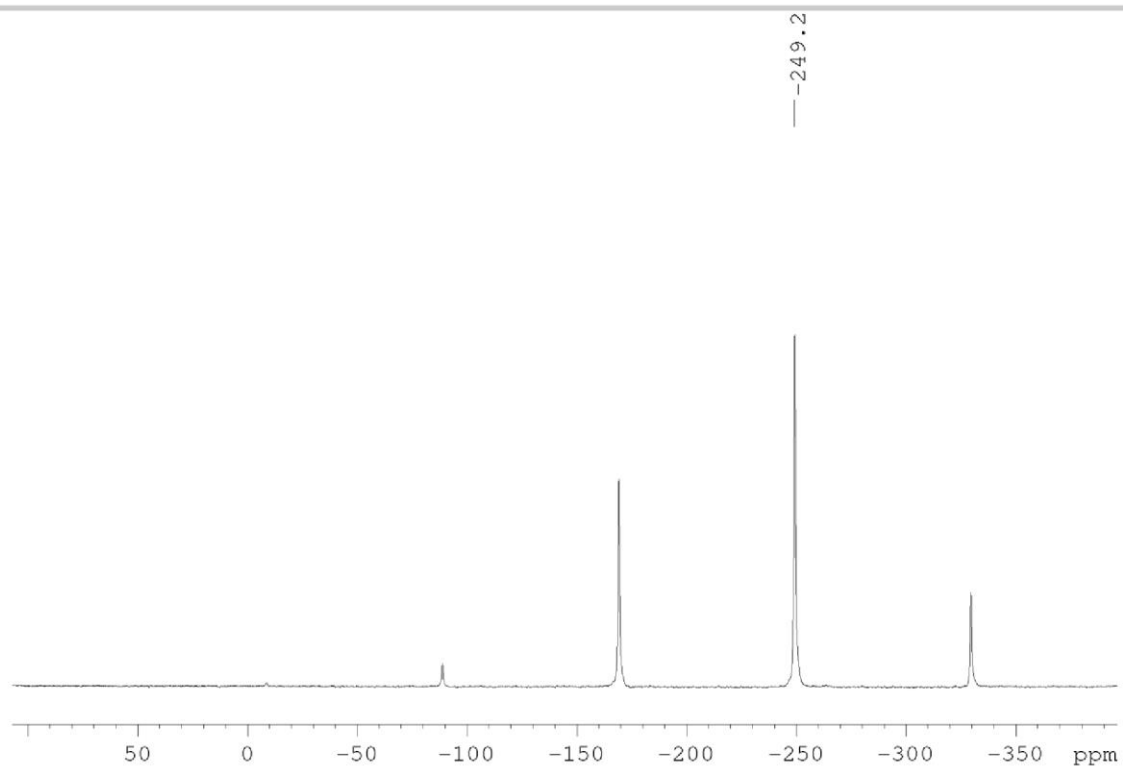


Figure S5: ^{31}P CP/MAS NMR spectrum of **5**.

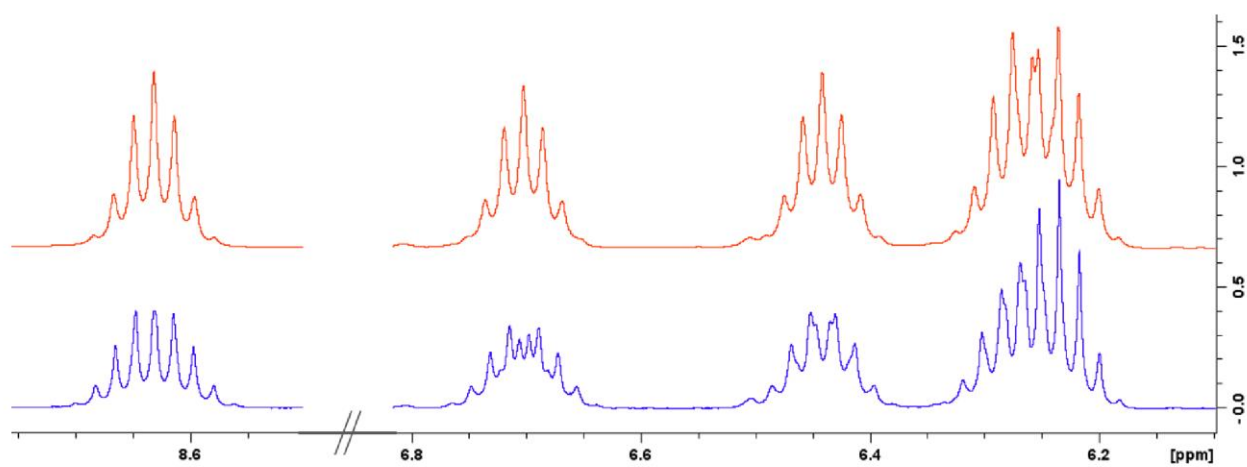


Figure S6: Comparison of selected signals of the ^1H NMR spectrum (blue) and the $^1\text{H}[^{31}\text{P}]$ NMR spectrum (red) of **5** that are affected by decoupling from the ^{31}P nucleus.

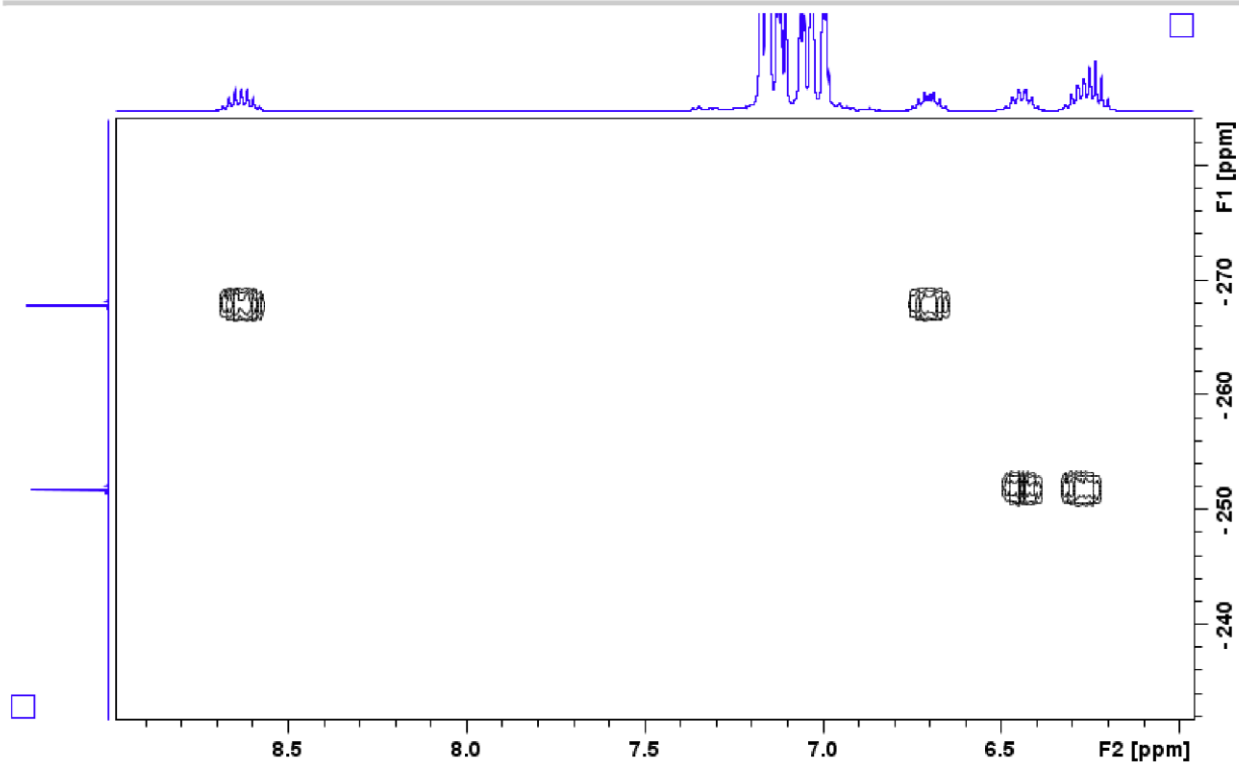


Figure S7: Selected section of the P-H correlation spectrum of 5.

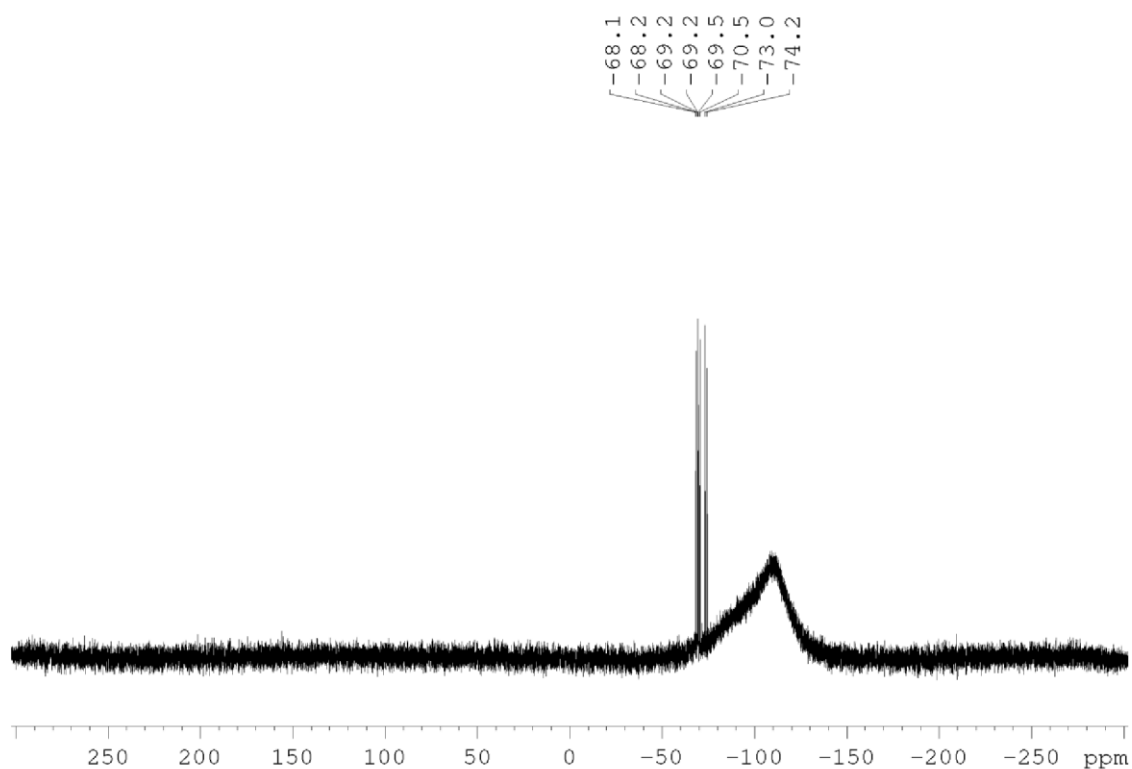


Figure S8: ^{29}Si NMR spectrum of 5 in C_6D_6 at 300 K.

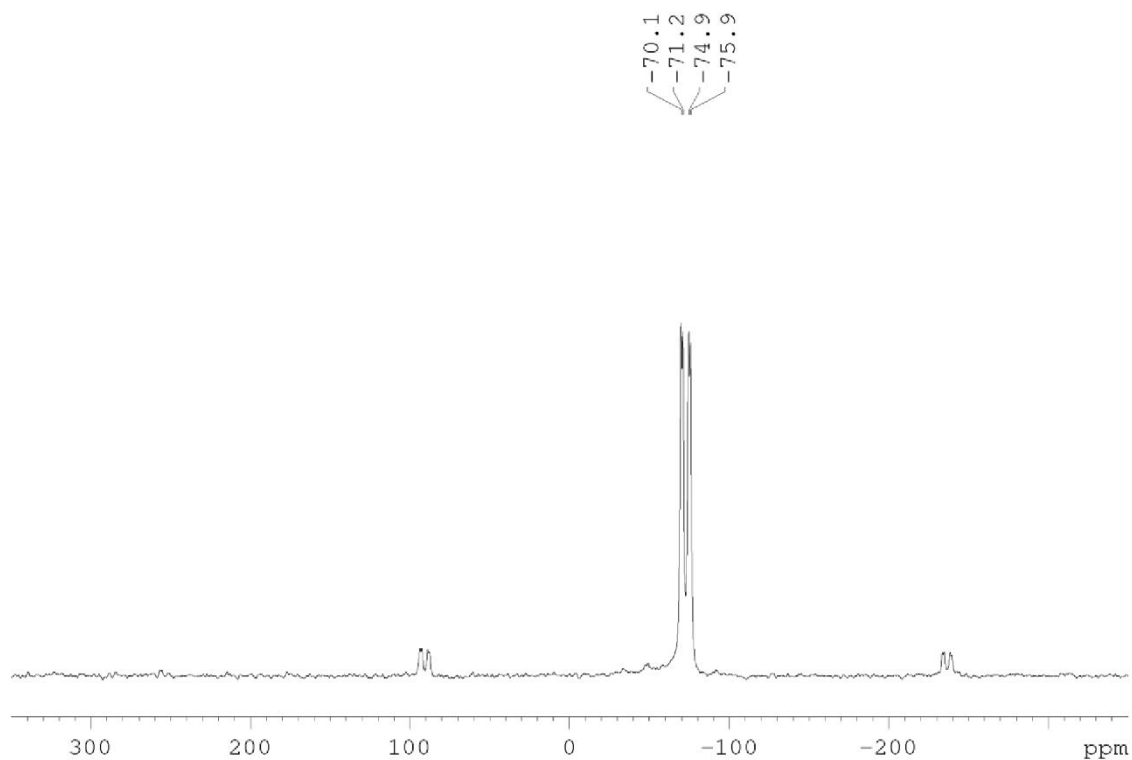


Figure S9: ^{29}Si CP/MAS NMR spectrum of 5.

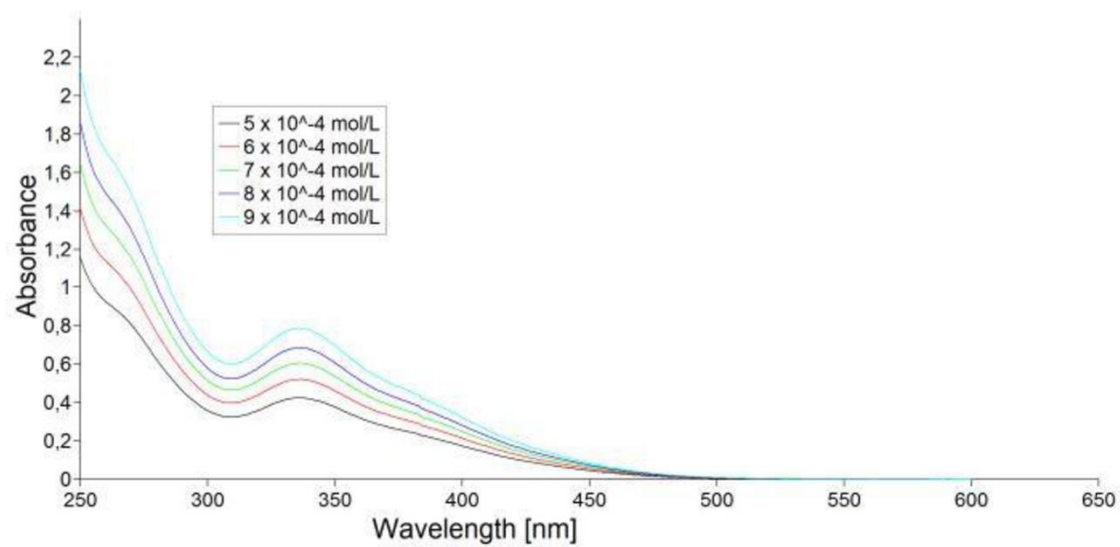


Figure S10: UV/Vis spectra of 5 in hexane at different concentrations ($5 \cdot 10^{-4}$ – $9 \cdot 10^{-4}$ mol/L).

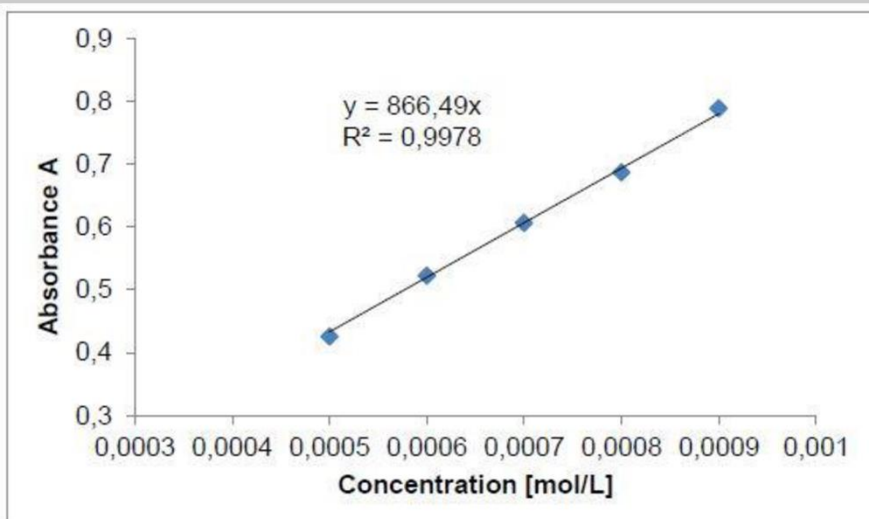


Figure S11: Determination of extinction coefficient ϵ ($8700 \text{ M}^{-1} \text{ cm}^{-1}$) by linear regression of absorbance ($\lambda = 336 \text{ nm}$) of **5** against concentration.

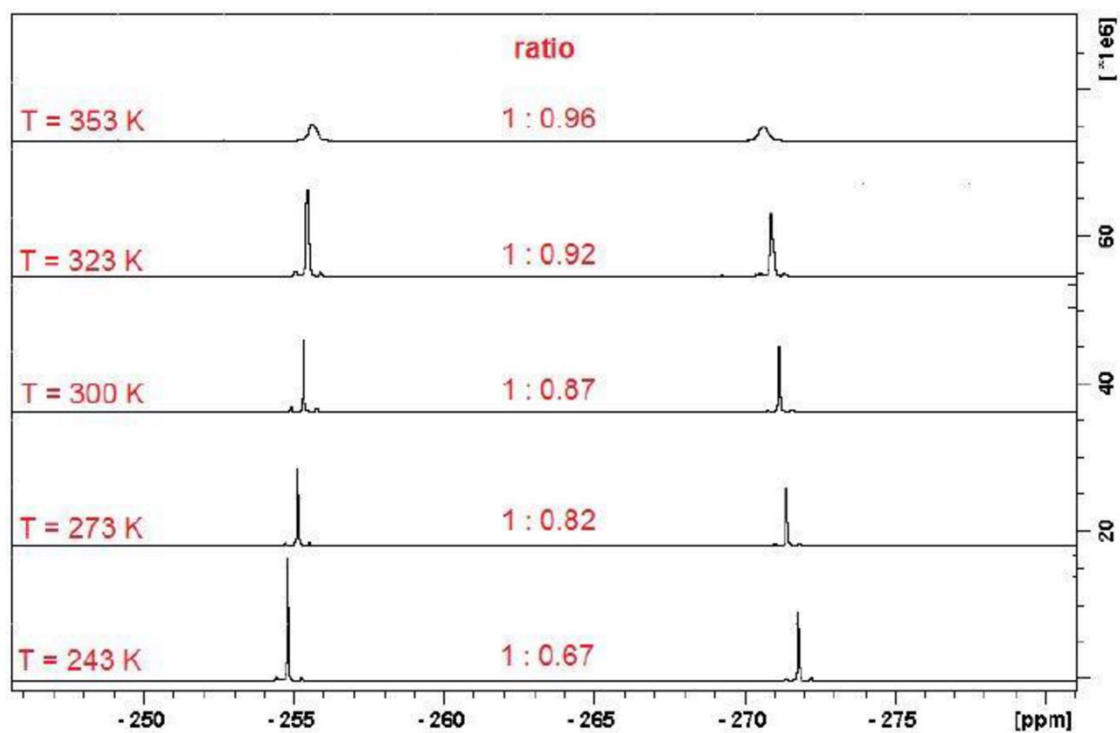


Figure S12: $^{31}\text{P}\{^1\text{H}\}$ NMR spectra of **5** at five different temperatures ($T = 243 - 353 \text{ K}$), numbers represent ratio of the intensity of the signals to each other.

2-(1,3-diisopropyl-4,5-dimethyl-1H-imidazol-3-ium-2-yl)-2,3,3-tris(2,4,6-triisopropylphenyl)-1,2,3-phosphadisiliran-1-ide tetracarbonyl iron 6

205 mg (0.23 mmol) of NHC-stabilized phosphasilene **5** and 100.5 mg (0.28 mmol) of diiron nonacarbonyl $\text{Fe}_2(\text{CO})_9$ are mixed and 1.5 mL toluene is added. After 15 minutes of stirring at room temperature, the yellow-orange suspension turns deep red. Stirring is continued for 12 h. Subsequently, all volatiles are removed in vacuo and 30 mL of toluene added to the solid residue. The red solution is filtered and the filtrate reduced to approximately 0.5 mL in vacuo. Standing overnight at room temperature affords 220 mg (91 %) of **6** as orange blocks. (m.p. 153°C, dec.).

^1H NMR (400.13 MHz, C_6D_6 , 300K): δ = 7.29, 7.22 (each d, each 1H, Tip-*H*), 7.07, 7.06 (each s, each 1H, Tip-*H*), 6.98 (d, 2H, Tip-*H*), 5.32 (sept, 1H, NHC-*Pr-CH*), 5.18 (br, 2H, Tip-*Pr-CH*), 4.71 (sept, 1H, NHC-*Pr-CH*), 3.95, 3.85, 3.45, 3.34 (each sept, each 1H, Tip-*Pr-CH*), 2.83 – 2.68 (m, 3H, Tip-*Pr-CH*), 1.83, 1.79, 1.72 (each d, each 3H, Tip-*Pr-CH}_3*), 1.57 – 1.44 (m, 18H, Tip-*Pr-CH}_3*, NHC-*Pr-CH}_3* and $\text{NC}(\text{CH}_3)=\text{C}(\text{CH}_3)\text{N}$), 1.38 (s, 3H, Tip-*Pr-CH}_3*), 1.32 (d, 3H, Tip-*Pr-CH}_3*), 1.26 – 1.22 (m, 12H, Tip-*Pr-CH}_3*), 1.15 (d, 6H, Tip-*Pr-CH}_3*), 1.10 (d, 3H, NHC-*Pr-CH}_3*), 0.75, 0.57 (each d, each 3H, Tip-*Pr-CH}_3*), 0.51, 0.31 (each d, each 6H, Tip-*Pr-CH}_3* overlapping with NHC-*Pr-CH}_3*).

^{13}C NMR (100.6 MHz, C_6D_6 , 300K): δ = 221.9 (d, $^2J_{\text{C-P}} = 11.3$ Hz, Fe-CO), 158.5 (Ar-C), 158.2 (d, $^2J_{\text{C-P}} = 19.1$ Hz, NCN), 157.5, 156.6 (Ar-C), 154.9 (d, $^3J_{\text{C-P}} = 3.8$ Hz, Ar-C), 153.4 (d, $^3J_{\text{C-P}} = 1.8$ Hz, Ar-C), 151.8 (d, $^3J_{\text{C-P}} = 1.9$ Hz, Ar-C), 151.3, 150.0, 149.1 (Ar-C), 137.9 (d, $^2J_{\text{C-P}} = 11.2$ Hz, Ar-*ipso-C*), 136.4 (d, $^2J_{\text{C-P}} = 9.3$ Hz, Ar-*ipso-C*), 132.8 (d, $^2J_{\text{C-P}} = 9.3$ Hz, Ar-*ipso-C*), 127.2 ($\text{NC}(\text{CH}_3)=\text{C}(\text{CH}_3)\text{N}$), 125.1, 125.0, 122.6, 122.0, 120.9, 120.8 (Ar-CH), 53.6, 53.2 (NHC-*Pr-CH*), 37.2, 36.2, 36.0, 35.7, 34.7, 34.6, 34.4, 33.1, 33.0, 32.9, 32.8, 28.7, 28.0, 26.7, 26.4, 26.4, 26.2, 25.6, 25.3, 25.2, 25.1, 24.2, 24.2, 24.1, 24.1, 24.0, 24.0, 24.0 (Tip-*Pr-CH* and Tip-*Pr-CH}_3*), 22.5, 21.6, 21.4, 19.9 (NHC-*Pr-CH}_3*), 10.3, 10.1 ($\text{NC}(\text{CH}_3)=\text{C}(\text{CH}_3)\text{N}$).

^{31}P NMR (162.0 MHz, C_6D_6 , 300K): δ = -244.8, -266.3 (ratio 10 : 1).

^{29}Si NMR (79.5 MHz, C_6D_6 , 300K): δ = -59.5 (d, $^1J_{\text{Si-P}} = 75.6$ Hz), -62.6 (d, $^1J_{\text{Si-P}} = 60.1$ Hz).

UV/Vis (hexane): λ = 460 – 340 nm (broad shoulder).

Elemental analysis: calculated for $\text{C}_{60}\text{H}_{89}\text{FeN}_2\text{O}_4\text{PSi}_2$: C, 68.94%; H, 8.58%; N, 2.68%. Found: C, 68.57; H, 8.63; N, 2.44.

IR: ν = 2020, 1930, 1906 and 1890 cm^{-1} .

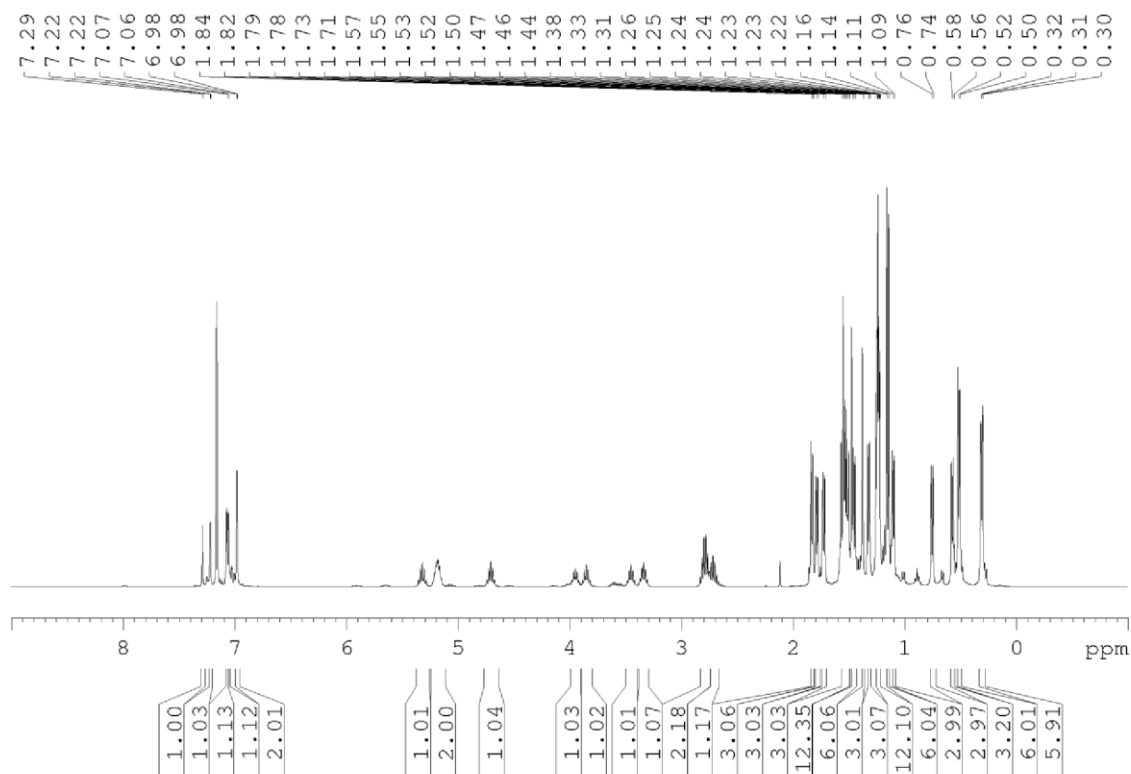


Figure S13: ^1H NMR spectrum of **6** in C_6D_6 at 300 K.

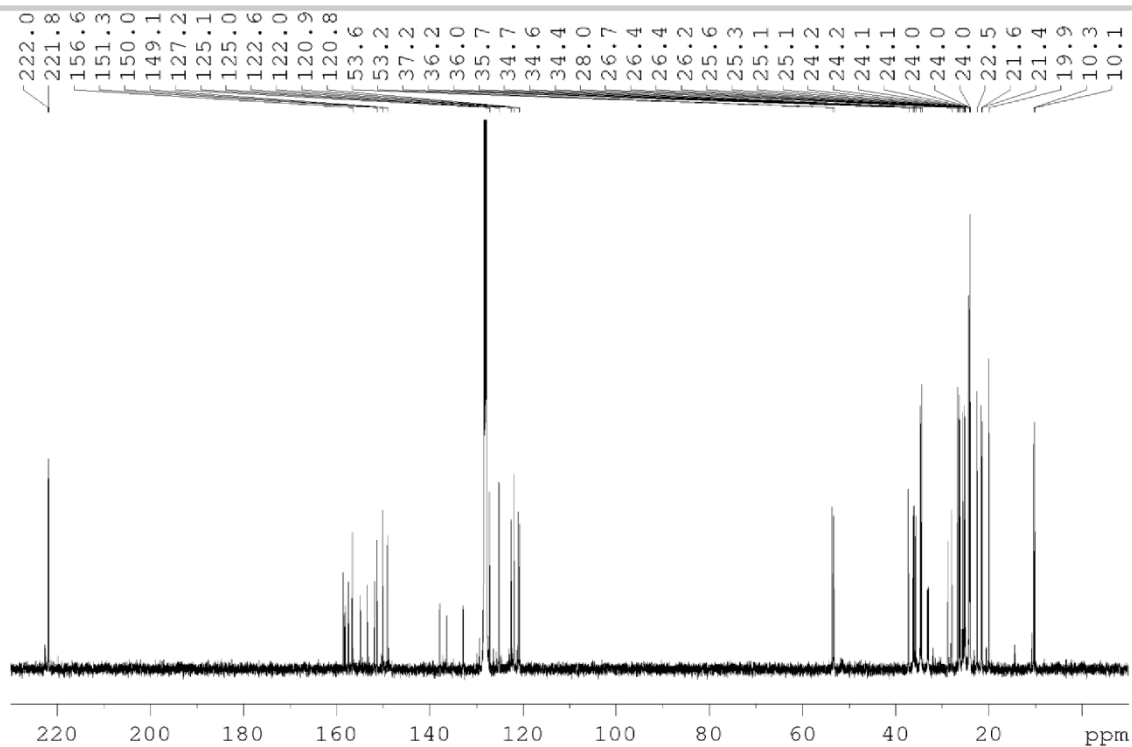


Figure S14: ^{13}C NMR spectrum of **6** in C_6D_6 at 300 K.

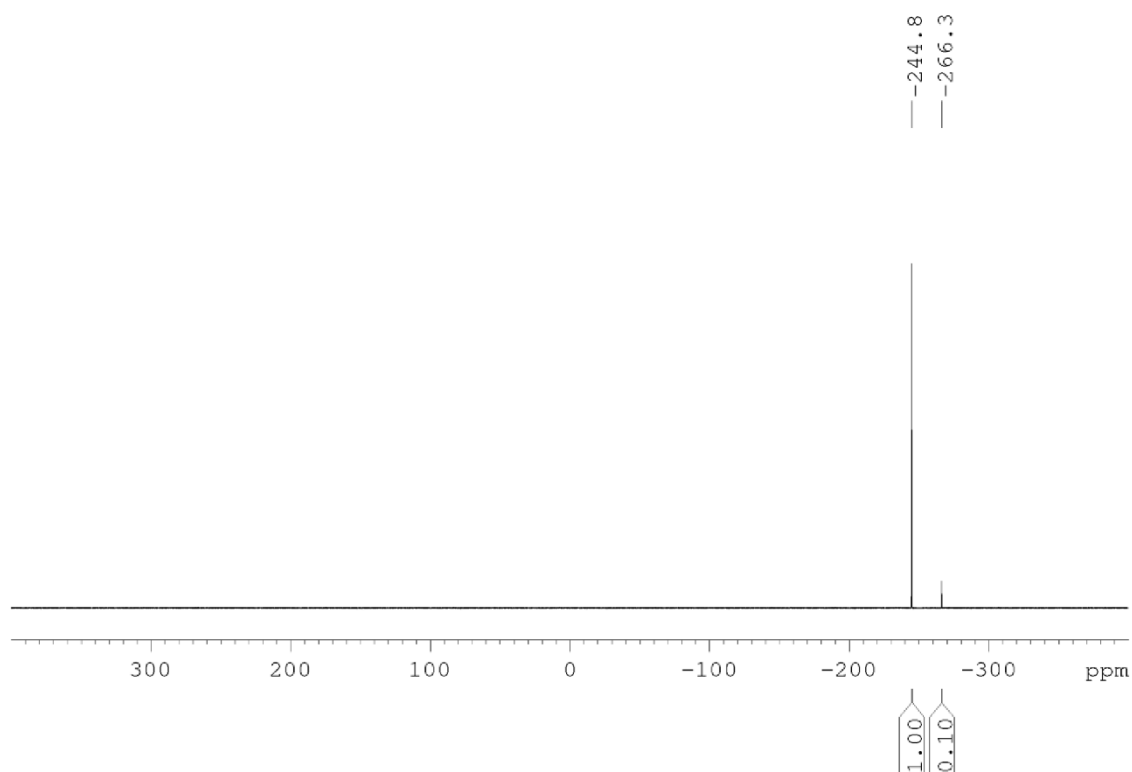


Figure S15: ^{31}P NMR spectrum of **6** in C_6D_6 at 300 K.

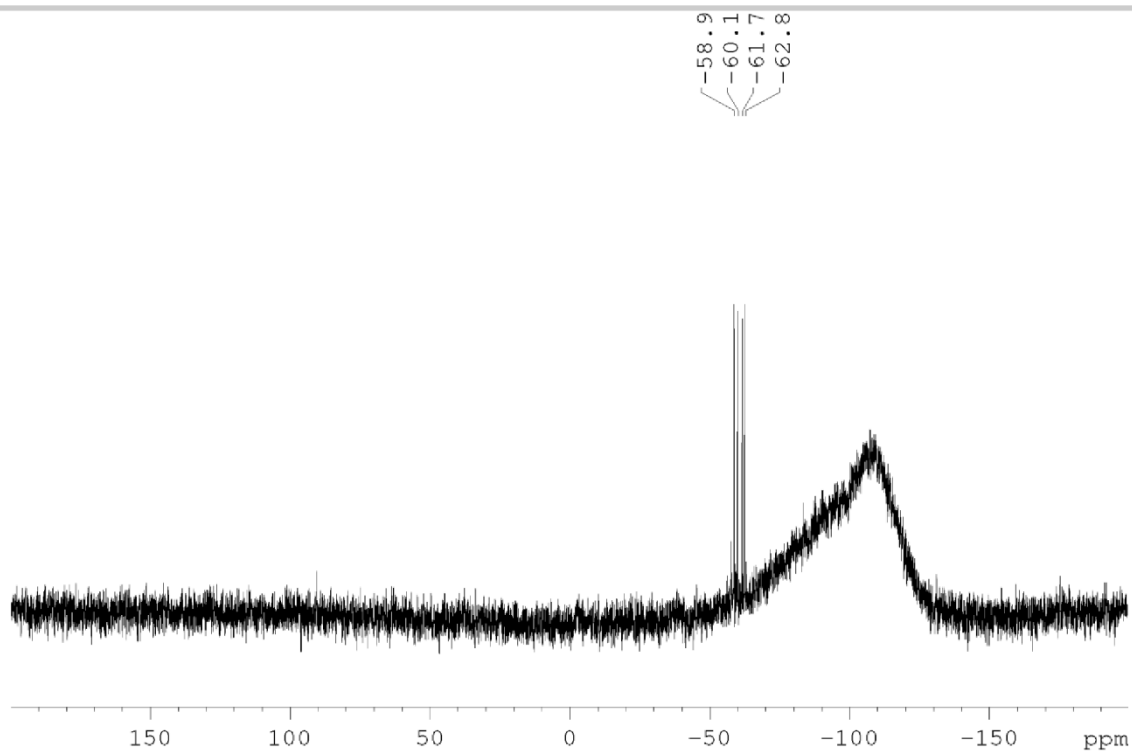


Figure S16: ^{29}Si NMR spectrum of **6** in C_6D_6 at 300 K.

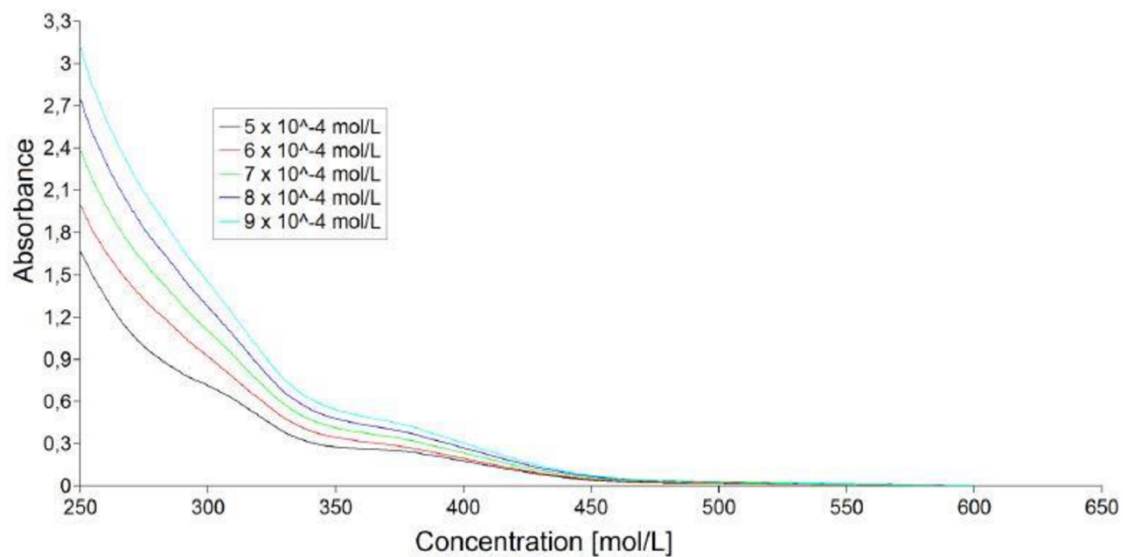


Figure S17: UV/Vis spectra of **6** in hexane at different concentrations ($5 \cdot 10^{-4}$ – $9 \cdot 10^{-4}$ mol/L).

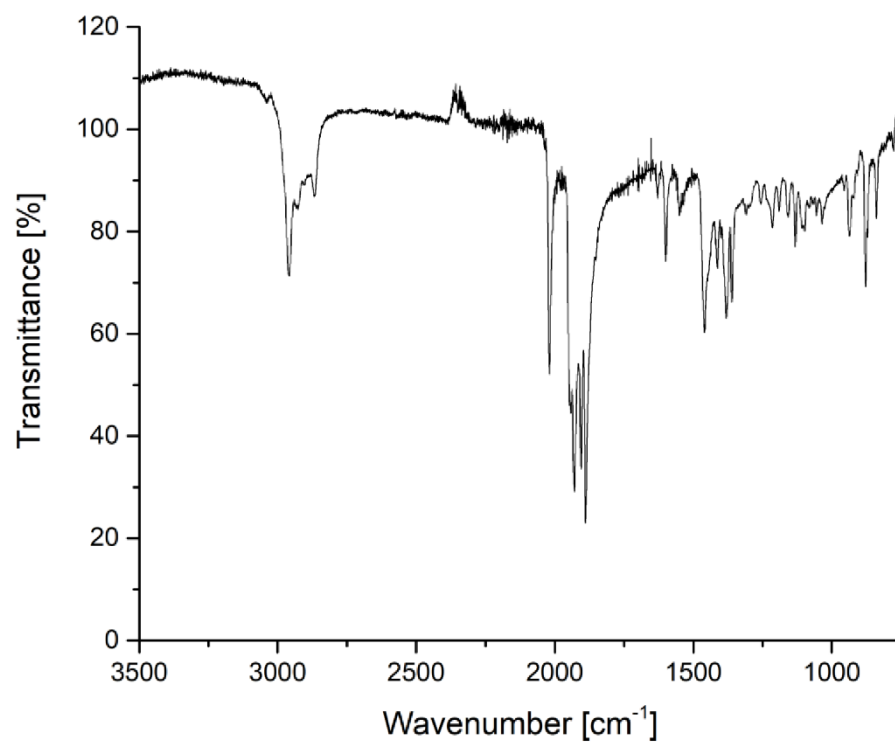


Figure S18: Infrared spectrum of **6** (powder).

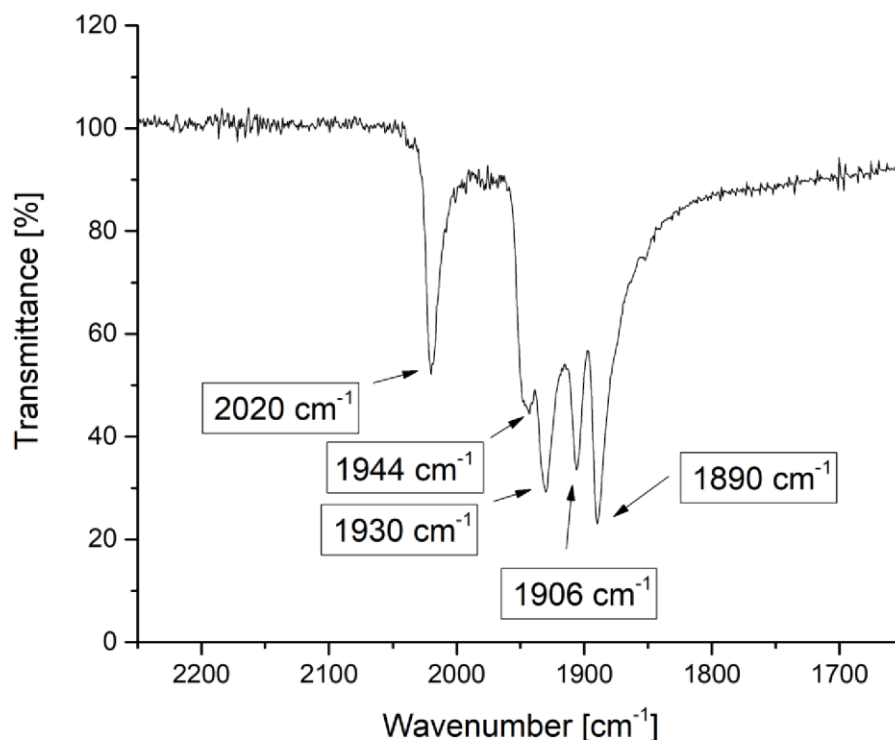


Figure S19: Selected section of Infrared spectrum of **6** (powder).

1,3-diisopropyl-4,5-dimethyl-2-(1,3,3-tris(2,4,6-triisopropylphenyl)disilaphosph-2-en-1-ylidene)-2,3-dihydro-1H-imidazole tricarbonyl iron **7**

387 mg (0.37 mmol) of tetracarbonyl complex **6** are dissolved in 8 mL of toluene and heated to 80°C upon stirring for 18h. All volatiles are removed in vacuo before the solid residue is again digested with 30 mL of toluene. The mixture is filtered and the filtrate reduced to approximately 2.5 mL. Standing at room temperature for three days affords 179 mg (48 %) of **7** as red plates. (m.p. 163°C, dec.).

¹H NMR (400.13 MHz, thf-*d*₈, 300K): δ = 7.07, 6.88 (each s, each 1H, Tip-*H*), 6.85 (s, 2H, Tip-*H*), 6.78, 6.77 (each s, each 1H, Tip-*H*), 5.79 (br, 2H, NHC-ⁱPr-*CH*), 4.51 (br sept), 4.29 (br) and 4.14 (sept) partially overlap (overall 4H, Tip-ⁱPr-*CH*), 3.85 (br sept, 1H, Tip-ⁱPr-*CH*), 3.58 (sept, 1H, Tip-ⁱPr-*CH* overlapping with thf-*d*₈), 2.83 – 2.61 (m, 3H, Tip-ⁱPr-*CH*), 2.28 (s, 6H, NC(CH₃)=C(CH₃)N), 1.29 (d, 6H, Tip-ⁱPr-*CH*₃), 1.21 – 1.15 (m, 30H, Tip-ⁱPr-*CH*₃ and NHC-ⁱPr-*CH*₃), 1.11 – 1.08 (m, 12H, Tip-ⁱPr-*CH*₃), 1.00 (d, 3H, Tip-ⁱPr-*CH*₃), 0.77 (br, 6H, Tip-ⁱPr-*CH*₃), 0.44 (d, 3H, Tip-ⁱPr-*CH*₃), 0.35 (d, 3H, Tip-ⁱPr-*CH*₃), 0.04 (d, 3H, Tip-ⁱPr-*CH*₃).

¹³C NMR (100.6 MHz, thf-*d*₈, 300K): δ = 219.9, 158.7 (d, ²J_{C-P} = 20.6 Hz, NCN), 156.3, 155.7, 154.7, 154.2, 154.0, 151.8, 148.9, 148.4 (Ar-*C*), 142.7 (br, Ar-*ipso-C*), 137.0 (Ar-*ipso-C*), 133.6 (d, ²J_{C-P} = 3.6 Hz, Ar-*ipso-C*), 130.7 (NC(CH₃)=C(CH₃)N), 123.4, 123.3, 122.2, 122.1 (Ar-*CH*), 51.9, 51.8 (NHC-ⁱPr-*CH*), 35.8, 35.5, 35.2, 34.8, 34.7, 34.6, 33.6, 26.3, 26.1, 25.7, 25.5, 24.7, 24.4, 24.2, 24.1, 24.0, 24.0, 23.9, 23.9, 23.9, 23.4, 22.6, 22.0 (Tip-ⁱPr-*CH*, Tip-ⁱPr-*CH*₃ and NHC-ⁱPr-*CH*₃), 11.1 (NC(CH₃)=C(CH₃)N).

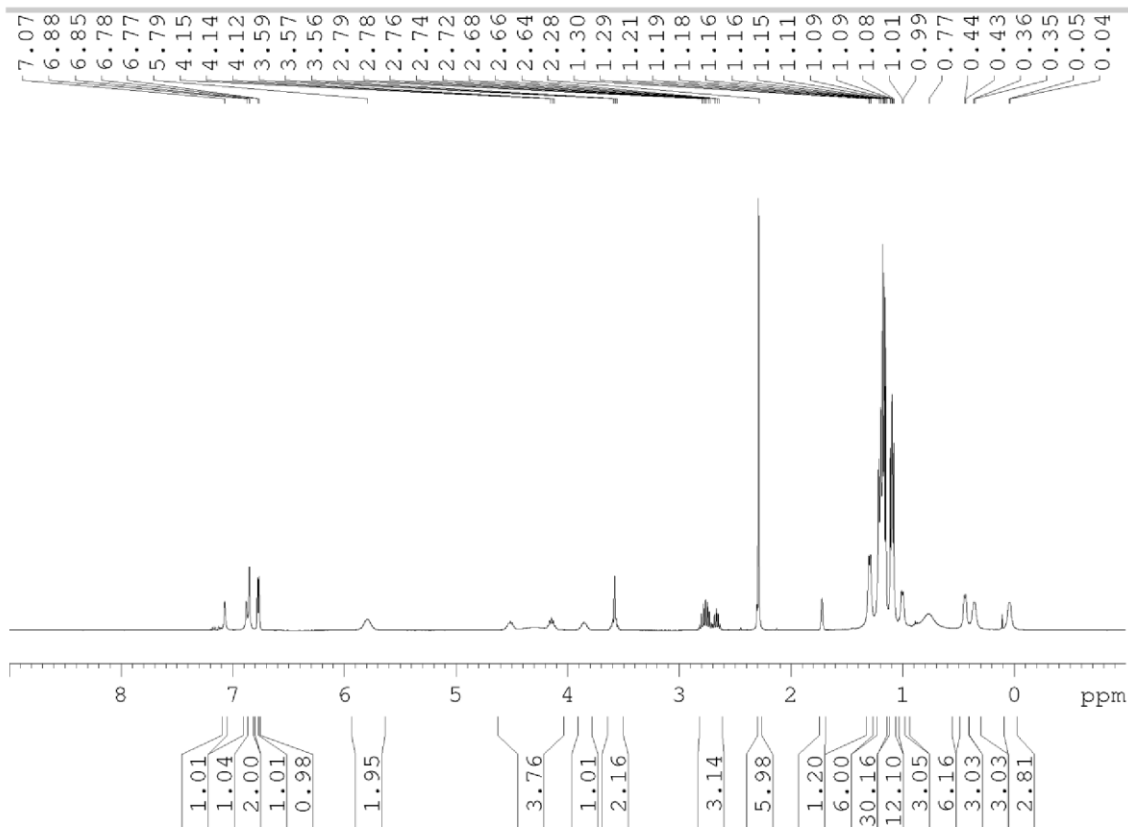
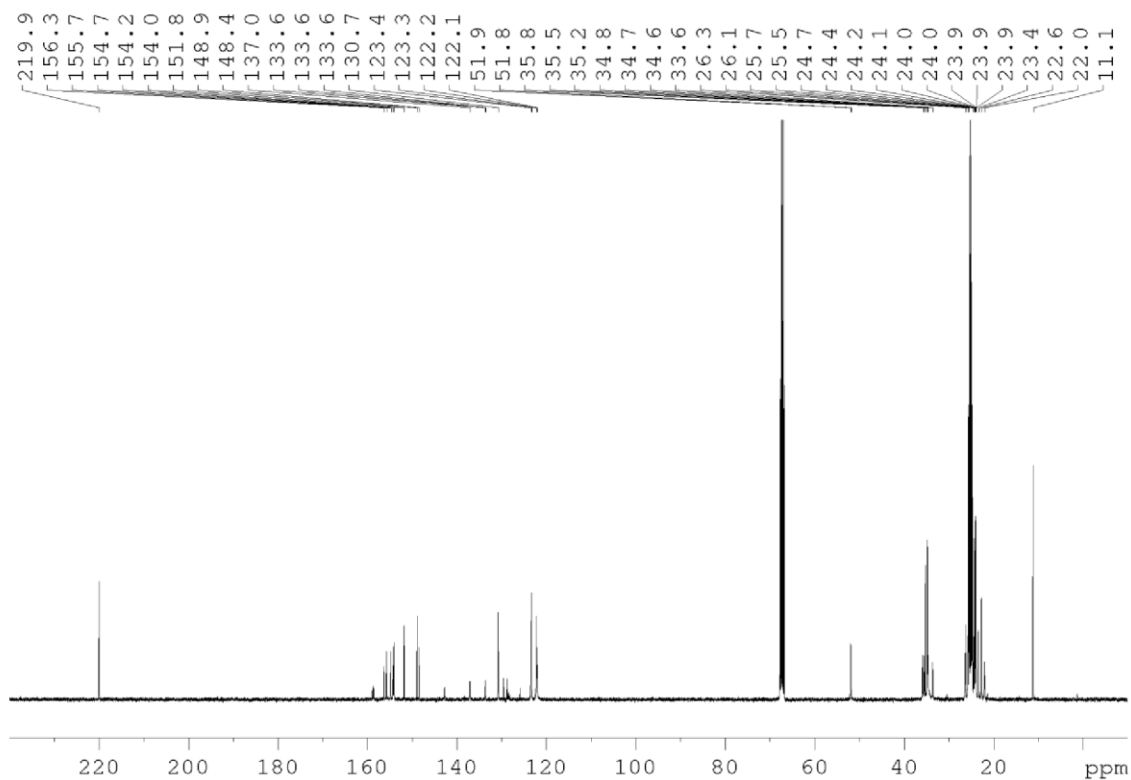
³¹P NMR (162.0 MHz, thf-*d*₈, 300K): δ = -378.6 (br).

²⁹Si NMR (79.5 MHz, thf-*d*₈, 300K): δ = 30.8 (br d, ¹J_{Si-P} = 110.9 Hz), 26.5 (d, ¹J_{Si-P} = 138.6 Hz).

UV/Vis (hexane): λ = 475 – 350 nm (broad shoulder).

Elemental analysis: calculated for C₅₉H₈₉FeN₂O₃PSi₂: C, 69.66%; H, 8.82%; N, 2.75%. Found: C, 69.40%; H, 8.73%; N, 2.62.

IR: ν = 1969, 1904 and 1878 cm⁻¹.

Figure S20: ¹H NMR spectrum of 7 in thf-d₈ at 300 K.Figure S21: ¹³C NMR spectrum of 7 in thf-d₈ at 300 K.

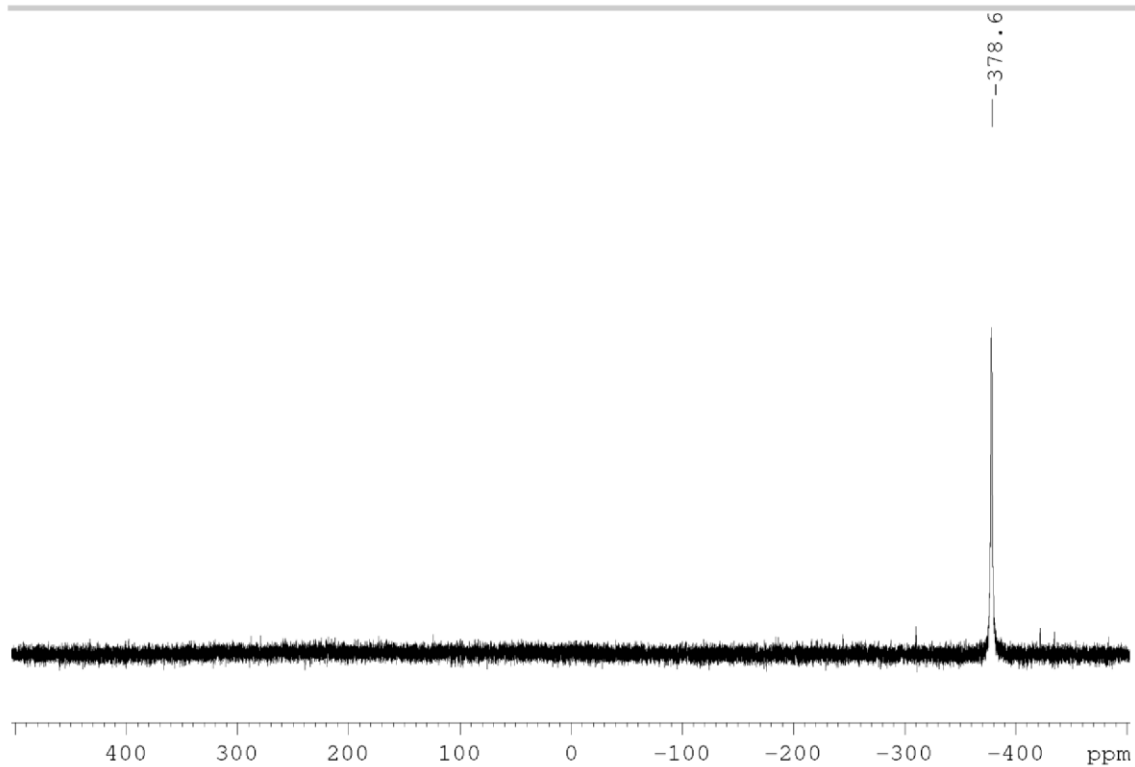


Figure S22: ^{31}P NMR spectrum of **7** in thf-d_8 at 300 K.

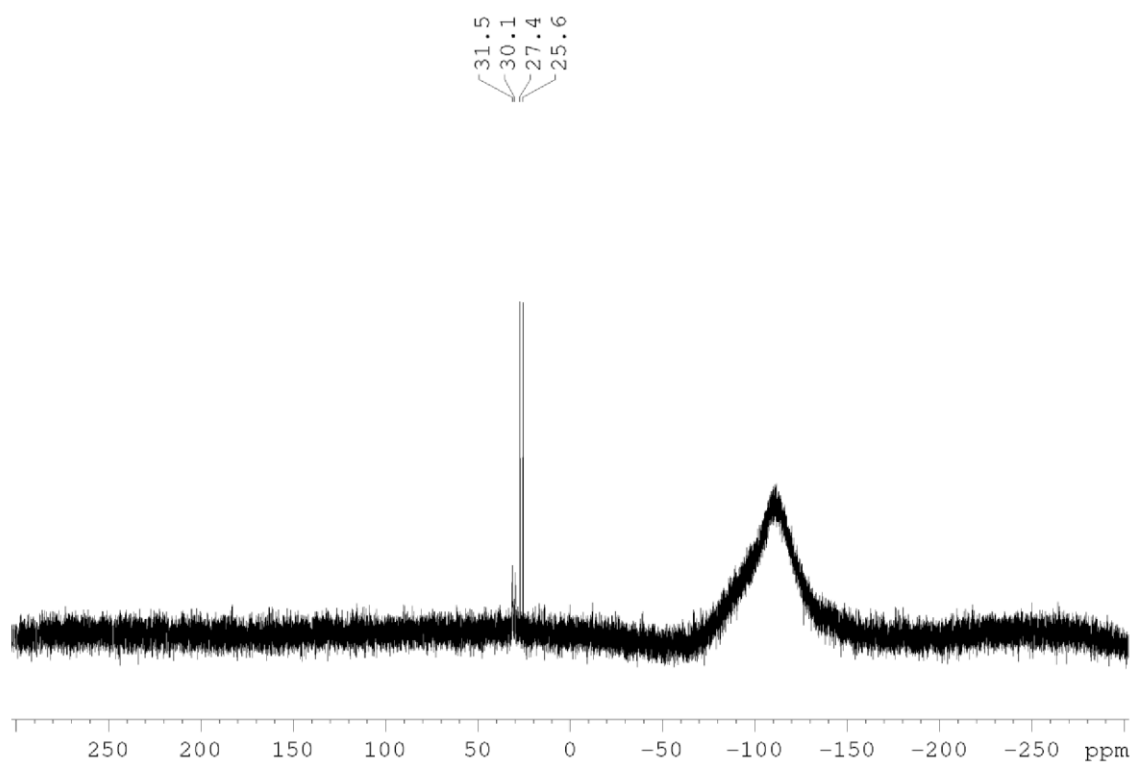


Figure S23: ^{29}Si NMR spectrum of **7** in thf-d_8 at 300 K.

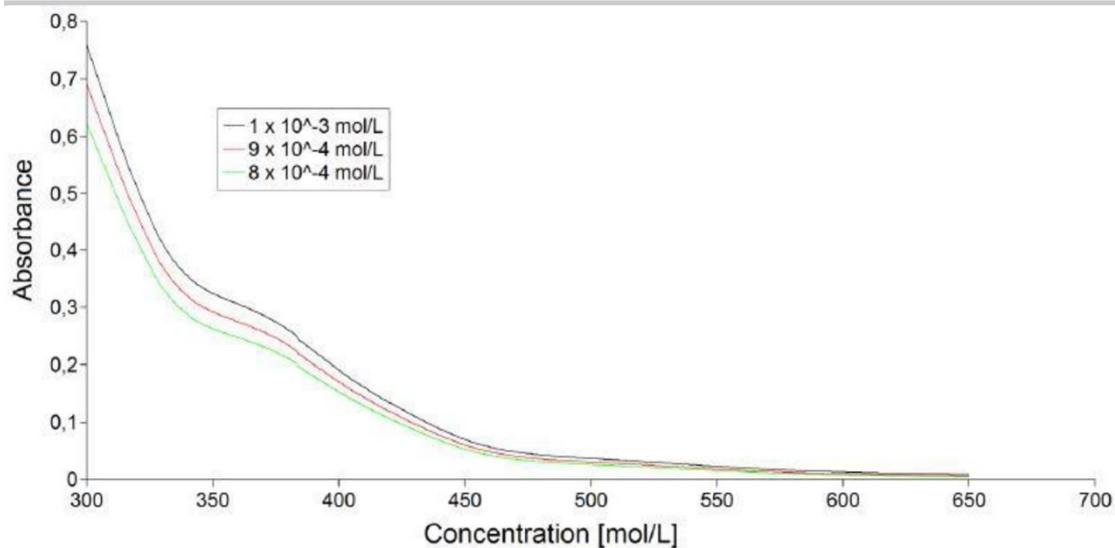


Figure S24: UV/Vis spectra of 7 in hexane at different concentrations ($8 \cdot 10^{-4}$ – $1 \cdot 10^{-3}$ mol/L).

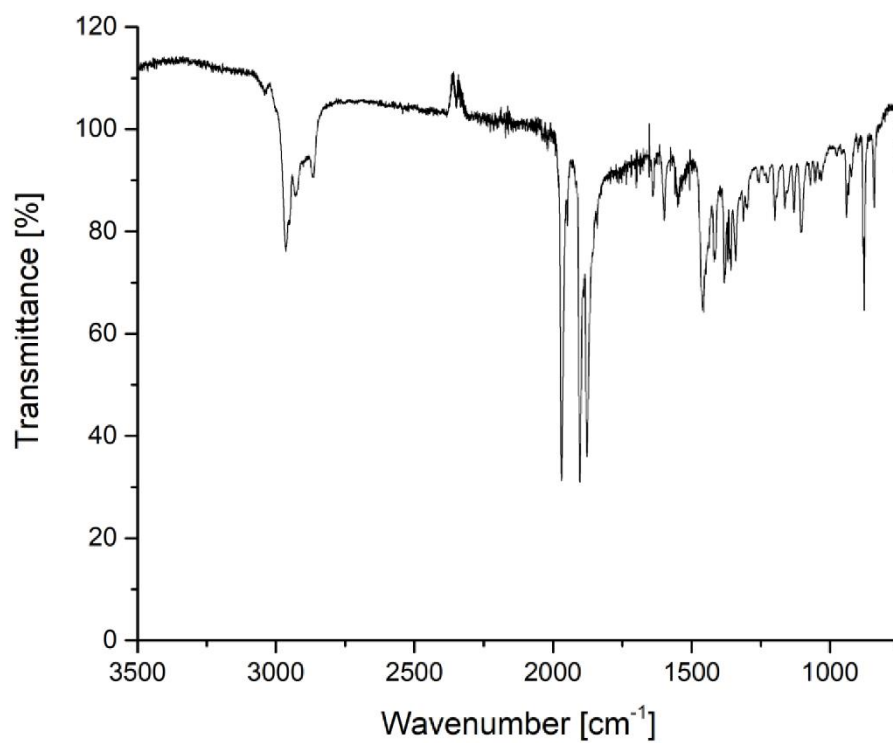


Figure S25: Infrared spectrum of 7 (powder).

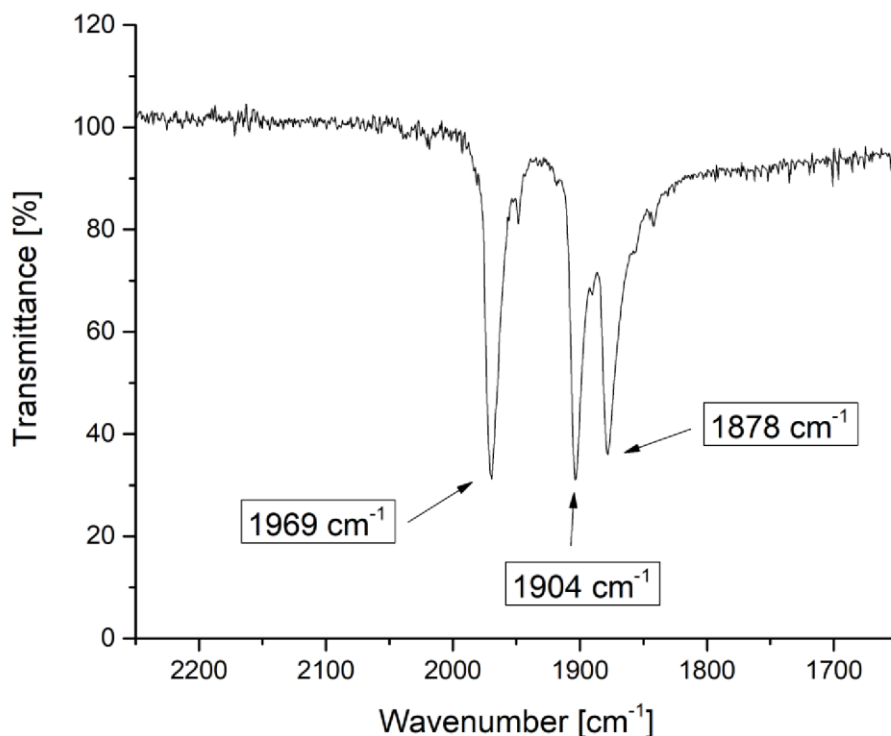


Figure S26: Selected section of infrared spectrum of **7** (powder).

3,3,4,5,6,6-hexakis(2,4,6-triisopropylphenyl)-1,2-diphospha-3,4,5,6-tetrasilatricyclo[2.2.0.02,5]hexane **8 and 2,3,3,5,6,6-hexakis(2,4,6-triisopropylphenyl)-1,4-diphospha-2,3,5,6-tetrasilatricyclo[3.1.0.02,4]hexane **9****

1.02 g (1.16 mmol) of cyclic phosphasilene **5** and 332 mg (1.37 mmol) of BPh₃ were mixed in a Schlenk flask and 12.5 mL of toluene were added. The resulting orange solution was heated to 100°C upon stirring which caused a slow color change from orange to yellow. Ongoing formation of the according NHC-borane adduct as desired side-product was monitored by ¹H NMR spectroscopy (characteristic resonances for NHC-BPh₃ at δ = 5.02 (sept., ¹PrCH), 1.56 (s, (CH₃)C=C(CH₃), 0.71 (d, ¹PrCH₃ in the ¹H NMR spectrum and at δ = -8.1 ppm in the ¹¹B NMR spectrum). After 17 hours no starting material **5** could be detected in the ³¹P NMR and the solvent was removed in vacuo. The solid residue was digested with hexane and kept at -80°C for 3 hours. After removing of the precipitated NHC-borane complex, the filtrate was reduced to approximately half of the volume and kept at -20°C overnight. A second filtration was followed by fractional crystallization to afford pale yellow single crystals of both Si₄P₂ isomers **8** and **9**. The main product **8** could not be completely separated from side products according to ¹H (NHC-BPh₃) and ³¹P NMR spectroscopy (**9**) even after several recrystallization steps. Thus, a full characterization including elemental analysis is still pending. (m.p. >220°C).

Si₄P₂ isomer **8** (m.p. >220°C):

³¹P NMR (162.0 MHz, C₆D₆, 300K): δ = -120.1, -121.1, -133.9, -134.9 (assigned to **8**) and -182.4 (assigned to **9**, ca. 5%)

³¹P CP/MAS NMR (162.0 MHz, 13kHz): -122.2, -136.9.

²⁹Si NMR (79.5 MHz, C₆D₆, 300K): δ = 32.1 (br), -1.4 (br).

²⁹Si CP/MAS NMR (79.5 MHz, 13kHz): δ = 32.2, -3.7.

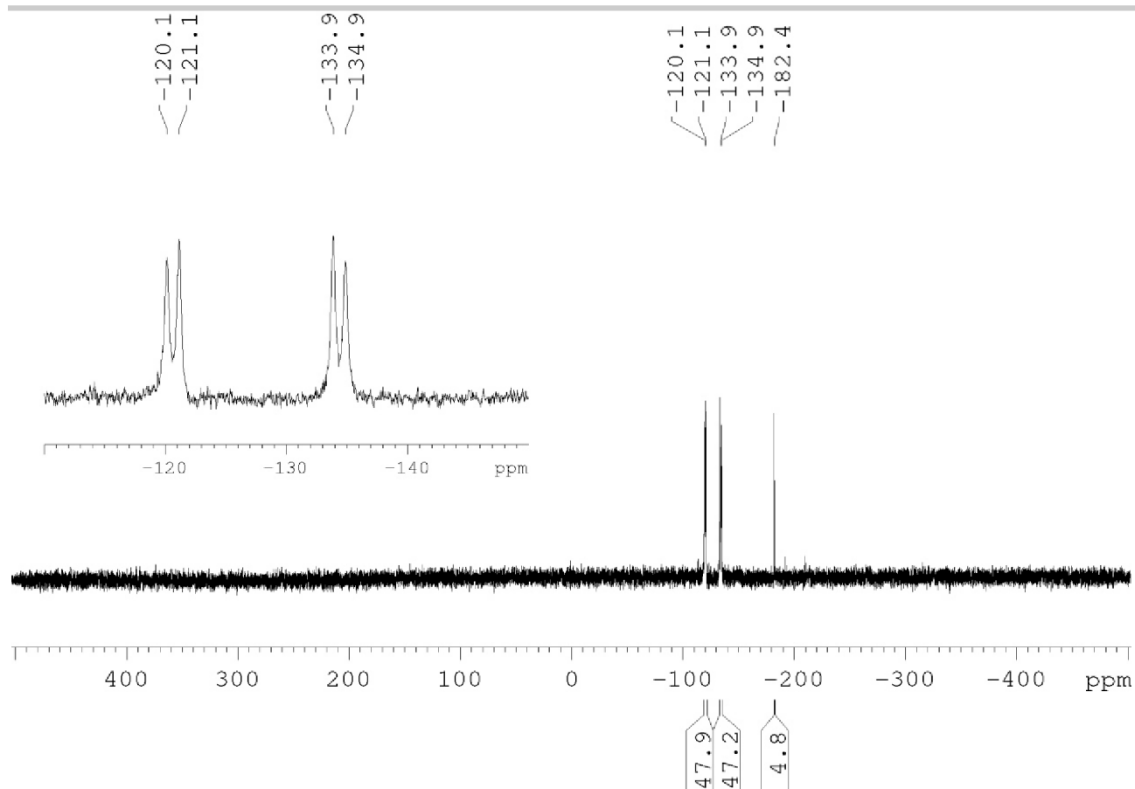


Figure S27: ^{31}P NMR spectrum of **8** in C_6D_6 at 300 K with residual amounts of **9** ($\delta = -182.4$ ppm).

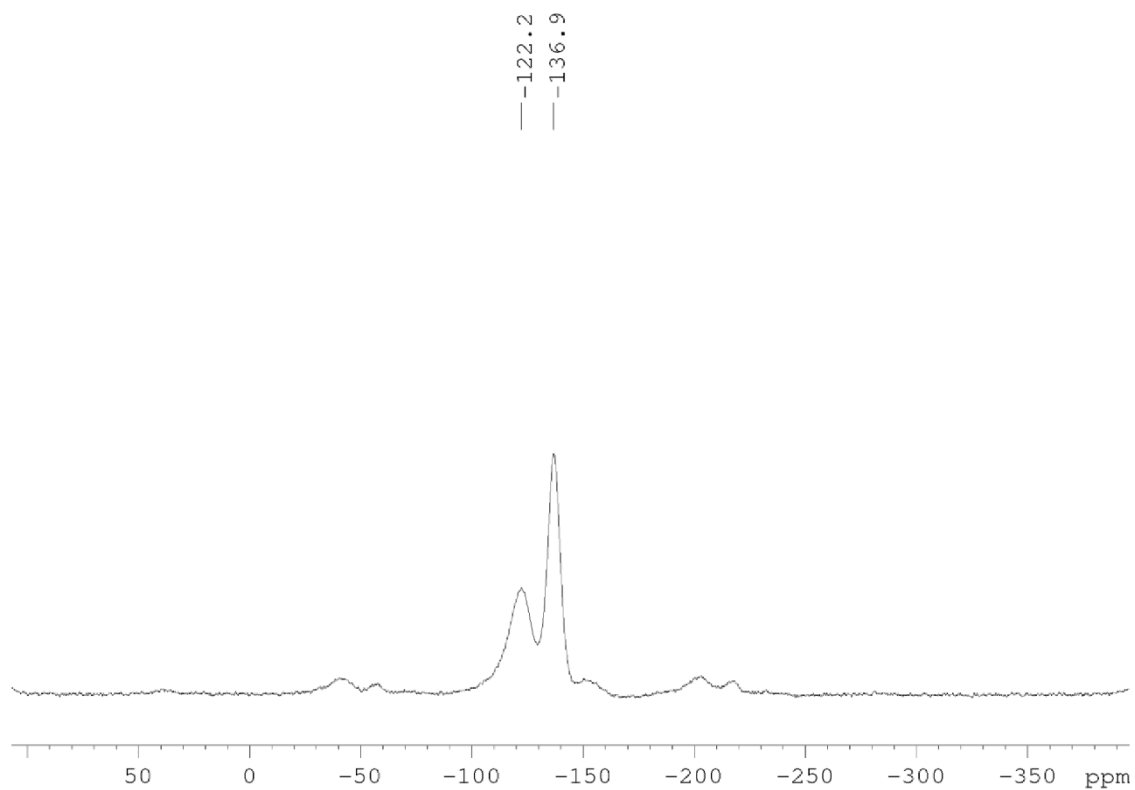


Figure S28: ^{31}P CP/MAS NMR spectrum of **8**.

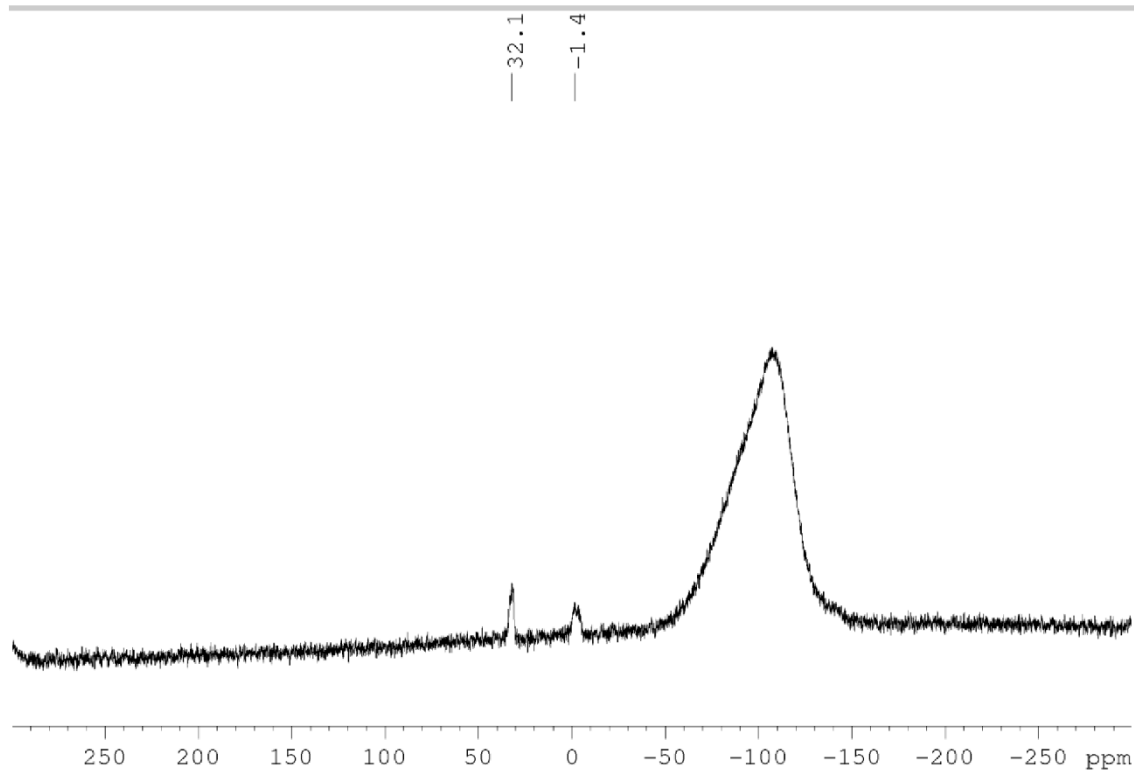


Figure S29: ^{29}Si NMR spectrum of **8** in C_6D_6 at 300K.

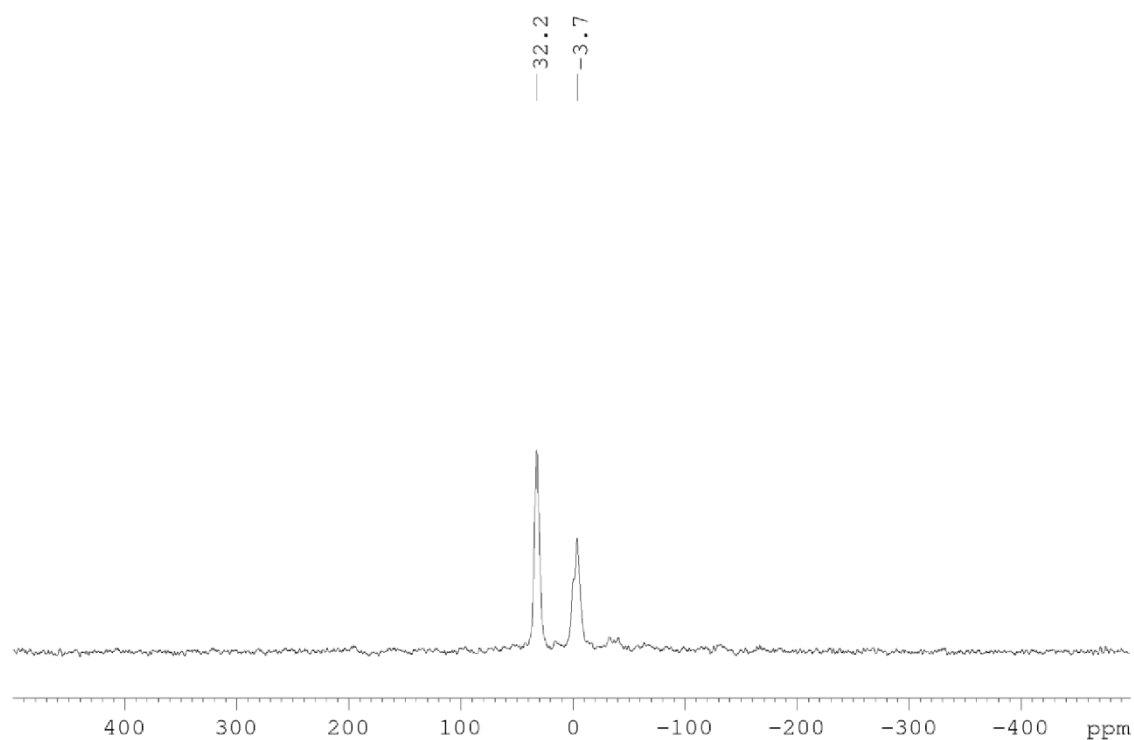


Figure S30: ^{29}Si CP/MAS NMR spectrum of **8**.

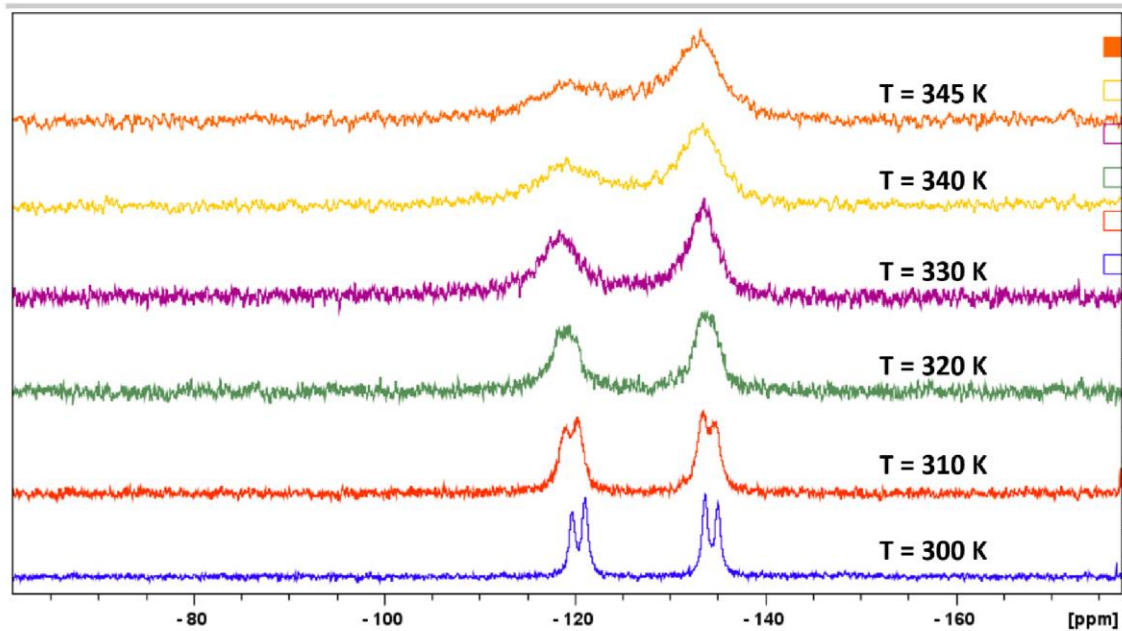


Figure S31: Selected section of $^{31}\text{P}\{^1\text{H}\}$ NMR spectra of **8** in C_6D_6 at six different temperatures ($T = 300 - 345$ K).

Si_4P_2 isomer **9** (m.p. $>220^\circ\text{C}$):

^1H NMR (400.13 MHz, thf-d_8 , 300K): $\delta = 7.09$ (s, 4H, Tip-*H*), 6.95, 6.73, 6.59, 6.39 (each s, each 2H, Tip-*H*), 5.39 (br. sept, 2H, Tip-*Pr-CH*), 4.91, 4.34, 3.76 (each sept, each 2H, Tip-*Pr-CH*), 3.62 – 3.56 (m, Tip-*Pr-CH* overlapping with thf-d_8), 2.86 (br. sept, 2H, Tip-*Pr-CH*), 2.74 – 2.64 (m, 6H, Tip-*Pr-CH*), 1.95 (d, 6H, Tip-*Pr-CH}_3*), 1.74 (br d, Tip-*Pr-CH}_3* overlapping with thf-d_8), 1.50 (d, 6H, Tip-*Pr-CH}_3*), 1.43 (t, 12H, Tip-*Pr-CH}_3*), 1.33 (d, 6H, Tip-*Pr-CH}_3*), 1.15 – 1.07 (m, 30H, Tip-*Pr-CH}_3*), 0.87 (d, 6H, Tip-*Pr-CH}_3*), 0.65 (d, 12H, Tip-*Pr-CH}_3*), 0.56, 0.38, -0.32 (each d, each 6H, Tip-*Pr-CH}_3*).

^{13}C NMR (100.6 MHz, thf-d_8 , 300K): $\delta = 158.6, 157.5, 157.3, 156.3, 156.2, 156.1, 150.4, 150.2, 149.9$ (each s, Tip-*C*), 130.7 (t, $^2J_{\text{C-P}} = 7.34$ Hz, Tip-*C*), 128.5 (br, Tip-*C*), 128.4 (s, Tip-*C*), 128.3 (br, Tip-*C*), 128.1 (br, Tip-*C*), 128.0, 125.4, 124.1, 122.4, 121.4, 121.3, 121.3 (each s, Tip-*C*), 37.8 (Tip-*Pr-CH* and Tip-*Pr-CH}_3*), 36.9 (t, $^4J_{\text{C-P}} = 6.7$ Hz, Tip-*Pr-CH*), 36.5, 36.0, 34.8, 34.7 (each s, Tip-*Pr-CH* and Tip-*Pr-CH}_3*), 34.5, 34.4 (each br, Tip-*Pr-CH* and Tip-*Pr-CH}_3*), 34.2 (t, $^4J_{\text{C-P}} = 6.3$ Hz, Tip-*Pr-CH*), 32.7 (d, $^4J_{\text{C-P}} = 6.9$ Hz, Tip-*Pr-CH*), 30.9, 30.8, 30.7 (each br, Tip-*Pr-CH* and Tip-*Pr-CH}_3*), 30.5(s), 30.1(br), 28.0 (Tip-*Pr-CH* and Tip-*Pr-CH}_3*), 27.7 (t, $^4J_{\text{C-P}} = 4.7$ Hz, Tip-*Pr-CH*), 27.5, 27.0, 26.8, 25.7, 25.5, 25.3, 25.2, 24.8, 24.5, 23.9, 23.9, 23.9, 23.8, 23.6 (Tip-*Pr-CH* and Tip-*Pr-CH}_3*).

^{31}P NMR (162.0 MHz, thf-d_8 , 300K): $\delta = -182.9$.

^{29}Si NMR (79.5 MHz, thf-d_8 , 300K): $\delta = -83.6$ (dd, $J_{\text{Si-P}} = 73.2$ Hz, $J_{\text{Si-P}} = 21.8$ Hz), -91.4 (dd, $J_{\text{Si-P}} = 107.1$ Hz, $J_{\text{Si-P}} = 21.7$ Hz).

Elemental analysis: calculated for $\text{C}_{90}\text{H}_{138}\text{P}_2\text{Si}_2$: C, 77.52%; H, 9.98%; N, 0.00%. Found: C, 77.07%; H, 10.20%; N, 0.00

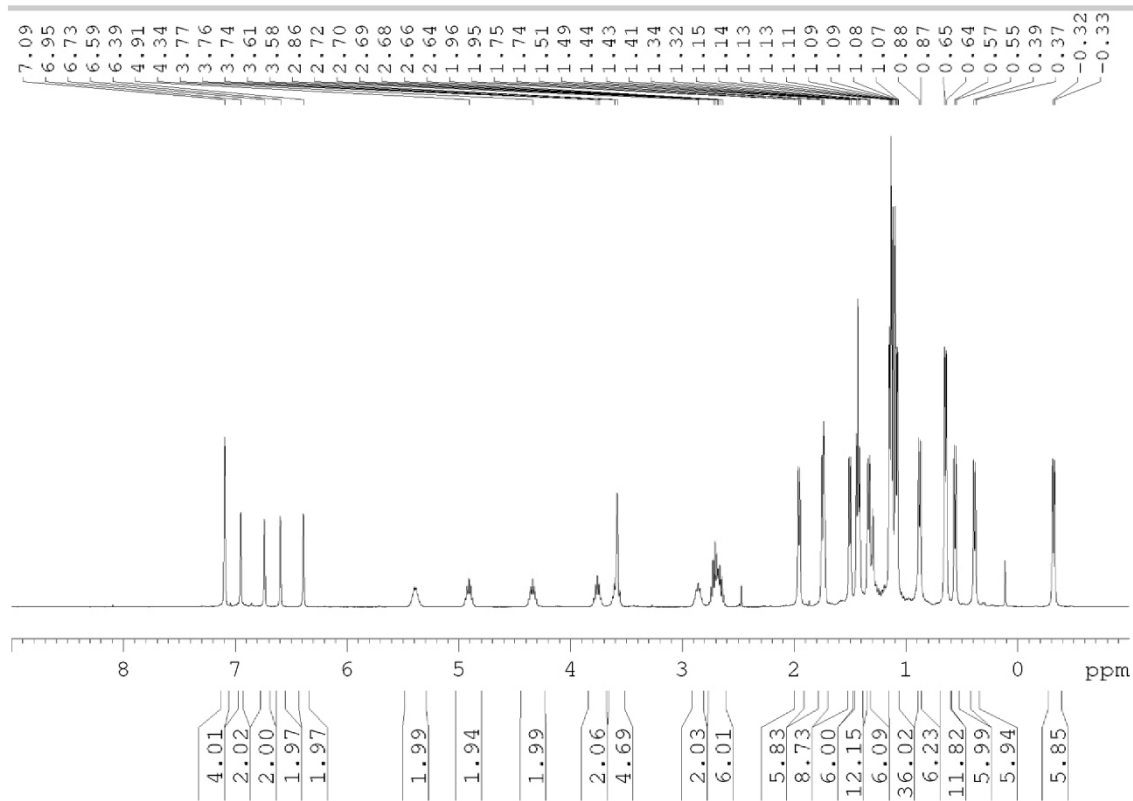


Figure S32: ¹H NMR spectrum of **9** in thf-d₈ at 300K.

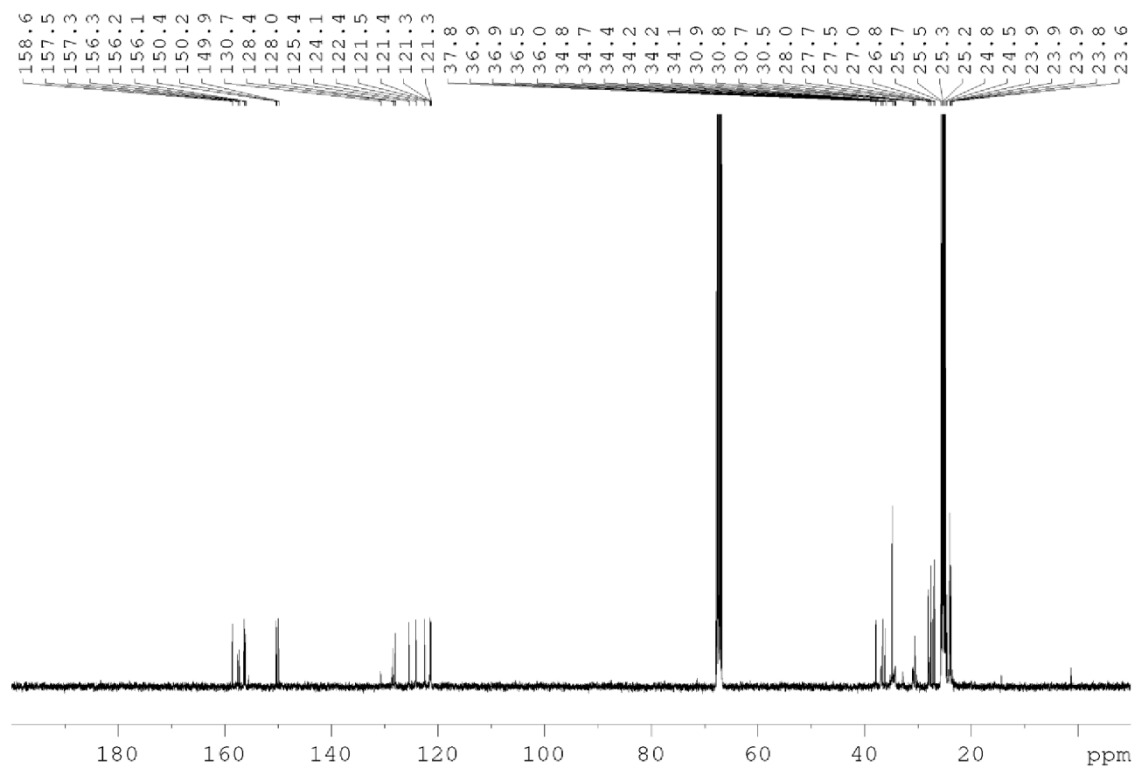


Figure S33: ¹³C NMR spectrum of **9** in thf-d₈ at 300K.

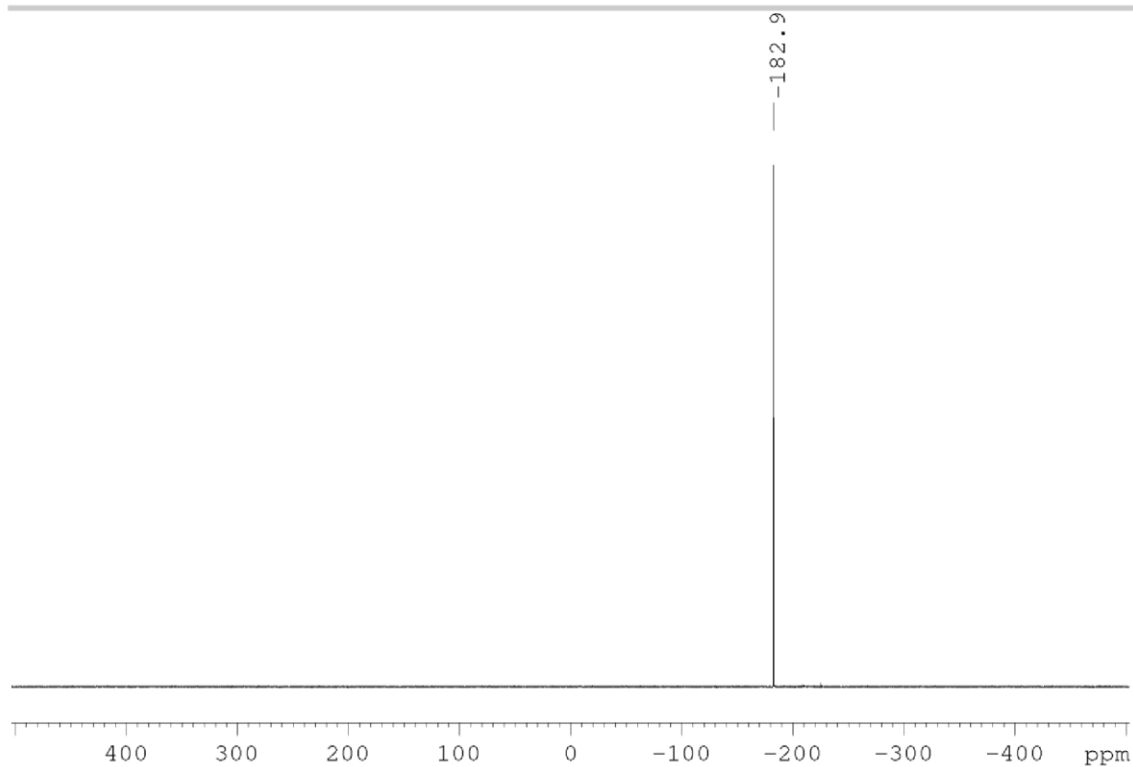


Figure S34: ^{31}P NMR spectrum of **9** in thf-d_8 at 300K.

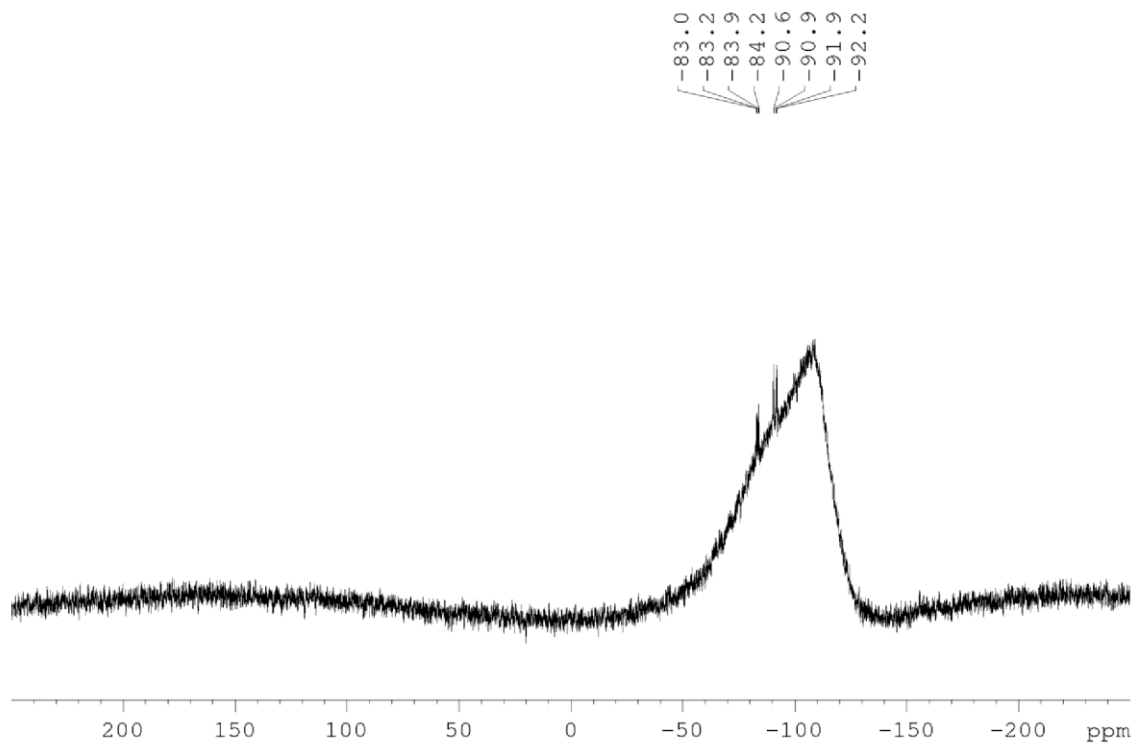


Figure S35: ^{29}Si NMR spectrum of **9** in thf-d_8 at 300K.

2. Details on X-ray Diffraction Studies**Table S1:** Crystal data and structure refinement for **5** (CCDC-1873591).

Identification code	sh3838	
Empirical formula	C ₅₆ H ₉₀ N ₂ P Si ₂	
Formula weight	874.41	
Temperature	152(2) K	
Wavelength	0.71073 Å	
Crystal system	Orthorhombic	
Space group	Pna2 ₁	
Unit cell dimensions	a = 19.4266(10) Å	a = 90°.
	b = 14.0309(7) Å	b = 90°.
	c = 19.8268(9) Å	g = 90°.
Volume	5404.2(5) Å ³	
Z	4	
Density (calculated)	1.075 Mg/m ³	
Absorption coefficient	0.131 mm ⁻¹	
F(000)	1916	
Crystal size	0.448 x 0.309 x 0.254 mm ³	
Theta range for data collection	1.778 to 26.509°.	
Index ranges	-24<=h<=24, -17<=k<=17, -21<=l<=24	
Reflections collected	70742	
Independent reflections	10500 [R(int) = 0.0595]	
Completeness to theta = 25.242°	100.0 %	
Absorption correction	Semi-empirical from equivalents	
Max. and min. transmission	0.7454 and 0.7044	
Refinement method	Full-matrix least-squares on F ²	
Data / restraints / parameters	10500 / 1 / 573	
Goodness-of-fit on F ²	1.018	
Final R indices [I>2sigma(I)]	R1 = 0.0448, wR2 = 0.0974	
R indices (all data)	R1 = 0.0674, wR2 = 0.1072	
Absolute structure parameter	0.03(3)	
Extinction coefficient	n/a	
Largest diff. peak and hole	0.528 and -0.325 e.Å ⁻³	

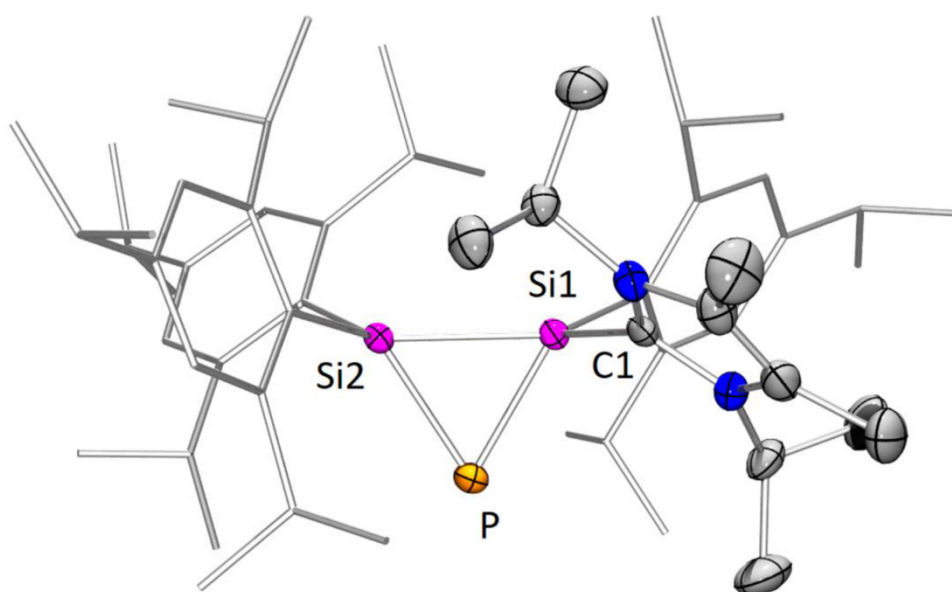


Figure S36: Molecular structure of **5** in the solid state (thermal ellipsoids at 50%, H atoms omitted); Selected bond lengths [Å] and angles [°]: Si1-C1 1.950(4), Si1-Si2 2.294(1), Si1-P 2.170(1), Si2-P 2.196(1), Si1-P-Si2 63.38(4).

Table S2: Crystal data and structure refinement for **6** (CCDC-1873592).

Identification code	sh3639	
Empirical formula	C ₆₀ H ₈₉ Fe N ₂ O ₄ P Si ₂ x 0.5(C ₆ H ₆)	
Formula weight	1084.38	
Temperature	122(2) K	
Wavelength	0.71073 Å	
Crystal system	Monoclinic	
Space group	P2 ₁ /n	
Unit cell dimensions	a = 13.7347(6) Å	a = 90°.
	b = 21.3829(10) Å	b = 100.853(3)°.
	c = 21.3318(10) Å	g = 90°.
Volume	6152.8(5) Å ³	
Z	4	
Density (calculated)	1.171 Mg/m ³	
Absorption coefficient	0.356 mm ⁻¹	
F(000)	2340	
Crystal size	0.755 x 0.664 x 0.204 mm ³	
Theta range for data collection	1.361 to 30.209°.	
Index ranges	-19<=h<=18, -30<=k<=27, -30<=l<=30	
Reflections collected	74588	
Independent reflections	18245 [R(int) = 0.0347]	
Completeness to theta = 25.242°	100.0 %	
Absorption correction	Semi-empirical from equivalents	
Max. and min. transmission	0.7460 and 0.6726	
Refinement method	Full-matrix least-squares on F ²	
Data / restraints / parameters	18245 / 271 / 811	
Goodness-of-fit on F ²	1.013	
Final R indices [I>2sigma(I)]	R1 = 0.0401, wR2 = 0.0956	
R indices (all data)	R1 = 0.0604, wR2 = 0.1066	
Extinction coefficient	n/a	
Largest diff. peak and hole	0.903 and -0.773 e.Å ⁻³	

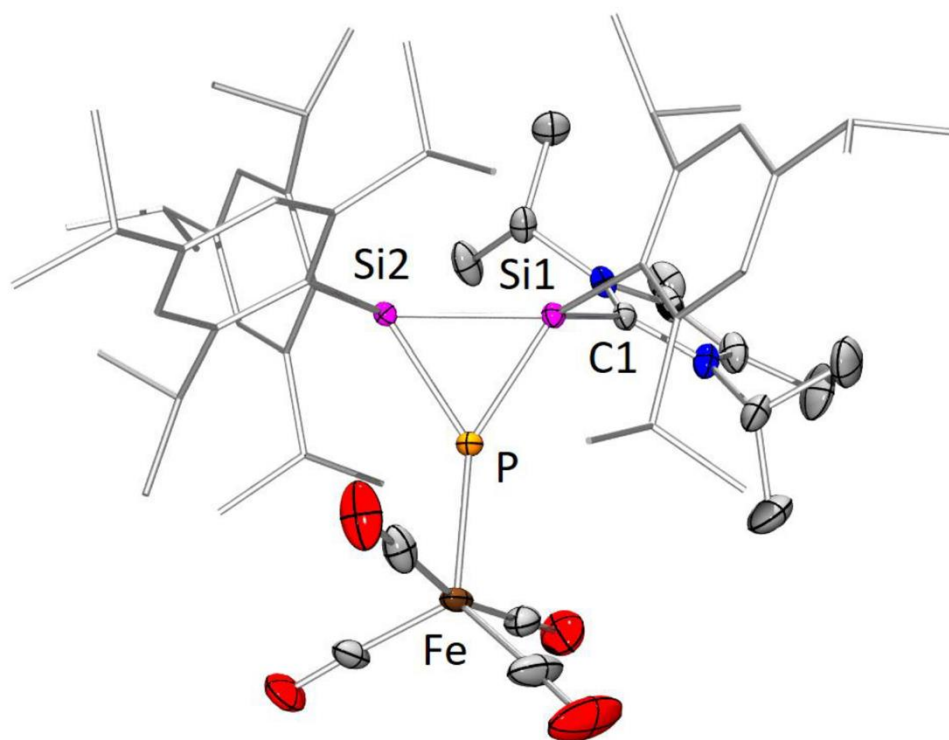


Figure S37: Molecular structure of **6** in the solid state (thermal ellipsoids at 50%, H atoms omitted); Selected bond lengths [Å]: Si1-C1 1.954(1), Si1-Si2 2.3755(5), Si1-P 2.1635(5), Si2-P 2.1838(5), P-Fe 2.2874(4), Si1-P-Si2 66.243(16).

Table S3: Crystal data and structure refinement for **7** (CCDC-1873593).

Identification code	sh3686	
Empirical formula	C ₅₉ H ₈₉ Fe N ₂ O ₃ P Si ₂	
Formula weight	1017.32	
Temperature	183(2) K	
Wavelength	0.71073 Å	
Crystal system	Monoclinic	
Space group	P2 ₁ /c	
Unit cell dimensions	a = 14.1247(13) Å	a = 90°.
	b = 15.5571(13) Å	b = 96.399(4)°.
	c = 26.3640(17) Å	g = 90°.
Volume	5757.1(8) Å ³	
Z	4	
Density (calculated)	1.174 Mg/m ³	
Absorption coefficient	0.375 mm ⁻¹	
F(000)	2200	
Crystal size	0.442 x 0.366 x 0.100 mm ³	
Theta range for data collection	1.451 to 26.553°.	
Index ranges	-17 ≤ h ≤ 17, 0 ≤ k ≤ 19, 0 ≤ l ≤ 33	
Reflections collected	19997	
Independent reflections	19997 [R(int) = 0]	
Completeness to theta = 25.242°	94.3 %	
Absorption correction	Semi-empirical from equivalents	
Max. and min. transmission	0.7454 and 0.6237	
Refinement method	Full-matrix least-squares on F ²	
Data / restraints / parameters	19997 / 0 / 638	
Goodness-of-fit on F ²	1.022	
Final R indices [I > 2σ(I)]	R1 = 0.0456, wR2 = 0.1156	
R indices (all data)	R1 = 0.0734, wR2 = 0.1308	
Extinction coefficient	n/a	
Largest diff. peak and hole	0.366 and -0.262 e.Å ⁻³	

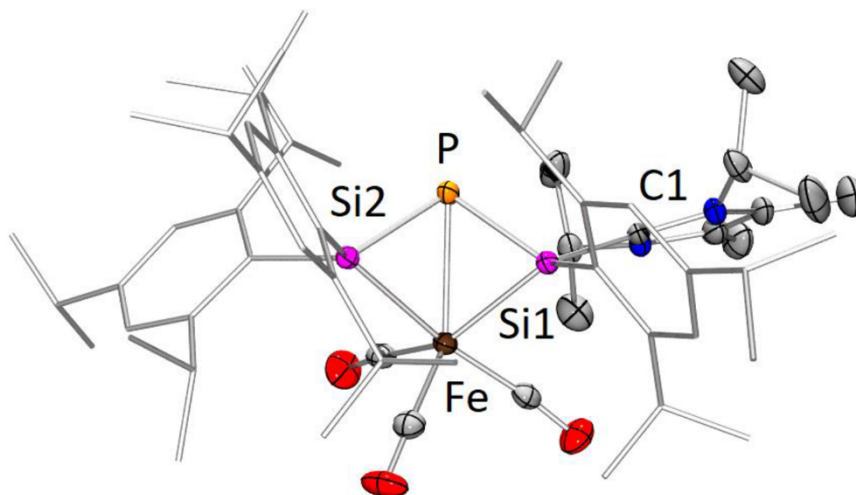


Figure S38: Molecular structure of **7** in the solid state (thermal ellipsoids at 50%, H atoms omitted); Selected bond lengths [Å]: Si1-C1 1.990(3), Si1-P 2.173(1), Si2-P 2.214(1), P-Fe 2.4981(8), Si1-Fe 2.3342(9), Si2-Fe 2.3958(9).

Table S4: Crystal data and structure refinement for **8** (CCDC-1873594).

Identification code	sh3933	
Empirical formula	C ₉₀ H ₁₃₈ P ₂ Si ₄	
Formula weight	1394.30	
Temperature	293(2) K	
Wavelength	0.71073 Å	
Crystal system	Orthorhombic	
Space group	P2 ₁ 2 ₁ 2 ₁	
Unit cell dimensions	a = 15.3043(9) Å	a = 90°.
	b = 21.7280(13) Å	b = 90°.
	c = 25.7918(15) Å	g = 90°.
Volume	8576.6(9) Å ³	
Z	4	
Density (calculated)	1.080 Mg/m ³	
Absorption coefficient	0.148 mm ⁻¹	
F(000)	3056	
Crystal size	0.316 x 0.178 x 0.156 mm ³	
Theta range for data collection	1.547 to 26.439°.	
Index ranges	-15<=h<=19, -27<=k<=27, -32<=l<=32	
Reflections collected	127326	
Independent reflections	17637 [R(int) = 0.1077]	
Completeness to theta = 25.242°	100.0 %	
Absorption correction	Semi-empirical from equivalents	
Max. and min. transmission	0.8620 and 0.7815	
Refinement method	Full-matrix least-squares on F ²	
Data / restraints / parameters	17637 / 213 / 1012	
Goodness-of-fit on F ²	1.005	
Final R indices [I>2sigma(I)]	R1 = 0.0567, wR2 = 0.1013	
R indices (all data)	R1 = 0.1237, wR2 = 0.1217	
Absolute structure parameter	0.00(4)	
Extinction coefficient	n/a	
Largest diff. peak and hole	0.312 and -0.223 e.Å ⁻³	

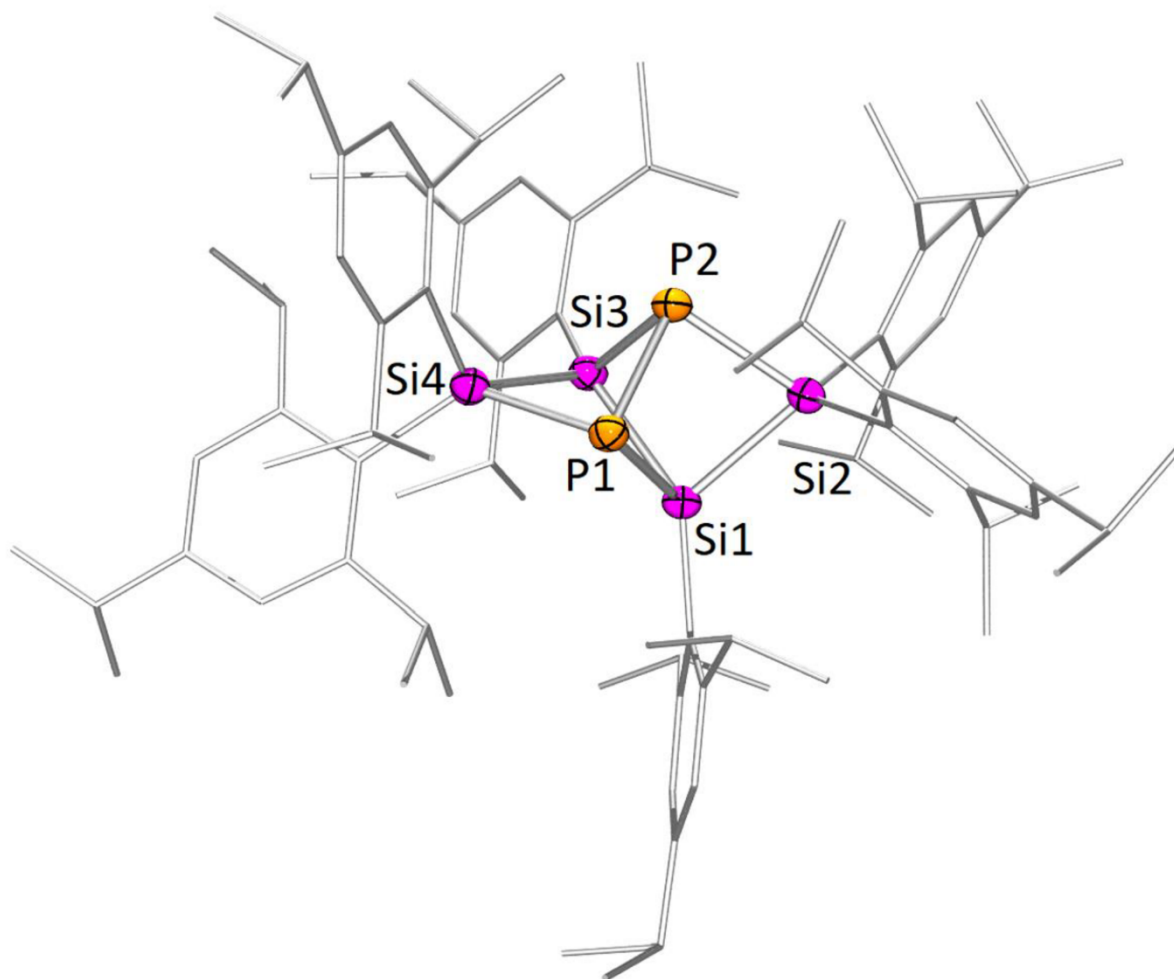


Figure S39: Molecular structure of **8** in the solid state (thermal ellipsoids at 50%, H atoms omitted); Selected bond lengths [Å] and angles [°]: P1-P2 2.243(1), P1-Si1 2.281(1), P1-Si4 2.3000(1), Si1-Si3 2.462(1), Si1-Si2 2.354(1), P1-Si4-Si3 76.12 (6), P2-P1-Si1 79.48(6), Si1-Si2-P2 76.83 (6).

Table S5: Crystal data and structure refinement for **9** (CCDC-1873595).

Identification code	sh4022	
Empirical formula	C ₉₀ H ₁₃₈ P ₂ Si ₄ , 2(C ₆ H ₆)	
Formula weight	1550.51	
Temperature	152(2) K	
Wavelength	0.71073 Å	
Crystal system	Triclinic	
Space group	P-1	
Unit cell dimensions	a = 12.4771(5) Å	a = 117.207(2)°.
	b = 14.7860(6) Å	b = 109.700(3)°.
	c = 16.1308(9) Å	g = 91.332(2)°.
Volume	2435.2(2) Å ³	
Z	1	
Density (calculated)	1.057 Mg/m ³	
Absorption coefficient	0.137 mm ⁻¹	
F(000)	848	
Crystal size	0.527 x 0.358 x 0.216 mm ³	
Theta range for data collection	1.542 to 35.871°.	
Index ranges	-20<=h<=20, -24<=k<=24, -26<=l<=26	
Reflections collected	88095	
Independent reflections	22714 [R(int) = 0.0447]	
Completeness to theta = 25.242°	100.0 %	
Absorption correction	Semi-empirical from equivalents	
Max. and min. transmission	0.7470 and 0.7112	
Refinement method	Full-matrix least-squares on F ²	
Data / restraints / parameters	22714 / 72 / 535	
Goodness-of-fit on F ²	1.035	
Final R indices [I>2sigma(I)]	R1 = 0.0530, wR2 = 0.1427	
R indices (all data)	R1 = 0.0824, wR2 = 0.1610	
Extinction coefficient	n/a	
Largest diff. peak and hole	0.999 and -0.580 e.Å ⁻³	

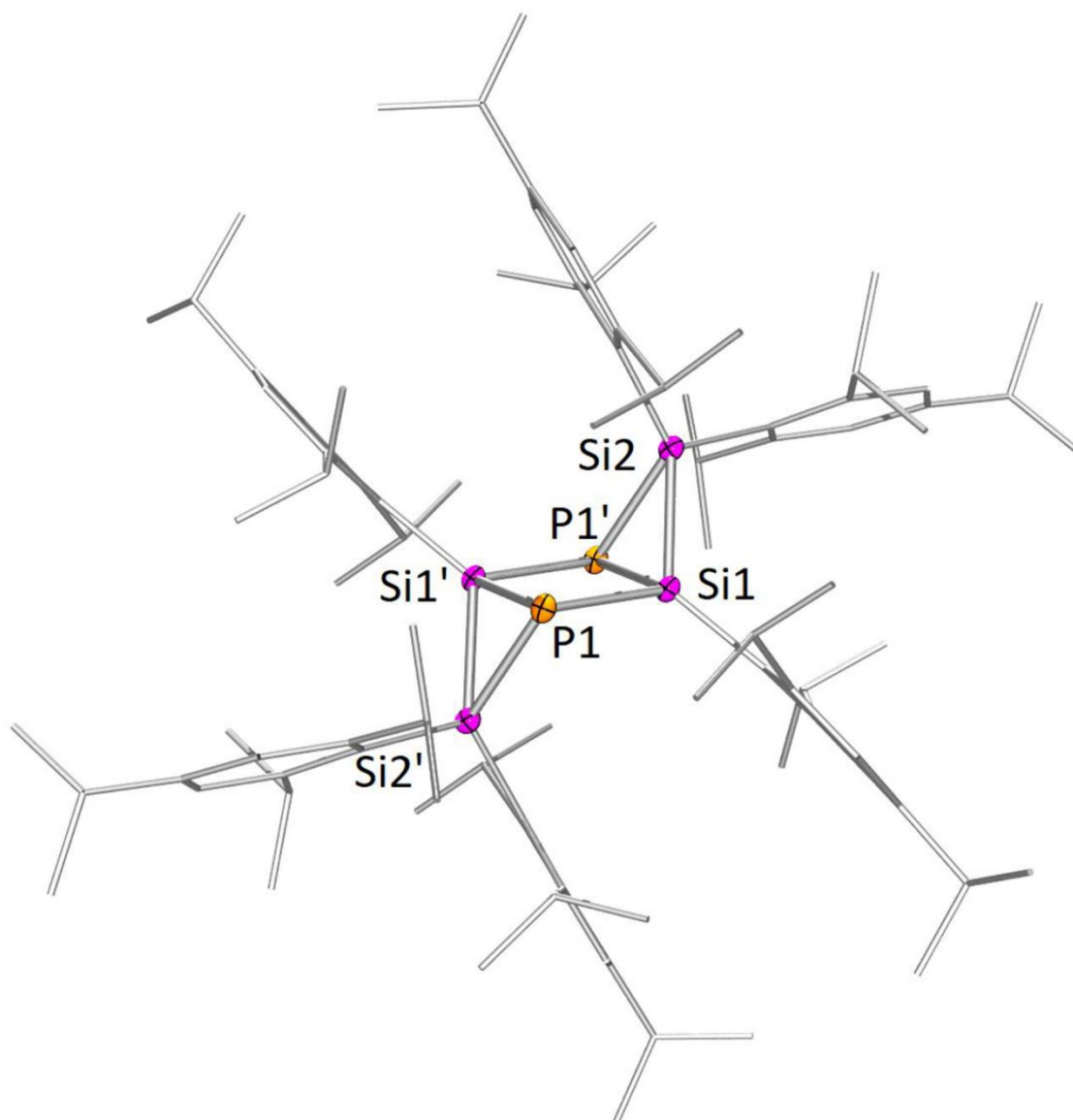


Figure S40: Molecular structure of **9** in the solid state (thermal ellipsoids at 50%, H atoms omitted); Selected bond lengths [Å] and angles [°]: P1-Si1 2.2372(4), P1-Si2' 2.3002(4), P1-Si1' 2.3210(4), Si1-Si2 2.3008(4), Si1-Si2-P1' 60.59(1), P1-Si1-P1' 97.56(1), Si1-P1-Si1' 82.44(1).

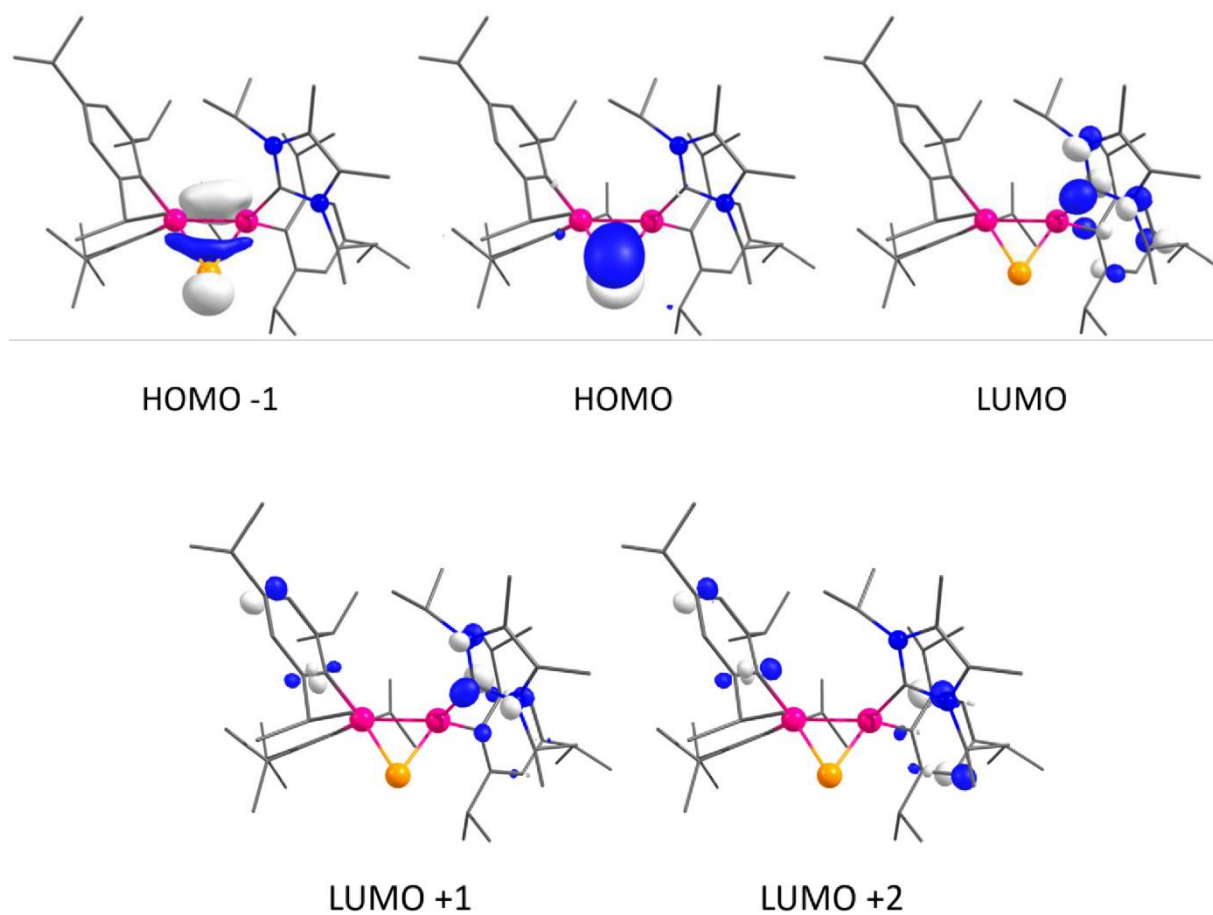
3. Details on theoretical calculations

Figure S41: Selected Kohn-Sham orbitals of **5** (isocontour value 0.07465; calculated on the (M06-ZX(D3)/def2-TZVPP//BP86(D3)/def2-SVP) level of theory).

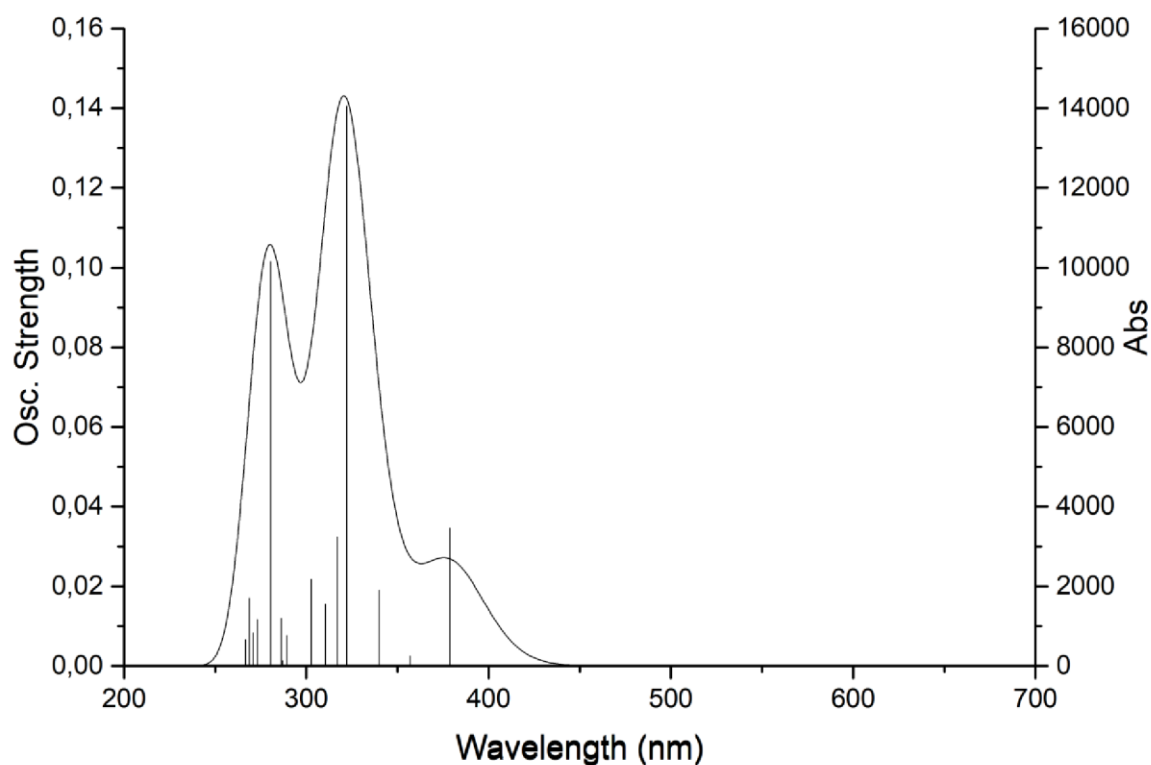


Figure S42: Calculated transitions (vertical bars) and simulated UV/Vis absorption spectrum of **5** (level of theory: (M06-2X(D3)/def2-TZVPP//BP86(D3)/def2-SVP)).

Table S6: Selected electronic transitions and optical parameters of the theoretical calculations of **5**.

Transition No.	Wavelength (nm)	Osc. Strength	Transitions with major contributions
1	378,7627	0,0346	HOMO->LUMO (49%), HOMO->L+1 (38%)
4	322,1205	0,1405	H-1->LUMO (27%), H-1->L+1 (43%), HOMO->L+2 (11%)
11	280,4374	0,1016	H-1->L+4 (29%), H-1->L+5 (12%), H-1->L+9 (20%)

3. References

- [1] D. Scheschkewitz, *Angew. Chem. Int. Ed.* **2004**, *43*, 2965–2967; *Angew. Chem.* **2004**, *116*, 3025-3028
- [2] B. D. Ellis, C. A. Dyker, A. Decken, C. L. B. Macdonald, *Chem. Commun.* **2005**, 1965.

4. Author Contributions

Y.H., P.W. and D.M. performed the synthetic work and data analysis, L.K. performed the theoretical calculations, V.H. performed the X-ray diffraction studies, M.Z. performed the VT-NMR studies, Y.H. and D.S. wrote the manuscript. D.S. conceived and coordinated the study.

6.3. Boron and Phosphorus Containing Heterosiliconoids: Stable p- and n-Doped Unsaturated Silicon Clusters (SI)

Boron and phosphorus containing heterosiliconoids: stable p- and n-doped unsaturated silicon clusters

Yannic Heider, Philipp Willmes, Volker Huch, Michael Zimmer, David Scheschkewitz*

Krupp-Chair for General and Inorganic Chemistry, Saarland University, 66123 Saarbrücken (Germany),

Supporting Information

Supporting Information

Table of Contents

1. General	S3
2. Experimental procedures, data and plots of spectra of:	S3
2.1. 2,3,3,4-Tetrakis(2,4,6-triisopropylphenyl)tricyclo[2.1.0.0 ^{2,5}]penta- silan-1,5-diyl)lithium (4)	S3
2.2. 2,3,3,4-Tetrakis(2,4,6-triisopropylphenyl)-1,5- bis(trimethylsilyl)tricyclo[2.1.0.0 ^{2,5}]pentasilane (7)	S10
2.3. <i>N,N</i> -Diisopropyl-4,5,5,6-tetrakis(2,4,6-triisopropylphenyl)-1,3,4,5,6-penta- sila-2-boratetracyclo[2.2.0.0 ^{1,3} .0 ^{3,6}]hexan-2-amine (8)	S13
2.4. <i>N,N</i> -Diisopropyl-4,5,5,6-tetrakis(2,4,6-triisopropylphenyl)-2-phospha- 1,3,4,5,6-pentasilatetracyclo[2.2.0.0 ^{1,3} .0 ^{3,6}]hexan-2-amine (9)	S17
3. Details on X-ray Diffraction Studies	S25
4. Computational Details	S35
5. References	S85

1. General

All manipulations were carried out under a protective atmosphere of argon, using Schlenk techniques or a glove box. Benzene was refluxed over sodium/benzophenone for purification. All other solvents used were purified by a PureSolvMD5 solvent purification system by Innovative Technology. Deuterated benzene (C_6D_6) and toluene- d_8 were refluxed over potassium, then distilled and stored under argon. Tetrahydrofuran- d_8 was refluxed over Na/K alloy, then distilled and stored under argon. UV/Vis spectra were acquired using a Shimadzu UV-2600 spectrometer and quartz cells with a path length of 0.1 cm. NMR spectra were recorded on a Bruker Avance III 300 MHz and/or a Bruker Avance III HD 400 MHz spectrometer. Solid-state NMR spectra were recorded on a Bruker AV400WB spectrometer. Elemental analyses were carried out with an elementar vario Micro Cube. Siliconoid **2** was prepared according to our published procedure. Me_3SiCl and $^iPr_2N-BCl_2$ were purchased from Sigma Aldrich and distilled prior to use. $^iPr_2N-PCl_2$ was prepared according to a literature known procedure.^[1]

2. Experimental procedures, data and plots of spectra of:

2.1. 2,3,3,4-Tetrakis(2,4,6-triisopropylphenyl)tricyclo[2.1.0.0^{2,5}]pentasilan-1,5-diyl)lithium (**4**)

To a suspension of 3.28 g (2,36 mmol) of perarylated hexasilabenzpolarene **2** in 30 mL of Et_2O , 20 mL of a $Li/C_{10}H_8$ solution in thf (0.53 M) are added at $-78^\circ C$. The resulting reaction mixture is allowed to slowly warm to room temperature overnight with vigorous stirring. All volatiles are removed in vacuum. The solid residue is dissolved in toluene, filtered and the solvent distilled off in vacuum. The residue is then digested with hexane and subsequently dried again under reduced pressure. Most naphthalene is removed by sublimation at $50^\circ C$ in vacuum. The crude product is washed with a hexane-benzene mixture (3:1). 1.92 g (69%) of the Si_5 dianion **4**

precipitates from hexane as ochre to olive coloured microcrystalline powder with variable residual amounts of naphthalene and 1,3,5-triisopropylbenzene. Single crystals suitable for an X-ray diffraction study were grown from a hexane/toluene solution after 3 days at r.t. Higher quality single crystals for X-ray diffraction studies were obtained after several weeks from a highly diluted hexane solution.

(**m.p.** > 220°C, dec.).

The dianion **4** is also accessible by reduction of the monoanionic siliconoid *privo-3* with 2.2 equivalents of a Li/C₁₀H₈ solution in thf. The experimental procedure used is similar to the one described above. Quantities: *privo-3*: 189.5 mg (0.14 mmol); Li/C₁₀H₈: 0.58 mL (0.52 M, 0.30 mmol).

¹H NMR (300.13 MHz, C₆D₆, 300K): δ = 7.64 – 7.61 (m, 2H, C₁₀H₈), 7.31 (d, 2H, Tip-*H*), 7.27 – 7.24 (m, 2H, C₁₀H₈), 6.99 (s, 0.5H, residual TipH = 1,3,5-Triisopropylbenzene), 6.93 (d, 2H, Tip-*H*), 6.86 (d, 2H, Tip-*H*), 6.83 (d, 2H, Tip-*H*), 5.30 (sept, 2H, Tip-*i*Pr-*CH*), 4.95 (sept, 2H, Tip-*i*Pr-*CH*), 4.62 (sept, 2H, Tip-*i*Pr-*CH*), 3.69 (br, 6H, thf), 3.24 (sept, 2H, Tip-*i*Pr-*CH*), 2.86 to 2.69 (m, 4.5H, Tip-*i*Pr-*CH* and residual TipH), 2.10 (d, 6H, Tip-*i*Pr-*CH*₃), 1.65 (d, 6H, Tip-*i*Pr-*CH*₃), 1.54 (d, 6H, Tip-*i*Pr-*CH*₃), 1.45 (br, 6H, thf), 1.39 (d, 6H, Tip-*i*Pr-*CH*₃), 1.25 (d, 21H, Tip-*i*Pr-*CH*₃ and residual TipH), 1.18 (d, 6H, Tip-*i*Pr-*CH*₃), 0.74 (br d, 6H, Tip-*i*Pr-*CH*₃), 0.67 – 0.61 (m, 12H, Tip-*i*Pr-*CH*₃), 0.37 (d, 6H, Tip-*i*Pr-*CH*₃).

¹³C NMR (100.6 MHz, C₆D₆, 300K): δ = 157.9, 154.8, 152.6, 151.9, 149.1, 148.7, 147.8, 142.3, 134.1 (Tip-*C* and Tip-*CH*), 133.7, 128.2, 126.1 (C₁₀H₈), 122.4 122.3, 122.2, 121.2, 120.6 (Tip-*C* and Tip-*CH*), 69.8 (thf), 36.5, 36.4, 35.1, 34.8, 34.8, 34.7, 34.1 (Tip-*i*Pr-*CH* and Tip-*i*Pr-*CH*₃) 32.0 (hexane), 29.8, 29.6 (Tip-*i*Pr-*CH* and Tip-*i*Pr-*CH*₃), 27.9 (thf), 25.6, 25.2, 24.9, 24.6, 24.5, 24.4, 24.2, 24.0, 23.8 (Tip-*i*Pr-*CH* and Tip-*i*Pr-*CH*₃), 23.1 (hexane), 22.4 (Tip-*i*Pr-*CH* and Tip-*i*Pr-*CH*₃), 14.4 (hexane).

²⁹Si NMR (79.5 MHz, C₆D₆, 300K): δ = 55.7 (*S*/Tip₂), -90.1 (*S*/Tip), -298.3 (*S*).

²⁹Si CP/MAS NMR (79.5 MHz, 13kHz): δ = 42.5 (*S*/Tip₂), -100.5 (*S*/Tip), -290.6 (*S*).

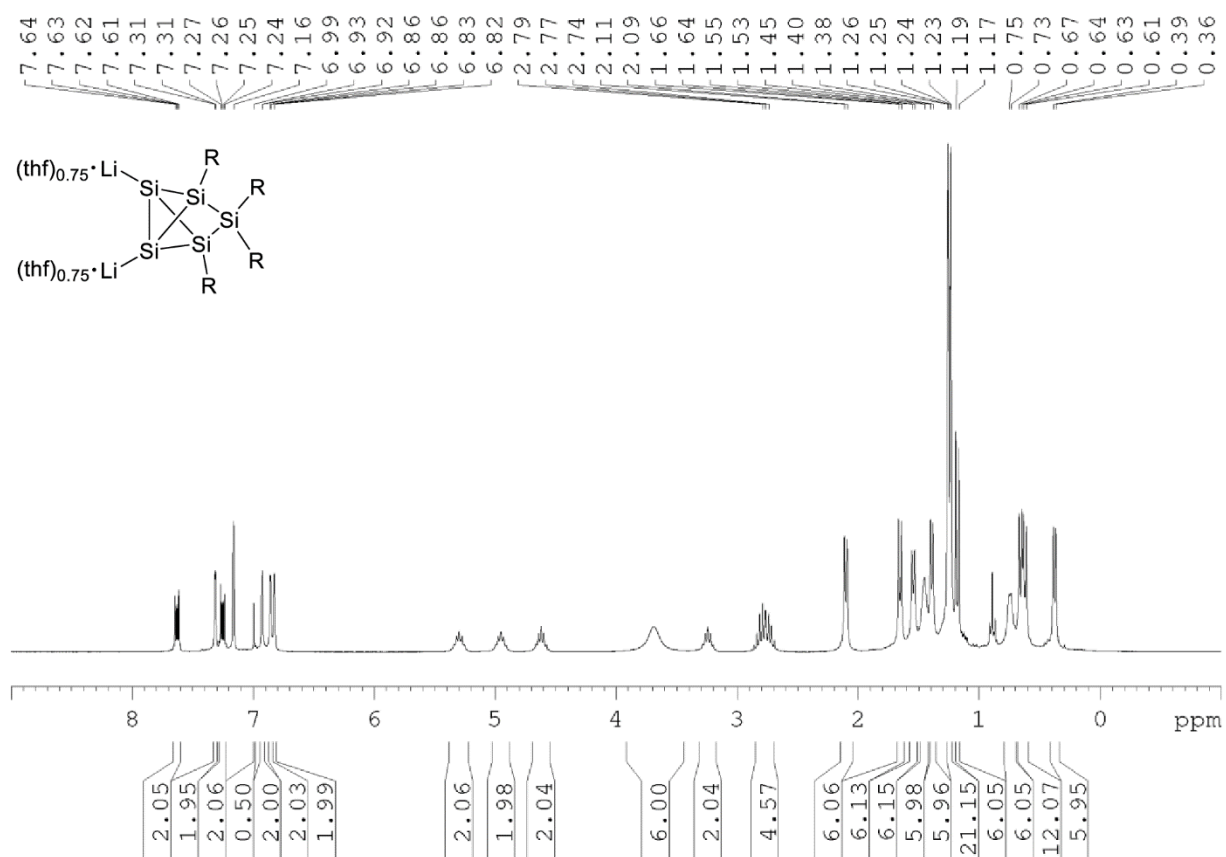
⁷Li NMR (116.6 MHz, C₆D₆, 300K): δ = 3.74 (br).

⁷Li{¹H} CP/MAS NMR (155.6 MHz, 13kHz): δ = 5.80, 2.28, -0.57.

UV/Vis (hexane): broad shoulders from $\lambda_{\text{max}} = 340 - 390$ nm and $\lambda_{\text{max}} = 260 - 285$ nm.

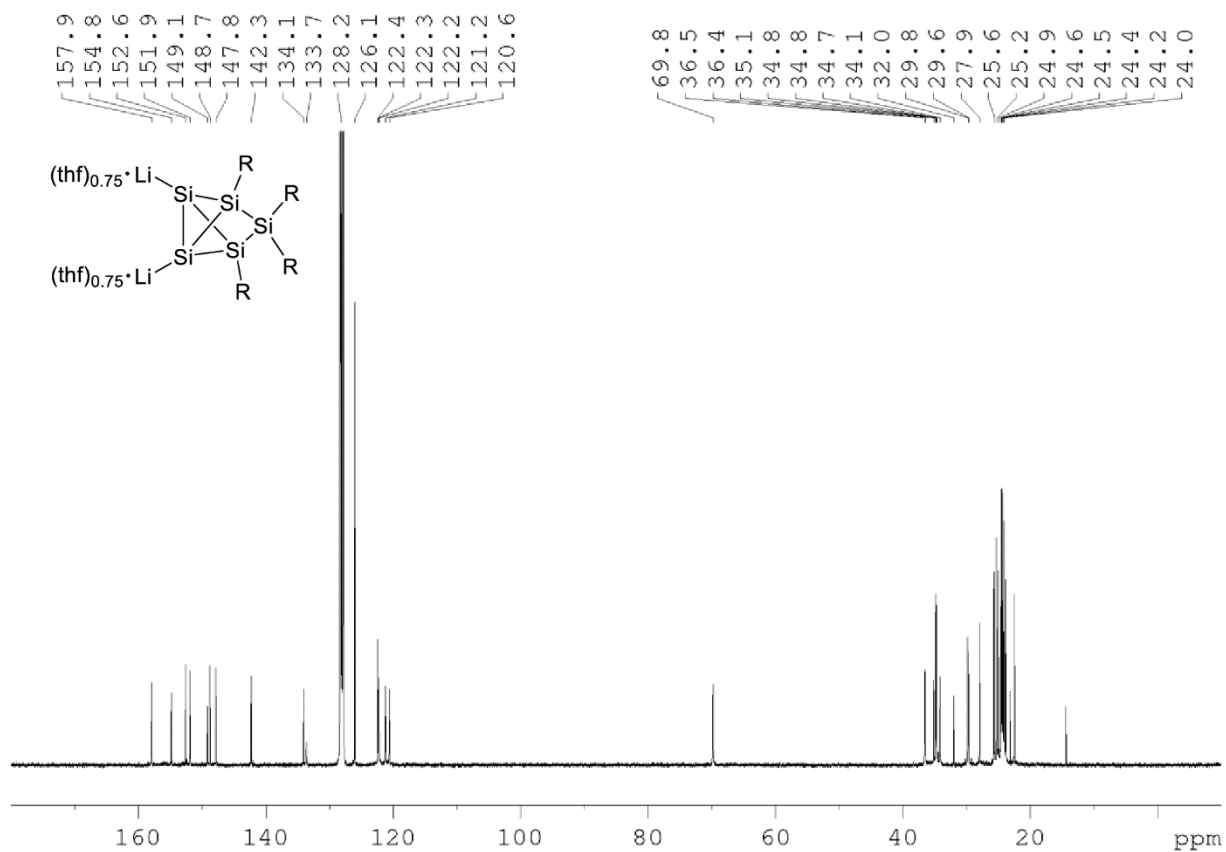
Elemental analysis: calculated for C₆₆H₁₀₄Li₂O_{1.5}Si₅: C, 73.68%; H, 9.74%; N, 0 %. Found: C, 73.33; H, 9.32; N, 0.

6. Supporting Information

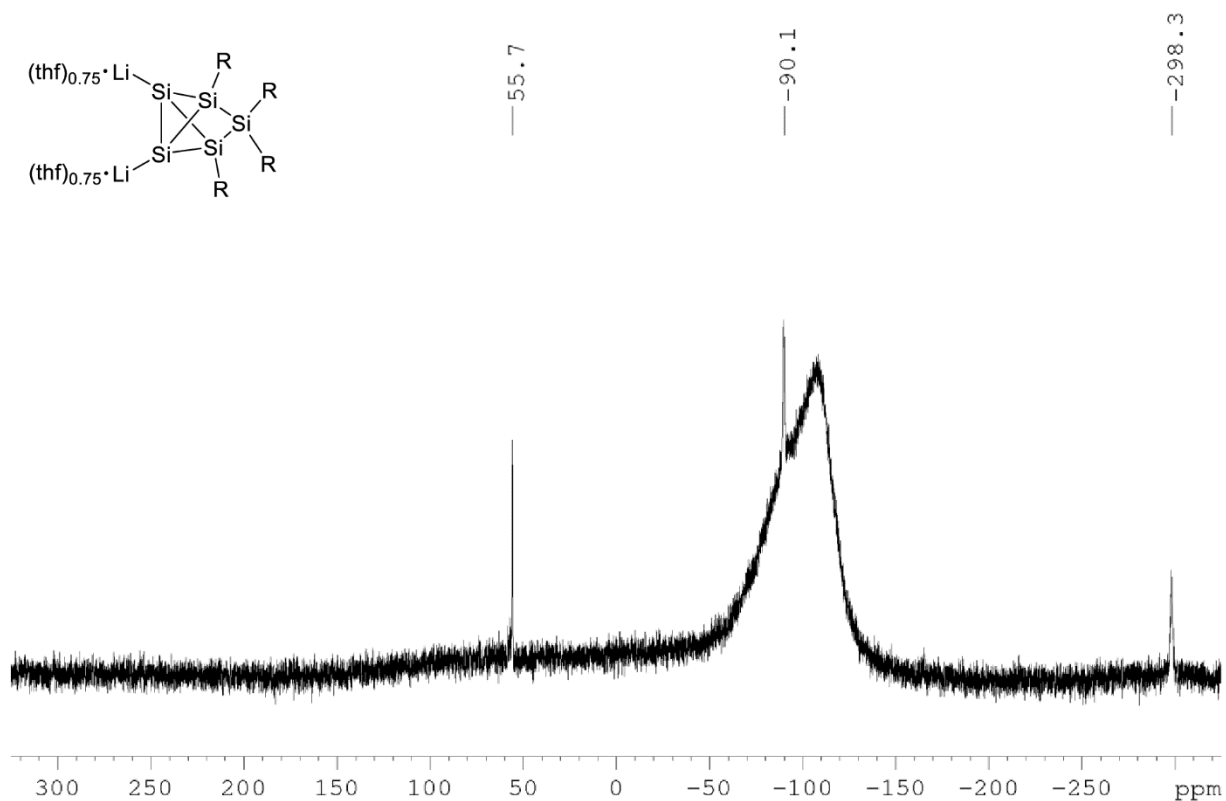


Supplementary Figure 1: ^1H NMR spectrum of 4 in C_6D_6 at 300 K.

6. Supporting Information

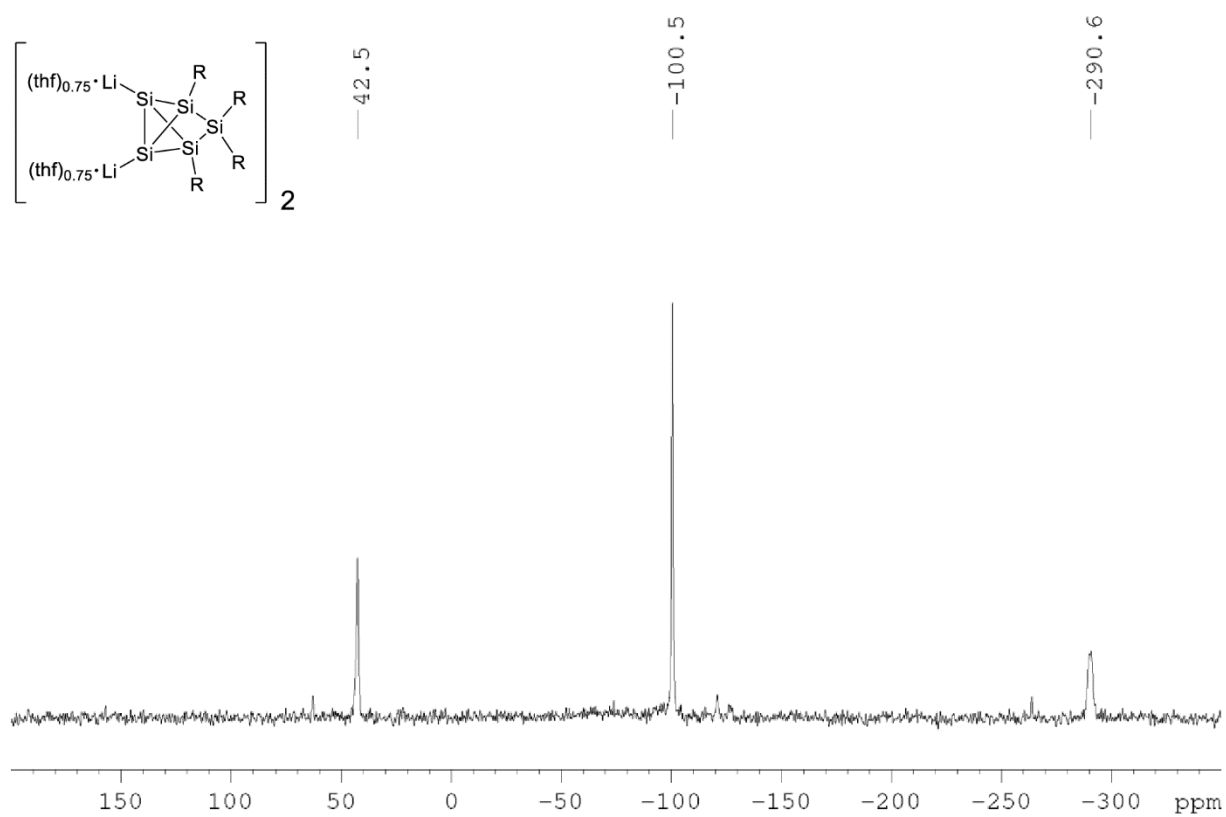


Supplementary Figure 2: ^{13}C NMR spectrum of **4** in C_6D_6 at 300 K.

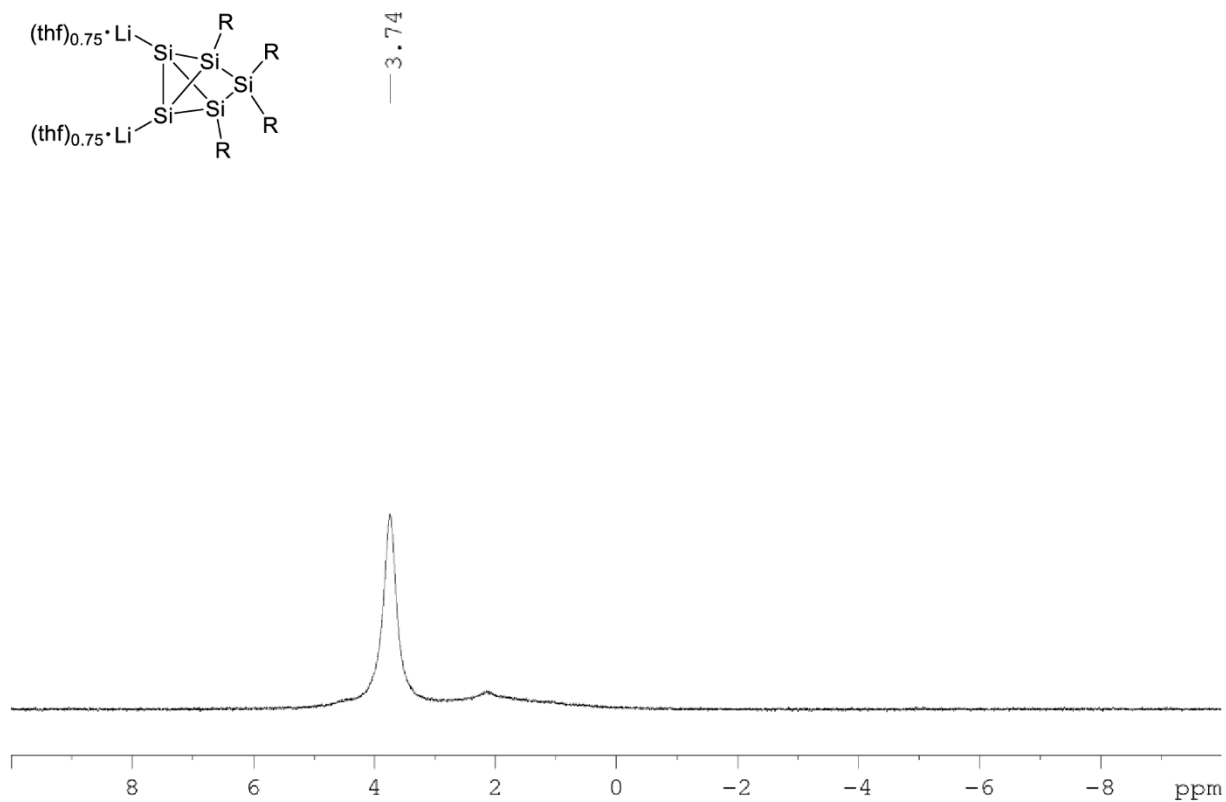


Supplementary Figure 3: ^{29}Si NMR spectrum of **4** in C_6D_6 at 300 K.

6. Supporting Information

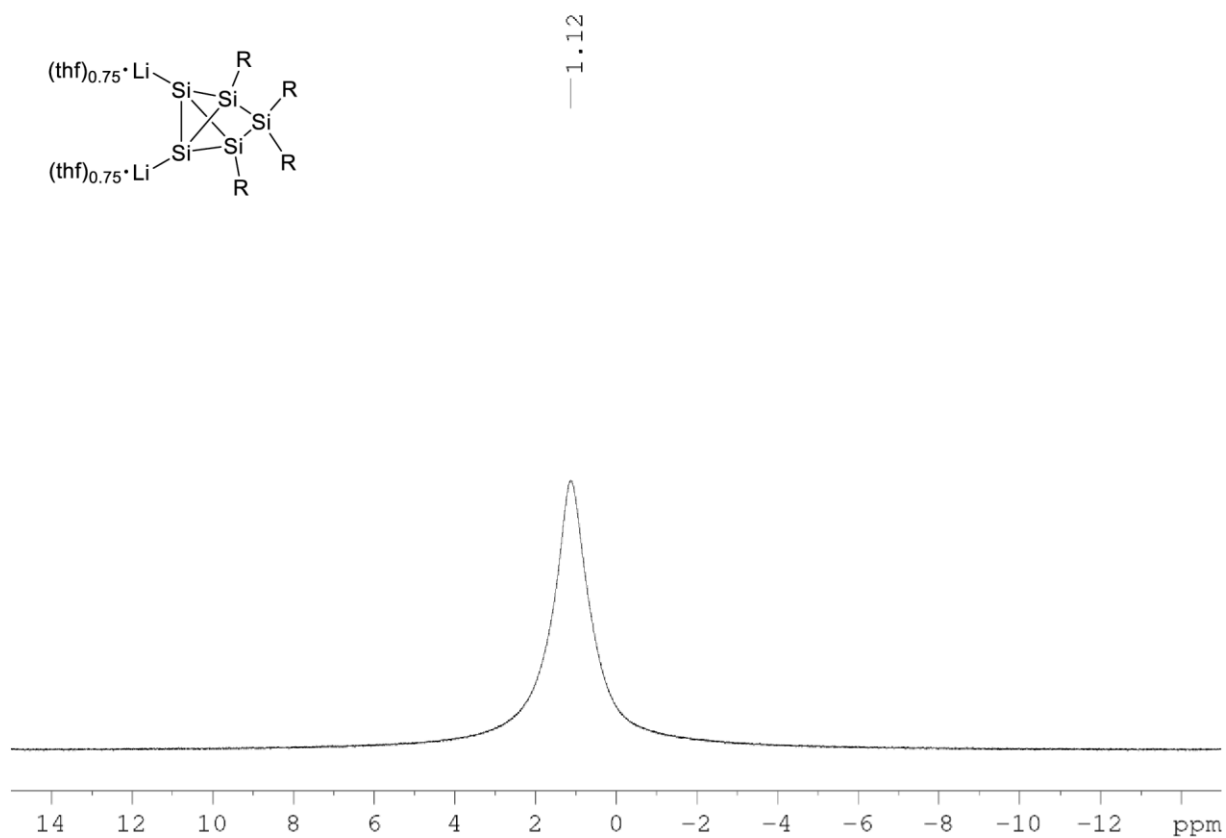


Supplementary Figure 4: ^{29}Si CP/MAS NMR spectrum of $[4]_2 \cdot (THF)_3$.

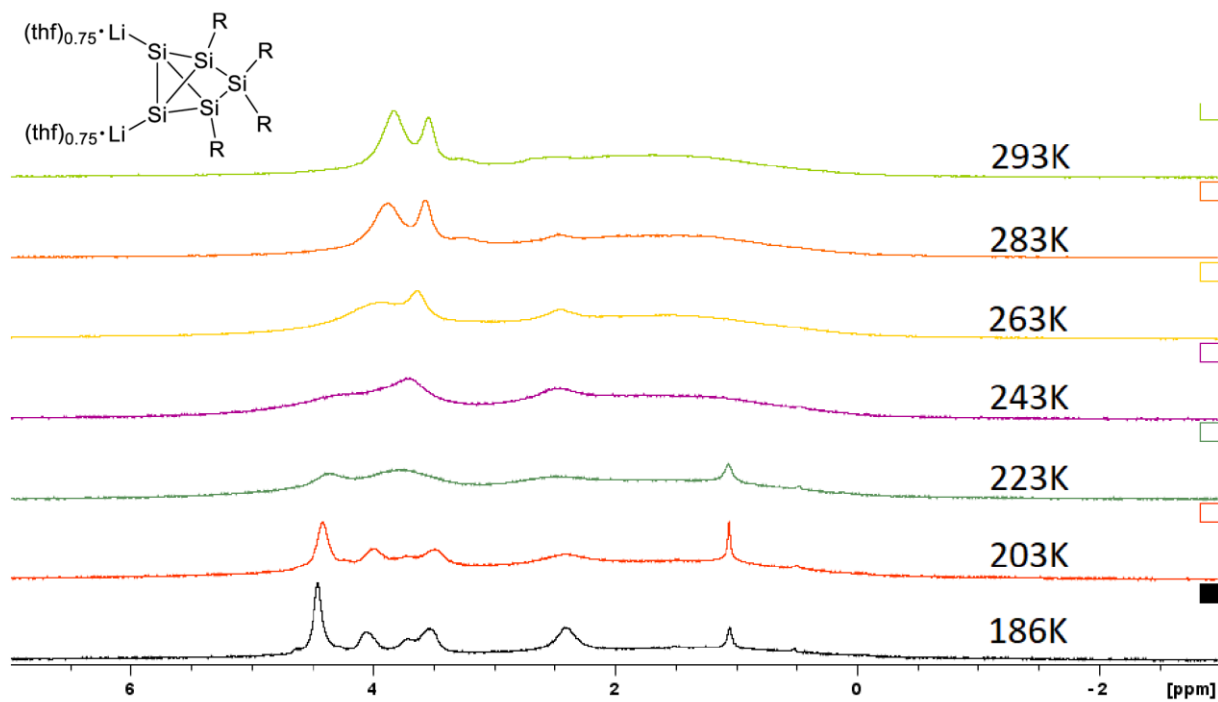


Supplementary Figure 5: 7Li NMR spectrum of **4** in C_6D_6 at 300 K.

6. Supporting Information

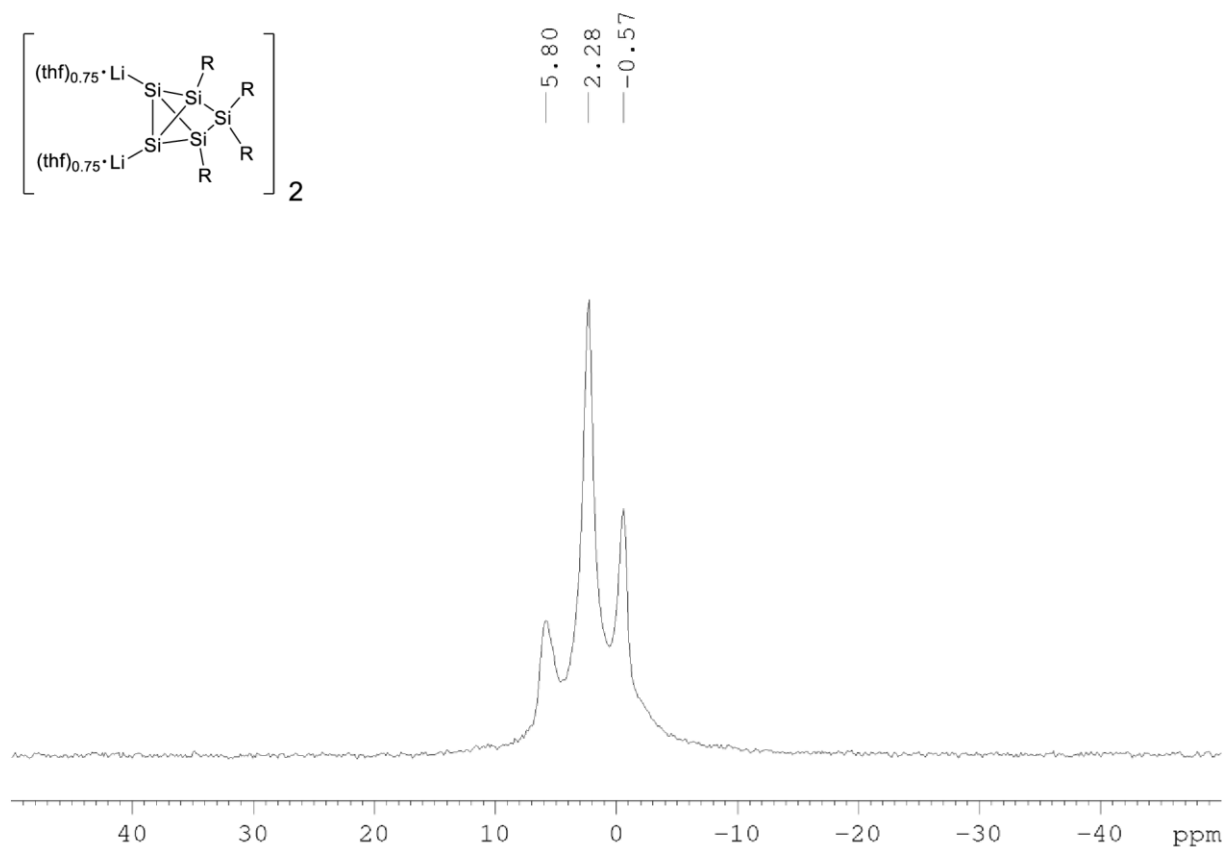


Supplementary Figure 6: ⁷Li NMR spectrum of **4** in thf-d₈ at 300 K.

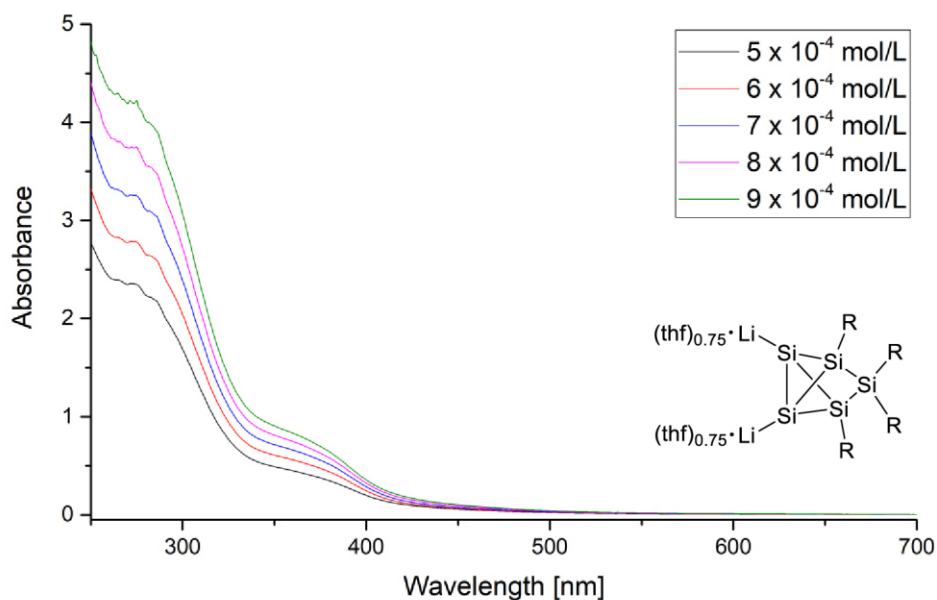


Supplementary Figure 7: ⁷Li NMR spectra of **4** in toluene-d₈ at different temperatures (186K – 293K).

6. Supporting Information



Supplementary Figure 8: $^7Li\{^1H\}$ CP/MAS NMR spectrum of $[4]_2 \cdot (THF)_3$.



Supplementary Figure 9: UV/Vis spectra of **4** in hexane at different concentrations ($5 \cdot 10^{-4}$ – $9 \cdot 10^{-4}$ mol/L).

2.2. 2,3,3,4-Tetrakis(2,4,6-triisopropylphenyl)-1,5-bis(trimethylsilyl)tricyclo[2.1.0.0^{2,5}]pentasilane (7)

230 mg (0.20 mmol) of dianionic Si₅-cluster **4** are dissolved in 2.5 mL of benzene. 51 μ L (0.40 mmol) of Me₃SiCl are added at room temperature. The resulting yellow-brownish reaction mixture is stirred for 30 minutes before all volatiles are removed under reduced pressure. The solid residue is digested with hexane and filtered. The filtrate is reduced to dryness in vacuo. Crystallization from pentane at -26°C afforded 59 mg (27%) of the Bis(trimethylsilyl)substituted Si₅-cluster **7** as yellow crystals. (**m.p.** > 220°C, dec.)

¹H NMR (400.13 MHz, C₆D₆, 300K): δ = 7.26, 7.12, 7.00, 6.81 (each d, each 2H, Tip-*H*), 4.92, 4.74, 3.78, 3.04 (each sept, each 2H, Tip-*i*Pr-CH), 2.77 to 2.67 (m, 4H, Tip-*i*Pr-CH), 2.07, 1.62, 1.57, 1.43, 1.38 (each d, each 6H, Tip-*i*Pr-CH₃) 1.28 to 1.22 (m, pentane), 1.20, 1.20 (overlapping d, each 6H, Tip-*i*Pr-CH₃) 1.14, 1.13 (overlapping d, each 6H, Tip-*i*Pr-CH₃), 0.88 (t, pentane), 0.64, 0.58 (each d, each 6H, Tip-*i*Pr-CH₃), 0.46 (s, 18H, Si(CH₃)₃), 0.23 (d, 6H, Tip-*i*Pr-CH₃).

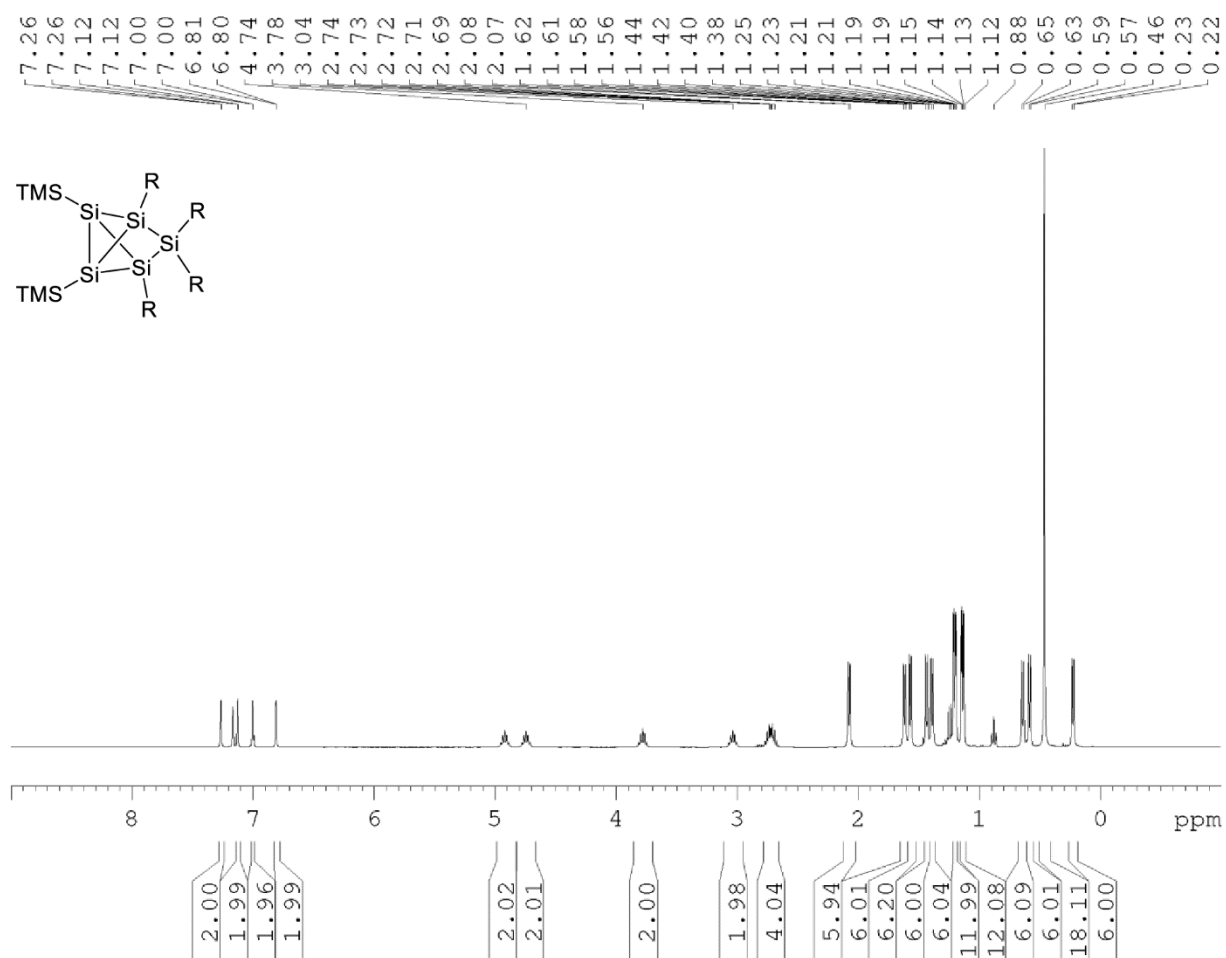
¹³C NMR (100.6 MHz, C₆D₆, 300K): δ = 158.2, 156.4, 153.5, 152.6, 150.8, 149.1, 138.4, 126.3 (Tip-Ar-C), 122.9, 122.8, 121.8, 120.9 (Tip-Ar-CH), 38.0, 37.6, 36.9, 34.8, 34.7, 34.7 (Tip-*i*Pr-CH), 34.5 (pentane), 29.5, 29.2, 27.6, 24.8, 24.7, 24.5, 24.2, 24.0, 23.8 (Tip-*i*Pr-CH₃), 22.7 (pentane), 22.6 (Tip-*i*Pr-CH₃), 14.3 (pentane), 5.5 (Si(CH₃)₃).

²⁹Si NMR (79.5 MHz, C₆D₆, 300K): δ = 34.7 (SiTip₂), 1.7 (Si(CH₃)₃), -81.3 (SiTip), -231.3 (Si).

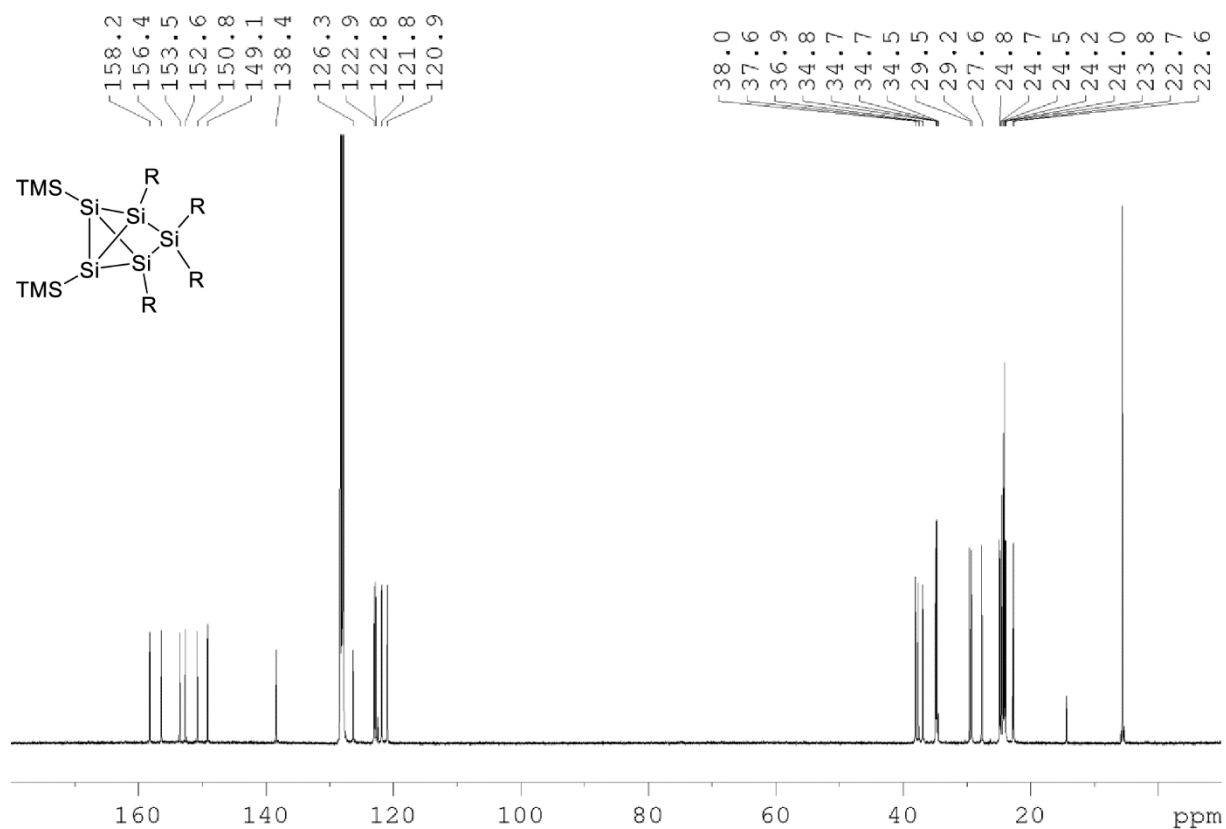
UV/Vis (hexane): broad shoulders from λ_{\max} = 320 - 390 nm and λ_{\max} = 260 - 285 nm.

Elemental analysis: calculated for C₆₆H₁₁₀Si₇: C, 72.05%; H, 10.08%; N, 0.00 %. Found: C, 73.89; H, 9.58; N, 1.38.

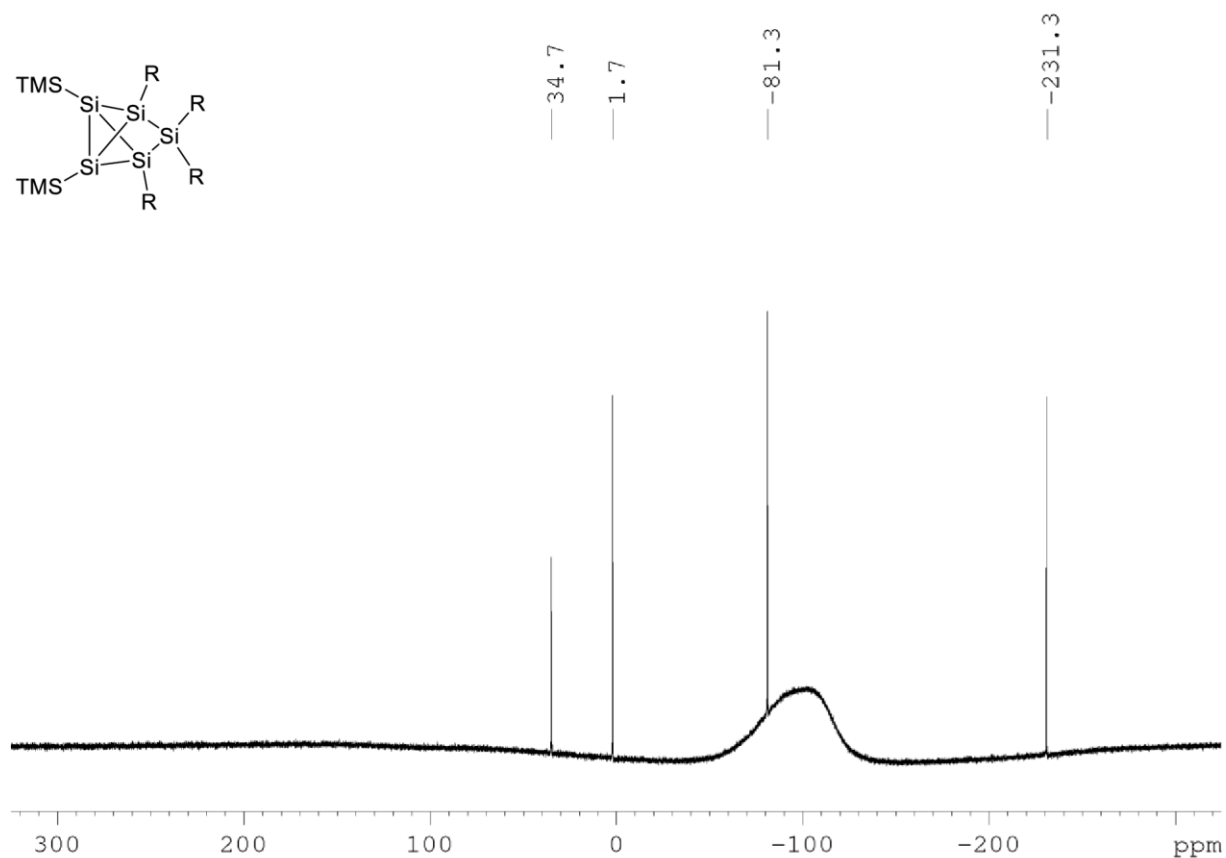
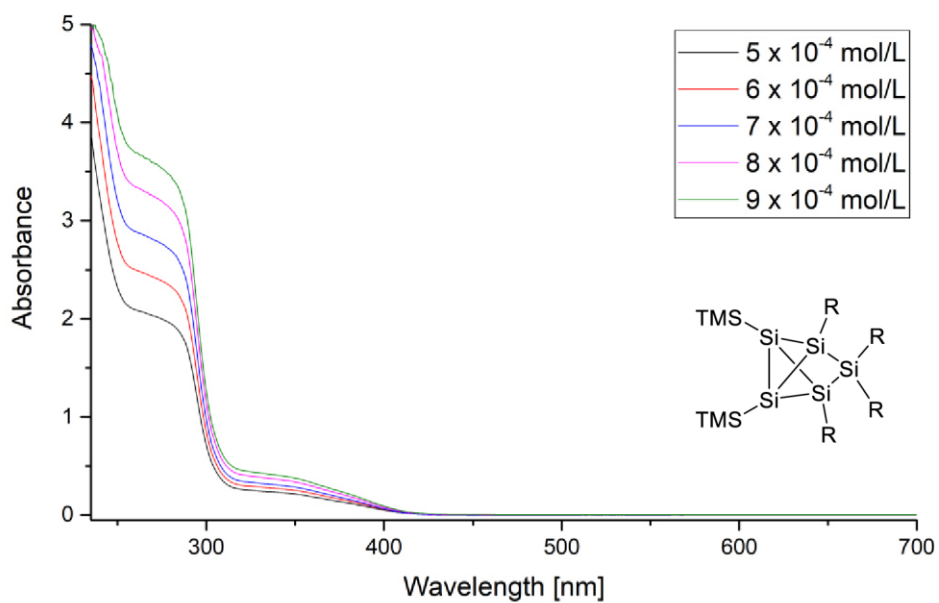
6. Supporting Information



Supplementary Figure 10: ¹H NMR spectrum of **7** in C₆D₆ at 300 K.



S11

Supplementary Figure 11: ^{13}C NMR spectrum of **7** in C_6D_6 at 300 K.**Supplementary Figure 12:** ^{29}Si NMR spectrum of **7** in C_6D_6 at 300 K.**Supplementary Figure 13:** UV/Vis spectra of **7** in hexane at different concentrations ($5 \cdot 10^{-4}$ – $9 \cdot 10^{-4}$ mol/L).

2.3. *N,N*-Diisopropyl-4,5,5,6-tetrakis(2,4,6-triisopropylphenyl)-1,3,4,5,6-pentasil-2-boratetracyclo[2.2.0.0^{1,3}.0^{3,6}]hexan-2-amine (8)

249 mg (0.21 mmol) of dianionic Si₅-cluster **4** are dissolved in 2.5 mL of benzene. 40 μL (0.23 mmol) of dichloro(diisopropylamino)borane are added at r.t. and the resulting reaction mixture is stirred for 30 minutes. All volatiles are removed in vacuo. The solid residue is digested with hexane and filtered. Crystallization from hexane at r.t. yields 132 mg (59%) of BSi₅ cluster **8** as orange crystals (**m.p.** > 220°C, stable).

¹H NMR (300.13 MHz, C₆D₆, 300K): δ = 7.25, 7.11, 6.99, 6.83 (each d, each 2H, Tip-*H*), 5.26, 4.66, 4.14 (each sept, each 2H, Tip-*i*Pr-CH), 3.43 (sept, 2H, B-N-*i*Pr-CH), 3.17 (sept, 2H, Tip-*i*Pr-CH), 2.84 to 2.63 (m, 4H, Tip-*i*Pr-CH), 2.10, 1.66, 1.57, 1.53 (each d, each 6H, Tip-*i*Pr-CH₃), 1.25 to 1.21 (m, 18H, Tip-*i*Pr-CH₃), 1.10 (dd, 12H, Tip-*i*Pr-CH₃), 0.95, 0.87 (each d, each 6H, B-N-*i*Pr-CH₃), 0.71, 0.62, 0.31 (each d, each 6H, Tip-*i*Pr-CH₃).

¹³C NMR (75.5 MHz, C₆D₆, 300K): δ = 157.7, 155.8, 153.3, 152.1, 150.3, 149.2, 139.5, 128.0, 123.0, 122.5, 121.3, 120.4 (Tip-C and Tip-CH), 53.9 (B-N-*i*Pr-CH), 37.3, 36.5, 36.0, 35.1, 34.7 (Tip-*i*Pr-CH and Tip-*i*Pr-CH₃) 32.0 (hexane), 30.1, 27.8, 27.3, 24.7, 24.5, 24.2, 24.2, 24.1, 24.0, 24.0, 23.5 (Tip-*i*Pr-CH and Tip-*i*Pr-CH₃), 23.4 (B-N-*i*Pr-CH₃), 23.06 (hexane), 21.4 (Tip-*i*Pr-CH₃), 14.4 (hexane).

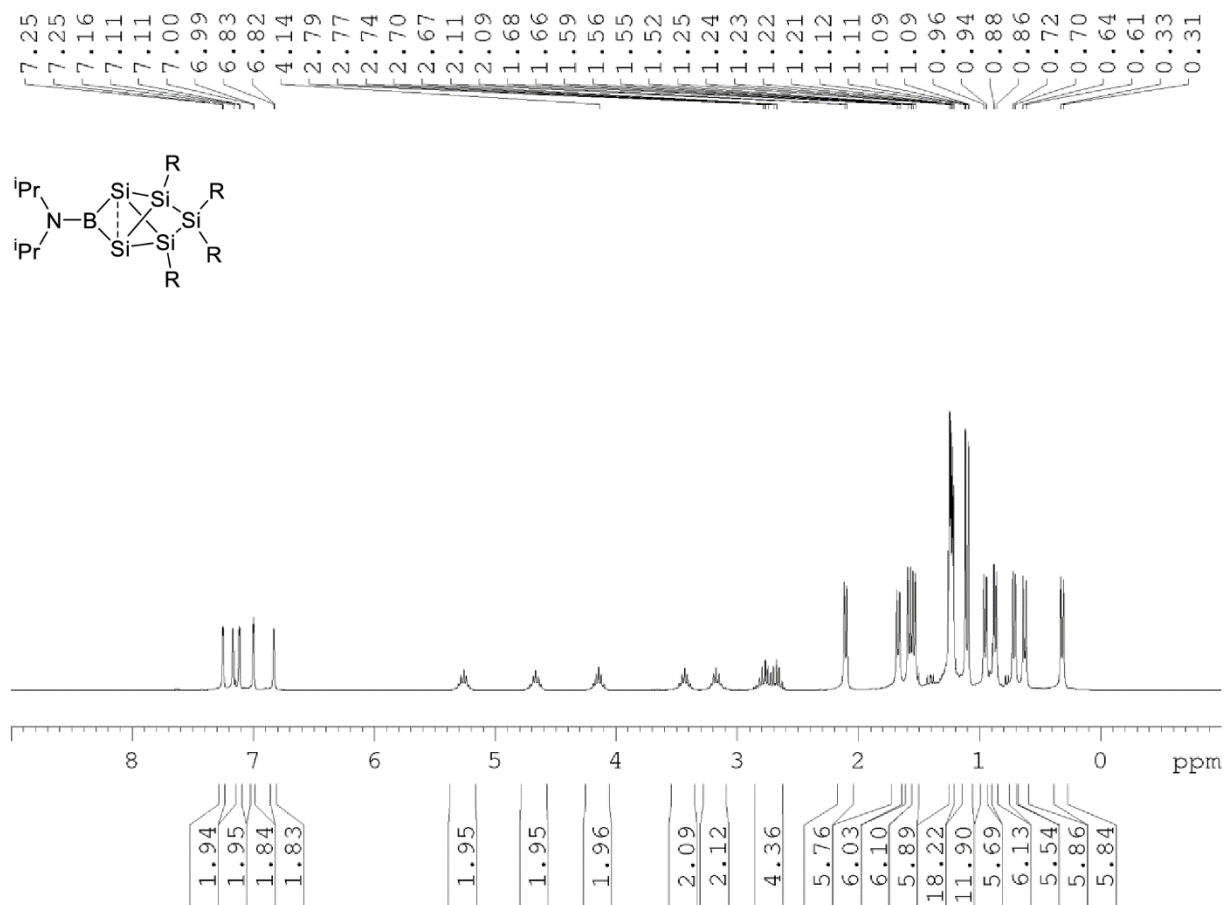
²⁹Si NMR (59.6 MHz, C₆D₆, 300K): δ = 39.0 (*Si*Tip₂), -43.4 (*Si*Tip), -288.6 (*Si*).

¹¹B NMR (128.4 MHz, C₆D₆, 300K): δ = 83.3.

UV/Vis (hexane): λ_{max} = 291 nm (ε = 37820 M⁻¹cm⁻¹); λ_{max} = 472 nm (very unintense).

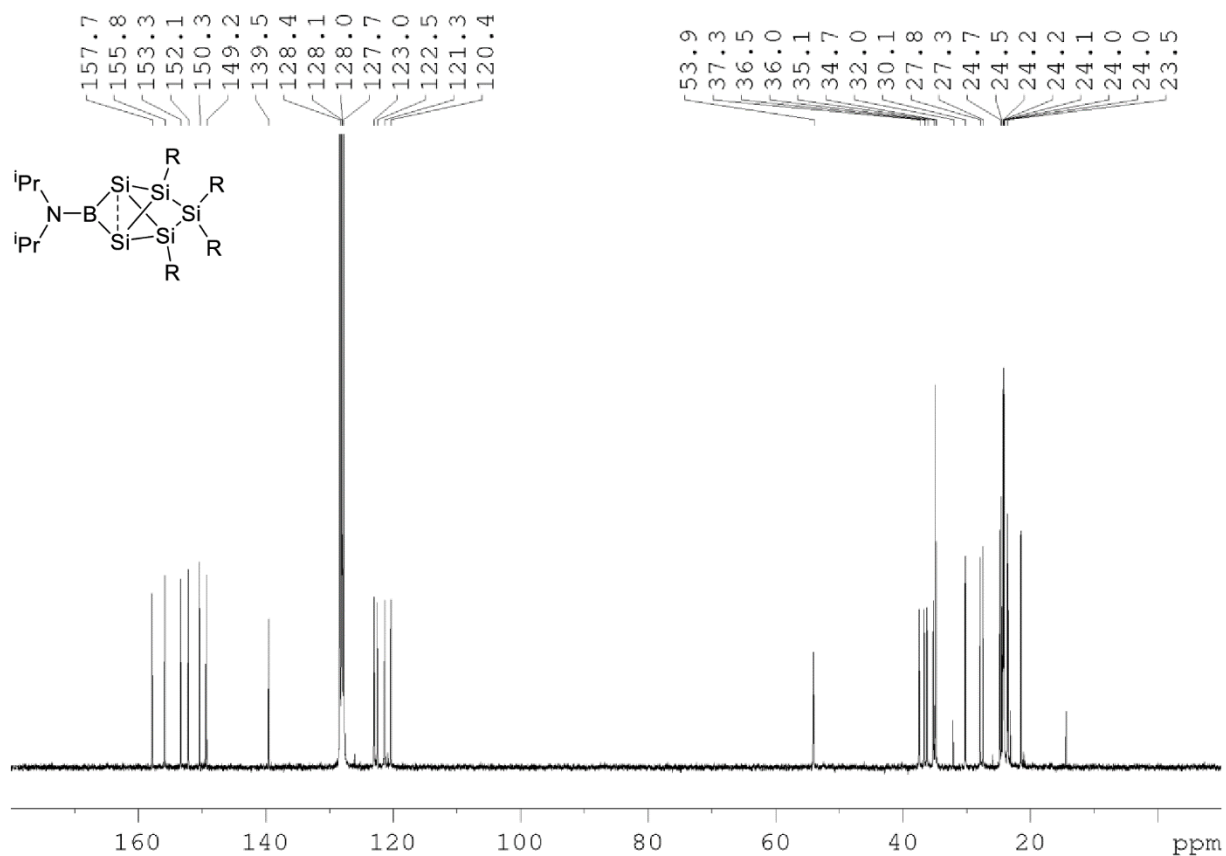
Elemental analysis: calculated for C₆₆H₁₀₆BNSi₅: C, 74.45%; H, 10.03%; N, 1.32 %. Found: C, 73.89; H, 9.58; N, 1.38.

6. Supporting Information

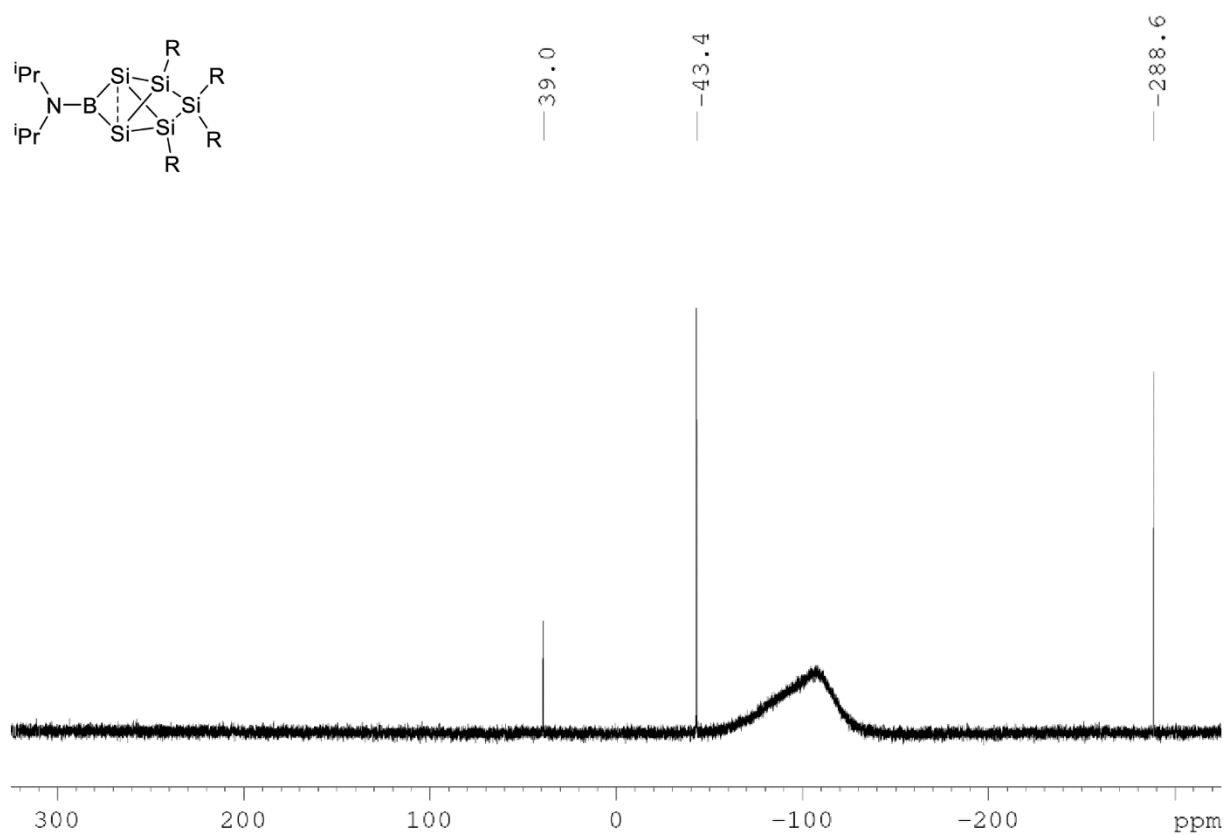


Supplementary Figure 14: ^1H NMR spectrum of **8** in C_6D_6 at 300 K.

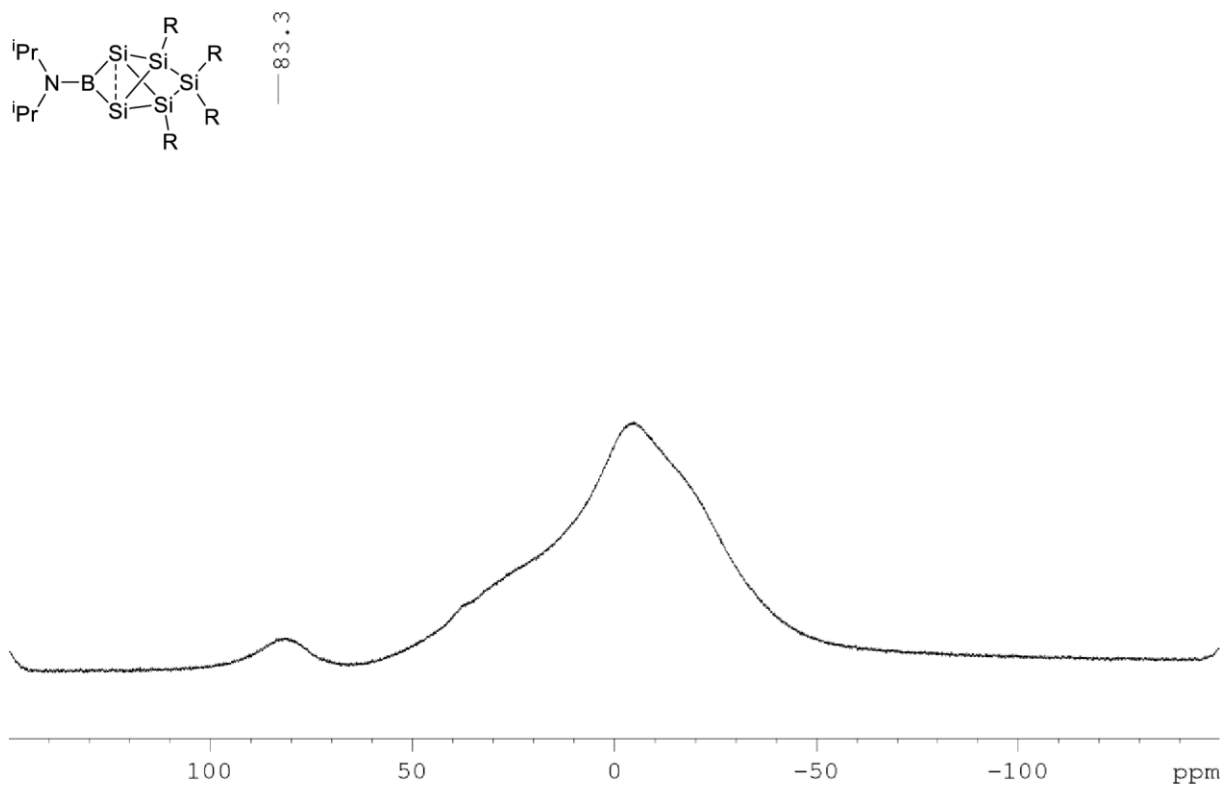
6. Supporting Information



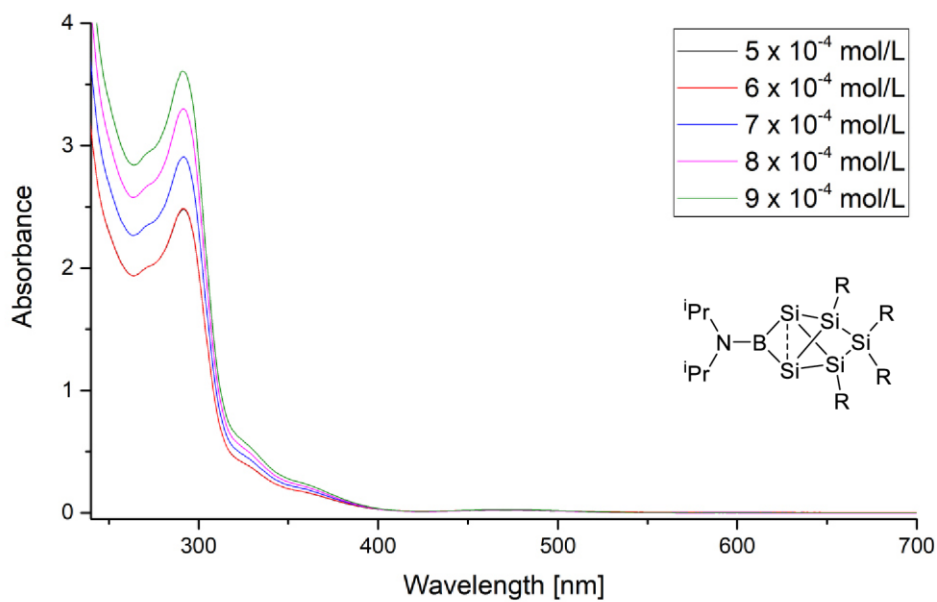
Supplementary Figure 15: ^{13}C NMR spectrum of **8** in C_6D_6 at 300 K.



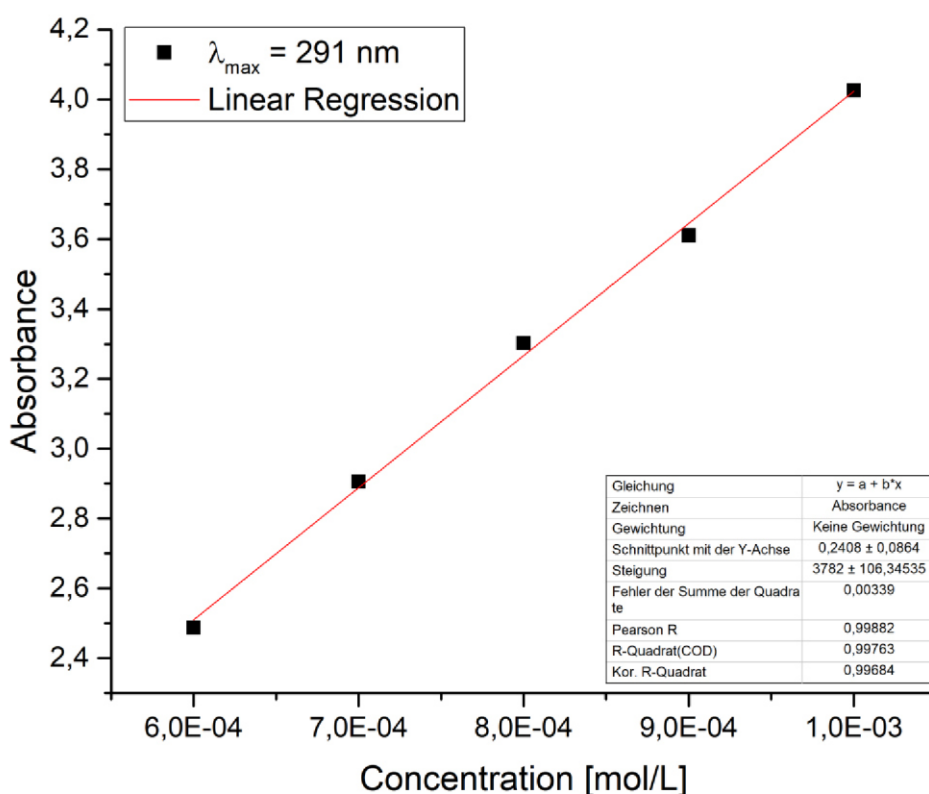
Supplementary Figure 16: ^{29}Si NMR spectrum of **8** in C_6D_6 at 300 K.



Supplementary Figure 17: ^{11}B NMR spectrum of **8** in C_6D_6 at 300 K.



Supplementary Figure 18: UV/Vis spectra of **8** in hexane at different concentrations ($5 \cdot 10^{-4}$ – $9 \cdot 10^{-4}$ mol/L).



Supplementary Figure 19: Determination of extinction coefficient ϵ ($37820 \text{ M}^{-1}\text{cm}^{-1}$) by linear regression of absorbance ($\lambda = 291 \text{ nm}$) of **8** against concentration.

2.4. *N,N*-Diisopropyl-4,5,5,6-tetrakis(2,4,6-triisopropylphenyl)-2-phospho-1,3,4,5,6-pentasilatetracyclo[2.2.0.0^{1,3}.0^{3,6}]hexan-2-amine (**9**)

257 mg (0.21 mmol) of dianionic Si₅-cluster **4** are dissolved in 4 mL of benzene. Following 38 μL (0.21 mmol) of dichloro(diisopropylamino)phosphine are added at r.t. and the resulting reaction mixture is stirred for 30 minutes. All volatiles are removed in vacuo. The solid residue is digested with hexane and filtered. Crystallization from hexane at -26°C yields 89 mg (42%) of PSi₅ cluster **9** (m.p. $> 220^\circ\text{C}$, dec.).

6. Supporting Information

¹H NMR (400.13 MHz, C₆D₆, 300K): δ = 7.25, 7.23, 7.13, 7.06 (each d, each 1H, Tip-*H*), 6.99 (s, 1,3,5-trisopropylbenzene), 6.97, 6.94, 6.85, 6.80 (each d, each 1H, Tip-*H*), 5.18 (sept, 1H, Tip-*i*Pr-CH), 4.65 to 4.54 (m, 2H, Tip-*i*Pr-CH), 4.06, 3.91, 3.46 (each sept, each 1H, Tip-*i*Pr-CH), 3.40 to 3.33 (m, 2H, Tip-*i*Pr-CH), 2.83 to 2.65 (m, 6H, overlapping septets of 1,3,5-trisopropylbenzene, Tip-*i*Pr-CH and P-N-*i*Pr-CH), 2.09, 1.98 (each d, each 3H, Tip-*i*Pr-CH₃), 1.63 to 1.56 (m, 18H, Tip-*i*Pr-CH₃), 1.50, 1.42 (each d, each 3H, Tip-*i*Pr-CH₃), 1.24 (d, 1,3,5-trisopropylbenzene), 1.22 to 1.18 (m, 12H, Tip-*i*Pr-CH₃ and hexane), 1.13 to 1.11 (m, 12H, Tip-*i*Pr-CH₃), 0.89 (m, 3H, Tip-*i*Pr-CH₃ and hexane), 0.83, 0.77 (each d, each 6H, P-N-*i*Pr-CH₃), 0.67 to 0.63 (m, 9H, Tip-*i*Pr-CH₃), 0.43 to 0.39 (m, 6H, Tip-*i*Pr-CH₃).

¹³C NMR (100.6 MHz, C₆D₆, 300K): δ = 157.9, 156.9, 156.5, 155.0, 154.0, 153.5, 152.5, 151.4, 151.0, 150.6, 149.5, 149.4, 149.1, 138.3, 136.8, 130.4, 125.1, 123.2, 123.1, 122.8, 122.5, 122.4 (Tip-*C* and Tip-CH), 122.2 (1,3,5-trisopropylbenzene), 122.0, 121.5, 121.4 (Tip-CH), 52.6 (br, P-N-*i*Pr-CH), 37.9, 37.9, 37.6, 37.2, 36.8, 36.2, 35.5, 35.0, 34.8, 34.6, 34.6, 34.6 (Tip-*i*Pr-CH and Tip-*i*Pr-CH₃), 32.0 (hexane), 28.6, 28.5, 27.6, 27.5, 27.3, 26.8, 26.6, 25.6, 25.2, 25.0, 24.8, 24.6, 24.5, 24.2, 24.2, 24.2, 24.1, 24.0, 24.0, 23.5 (Tip-*i*Pr-CH and Tip-*i*Pr-CH₃), 23.3 (br, P-N-*i*Pr-CH₃), 23.1 (hexane), 21.7 (br, P-N-*i*Pr-CH₃), 14.4 (hexane).

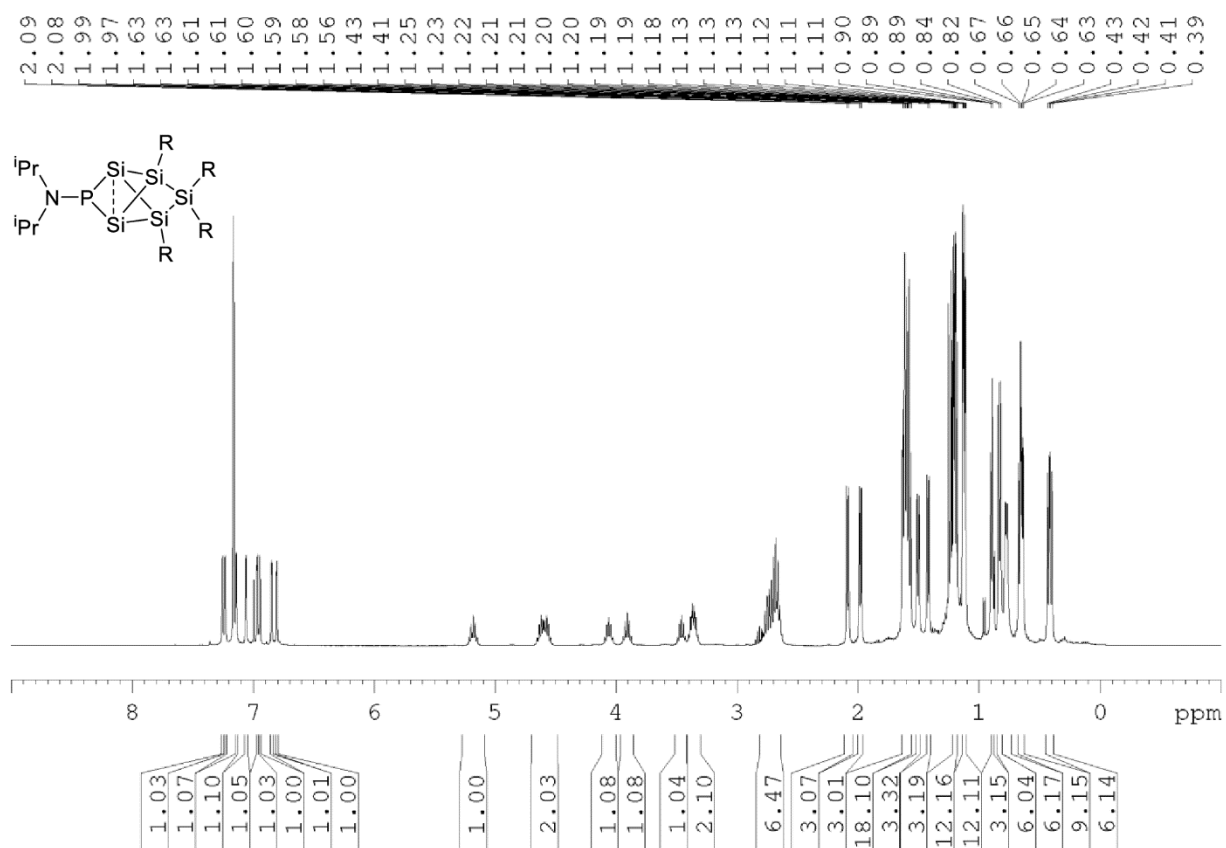
²⁹Si NMR (79.5 MHz, C₆D₆, 300K): δ = 153.7 (s, *Si*Tip), 8.2 (d, ³J_{Si-P} = 29.6 Hz, *Si*Tip₂), -76.7 (d, ²J_{Si-P} = 41.0 Hz, *Si*Tip), -225.8 (d, ¹J_{Si-P} = 124.4 Hz, *Si*), -240.0 (d, ¹J_{Si-P} = 105.4 Hz, *Si*).

³¹P NMR (162.0 MHz, C₆D₆, 300K): δ = 386.7.

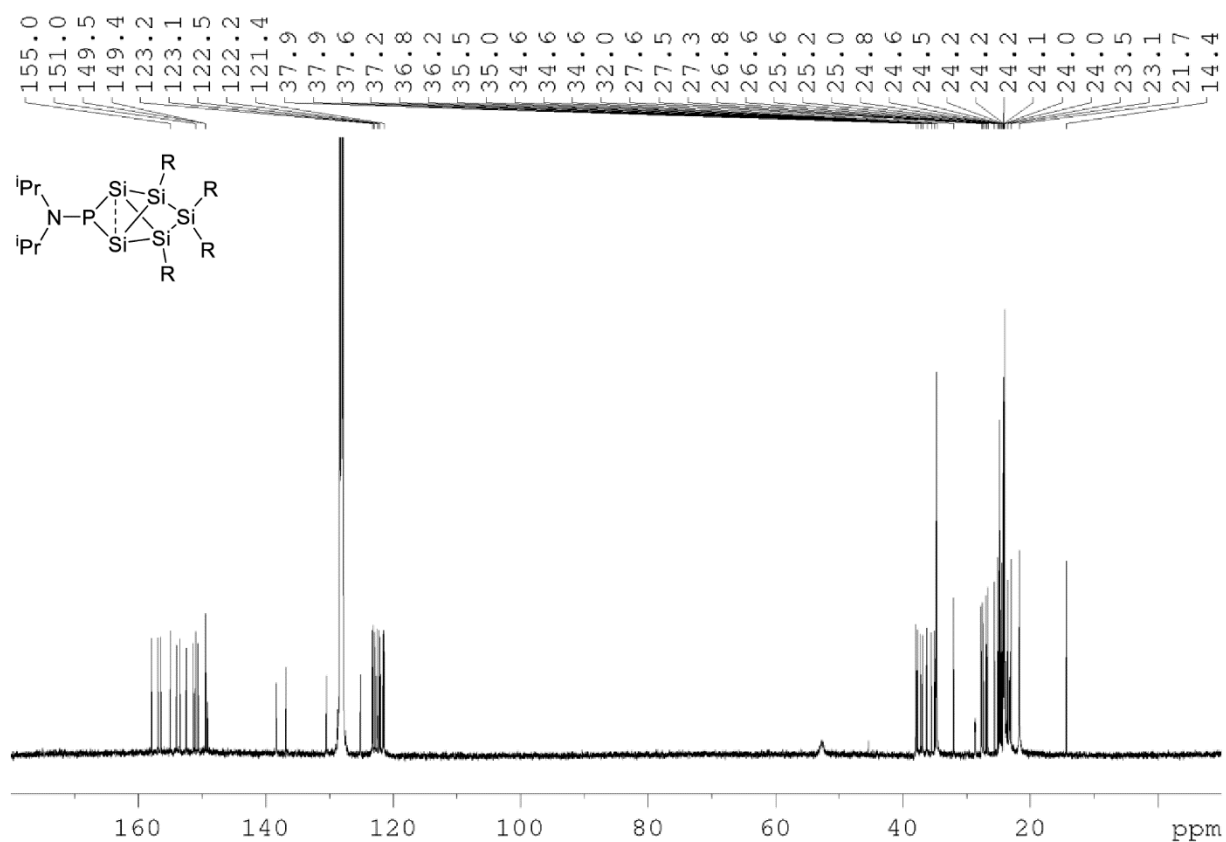
UV/Vis (hexane): broad plateau at λ_{\max} = 250 - 265 nm (ϵ = 40930 M⁻¹cm⁻¹); λ_{\max} = 355 nm (ϵ = 2860 M⁻¹cm⁻¹); λ_{\max} = 412 nm (ϵ = 5010 M⁻¹cm⁻¹); λ_{\max} = 511 nm (very unintense).

Elemental analysis: calculated for C₆₆H₁₀₆NPSi₅: C, 73.06%; H, 9.85%; N, 1.29 %. Found: C, 72.74; H, 9.43; N, 1.22.

6. Supporting Information

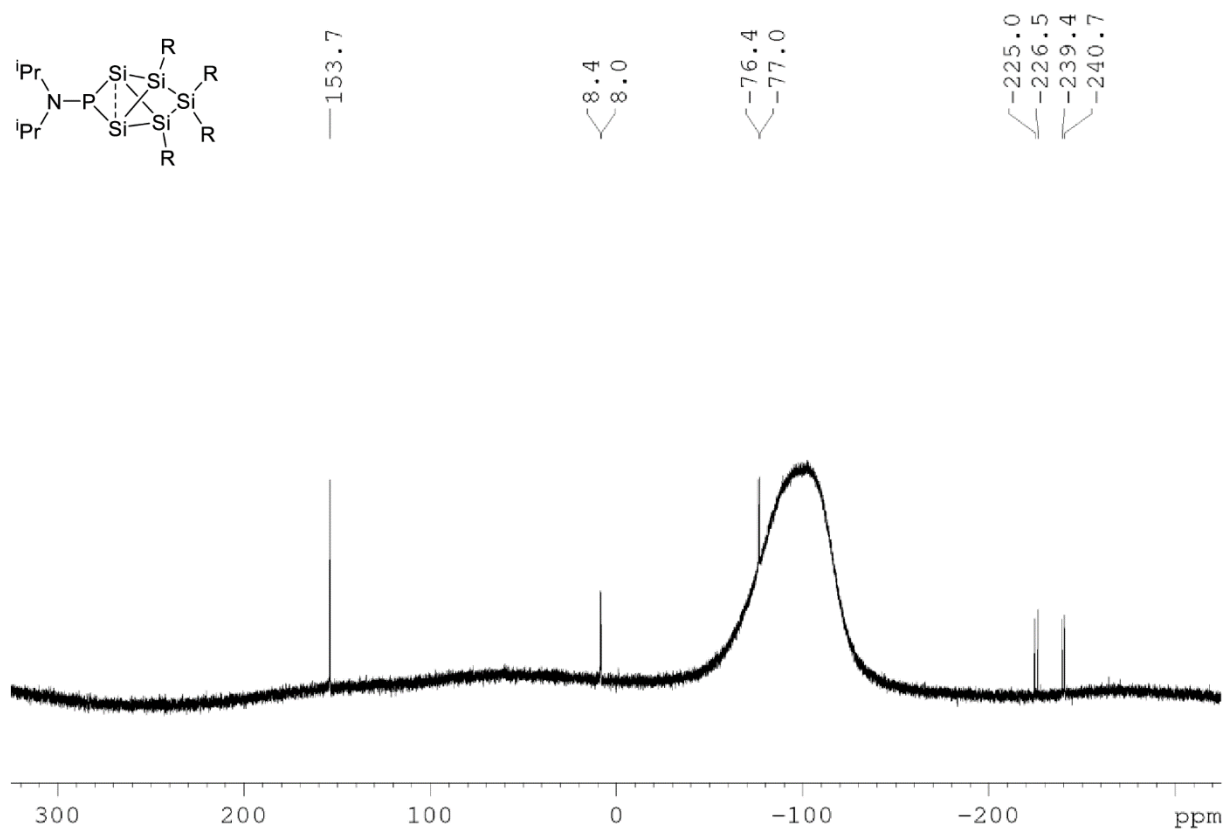


Supplementary Figure 20: ¹H NMR spectrum of **9** in C₆D₆ at 300 K.

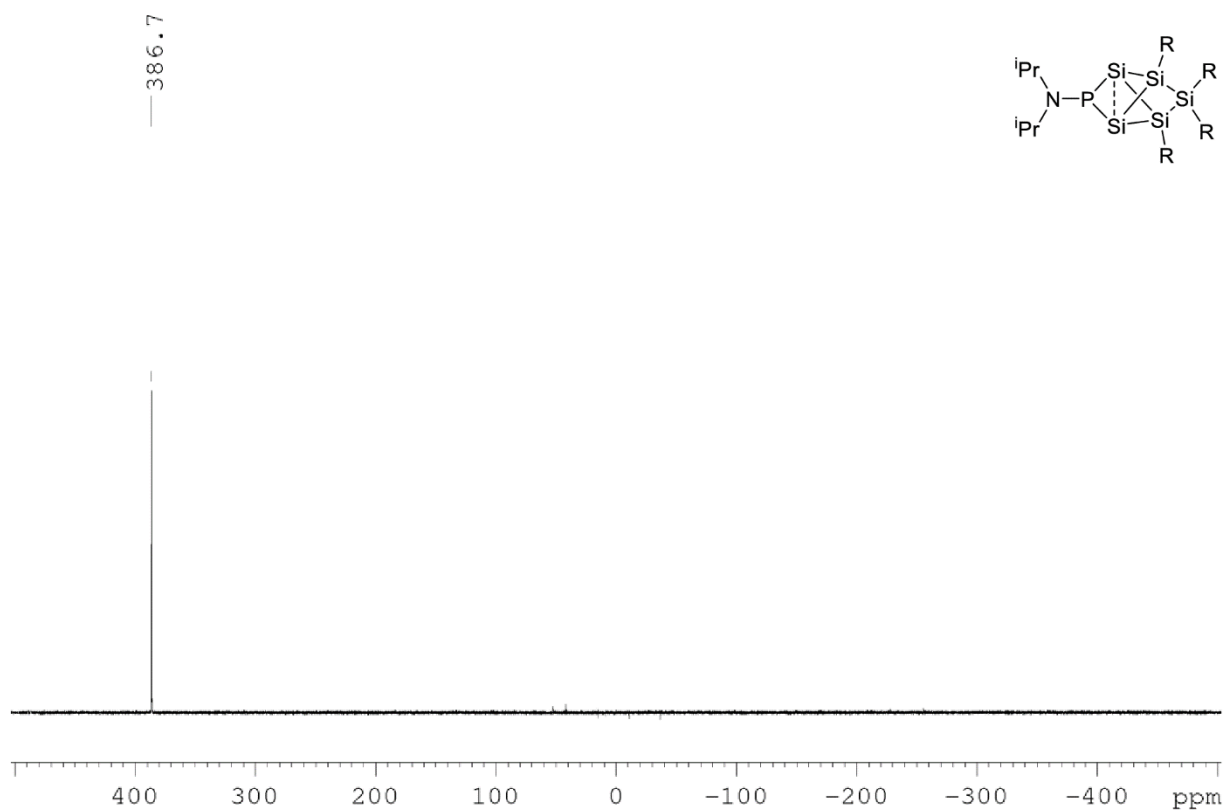


Supplementary Figure 21: ¹³C NMR spectrum of **9** in C₆D₆ at 300 K.

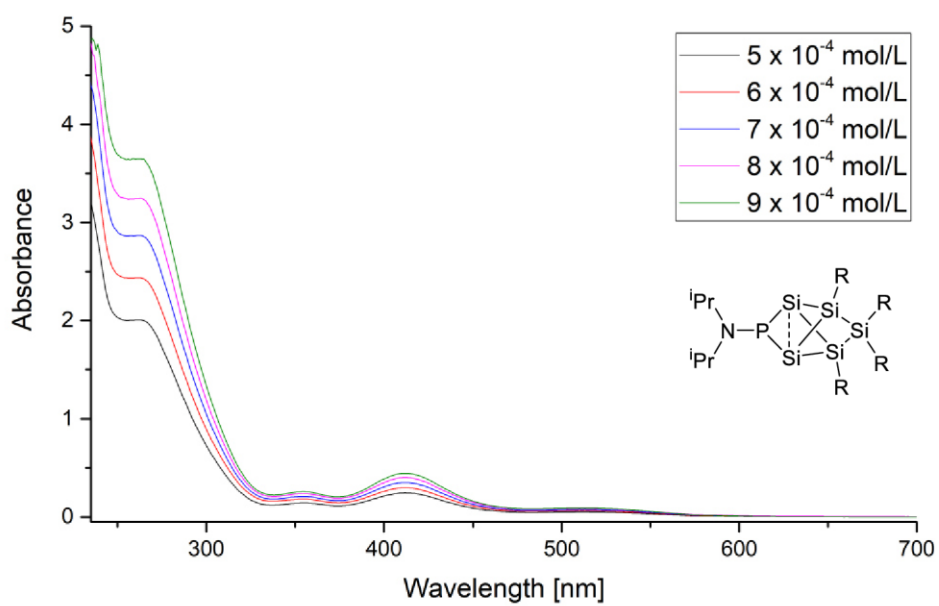
6. Supporting Information



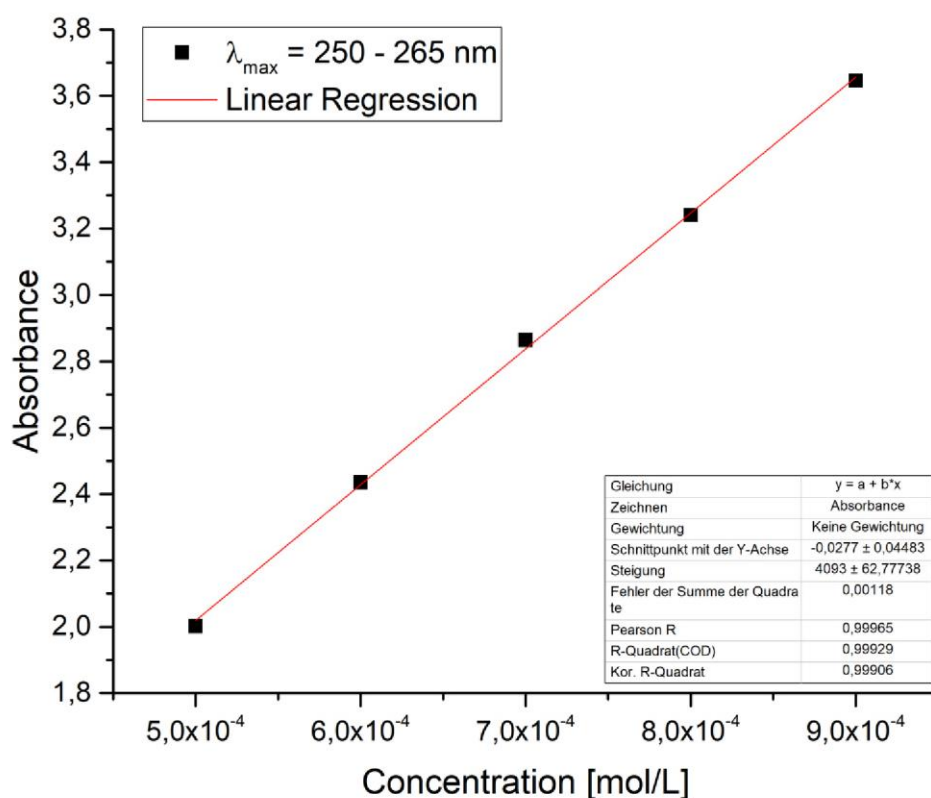
Supplementary Figure 22: ^{29}Si NMR spectrum of **9** in C_6D_6 at 300 K.



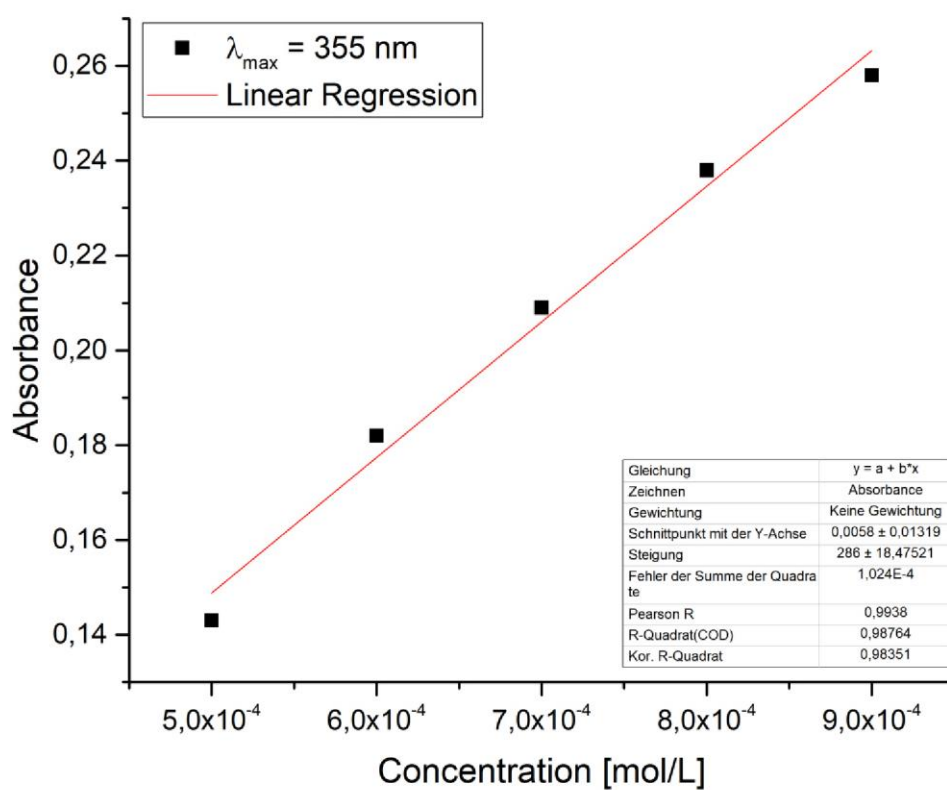
Supplementary Figure 23: ^{31}P NMR spectrum of **9** in C_6D_6 at 300 K.



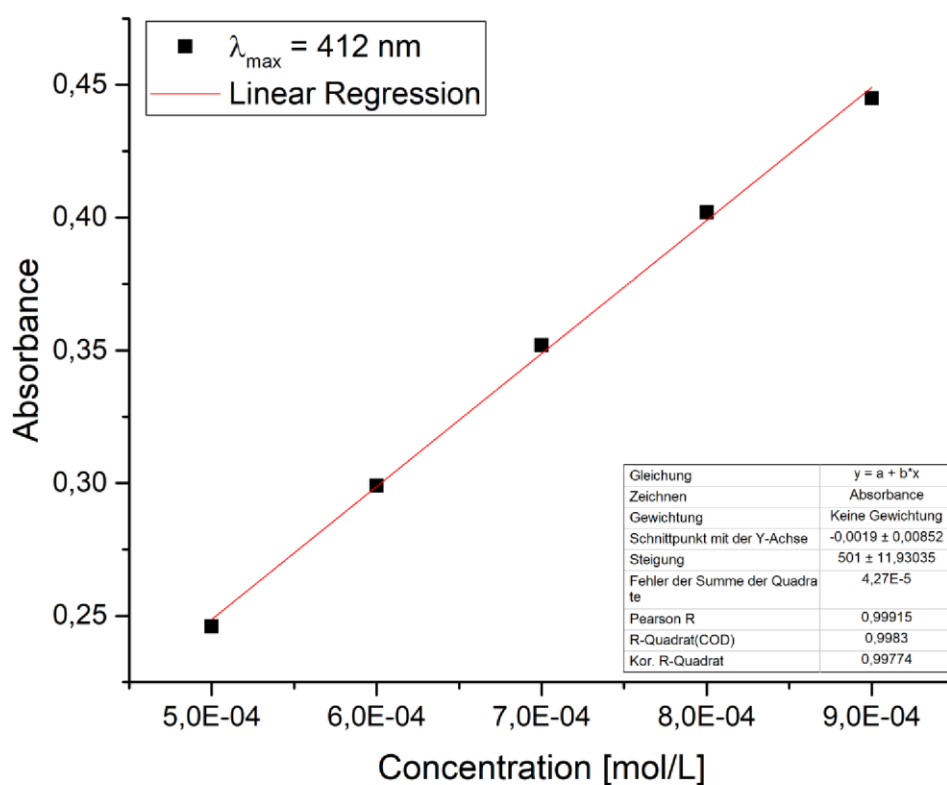
Supplementary Figure 24: UV/Vis spectra of **9** in hexane at different concentrations ($5 \cdot 10^{-4}$ – $9 \cdot 10^{-4}$ mol/L).



Supplementary Figure 25: Determination of extinction coefficient ε ($40930 \text{ M}^{-1}\text{cm}^{-1}$) by linear regression of absorbance ($\lambda_{\text{max}} = 250 - 265 \text{ nm}$) of **9** against concentration.



Supplementary Figure 26: Determination of extinction coefficient ϵ ($2860 \text{ M}^{-1}\text{cm}^{-1}$) by linear regression of absorbance ($\lambda_{\text{max}} = 355 \text{ nm}$) of **9** against concentration.

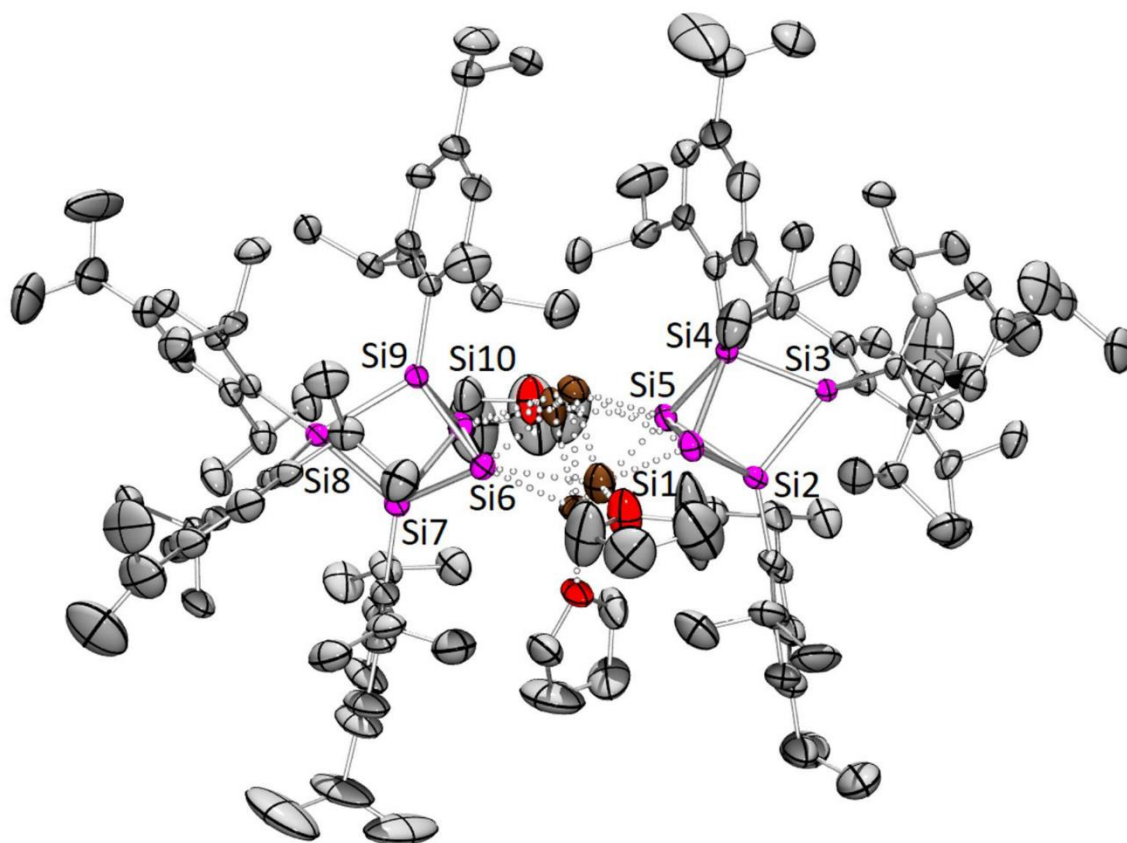


Supplementary Figure 27: Determination of extinction coefficient ϵ ($5010 \text{ M}^{-1}\text{cm}^{-1}$) by linear regression of absorbance ($\lambda_{\max} = 412 \text{ nm}$) of **9** against concentration.

3. Details on X-ray Diffraction Studies

Supplementary Table 1: Crystal data and structure refinement for [4]₂·(THF)₃ (CCDC-1953248).

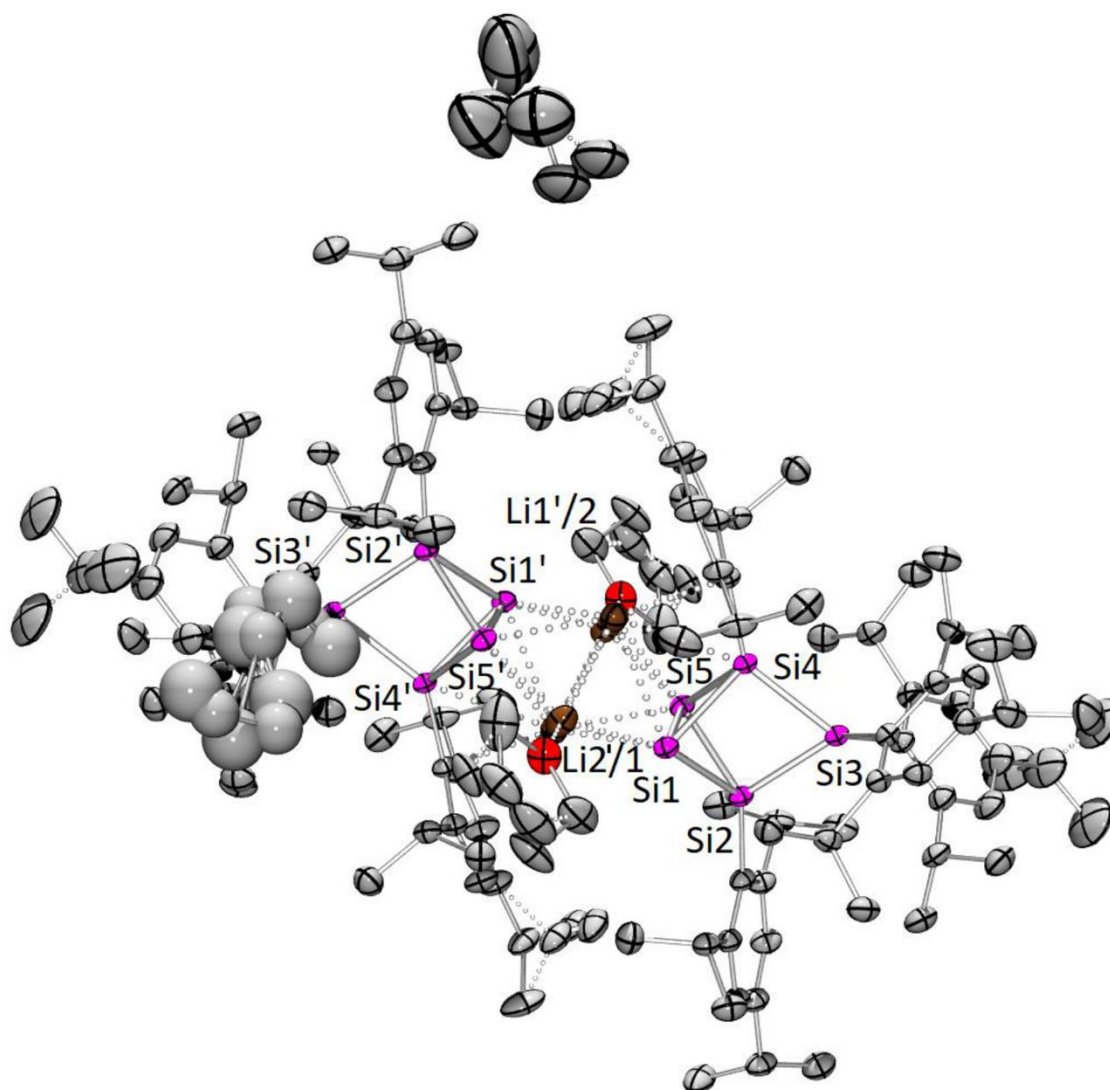
Identification code	sh3898	
Empirical formula	C ₁₃₂ H ₂₀₈ Li ₄ O ₃ Si ₁₀ , 1.125 (C ₆ H ₁₄)	
Formula weight	2248.57	
Temperature	152(2) K	
Wavelength	0.71073 Å	
Crystal system	Triclinic	
Space group	P-1	
Unit cell dimensions	a = 16.0030(11) Å	α = 107.539(3)°.
	b = 29.9444(19) Å	β = 97.162(3)°.
	c = 31.757(2) Å	γ = 93.935(3)°.
Volume	14306.2(17) Å ³	
Z	4	
Density (calculated)	1.044 Mg/m ³	
Absorption coefficient	0.138 mm ⁻¹	
F(000)	4929	
Crystal size	0.345 x 0.276 x 0.200 mm ³	
Theta range for data collection	1.133 to 28.002°.	
Index ranges	-21 ≤ h ≤ 21, -37 ≤ k ≤ 39, -41 ≤ l ≤ 41	
Reflections collected	256396	
Independent reflections	67386 [R(int) = 0.0579]	
Completeness to theta = 25.242°	99.4 %	
Absorption correction	Semi-empirical from equivalents	
Max. and min. transmission	0.7456 and 0.6979	
Refinement method	Full-matrix least-squares on F ²	
Data / restraints / parameters	67386 / 282 / 2908	
Goodness-of-fit on F ²	1.019	
Final R indices [I > 2σ(I)]	R1 = 0.0716, wR2 = 0.1646	
R indices (all data)	R1 = 0.1407, wR2 = 0.1988	
Extinction coefficient	n/a	
Largest diff. peak and hole	0.935 and -0.619 e.Å ⁻³	



Supplementary Figure 28: Molecular structure of $[4]_2 \cdot (THF)_3$ in the solid state. Thermal ellipsoids are displayed at 50% probability. Hydrogen atoms, and co-crystallized solvent molecules are omitted for clarity. Lithium bonds are drawn with dotted lines. Selected bond lengths [\AA]: Si1-Si5 2.572(1), Si6-Si10 2.575(1), Si1-Si4 2.347(1), Si1-Li1 2.633(6), Si1-Li2 3.021(6), Li1-Li4 3.067(8), Li2-Li4 2.571(7).

Supplementary Table 2: Crystal data and structure refinement for [4]₂·(THF)₂ (CCDC-1953249).

Identification code	sh4162cu	
Empirical formula	C128 H200 Li4 O2 Si10, 3(C6 H14)	
Formula weight	2338.04	
Temperature	133(2) K	
Wavelength	1.54178 Å	
Crystal system	Triclinic	
Space group	P-1	
Unit cell dimensions	a = 13.6454(5) Å	α = 76.3140(10)°.
	b = 15.2125(5) Å	β = 74.2330(10)°.
	c = 19.0933(7) Å	γ = 76.5130(10)°.
Volume	3645.0(2) Å ³	
Z	1	
Density (calculated)	1.065 Mg/m ³	
Absorption coefficient	1.197 mm ⁻¹	
F(000)	1286	
Crystal size	0.251 x 0.083 x 0.040 mm ³	
Theta range for data collection	4.074 to 80.513°.	
Index ranges	-17 ≤ h ≤ 17, -18 ≤ k ≤ 19, -24 ≤ l ≤ 24	
Reflections collected	73063	
Independent reflections	15601 [R(int) = 0.0381]	
Completeness to theta = 67.679°	99.4 %	
Absorption correction	Semi-empirical from equivalents	
Max. and min. transmission	0.7543 and 0.6614	
Refinement method	Full-matrix least-squares on F ²	
Data / restraints / parameters	15601 / 231 / 804	
Goodness-of-fit on F ²	1.049	
Final R indices [I > 2σ(I)]	R1 = 0.0544, wR2 = 0.1504	
R indices (all data)	R1 = 0.0582, wR2 = 0.1548	
Extinction coefficient	n/a	
Largest diff. peak and hole	0.961 and -0.758 e.Å ⁻³	



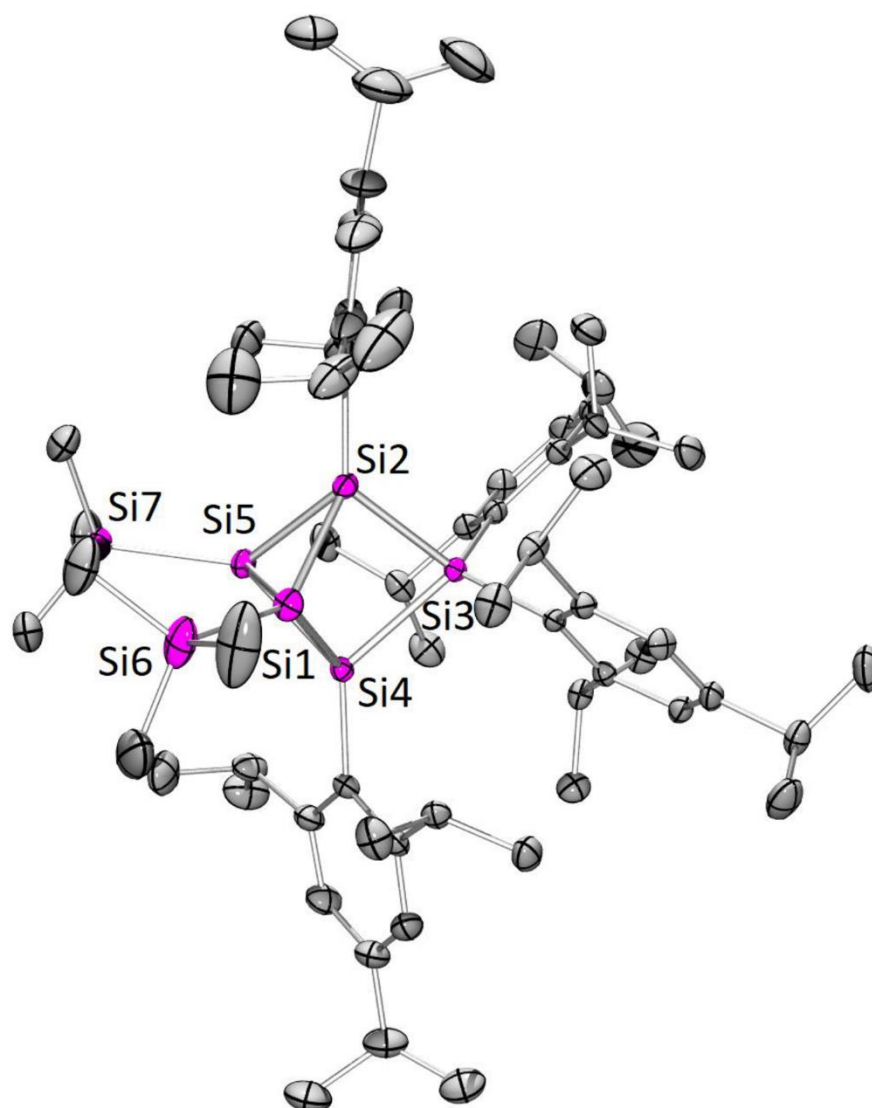
Supplementary Figure 29: Molecular structure of $[4]_2 \cdot (\text{THF})_2$ in the solid state

Thermal ellipsoids are displayed at 50% probability. Hydrogen atoms are omitted for clarity. Split positions are drawn with small dotted lines. Lithium bonds are drawn with bigger dotted lines. Selected bond lengths [Å]: Si1-Si5 2.5524(6), Si1-Si2 2.3822(6), Si1-Si4 2.3229(6), Si1-Li1 2.858(3), Si2-Li1 2.785(3), Li1-Li1' 2.793(7).

Supplementary Table 3: Crystal data and structure refinement for **7**

(CCDC-1953250).

Identification code	sh4075	
Empirical formula	C ₆₆ H ₁₁₀ Si ₇ , C ₅ H ₁₂	
Formula weight	1172.31	
Temperature	142(2) K	
Wavelength	0.71073 Å	
Crystal system	Monoclinic	
Space group	P2 ₁ /c	
Unit cell dimensions	a = 24.7021(9) Å	α = 90°.
	b = 27.0801(8) Å	β = 113.3692(15)°.
	c = 24.4934(7) Å	γ = 90°.
Volume	15040.4(8) Å ³	
Z	8	
Density (calculated)	1.035 Mg/m ³	
Absorption coefficient	0.163 mm ⁻¹	
F(000)	5168	
Crystal size	0.522 x 0.494 x 0.376 mm ³	
Theta range for data collection	1.171 to 29.689°.	
Index ranges	-31 ≤ h ≤ 34, -35 ≤ k ≤ 37, -34 ≤ l ≤ 33	
Reflections collected	133330	
Independent reflections	42515 [R(int) = 0.0677]	
Completeness to theta = 25.242°	100.0 %	
Absorption correction	Semi-empirical from equivalents	
Max. and min. transmission	0.7459 and 0.6764	
Refinement method	Full-matrix least-squares on F ²	
Data / restraints / parameters	42515 / 290 / 1522	
Goodness-of-fit on F ²	1.024	
Final R indices [I > 2σ(I)]	R1 = 0.0739, wR2 = 0.1395	
R indices (all data)	R1 = 0.1520, wR2 = 0.1733	
Extinction coefficient	n/a	
Largest diff. peak and hole	0.917 and -0.823 e.Å ⁻³	

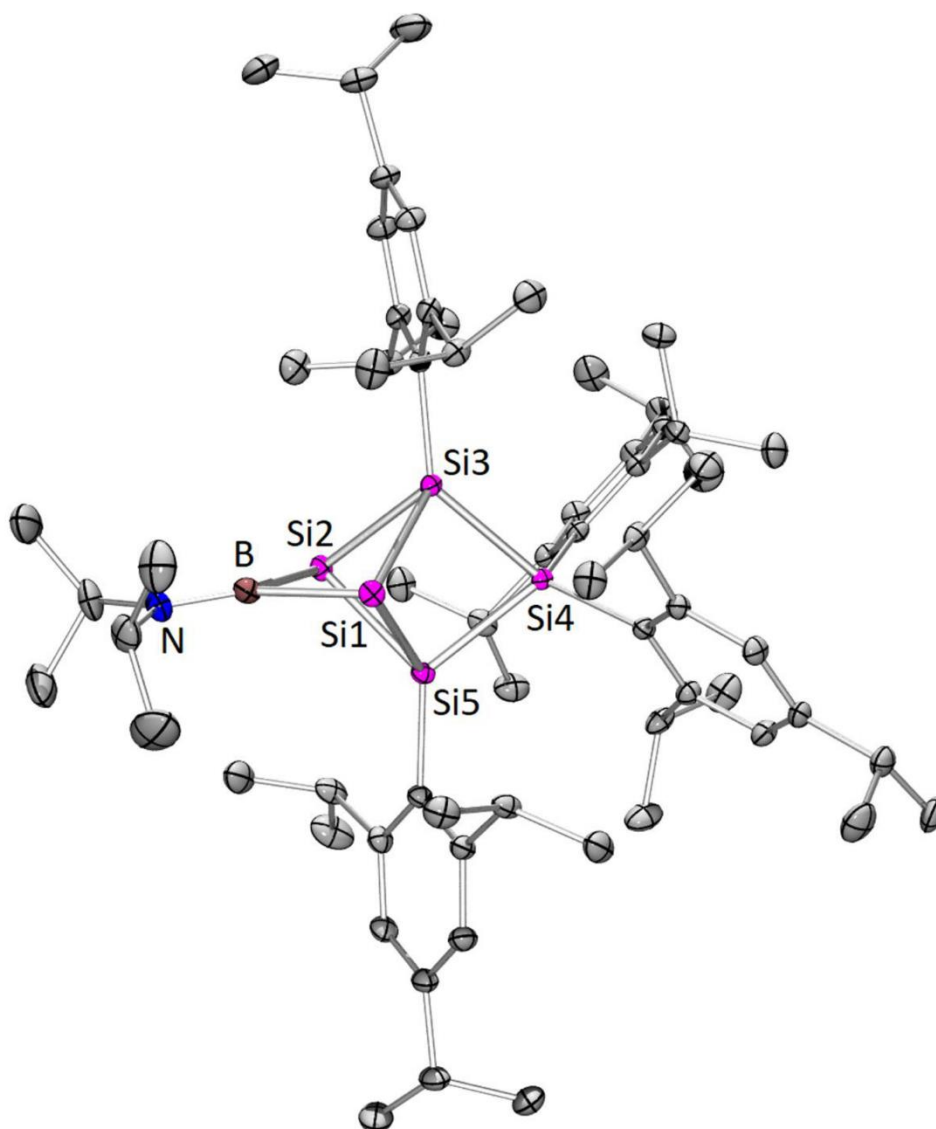


Supplementary Figure 30: Molecular structure of **7** in the solid state. Thermal ellipsoids are displayed at 50% probability. Hydrogen atoms and co-crystallized solvent molecules are omitted for clarity. Selected bond lengths [\AA]: Si1-Si5 2.469(1), Si1-Si2 2.302(1) Si1-Si4 2.338(1), Si1-Si6 2.332(1), Si2-Si3 2.376(1).

Supplementary Table 4: Crystal data and structure refinement for **8**

(CCDC-1953251).

Identification code	sh4060	
Empirical formula	C ₆₆ H ₁₀₆ B N Si ₅	
Formula weight	1064.77	
Temperature	132(2) K	
Wavelength	0.71073 Å	
Crystal system	Triclinic	
Space group	P-1	
Unit cell dimensions	a = 13.5006(6) Å	α = 98.387(2)°.
	b = 13.5798(6) Å	β = 92.938(2)°.
	c = 18.9871(8) Å	γ = 106.305(2)°.
Volume	3289.7(3) Å ³	
Z	2	
Density (calculated)	1.075 Mg/m ³	
Absorption coefficient	0.146 mm ⁻¹	
F(000)	1168	
Crystal size	0.652 x 0.377 x 0.120 mm ³	
Theta range for data collection	1.089 to 30.988°.	
Index ranges	-19 ≤ h ≤ 19, -19 ≤ k ≤ 19, -27 ≤ l ≤ 27	
Reflections collected	76421	
Independent reflections	20730 [R(int) = 0.0277]	
Completeness to theta = 25.242°	100.0 %	
Absorption correction	Semi-empirical from equivalents	
Max. and min. transmission	0.7461 and 0.7190	
Refinement method	Full-matrix least-squares on F ²	
Data / restraints / parameters	20730 / 0 / 1082	
Goodness-of-fit on F ²	1.027	
Final R indices [I > 2σ(I)]	R1 = 0.0373, wR2 = 0.0888	
R indices (all data)	R1 = 0.0527, wR2 = 0.0965	
Extinction coefficient	n/a	
Largest diff. peak and hole	0.402 and -0.228 e.Å ⁻³	

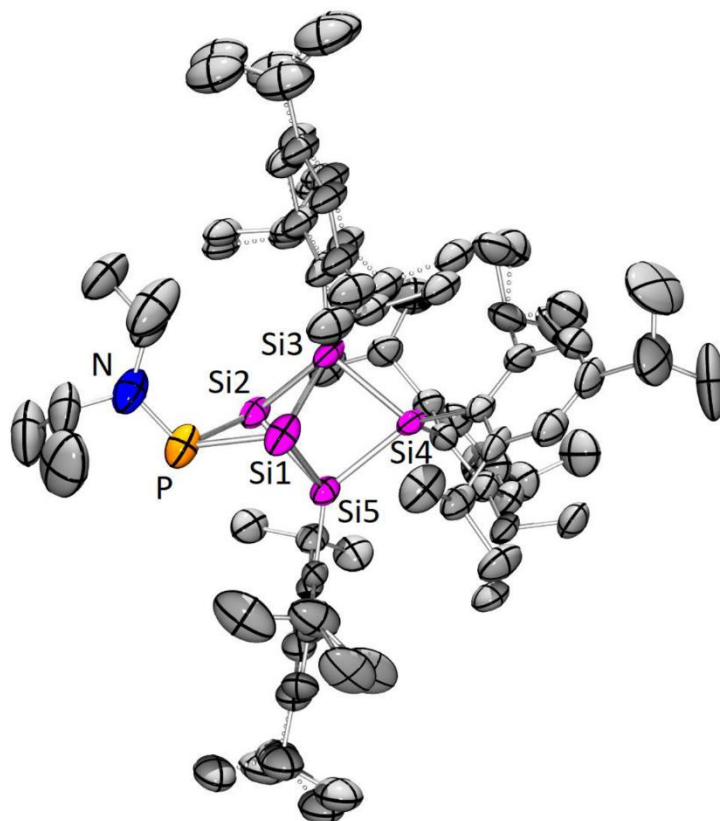


Supplementary Figure 31: Molecular structure of **8** in the solid state. Thermal ellipsoids are displayed at 50% probability. Hydrogen atoms are omitted for clarity. Selected bond lengths [Å]: Si1-B 2.031(1), Si1-Si2 2.5911(4), Si1-Si3 2.3270(4), Si3-Si4 2.3816(4), B-N 1.374(2).

Supplementary Table 5: Crystal data and structure refinement for **9**

(CCDC-1953252).

Identification code	sh4073	
Empirical formula	C ₆₆ H ₁₀₆ N P Si ₅	
Formula weight	1084.93	
Temperature	142(2) K	
Wavelength	0.71073 Å	
Crystal system	Monoclinic	
Space group	P2 ₁ /n	
Unit cell dimensions	a = 20.5557(11) Å	α = 90°.
	b = 13.3994(10) Å	β = 90.261(2)°.
	c = 24.2831(17) Å	γ = 90°.
Volume	6688.3(8) Å ³	
Z	4	
Density (calculated)	1.077 Mg/m ³	
Absorption coefficient	0.168 mm ⁻¹	
F(000)	2376	
Crystal size	0.201 x 0.200 x 0.184 mm ³	
Theta range for data collection	1.301 to 26.615°.	
Index ranges	-20 ≤ h ≤ 25, -16 ≤ k ≤ 16, -30 ≤ l ≤ 29	
Reflections collected	101267	
Independent reflections	13657 [R(int) = 0.0857]	
Completeness to theta = 25.242°	99.6 %	
Absorption correction	Semi-empirical from equivalents	
Max. and min. transmission	0.7454 and 0.7211	
Refinement method	Full-matrix least-squares on F ²	
Data / restraints / parameters	13657 / 601 / 899	
Goodness-of-fit on F ²	1.383	
Final R indices [I > 2σ(I)]	R1 = 0.0776, wR2 = 0.1784	
R indices (all data)	R1 = 0.1617, wR2 = 0.2022	
Extinction coefficient	n/a	
Largest diff. peak and hole	0.544 and -0.456 e.Å ⁻³	



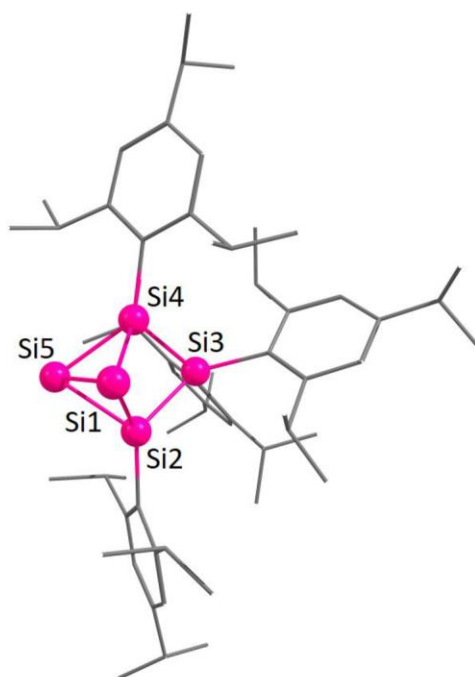
Supplementary Figure 32: Molecular structure of **9** in the solid state. Thermal ellipsoids are displayed at 50% probability. Hydrogen atoms and co-crystallized solvent molecules are omitted for clarity. Split positions are drawn with dotted lines. Selected bond lengths [Å]: Si1-P 2.314(2), Si1-Si2 2.613(1), Si1-Si3 2.391(2), Si3-Si4 2.38(1), P-N 1.651(3).

Comment on structure refinement:

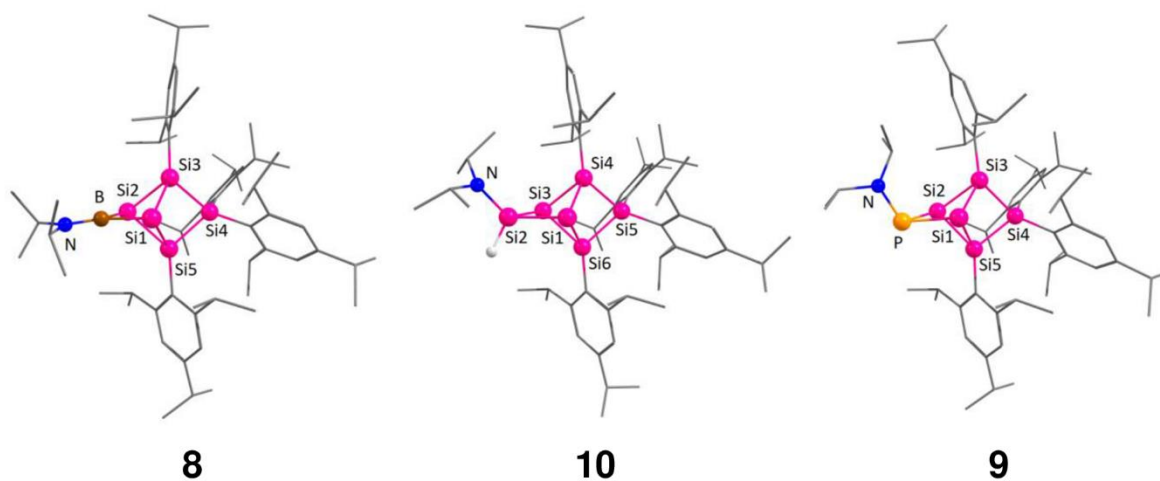
Level B alerts caused by many positionally disordered parts of the molecule, which were refined on split positions. All attempts treating the problem as pseudo-merohedral twinning in the higher orthorhombic symmetry remained unsuccessful.

4. Computational Details

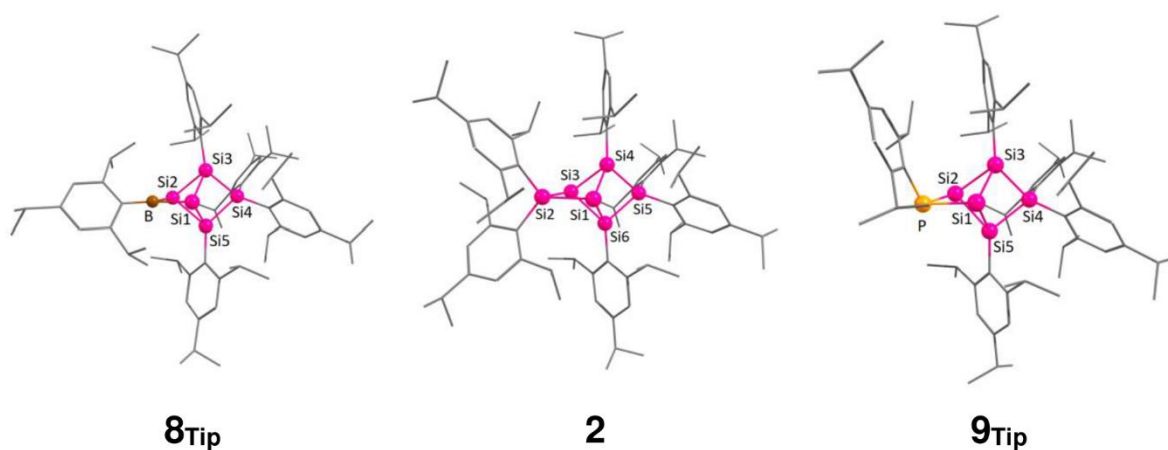
Structural optimizations were carried out using the Gaussian 09 program package^[2] and the functional BP86^[3,4] with Grimme dispersion corrections D3^[5] in combination with the def2-SVP basis set.^[6] To ensure the presence of a local minimum a subsequent frequency analysis at the same level was performed for each structure. Optimized structures were plotted using ChemCraft 1.8.^[7] Molecular orbitals were calculated using the functional M06-2X^[8] with the Grimme dispersion corrections D3^[5] in combination with the def2-SVPP basis set.^[6] Chemical shifts were calculated with GIAO^[9-13] as implemented in the Gaussian 09 program package using the functional OLYP^[14-17] in combination with the two different basis sets def2-TZVPP^[18] and pcS-2.^[19-21] All chemical shifts were referenced to the values calculated for Si(CH₃)₄, H₃PO₄ and BF₃·Et₂O at the same level of theory.



Supplementary Figure 33: Optimized structure of **4'** (**4** was calculated as the monomeric dianionic Si₅-cluster core without lithium counter cations and coordinated donor molecules; level of theory: BP86/def2-SVP)



Supplementary Figure 34: Optimized structures of **8**, **10** and **9** (level of theory: BP86/def2-SVP).



Supplementary Figure 35: Optimized structures of **8_{Tip}**, **2** and **9_{Tip}** (level of theory: BP86/def2-SVP).

Supplementary Table 6: Atomic coordinates of the optimized structure of **4'**.

C	-3.697038000	-2.772747000	-2.417484000
C	3.665859000	-4.319457000	-2.403690000
C	-0.242282000	-4.138826000	-0.884223000
C	-3.707128000	-4.973775000	3.290269000
C	3.106647000	-2.668191000	-4.240802000
C	-4.007807000	-2.734506000	0.099492000
C	3.147241000	-2.907602000	-2.716404000
C	1.594819000	-4.144551000	0.877587000
C	-3.481618000	-1.965218000	-1.122137000
C	-1.705298000	-4.896834000	4.861343000
C	0.494820000	-3.315623000	0.188480000
C	-2.709498000	-4.064530000	4.039060000
C	-1.112097000	-3.565163000	2.104446000
C	-8.477308000	0.167122000	-1.464514000
C	-5.425136000	-0.357879000	-1.010282000
C	-2.019595000	-3.105342000	3.074663000
C	-0.488585000	-2.697945000	1.184437000
C	-4.059223000	-0.560041000	-1.292620000
C	3.907913000	-1.772198000	-2.036389000
C	5.272916000	-1.937692000	-1.719201000
C	7.635139000	-1.028160000	0.775811000
C	-7.493380000	1.122823000	-0.759673000
C	-6.046728000	0.892778000	-1.185047000
C	-3.255575000	0.522199000	-1.781095000
C	-2.320089000	-1.733226000	3.078265000
C	-0.782080000	-1.298624000	1.201312000
C	7.493603000	-1.123112000	-0.758877000
C	3.255777000	-0.522847000	-1.780509000
C	-7.633855000	1.030796000	0.775302000
C	6.046831000	-0.893353000	-1.183995000
C	-1.744583000	-0.835731000	2.154883000
C	-5.272792000	1.936968000	-1.720500000

6. Supporting Information

C	-3.907742000	1.771442000	-2.037465000
C	-3.106317000	2.666739000	-4.242093000
C	1.663214000	-1.296054000	3.528583000
C	5.425285000	0.357399000	-1.009752000
C	4.059409000	0.559518000	-1.292276000
C	8.477343000	-0.169072000	-1.466260000
C	-3.705440000	0.808103000	2.079636000
C	2.182661000	-0.630123000	2.238686000
C	3.705160000	-0.807437000	2.080562000
C	-3.147089000	2.906676000	-2.717780000
C	-2.182970000	0.630829000	2.238096000
C	0.781872000	1.298955000	1.201147000
C	3.481804000	1.964750000	-1.122286000
C	1.744292000	0.836401000	2.154959000
C	-3.665842000	4.318599000	-2.405605000
C	-1.663786000	1.297189000	3.527876000
C	3.697381000	2.771861000	-2.417871000
C	0.488362000	2.698270000	1.183774000
C	-0.494867000	3.315610000	0.187447000
C	4.007851000	2.734433000	0.099149000
C	2.319711000	1.734218000	3.078085000
C	0.242486000	4.138430000	-0.885373000
C	-1.595000000	4.144799000	0.876012000
C	1.111700000	3.565802000	2.103601000
C	2.019125000	3.106320000	3.074038000
C	2.708931000	4.065847000	4.038159000
C	1.704671000	4.898324000	4.860198000
C	3.706465000	4.975017000	3.289103000
H	-3.260199000	-3.790858000	-2.322212000
H	2.943436000	-5.080557000	-2.769227000
H	2.497001000	-3.447758000	-4.746886000
H	-3.172349000	-5.622532000	2.563707000
H	-4.783726000	-2.875777000	-2.640212000
H	-0.842010000	-4.959538000	-0.428247000

6. Supporting Information

H	0.481776000	-4.589594000	-1.596859000
H	-4.267457000	-5.633520000	3.990549000
H	4.641201000	-4.531571000	-2.898185000
H	-3.192645000	-2.273161000	-3.270549000
H	4.135663000	-2.682138000	-4.667373000
H	-4.435003000	-4.368284000	2.712485000
H	-0.907852000	-3.482885000	-1.482320000
H	-3.387930000	-3.640041000	0.267170000
H	-5.062429000	-3.070534000	-0.030221000
H	3.802795000	-4.476070000	-1.313119000
H	-1.092063000	-5.546466000	4.201019000
H	1.186244000	-5.043039000	1.391993000
H	2.331694000	-4.499818000	0.128390000
H	-0.876119000	-4.642646000	2.057698000
H	2.639290000	-1.688067000	-4.469425000
H	-2.226664000	-5.556776000	5.590296000
H	-8.266163000	-0.890054000	-1.195652000
H	2.089195000	-2.828107000	-2.369346000
H	-6.015393000	-1.202455000	-0.616161000
H	-8.392250000	0.251322000	-2.567929000
H	-2.383031000	-1.839370000	-0.999061000
H	5.758274000	-2.914568000	-1.887703000
H	-3.947289000	-2.124497000	1.022390000
H	-9.530555000	0.382426000	-1.175503000
H	6.938840000	-1.729457000	1.280064000
H	0.988955000	-2.476428000	-0.353499000
H	2.142009000	-3.544485000	1.632881000
H	-3.294853000	-3.441814000	4.754789000
H	-1.006351000	-4.239525000	5.418984000
H	8.672974000	-1.256570000	1.108747000
H	7.762643000	-2.163186000	-1.057508000
H	-7.376603000	0.009856000	1.130257000
H	7.379235000	-0.006254000	1.128981000
H	-2.638794000	1.686603000	-4.470320000

6. Supporting Information

H	-7.762932000	2.162238000	-1.060138000
H	-8.671701000	1.258816000	1.108476000
H	-3.047487000	-1.354553000	3.818836000
H	1.917340000	-2.377774000	3.547778000
H	-4.135299000	2.680377000	-4.668757000
H	3.970415000	-1.887074000	2.084932000
H	1.723376000	-1.158226000	1.379664000
H	-4.059150000	0.383565000	1.119811000
H	-6.937938000	1.733800000	1.277703000
H	-5.758170000	2.913776000	-1.889333000
H	-4.271503000	0.322388000	2.905116000
H	0.560604000	-1.211235000	3.603959000
H	9.530710000	-0.383739000	-1.177203000
H	-2.496740000	3.446215000	-4.748401000
H	4.059042000	-0.383088000	1.120716000
H	8.391830000	-0.255791000	-2.569446000
H	-2.089074000	2.827402000	-2.370575000
H	8.266259000	0.888706000	-1.199732000
H	2.113657000	-0.823384000	4.429833000
H	-1.723536000	1.158664000	1.378993000
H	6.015567000	1.202087000	-0.615908000
H	-3.970693000	1.887740000	2.083746000
H	4.271052000	-0.321544000	2.906054000
H	3.193094000	2.271999000	-3.270835000
H	2.383205000	1.838933000	-0.999284000
H	-4.641102000	4.530513000	-2.900348000
H	-2.114369000	0.824780000	4.429191000
H	-0.988894000	2.476226000	-0.354335000
H	-0.561183000	1.212477000	3.603486000
H	4.784098000	2.874815000	-2.640483000
H	-3.802993000	4.475542000	-1.315108000
H	-2.943388000	5.079619000	-2.771244000
H	3.947350000	2.124701000	1.022235000
H	-1.917994000	2.378898000	3.546677000

6. Supporting Information

H	0.908501000	3.482340000	-1.482799000
H	3.260524000	3.789999000	-2.322986000
H	3.047091000	1.355816000	3.818813000
H	5.062444000	3.070533000	-0.030600000
H	-2.142419000	3.545018000	1.631369000
H	-0.481371000	4.588621000	-1.598577000
H	-2.331667000	4.499844000	0.126506000
H	3.387866000	3.639955000	0.266496000
H	0.841793000	4.959532000	-0.429555000
H	-1.186521000	5.043445000	1.390217000
H	1.005819000	4.241164000	5.418134000
H	0.875688000	4.643253000	2.056512000
H	3.294364000	3.443406000	4.754059000
H	1.091324000	5.547641000	4.199660000
H	2.225985000	5.558626000	5.588868000
H	4.434246000	4.369472000	2.711258000
H	3.171536000	5.623690000	2.562575000
H	4.266915000	5.634829000	3.989214000
Si	-0.289113000	-1.253126000	-3.435604000
Si	1.334544000	-0.309578000	-1.948715000
Si	-1.334280000	0.309041000	-1.948905000
Si	0.289503000	1.252165000	-3.435943000
Si	0.000040000	-0.000002000	-0.040809000

Supplementary Table 7: Atomic coordinates of the optimized structure of **8**.

C	2.243354000	-6.203454000	-3.925362000
C	7.709839000	-1.254569000	1.524389000
C	-1.731665000	-5.631490000	4.787893000
C	1.559395000	-4.287978000	1.087387000
C	2.448660000	-4.725891000	-4.312830000
C	3.626302000	-2.883013000	0.566796000
C	8.412978000	1.190616000	1.381760000
C	3.944931000	-4.392857000	-4.495205000
C	2.153313000	-3.800187000	-1.951644000
C	7.566320000	0.071372000	0.746043000
C	2.095890000	-3.000727000	0.429553000
C	1.804114000	-3.772769000	-3.313111000
C	1.652543000	-1.721600000	3.989229000
C	-2.749182000	-4.781220000	4.002757000
C	1.618932000	-2.889189000	-1.021169000
C	6.093886000	0.443109000	0.610315000
C	-2.075236000	-3.809233000	3.041258000
C	-3.707946000	-4.029756000	4.950725000
C	-1.117064000	-2.882931000	3.489223000
C	5.353476000	0.914357000	1.711610000
C	5.421365000	0.273656000	-0.610771000
C	3.861101000	1.474473000	4.190455000
C	-1.887078000	-4.166349000	-1.372370000
C	0.881735000	-2.798999000	-3.726369000
C	-2.432251000	-3.768883000	1.684254000
C	3.910262000	-0.851837000	-2.935371000
C	0.526988000	-1.001851000	3.224657000
C	-0.502800000	-1.957688000	2.623835000
C	0.655645000	-1.922178000	-1.449305000
C	3.974740000	1.182316000	1.624877000
C	-1.868067000	-2.841480000	0.784967000
C	4.038490000	0.511293000	-0.745485000

6. Supporting Information

C	-0.866289000	-1.932426000	1.244644000
C	0.298487000	-1.881909000	-2.828078000
C	3.242236000	1.791097000	2.819883000
C	3.291909000	0.949288000	0.390594000
C	-0.159041000	0.057618000	4.107457000
C	-2.352761000	-2.876738000	-0.667069000
C	3.397626000	0.348832000	-2.123244000
C	-3.874490000	-2.669832000	-0.796656000
C	3.106083000	3.317455000	2.624764000
C	3.553605000	1.660114000	-2.920062000
C	-0.686936000	-0.862756000	-3.397076000
C	-1.838058000	-1.506038000	-4.190975000
C	0.048024000	0.197872000	-4.237688000
C	-4.059940000	-0.784778000	2.756096000
C	-3.497489000	0.437407000	2.011507000
C	-3.597437000	1.706838000	2.881460000
C	-3.370325000	1.133919000	-0.480390000
C	-4.135182000	0.698549000	0.646668000
C	2.153942000	5.817374000	-1.522096000
C	-3.918296000	1.752246000	-4.260449000
C	-3.284861000	2.036394000	-2.888668000
C	-4.043779000	1.450375000	-1.698973000
C	1.420039000	6.731028000	1.896611000
C	-5.529766000	0.555477000	0.518854000
C	0.125843000	6.063658000	1.405386000
C	0.741458000	6.193705000	-1.051081000
C	-5.440577000	1.280900000	-1.777385000
C	-6.201429000	0.822342000	-0.687557000
C	-3.084705000	3.554384000	-2.688720000
C	-8.055288000	-0.895205000	-0.673283000
C	-0.291566000	6.148106000	-2.185550000
C	-1.057829000	7.041219000	1.336329000
C	-7.704323000	0.600838000	-0.815940000
C	-8.502623000	1.463400000	0.182270000

6. Supporting Information

H	2.658953000	-6.878235000	-4.703393000
H	1.166905000	-6.439895000	-3.798650000
H	2.754990000	-6.445352000	-2.969538000
H	8.771701000	-1.576824000	1.577126000
H	7.335721000	-1.141416000	2.564487000
H	1.982677000	-5.188605000	0.593487000
H	-1.048799000	-6.175056000	4.103065000
H	-2.249555000	-6.377073000	5.427496000
H	1.832937000	-4.329094000	2.162245000
H	4.153210000	-3.715833000	0.054586000
H	7.122014000	-2.064392000	1.045136000
H	-1.106213000	-5.001093000	5.455180000
H	2.887093000	-4.545066000	-1.602490000
H	9.488935000	0.916184000	1.385344000
H	3.920864000	-2.913619000	1.636950000
H	4.411303000	-5.048911000	-5.260714000
H	8.118475000	1.375458000	2.436776000
H	1.945366000	-4.561441000	-5.292450000
H	0.454763000	-4.342911000	1.019388000
H	4.500329000	-4.533802000	-3.543407000
H	2.172109000	-2.459517000	3.346502000
H	1.269584000	-2.260235000	4.881537000
H	3.996102000	-1.928161000	0.145148000
H	7.954003000	-0.099994000	-0.283567000
H	8.300446000	2.145511000	0.828234000
H	2.404163000	-0.988207000	4.344389000
H	-3.363034000	-5.475562000	3.385622000
H	4.085571000	-3.337622000	-4.806747000
H	4.058915000	0.389911000	4.312537000
H	-4.254020000	-4.736524000	5.611273000
H	1.674994000	-2.140288000	0.990608000
H	-0.833966000	-2.879267000	4.554485000
H	5.871718000	1.075723000	2.668760000
H	-0.785727000	-4.277398000	-1.318238000

6. Supporting Information

H	3.881180000	-1.786930000	-2.343254000
H	-3.147462000	-3.323805000	5.600580000
H	-2.350148000	-5.061646000	-0.905376000
H	5.994528000	-0.076012000	-1.484703000
H	4.947662000	-0.700521000	-3.303249000
H	4.820369000	2.012053000	4.349831000
H	-3.193840000	-4.478102000	1.318467000
H	3.174096000	1.791043000	5.002644000
H	-2.173193000	-4.157315000	-2.444905000
H	0.607913000	-2.754189000	-4.794019000
H	3.261207000	-1.005529000	-3.822043000
H	1.001898000	-0.456271000	2.378725000
H	-4.452419000	-3.437533000	4.380099000
H	-0.665082000	-0.410658000	4.979001000
H	2.210278000	1.374590000	2.811299000
H	0.578804000	0.793040000	4.493586000
H	2.310541000	0.178814000	-1.961015000
H	-1.885107000	-2.021515000	-1.198917000
H	-4.446474000	-3.482338000	-0.300699000
H	-1.472634000	-2.029221000	-5.099450000
H	-2.392480000	-2.242847000	-3.576748000
H	4.628149000	1.886843000	-3.088647000
H	-0.922962000	0.618452000	3.531682000
H	4.106256000	3.801694000	2.629789000
H	0.540782000	-0.259572000	-5.122320000
H	2.492812000	3.769187000	3.433345000
H	-4.170588000	-2.661499000	-1.866859000
H	-3.411282000	-1.029094000	3.622209000
H	3.056381000	1.586137000	-3.910657000
H	-1.140766000	-0.329386000	-2.532356000
H	-4.085040000	-1.679734000	2.105144000
H	-4.190420000	-1.704395000	-0.355249000
H	2.618614000	3.556797000	1.656836000
H	0.830428000	0.703919000	-3.636684000

6. Supporting Information

H	3.105718000	2.515439000	-2.372381000
H	-2.555899000	-0.729783000	-4.523765000
H	-2.418206000	0.231341000	1.838282000
H	-5.084385000	-0.604919000	3.147007000
H	-0.656414000	0.976256000	-4.601062000
H	-3.115750000	1.549346000	3.869961000
H	-2.272367000	1.574635000	-2.882951000
H	-4.173961000	0.679867000	-4.381599000
H	2.243875000	5.992308000	1.954231000
H	2.169912000	4.777121000	-1.909028000
H	2.879459000	5.881188000	-0.686335000
H	-3.101694000	2.569638000	2.389643000
H	-4.661542000	1.975542000	3.054806000
H	-3.214698000	2.032096000	-5.071987000
H	-0.136707000	5.261484000	2.126476000
H	-6.108383000	0.210184000	1.390104000
H	1.265556000	7.159078000	2.908435000
H	2.490408000	6.494462000	-2.334367000
H	1.741668000	7.561321000	1.232952000
H	-7.493319000	-1.510310000	-1.405874000
H	-4.847022000	2.340523000	-4.420416000
H	-0.358057000	5.126813000	-2.613330000
H	-7.799828000	-1.268299000	0.341354000
H	-2.571955000	3.772735000	-1.729220000
H	-2.469471000	3.985173000	-3.506937000
H	0.779325000	7.239497000	-0.678445000
H	-5.963814000	1.512151000	-2.718727000
H	-4.065444000	4.076586000	-2.676549000
H	-1.241574000	7.491923000	2.333395000
H	-0.005894000	6.846930000	-2.998837000
H	-1.979691000	6.515271000	1.015529000
H	-9.141044000	-1.067048000	-0.832545000
H	-1.298378000	6.429153000	-1.815794000
H	-7.994870000	0.918706000	-1.842736000

6. Supporting Information

H	-0.868734000	7.874534000	0.626421000
H	-8.276228000	1.178124000	1.231632000
H	-8.259606000	2.539825000	0.067573000
H	-9.595456000	1.335269000	0.031071000
N	0.321710000	5.352880000	0.111239000
B	0.130231000	3.978057000	0.016882000
Si	-0.081036000	-0.779735000	-0.083556000
Si	1.392353000	1.052237000	0.258757000
Si	-0.263260000	2.410358000	1.286932000
Si	-1.468825000	1.137268000	-0.351219000
Si	0.255155000	2.440918000	-1.329754000

Supplementary Table 8: Atomic coordinates of the optimized structure of **10**.

C	8.384343000	-0.119258000	0.027100000
C	3.478430000	2.318572000	3.142632000
C	7.562253000	-0.966323000	1.020486000
C	3.684301000	0.138283000	4.420352000
C	5.348670000	-0.122238000	1.968374000
C	7.860867000	-2.471059000	0.860167000
C	6.071932000	-0.671728000	0.896153000
C	3.273643000	0.790928000	3.087199000
C	3.974968000	0.178471000	1.874254000
C	5.375581000	-0.940900000	-0.296220000
C	3.293179000	-0.064935000	0.644450000
C	4.006921000	-0.652297000	-0.446896000
C	3.809046000	0.090852000	-2.855154000
C	-0.601301000	0.320536000	4.149969000
C	3.359182000	-0.941885000	-1.802674000
C	0.549668000	-1.940358000	4.259992000
C	-0.226382000	-0.953345000	3.369373000
C	3.611418000	-2.374871000	-2.308411000
C	-3.200887000	2.918022000	2.506865000
C	2.376586000	-3.752136000	1.095673000
C	-1.840549000	3.975903000	-3.108456000
C	-1.456037000	-1.578534000	2.713671000
C	-3.455071000	1.595803000	1.754818000
C	0.885963000	-3.487114000	0.808375000
C	-2.968234000	1.980140000	-0.759705000
C	0.163082000	-0.220363000	-4.217731000
C	-2.472701000	2.571741000	-3.218119000
C	-3.898631000	1.894564000	0.322953000
C	-1.684038000	-1.547277000	1.305353000
C	-2.398584000	-2.193147000	3.559996000
C	-0.032501000	-2.191773000	-1.247779000
C	-3.440789000	2.345713000	-2.057133000

6. Supporting Information

C	0.579267000	-3.356061000	-0.685876000
C	-4.410771000	0.684713000	2.542182000
C	-0.031896000	-4.537265000	1.465182000
C	-5.263372000	2.138777000	0.080287000
C	-0.885431000	-0.953599000	-3.360898000
C	-0.266387000	-2.157077000	-2.652310000
C	0.895155000	-4.449169000	-1.513313000
C	-4.819552000	2.565209000	-2.248882000
C	-3.081179000	2.364735000	-4.614637000
C	-5.749715000	2.454086000	-1.200630000
C	-7.858062000	3.737888000	-0.575696000
C	-3.565560000	-2.802846000	3.068955000
C	-2.885822000	-2.130320000	0.797797000
C	2.556314000	-5.865985000	-3.773831000
C	0.091736000	-3.268314000	-3.444178000
C	-3.966495000	-4.439630000	4.982737000
C	0.661722000	-4.429763000	-2.899248000
C	-5.362627000	-2.319333000	4.765752000
C	-7.242723000	2.629846000	-1.453263000
C	-3.784131000	-2.759913000	1.683284000
C	-4.592752000	-3.423200000	4.008601000
C	-2.126533000	-1.317678000	-4.196316000
C	-3.248728000	-2.127187000	-0.688895000
C	1.033480000	-5.617718000	-3.778763000
C	-4.621501000	-1.483136000	-0.967263000
C	-3.148069000	-3.548528000	-1.279096000
C	-7.985894000	1.289104000	-1.270678000
C	0.255454000	-6.886910000	-3.375566000
H	9.473237000	-0.289290000	0.164886000
H	8.181225000	0.963400000	0.159999000
H	4.555424000	2.563631000	3.266944000
H	7.869176000	-0.670345000	2.049034000
H	4.715292000	0.421098000	4.721843000
H	8.134465000	-0.380495000	-1.023258000

6. Supporting Information

H	2.925008000	2.759357000	3.999292000
H	5.882975000	0.080884000	2.910896000
H	8.940292000	-2.680260000	1.016865000
H	3.125533000	2.815987000	2.215939000
H	3.008021000	0.469905000	5.235987000
H	3.643516000	-0.968432000	4.361589000
H	7.280666000	-3.075027000	1.587752000
H	7.595648000	-2.827178000	-0.158116000
H	2.184406000	0.612286000	2.951610000
H	5.919079000	-1.384567000	-1.146268000
H	4.913876000	0.082341000	-2.970325000
H	3.506678000	1.119106000	-2.568280000
H	0.304515000	0.815188000	4.561238000
H	1.465554000	-1.462188000	4.659379000
H	3.359962000	-0.133950000	-3.845243000
H	-1.118733000	1.051596000	3.496342000
H	-1.279393000	0.087808000	4.999088000
H	4.663130000	-2.523170000	-2.634650000
H	-2.444606000	3.538978000	1.982967000
H	0.456996000	-0.639026000	2.548900000
H	-2.834989000	2.725773000	3.537943000
H	-0.054377000	-2.274105000	5.129823000
H	2.258784000	-0.839380000	-1.678809000
H	3.011438000	-2.931716000	0.704534000
H	-1.346183000	4.121416000	-2.126606000
H	0.853721000	-2.843920000	3.695788000
H	2.551831000	-3.818471000	2.190230000
H	-4.138000000	3.510582000	2.579358000
H	-1.075628000	4.130928000	-3.898673000
H	3.380619000	-3.129712000	-1.533291000
H	2.953136000	-2.585723000	-3.176065000
H	-2.619226000	4.761246000	-3.213860000
H	2.723470000	-4.706184000	0.645531000
H	0.658962000	-2.511824000	1.286077000

6. Supporting Information

H	1.022346000	0.108591000	-3.598539000
H	-2.487633000	1.051359000	1.692402000
H	-2.212144000	-2.194273000	4.646169000
H	-1.647609000	1.835312000	-3.099308000
H	-0.273327000	0.681719000	-4.696892000
H	-3.926188000	0.356260000	3.484030000
H	0.140596000	-4.587792000	2.560572000
H	0.555837000	-0.878748000	-5.021785000
H	-1.214307000	-0.243480000	-2.569530000
H	-7.328202000	4.702606000	-0.714762000
H	-5.355340000	1.200826000	2.817619000
H	-3.262006000	-3.946149000	5.685645000
H	-2.280071000	2.352696000	-5.382707000
H	-5.972712000	2.058470000	0.918363000
H	3.113559000	-4.959665000	-4.087559000
H	-7.803089000	3.476441000	0.502485000
H	0.154722000	-5.548368000	1.044702000
H	1.352138000	-5.343259000	-1.058636000
H	-4.673922000	-1.733001000	5.411092000
H	-1.099737000	-4.286293000	1.304232000
H	2.913303000	-6.140556000	-2.758277000
H	-3.779548000	3.183858000	-4.889160000
H	-4.663060000	-0.228313000	1.968306000
H	-5.192671000	2.832038000	-3.250160000
H	-3.403404000	-5.225458000	4.438581000
H	-2.506785000	-1.491843000	-1.216951000
H	-8.929346000	3.890674000	-0.825391000
H	-3.638993000	1.408735000	-4.684896000
H	-0.085730000	-3.231860000	-4.532304000
H	2.826701000	-6.696172000	-4.460352000
H	-2.579156000	-0.403861000	-4.629670000
H	-4.749959000	-4.933478000	5.595430000
H	-4.670515000	-0.451238000	-0.567119000
H	-7.360492000	2.937879000	-2.516718000

6. Supporting Information

H	-5.842405000	-1.609339000	4.061388000
H	-6.151539000	-2.753499000	5.416147000
H	-1.873784000	-1.993392000	-5.040376000
H	-2.896297000	-1.822147000	-3.580521000
H	0.737391000	-5.358077000	-4.820245000
H	-2.135202000	-3.974470000	-1.131298000
H	-7.914775000	0.936361000	-0.219570000
H	-4.702060000	-3.219828000	1.280281000
H	-5.325846000	-3.970385000	3.373997000
H	0.524596000	-7.212766000	-2.348193000
H	-4.805684000	-1.426994000	-2.060778000
H	-5.453348000	-2.068112000	-0.520975000
H	-3.356153000	-3.542861000	-2.369275000
H	-9.063283000	1.391687000	-1.520958000
H	-7.550915000	0.498997000	-1.916797000
H	-3.884149000	-4.227236000	-0.797982000
H	0.484026000	-7.728557000	-4.063279000
H	-0.839533000	-6.709543000	-3.394425000
Si	1.238891000	3.989759000	-0.204430000
Si	0.288359000	2.335042000	1.243696000
Si	1.488100000	0.482063000	0.389106000
Si	0.930090000	1.979640000	-1.435554000
Si	-1.165620000	1.444014000	-0.452053000
Si	-0.479732000	-0.795373000	0.001049000
H	0.249903000	5.102928000	-0.474324000
N	2.833176000	4.688749000	0.057612000
C	2.963208000	5.916948000	0.881220000
H	3.996132000	5.889997000	1.303843000
C	2.000335000	5.924912000	2.079384000
C	2.826617000	7.202019000	0.040369000
H	3.565742000	7.221939000	-0.786669000
H	1.811888000	7.264497000	-0.406897000
H	2.987705000	8.109187000	0.660723000
H	0.938889000	6.004290000	1.761102000

6. Supporting Information

H	2.211131000	6.800116000	2.727875000
H	2.108604000	5.003901000	2.686689000
C	4.044558000	4.342001000	-0.735260000
H	4.803244000	5.104903000	-0.446280000
C	3.832761000	4.478616000	-2.254639000
C	4.619342000	2.968468000	-0.364062000
H	4.869032000	2.908739000	0.712490000
H	3.891129000	2.160842000	-0.574548000
H	5.536435000	2.744533000	-0.947787000
H	3.113225000	3.719055000	-2.627539000
H	4.787597000	4.329001000	-2.801133000
H	3.433626000	5.480698000	-2.512913000

Supplementary Table 9: Atomic coordinates of the optimized structure of **9**.

C	5.590711000	-4.372327000	-3.619296000
C	7.539100000	2.292282000	1.779653000
C	0.919956000	-5.903560000	4.666994000
C	3.605412000	-3.085988000	1.259081000
C	5.100434000	-2.968588000	-4.025408000
C	4.792791000	-0.853266000	0.873818000
C	7.076446000	4.798796000	1.777442000
C	6.264742000	-1.956732000	-4.080319000
C	4.184992000	-2.328199000	-1.728604000
C	6.853384000	3.463629000	1.042316000
C	3.525256000	-1.689342000	0.610065000
C	3.988179000	-2.464091000	-3.113785000
C	2.310562000	-0.904880000	4.080368000
C	-0.366188000	-5.525113000	3.904450000
C	3.190823000	-1.808678000	-0.877849000
C	5.380056000	3.142167000	0.819214000
C	-0.132792000	-4.352358000	2.958134000
C	-1.532471000	-5.243849000	4.874503000
C	0.304633000	-3.104797000	3.437500000
C	4.452725000	3.187294000	1.877382000
C	4.920929000	2.726332000	-0.441311000
C	2.766942000	2.899993000	4.269392000
C	0.608989000	-4.637299000	-1.382720000
C	2.746460000	-2.067412000	-3.633420000
C	-0.356592000	-4.473759000	1.577753000
C	4.212239000	1.120483000	-2.852835000
C	1.039044000	-0.712950000	3.233099000
C	0.549431000	-2.009563000	2.586033000
C	1.919210000	-1.436996000	-1.415338000
C	3.109048000	2.801907000	1.712957000
C	-0.150538000	-3.401056000	0.687770000
C	3.591301000	2.311147000	-0.654487000

6. Supporting Information

C	0.330013000	-2.149810000	1.183129000
C	1.710848000	-1.566228000	-2.818441000
C	2.128372000	2.970407000	2.872835000
C	2.673200000	2.322296000	0.438679000
C	-0.079195000	-0.056507000	4.063531000
C	-0.418586000	-3.647882000	-0.799292000
C	3.159321000	1.915188000	-2.064931000
C	-1.873448000	-4.061906000	-1.089570000
C	1.341220000	4.288968000	2.707566000
C	2.709968000	3.170448000	-2.840771000
C	0.403335000	-1.167348000	-3.497767000
C	-0.180787000	-2.291234000	-4.372153000
C	0.559741000	0.137114000	-4.301320000
C	-3.368604000	-2.732054000	2.271866000
C	-3.248507000	-1.248130000	1.870107000
C	-3.688299000	-0.331726000	3.025596000
C	-3.317967000	-0.565129000	-0.626887000
C	-3.994715000	-0.960615000	0.566538000
C	-3.542288000	5.831054000	1.516966000
C	-3.719026000	-1.446678000	-4.165182000
C	-3.343274000	-0.305872000	-3.197711000
C	-4.044253000	-0.488852000	-1.850706000
C	-4.963549000	2.571764000	0.853347000
C	-5.391443000	-1.134194000	0.534042000
C	-4.224545000	2.945678000	-0.442006000
C	-3.810002000	5.396235000	0.064664000
C	-5.445106000	-0.637160000	-1.824171000
C	-6.143762000	-0.928499000	-0.638370000
C	-3.589577000	1.072044000	-3.833734000
C	-8.226588000	-2.236398000	0.063025000
C	-3.324275000	6.439083000	-0.954904000
C	-5.204381000	3.223263000	-1.593415000
C	-7.667627000	-0.977362000	-0.626228000
C	-8.231174000	0.310759000	0.013546000

6. Supporting Information

H	6.357447000	-4.745655000	-4.330651000
H	4.753043000	-5.099464000	-3.597746000
H	6.052172000	-4.361876000	-2.608956000
H	8.629259000	2.472181000	1.895327000
H	7.104486000	2.160970000	2.793817000
H	4.430651000	-3.679542000	0.811138000
H	1.754846000	-6.112486000	3.966903000
H	0.758671000	-6.804870000	5.295492000
H	3.794602000	-3.011586000	2.350027000
H	5.704961000	-1.346517000	0.476033000
H	7.397363000	1.338257000	1.231087000
H	1.244521000	-5.081407000	5.339768000
H	5.154858000	-2.619322000	-1.293175000
H	8.159410000	5.034616000	1.843596000
H	4.941972000	-0.712988000	1.964948000
H	7.050307000	-2.290219000	-4.791245000
H	6.685272000	4.762497000	2.816431000
H	4.672548000	-3.044610000	-5.050584000
H	2.659697000	-3.647079000	1.118506000
H	6.738862000	-1.842298000	-3.082022000
H	3.135707000	-1.341877000	3.485397000
H	2.130758000	-1.572814000	4.949066000
H	4.714165000	0.151540000	0.413985000
H	7.323281000	3.549349000	0.036537000
H	6.570037000	5.636656000	1.255608000
H	2.655650000	0.069299000	4.480320000
H	-0.654674000	-6.397813000	3.276292000
H	5.910066000	-0.954452000	-4.396492000
H	3.428430000	2.016496000	4.378538000
H	-1.717004000	-6.114095000	5.539593000
H	2.693488000	-1.138189000	1.098032000
H	0.475226000	-2.980432000	4.519391000
H	4.792659000	3.532182000	2.865116000
H	1.642466000	-4.262654000	-1.234750000

6. Supporting Information

H	4.596134000	0.265317000	-2.263225000
H	-1.310169000	-4.367904000	5.520686000
H	0.527091000	-5.633200000	-0.897741000
H	5.633565000	2.706396000	-1.281609000
H	5.073669000	1.751570000	-3.159421000
H	3.371741000	3.804329000	4.494534000
H	-0.709721000	-5.441350000	1.182621000
H	1.978425000	2.838187000	5.048057000
H	0.453686000	-4.777009000	-2.472927000
H	2.582236000	-2.150893000	-4.720853000
H	3.759126000	0.707307000	-3.777276000
H	1.289954000	-0.004465000	2.412407000
H	-2.469896000	-5.025042000	4.323512000
H	-0.391380000	-0.709692000	4.906406000
H	1.391452000	2.140382000	2.796140000
H	0.257300000	0.912660000	4.488826000
H	2.274423000	1.248449000	-1.957546000
H	-0.274887000	-2.684770000	-1.330746000
H	-2.144483000	-5.017047000	-0.592265000
H	0.489587000	-2.544018000	-5.219919000
H	-0.344741000	-3.217021000	-3.785782000
H	3.556440000	3.882340000	-2.945620000
H	-0.974086000	0.139482000	3.439365000
H	2.030136000	5.158774000	2.765716000
H	1.260721000	0.000473000	-5.152359000
H	0.574865000	4.395196000	3.504546000
H	-2.023259000	-4.201169000	-2.181454000
H	-2.696605000	-2.944202000	3.128481000
H	2.356248000	2.903359000	-3.859443000
H	-0.332244000	-0.959150000	-2.688119000
H	-3.066201000	-3.401465000	1.444196000
H	-2.582986000	-3.279321000	-0.751015000
H	0.817485000	4.337363000	1.730916000
H	0.953646000	0.955401000	-3.666186000

6. Supporting Information

H	1.885102000	3.695683000	-2.315829000
H	-1.152445000	-1.982594000	-4.803452000
H	-2.167466000	-1.061478000	1.682656000
H	-4.407286000	-2.992543000	2.568595000
H	-0.418337000	0.469281000	-4.709969000
H	-3.171516000	-0.614653000	3.965712000
H	-2.249647000	-0.382786000	-3.004272000
H	-3.485254000	-2.438135000	-3.725947000
H	-4.241146000	2.396817000	1.675732000
H	-2.454108000	5.967796000	1.691046000
H	-3.909064000	5.066181000	2.230996000
H	-3.447016000	0.729425000	2.809590000
H	-4.781383000	-0.401389000	3.208561000
H	-3.163840000	-1.347857000	-5.121307000
H	-3.614359000	2.068551000	-0.741303000
H	-5.910672000	-1.421994000	1.462412000
H	-5.544701000	1.638641000	0.709117000
H	-4.049686000	6.793225000	1.740185000
H	-5.662827000	3.375751000	1.168032000
H	-7.806494000	-3.161417000	-0.382529000
H	-4.800706000	-1.431733000	-4.414221000
H	-2.221657000	6.558310000	-0.893505000
H	-7.990200000	-2.246574000	1.148170000
H	-3.200226000	1.881431000	-3.184281000
H	-3.073436000	1.148195000	-4.814153000
H	-4.910535000	5.300757000	-0.054312000
H	-6.017167000	-0.531975000	-2.761939000
H	-4.671687000	1.254720000	-4.001768000
H	-5.757164000	2.292131000	-1.835902000
H	-3.788406000	7.429198000	-0.762448000
H	-4.667051000	3.557193000	-2.502751000
H	-9.332073000	-2.276769000	-0.031049000
H	-3.578050000	6.124040000	-1.987286000
H	-8.000310000	-0.998390000	-1.688550000

6. Supporting Information

H	-5.951560000	4.000153000	-1.325974000
H	-7.917107000	0.389966000	1.076397000
H	-7.860233000	1.215381000	-0.511137000
H	-9.341477000	0.321609000	-0.016374000
N	-3.258571000	4.046907000	-0.237445000
P	-1.568002000	3.819743000	-0.012275000
Si	0.612353000	-0.791860000	-0.154762000
Si	0.960026000	1.529544000	0.203172000
Si	-1.160714000	1.823839000	1.179816000
Si	-1.553428000	0.138485000	-0.520858000
Si	-0.699151000	2.158323000	-1.440333000

Supplementary Table 10: Atomic coordinates of the optimized structure of **8_{Tip}**.

C	7.427558000	1.769045000	-3.582034000
C	1.025133000	8.151007000	2.219037000
C	5.903429000	-3.430614000	4.653162000
C	5.349309000	0.755872000	1.319085000
C	6.017103000	2.314307000	-3.885611000
C	4.102003000	2.988045000	1.110252000
C	-1.373388000	8.078547000	1.358287000
C	5.973322000	3.852600000	-3.777773000
C	4.988189000	1.822353000	-1.601153000
C	0.081770000	7.625884000	1.117818000
C	4.126624000	1.493369000	0.739599000
C	4.963174000	1.662208000	-2.997694000
C	2.835833000	0.735950000	4.233502000
C	4.887768000	-4.163369000	3.754157000
C	4.012720000	1.248061000	-0.766242000
C	0.168746000	6.110793000	0.970734000
C	4.115341000	-3.199011000	2.860514000
C	3.925774000	-5.036220000	4.587360000
C	3.384549000	-2.126286000	3.402401000
C	-0.155755000	5.256382000	2.041193000
C	0.578481000	5.522809000	-0.237729000
C	0.290128000	3.513068000	4.422131000
C	4.775849000	-2.514844000	-1.461717000
C	3.922017000	0.895009000	-3.544425000
C	4.082917000	-3.367355000	1.467564000
C	2.398261000	4.139976000	-2.267476000
C	1.922713000	-0.085209000	3.304274000
C	2.662172000	-1.221995000	2.599567000
C	2.973374000	0.447030000	-1.332278000
C	-0.103476000	3.854722000	1.924114000
C	3.351662000	-2.506068000	0.625679000
C	0.626324000	4.125595000	-0.414729000

6. Supporting Information

C	2.642732000	-1.400402000	1.184508000
C	2.933462000	0.281396000	-2.746687000
C	-0.426603000	3.007225000	3.155490000
C	0.250947000	3.274272000	0.667573000
C	0.688895000	-0.611902000	4.059998000
C	3.375755000	-2.787517000	-0.878008000
C	1.047210000	3.584594000	-1.781222000
C	2.848706000	-4.190588000	-1.233647000
C	-1.943606000	2.885779000	3.393349000
C	-0.059605000	3.831237000	-2.822994000
C	1.852204000	-0.530252000	-3.459013000
C	2.431223000	-1.630084000	-4.367684000
C	0.890377000	0.385589000	-4.237966000
C	0.845271000	-4.668377000	2.128784000
C	-0.238366000	-3.688760000	1.642961000
C	-1.355413000	-3.532764000	2.690601000
C	-0.860924000	-3.159041000	-0.819043000
C	-0.824329000	-4.068316000	0.282552000
C	-0.855560000	-3.461964000	-4.563087000
C	-1.374492000	-2.715081000	-3.319400000
C	-1.386398000	-3.597690000	-2.070869000
C	-1.371201000	-5.355516000	0.128694000
C	-1.938761000	-4.890975000	-2.166080000
C	-1.957561000	-5.780240000	-1.078299000
C	-2.751274000	-2.080329000	-3.591490000
C	-1.576496000	-8.288585000	-0.935065000
C	-2.593804000	-7.160388000	-1.200679000
C	-3.825577000	-7.284620000	-0.279478000
H	8.178735000	2.200364000	-4.277259000
H	7.459752000	0.664189000	-3.677155000
H	7.742837000	2.026119000	-2.548129000
H	0.995333000	9.259989000	2.270705000
H	0.733296000	7.762493000	3.217905000
H	6.292195000	1.128729000	0.865655000

6. Supporting Information

H	6.592489000	-2.802011000	4.052386000
H	6.511324000	-4.154660000	5.235722000
H	5.421044000	0.900904000	2.417296000
H	4.962396000	3.540445000	0.676789000
H	2.073504000	7.840295000	2.031552000
H	5.391316000	-2.766396000	5.381335000
H	5.788009000	2.428712000	-1.144609000
H	-1.444853000	9.186267000	1.397351000
H	4.149052000	3.110843000	2.212875000
H	6.710649000	4.320440000	-4.464053000
H	-1.761869000	7.683006000	2.321038000
H	5.771048000	2.043225000	-4.937193000
H	5.276839000	-0.333992000	1.125775000
H	6.214372000	4.188361000	-2.746677000
H	3.729276000	1.109918000	3.695717000
H	3.190363000	0.135854000	5.097824000
H	3.166597000	3.469163000	0.758913000
H	0.415576000	8.066501000	0.151424000
H	-2.044295000	7.715036000	0.552885000
H	2.287954000	1.608024000	4.640906000
H	5.460097000	-4.841930000	3.082221000
H	4.967052000	4.246065000	-4.028181000
H	1.371760000	3.675845000	4.238074000
H	4.486523000	-5.757784000	5.218891000
H	3.228444000	1.054117000	1.221041000
H	3.383047000	-1.981814000	4.495130000
H	-0.456754000	5.699086000	3.004514000
H	5.080917000	-1.464442000	-1.278051000
H	3.193124000	4.005233000	-1.508894000
H	3.304791000	-4.408072000	5.261512000
H	5.535890000	-3.183357000	-1.004640000
H	0.860144000	6.181401000	-1.076622000
H	2.338531000	5.220006000	-2.520943000
H	-0.136584000	4.471450000	4.787086000

6. Supporting Information

H	4.641172000	-4.208751000	1.022985000
H	0.182115000	2.777320000	5.246694000
H	4.791632000	-2.684793000	-2.558559000
H	3.882027000	0.769141000	-4.639547000
H	2.718827000	3.593022000	-3.177843000
H	1.548144000	0.603574000	2.513991000
H	3.235770000	-5.608522000	3.934310000
H	0.981316000	-1.342979000	4.843644000
H	-0.050093000	1.982630000	2.946214000
H	0.137653000	0.217153000	4.552698000
H	1.176231000	2.483671000	-1.680981000
H	2.678211000	-2.074710000	-1.365854000
H	3.475025000	-4.994230000	-0.792067000
H	3.010063000	-1.202301000	-5.213308000
H	3.106799000	-2.306047000	-3.807481000
H	-0.267620000	4.917068000	-2.931778000
H	-0.013489000	-1.116714000	3.366414000
H	-2.401644000	3.886543000	3.546451000
H	1.422219000	0.938310000	-5.041688000
H	-2.153018000	2.268207000	4.292525000
H	2.848525000	-4.334403000	-2.334810000
H	1.333795000	-4.264061000	3.038869000
H	0.236312000	3.439500000	-3.818559000
H	1.245067000	-1.031055000	-2.671936000
H	1.635943000	-4.810418000	1.367028000
H	1.807355000	-4.327002000	-0.877537000
H	-2.448861000	2.406685000	2.530792000
H	0.421761000	1.129954000	-3.563701000
H	-1.002748000	3.332449000	-2.522837000
H	1.615784000	-2.241288000	-4.801831000
H	0.257754000	-2.698971000	1.528059000
H	0.422765000	-5.664267000	2.382518000
H	0.075022000	-0.204013000	-4.708827000
H	-0.936255000	-3.260151000	3.681475000

6. Supporting Information

H	-0.667902000	-1.881412000	-3.115061000
H	0.107250000	-3.972592000	-4.356621000
H	-2.071932000	-2.742029000	2.389689000
H	-1.924361000	-4.479371000	2.809644000
H	-0.701641000	-2.751996000	-5.402844000
H	-1.350397000	-6.047116000	0.986986000
H	-0.697506000	-8.203356000	-1.606465000
H	-1.574890000	-4.230237000	-4.917970000
H	-1.203867000	-8.256989000	0.110954000
H	-3.072452000	-1.440411000	-2.745221000
H	-2.718778000	-1.444303000	-4.501497000
H	-2.371343000	-5.223730000	-3.124262000
H	-3.526420000	-2.861847000	-3.743302000
H	-2.040267000	-9.285151000	-1.093559000
H	-2.946703000	-7.265378000	-2.251352000
H	-3.533153000	-7.201058000	0.789028000
H	-4.564729000	-6.483843000	-0.488266000
H	-4.327958000	-8.265980000	-0.414774000
B	-3.026176000	0.518097000	-0.085032000
Si	1.709670000	-0.285493000	-0.078970000
Si	0.093339000	1.402736000	0.363912000
Si	-1.522353000	-0.099826000	1.185881000
Si	-0.366788000	-1.343221000	-0.539970000
Si	-1.404460000	0.605700000	-1.360568000
C	-4.557768000	0.787744000	-0.082425000
C	-5.501729000	-0.235338000	0.306553000
C	-5.097220000	2.071567000	-0.463675000
C	-6.881362000	0.037204000	0.290349000
C	-6.488598000	2.287380000	-0.424290000
C	-7.407508000	1.292137000	-0.059974000
H	-7.571496000	-0.773819000	0.578280000
H	-6.871682000	3.283891000	-0.704897000
C	-4.270986000	3.267805000	-0.954134000
H	-4.964904000	4.136970000	-0.920984000

6. Supporting Information

C	-3.876246000	3.096718000	-2.436940000
C	-3.089229000	3.635371000	-0.046591000
H	-3.428302000	3.869968000	0.981566000
H	-2.354546000	2.807666000	0.030392000
H	-2.523564000	4.507410000	-0.435472000
H	-3.203042000	2.226571000	-2.581165000
H	-3.348540000	3.999712000	-2.808934000
H	-4.776307000	2.934492000	-3.064935000
C	-5.125114000	-1.644313000	0.783536000
H	-6.068905000	-2.232198000	0.738578000
C	-4.704292000	-1.624647000	2.269113000
C	-4.125272000	-2.373972000	-0.122345000
H	-4.506135000	-2.461430000	-1.158975000
H	-3.153026000	-1.841403000	-0.172022000
H	-3.891918000	-3.392335000	0.252420000
H	-3.783809000	-1.023959000	2.420900000
H	-4.504496000	-2.653089000	2.635796000
H	-5.504232000	-1.179255000	2.895663000
C	-8.907396000	1.558488000	-0.053320000
H	-9.050041000	2.625890000	-0.335790000
C	-9.514327000	1.361231000	1.351295000
C	-9.634762000	0.695204000	-1.105360000
H	-9.213144000	0.856054000	-2.118767000
H	-9.539492000	-0.386149000	-0.869520000
H	-10.718066000	0.938099000	-1.136877000
H	-9.425227000	0.304573000	1.682200000
H	-10.593643000	1.622721000	1.355840000
H	-9.000506000	1.993556000	2.104177000

Supplementary Table 11: Atomic coordinates of the optimized structure of **2**.

C	-6.467679000	5.945015000	1.920427000
C	-7.870427000	4.763139000	0.149893000
C	-6.999330000	4.589816000	1.412123000
C	-5.876808000	3.592003000	1.155282000
C	-5.840788000	2.346875000	1.800013000
C	-4.838888000	3.879716000	0.253645000
C	-6.186243000	-0.687764000	2.157996000
C	-4.526903000	0.363030000	3.798475000
C	-8.413969000	-3.811530000	0.060922000
C	-4.850182000	1.387442000	1.512694000
C	0.212234000	8.304475000	-0.223288000
C	-4.870634000	0.093648000	2.319993000
C	-3.813574000	2.963929000	-0.053366000
C	-6.131706000	1.409483000	-2.043089000
C	-2.152317000	4.824648000	-0.520164000
C	-3.843377000	1.659987000	0.535700000
C	-1.558962000	3.119585000	2.907835000
C	1.221013000	7.616588000	0.720435000
C	-3.196763000	3.585079000	-2.457891000
C	-2.717185000	3.470859000	-0.995266000
C	-7.600094000	-3.716446000	-1.246931000
C	0.464163000	3.820361000	4.253108000
C	0.657331000	5.348493000	1.744191000
C	2.663613000	8.086187000	0.445352000
C	-6.171625000	-1.646803000	-1.692028000
C	1.092397000	6.100221000	0.640538000
C	-4.937936000	0.462200000	-2.257642000
C	-0.021095000	3.215549000	2.923273000
C	-6.345103000	-2.877078000	-1.040771000
C	-7.276677000	-5.113919000	-1.812354000
C	-5.052023000	-0.826908000	-1.450535000
C	0.495106000	3.949462000	1.684854000

6. Supporting Information

C	-5.316326000	-3.301664000	-0.183718000
C	-4.051177000	-1.230023000	-0.513587000
C	1.389056000	5.410160000	-0.547648000
C	-4.694415000	0.156747000	-3.748845000
C	-3.549849000	-3.253913000	2.449441000
C	-4.168162000	-2.528333000	0.076744000
C	0.770918000	3.266403000	0.461325000
C	1.242411000	4.015298000	-0.664070000
C	-3.107834000	-3.173722000	0.973119000
C	0.396873000	3.501128000	-2.997908000
C	1.533253000	-0.277050000	4.138213000
C	1.576410000	3.376841000	-2.015429000
C	-2.719497000	-4.575125000	0.460288000
C	3.377722000	1.467700000	4.079537000
C	2.621516000	0.392517000	3.279182000
C	2.857575000	3.932457000	-2.665425000
C	0.040610000	-3.587165000	2.897657000
C	4.596329000	3.456668000	0.711945000
C	-1.966548000	-2.922453000	-2.951187000
C	3.542782000	-0.656638000	2.658470000
C	1.212679000	-3.613834000	1.899504000
C	4.672529000	1.925903000	0.552469000
C	0.381375000	-3.380821000	-0.556475000
C	1.507826000	0.074203000	-4.202570000
C	-0.451773000	-3.202303000	-2.997243000
C	0.773110000	-4.195592000	0.553738000
C	3.503934000	-0.999493000	1.273912000
C	4.452913000	-1.308339000	3.512677000
C	3.581739000	0.559151000	-1.376309000
C	-0.010191000	-4.010095000	-1.776888000
C	4.582034000	1.467117000	-0.905828000
C	2.419365000	-4.333898000	2.529513000
C	5.930563000	1.345575000	1.230495000
C	0.720752000	-5.596530000	0.429014000

6. Supporting Information

C	2.531100000	-0.720935000	-3.371600000
C	3.574185000	0.211528000	-2.758499000
C	5.557030000	1.952818000	-1.797009000
C	-0.046048000	-5.417259000	-1.845592000
C	-0.062516000	-3.841596000	-4.342150000
C	0.297964000	-6.229605000	-0.752887000
C	-0.998570000	-8.226744000	0.060740000
C	5.357673000	-2.279169000	3.048622000
C	4.389364000	-2.016325000	0.798058000
C	6.391212000	3.707565000	-4.298182000
C	4.555293000	0.749056000	-3.617207000
C	7.195381000	-1.983454000	4.785632000
C	5.565240000	1.609913000	-3.159627000
C	5.566805000	-3.937768000	4.940440000
C	0.167508000	-7.745874000	-0.829770000
C	5.305146000	-2.614233000	1.687036000
C	6.324327000	-2.980143000	3.996271000
C	3.147757000	-1.865374000	-4.195241000
C	4.420670000	-2.476213000	-0.662160000
C	6.603220000	2.189877000	-4.113330000
C	4.165549000	-3.986427000	-0.832123000
C	5.733525000	-2.040609000	-1.344350000
C	1.482443000	-8.468761000	-0.478715000
C	8.043081000	1.872438000	-3.663270000
H	-7.304866000	6.631391000	2.167902000
H	-8.726599000	5.443678000	0.344270000
H	-5.843623000	5.816915000	2.828715000
H	-5.842534000	6.447534000	1.151852000
H	-7.277197000	5.195552000	-0.684043000
H	-8.271080000	3.788428000	-0.196962000
H	-6.614790000	2.112473000	2.549910000
H	-4.824066000	4.865684000	-0.236858000
H	-7.040624000	-0.136220000	2.604869000
H	-5.286268000	1.015579000	4.279017000

6. Supporting Information

H	-8.658970000	-2.803523000	0.454469000
H	-9.363638000	-4.364804000	-0.098889000
H	0.257148000	9.409329000	-0.118998000
H	-0.825440000	7.975318000	-0.009006000
H	-2.884970000	5.648122000	-0.655741000
H	-6.281371000	1.623426000	-0.965855000
H	-2.020378000	4.129612000	2.938189000
H	-7.840235000	-4.346183000	0.847778000
H	-6.411345000	-0.867299000	1.087869000
H	-6.122535000	-1.673446000	2.662796000
H	-4.486830000	-0.586926000	4.372805000
H	-3.541298000	0.864220000	3.887670000
H	-4.132789000	4.179412000	-2.520163000
H	-7.070986000	0.973934000	-2.445151000
H	0.963201000	7.912120000	1.762442000
H	-5.961366000	2.375388000	-2.561105000
H	-1.862185000	4.793561000	0.546762000
H	-0.057811000	4.771900000	4.489915000
H	0.428404000	8.057514000	-1.284649000
H	-1.926984000	2.549756000	3.787077000
H	0.428848000	5.880475000	2.681296000
H	-8.228319000	-3.185782000	-1.997466000
H	2.754360000	9.185669000	0.573241000
H	-1.246633000	5.087867000	-1.099769000
H	-1.935129000	2.611162000	1.999357000
H	0.253972000	3.122150000	5.089994000
H	-4.054091000	-0.551475000	1.931382000
H	-6.939315000	-1.311352000	-2.409387000
H	-3.390182000	2.595265000	-2.913741000
H	-8.207634000	-5.686854000	-2.008757000
H	-2.434989000	4.095153000	-3.081190000
H	-4.030579000	0.995010000	-1.902515000
H	-1.878146000	2.742165000	-0.960666000
H	1.553230000	4.028900000	4.239687000

6. Supporting Information

H	-3.624974000	-2.253441000	2.916479000
H	3.383203000	7.595699000	1.132658000
H	-6.665956000	-5.705898000	-1.097962000
H	2.974871000	7.844789000	-0.593292000
H	-4.540077000	-3.748716000	2.537907000
H	-5.550009000	-0.392698000	-4.195294000
H	-4.559210000	1.095846000	-4.326570000
H	0.368560000	2.174820000	2.864742000
H	-5.410396000	-4.281845000	0.310177000
H	-6.706429000	-5.041598000	-2.761187000
H	1.741607000	5.978250000	-1.422755000
H	-2.825574000	-3.846142000	3.043934000
H	0.096233000	4.563526000	-3.119315000
H	-0.483848000	2.929423000	-2.646080000
H	0.807059000	0.471838000	4.520251000
H	-3.784747000	-0.464468000	-3.879900000
H	2.669799000	2.225808000	4.467120000
H	-2.192649000	-2.544217000	0.919270000
H	-3.544349000	-5.306328000	0.595267000
H	0.675653000	3.110202000	-3.998588000
H	0.968769000	-1.024397000	3.546350000
H	1.977869000	-0.801608000	5.011172000
H	2.698819000	4.941738000	-3.101980000
H	-0.767139000	-2.916933000	2.545174000
H	2.099310000	0.909490000	2.442674000
H	0.375576000	-3.221689000	3.890710000
H	3.908754000	1.036601000	4.954026000
H	1.754336000	2.294734000	-1.837095000
H	3.640949000	3.857234000	0.320270000
H	-2.264241000	-2.403281000	-2.019763000
H	4.127910000	1.988925000	3.452953000
H	4.657953000	3.733926000	1.785469000
H	-1.841801000	-4.959680000	1.014544000
H	-2.448605000	-4.555997000	-0.611884000

6. Supporting Information

H	-0.384595000	-4.604293000	3.034631000
H	-2.276353000	-2.282700000	-3.804402000
H	3.695592000	3.994415000	-1.946692000
H	3.177142000	3.258585000	-3.486119000
H	-2.545458000	-3.869144000	-3.002728000
H	5.430893000	3.969984000	0.188863000
H	3.786178000	1.524815000	1.085914000
H	1.014722000	0.849594000	-3.583279000
H	1.525965000	-2.563100000	1.720673000
H	4.459987000	-1.039743000	4.581499000
H	0.061183000	-2.217383000	-2.932401000
H	0.715521000	-0.592638000	-4.604434000
H	2.811552000	-3.727520000	3.370835000
H	5.950784000	1.595022000	2.311496000
H	1.997386000	0.584405000	-5.059660000
H	1.970757000	-1.183404000	-2.527914000
H	-1.943650000	-7.710720000	-0.206672000
H	2.142327000	-5.330424000	2.935494000
H	6.580059000	-1.357805000	5.466833000
H	-0.201263000	-3.112566000	-5.167624000
H	1.007300000	-6.215255000	1.293718000
H	5.367870000	3.928386000	-4.664842000
H	-0.793098000	-8.010579000	1.131063000
H	6.852892000	1.759420000	0.770034000
H	6.329589000	2.639256000	-1.413468000
H	4.865939000	-3.375521000	5.594325000
H	5.964796000	0.241792000	1.139939000
H	6.521549000	4.246408000	-3.335473000
H	-0.695513000	-4.722454000	-4.581670000
H	3.245779000	-4.470885000	1.807366000
H	-0.369143000	-5.905201000	-2.779060000
H	7.741422000	-1.299435000	4.103973000
H	3.584205000	-1.971305000	-1.187860000
H	-1.155478000	-9.321746000	-0.039999000

6. Supporting Information

H	0.994704000	-4.176298000	-4.348582000
H	4.538369000	0.481930000	-4.687091000
H	7.119765000	4.127876000	-5.023684000
H	2.355470000	-2.552369000	-4.551302000
H	7.940010000	-2.518990000	5.411666000
H	3.172307000	-4.275776000	-0.436948000
H	-0.087032000	-7.999021000	-1.883629000
H	4.969570000	-4.676462000	4.367572000
H	6.270645000	-4.491999000	5.597220000
H	3.682461000	-1.487851000	-5.091897000
H	3.868722000	-2.455602000	-3.595950000
H	6.445138000	1.704810000	-5.103109000
H	5.890922000	-0.947507000	-1.253976000
H	1.775230000	-8.286225000	0.577047000
H	5.997322000	-3.384200000	1.306810000
H	7.005183000	-3.597603000	3.367836000
H	8.281167000	2.363215000	-2.695609000
H	4.187600000	-4.258360000	-1.908510000
H	4.937328000	-4.599265000	-0.320013000
H	5.721294000	-2.291182000	-2.425502000
H	1.376329000	-9.566654000	-0.607441000
H	2.316399000	-8.122243000	-1.123057000
H	6.605417000	-2.555686000	-0.887703000
H	8.780808000	2.236005000	-4.409527000
H	8.190958000	0.780892000	-3.530898000
Si	-2.779501000	0.136270000	-0.005929000
Si	-0.801690000	-0.285235000	1.323254000
Si	0.587345000	1.375152000	0.305840000
Si	-0.793485000	0.317828000	-1.370125000
Si	0.433149000	-1.482983000	-0.384788000
Si	2.380771000	-0.153819000	-0.046159000
H	-7.644216000	4.159061000	2.211033000

Supplementary Table 12: Atomic coordinates of the optimized structure of **9_{Tip}**.

C	-6.031921000	1.492084000	-5.421443000
C	-7.419290000	-3.933609000	2.251525000
C	-3.893954000	6.796818000	2.424496000
C	-4.962623000	2.407253000	-0.191005000
C	-5.157608000	0.236879000	-5.228923000
C	-5.454512000	-0.083612000	0.102826000
C	-6.046758000	-6.040400000	2.669222000
C	-6.020697000	-1.032063000	-5.064539000
C	-4.652070000	0.634142000	-2.758253000
C	-6.273548000	-4.831167000	1.739407000
C	-4.401410000	0.973944000	-0.281371000
C	-4.188565000	0.389943000	-4.062707000
C	-3.807290000	1.711961000	3.405421000
C	-2.465503000	6.634326000	1.868847000
C	-3.780113000	0.725504000	-1.657407000
C	-4.995931000	-4.025051000	1.532527000
C	-2.194463000	5.216183000	1.379146000
C	-1.404856000	7.067947000	2.902876000
C	-2.387184000	4.103725000	2.217781000
C	-4.335217000	-3.420097000	2.618979000
C	-4.448886000	-3.852785000	0.250487000
C	-3.363350000	-1.789180000	4.873398000
C	-1.950138000	3.892417000	-2.832527000
C	-2.804101000	0.247490000	-4.241788000
C	-1.700331000	4.977649000	0.087151000
C	-3.807803000	-2.836834000	-2.490173000
C	-2.397098000	1.656693000	2.790463000
C	-2.131905000	2.784920000	1.794053000
C	-2.368696000	0.609879000	-1.858472000
C	-3.172497000	-2.646299000	2.449939000
C	-1.402008000	3.680314000	-0.373606000
C	-3.294669000	-3.076063000	0.024425000

6. Supporting Information

C	-1.636066000	2.556740000	0.476063000
C	-1.886830000	0.358256000	-3.176145000
C	-2.447127000	-2.096445000	3.677098000
C	-2.651987000	-2.448713000	1.134010000
C	-1.312421000	1.622767000	3.882540000
C	-0.864878000	3.533161000	-1.798581000
C	-2.738091000	-2.983387000	-1.395976000
C	0.448468000	4.304327000	-2.031553000
C	-1.313393000	-3.057787000	4.095680000
C	-1.820283000	-4.192427000	-1.671618000
C	-0.405093000	0.183180000	-3.503532000
C	0.086416000	1.144153000	-4.601445000
C	-0.079962000	-1.279253000	-3.860608000
C	1.360985000	4.466576000	1.714305000
C	1.762442000	2.979199000	1.697837000
C	2.253026000	2.544541000	3.091156000
C	2.591770000	1.595449000	-0.337249000
C	2.786892000	2.648700000	0.609823000
C	3.745148000	0.852778000	-3.859622000
C	3.362678000	0.336237000	-2.459704000
C	3.555914000	1.387531000	-1.366622000
C	3.962853000	3.416957000	0.545117000
C	4.726204000	2.173932000	-1.372955000
C	4.957866000	3.182815000	-0.421770000
C	4.112124000	-0.965854000	-2.128497000
C	6.008968000	5.495904000	-0.552852000
C	6.257077000	3.979904000	-0.421238000
C	7.097720000	3.653454000	0.831551000
H	-6.681296000	1.389116000	-6.316439000
H	-5.408103000	2.400827000	-5.547438000
H	-6.696114000	1.659591000	-4.546881000
H	-8.365864000	-4.507920000	2.339657000
H	-7.182962000	-3.518741000	3.254666000
H	-5.799426000	2.546867000	-0.907975000

6. Supporting Information

H	-4.653225000	6.481895000	1.679437000
H	-4.093326000	7.854034000	2.699414000
H	-5.348637000	2.622695000	0.826965000
H	-6.340006000	-0.050097000	-0.566910000
H	-7.593095000	-3.077546000	1.567602000
H	-4.045277000	6.183475000	3.337971000
H	-5.735591000	0.738684000	-2.585366000
H	-6.970466000	-6.650711000	2.757473000
H	-5.815570000	0.092643000	1.137833000
H	-6.691600000	-1.174688000	-5.938153000
H	-5.764522000	-5.714013000	3.692873000
H	-4.543914000	0.109695000	-6.149205000
H	-4.181338000	3.158972000	-0.421179000
H	-6.657481000	-0.964315000	-4.156704000
H	-4.591187000	1.721630000	2.622681000
H	-3.949699000	2.613493000	4.037577000
H	-5.029910000	-1.106373000	0.065632000
H	-6.574668000	-5.224816000	0.742516000
H	-5.234434000	-6.693704000	2.289689000
H	-3.978241000	0.827877000	4.050933000
H	-2.368462000	7.306870000	0.986980000
H	-5.388380000	-1.937109000	-4.959107000
H	-4.252833000	-1.199736000	4.570864000
H	-1.573762000	8.114502000	3.234582000
H	-3.593458000	0.880375000	0.474817000
H	-2.759613000	4.267188000	3.242004000
H	-4.740927000	-3.559114000	3.632601000
H	-2.853634000	3.265155000	-2.691393000
H	-4.514881000	-2.017334000	-2.256596000
H	-1.441005000	6.417266000	3.802808000
H	-2.249022000	4.958374000	-2.743537000
H	-4.948894000	-4.334246000	-0.605387000
H	-4.389074000	-3.771533000	-2.639606000
H	-3.725338000	-2.716383000	5.366548000

6. Supporting Information

H	-1.531998000	5.838422000	-0.581930000
H	-2.810154000	-1.210727000	5.642224000
H	-1.583957000	3.728361000	-3.867366000
H	-2.424397000	0.041860000	-5.256940000
H	-3.323511000	-2.587392000	-3.456590000
H	-2.320026000	0.697415000	2.230821000
H	-0.381503000	6.997999000	2.480768000
H	-1.289369000	2.574905000	4.454660000
H	-1.964143000	-1.142769000	3.366812000
H	-1.493746000	0.795767000	4.601090000
H	-2.111528000	-2.065895000	-1.444026000
H	-0.611122000	2.463431000	-1.950905000
H	0.319822000	5.398823000	-1.894145000
H	-0.418261000	0.953415000	-5.571654000
H	-0.098699000	2.201801000	-4.328752000
H	-2.397332000	-5.140007000	-1.613081000
H	-0.309732000	1.467259000	3.437135000
H	-1.733052000	-4.038183000	4.407127000
H	-0.599221000	-1.588702000	-4.792611000
H	-0.733939000	-2.639169000	4.945563000
H	0.811954000	4.140027000	-3.067909000
H	0.492770000	4.612414000	2.388797000
H	-1.367169000	-4.126313000	-2.683724000
H	0.162824000	0.422913000	-2.576177000
H	1.062009000	4.821598000	0.710320000
H	1.243217000	3.957218000	-1.340559000
H	-0.603928000	-3.245063000	3.263463000
H	-0.395595000	-1.969348000	-3.051777000
H	-0.997417000	-4.250168000	-0.928460000
H	1.174585000	1.019564000	-4.765462000
H	0.835384000	2.407209000	1.466317000
H	2.187688000	5.112579000	2.079491000
H	1.011972000	-1.417138000	-4.013258000
H	1.516513000	2.824468000	3.872075000

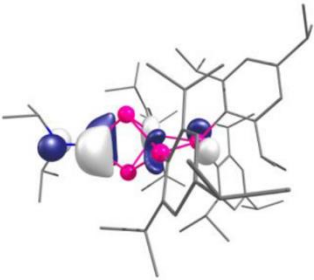
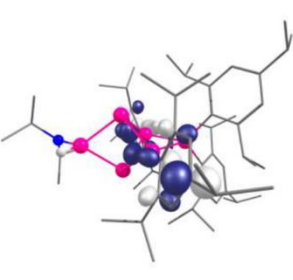
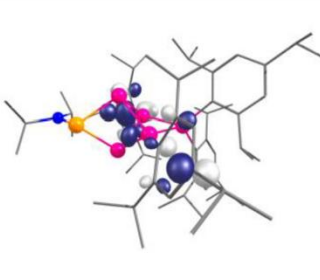
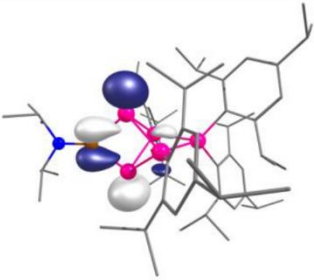
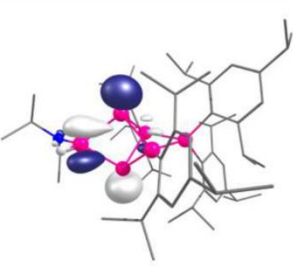
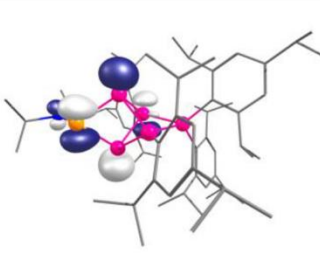
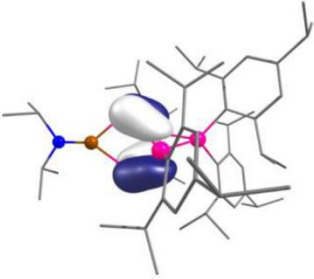
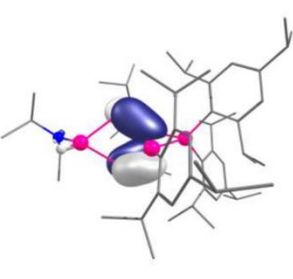
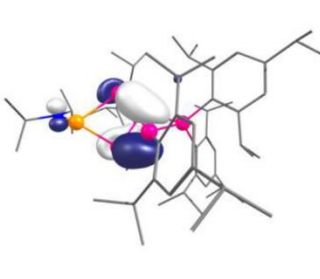
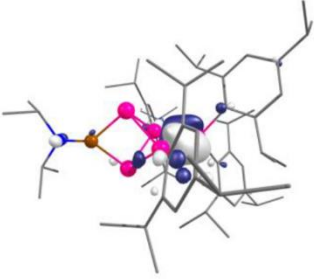
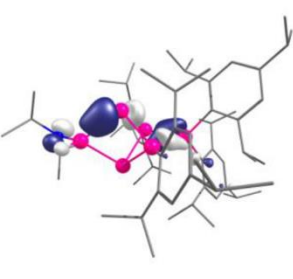
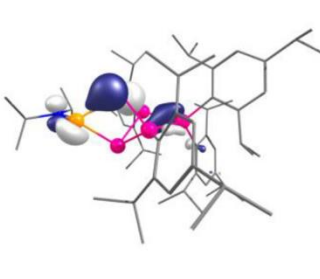
6. Supporting Information

H	2.276121000	0.093972000	-2.482172000
H	3.270194000	1.830582000	-4.080532000
H	2.407233000	1.447555000	3.143476000
H	3.214882000	3.040162000	3.341052000
H	3.428339000	0.125248000	-4.636066000
H	4.113832000	4.217189000	1.287551000
H	5.411258000	5.728859000	-1.457964000
H	4.843360000	0.977782000	-3.967033000
H	5.457253000	5.892683000	0.325744000
H	3.782734000	-1.388122000	-1.160251000
H	3.943073000	-1.735113000	-2.911165000
H	5.489030000	1.998153000	-2.148904000
H	5.204156000	-0.786845000	-2.050169000
H	6.969816000	6.048693000	-0.618542000
H	6.840425000	3.655663000	-1.312414000
H	6.560805000	3.949971000	1.757779000
H	7.307076000	2.566710000	0.904071000
H	8.066832000	4.195718000	0.813483000
P	1.817405000	-2.804722000	1.439182000
Si	-1.265238000	0.834832000	-0.293969000
Si	-1.192278000	-1.272051000	0.822657000
Si	0.826635000	-0.751886000	1.940920000
Si	1.094918000	0.444348000	-0.132370000
Si	0.760018000	-1.878454000	-0.397458000
C	3.628264000	-2.769999000	0.938852000
C	4.030760000	-3.857180000	0.103017000
C	4.603666000	-1.802163000	1.339112000
C	5.363970000	-3.933208000	-0.347675000
C	5.923878000	-1.944594000	0.874380000
C	6.330572000	-2.987216000	0.021213000
H	5.643178000	-4.761165000	-1.016696000
H	6.677603000	-1.200390000	1.173423000
C	3.052334000	-4.928138000	-0.387351000
H	2.102337000	-4.796584000	0.178351000

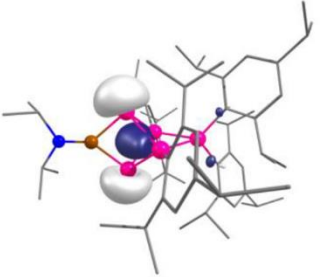
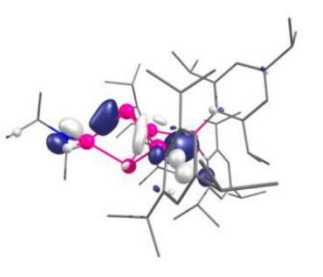
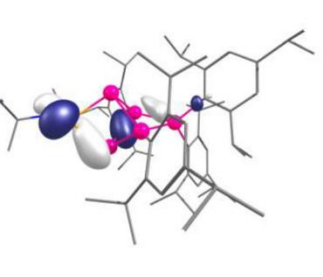
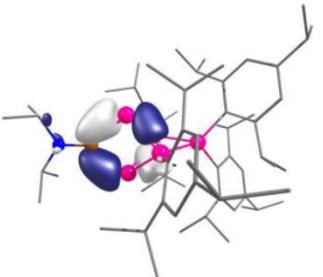
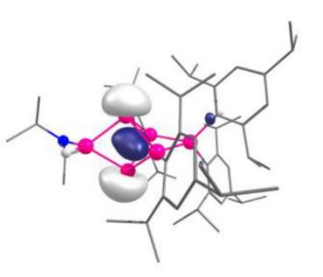
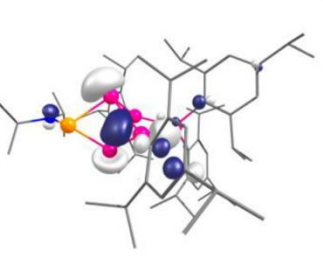
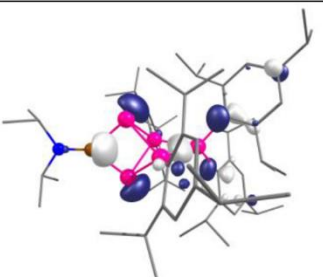
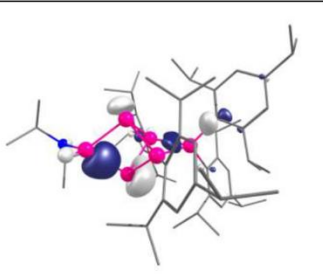
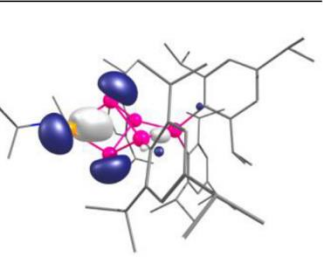
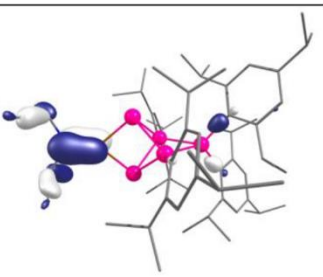
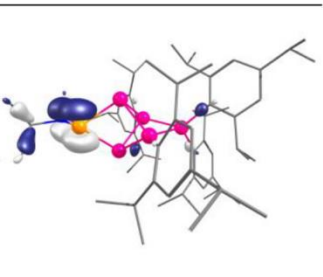
6. Supporting Information

C	3.544345000	-6.358497000	-0.096851000
C	2.722008000	-4.727491000	-1.879364000
H	2.323345000	-3.707493000	-2.065694000
H	3.628709000	-4.851191000	-2.509711000
H	1.961063000	-5.460244000	-2.222081000
H	4.461190000	-6.608851000	-0.672042000
H	2.767382000	-7.100413000	-0.377976000
H	3.774832000	-6.490295000	0.980193000
C	4.266806000	-0.631239000	2.258118000
H	3.268875000	-0.255590000	1.933403000
C	5.230513000	0.557964000	2.140230000
C	4.133692000	-1.100348000	3.721033000
H	3.395172000	-1.922636000	3.821705000
H	5.110141000	-1.473268000	4.097183000
H	3.804547000	-0.265333000	4.375679000
H	6.237964000	0.323920000	2.546062000
H	4.842773000	1.421839000	2.713623000
H	5.339219000	0.883594000	1.086425000
C	7.760269000	-3.007870000	-0.513574000
H	8.415187000	-2.643512000	0.311297000
C	7.897605000	-2.010555000	-1.686330000
C	8.257838000	-4.404283000	-0.920715000
H	8.120256000	-5.141880000	-0.103393000
H	7.719233000	-4.784151000	-1.815091000
H	9.336201000	-4.373207000	-1.181184000
H	7.242880000	-2.316319000	-2.530082000
H	8.943573000	-1.966694000	-2.057925000
H	7.594681000	-0.987400000	-1.382014000

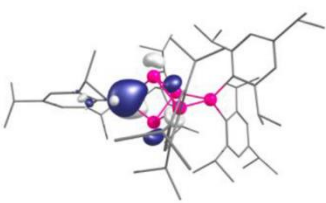
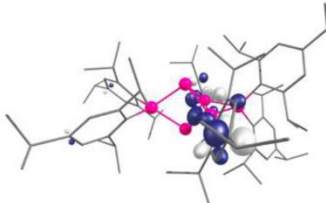
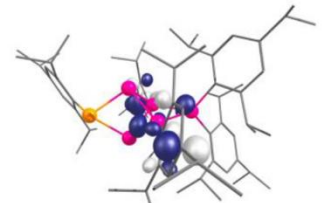
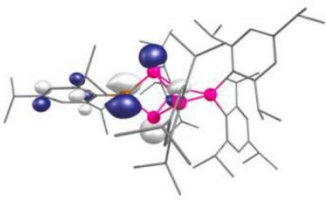
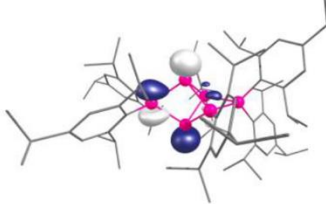
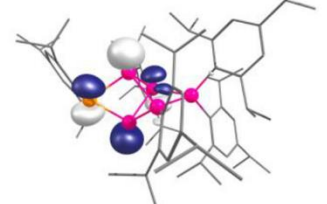
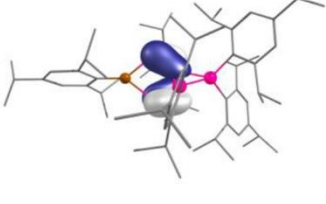
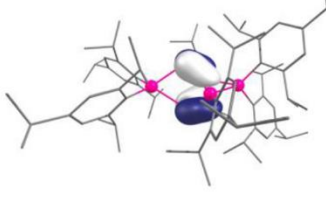
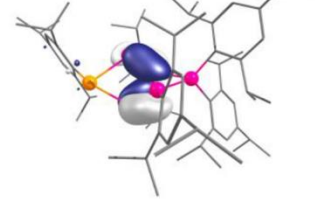
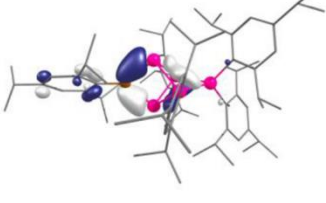
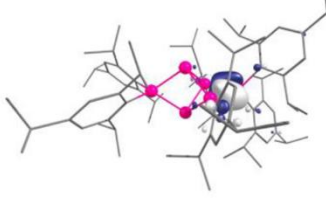
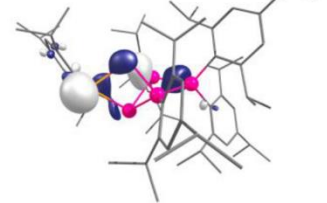
Supplementary Table 13: Comparison of Kohn-Sham frontier orbitals of **8**, **9** and the hypothetical diisopropylamino substituted Si₆ siliconoid **10** (level of theory: M06-2X/def2-SVPP//BP86/def2-SVP).

	8	10	9
LUMO+1	 -0.17 eV	 -0.05 eV	 -0.12 eV
LUMO	 -1.02 eV	 -1.26 eV	 -1.42 eV
HOMO	 -6.02 eV	 -6.31 eV	 -6.22 eV
HOMO-1	 -6.61 eV	 -6.64 eV	 -6.53 eV

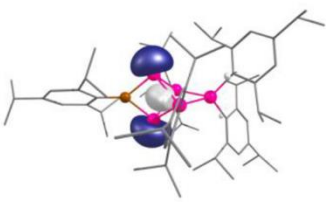
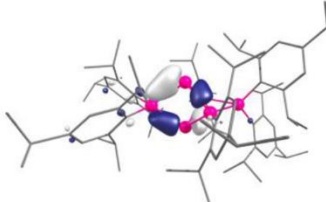
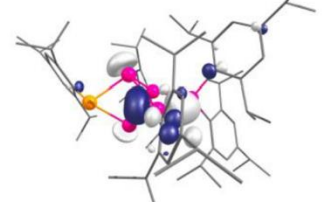
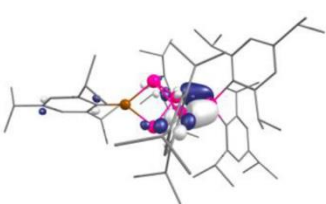
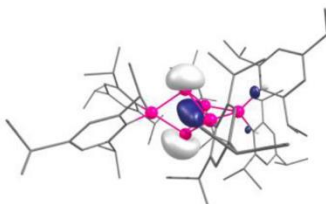
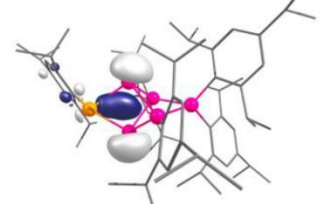
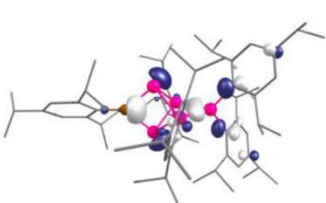
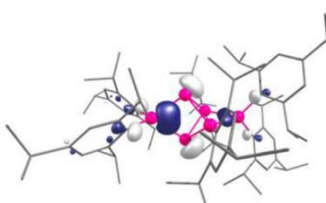
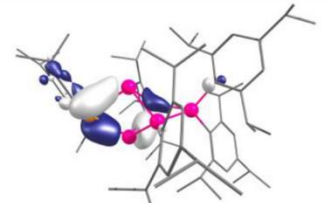
6. Supporting Information

HOMO-2	 -6.71 eV	 -6.81 eV	 -6.65 eV
HOMO-3	 -6.93 eV	 -6.92 eV	 -6.92 eV
HOMO-4	 -7.30 eV	 -7.28 eV	 -7.15 eV
HOMO-14	 -9.08 eV		 -8.89 eV

Supplementary Table 14: Comparison of Kohn-Sham frontier orbitals of the hypothetical all-Tip substituted doped siliconoids **8_{Tip}** (BSi₅Tip₅), **9_{Tip}** (PSi₅Tip₅) and hexasilabenzpolarene **2** (level of theory: M06-2X/def2-SVPP//BP86/def2-SVP).

	8_{Tip}	2	9_{Tip}
LUMO+1	 -0.96 eV	 -0.12 eV	 -0.20 eV
LUMO	 -1.34 eV	 -1.33 eV	 -1.61 eV
HOMO	 -6.11 eV	 -6.24 eV	 -6.28 eV
HOMO-1	 -6.62 eV	 -6.69 eV	 -6.50 eV

6. Supporting Information

HOMO-2	 -6.68 eV	 -6.89 eV	 -6.85 eV
HOMO-3	 -6.90 eV	 -6.90 eV	 -7.02 eV
HOMO-4	 -7.39 eV	 -7.12 eV	 -7.40 eV

6. Supporting Information

Supplementary Table 15: Comparison of selected calculated and experimentally observed bond lengths of **8** and **9** (level of theory: BP86/def2-SVP).

	8 (E = B)		9 (E = P)	
	calc. [Å]	exp. [Å]	calc. [Å]	exp. [Å]
Si1-E	2.0474	2.031(1)	2.3568	2.314(2)
Si1-Si3	2.3726	2.3270(4)	2.3780	2.391(avg.)
Si1-Si5	2.3969	2.3602(4)	2.4185	2.315(1)
Si1-Si2	2.6677	2.5911(4)	2.6814	2.613(1)
Si2-E	2.0556	2.038(1)	2.3602	2.303(2)
Si2-Si3	2.3995	2.3617(4)	2.4263	2.322(avg.)
Si2-Si5	2.3754	2.3215(4)	2.3533	2.370(1)
Si3-Si4	2.3817	2.3816(4)	2.3854	2.382(avg.)
Si4-Si5	2.3758	2.3594(4)	2.3744	2.357(1)
E-N	1.3913	1.374(2)	1.7206	1.651(3)

Supplementary Table 16: Comparison of calculated and experimentally observed ²⁹Si, ³¹P and ¹¹B NMR chemical shifts of **8** and **9** (δ values are given in ppm; level of theory: OLYP/def2-TZVPP//BP86/def2-SVP and OLYP/pcS-2//BP86/def2-SVP).

	8			9		
	δ_{calc} (def2tzvpp)	δ_{calc} (pcS-2)	δ_{exp}	δ_{calc} (def2tzvpp)	δ_{calc} (pcS-2)	δ_{exp}
<i>nudo</i> -Si	-290.9 _{avg}	-281.6 _{avg}	-288.6	-227.9	-221.9	-240.0
<i>nudo</i> -Si				-219.6	-214.8	-225.8
<i>ligato</i> -Si	-39.9 _{avg}	-37.4 _{avg}	-43.3	-66.4	-64.6	-76.7
<i>ligato</i> -Si				-6.1	-2.5	8.2
<i>remoto</i> -Si	22.8	29.2	39.0	148.3	148.8	153.7
<i>privo</i> -B	75.6	77.1	83.3	/	/	/
<i>privo</i> -P	/	/	/	448.6	439.0	386.7

6. Supporting Information

Supplementary Table 17: Comparison of calculated (**4'**) and experimentally observed ^{29}Si NMR chemical shifts of **4** (δ values are given in ppm; level of theory: OLYP/def2-TZVPP//BP86/def2-SVP and OLYP/pcS-2//BP86/def2-SVP).

	4'		4
	$\delta_{\text{calc}}(\text{def2tzvpp})$	$\delta_{\text{calc}}(\text{pcS-2})$	δ_{exp}
Si ⁻	-248.2 _{avg}	-237.4 _{avg}	-298.3
Si ⁻			
SiTip	-100.4 _{avg}	-98.3 _{avg}	-90.1
SiTip			
SiTip ₂	25.5	28.6	55.7

5. References

- [1] Song, F., Zhang, J., Zhao, Y., Chen, W., Li, L. & Xi, Z. Synthesis and antitumor activity of inositol phosphotriester analogues. *Org. Biomol. Chem.* **10**, 3642-3654 (2012).
- [2] *Gaussian 09*, Revision D.01, M. J. Frisch, G. W. Trucks, H. B. Schlegel, G. E. Scuseria, M. A. Robb, J. R. Cheeseman, G. Scalmani, V. Barone, B. Mennucci, G. A. Petersson, H. Nakatsuji, M. Caricato, X. Li, H. P. Hratchian, A. F. Izmaylov, J. Bloino, G. Zheng, J. L. Sonnenberg, M. Hada, M. Ehara, K. Toyota, R. Fukuda, J. Hasegawa, M. Ishida, T. Nakajima, Y. Honda, O. Kitao, H. Nakai, T. Vreven, J. A. Montgomery, Jr., J. E. Peralta, F. Ogliaro, M. Bearpark, J. J. Heyd, E. Brothers, K. N. Kudin, V. N. Staroverov, R. Kobayashi, J. Normand, K. Raghavachari, A. Rendell, J. C. Burant, S. S. Iyengar, J. Tomasi, M. Cossi, N. Rega, J. M. Millam, M. Klene, J. E. Knox, J.B. Cross, V. Bakken, C. Adamo, J. Jaramillo, R. Gomperts, R. E. Stratmann, O. Yazyev, A. J. Austin, R. Cammi, C. Pomelli, J. W. Ochterski, R. L. Martin, K. Morokuma, V. G. Zakrzewski, G. A. Voth, P. Salvador, J. J. Dannenberg, S. Dapprich, A. D. Daniels, Ö. Farkas, J. B. Foresman, J. V. Ortiz, J. Cioslowski, and D. J. Fox, Gaussian, Inc., Wallingford CT, **2009**.
- [3] Becke, A. D. Density-functional exchange-energy approximation with correct asymptotic-behavior. *Phys. Rev. A* **38**, 3098-3100 (1988).
- [4] Perdew, J. P. Density-functional approximation for the correlation energy of the inhomogeneous electron gas. *Phys. Rev. B* **33**, 8822-8824 (1986).
- [5] Grimme, S., Antony, J., Ehrlich S. and Krieg H. A consistent and accurate ab initio parameterization of density functional dispersion correction (DFT-D) for the 94 elements H-Pu. *J. Chem. Phys.* **132**, 154104 (2010).
- [6] Weigend, F. and Ahlrichs, R. Balanced basis sets of split valence, triple zeta valence and quadruple zeta valence quality for H to Rn: Design and assessment of accuracy. *Phys. Chem. Chem. Phys.* **7**, 3297-3305 (2005).
- [7] <http://www.chemcraftprog.com>.
- [8] Zhao, Y. and Truhlar, D. G. The M06 suite of density functionals for main group thermochemistry, thermochemical kinetics, noncovalent interactions, excited states, and transition elements: two new functionals and systematic

- testing of four M06-class functionals and 12 other functionals. *Theor. Chem. Acc.* **120**, 215-241 (2008).
- [9] London, F. The quantic theory of inter-atomic currents in aromatic combinations. *J. Phys. Radium.* **8**, 397-409 (1937).
- [10] McWeeny, R. Perturbation theory for Fock-Dirac density matrix. *Phys. Rev.* **126**, 1028 (1962).
- [11] Ditchfield, R. Self-consistent perturbation theory of diamagnetism. 1. Gauge-invariant LCAO method for N.M.R. chemical shifts. *Mol. Phys.* **27**, 789-807 (1974).
- [12] Wolinski, K., Hilton, J. F., and Pulay, P. Efficient implementation of the Gauge-independent atomic orbital method for NMR chemical shift calculations. *J. Am. Chem. Soc.* **112**, 8251-8260 (1990).
- [13] Cheeseman, J. R., Trucks, G. W., Keith, T. A., and Frisch, M. J. A comparison of models for calculating nuclear magnetic resonance shielding tensors. *J. Chem. Phys.* **104**, 5497-5509 (1996).
- [14] Handy, N. C. and Cohen, A. J. Left-right correlation energy. *Mol. Phys.* **99**, 403-412 (2001).
- [15] Hoe, W.-M., Cohen, A., and Handy, N. C. Assessment of a new local exchange functional OPTX. *Chem. Phys. Lett.* **341**, 319-328 (2001).
- [16] Lee, C., Yang, W. and Parr, R. G. Development of the Colle-Salvetti correlation-energy formula into a functional of the electron density. *Phys. Rev. B* **37**, 785-789 (1988).
- [17] Miehlich, B., Savin, A., Stoll, H. and Preuss, H. Results obtained with the correlation-energy density functionals of Becke and Lee, Yang and Parr. *Chem. Phys. Lett.* **157**, 200-206 (1989).
- [18] Weigend, F. Accurate Coulomb-fitting basis sets for H to Rn. *Phys. Chem. Chem. Phys.* **8**, 1057-1065 (2006).
- [19] Feller, D. The role of databases in support of computational chemistry calculations. *J. Comp. Chem.* **17**, 1571-1586 (1996).
- [20] Schuchardt, K. L., Didier, B. T., Elsethagen, T., Sun, L., Gurumoorthi, V., Chase, J. and Windus, T. L. Basis set exchange: a community database for computational sciences. *J. Chem. Inf. Model.* **47**, 1045-1052 (2007).

- [21] Jensen, F. Basis set convergence of nuclear magnetic shielding constants calculated by density functional methods. *J. Chem. Theory Comput.*, **4**, 719-727 (2008).

7. Curriculum Vitae